Bulletin
of
The Geological Society of America

VOLUME 70 March 1959 NUMBER 3

CONTENTS

	Pages
Determination of crustal structure from phase velocity of Rayleigh waves. By Maurice Ewing and Frank Press	229–244
Experimental deformation of dolomite single crystals. By Donald V. Higgs and John Handin	245–278
Turbidity-current deposits in San Pedro and Santa Monica basins off southern California. By Donn S. Gorsline and K. O. Emery	279–290
Seismic-refraction measurements in the Atlantic Ocean basins, in the Mediterranean Sea, on the Mid-Atlantic Ridge, and in the Norwegian Sea. By John Ewing and Maurice Ewing	291–318
Quaternary geology of the Bengal Basin, East Pakistan and India. By James P. Morgan and William G. McIntire	319–342
Pleistocene climates in eastern and southern Africa. By Richard Foster Flint	343–374
Short Notes	
Blancan mammalian fauna from Rio Grande Valley, Hudspeth County, Texas. By W. S. Strain	375–378
Quantitative study of columnar jointing. By C. Noble Beard	379–382

Subscription $15.00 per year.

Printing Office: Mt. Royal & Guilford Aves., Baltimore 2, Md.

Communications for publications should be addressed to The Geological Society of America, Dr. H. R. Aldrich, Secretary, 419 West 117 Street, New York, N. Y.

Please give notice of change of address 4 weeks in advance. Claims for nonreceipt of the Bulletin of a given month must be sent to the Secretary of the Society before the end of the second succeeding month.

Second-class Postage paid at Baltimore, Md.
Accepted for mailing at special rate of postage provided for in Section 1103
Act of October 3, 1917, authorized on July 8, 1918.

PAPERS IN PRESS FOR FORTHCOMING ISSUES

Geophysical Investigation of the Continental Margin Between Cape Henry, Virginia, and Jacksonville, Florida. By J. B. Hersey *et al.*

Rock Glaciers in the Alaska Range. By Clyde Wahrhaftig and Allan Cox

Geologic Evolution of the Beartooth Mountains, Montana and Wyoming. Part 2. Fracture Patterns. By Edgar Winston Spencer

Overthrust Ordovician and the Nannie's Peak Intrusive, Lone Mountain, Elko County, Nevada. By Donald W. Lovejoy

Eocene Stratigraphy and Paleontology, Orocopia Mountains, Southeastern California. By John C. Crowell and Takeo Susuki

Re-evaluation of the Salt Chronology of Several Great Basin Lakes. By Wallace S. Broecker and Alan F. Walton

BULLETIN OF THE GEOLOGICAL SOCIETY OF AMERICA
VOL. 70, PP. 229-244, 11 FIGS. MARCH 1959

DETERMINATION OF CRUSTAL STRUCTURE FROM PHASE VELOCITY OF RAYLEIGH WAVES

PART III: THE UNITED STATES

BY MAURICE EWING AND FRANK PRESS

ABSTRACT

Variations in phase velocity of Rayleigh waves from the Samoa earthquake of April 14, 1957 are reported for the United States. These variations are correlated with topography and Bouguer gravity anomaly on a continental scale, demonstrating regional isostatic compensation. The correlation of phase-velocity variations with crustal-thickness changes is justified, and permits specification of the mechanism of compensation as the regional Airy system.

Regional average crustal thicknesses are: Peninsular Ranges and Southwestern Desert, 40 km; Basin and Range Province, 48 km; Rocky Mountains, 47 km; Interior Plains, 35–41 km; Appalachian Mountains, 40 km.

CONTENTS

TEXT

	Page
Introduction	229
Acknowledgments	230
Method	230
Use of dispersed waves	230
Use and advantages of seismograph networks	234
Difficulties of "interferences"	237
Results: Wave-front chart	238
Regional results	243
Peninsular ranges—Southwestern Desert region	243
Basin and Range province	243
Rocky Mountain region	243
Interior Plains region	243
Appalachian region	243
Discussion	243
References cited	244

ILLUSTRATIONS

Figure	Page
1. Index map of station locations with reference to topography	232
2. Correlation chart of Rayleigh-wave crests	234
3. Progress of fifth Pasadena crest to Rapid City	235
4. Wave-front chart for fifth Pasadena crest	236
5. Phase-velocity determinations for Peninsular Ranges-Southwest Desert region	240
6. Phase-velocity determinations for Basin and Range Province	240
7. Phase-velocity determinations for Rocky Mountain region	241
8. Phase-velocity determinations for Interior Plains and Rocky Mountain regions	241
9. Phase-velocity determinations for Appalachian region	242
10. Phase-velocity determinations for Appalachian region	242
11. Transcontinental section	243

TABLES

Table	Page
1. Seismograph stations, co-ordinates, epicentral distances, and azimuths	231
2. Crustal-thickness determinations for selected segments	238
3. Crustal-thickness results by region	239

INTRODUCTION

The regional crustal structure of the United States was determined from phase-velocity measurements on the Rayleigh waves from the Samoa earthquake of April 14, 1957. Individual crests of the Rayleigh-wave train were traced across the United States, and crustal structure was inferred from variations in the velocity of each crest. Previous crustal-structure studies using the phase-velocity method (Press, 1956a, 1957) were restricted to California, where numerous seismograph stations with identical instruments permit identification and correlation of individual crests without difficulty. As an extension of that method, a system of correlation is used in the present paper which permits a positive identification and correlation

over triangles an order of magnitude larger. When small triangles are used, the instrumental constants for all the seismograms must be as nearly equal as possible, because a small phase shift would introduce a significant error in the observed travel time. With the larger triangles, small phase shifts are negligible, and seismograms from any of the various types of short-period vertical instruments in this country can be used. Thus data from the existing seismological stations of the United States become available for use in determining regional crustal structure. Variations in the observed velocity can be measured with considerable precision, and from these velocities, regional variations in crustal structure can be deduced. The significance of this method of investigating crustal structure is demonstrated by the fact that a single earthquake and the existing network of stations provide a more comprehensive survey of the crustal-structure variations in the United States than that provided by all previous studies.

Acknowledgments

It is a pleasure to acknowledge the co-operation of seismologists from stations cited in the text in making their records available to us. Manik Talwani assisted in all phases of this study, and John Nordquist participated in the calculations. This study was supported by a grant from the Basic Science Program of the Alfred P. Sloan Foundation.

Method

Use of Dispersed Waves

The phase-velocity method (Press, 1956a) is based on the dispersion of Rayleigh waves, which is governed by the structure of the crustal layer. Owing to dispersion, the velocity with which a given Rayleigh-wave crest advances depends upon the wave length or the period associated with that particular crest and upon the variation in elastic properties with depth. Theoretical methods (Ewing, Jardetzky, and Press, 1957, Ch. 4) permit calculation of the dispersion for various types of layering in the earth's crust. Thus, in principle, variations in the velocity of a Rayleigh-wave crest can be used to infer variations in the thickness of the crust. The procedure is particularly simple if thickness is the only parameter of the crust which is variable. In practical application of the phase-velocity method, the velocities can be readily measured with the desired accuracy if the Rayleigh waves have traversed a long oceanic path before entering the area to be investigated. Dispersion over the long oceanic path provides a long train of nearly sinusoidal oscillations with gradually varying period. The propagation of such a train of waves across the area to be investigated can be measured with adequate accuracy. The Rayleigh-wave train provided by a distant oceanic earthquake contains waves from 35 seconds to 15 seconds in period and from 150 km to 50 km in length. With an ideal distribution of stations, the method is effective for the study of a region with dimensions of the order of 1 wave length or larger. Thus with an ideal network of seismographs, it is feasible to study the average crustal structure over geological provinces of the order of only 50 to 100 km in dimension, but in the present work, in which only the existing network of permanent seismograph stations is used, the units investigated are somewhat larger and in many cases contain parts of two or more geological provinces. The results for each area will be given in terms of a phase velocity associated with each available Rayleigh-wave period and a crustal thickness for each of these periods. In general the values of thickness deduced for the various periods are the same within the limits of measurement, thus providing internal evidence of the validity of the method.

Reduction of velocity to crustal thickness involves the assumption that the elastic constants of the mantle and crust show no significant variation and that the thickness of the crust is the only parameter which changes. This assumption is supported by the fact that elastic velocities in the upper crust and mantle show no significant variations between mountain and shield areas. Press (1956b) reports that the velocity of earthquake-generated Lg waves for paths traversing the Sierra Nevada block is 3.53 km/sec. Using observations to distances of 1000 km from Nevada explosions, Bailey and Romney (1958) report velocities of 3.5 km/sec. and 8.0 km/sec. respectively for Lg shear waves in the crust and compressional waves in the upper mantle (Pn). Carder and Bailey (in press) give 6.15 and 8.2 km/sec. for compressional velocities in the crust and mantle respectively for Nevada explosions detected in the Basin and Range province. Press (unpublished report) observed velocities of 6.0 km/sec. and 3.45 km/sec. for explosion-generated compressional and shear waves in the upper crust along paths in southern California and Nevada.

TABLE 1.—SEISMOGRAPH STATIONS, CO-ORDINATES, EPICENTRAL DISTANCES, AND AZIMUTHS

TABLE 1.—SEISMOGRAPH STATIONS, CO-ORDINATES, EPICENTRAL DISTANCES, AND AZIMUTHS

Station	Abbreviations	Latitude	Longitude	Correlation Path	Great-Circle Distance in Degrees	Great-Circle Distance in Km	Azimuth to Epicenter	Fifth (Pas) Crest Period in Seconds	Fifth (Pas) Crest Arrival Time
									h m s
Ann Arbor	A.A.	42° 17′ 00″N	83° 44′ 00″ W	D	99.83°	11,100	257° 56′	30.3	20 06 42.0
Barrett	Bar.	32 40 48	116 40 18	C	72.22	8,030	237 22	21.5	19 52 44.5
Berkeley	Ber.	37 52 18	122 15 36	C	71.50	7,950	231 53	22.0	19 52 20.5
Boulder	Bou.	40 00 30	105 16 15	C	83.80	9,319	243 46	24.6	19 58 53.0
Boulder City	Bo. C.	35 58 51	114 50 02	C	75.27	8,369	237 50	22.9	19 54 21.0
Bozeman	Boz.	45 40 01	111 02 43	C	82.79	9,206	239 01	24.1	19 58 20.5
Butte	Butte	46 00 48	112 33 48	C	82.07	9,126	237 48	25.3	19 57 57.5
Chapel Hill	Ch. H.	35 54 45	79 03 10	E	102.15	11,359	259 32	31.2	20 07 51.0
China Lake	C. L.	35 49 00	117 35 48	C	73.30	8,151	235 55	22.5	19 53 21.0
Cleveland	Cle.	41 29 27	81 31 52	D	101.28	11,261	259 12	29.6	20 07 24.0
Columbia	Col.	34 00 00	81 02 00	E	100.19	11,140	258 06	28.8	20 06 51.0
Corvallis	Cor.	44 35 06	123 18 12	B	75.15	8,356	229 29	23.0	19 54 12.5
Dallas	Dal.	32 48 40	96 48 10	E	87.22	9,699	249 32	24.7	20 00 29.0
Eureka	Eur.	39 30 09	115 59 42	C	76.41	8,497	236 15	23.5	19 55 00.0
Fayetteville	Fay.	36 05 24	94 11 24	D	90.36	10,048	250 58	26.3	20 02 06.0
Fresno	Fre.	36 46 06	119 47 48	C	72.40	8,050	234 03	22.0	19 52 51.5
Halifax	Hal.	44 38 00	63 36 00	D	114.55	12,738	267 49	35.5	20 13 42.0
Horseshoe Bay	Ho. B.	49 22 39	123 16 33	A	78.30	8,707	228 40	24.0	19 55 39.5
Hungry Horse	H. H.	48 20 58	114 01 39	B	82.51	9,174	236 24	25.0	19 58 00.0
King Ranch	K. R.	35 19 42	119 44 42	C	71.59	7,961	234 28	22.0	19 52 28.5
Kirkland Lake	K. L.	48 08 41	80 01 45	C	103.44	11,502	261 39	31.8	20 08 31.0
Laramie	Lar.	41 19 00	105 35 00	C	84.17	9,360	243 26	24.9	19 59 06.0
Lawrence	Law.	38 58 00	95 15 00	D	90.52	10,065	250 21	25.4	20 02 11.5
Lubbock	Lub.	33 35 00	101 51 00	D	83.65	9,293	240 30	23.6	19 58 41.5
Mineral	Min.	40 20 48	121 36 06	C	73.43	8,165	231 47	23.0	19 53 24.0
Montreal	Mon.	45 30 09	73 37 26	D	107.50	11,953	265 28	33.8	20 10 24.0
Ottawa	Ott.	45 23 38	75 42 57	D	106.03	11,789	263 59	32.4	20 09 42.0
Palisades	Pal.	41 00 25	73 54 31	D	106.87	11,884	263 54	30.6	20 10 07.5
Pasadena	Pas.	34 08 54	118 10 18	C	71.98	8,004	235 56	21.9	19 52 39.5
Rapid City	R. C.	44 04 36	103 12 00	C	86.95	9,669	244 55	26.8	20 00 31.0
Reno	Reno	39 32 18	119 48 48	C	74.03	8,231	233 22	22.3	19 53 42.5
St. Louis	St. L.	38 33 10	90 14 00	D	94.13	10,467	253 26	27.8	20 03 56.0
Salt Lake City	S. L. C.	40 45 55	111 50 54	D	79.77	8,870	239 03	24.3	19 56 45.0
Shasta	Sha.	40 41 44	122 23 19	C	73.18	8,137	231 05	22.4	19 53 15.5
Shawinigan Falls	Sh. F.	46 33 06	72 45 48	D	108.17	12,028	266 25	32.2	20 10 42.5
State College	St. C.	40 48 00	77 52 00	D	103.88	11,551	261 21	31.2	20 08 39.0
Tinemaha	Tin.	37 03 18	118 30 42	C	73.59	8,182	235 09	22.6	19 53 28.5
Tucson	Tuc.	32 14 48	110 50 06	D	76.23	8,477	241 19	22.4	19 54 47.5
Ukiah	Uki.	39 08 00	123 13 00	C	71.70	7,973	230 48	22.3	19 52 30.0
Victoria	Vic.	48 31 12	123 24 54	A	77.67	8,636	228 41	23.0	19 55 20.5
Weston	Wes.	42 23 04	71 19 19	D	108.92	12,111	266 00	32.5	20 11 05.0
Woody	Wood.	35 42 00	118 50 48	C	72.40	8,051	235 02	22.0	19 52 51.5

FIGURE 1.—INDEX MAP OF STATIO

These Lg velocities depart insignificantly (less than 0.05 km/sec.) from those reported for shield areas. Similarly the compressional waves fall within the range of velocities 5.9–6.2 km/sec. and 8.0–8.2 km/sec. reported respectively for P and Pn in shield areas (Gutenberg, 1955). To account for the observed phase-velocity variations in terms of velocity changes rather than thickness changes would require reduced crustal and mantle-shear velocities in topographically high regions of about 3.34 and 4.45 km/sec. The corresponding compressional velocities would be reduced to 5.78 and 7.71 km/sec. These are significantly below the reported values. The striking similarity between most observed phase-velocity data and the reference phase-velocity curves lends further support to the correlation of phase-velocity variations with thickness changes.

In the phase-velocity method, as in other methods, lateral variations of the elastic parameters can be allowed for, and variations in crustal thickness can be separated from these, if the analysis must be carried out in this fashion.

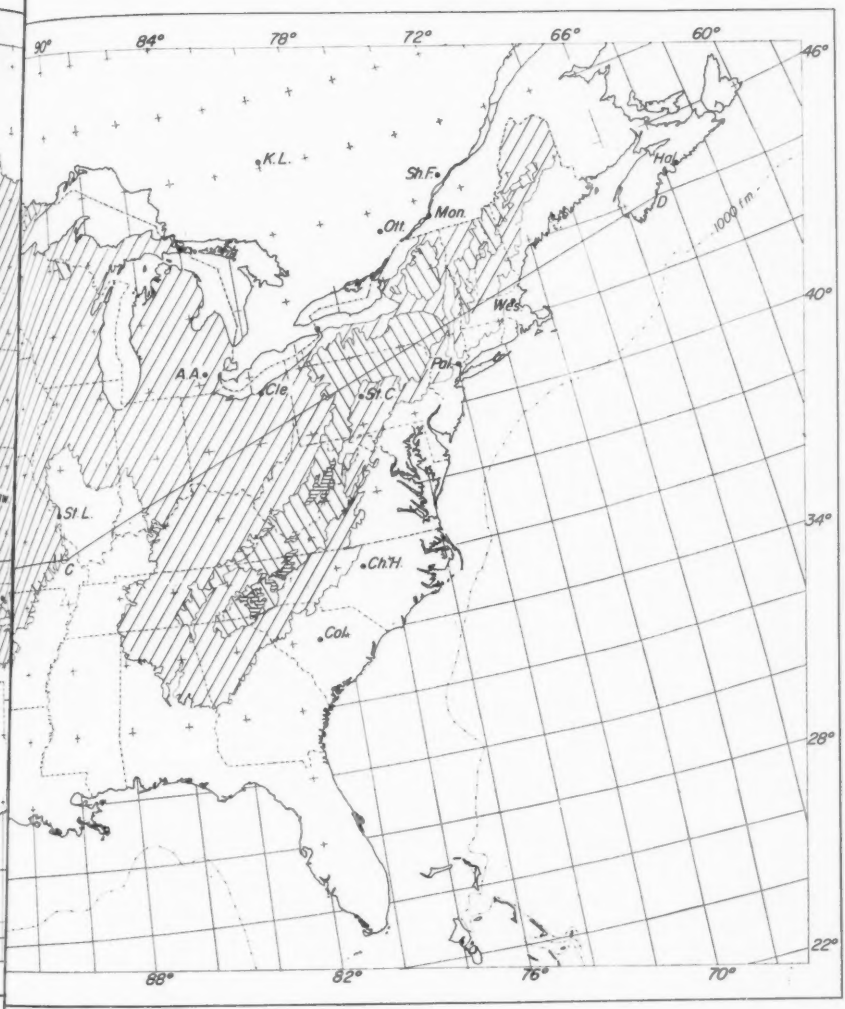

LOCATIONS WITH REFERENCE TO TOPOGRAPHY

Two other effects of dispersion must be considered if application of the phase-velocity method to crustal investigations is to be understood. In the dispersion of Rayleigh waves, the wave train lengthens as it travels outward. Thus not only the velocity of propagation of the crest but also the gradually changing period associated with it must be determined. This is usually done by plotting the sequential number of each wave in the train against the time of arrival. The measurement of the period is easily obtained from the slope of this curve except for the waves at the very beginning of the train, which may be of low amplitude. In general no difficulty is introduced into this study by the necessity of measuring the gradually changing period.

Since the period of a given wave in the train changes gradually as the wave moves along, another concept of wave propagation, that of group velocity, must be introduced. If at each seismograph station of the network, the recorded train of waves is examined and the time at which waves of a given period arrive is

measured, the velocity computed from these arrival times for the whole network would be the group velocity for waves of the chosen period. The group-velocity method has been used for North America by Brilliant and Ewing (1954) and for Africa by Press, Ewing, and Oliver (1956). It does not require the identification of the same crest at the various stations of the network; however, its precision is much less than that for the phase-velocity method. The precision is lowered because the rate of progress being measured is of a less definite feature of the wave train than in the case of the phase velocity.

The deduction of crustal thickness from the observed relationship between phase velocity and period is carried out by means of a grid similar to that shown in Figure 5. The method of construction of the grid has been described by Press (1956a). It is important to point out that these grids have an empirical basis but are compatible with theoretical dispersion curves and other seismological data. They depend on observations of group velocity of Rayleigh waves traversing long continental paths and on shear-wave velocities in the crust and mantle.

Use and Advantages of Seismograph Networks

Table 1 lists the seismograph stations used in this study, together with their co-ordinates,

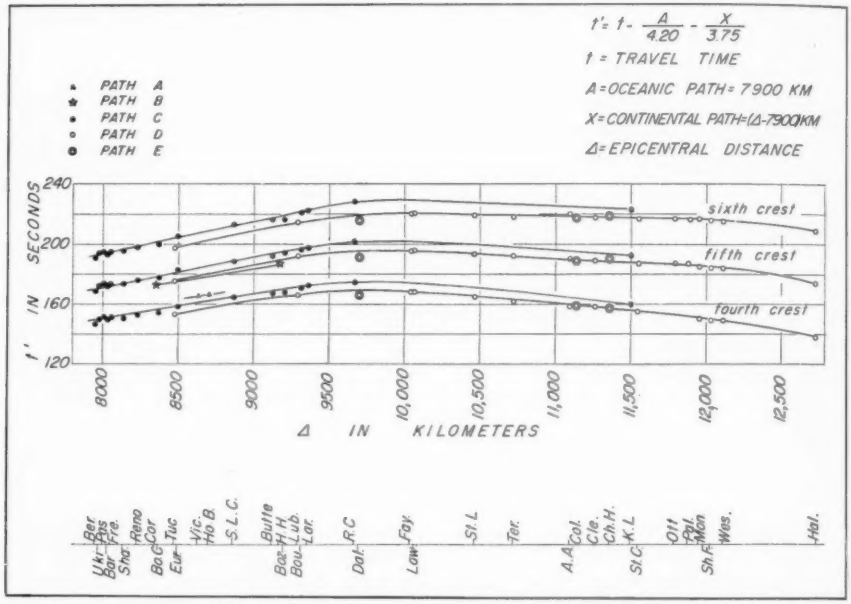

FIGURE 2.—CORRELATION CHART OF RAYLEIGH-WAVE CRESTS

Fourth, fifth, and sixth Rayleigh-wave crests correspond to systematic curves, each appropriate to a definite path acros the continent.

distances, and azimuths from the epicenter. Figure 1 is an index map showing station locations with reference to topography. This network system provides a means for correlation or positive identification of an individual crest when the distances between stations are considerably larger than the wave length. Given a triangular array of three seismograph stations, separated from each other by distances on the order of several wave lengths, one must identify the same wave crest in the seismograms written at each of the stations. For triangles of the size used in this study the correlation can be made in most cases to within ±1 wave length on the basis of record character alone by superposing the two seismograms and seeking a similarity in pattern. Since the greatest and the least known or admissible values of phase velocity for waves in the range of periods used in correlation are 3.3–4.1 km/sec., uniqueness may be established if only one of the possible correlations yields a velocity in this range. A formal network solution will not be given here; how-

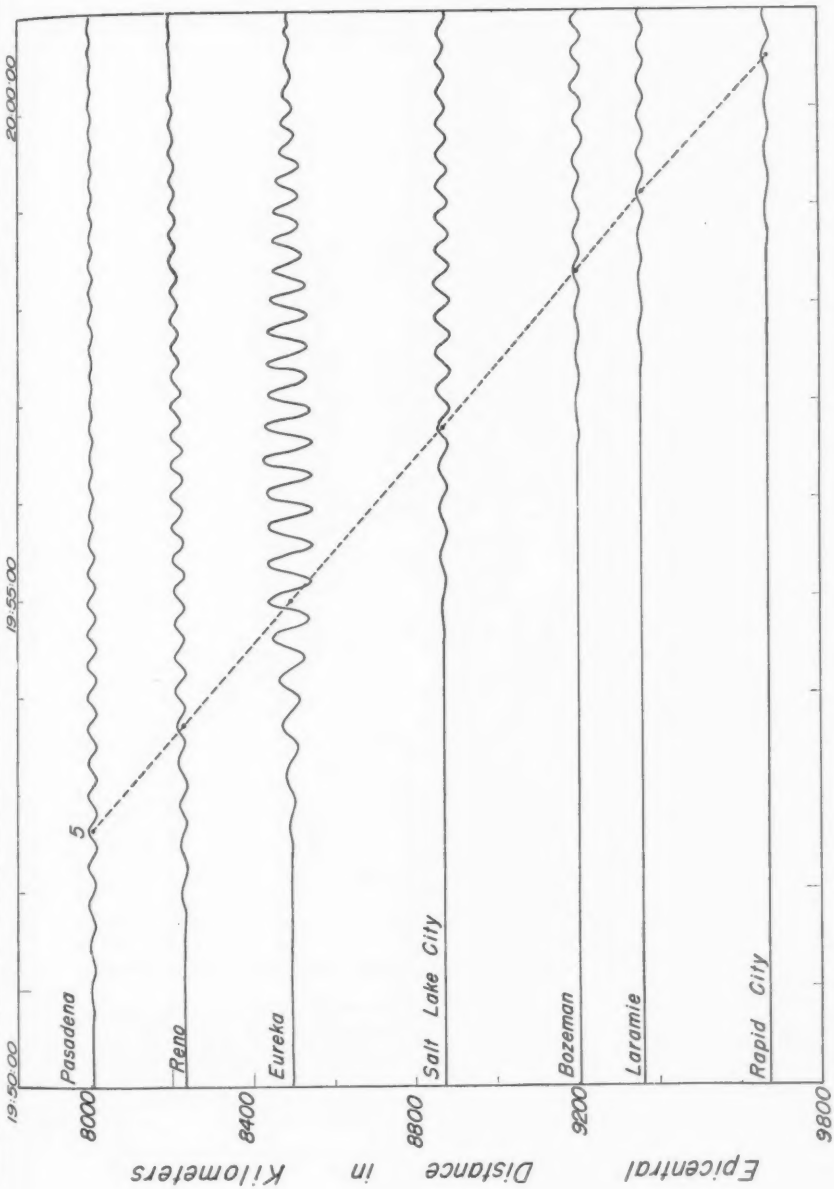

FIGURE 3.—PROGRESS OF FIFTH PASADENA CREST TO RAPID CITY

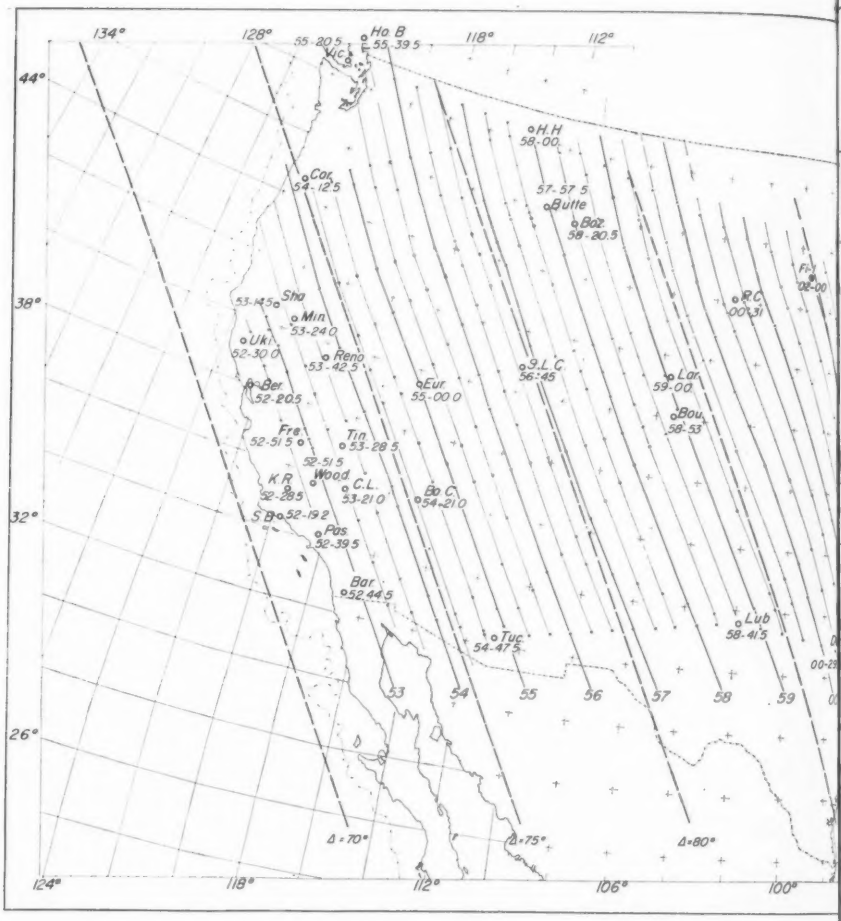

FIGURE 4.—WAVE-FRONT CHART FOR FIRST 20 SECONDS
Position of wave front is shown for successive increments in travel time

ever, in no case was there difficulty in establishing uniqueness within the network as defined. If two or three possible correlations existed for a given triangle, a new triangle was formed from two of the stations and one new station; in all cases, this was sufficient to give a unique solution. In this manner correlation of the waves could be established across the entire continent.

Passage of the wave front from ocean to continent is accompanied by refraction which is negligible when the wave front is nearly parallel to the continental margin. Under these circumstances another powerful criterion for establishing positive correlation is the requirement that the local direction of propagation deviate not more than a few degrees from the great-circle path from the epicenter.

Demonstration of proper correlation can be made with the chart shown in Figure 2, where reduced travel times of the fourth, fifth, and sixth crests are plotted against distance from epicenter for all the seismograph stations. The time reduction is made according to the equation

$$t' = t - \frac{A}{4.20} - \frac{X}{3.75}$$

where t is travel time, A is oceanic path taken as 7900 km, X is continental path (Δ − 7900 km), with Δ as epicentral distance. The factor

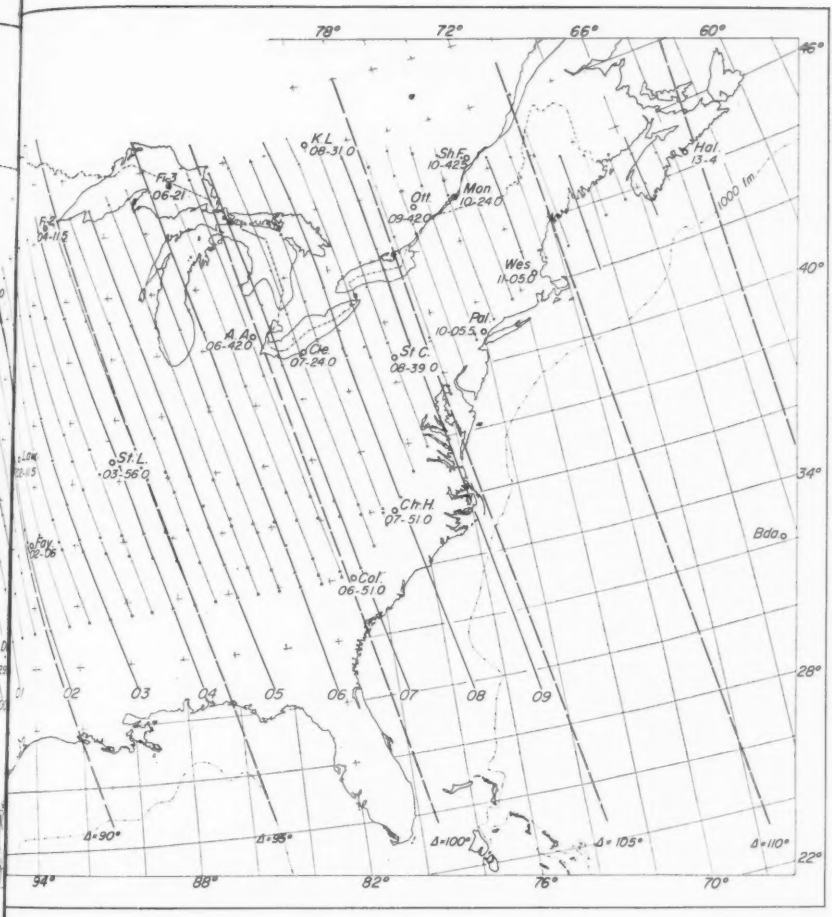

FOR FIFTH PASADENA CREST
of 20 seconds. Dashed lines indicate epicentral distances at 5° intervals.

$A/4.20$ corrects approximately for the oceanic path. Here 4.20 km/sec. is approximately the phase velocity of 20-second oceanic Rayleigh waves. Similarly the factor $X/3.75$ allows approximately for propagation across the continent at the mean phase velocity of 3.75 km/sec. With the open time scale permitted by use of reduced times it can be seen in Figure 2 that the travel times plot on a series of systematic curves, each appropriate to a definite path across the continent. Each station falls on one of these paths as indicated in Table 1. The change in t' from station to station on any of the correlation curves of Figure 2 is so small with respect to the time between crests as to preclude the possibility of miscorrelation.

In Figure 3, the passage of Pasadena crest number five from station to station is depicted by means of tracings from seismograms.

Difficulties of "Interferences"

A long-standing problem in surface wave investigations is significant in the present study. This is the problem of the "interferences" observed in an otherwise uniform and gradually varying train of sinusoidal surface waves. Interferences are characterized by a strong decrease in amplitude over an extent of a few cycles, with the amplitude commonly vanishing so that no waves can be counted through it. The plots of period versus arrival time for the

various seismograms indicate that the factor which causes the large change in amplitude also disturbs the phase in the neighborhood of extracting phase velocity from seismograms, involving amplitude as well as phase, may solve the problem.

TABLE 2.—CRUSTAL-THICKNESS DETERMINATIONS FOR SELECTED SEGMENTS

(See Table 1 for explanation of station abbreviations.)

Stations	Distances (km)	Mean Period (seconds)	Travel Time (seconds)	Velocity (km/sec.)	Thickness (km)	Mean Thickness (km)
Pas.-Bo.C.	365	30.0	97.3	3.76	42	
		25.0	99.5	3.68	39	39
		19.9	102.5	3.57	36	
Fre.-R.C.	1619	29.7	445.5	3.63	50	
		25.0	457.0	3.54	47	48
		20.0	476.0	3.40	48	
Cor.-H.H.	818	29.5	218.0	3.75	42	
		25.0	225.0	3.64	41	41
		20.1	231.5	3.53	39	
Min.-Butte	961	29.9	264.5	3.63	50	
		25.3	272.0	3.53	48	48
		20.3	280.0	3.43	46	
Bo.C.-Bou.	950	31.6	262.5	3.62	53	
		24.9	270.0	3.52	49	49
		20.0	276.0	3.44	45	
R.C.-K.L.	1833	30.0	477.5	3.84	37	
		25.0	493.0	3.72	37	36
		19.7	508.0	3.61	34	
Law.-Cle.	1196	30.5	309.0	3.87	36	
		25.4	320.0	3.74	37	36
		19.5	332.0	3.60	34	
Dal.-Col.	1441	30.2	375.5	3.84	38	
		24.7	391.0	3.69	38	38
		20.0	409.5	3.52	39	
Cle.-W.	850	31.0	221.0	3.85	38	
		25.0	228.0	3.73	37	36
		19.9	235.5	3.61	34	
Mon.-Hal.	785	29.8	204.0	3.85	37	38
		26.2	212.0	3.70	39	

the interference. Fortunately these interferences generally occur sufficiently late in the wave train to permit correlations for periods down to 16 or 17 seconds. It was found that values of phase velocity versus period follow the trend indicated by the phase-velocity grids from the beginning of the wave train out to the occurrence of the first interference, but that beyond an interference, the points usually diverge wildly from an acceptable pattern. At the present time data from portions of seismograms showing obvious interferences are rejected. Perhaps more sophisticated methods of

RESULTS: WAVE-FRONT CHART

The arrival times for the crest identified as wave number five in the train at Pasadena are listed in Table 1. Figure 4 is a wave-front chart constructed from these data. The locations of the seismograph stations are indicated on the chart together with the arrival time of the same wave at each station. The position of the wave was plotted for successive increments in travel time of 20 seconds on the basis of the correlated arrival times for all stations. Even on this diagram a systematic regional variation in the spacing of the wave fronts may be seen.

The deviation of the wave fronts from a circular form with center at the epicenter is not large. Lines showing epicentral distances from 70° to 95° have been placed on Figure 4 for comparison. This simple wave-front pattern follows from the choice of an earthquake with Rayleigh waves incident upon the continent at almost normal incidence for the greater part of the coast line. Evernden (1954) has observed much greater deviations from great-circle propagation in studying waves incident upon the continental border at an oblique angle.

The refraction at a continental margin is clearly demonstrated in the northwestern part of the chart, where the coast line is not parallel to the wave fronts. An approximate velocity computed for the oceanic part of this segment for travel from the great circle through Corvallis to Victoria showed 4.12 km/sec., nearly equal to 4.2 km/sec., the expected high velocity for the oceanic segment of the path to Victoria.

An attractive feature of the wave-front chart is its availability for the measurement of phase velocity across segments of the continent chosen for their geological interest. This rough measurement is accomplished by using the distance traversed normal to the wave fronts in an interval of time chosen that is long enough to minimize the errors inherent in the graphic method. This simple procedure is in most cases adequate for revealing the main features of variation of crustal structure to be discussed later. Results are shown in Table 2. For example, Pasadena wave number five traversed a 1619-km path from Fresno to Rapid City in 476 sec., giving a mean phase velocity of 3.40 km/sec. For the average period of 20 seconds, this corresponds to a crustal thickness of 48 km.

In addition to measurement of phase velocity by this rough graphical method, more accurate values can be obtained by considering individual triangles suitably chosen with respect to the topography of the geological provinces.

TABLE 3.—CRUSTAL THICKNESS RESULTS BY REGION

(See Table 1 for explanation of station abbreviations.)

Array	Province	Mean Crustal Thickness (in km)	Standard Deviation (in km)	Standard Error of Mean
Pas., Bar., Bo. C.	Peninsular Range-S. W. Desert	38.1	1.9	0.6
Bar., Bo. C., Tuc.	Peninsular Range-S. W. Desert	42.1	2.2	0.6
Pas., Bar., Tuc.	Peninsular Range-S. W. Desert	47.1	3.4	1.0
Pas., Bo. C., Tuc.	Peninsular Range-S. W. Desert	39.0	1.7	0.4
Pas., Reno, Bo. C.	Basin and Range	40.1	1.7	0.5
Reno, Bo. C., Eur.	Basin and Range	51.3	2.3	0.8
Eur., S. L. C., Butte	Basin and Range	47.8	2.5	0.7
Bo. C., Eur., S. L. C.	Basin and Range	49.0	2.2	0.7
Tuc., Bou., Lub.	Rocky Mountain	47.2	5.4	1.5
S. L. C., Butte, Bou.	Rocky Mountain	41.7	9.8	3.0
R. C., S. L. C., Boz.	Rocky Mountain	48.7	2.2	1.0
R. C., Bou., Boz.	Rocky Mountain	47.8	2.8	0.9
S. L. C., Lar., Boz.	Rocky Mountain	47.5	4.2	1.1
R. C., Lar., Boz.	Rocky Mountain	47.7	3.3	1.0
S. L. C., Lar., R. C.	Rocky Mountain	49.0	1.1	0.3
Lub., Dal., Law.	Interior Plains	40.6	3.4	0.9
Lub., Dal., Fay.	Interior Plains	40.9	2.3	0.7
Lub., Bou., Law.	Interior Plains	39.3	2.9	0.7
Fay., Law., St. L.	Interior Plains	34.5	2.8	0.7
Cle., Ch. H., Pal.	Appalachian Mts.	40.1	2.4	0.6
Ch. H., St. L., Pal.	Appalachian Mts.	40.4	2.0	0.5
Cle., K. L., Pal.	Appalachian Mts.	41.0	1.6	0.4
Pal., Sh. F., Wes.	Appalachian Mts.	37.1	2.9	1.0
Sh. F., Wes., Hal.	Maritime	38.2	3.0	1.0

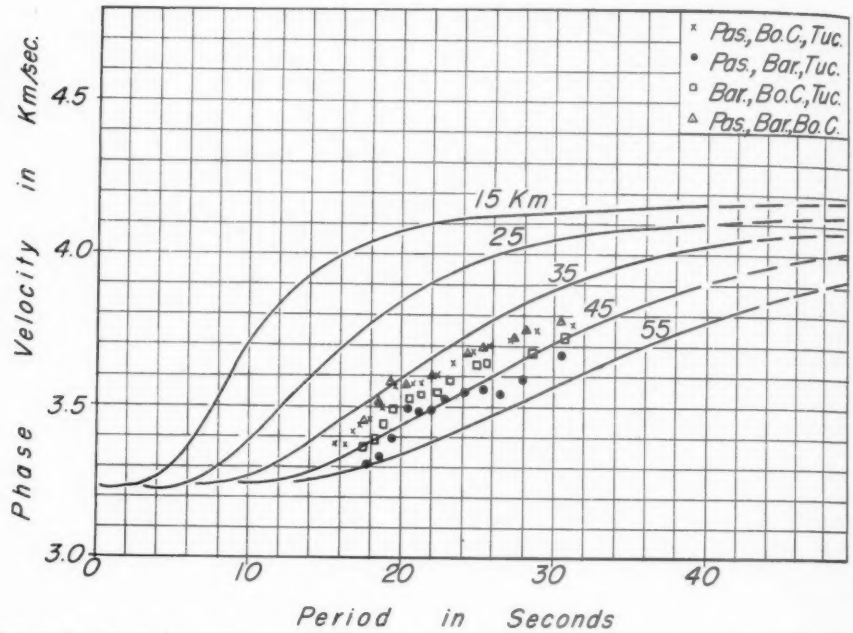

FIGURE 5.—PHASE-VELOCITY DETERMINATIONS FOR PENINSULAR RANGES-SOUTHWEST DESERT REGION

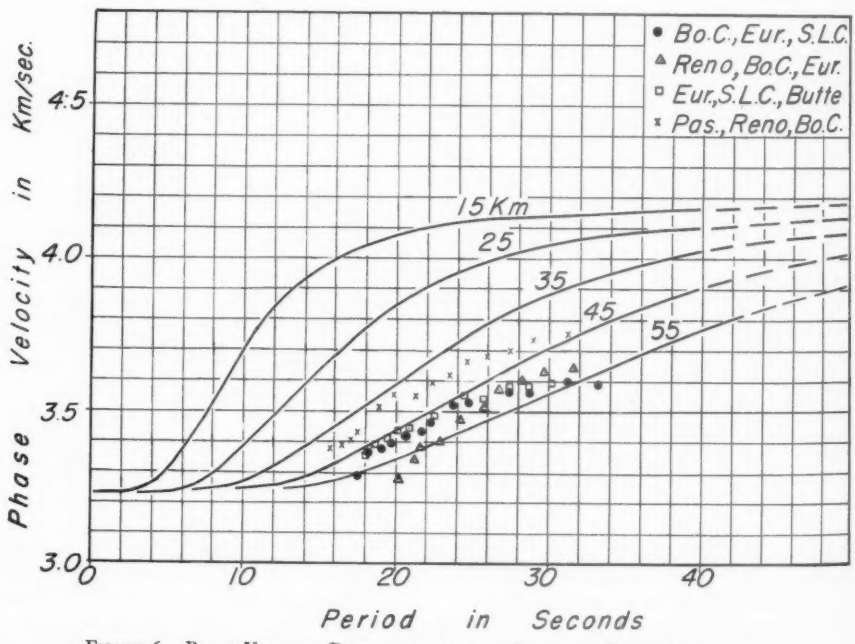

FIGURE 6.—PHASE-VELOCITY DETERMINATIONS FOR BASIN AND RANGE PROVINCE

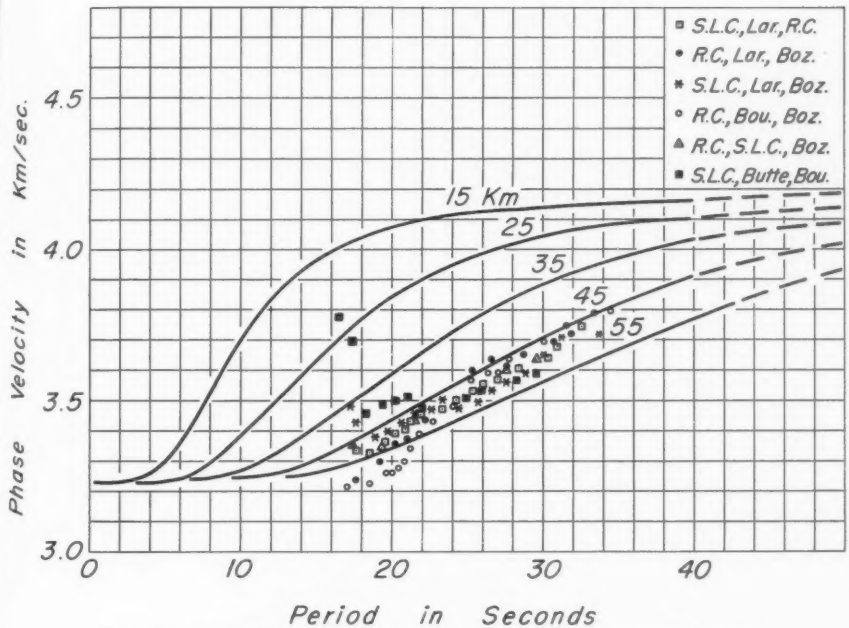

FIGURE 7.—PHASE-VELOCITY DETERMINATIONS FOR ROCKY MOUNTAIN REGION

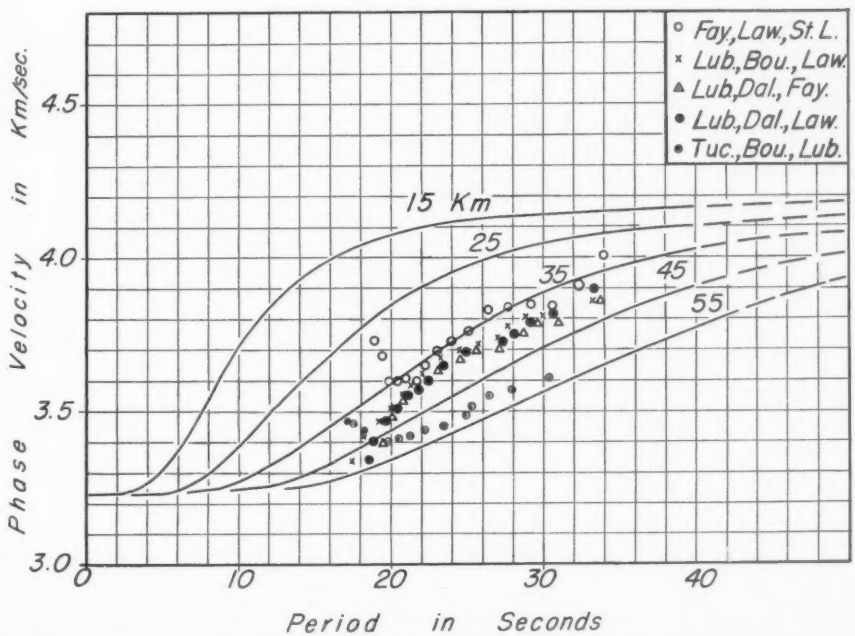

FIGURE 8.—PHASE-VELOCITY DETERMINATIONS FOR INTERIOR PLAINS AND ROCKY MOUNTAIN REGIONS

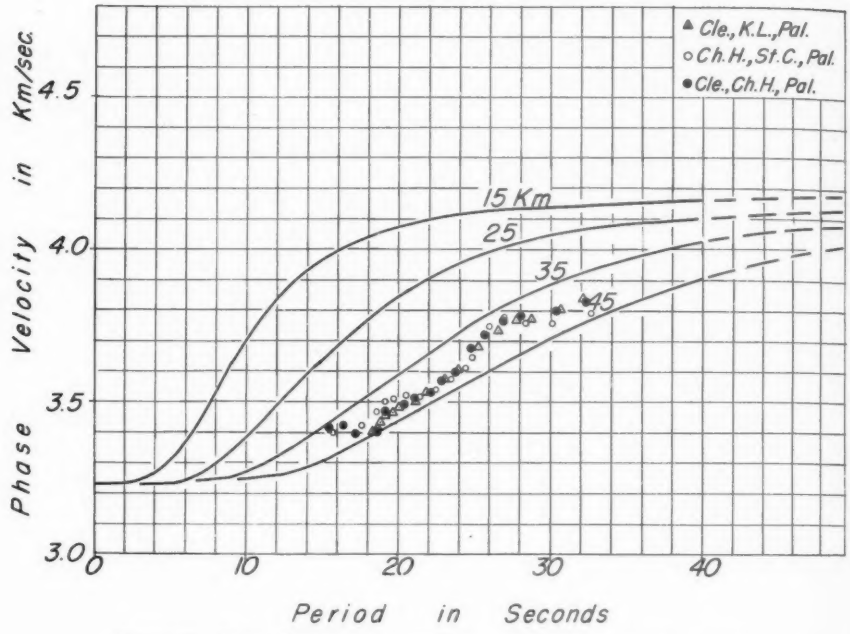

FIGURE 9.—PHASE-VELOCITY DETERMINATIONS FOR APPALACHIAN REGION

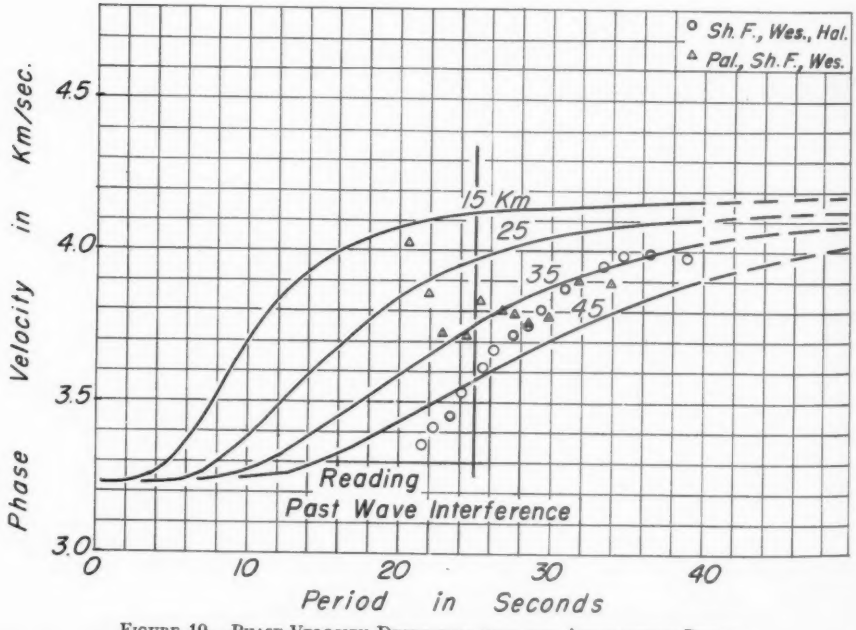

FIGURE 10.—PHASE-VELOCITY DETERMINATIONS FOR APPALACHIAN REGION

Regional Results

Peninsular Ranges—Southwestern Desert Region (Figure 5)

The triangles cover a composite region made up of parts of the Peninsular Ranges, and the Colorado and Mohave deserts. A crustal thickness of 38–42 km is indicated for this region, the average being 40 km. A determination of 47 km for the triangle Pasadena, Barrett, and Tucson is excluded because of the uncertain effect on phase velocity of the Gulf of Lower California, which lies in the path of the wave front. (See Table 3.)

Basin and Range Province (Figure 6)

Crustal thickness ranges from 40 to 51 km in the Basin and Range province; it averages 47 km. The value 39 km determined for a path between Pasadena and Boulder City indicates a thickening of the crust as one enters this province from the southwest.

Rocky Mountain Region (Figures 7 and 8)

Data from seven triangles indicate crustal thickness in the range 42–49 km, with an average value of 47 km.

Interior Plains Region (Figure 8)

Crustal thickness in the Interior Plains region ranges from 35 to 41 km, the larger values occurring under the higher plains in the western part.

Appalachian Region (Figures 9 and 10)

The triangle Chapel Hill-State College-Palisades includes the Appalachian Mountains and gives a crustal thickness of 40 km. A thickness of about 40 km is indicated for the triangle Cleveland-Kirkland Lake-Palisades, which also includes part of the Canadian Shield. In Figure 10 the data for periods smaller than 25 seconds scatter because of interferences on the seismograms. If these data are neglected, the triangle Palisades-Shawinigan Falls-Weston shows a thickness of 37 km.

A thickness of 38 km is indicated for the triangle Shawinigan Falls-Weston-Halifax. This region includes the Maritime Province as well as highlands associated with the Appalachian trend.

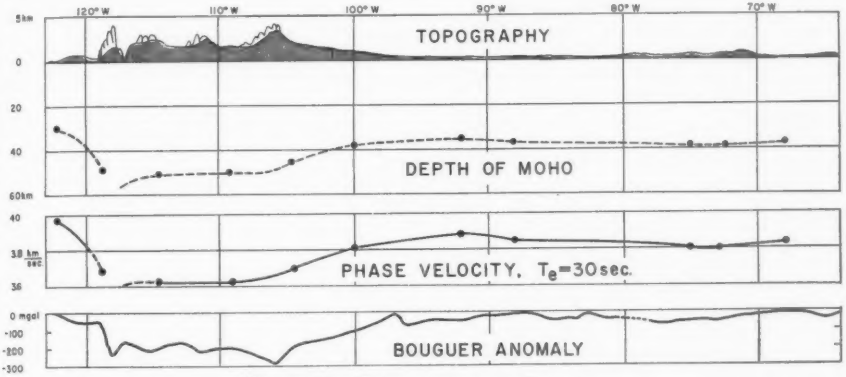

FIGURE 11.—TRANSCONTINENTAL SECTION
Topography, phase velocity, and Bouguer anomaly show correlation based on experimental data only.

Discussion

The measurements demonstrate clearly a relationship between phase velocity and mean elevation. Figure 11 shows a transcontinental section of topography and phase velocity of Rayleigh waves with periods of 30 seconds. The depths of the Mohorovičić discontinuity deduced from the phase-velocity curves in Figures 5–10 and the Bouguer gravity anomalies (Woollard, 1943, 1948) are shown. Some results from earlier studies (Press, 1956a, 1957) are also included. Location of the section is indicated on Figure 1 as *ABB'CD*.

The phase velocities are lowest in the regions of greatest elevation. Thus the phase velocity is least in the Basin and Range and Rocky Mountain areas, much greater in the mid-

continent and coastal areas, and has intermediate values in the Appalachian areas. It must be emphasized that this correlation has been established on a purely observational basis and involves no interpretation of phase-velocity variations in terms of thickness or composition of the various continental layers. The comparison of phase velocities with Bouguer anomalies establishes on a continental scale a correlation between a seismic parameter and a gravity parameter. The known correlation of gravity with topography is a proof of regional isostatic compensation. The additional correlation with phase velocity demonstrates the significance of phase velocity as an indication of crustal structure.

Interpretation of phase velocity in terms of crustal thickness allows specification of the mechanism of isostatic compensation. The regional Airy system of compensation is a good approximation. From Figure 11 in the region 95°–100°W. longitude it is seen that regional Bouguer anomalies as small as 50 milligals can be compensated as shown by the clear reduction in phase velocity.

References Cited

Bailey, Leslie F., and Romney, Carl, 1958, Seismic waves from the Nevada underground explosion of September 19, 1957 (Abstract): Geol. Soc. America Bull., v. 69, p. 1672

Brilliant, R. M., and Ewing, Maurice, 1954, Dispersion of Rayleigh waves across the U.S.: Seismol. Soc. America Bull., v. 44, p. 149–158

Carder, D. S., and Bailey, L. R., (in press), Seismic wave travel times from nuclear explosions: Seismol. Soc. America Bull.

Evernden, Jack, 1954, Direction of approach of Rayleigh waves and related problems, Part II: Seismol. Soc. America Bull., v. 44, p. 159–184

Ewing, Maurice, Jardetzky, W. S., and Press, Frank, 1957, Elastic waves in layered media: N.Y., McGraw-Hill Book Co., 380 p.

Gutenberg, Beno, 1955, Wave velocities in the earth's crust, p. 19–34 *in* Poldervaart, Arie, Crust of the earth: Geol. Soc. America Special Paper 62, 762 p.

Press, Frank, 1956a, Determination of crustal structure from phase velocity of Rayleigh waves, Part I: Southern California: Geol. Soc. America Bull., v. 67, p. 1647–1658

—— 1956b, Velocity of Lg waves in California: Am. Geophys. Union Trans. v. 37, p. 615–618

—— 1957, Determination of crustal structure from phase velocity of Rayleigh waves, Part II: San Francisco Bay Region: Seismol. Soc. America Bull., v. 47, p. 87–88

Press, Frank, Ewing, Maurice, and Oliver, Jack, 1956, Crustal structure and surface wave dispersion in Africa: Seismol. Soc. America Bull., v. 46, p. 97–103

Woollard, George P., 1943, Transcontinental gravitational and magnetic profile of North America and its relation to geologic structure: Geol. Soc. America Bull., v. 54, p. 747–790

—— 1948, Gravity and magnetic investigations in New England: Am. Geophys. Union Trans., v. 29, p. 306–317

Lamont Geological Observatory, Columbia University, Palisades, New York; Seismological Laboratory, California Institute of Technology, 220 North San Rafael Ave., Pasadena, California

Manuscript Received by the Secretary of the Society, April 21, 1958

Lamont Geological Observatory Contribution No. 238

Division of Geological Sciences, California Institute of Technology, Contribution No. 874

BULLETIN OF THE GEOLOGICAL SOCIETY OF AMERICA
VOL. 70, PP. 245–278, 20 FIGS., 6 PLS. MARCH 1959

EXPERIMENTAL DEFORMATION OF DOLOMITE SINGLE CRYSTALS

BY DONALD V. HIGGS AND JOHN HANDIN

ABSTRACT

Jacketed cylindrical specimens of dolomite single crystals were deformed dry under a constant confining pressure of 5000 bars at a strain rate of 1 per cent per minute at temperatures from 24°C. to 500°C. Uniaxial compression and extension experiments were carried out with the load oriented (1) parallel to the optic axis c_v, (2) parallel to a horizontal axis a, (3) perpendicular to a cleavage r, and (4) parallel to an edge $[f:f]$.

In orientations (1) and (2), unfavorable for basal translation, crystals loaded at temperatures below 400°C. are brittle and fail on shear fractures inclined at about 30° to the direction of greatest principal pressure. At 400°C. and above, specimens of orientations (1) and (2) flow in compression and extension, respectively. Large permanent deformations are achieved in orientations (3) and (4), favorable for translation gliding, at all temperatures.

Petrographic studies by the techniques developed by Turner in his investigation of calcite crystals (Turner *et al.*, 1954a) reveal that translation gliding on $c\{0001\}$ along the gliding line parallel to an a axis is the flow mechanism for orientations (3) and (4) below 400°C. This confirms Johnsen's (1902) first discovery and the results of the later work of Turner *et al.* (1954b) on dolomite rock. The intracrystalline slip mechanism for orientations (1) and (2) is twin gliding on $f\{02\bar{2}1\}$ in a negative direction sense (in contrast to the positive sense of $e\{01\bar{1}2\}$ twinning in calcite), which, however, occurs only at about 400°C. and above. This confirms the hypothesis of Fairbairn and Hawkes (1941) and the data of Turner *et al.* (1954b) and Handin and Fairbairn (1955) for dolomite rocks. In orientations (3) and (4) twinning occurs to the exclusion of translation at 500°C., and both mechanisms are operative at 400°C.

The critical resolved shear stress for translation increases with temperature up to 400°C. at least, a most unusual behavior. The critical stress for twinning decreases at least in the range of 400°C. to 500°C., and the two critical stresses are equal at about 400°C.

A few magnesite crystals were deformed parallel to c_v under similar conditions. Basal translation cannot occur in this orientation, but translation on $r\{10\bar{1}1\}$ along the line $[10\bar{1}1:02\bar{2}1]$ does occur. No twinning was detected.

CONTENTS

TEXT

	Page
Introduction	246
Acknowledgments	247
Intragranular rotation phenomena	247
Notation conventions	249
Crystallographic notation	249
Notation for rotated lamellae	249
Gliding mechanisms	250
Selection and preparation of material	253
Experimental work	254
Apparatus and procedures	254
Results	256
Petrographic observations	263
Laboratory procedure	263
Results for dolomite	263
Parallel to c_v	263
Parallel to a	266
Perpendicular to r_1	267
Parallel to $[f_2:f_3]$	271
Results for magnesite	272
Discussion	273
Conclusions	276
References cited	277

ILLUSTRATIONS

Figure		Page
1.	Schematic illustration of internal and external rotations	248
2.	Crystallography of dolomite	249
3.	Diagram illustrating simple shear	250
4.	Section through hypothetical lattice	251
5.	Section through dolomite structure parallel to (11$\bar{2}$0)	252
6.	Stress-strain curves for dolomite single crystals loaded parallel to c_v	258
7.	Stress-strain curves for dolomite single crystals loaded parallel to a	259
8.	Stress-strain curves for dolomite single crystals compressed normal to r_1	260

Figure — Page
9. Stress-strain curves for dolomite single crystals extended normal to r_1 260
10. Stress-strain curves for dolomite single crystals loaded parallel to $[f_2{:}f_3]$ 261
11. Stress-strain curves for magnesite single crystals loaded parallel to c_v 262
12. Critical resolved shear stresses as functions of temperature for basal translation and $f\{02\bar{2}1\}$ twinning 262
13. Changes of resolved shear-stress coefficients (S_0) for $c\{0001\}$ and $f\{02\bar{2}1\}$ 263
14. Stereograms for specimens compressed parallel to c_v 265
15. Stereograms for specimens extended parallel to a 267
16. Stereograms for specimens extended perpendicular to r_1 268
17. Stereograms for specimens compressed perpendicular to r_1 270
18. Stereograms for specimens loaded parallel to $[f_2{:}f_3]$ 272
19. Stereogram for magnesite specimen 123 loaded parallel to c_v 272
20. Generalized lattice for calcite, dolomite, and magnesite 273

Plate — Facing page
1. Dolomite specimens 264
2. Thin sections of specimens loaded parallel to c_v and a 265

Following page
3. Thin sections of specimens loaded perpendicular to r_1 274

Plate — Following page
4. Photomicrographs of specimens 170, 174, and 161 274
5. Photomicrographs of specimens loaded perpendicular to r_1 274
6. Thin sections of dolomite specimens loaded parallel to $[f_2{:}f_3]$ and magnesite loaded parallel to c_v 274

TABLES

Table — Page
1. Notations of individual planes for each of the four common crystallographic forms in dolomite 249
2. Useful interfacial angles in dolomite 250
3. Calculated angles of internal rotation of e_1, r_1, m_1, $c(0001)$, f_2, e_2, and r_2 by complete twinning on f_1 253
4. Chemical analyses of crystals A, B, C_1, and C_2 expressed in weight per cent 254
5. CaO/MgO ratios for the crystals A, B, C_1, and C_2 254
6. Crystallographic data relative to load axes 255
7. Resolved shear-stress coefficient for postulated gliding elements for different directions of loading 255
8. Summary of experiments 256
9. Yield stresses of dolomite crystals and corresponding resolved shearing stresses for translation gliding on $c\{0001\}$ and twin gliding on $f\{02\bar{2}1\}$ 264

Introduction

The intracrystalline flow of an aggregate is better understood in the light of information about the deformation of single crystals of the species comprising this aggregate. Thus the knowledge of gliding flow of limestone is much enhanced by the work of Turner *et al.* (1954a) on calcite single crystals. The primary purpose of the present investigation of dolomite crystals is to build a firmer foundation for the understanding of the deformation of dolomite rock.

Johnsen (1902) first successfully deformed dolomite single crystals in the laboratory. Tschermak's (1881) earlier efforts to produce twin gliding had been inconclusive, and Johnsen's experiments were designed to induce mechanical twinning. He was unsuccessful despite repeated attempts, but he did achieve basal translation gliding (T = $\{0001\}$, t = $[10\bar{1}0]$). The experiments were conducted at room temperature and atmospheric confining pressure.

From studies of naturally deformed dolomite rocks, Fairbairn and Hawkes (1941) concluded that dolomite did twin mechanically on $f\{02\bar{2}1\}$ and postulated a direction sense of gliding (negative) opposite to that of the well-known $e\{01\bar{1}2\}$ twin in calcite (positive).

Turner *et al.* (1954b) and Handin and Fairbairn (1953; 1955) independently and at about the same time deformed dolomite rocks under high confining pressures at high temperatures. Both produced mechanical twins on $f\{02\bar{2}1\}$ and reported a negative direction sense. Turner *et al.* also detected basal translation in their specimen, confirming Johnsen's discovery. Translation was not noted by Handin and Fairbairn, because in their specimens most of the dolomite grains were oriented relative to the applied load such that the resolved shear stress on $c\{0001\}$ was very low.

Under similar test conditions dolomite rock is stronger and less ductile than limestone. (*Cf.* Handin and Fairbairn, 1955, Fig. 5; Griggs *et al.*, 1951, Fig. 1; 1953, Fig. 1.) The ultimate strength of limestone (Yule marble) at room temperature exceeds that at 300°C. by about 50 per cent (under 5000 bars confining pressure). An increase of temperature from 24°C. to 300°C. reduces the ultimate strength of dolomite less than 10 per cent. Heating influences the ductility of dolomite very little (up to 300°C.), whereas the ductility of lime-

stone is enhanced. The Yule marble has a pronounced strength anisotropy which can be correlated qualitatively at least with its marked preferred orientation of calcite optic axes (Griggs and Miller, 1951, Table 3). However, the Hasmark dolomite has little strength anisotropy despite the fact that its preferred orientation is as strong as that of the Yule marble (Handin and Fairbairn, 1955, p. 1264).

Although it has not been possible to predict the behavior of the limestone precisely from the properties of single calcite crystals, the effects of temperature and of orientation of load relative to the rock fabric are better understood now that the gliding systems of calcite crystals are known as well as the temperature dependence of the critical resolved shear stresses of these systems. The success of the monumental calcite crystal study is due largely to Turner's method (1954a) of identifying the gliding elements for both twinning and translation. This technique makes use of internal rotations of the crystal structure resulting from the simple shear of the intragranular gliding process. The method had already been applied successfully in the study of dolomite rock (Turner *et al.*, 1954b) and is used in this single crystal investigation.

In order to accomplish our purpose we consider it necessary (1) to obtain stress-strain relations of dolomite crystals for a wide range of temperatures (24°C.–500°C.), (2) to identify the operative gliding systems to confirm the data of experiments on dolomite rocks and to discover unreported systems, if any, (3) to correlate the stress-strain data with the gliding mechanisms, especially to determine the critical resolved shear stresses as functions of temperature. Having done this, we will show that the behavior of dolomite rock, especially in contrast with limestone, is more readily understandable.

Acknowledgments

We are grateful indeed to Mr. Ronald E. Januzzi of Danbury, Connecticut, who donated several beautiful dolomite specimens (Pl. 1, fig. 1) from his private collection. Mr. Januzzi's generosity has in fact made this work possible. Mrs. E. B. Knopf has followed our work with interest, and it was through her efforts that a source of satisfactory experimental material was finally discovered. We wish to express our appreciation for the time and effort devoted by Prof. F. J. Turner to our understanding of his techniques for measuring internal rotations in deformed carbonate minerals. Higgs spent 6 weeks with Turner at the Department of Geological Sciences of the University of California, Berkeley, where facilities for petrographic work were kindly made available. Thanks are due Prof. David Griggs of the Institute of Geophysics, University of California, Los Angeles, for spot checking the stress-strain curves of the dolomite crystals. John Sosoka, R. V. Hager, Jr., and J. N. Feather contributed to the experimental results.

Intragranular Rotation Phenomena

Turner's important new technique merits a review of its underlying principles. When a mineral is deformed by translation or twin gliding, lamellae present before deformation are rotated during the gliding process. This is analogous to shear folding, if the process is thought of as a simple shear.

A lamella P (Fig. 1*A*) in existence before deformation is rotated to a new position by gliding on the set of parallel planes T. Two kinds of rotation are recognized: external rotation is defined as rotation of crystallographic elements relative to external co-ordinates (*e.g.*, rotation of the gliding plane relative to the loading axis); internal rotation is defined as rotation of elements relative to internal co-ordinates (*e.g.*, rotation of twin lamellae relative to the optic axis). In Figures 1*B* and 1*C* the lamella P has been rotated internally to the position L in the deformed sector of the crystal. This is the simplest case, and the lattice in the deformed sector has remained unchanged in orientation (*i.e.*, the optic axis, the gliding plane T, and the rational position of P remain unchanged) because the ends of the specimen were free to move laterally during deformation. External rotation occurs when the crystal is under constraint (*i.e.*, the ends are not free to move laterally), and the active gliding plane must rotate to accommodate the shear.[1] This is illustrated in Figures 1*D* and 1*E* which show that the gliding plane T and the lamella P in the deformed sector have been rotated relative to the load axis to T_1 and P_1, respectively. Here the lamella P has been rotated internally

[1] This can be demonstrated by the reader. Mark a line on the side of a pack of 3 by 5 index cards and hold one end of the pack in place on a desk top. If the gliding plane is parallel to the planes separating the individual cards, it must be rotated (externally) to produce shear along that plane when one end of the pack is fixed in position. If the shear is uniform throughout the pack, the line marked on the edge will have been rotated internally.

relative to the externally rotated P_1 in the deformed sector. The angle of internal rotation is the angle between the internally rotated lamella L and its rational position P_1 in the deformed sector.

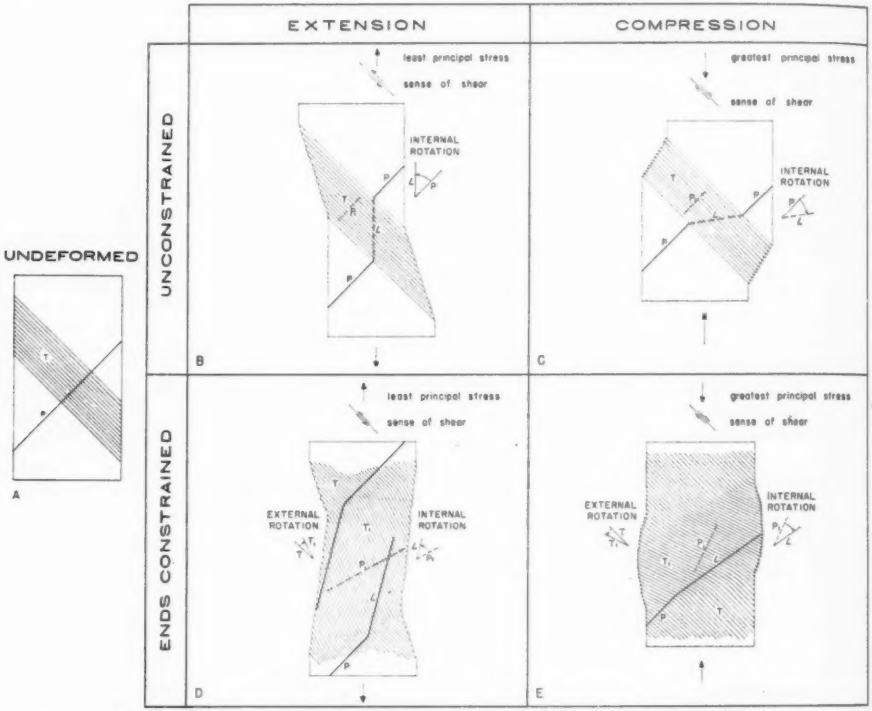

FIGURE 1.—SCHEMATIC ILLUSTRATION OF INTERNAL AND EXTERNAL ROTATIONS
The sense of shear and the direction of loading are indicated by arrows at ends of the sections. Direction senses of internal and external rotations are shown by curved arrows.

The several geometric relations which hold for gliding processes are:

(1) External rotation of a lamella is always toward parallelism with the least principal stress direction.
(2) Internal rotations of lamellae are always opposite in direction sense to that of the external rotation.
(3) The axis of external rotation lies in the gliding plane and is normal to the gliding direction, when a specimen is constrained and kink bands are developed.
(4) The axis of internal rotation is the intersection of the gliding plane and the rotated lamella.
(5) The axis of internal rotation is the zone axis of the zone defined by the gliding plane and a rotated lamella in all positions of rotation. (The poles of the gliding plane and the rotated lamella in all positions of rotation will fall on a great circle when plotted on either the stereographic or equal-area net.)

Turner *et al.* (1954a, p. 900) have shown that, if the magnitude of the shear strain and the gliding system[2] are known, the angle of internal rotation can be calculated for any lamella rotated during deformation from the equation

$$\cot \alpha - \cot \beta = s \sin \gamma, \qquad (1)$$

where α and β are the angles between the lamella and the gliding plane before and after rotation (β always taken as the larger angle), γ is the angle between the gliding direction

[2] The active gliding plane, the direction of gliding, and the direction sense of gliding define a gliding system.

and the axis of internal rotation, and s is the shear strain ($2\tan(\psi/2)$, where ψ is the angle of shear). The longitudinal strain ϵ, the shear strain s, and the coefficient of resolved shear stress (S_0) for a single crystal are related (Handin and Griggs, 1951, p. 867) by the equations

$$1 + \epsilon = \sqrt{1 + 2sS_0 + s^2 \sin^2 \chi_0} \text{ for extension,}$$

and

$$1 - \epsilon = \sqrt{1 - 2sS_0 + s^2 \sin^2 \chi_0} \text{ for compression,}$$

where χ_0 is the angle between the gliding plane and the load axis before deformation. The strain ϵ can be calculated from measurements of internal rotations in a crystal if the gliding system is known. Where ϵ and s are small these formulas can be reduced to the form $\epsilon = sS_0$. By substitution, then,

$$\epsilon = \frac{S_0(\cot \alpha - \cot \beta)}{\sin \gamma} . \qquad (2)$$

TABLE 1.—NOTATIONS OF INDIVIDUAL PLANES FOR EACH OF THE FOUR COMMON CRYSTALLOGRAPHIC FORMS IN DOLOMITE

Zone 1 a_2 = zone axis		Zone 2 a_3 = zone axis		Zone 3 a_1 = zone axis	
form	indices	form	indices	form	indices
f_1	$(\bar{2}021)$	f_2	$(2\bar{2}01)$	f_3	$(02\bar{2}1)$
e_1	$(\bar{1}012)$	e_2	$(1\bar{1}02)$	e_3	$(01\bar{1}2)$
r_1	$(10\bar{1}1)$	r_2	$(\bar{1}101)$	r_3	$(01\bar{1}1)$
m_1	$(10\bar{1}0)$	m_2	$(\bar{1}100)$	m_3	$(0\bar{1}10)$

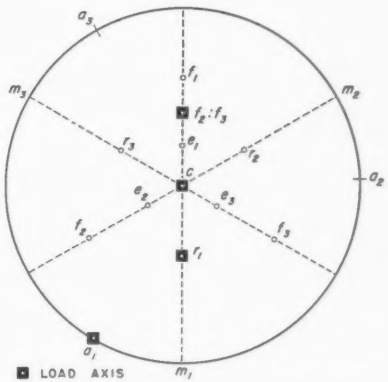

FIGURE 2.—CRYSTALLOGRAPHY OF DOLOMITE
Stereographic projection (upper hemisphere) of the common forms and the crystallographic axes. The load axes are projected also.

NOTATION CONVENTIONS

Crystallographic Notation

The four common crystallographic forms of dolomite are $f\{02\bar{2}1\}$, $e\{01\bar{1}2\}$, $r\{10\bar{1}1\}$, and $m\{10\bar{1}0\}$. It is necessary, however, to designate specific planes. The convention used by Turner *et* al. (1954a, p. 886) in their study of calcite single crystals is followed here. All the common forms that are cozonal with one another and with {0001} have the same subscript number appended to the form designator. Thus f_1, e_1, and r_1 are cozonal. The forms and their notations are listed in Table 1, and their crystallographic relationships are illustrated graphically in Figure 2.

For identification of various planar structures the interfacial angles listed in Table 2 are useful.

Notation for Rotated Lamellae

Since this notation for rotated lamellae was introduced only recently (Handin *et al.*, 1957, p. 1203) to replace the less flexible system used previously (Borg and Turner, 1953; Turner *et al.*, 1954a; 1954b), a brief description seems warranted.

Rotated lamellae are identified by the symbol L. Specific rotated lamellae are identified by subscripts (f_3, r_1, s) which relate them directly to their original rational positions in terms of accepted (Palache *et al.*, 1951) crystallographic notation for forms of the particular crystal involved. These crystallographic notations are used also as superscripts to identify the active gliding planes. Hence $L^{n_j}_{m_i}$ identifies an m_i lamella that has been rotated by gliding on the n_j plane. The lamella that is rotated is identified by the subscript, the operator (or active gliding plane) by the superscript. Since lamellae may be rotated by successive or simultaneous gliding on two or more gliding planes,

additional operators are added in superscript where the individual operations are identified, and they are separated by bars. For example, $L_{m_i}^{n_j|o_k|p_l}$ identifies the lamella which results from rotation of an m_i lamella by gliding on each of the three plains n_j, o_k, p_l. Chronological order of gliding is not implied by sequences of letters in the superscript because in many cases it cannot be determined. An e lamella in calcite may be rotated by twin gliding on another e plane followed by translation gliding on an r plane. The resulting rotated lamella would be identified as $L_{e_2}^{e_1|r_3}$, where the specific e and r planes are identified. This system does not distinguish between twin gliding and translation gliding. The type of gliding must be specified in the text.

TABLE 2.—USEFUL INTERFACIAL ANGLES IN DOLOMITE

$c \wedge f$ = 62 1/2°	$f_1 \wedge f_2$ = 80°
$c \wedge e$ = 25 1/2°	$f_1 \wedge e_2$ = 76 1/2°
$c \wedge r$ = 44°	$f_1 \wedge r_2$ = 50°
$c \wedge m_1$ = 90°	$f_1 \wedge m_2$ = 63 1/2°
$f_1 \wedge e_1$ = 37°	$r_1 \wedge r_2$ = 74°
$f_1 \wedge r_1$ = 73 1/3°	$e_1 \wedge e_2$ = 44°
$f_1 \wedge m_1$ = 27 1/2°	

GLIDING MECHANISMS

The established gliding systems in dolomite are (1) translation on $c\{0001\}$ in a direction parallel to an a axis, and (2) twin gliding on $f\{02\bar{2}1\}$ with $K_1 = (2\bar{2}01)$, $N_1 = [1\bar{1}04]$. (*See* Fig. 3.) The direction sense of twinning is negative in contrast to the positive sense of twin gliding on $e\{01\bar{1}2\}$ in calcite as defined by Turner *et al.* (1954a, p. 887).

As Turner *et al.* (1954a, p. 926) state,

"All the petrographic data [regarding deformed crystals], and especially those relating to internal rotation, can best be explained on the orthodox assumption that the essence of plastic deformation in ionic crystals is gliding on one or more gliding systems. Each system comprises a glide plane and within it a glide direction, both of some simple crystallographic orientation. We make no specific assumptions regarding relative motions of ions during gliding. Whether this involves the generation and migration of dislocations along fixed paths in the lattice, or some other mechanism, the ultimate result of gliding is as if successive thin layers parallel to the glide plane were relatively displaced along the glide line in a uniform sense. In translation gliding each displacement is through an integral number of interionic distances, so that the configuration of the lattice remains unchanged. In twin gliding each layer has moved through a constant appropriate fraction of an interionic distance so that the deformed lattice is in twinned relation to the initial lattice."

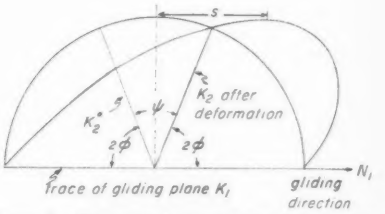

FIGURE 3.—DIAGRAM ILLUSTRATING SIMPLE SHEAR (After Bell, 1941, Fig. 5). The plane of deformation is the projection plane.

Hence, the shear s in translation gliding is not fixed. Shear in twin gliding is fixed according to the symmetry requirements of the lattice across the twin plane and to the direction sense of gliding.

From symmetry considerations alone, the shear must be such that all positions of the twinned lattice are satisfied. The shear depends, therefore, upon the selection of "the other plane of no distortion", K_2 (*cf.* Bell, 1941, p. 252; Pabst, 1955, p. 898), since $s = 2/\tan 2\phi = 2\tan(\psi/2)$, where 2ϕ is the angle between K_1 and K_2^0 (Fig. 3) and ψ the angle between K_2^0 and its position after gliding. If one visualizes the twin gliding process as one of simple shear with gliding on successive ionic layers, the shear must be such that all ionic positions in that part of the lattice where gliding occurs are in twinned positions relative to their positions in the host lattice. If the movement is from left to right (Fig. 4), the atom at position *1* (original position) will move to position *3*, and the trace of K_2 will be defined by the line x. If the movement is from right to left, the atom at position *2* (original position) will move to position *3*, and the trace of K_2 will be defined by the line y. In either event the symmetry requirements of the twinned lattice are satisfied.

The direction sense of twin gliding places an additional restriction on selection of the "other plane of no distortion." Because of steric hindrances or charge barriers, twin gliding can occur on a particular plane by gliding in one

direction sense only. Thus (Fig. 4) charge barriers prohibit the atom at position *2* from moving to position *3*, since it would necessarily pass too close to the ion of opposite charge at position *4*. The proper direction sense is indicated by the arrows on the figure—the atom at *1* moves to *3* during the gliding process. Hence, the correct selection of K_2 is dependent first upon the symmetry requirements and secondly upon the direction sense of gliding. The value of shear for twin gliding on a specific plane is, therefore, fixed.

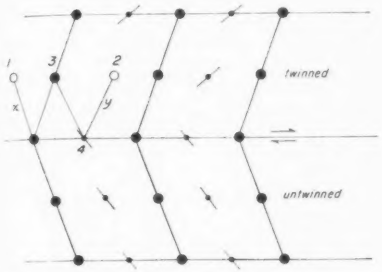

FIGURE 4.—SECTION THROUGH HYPOTHETICAL LATTICE
Illustrating selection of "other plane of no distortion" (K_2) depending upon the direction sense of gliding.

According to Pabst (1955, p. 907–908), if the direction sense of twin gliding on $f\{02\bar{2}1\}$ in dolomite is negative, $s = 0.5874$, and if the direction sense is positive, $s = 1.0408$. Handin and Fairbairn (1955, p. 1268) give the value 0.59 for negative sense. They indicate the relative magnitude of shear for the positive sense in their Figure 7, from which the angle of shear ψ for the positive sense is the angle between $(01\bar{1}2)$ in the initial structure and $(01\bar{1}2)$ in the twinned lattice; s would be 2.6686.

Figure 5 is a section through the dolomite structure parallel to $(11\bar{2}0)$ with $(2\bar{2}01)$ as the gliding plane. The gliding direction is parallel to the plane of the section which is, therefore, the plane of deformation S as defined by Pabst (1955, p. 898). The positive and negative direction senses are indicated, and the three planes under consideration are labeled e_2, r_2, and (0001). If the direction sense is negative, $K_2 = r_2$ $(\bar{1}101)$ and $s = 2 \tan(32°44'/2)$ or 0.5874. The CO_3 group at position *1* of the host structure moves to position *2* of the twinned structure. During the movement of the layer of CO_3 groups, all layers above will move as a unit (*e.g.*, the Mg ion at *A* will move to *B*). Then twin gliding of the Mg layer must move the Mg ion at *B* to *C*, which is a Mg position in the twinned structure. If the direction sense is positive, $K_2 = e_2$ $(1\bar{1}02)$ and $s = 2 \tan(106°18'/2)$ or 2.6686. The CO_3 group at position *3* moves to position *2*, and at the same time all layers above this layer will move as a unit (*e.g.*, the Mg ion at *E* moves to position *D*). Then twin gliding of the Mg layer will move the Mg ion at *D* to *C*, again a Mg position in the twinned structure.

As postulated by Pabst (1955, p. 907) and Turner *et al.* (1954b, p. 485), if the direction sense is positive (Fig. 5) and $K_2 = c(0001)$, then $s = 2 \tan(54°59'/2)$ or 1.0408. Now, however, when the Mg ion at *A* moves to *F*, the CO_3 group at position *1* moves to position *4* which is not a rational position for the CO_3 group in the twinned structure; that is, the structure would no longer be that of dolomite. The two possible "other planes of no distortion" in dolomite, therefore, are $r\{10\bar{1}1\}$ and $e\{01\bar{1}2\}$ for the negative and positive direction senses respectively, and the values of shear are 0.5874 and 2.6686, respectively. All CO_3 positions, as well as Mg and Ca positions, must be taken into account.

Handin and Fairbairn (1955, p. 1271) present evidence for a negative direction sense. They find that "compression at 300°C. of specimens favorably oriented for twinning on $\{02\bar{2}1\}$ in a negative sense results in a profusion of lamellae. . . ." and "plots of lamellae spacing index vs. resolved shear stress consistently show that lamellae develop most profusely parallel to $\{02\bar{2}1\}$ planes of highest resolved shear stress in the negative sense."

Turner *et al.* (1954b, p. 486) conclude that "the sense of shear for twinning on $\{02\bar{2}1\}$ is negative. . . .," and "the conspicuous twinning is restricted to grains whose *c* axes were originally inclined to the axis of compression at angles between zero and 25°." Their evidence is based in part on internal rotations of lamellae that were in existence before the experimental deformation. They show how (p. 485)

". . . . a pre-existing $\{02\bar{2}1\}$ lamella f_2 in dolomite will rotate internally to a new orientation during twin gliding on f_1. And this new orientation can be computed from the geometry and sense of twinning on $\{02\bar{2}1\}$. It can be shown that if shear on f_1 is negative, an original f_2 lamella rotates internally through 21° and so comes to coincide with f_2 of the twinned lattice. . . . If shear on f_1 were positive the angle of rotation in the opposite sense would be 28° and the ultimate position of the rotated f_2

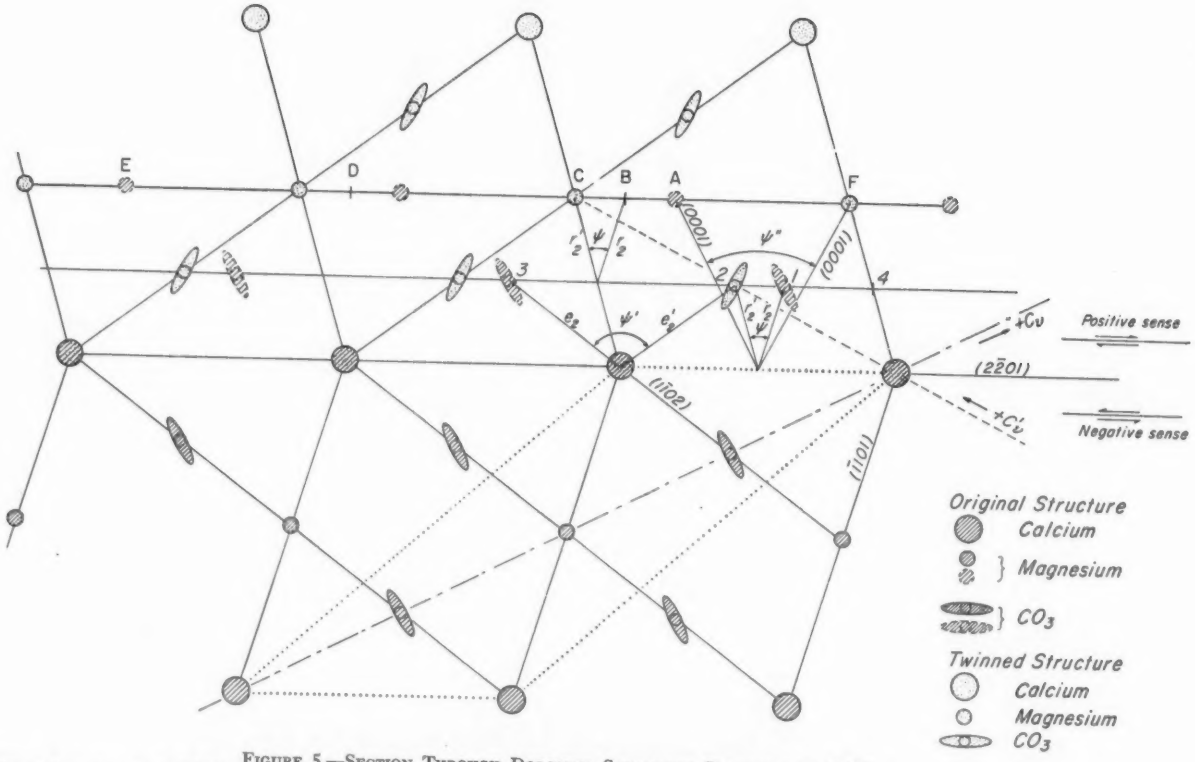

FIGURE 5.—SECTION THROUGH DOLOMITE STRUCTURE PARALLEL TO (11$\bar{2}$0)
The gliding plane is f_2 (22$\bar{0}$1). The gliding direction $[f_2 : r_1]$ lies in the plane of the section. One structure cell is outlined by the dotted lines.

structure would coincide with r_3 of the twinned lattice.... We have measured a number of dolomite grains in which an early set of f_2 lamellae are deflected within broad f_1 lamellae of later origin. In every instance the deflected lamella is parallel to f_2 of the lattice formed by twinning on f_1. The sense of shear must be negative."

indeed to obtain several excellent specimens from the private collection of Mr. Ronald E. Januzzi, who collected the crystals from the old Tilly Foster mine in Putnam County, New York. There were two individual cleavage rhombs about 2 inches on a side which we

TABLE 3.—CALCULATED ANGLES OF INTERNAL ROTATION OF e_1, r_1, m_1, $c(0001)$, f_2, e_2, AND r_2 BY COMPLETE TWINNING ON f_1

Identity before rotation	Angle of rotation	Rotated lamella coincides with	Remarks
e_1	9° 21 1/2′	* m_1'	$e_1 \wedge m_1' = 9°\ 21\ 1/2'$
r_1	32°44′	r_1'	$r_1 \wedge r_1' = 32°44'$
m_1	9° 21 1/2′	e_1'	$m_1 \wedge e_1' = 9°\ 21\ 1/2'$
$c(0001)$	42°4′	M'	$c(0001) \wedge M' = 42°4'$
f_2	20°47′	f_2'	$f_2 \wedge f_2' = 20°48'$
e_2	24°36′	v'	$e_2 \wedge v' = 24°35.4'$
r_2	10°24′	$-e_1'$	$r_2 \wedge -e_1' = 10°24'$

*The prime symbol is used here to distinguish the form in the twinned part of a crystal.

Their argument is not invalidated by using an incorrect value of shear (1.0408) for the positive sense; based on the correct value (2.6686) for positive sense, the angle of internal rotation would be much greater (51°12.5′) and would only enhance their point.

The amounts of internal rotations due to complete twinning on f_1 in the negative sense were computed for the forms e_1, r_1, m_1, $c(0001)$, f_2, e_2, and r_2 by equation (1). The rotated lamellae coincide with rational crystallographic forms of either the twinned or host structure as indicated in Table 3. Since the shear is not fixed in translation gliding, the amount of internal rotation is variable, and the positions of rotated lamellae do not necessarily coincide with rational forms.

Thus the experimental work on dolomite rock confirms the hypothesis of Fairbairn and Hawkes (1941, p. 621) that the direction sense of twinning in dolomite would be the opposite of that in calcite. The fact that in dolomite the sense is negative rather than positive is to be expected in view of the much smaller shear required to bring the twinned structure into proper relationship with the host.

SELECTION AND PREPARATION OF MATERIAL

In nature, dolomite single crystals sufficiently large and flawless for experimental deformation studies are extremely rare. We were fortunate

labeled *A* and *B* and a huge specimen consisting of an intergrowth of three large crystals (Pl. 1, fig. 1), which we denoted C_1, C_2, and C_3.

None of the translucent crystals was optically flawless. There was much incipient cleavage, and the crystals contained a few veinlets filled with kaolinite. Few of the test specimens, however, contained macroscopic impurities, since it was almost always possible to avoid concentrations of foreign matter when coring the test cylinders, except in crystal C_3 which was not used.

A chemical analysis was made of each crystal from which experimental material was procured (Table 4). Crystal *B* turned out to be magnesite. Since several experiments were conducted on test pieces cut from this crystal before it was identified, the results for magnesite are included in this paper. The other three crystals have CaO/MgO ratios (Table 5) close to the value of 1.38:1 for the ideal dolomite structure. Ferrous iron, the chief impurity, is present in the amount of 2 per cent in the dolomite crystals. All other impurities constitute less than 1 per cent of the weight of the crystals. The magnesite contains 3 per cent ferrous iron and 4 per cent other impurity oxides. Very fine grains of magnetite and kaolinite were scattered sparsely throughout all the crystals.

Cylindrical test specimens were drilled from the crystals with a diamond core bit. Most of the specimens had a diameter of half an inch.

These were cut to a length of 1 inch if possible. However, in order to use the available material most economically, it was necessary to test some cylinders with a length of as little as half an inch. Fortunately, the length/diameter ratio appears to have no influence on the stress-strain curves. During the coring operation, small chips were dislodged from the cylindrical surfaces of the specimens. In order to prevent the thin copper jacket from intruding into the voids where it often failed, it was necessary to wrap the test pieces with brass foil before surrounding them with the jacket of seamless, annealed copper tubing of 0.01-inch wall thickness.

Because of surface imperfections due to chipping and because of impurities, it was impossible to prevent jacket leaks when using thin-walled tubing for tests at 500°C. Accordingly, undersized specimens 0.375 inch in diameter and 0.75 inch long were prepared for high-temperature experiments. The space between the sample and the standard half-inch copper jacket was filled by a brass sleeve. At 500°C. the strength of the brass is small, and the correction for the contribution of the sleeve to the applied load is less than 10 per cent of the total load. The strength of the copper jacket is negligibly small at all temperatures.

The choice of the orientations of the specimens relative to the applied load was dictated by previous investigations on dolomite rock. Cylinders were cored in four directions (1) parallel to the optic axis c_v and normal to the base $c(0001)$, (2) parallel to the axis a, (3) normal to the cleavage r_1 $(10\bar{1}1)$, and (4) parallel to the intersection $[f_2{:}f_3]$. (*See* Fig. 2.) Table 6 summarizes the gliding mechanisms to be expected for each of these orientations, and Table 7 lists the resolved shearing-stress coefficients for some postulated gliding elements for the four loading directions.

TABLE 4.—CHEMICAL ANALYSES OF CRYSTALS A, B, C_1, AND C_2 EXPRESSED IN WEIGHT PER CENT

Oxide (Method)	A	B	C_1	C_2
CaO (Gravimetric)	28.9	1.8	29.8	29.4
MgO (Gravimetric)	21.2	42.8	21.1	20.9
FeO (Titrometric)	2.0	3.0	1.9	2.0
MnO (Spectrochemical)	0.3	0.5	0.3	0.3
CO_2 (Gravimetric)	46.3	48.5	47.2	47.0
Rem*	1.1	3.5	0.1	0.1
Total	99.8	100.1	100.4	99.7

*Rem includes SiO_2, Fe_2O_3, Al_2O_3, Na_2O, and SrO.

TABLE 5.—CaO/MgO RATIOS FOR THE CRYSTALS A, B, C_1, AND C_2

Ratio	A	B	C_1	C_2
CaO/MgO	1.36:1	.04:1	1.41:1	1.40:1

EXPERIMENTAL WORK

Apparatus and Procedures

The apparatus, procedures, and techniques for triaxial compression tests have been described in detail (Handin, 1953; Handin and Hager, 1957). The jacketed, cylindrical specimens are first subjected to a hydrostatic confining pressure of 5000 bars. In a compression test a load is superposed so that the greatest principal stress is parallel to the cylinder axis. In an extension test the end load is relieved, and the least principal stress is longitudinal.

In practice the desired confining pressure is applied first. The test chamber is then heated externally to bring the specimen to the desired temperature. The sample is then deformed at a constant strain rate of 1 per cent per minute. The apparatus is allowed to cool, the pressure is relieved, and the test piece is removed from the apparatus. Measurements are made of the final length and of the major and minor diameters of the central sector of the deformed specimen and also of the inclination of shear fractures when present.

Stress-strain curves are derived from recorded measurements of press motion and differential force. The latter is corrected for friction and the "true" longitudinal differential stress is computed for a given strain on the assumption that the deformation is homogeneous and that no volume changes result from permanent straining. The piston displacement is corrected for apparatus distortion, and the conventional longitudinal strain is computed.

TABLE 6.—CRYSTALLOGRAPHIC DATA RELATIVE TO LOAD AXES

The axis of a cored cylinder is parallel to the greatest principal stress in compression experiments and parallel to the least principal stress in extension experiments.

Orientation of Cylinders	Remarks
A. Favorable for twin gliding:	
1) Parallel to c_v	Resolved shear stress high for all three f planes, zero on {0001}. Favorable for twin gliding on $f\{02\bar{2}1\}$ in compression only, if negative direction sense is assumed. Translation gliding on {0001} is impossible.
2) Parallel to a_1	Resolved shear stress high on two f planes, zero on third f plane and on {0001}. Favorable for twin gliding on two f planes in extension only, if negative direction sense is assumed. Twin gliding on third f plane and translation gliding on {0001} are impossible.
B. Favorable for translation gliding:	
3) Normal to r_1	Resolved shear stress near maximum value on {0001} and lower on $f\{02\bar{2}1\}$. Favorable for translation gliding in compression and extension. Twin gliding less likely but possible on f_1 in extension and on f_2 and f_3 in compression if negative direction sense is assumed.
4) Parallel to $[f_2:f_3]$	Resolved shear stress near maximum on {0001}, zero on f_2 and f_3, and moderate on f_1. Favorable for translation gliding in compression and extension. Twin gliding impossible on f_2 and f_3. Twin gliding on f_1 possible in compression only if negative direction sense is assumed.

TABLE 7.—RESOLVED SHEAR-STRESS COEFFICIENT FOR POSTULATED GLIDING ELEMENTS FOR DIFFERENT DIRECTIONS OF LOADING

$S_0 = \sin \chi_0 \cos \chi_0 \cos \phi$, where χ_0 = angle between load axis and gliding plane before deformation, and ϕ = angle between gliding line and projection of load axis on gliding plane. *C* and *E* signify that twin gliding in the negative sense can occur only in compression and extension, respectively.

Postulated gliding elements		Direction of loading											
Plane	Direction	$\parallel c_v$			$\parallel a_1$			$\parallel [f_2:f_3]$			$\perp r_1$		
T	t	χ_0	ϕ	S_0	χ_0	ϕ	S_0	χ_0	ϕ	S_0	χ_0	ϕ	S_0
Translation													
c(0001)	a_1 [0001:0$\bar{1}$11]	90	–	0	0	0	0	44	30	.43	46	30	.43
	a_2 [0001:$\bar{1}$01$\bar{1}$]	90	–	0	0	60	0	44	90	0	46	90	0
	a_3 [0001:$\bar{1}$$\bar{1}$01]	90	–	0	0	60	0	44	30	.43	46	30	.43
Twinning													
f_1($\bar{2}$021)	[$\bar{2}$021:$\bar{1}$2$\bar{1}$0]	28	0	.40C	50	51	.31E	74	0	.26C	17	0	.27E
f_2(2$\bar{2}$01)	[2$\bar{2}$01:11$\bar{2}$0]	28	0	.40C	0	90	0	0	39	0	40	51	.31C
f_3(02$\bar{2}$1)	[02$\bar{2}$1:$\bar{2}$110]	28	0	.40C	50	51	.31E	0	39	0	40	51	.31C
Translation													
e_1($\bar{1}$012)	[$\bar{1}$012:$\bar{1}$2$\bar{1}$0]	64	90	0	22	57	.19	69	90	0	20	90	0
e_2(1$\bar{1}$02)	[1$\bar{1}$02:11$\bar{2}$0]	64	90	0	0	0	0	29	46	.30	53	0	.48
e_3(01$\bar{1}$2)	[01$\bar{1}$2:$\bar{2}$110]	64	90	0	22	57	.19	29	46	.30	53	0	.48
Translation													
r_1(10$\bar{1}$1)	[10$\bar{1}$1:$\bar{1}$2$\bar{1}$0]	46	0	.50	37	39	.37	0	0	0	90	–	0
r_2($\bar{1}$101)	[$\bar{1}$101:11$\bar{2}$0]	46	0	.50	0	90	0	48	70	.17	16	38	.21
r_3(0$\bar{1}$11)	[0$\bar{1}$11:$\bar{2}$110]	46	0	.50	37	39	.37	48	70	.17	16	38	.21
Translation													
r_1(10$\bar{1}$1)	[10$\bar{1}$1:0001]	46	90	0	37	51	.30	0	90	0	90	–	0
r_2($\bar{1}$101)	[$\bar{1}$101:0001]	46	90	0	0	0	0	48	20	.47	16	52	.16
r_3(0$\bar{1}$11)	[0$\bar{1}$11:0001]	46	90	0	37	51	.30	48	20	.47	16	52	.16

Since the permanent strains achieved in the dolomite crystals are relatively small, these assumptions lead to no great errors in the stress-strain curves.

Results

Sixty-seven experiments on dolomite and six on magnesite have been conducted under 5000 bars confining pressure and at temperatures from 24°C. to 500°C. In the summary of experiments (Table 8) specimens are grouped according to their four directions of loading. The stress-strain curves are cut off at 10 per cent; the total strain achieved, the ultimate strength, and a brief description of the fracture are indicated in the summary. Experiment and specimen numbers coincide.

TABLE 8.—SUMMARY OF EXPERIMENTS

All experiments were made on dry, jacketed crystals under 5000 bars confining pressure at a constant strain rate of 1 per cent per minute.

	Exp. No.	Crystal	Type	Temp. (°C)	Total strain (%)	Ultimate strength (kg/cm^2)	Thin section	Remarks
Dolomite								
Load parallel to c_y	108	A	Comp.	24	3.0	5710		30° shear fracture.
	580	c_2	Comp.	24	1.7	6550		34° shear fracture.
	583	c_2	Comp.	300	1.5	4320		Broke on cleavage.
	587	c_2	Comp.	300	0.7	3100	X	Terminated before fracture.
	582	c_1	Comp.	400	13.5	5200		43° shear fracture.
	586	c_2	Comp.	400	2.5	3200	X	Terminated before fracture.
	557	c_2*	Comp.	500	16.7	6700	X	Incipient shear fracture.
	567	c_1*	Comp.	500	12.5	4500		Incipient shear fracture.
	109	A	Ext.	24	1.9	3090		Incipient fracture. Jacket broke.
	579	c_2	Ext.	24	1.7	3000		Incipient shear fracture.
	589	c_2	Ext.	300	1.1	3300		"Tensile" fracture.
	592	c_1	Ext.	300	0.1	2460		Terminated before fracture.
	588	c_1	Ext.	400	3.0	3500		33° shear fracture.
	591	c_1	Ext.	400	0.2	3300		Terminated before fracture.
	593	c_2*	Ext.	500	2.6	3080		33° shear fracture.
	595	c_2*	Ext.	500	2.3	3000	X	Incipient shear fracture.
Load parallel to a	145	c_2	Comp.	24	2.1	6560	X	Incipient shear fracture.
	576	c_2	Comp.	24	1.1	4920		33° shear fracture.
	526	c_2	Comp.	24	2.8	4600		36° shear fracture.
	149	c_2	Comp.	300	1.1	5190	X	Incipient 30° shear fracture.
	530	c_2	Comp.	400	0.7	5450		Terminated before fracture.
	577	c_2	Comp.	400	1.6	6680		37° shear fracture.
	558	c_2*	Comp.	500	8.9	6350	X	30° shear fracture.
	598	c_1*	Comp.	500	4.8	5850	X	Terminated before fracture.
	162	c_2	Ext.	24	2.2	2520	X	Incipient shear & "tensile" break.
	527	c_2	Ext.	24	1.1	2880		Terminated before fracture.
	165	c_2	Ext.	300	1.6	3450	X	Incipient shear. Jacket broke.
	531	c_2	Ext.	400	1.5	2710	X	Terminated before fracture.
	578	c_2	Ext.	400	0.6	3410		38° shear fracture.
	622	c_1*	Ext.	450	30.0	3100	X	Terminated before fracture.
	594	c_1*	Ext.	500	13.1	3060	X	33° shear fracture.
	596	c_1*	Ext.	500	8.1	3200	X	Terminated before fracture.
Load normal to r_1	105	A	Comp.	24	12.9	3860		Accidentally broken.
	106	A	Comp.	24	7.8	3050	X	Terminated before fracture.
	146	c_2	Comp.	24	14.6	4650	X	Terminated before fracture.
	155	c_2	Comp.	24	18.8	4820	X	Terminated before fracture.
	568	c_2	Comp.	24	17.2	5750		Terminated. Bulged and bent.
	156	c_2	Comp.	300	7.8	5990	X	Terminated before fracture.
	169	c_2	Comp.	300	6.1	4390		30° shear fracture.

TABLE 8—*Continued*

	Exp. No.	Crystal	Type	Temp. (°C)	Total strain (%)	Ultimate strength (kg/cm²)	Thin section	Remarks
Load normal to r_1	584	C_2	Comp.	300	9.7	6100		33° shear fracture.
	528	C_2	Comp.	400	9.1	3260		27° shear fracture.
	529	C_2	Comp.	400	6.5	2840	X	Terminated before fracture.
	555	C_2*	Comp.	500	7.0	5850		40° shear fracture.
	556	C_2*	Comp.	500	9.3	6050	X	40° shear fracture.
	620	C_2*	Comp.	500	6.7	6100		35° shear fracture.
	107	A	Ext.	24	8.3	2310		Accidentally broken.
	160	C_2	Ext.	24	11.9	2610	X	Jacket failed.
	163	C_2	Ext.	300	8.2	3110		Accidentally broken.
	170	C_2	Ext.	300	10.4	4000	X	Terminated before fracture.
	574	C_2*	Ext.	300	25.6	3700		Jacket failed.
	174	C_2	Ext.	400	4.2	4250	X	Jacket failed.
	573	C_2*	Ext.	400	6.2	4000		40° shear fracture.
	554	C_2*	Ext.	500	2.5	2100		Terminated before fracture.
	559	C_2*	Ext.	500	7.1	4200	X	Terminated before fracture.
Load parallel to $[f_2:f_3]$	110	A	Comp.	24	8.9	2530	X	Terminated before fracture.
	141	C_1	Comp.	24	14.6	3080		Shattered suddenly.
	153	C_1	Comp.	24	12.0	2890	X	Terminated before fracture.
	142	C_1	Comp.	300	4.4	2280	X	35° shear fracture.
	147	C_1	Comp.	300	6.5	2650	X	30° shear fracture.
	112	A	Ext.	24	5.1	3050	X	20° shear fracture.
	161	C_1	Ext.	24	7.5	2440	X	Terminated before fracture.
	166	C_1	Ext.	300	3.2	2550		Specimen accidentally broken.
	179	C_1	Ext.	300	3.1	2660		Jacket failed.
	575	C_1	Ext.	300	5.2	2840	X	Terminated before fracture.
	647	C_2*	Ext.	400	5.2	3380		Sheared near one end.
Magnesite								
Load parallel to C_v	123	B	Comp.	24	7.9	6760	X	Possible jacket failure.
	150	B	Comp.	24	7.1	6450	X	Incipient shear fracture.
	168	B	Comp.	300	2.4	5950		Accidentally broken.
	597	B	Comp.	500	1.1	4350		40° shear fracture.
	158	B	Ext.	24	1.5	2330	X	25° shear fracture.
	159	B	Ext.	300	0.9	2770	X	25° shear fracture.

*Denotes undersized specimen with brass sleeve

Most of the stress-strain curves presented (Figs. 6–10) represent average curves based on two or more experiments conducted under identical test conditions. Most of the curves reflecting large permanent deformations have well-defined breaks or "knees", marking the onset of flow. For these the yield stress is taken as the differential stress at the discontinuity. If there is no sharp break in the curve, the choice of a yield stress is arbitrary. A value has been picked at a strain of one per cent where the curves have clearly departed from the linearity associated with elastic distortion.

In crystals loaded parallel to the optic axis, basal translation is impossible, and if the sense of *f* twinning is negative, twin gliding can occur only in compression (Table 6). Extended specimens of this orientation are essentially brittle at all temperatures, and compressed specimens are brittle up to 400°C. (Fig. 6). Failure occurred by violent shear fracturing on surfaces inclined at about 30° to the direction of maximum principal stress; that is, at 30° to the cylinder axis in a compression test and 60° to the axis in extension (Pl. 1, fig. 2). The critical resolved shearing stress for twinning below 400°C. must exceed 2000 kg/cm² (Table 9) in compression. This is of the order of 100 times that required for *e* twinning in calcite under similar conditions (Turner *et al.*, 1954a, p. 889). At 400°C. the dolomite suddenly acquires ductility; the resolved shearing stress for twin-

ning is about 1160 kg/cm². This stress drops rapidly with increasing temperature to 500 kg/cm² at 500°C. The stress-strain relations suggest that the only operative gliding mechanism in this orientation is *f* twinning in the negative sense. Flow at high temperature is made possible by a reduction of the resolved shearing stress required to initiate this mechanism.

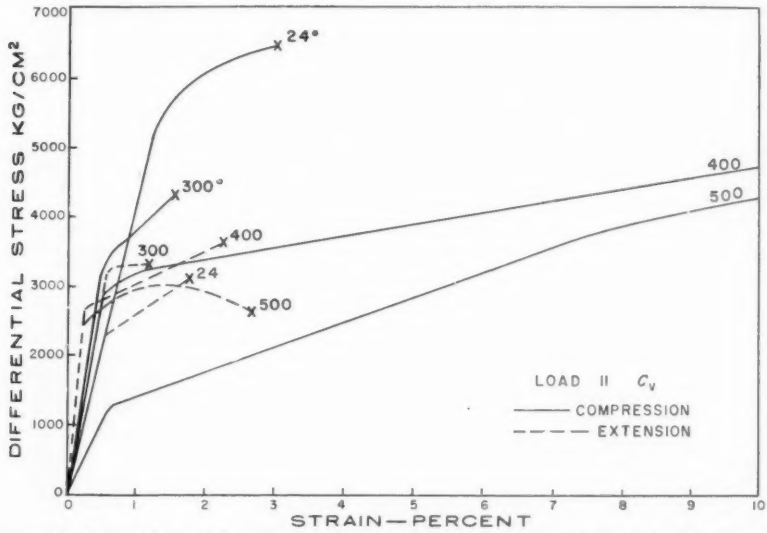

FIGURE 6.—STRESS-STRAIN CURVES FOR DOLOMITE SINGLE CRYSTALS LOADED PARALLEL TO c_v Under 5000 bars confining pressure at different temperatures.

Since fracture tends to be capricious, the reproducibility of the breaking stress of the brittle material is poor. However, the high-temperature compression curves are reproducible to within better than 10 per cent. It appears that work hardening becomes more important as the temperature rises (Fig. 6).

Basal translation is excluded also from crystals loaded parallel to an *a* axis, and twinning in the negative sense can occur only in extension (Table 6). In this orientation the dolomite is brittle at low temperature. Ductility is acquired between 400°C. and 450°C. in extension (Fig. 7). Petrographic studies confirm that the flow is due to *f* twin gliding, and the resolved shearing stress to initiate gliding at 450°C. and 500°C. is 570 kg/cm², or about the same value measured in crystals compressed parallel to c_v. Crystals in the brittle state again failed by sudden shear fracturing along surfaces inclined at 30°–40° to the direction of greatest principal pressure.

The reproducibility of the brittle stress-strain curves is again poor, but that of the curves exhibiting large permanent strain is about 5 per cent. From the standpoint of the stress-strain curve the specimens compressed at 500°C. appear to have flowed. However, the thin-section examination reveals that failure occurs by large offset on conjugate macroscopic shears (Pl. 2, fig. 2*A*). Cohesion was maintained; the large offsets were permitted by the thick brass jackets. By macroscopic shearing the writers mean shear "fracturing" without permanent loss of cohesion. Fracturing in the ordinary sense implies permanent loss of cohesion, separation into two or more parts, and loss of resistance to differential stress. However, under high confining pressure a large offset can occur before fracture ensues and the differential force drops suddenly to zero. Thus in Table 8 "shear fracture" implies loss of cohesion and hence a drastic reduction of differential force at the stated total strain. "Incipient fracture" conveys the idea that shearing offset has occurred, but cohesion has been retained. Macroscopic shears are not necessarily visible without the aid of a microscope but are distinct from the intracrystalline shear due to gliding processes. These two mechanisms of flow are not always distinguishable by the form of the stress-strain curve. (For a fuller discussion *see* Handin and Hager, 1957, p. 44–45.)

In crystals loaded perpendicular to a cleavage face a high resolved shearing stress on the basal plane favors translation gliding. Twinning in the negative sense can occur in either compression or extension (Table 6).

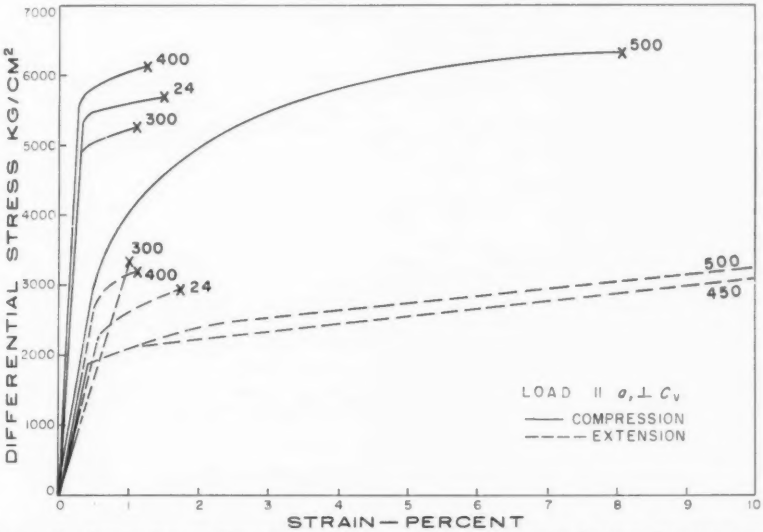

FIGURE 7.—STRESS-STRAIN CURVES FOR DOLOMITE SINGLE CRYSTALS LOADED PARALLEL TO *a* Under 5000 bars confining pressure at different temperatures.

The stress-strain curves (Figs. 8, 9) reveal a rare phenomenon: the yield stress of the crystal *increases* with temperature up to 400°C. at least. Petrographic examinations reveal that the principal gliding mechanism from 24°C. to 300°C. is basal translation. At 400°C. both translation and twin gliding occur, and at 500°C. twinning operates alone. Experiments on crystals oriented to exclude translation have shown that the resolved shearing stress required to initiate twinning decreases with increasing temperature. The stress for basal translation must at the same time be *increasing*.

At room temperature the critical resolved shearing stress for translation is essentially the same in compression and extension (Table 9), and the stress-strain curves are reproducible to better than 5 per cent. This stress of about 900 kg/cm² is of the same order as that for *r* translation in calcite (Turner *et al.*, 1954a, Fig. 7). At 300°C. the stress measured in compression tests, 1330 kg/cm², exceeds that measured in extension experiments, 950 kg/cm². The reproducibility of the 300°C. stress-strain curves is also good; the reason for the difference is not known. The recorded critical stresses at 400°C. also differ in compression and extension, but here the picture is confused because the resolved shearing stress on the twin plane is high enough to initiate twinning, and both mechanisms operate together. At 500°C. twinning occurs alone, and the resolved shearing stress required in extension, 540 kg/cm², agrees with that measured in the crystals loaded parallel to c_v and to *a*.

All the extension stress-strain curves of crystals loaded normal to r_1 are reproducible to better than 7 per cent, as are the compression curves for 24°C., 300°C., and 400°C. The 24°C. compression curve agrees very well with that obtained by Griggs for similar test conditions (Fig. 8). The 500°C. compression curves are very erratic; this is not understood in view of the good reproducibility of the 500°C. curves for all other orientations. Our average curve differs widely from the curve of Griggs based on only one experiment. However, Griggs' curve has a yield stress giving a resolved shearing stress for twinning (740 kg/cm²) much closer to the value measured in other orientations (about 550 kg/cm²) than does our average curve (1390 kg/cm²). All the stress-strain curves for *r* cylinders exhibit work hardening except the 400°C. compression curve. The uniqueness of this curve is not understood, but there can be little doubt that the effect is real.

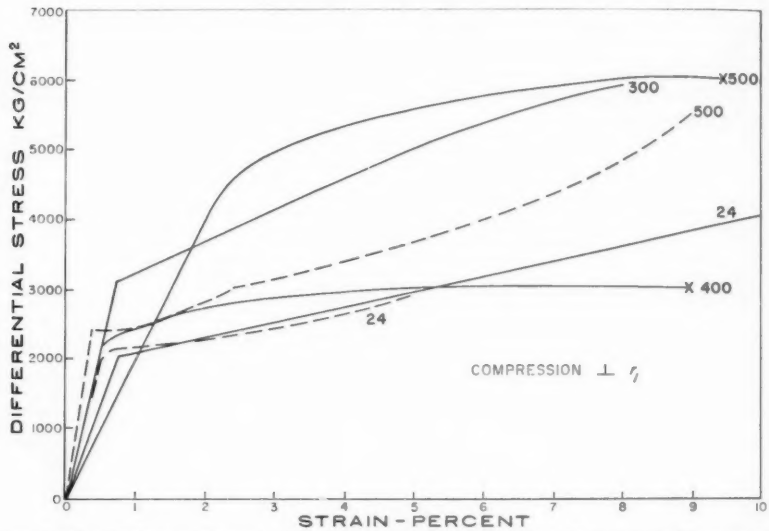

FIGURE 8.—STRESS-STRAIN CURVES FOR DOLOMITE SINGLE CRYSTALS COMPRESSED NORMAL TO r_1 Under 5000 bars confining pressure at different temperatures.

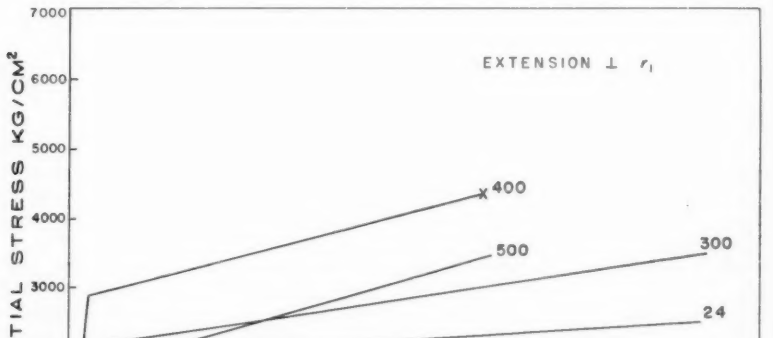

FIGURE 9.—STRESS-STRAIN CURVES FOR DOLOMITE SINGLE CRYSTALS EXTENDED NORMAL TO r_1 Under 5000 bars confining pressure at different temperatures.

In crystals loaded parallel to the intersection of two f planes, $[f_2:f_3]$, the resolved shearing stress on the basal plane is high, and twinning on f_1 in the negative sense can occur only in compression (Table 6). No twinning occurs at 24°C. and 300°C.; the only gliding mechanism observed is basal translation. In extension the critical resolved shearing stress for translation, 950 kg/cm² at 24°C. and 970 kg/cm² at 300°C., is about the same as that measured in crystals loaded normal to r (Table 9). In compression at 300°C. the stress is 840 kg/cm², not very

different from the results of the extension experiments. However, the low room-temperature value of 650 kg/cm² in compression is not understood. Turner *et al.* (1954a, p. 891) found creases. The curves intersect at about 400°C., at which temperature twinning and translation should occur together if the resolved shearing-stress coefficients for each are about the same.

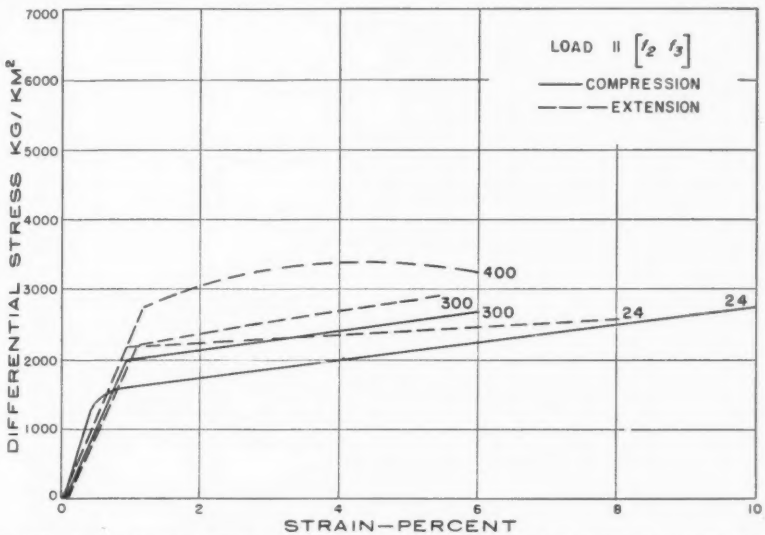

FIGURE 10.—STRESS-STRAIN CURVES FOR DOLOMITE SINGLE CRYSTALS LOADED PARALLEL TO $[f_2{:}f_3]$ Under 5000 bars confining pressure at different temperatures.

that at room temperature the critical resolved shearing stress for r translation in calcite was also inconsistent for different orientations of load. At 300°C., however, this stress proved to be nearly constant, independent of crystal orientation (Turner *et al.*, 1954a, Fig 6).

Because of unfavorable orientation, twinning cannot occur in cylinders extended parallel to $[f_2{:}f_3]$. The flow at 400°C. is due to basal translation only, so that the critical resolved shearing stress can be determined without ambiguity. Attempts to deform specimens of this orientation at 500°C. were not successful before all available experimental material was exhausted. The reproducibility of the stress-strain curves for this orientation is the best of any, better than 2 per cent at 24°C., and 6 per cent at high temperatures. All the stress-strain curves (Fig. 10) except the 400°C. curve exhibit work hardening.

Figure 12 shows a plot of resolved shearing stress against temperature based on the data for all four orientations. Although the precision of the curves is uncertain, they indicate surely that the critical stress for translation increases with temperature while for twinning it de-

In calcite the critical stress for twinning is so low even at room temperature, about 30 kg/cm² (Turner *et al.*, 1954a, p. 889), that it is difficult to measure the temperature effect; however, there is little doubt that it decreases with increasing temperature. In calcite the critical stress for r translation drops from about 1500 kg/cm² at 24°C. to about 50 at 500°C. (Turner *et al.*, 1954a, Figs. 7, 8). It is surprising that the behaviors of two isostructural crystals, calcite and dolomite, are vastly different.

The stress-strain curves for all orientations and temperatures, except for specimens compressed normal to r_1 at 500°C., are well reproducible despite any differences from crystal to crystal, impurities and imperfections in each crystal, and variable ratios of specimen length to diameter. Incipient cleavage does not influence fracture. In specimens loaded parallel to c_0 and a, the cleavage planes very nearly parallel planes of maximum shearing stress. Yet under confining pressure, shear fracturing occurs along surfaces inclined not at 45° but at 30°–40° to the direction of greatest principal stress. Potential cleavages are ignored.

The ductility of the dolomite crystals is

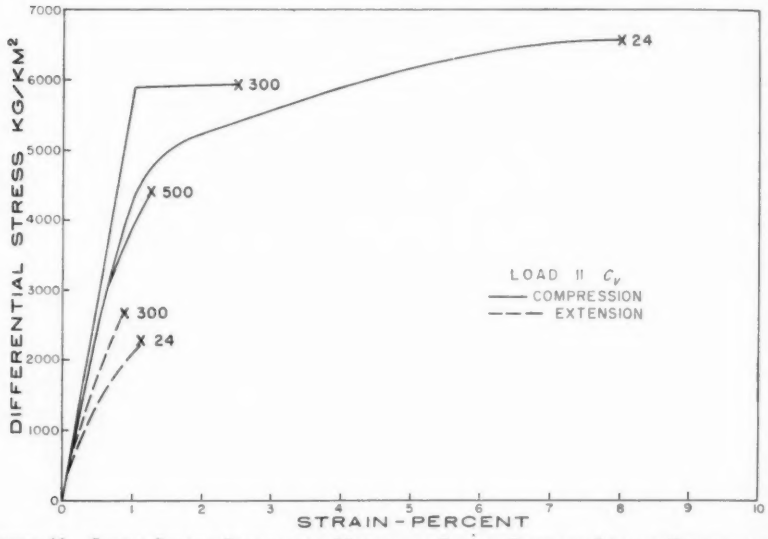

FIGURE 11.—STRESS-STRAIN CURVES FOR MAGNESITE SINGLE CRYSTALS LOADED PARALLEL TO c_v Under 5000 bars confining pressure at different temperatures.

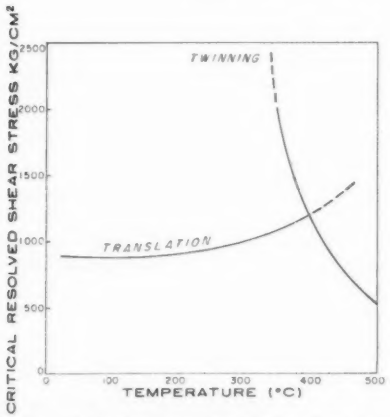

FIGURE 12.—CRITICAL RESOLVED SHEARING STRESSES AS FUNCTIONS OF TEMPERATURE FOR BASAL TRANSLATION AND $f\{0221\}$ TWINNING

enhanced by heating when basal translation is excluded, and twinning becomes possible at high temperature as in specimens loaded parallel to c_v and a (Figs. 6, 7). In these orientations the dolomite crystals are brittle at low temperature. Fracture is sudden, violent, and accompanied by release of stored elastic energy. The breaking stress is evidently strongly dependent on mean pressure, since the strength is always lower in extension than in compression.

The critical resolved shearing stresses for twinning and translation, and hence the yield stress of the crystal, appear to be largely independent of mean pressure. However, in crystals loaded parallel to $[f_2{:}f_3]$ and normal to r_1 the ductility is reduced by heating, probably because the breaking stress is only slightly influenced by temperature, while the yield stress for translation gliding is increased.

At high temperatures the strength of the brass sleeves surrounding the undersized specimens is low, and the brass appears to have no influence on the stress-strain curves of the dolomite crystals. The curves for experiment 170 without, and 574 with, a brass sleeve are practically identical (for crystals extended normal to r_1 at 300°C.) as are those for experiments 174 and 573 (extension normal to r_1 at 400°C.). The sleeves do influence ductility by permitting greater macroscopic shearing offsets before the splitting of the copper jackets. This effect is important only in crystals compressed parallel to a. The stress-strain curve for 500°C. suggests that intracrystalline gliding may have occurred, when in fact the deformation was due to macroscopic shearing without permanent loss of cohesion and hence without loss of differential load (Pl. 2, fig. 2*A*).

At least part of the apparent work hardening exhibited by most of the stress-strain curves is due to the external rotation of the active gliding plane. For example, in crystals loaded normal

to r_1, the resolved shearing-stress coefficient on $c\{0001\}$ decreases as the deformation progresses, while the coefficient on at least one f

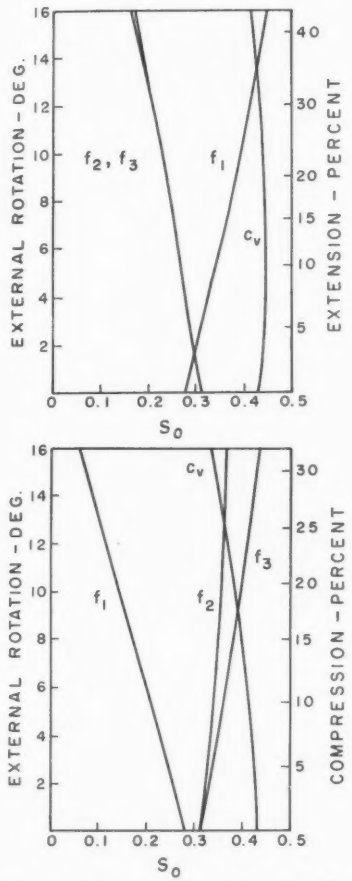

FIGURE 13.—CHANGES OF RESOLVED SHEAR-STRESS COEFFICIENTS (S_0) FOR $c\{0001\}$ AND $f\{02\bar{2}1\}$
Changes resulting from external rotations in specimens extended and compressed normal to r_1, basal translation assumed. The curves were constructed according to principles fully discussed by Handin and Griggs (1951, p. 866–869).

twin plane increases (Fig. 13). This means that basal translation becomes more difficult and the differential stress increases. Also because of these rotations, twinning may occur late in the deformation history, although initially the resolved shearing stress may be too low.

No effort was made to investigate magnesite thoroughly. Neither e nor f twinning was observed up to 300°C. Basal translation was excluded by the orientation of the load normal to $c\{0001\}$. At room temperature in compression the gliding mechanism is r translation of the kind observed in calcite. The magnesite does not flow at 300°C. and above, so that the critical resolved shearing stress for translation appears to increase with temperature, while the ductility is lower in the heated crystals (Fig. 11).

PETROGRAPHIC OBSERVATIONS

Laboratory Procedure

Thin sections of the deformed crystals were studied to check the deformation mechanisms, and the results are grouped according to the four orientations.

The measurements are made on a petrographic microscope equipped with a Zeiss-Winkel universal stage and object traverser. The errors in measurements of c_v are about 1°, where c_v is inclined to the plane of the thin section at 20° or less, and about 2° where the angle of inclination is 35°–45°. Planar elements inclined 70° or more to the plane of the section can be measured to about 1°. The error may be about 2° where they are inclined 45°–70°.

All measured data are plotted on a stereographic net of 20 cm diameter, and all recorded interfacial and zonal measurements are made on this net. The lower hemisphere of the projection sphere is projected on the horizontal plane (Figs. 14–19). (In Figure 2 of the crystallographic data the upper hemisphere is projected.)

The thin sections are cut parallel to the cylinder axes of the deformed specimens. Moreover, the plane of the thin section is parallel to the plane of deformation, *i.e.*, the plane of the thin section contains the maximum or minimum diameters of the specimens deformed in compression or extension, respectively, when these can be identified. Table 8 indicates the specimens from which thin sections were prepared.

Results for Dolomite

Parallel to c_v.—Translation gliding on $c\{0001\}$ is impossible, and twin gliding on $f\{02\bar{2}1\}$ (in a negative direction sense) is possible in compression experiments only (Table 6). All cylinders were brittle except those compressed at 400°C. and 500°C. which were ductile. The brittle specimens are characterized by shear fractures or incipient shear fractures (Table 8) and very small strains. Specimens

595 and 587 are considered to be representative of the brittle material.

Specimen 595 (Pl. 2, fig. 1*A*) was extended 2.3 per cent[3] at 500°C. Microscopic examination with the presence of numerous shear fract ures and bodily rotations of small but discrete pa t of the crystal, discredit the possibility of portant intracrystalline gliding. Probably

TABLE 9.—YIELD STRESSES OF DOLOMITE CRYSTALS AND CORRESPONDING RESOLVED SHEARING STRESSES FOR TRANSLATION GLIDING ON $c\{0001\}$ AND TWIN GLIDING ON $f\{02\bar{2}1\}$

Orientation	Temp. (°C)	Yield stress (kg/cm²)		Resolved shearing stress (kg/cm²)			
				$c\{0001\}$		$f\{02\bar{2}1\}$	
		Comp.	Ext.	Comp.	Ext.	Comp.	Ext.
$\parallel c_v$	24	>5500*	>3000*			>2200	
	300	>4300*	>3250*			>1720	
	400	2900	>2700*			1160	
	500	1250	>2450*			500	
$\parallel a$	24	>5720*	>2930*				> 910
	300	>5270*	>3350*				>1040
	400	>6150*	>3220*				>1000
	450		1850				570
	500	3250	1850				570
$\perp r_1$	24	2030	2000	870	860	630	540
	300	3100	2200	1330	950	960	590
	400	2250	2850	970	1230	700	740
	500	4500	2000	1940	860	1390	540
	500**	2400		1030		740	
$\parallel [f_2 : f_3]$	24	1500	2200	650	950	390	
	300	1950	2250	840	970	510	
	400		2750		1180		

*Breaking strength. Crystal is essentially brittle.
**From D. Griggs (his specimen 504).

revealed the development of numerous small conjugate shear fractures, particularly in the lower half of the specimen, inclined at about 60° to the least principal stress. Incipient f_1 and f_2 lamellae occur adjacent to the shear fractures and are thought to be associated with local stress concentrations. Although slight bending of these f lamellae near fractures was noticed, measurable internal rotations of pre-existent lamellae were absent. This absence, together with the presence of numerous shear fractures and bodily rotations of small but discrete parts of the crystal, discredit the possibility of important intracrystalline gliding. Probably the strain is accounted for by macroscopic shear on irregular surfaces.

One major shear fracture, inclined at about 40° to the maximum principal stress, extends part way through specimen 587 (Pl. 2, fig. 1*B*) which was compressed 0.7 per cent at 300°C. The specimen consists of parts of two individual crystals. (Fortunately, this accident in preparing a specimen did not often occur.) The origin of the many small fractures occurring near the major shear fracture is unknown. The greatest concentration of the small fractures occurs near the intersection of the major shear fracture and the boundary between the two crystals. Sparse and incipiently developed lamellae occur parallel to f_1, f_2, and f_3 throughout the area of the larger crystal. None could be identified optically

[3] All the measured values of longitudinal strain are for total strain. Of this about 1 per cent is recoverable elastic strain, so that the permanent strain (flow), with which the values computed from microscopic data should be compared, is a little less than the values quoted. However, this discrepancy is unimportant in view of the precision of measurements.

PLATE 1.—DOLOMITE SPECIMENS

FIGURE 1.—Dolomite specimen, supplied by Mr. R. E. Januzzi, consisting of three crystals C_1, C_2, and C_3. Cylinders of C_1 and C_2 were used in most of the experiments.

FIGURE 2.—Deformed specimens compared with undeformed cylinder (C). Cylinders A and B, loaded parallel to c_v, were brittle, and cylinders D and E, loaded perpendicular to r_1, were ductile.

FIGURE 1

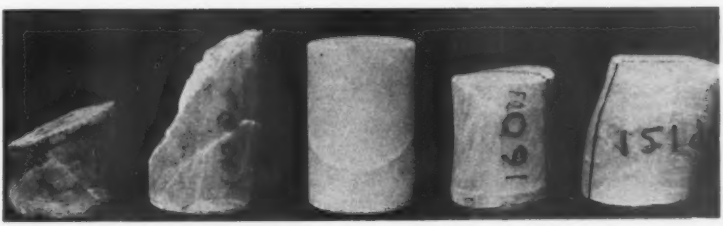

FIGURE 2

DOLOMITE SPECIMENS

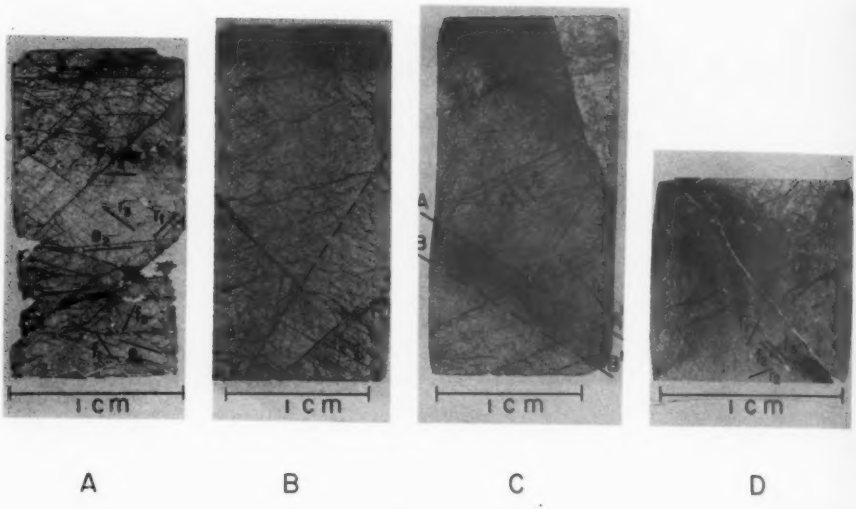

FIGURE 1

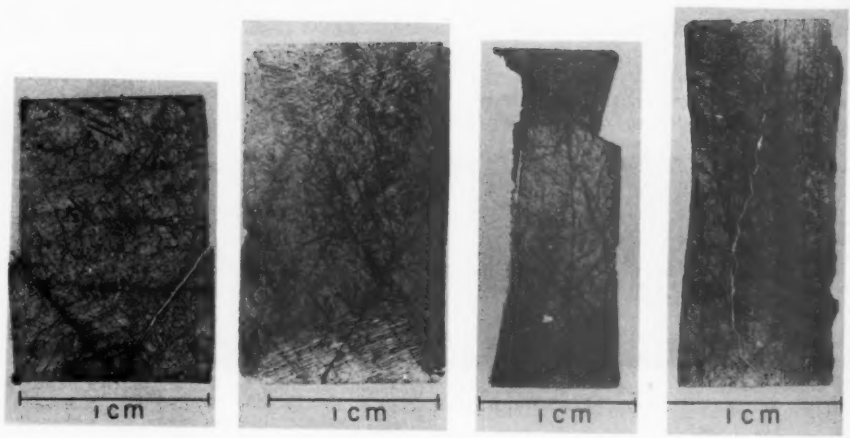

FIGURE 2

THIN SECTIONS OF SPECIMENS LOADED PARALLEL TO c_V AND a

as twin lamellae. Despite their presence, most, if not all, of the small strain is accounted for by macroscopic shearing.

Specimen 586 compressed 2.5 per cent at 400°C. exhibits a marked development of f_1 lamellae and a narrow but well-defined kink band (Pl. 2, fig. 1*C*, *AA'–BB'*). Measurements were confined to the lower half of the section, because the upper half contains a small portion of a second individual. Although f_1 lamellae occur throughout the section, optically recognizable f_1 twins are limited to the region of the kink band and constitute about 30 per cent of the band. Clockwise external and counterclockwise internal rotations occurred. Internal rotation of r_1 lamellae in the kink band amounts to 9°. Assuming that r_1 was rotated by twin gliding on f_1, one can calculate the strain as 6.6 per cent. This value may appear to be high but is in accord with the measured strain because most of the deformation was confined to the narrow kink band of which the twins constitute only about 30 per cent. The senses of observed external and internal rotations are consistent with a negative sense of shear on f_1 (Fig. 14*A*, insert).

Specimen 557 (Pl. 2, fig. 1*D*), compressed 16.7 per cent at 500°C., was barrel-shaped

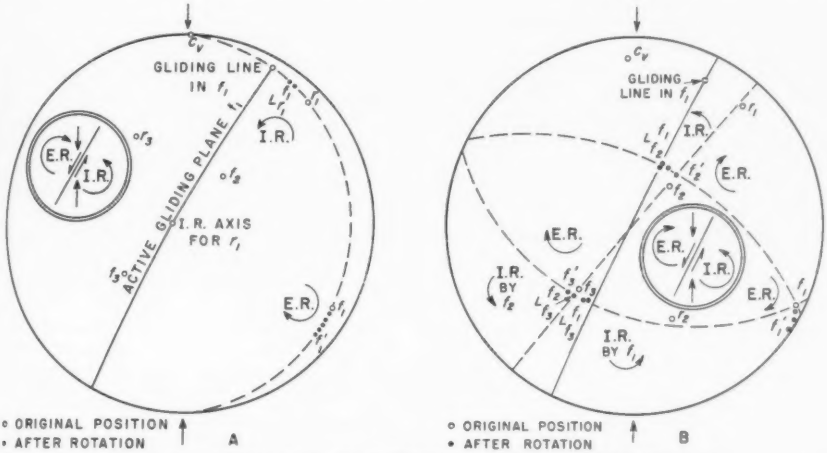

FIGURE 14.—STEREOGRAMS FOR SPECIMENS COMPRESSED PARALLEL TO c_v

A. Specimen 586 showing external rotation of f_1, and internal rotation of r_1 to $L_{r_1}^{f_1}$. The senses of shear and of the rotations are shown in the insert.

B. Specimen 557 showing external and internal rotations. The senses of shear and of the rotations are shown in the insert.

PLATE 2.—THIN SECTIONS OF SPECIMENS LOADED PARALLEL TO c_v AND a

FIGURE 1.—Thin sections of specimens loaded parallel to c_v. *A*. Specimen 595 extended 2.3 per cent at 500°C. The plane of the section is almost normal to a macroscopic shear. *B*. Specimen 587 compressed 0.7 per cent at 300°C. The plane of the section is almost perpendicular to a macroscopic shear inclined about 40° to the greatest principal pressure. Line *XY* is the contact between parts of the two individual crystals. *C*. Specimen 586 compressed 2.5 per cent at 400°C. The plane of the section is approximately parallel to the plane of deformation, *S*. (*See* Fig. 3.) *D*. Specimen 557 compressed 16.7 per cent at 500°C. The plane of the section is approximately perpendicular to f_1.

FIGURE 2.—Thin sections of specimens loaded parallel to a_1. *A*. Specimen 558 compressed 8.9 per cent at 500°C. The section is almost perpendicular to the macroscopic shear fractures. *B*. Specimen 531 extended 1.5 per cent at 400°C. The section is approximately parallel to the plane of deformation. *C*. Specimen 622 extended 30.0 per cent at 450°C. The section is approximately parallel to the plane of deformation. *D*. Specimen 596 extended 8.1 per cent at 500°C. The section is approximately parallel to the plane of deformation.

after deformation, and the cross section was everywhere circular. Apparently an incipient shear fracture had developed. Since a unique deformation plane could not be identified, the thin section was cut approximately perpendicular to the incipient shear fracture. In view of the shape and of the fact that all three f planes have the same resolved shear stress ($S_0 = .40$), it was not surprising to find that lamellae parallel to f_1, f_2, and f_3 were about equally developed. All three have been rotated internally through angles up to 10°. Sequential rotations, however, could not be identified. The senses of shear and of the rotations (*see* Fig. 14*B*, insert) are consistent and indicate negative gliding on the f planes. The maximum calculated strain of 9.7 per cent appears low when compared with measured strain of 16.7 per cent. Some of the measured strain may be accounted for by the macroscopic shear. Possibly sequential rotation of an f_2 lamella (for example) occurred by gliding first on f_1 and then on f_3. The resulting calculated strains would be cumulative and in better agreement with the measured strain.

In summary, macroscopic shearing accounts for the strain in those crystals that were brittle. Ductile behavior of specimens compressed at 400°C. and 500°C. reflects intracrystalline gliding, and twin gliding on $f\{02\bar{2}1\}$, direction sense negative, is the only mechanism.

Parallel to a.—Translation gliding on $c\{0001\}$ is impossible, and twin gliding on $f\{02\bar{2}1\}$ (in a negative direction sense) is possible in extension experiments only (Table 6). All cylinders were brittle except those extended at 400°C., 450°C., and 500°C.

Since the microscopic features of the brittle specimens are much the same regardless of orientation, they need not be redescribed. It is necessary only to describe specimen 558 (Pl. 2, fig. 2*A*), compressed 8.9 per cent at 500°C., because, from the experimental record, its behavior is apparently anomalous. Intracrystalline gliding should not occur, but the stress-strain curve indicates that the specimen flowed. Microscopic examination revealed that despite a slight bulging of the specimen, most of the strain was due to macroscopic shearing. At least 7.0 per cent of the strain is accounted for by displacements on the shear surfaces. Since the measured strain is 8.9 per cent, only a very small amount could be due to intracrystalline gliding. If gliding occurred, it could not be detected microscopically because strains of 1 or 2 per cent would be reflected in internal rotations of only 1° or 2°, and such small rotations are not in excess of errors in measurement.

Cylinders extended at 400°C., 450°C., and 500°C. were ductile. In contrast to deformation by macroscopic shearing, intracrystalline gliding is the dominant mechanism in the ductile crystals.

Specimen 531 (Pl. 2, fig. 2*B*), extended 1.5 per cent at 400°C., exhibits the onset of twin gliding. Lamellae parallel to f_1 are developed profusely although only a few very narrow bands can be identified optically as distinct twins. Locally, r_1 lamellae were rotated internally through 8°. The resulting calculated strain of 4.5 per cent is of the right order of magnitude. Observed clockwise internal rotation (*see* Fig. 15*A*, insert) is consistent with the sense of shear that reflects negative gliding on f_1.

Specimen 622 (Pl. 2, fig. 2*C*), extended 30.0 per cent at 450°C., is characterized by a kink band the boundaries of which approximate the two shear fractures (one is offset) near the ends of the crystal. Almost complete twinning on f_1 occurred in the kink band. This was accompanied by external and internal rotations as indicated in Figure 15*B*. Specifically, the external rotated r_1' and f_2' were rotated internally through about 34° and 22° respectively. The calculated angles for complete f_1 twinning are 32°44′ and 20°47′. The strains, calculated from internal rotations of r_1 and f_2 are 19.9 per cent and 20.4 per cent, in good agreement with the measured strain after subtraction of the amount due to macroscopic shearing (about 5 per cent).

Specimen 596 (Pl. 2, fig. 2*D*), extended 8.1 per cent at 500°C., is similar to 622, the only essential difference being in the amount of strain. There is profuse development of f_1 lamellae throughout the section. Optically recognizable f_1 twins constitute about one-third of the total area of the section. Clockwise internal rotations (*see* Fig. 15*C*, insert) of r_1 and f_2 amount to 12° and 8° respectively. The corresponding calculated strains are 6.7 per cent and 7.1 per cent which are in good agreement with the measured strain. The senses of shear and of rotations are consistent with negative twin gliding on $f\{02\bar{2}1\}$.

In summary, the brittle and ductile behaviors of cylinders in this orientation are consistent with behaviors of cylinders loaded parallel to c_v. All cylinders compressed parallel to a or extended parallel to c_v were brittle, whereas above 400°C. cylinders extended parallel to a

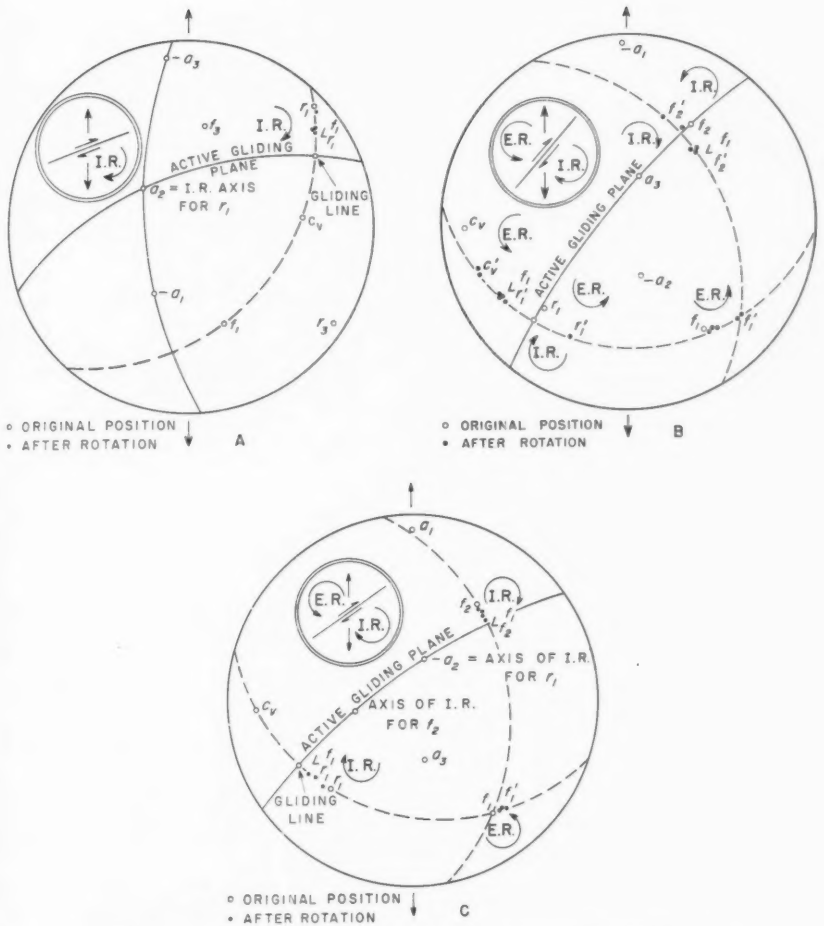

FIGURE 15.—STEREOGRAMS FOR SPECIMENS EXTENDED PARALLEL TO *a*

A. Specimen 531 showing internal rotation of r_1 by f_1 twin gliding. Senses of shear and of internal rotation are shown in the insert.

B. Specimen 622 showing external and internal rotations; f_1, f_2, and r_1 are rotated externally to f_1', f_2', and r_1' respectively. Internal rotations of f_2' and r_1' are consistent with twin gliding on f_1. The senses of shear and of rotations are shown in the insert.

C. Specimen 596 showing rotations of lamellae. Senses of shear and of rotations are shown in the insert.

or compressed parallel to c_v were ductile, and the deformation mechanism was twin gliding on $f\{02\bar{2}1\}$. As predicted, the direction sense must be negative. The gliding line could not be established without ambiguity because of lack of assurance that the thin sections were exactly parallel to the plane of deformation. Nevertheless, for each of the sections examined, the predicted gliding line $[1\bar{1}04]$ lies near the plane of the section.

Perpendicular to r_1.—Translation gliding on $c\{0001\}$ is possible in both compression and extension experiments, whereas twin gliding on f_1 is possible in extension only and on f_2 and f_3 in compression only (Table 6). The resolved shear-stress coefficient (Table 7) is higher on $c\{0001\}$ than on $f\{02\bar{2}1\}$, and, accordingly, translation gliding would be favored if the critical resolved shear stresses were the same for translation and twinning.

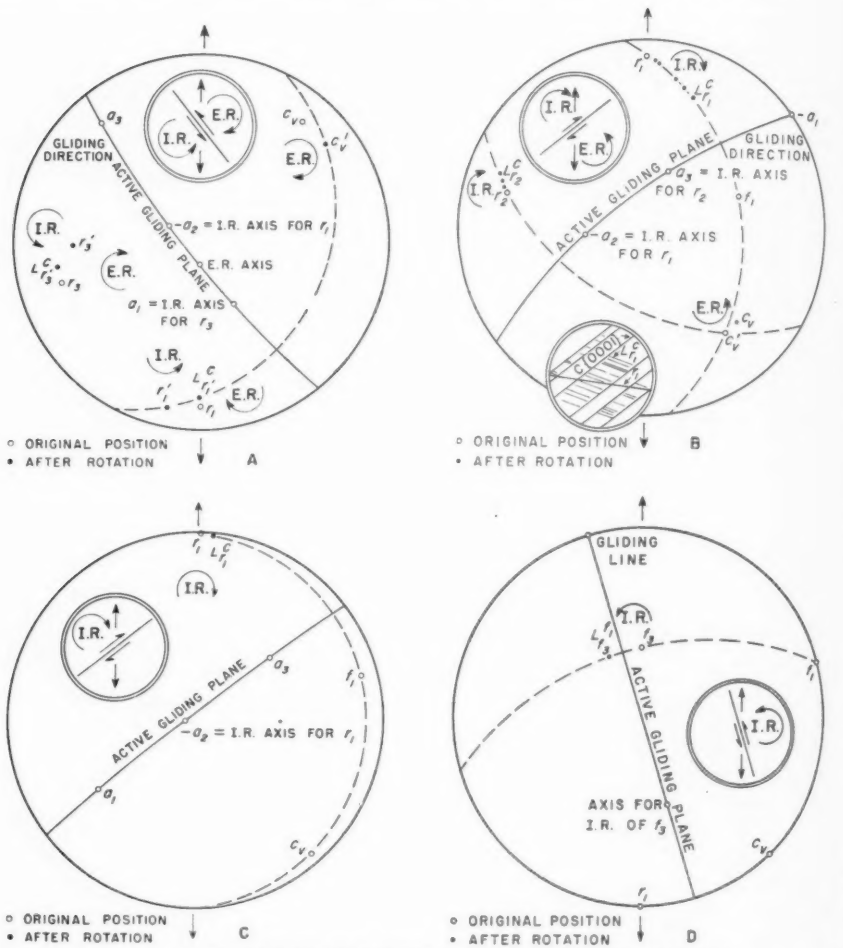

FIGURE 16.—STEREOGRAMS OF SPECIMENS EXTENDED PERPENDICULAR TO r_1

A. Specimen 160 showing rotations of r lamellae. r_1, r_2, and c_v were rotated externally to r_1', r_2', and c_v'. r_1' and r_2' were rotated internally to $L^{c_v}_{r_1'}$ and $L^{c_v}_{r_2'}$. The senses of shear and of the rotations are shown in the insert.

B. Specimen 170 showing rotation of r lamellae. The senses of shear and of internal rotation are indicated. Rotation of r_1 lamellae in alternate slip bands (*see* Pl. 4*A*, *B*) is shown diagramatically in the insert.

C. Specimen 174 showing internal rotation of r_1 lamellae. Senses of shear and of internal rotation are indicated in the insert. The section is perpendicular to r_1.

D. Specimen 559 showing internal rotation of f_3 lamellae. Senses of shear and of rotation are indicated in the insert.

Specimen 160 (Pl. 3, fig. 1*A*), extended 11.9 per cent at 24°C., is characterized by a kink band (Pl. 3, fig. 1*A*, *WX-YZ*) transverse to $c\{0001\}$ and by externally and internally rotated elements. Sharply defined to indistinct deformation bands occur within the kink band and are scattered irregularly through it. Their trends are subparallel to the boundaries of the kink band; their normals are almost parallel to a_2. External rotation (*see* Fig. 16*A*) of about 12° was identified. This is reflected in rotations of c_v, r_1, and r_3 to c_v', r_1', and r_3' respectively.

The axis of external rotation lies in $c\{0001\}$ and bisects the angle between a_1 and a_2. Since this axis is normal to the gliding line, it follows that the latter is parallel to a_3. Counterclockwise internal rotations (Fig. 16*A*) of r_1' and r_3' to $L_{r_1'}^{c}$ and $L_{r_3'}^{c}$ amount to 10°–11° in the kink band and 6°–7° outside the band. Corresponding calculated strains of 14.9 per cent and 9.2–12 per cent compare favorably with the measured strain. Senses of rotations are consistent with the sense of shear on $c\{0001\}$. Twin gliding was not detected.

Specimen 170 (Pl. 3, fig. 1*B*), extended 10.4 per cent at 300°C., is characterized by a poorly developed kink bank which traverses the section, and by well-developed, sharply defined slip bands (Pl. 4*A*, *B*) which are parallel to $c\{0001\}$. These slip bands are almost identical in appearance to those described by Turner *et al* (1954a, Pl. 10*C*). In their illustration, the slip bands are parallel to r_2 which is a possible translation gliding plane in calcite. Counterclockwise external rotation of about 7° was determined from *c*-axis measurements on each side of the boundaries of the kink band. The *c* axis in the deformed part of the specimen (in the kink band) has been rotated externally from the position c_v to c_v' (Fig. 16*B*). Two values, clockwise in sense, were determined for internal rotation. Throughout the central deformed area, r_2 lamellae exhibit internal rotations of up to 9°. The calculated strain is 12.3 per cent, in good agreement with the measured strain. Internal rotations of r_1 lamellae amounting to 20° were measured in alternate slip bands (Fig. 16*B*, insert; Pl. 3, fig. 1*B*; Pl. 4*A*, *B*). Moreover, f_1 lamellae, which are sparsely developed, occur only in those slip bands containing the rotated lamellae $L_{r_1}^{c}$. The slip bands containing these lamellae constitute only about a third of the area of the deformed part of the specimen, so that the calculated strain of 27 per cent is reasonable. The senses of external and internal rotations are consistent with translation gliding on $c\{0001\}$. The slip bands parallel to $c\{0001\}$ are additional evidence for basal translation, and agreement between calculated and measured strains lends credence to this mechanism. The gliding line is a_1.

Specimen 174 (Pl. 3, fig. 1*C*), extended 4.2 per cent at 400°C., contains slip bands (Pl. 4*C*, *D*) that are parallel to $c\{0001\}$, but these bands are not so well defined as those in 170. Moreover, *f* lamellae are not confined to alternate slip bands; they do exhibit an en echelon arrangement associated with the bands. Concentrations of rotated *r* lamellae in alternate bands are lacking also. Internal rotation of r_1 to $L_{r_1}^{c}$ (Fig. 16*C*) amounts to 4°, and the calculated strain of 4.3 per cent is in good agreement with the measured strain. This indicates that nearly all the strain is accounted for by basal translation, despite the presence of *f* lamellae. In support of this, the sense of internal rotation is consistent with shear on $c\{0001\}$.

Specimen 559 (Pl. 3, fig. 1*D*), extended 7.1 per cent at 500°C., is characterized by profuse development of f_1 lamellae throughout the section. Counterclockwise internal rotation of f_3 lamellae amounts to about 18°. The resulting calculated strain of 17 per cent is in agreement with predicted strain of 15.9 per cent for complete twinning in this orientation. Measured on a traverse normal to f_1, the host-to-twin ratio is between 10:3 and 10:4. Using these ratios, one calculates strains of 4.8 per cent and 6.4 per cent, not appreciably different from the measured strain. Translation gliding cannot be excluded and may account for the small differences between calculated and measured strains. Any translation, however, would cause internal rotations of less than 2° which would not be detectable with assurance. The counterclockwise internal rotation of f_3 (*see* Fig. 16*D*, insert) is consistent with negative slip on f_1.

Specimen 146 (Pl. 3, fig. 2*A*), compressed 14.6 per cent at 24°C., contains a well-developed kink band that is transverse to $c\{0001\}$. The kink band contains sparse, indistinct deformation bands (visible only under crossed nicols), with trends subparallel to the kink band, and sharply defined slip bands (Pl. 5*A*) that are parallel to $c\{0001\}$. Clockwise external rotation of about 5° was determined from *c*-axis measurements on both sides of the kink-band boundaries. The axis of external rotation, however, could not be identified. Counterclockwise internal rotation amounts to 11°–12° (Fig. 17*A*); r_1 and r_2 lamellae (Pl. 5*A*, *B*) were rotated to L_{r1}^{c} and L_{r2}^{c}, respectively. The axes of internal rotations for r_1 and r_2 are a_2 and a_1 respectively, and a_3 is the gliding direction. The calculated strain of 16.7 per cent is in good agreement with the measured strain.

Specimen 156 (Pl. 3, fig. 2*B*), compressed 7.8 per cent at 300°C., is characterized by both deformation bands and slip bands. The shadowy to indistinct deformation bands occur only in small sparsely scattered areas. Their trends are about normal to $c\{0001\}$. Faint but sharply defined slip bands parallel to $c\{0001\}$ are emphasized by concentrations of *f* lamellae

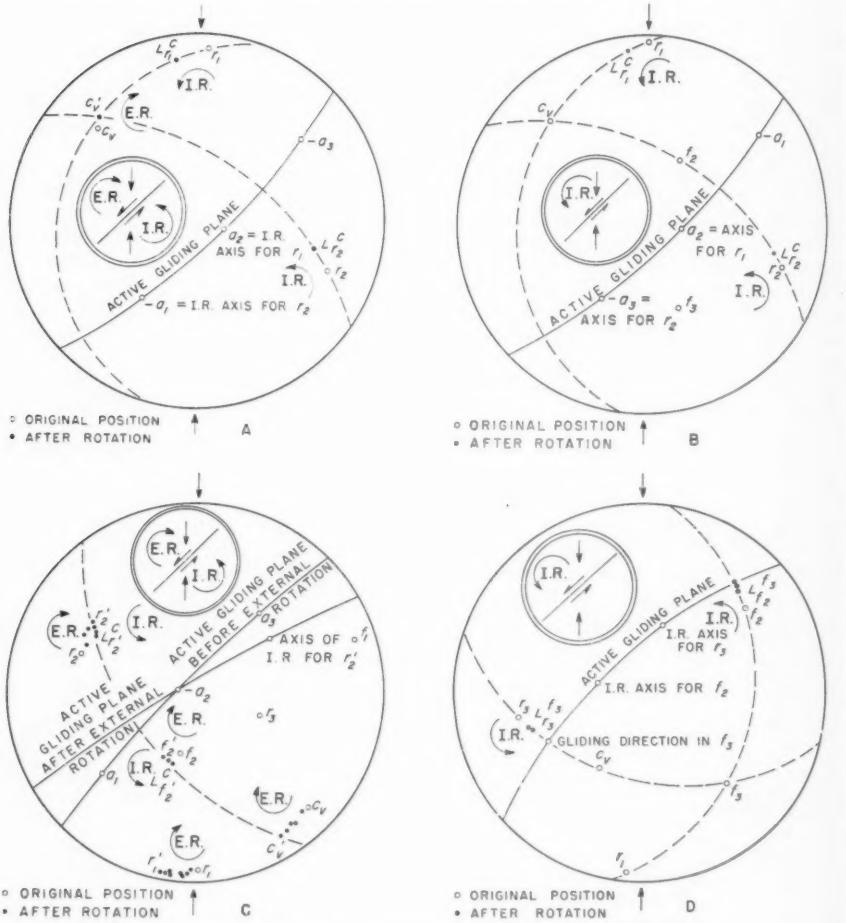

FIGURE 17.—STEREOGRAMS FOR SPECIMENS COMPRESSED PERPENDICULAR TO r_1

A. Specimen 146 illustrating external rotation of c_v to c_v' and internal rotations of r_1 and r_2 to $L^c_{r_1}$ and $L^c_{r_2}$ respectively. The senses of shear and of rotations are indicated in the insert.

B. Specimen 156 illustrating external rotation of c_v and internal rotations of r_1 and r_2 to $L^c_{r_1}$ and $L^c_{r_2}$ respectively. Senses of shear and of rotations are shown in the insert.

C. Specimen 529 illustrating external rotations of c_v, r_1, r_2, and f_2 to c_v', r_1', r_2', and f_2' respectively. Internal rotations of r_2' and f_2' are shown. Senses of shear and of rotations are shown in the insert.

D. Specimen 504 (Griggs) illustrating internal rotations of r_3 and f_2 lamellae to $L^{f_3}_{r_3}$ and $L^{f_3}_{f_2}$ respectively. The senses of shear and of rotations are shown in the insert.

in alternate bands (Pl. 5*D*). A kink band did not develop in this specimen. External rotation of the *c* axis amounts to about 10°. This rotation is restricted to the small local areas of shadowy deformation bands. The direction sense is clockwise. Counterclockwise internal rotation amounts to 7°. The r_1 and r_2 lamellae (Fig. 17*B*; Pl. 5*C*) were rotated to L^c_{r1} and L^c_{r2} respectively, and their corresponding rotation axes are a_2 and a_3. The calculated strain of 12.0 per cent is in fair agreement with the measured strain, since slip did not occur throughout the crystal.

Specimen 529 (Pl. 3, fig. 2*C*), compressed

6.5 per cent at 400°C., is characterized by marked external rotation (up to 14°) and by a moderate development of f_2 and f_3 lamellae, although few of these are optically recognizable as twins. Internal rotations amount to about 6° and are typified by rotation of r_2. The externally rotated r_2 has been rotated internally to $L^{c}_{r_2'}$ (Fig. 17*C*). Calculated strain based on $c\{0001\}$ gliding in a direction parallel to a_1 amounts to 9 per cent. Since the deformation is restricted to about 70 per cent of the specimen, this value is high, and the corrected value of 6.3 per cent is in good agreement with the measured strain. It should be pointed out that twin gliding (on f_2 and f_3) was operative but of secondary importance at 400°C. The critical resolved shear stresses for the gliding mechanisms are evidently temperature-dependent. Moreover, twin gliding in 529 occurred on f_2 and f_3 in contrast to gliding on f_1 in the extended specimen (559). This is in accord with a negative sense of gliding on $f\{02\bar{2}1\}$. The observed senses of rotation (clockwise external and counterclockwise internal) are consistent with basal translation where the sense of shear is as indicated in the insert of Figure 17*C*.

Specimen 504 (Griggs' experiment number), compressed 10.8 per cent at 500°C., is characterized by profuse development of two sets of twin lamellae (Pl. 3, fig. 2*D*; Pl. 5, *E*, *F*). These are developed to a much greater extent than any other of the experimentally deformed crystals. The f_3 lamellae are more profuse than f_2. In both sets the lamellae are broad enough to be identified as twins. Counterclockwise internal rotation of f_2 lamellae amounts to 14°. The f_3, f_2, and rotated lamellae L_{f_2} are cozonal (Fig. 17*D*). Calculated strain is 11.3 per cent, based on f_3 as the gliding plane with $[02\bar{2}1:\bar{2}110]$ the assumed gliding direction. Since external rotation was not identified, the gliding direction could not be established uniquely. Nevertheless, this assumption appears to be valid since the calculated strain of 11.3 per cent compares so favorably with the experimentally measured strain. The direction sense of gliding on f_3 must be negative to account for the clockwise internal rotation of f_2 to $L^{f_3}_{f_2'}$.

In summary, petrographic evidence supports translation gliding with $T\{0001\}$, $l[10\bar{1}0]$ as the operative mechanism for specimens compressed or extended perpendicular to r in the temperature range of 24°C. to 400°C. The senses of internal and external rotations, the high resolved shear stress on $c\{0001\}$, and the agreements between measured and calculated strains are in accord with basal translation.

Although the resolved shear stress on $c\{0001\}$ is higher than on f_1 in compression (0.43 compared to 0.27) and on f_2 and f_3 in extenson (0.43 compared to 0.31), twin gliding on f_3 accounts for the strain in the specimen compressed at 500°C. The gliding direction could not be defined uniquely since external rotation was not recognized. The direction sense must be negative to account for the counterclockwise internal rotation of f_2 lamellae. The critical resolve shear stress for translation gliding on $c\{0001\}$ must be higher than for twin gliding on f at 500°C. The reverse is true at lower temperature.

Parallel to $[f_2:f_3]$.—Translation gliding on $c\{0001\}$ is possible in both extension and compression experiments, whereas twin gliding is possible only on f_1 and is restricted to compression experiments if the direction sense is negative (Table 6). Behaviors were consistent for both extended and compressed specimens.

Specimen 161 (Pl. 6, fig. 1*A*), extended 7.5 per cent at 24°C., is characterized by a narrow, sharply defined kink band (*WXYZ*) trending at right angles to $c\{0001\}$ and by externally and internally rotated elements. As in specimen 160, slip bands parallel to $c\{0001\}$ are absent. Counter-clockwise external rotation amounts to about 10°. The c axis and r_1 and r_2 lamellae were rotated to the positions c_v', r_1', and r_2' respectively (Fig. 18*A*). Clockwise internal rotation amounts to 7°. The r_1' lamellae were rotated to $L^{c}_{r_1'}$ (Pl. 4*E*, *F*); $c\{0001\}$, r_1' and $L_{r_1'}$ are cozonal, which is in agreement with gliding on $c\{0001\}$. The gliding direction was not defined uniquely because neither the axis of external rotation nor the plane of deformation could be identified with assurance. Nevertheless, on the assumption that the gliding direction is parallel to an a axis (established in other specimens), the calculated strains of 7.9 per cent and 9.0 per cent agree favorably with the measured strain. Moreover, the senses of rotations are consistent with the sense of shear on $c\{0001\}$.

Specimen 153 (Pl. 6, fig. 1*B*), compressed 12.0 per cent at 24°C., is characterized by indistinct deformation bands that are scattered throughout the section, and by externally and internally rotated elements. Counterclockwise external rotation is exhibited by rotations of c_v, r lamellae, and the normals to deformation bands. This ranges from about 8° for c_v to 4°–6° for the r lamellae. All r lamellae were

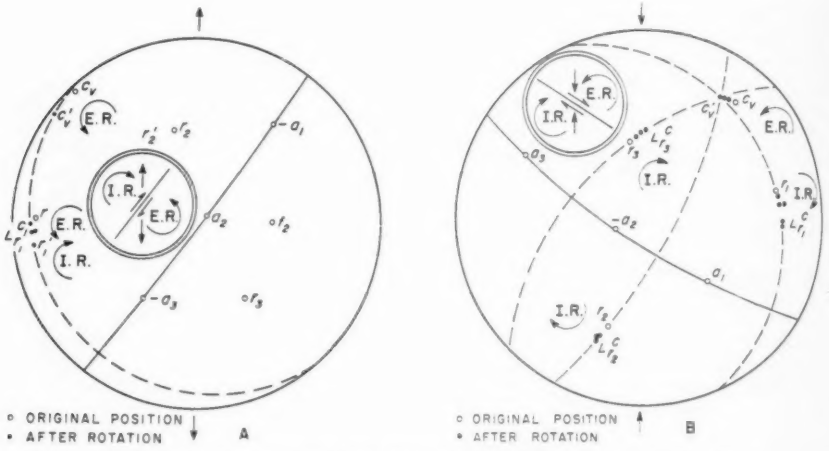

FIGURE 18.—STEREOGRAMS FOR SPECIMENS LOADED PARALLEL TO $[f_2{:}f_3]$

A. Specimen 161 illustrating internal and external rotations. c_v, r_1, and r_2 were rotated externally to c'_v, r'_1, and r'_2 respectively. r'_1 was rotated internally to $L^{c,r'_1}_{r'_1}$. The senses of shear and of rotations are indicated in the insert.

B. Specimen 153 illustrating external and internal rotations. c_v was rotated externally to c'_v. The three *r* lamellae were rotated to $L^{c}_{r_1}$, $L^{c}_{r_2}$, and $L^{c}_{r_3}$. Senses of shear and of rotations shown in the insert were determined by rotating r_3, r_1, and $L^{r_3}_{r_1}$ to the periphery.

rotated internally (Fig. 18*B*). The maximum rotation of 13° affected r_1 lamellae. Calculated strain, basal translation assumed, amounts to 14.2 per cent and is in good agreement with measured strain. The senses of rotations are consistent with the sense of shear on $c\{0001\}$.

Results for Magnesite

Johnsen (1902, p. 139–144) reported possible twin gliding in naturally deformed rhombs collected from talc and chlorite schists and labeled "Zillerthal." He recognized the lack of convincing evidence but predicted that if twinning occurred it would be on $e\{01\bar{1}2\}$ as in calcite. This is in contrast to his reported twin gliding on $f\{02\bar{2}1\}$ in dolomite. He also identified translation gliding with $T = (0001)$, $t = [10\bar{1}1{:}0001]$, as in dolomite.

The few cylinders deformed in this study were loaded parallel to c_v. Thus, translation gliding on $c\{0001\}$ was impossible, whereas twin gliding on $e\{01\bar{1}2\}$ would be possible only in extension if the sense was the same as in calcite. Translation gliding on $r\{10\bar{1}1\}$ would be possible only in compression if the sense was negative as in calcite. (*See* Turner *et al.*, 1954a, p. 931.)

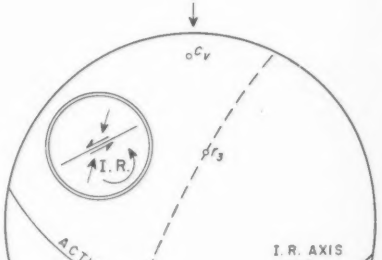

FIGURE 19.—STEREOGRAM FOR MAGNESITE SPECIMEN 123 LOADED PARALLEL TO c_v

Illustrating internal rotation. Senses of shear and rotations are shown in the insert.

Specimens extended at 24°C. (158) and at 300°C. (159) were brittle; total strains were of the order of 1 per cent. This of course is in marked contrast to the behavior of calcite

which twins easily in extension parallel to c_v even at room temperature.

A deformation mechanism was identified in only one specimen (123), which was ductile little doubt that r translation analogous to that in calcite has occurred. However, no $e\{01\bar{1}2\}$ twinning was produced at any temperature. Basal translation cannot be ruled out.

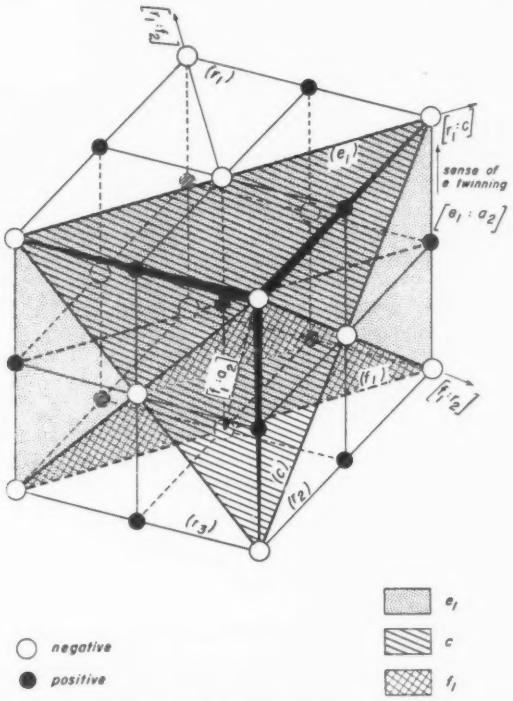

FIGURE 20.—GENERALIZED LATTICE FOR CALCITE, DOLOMITE, AND MAGNESITE

(Pl. 6, fig. 2). This specimen was compressed 7.9 per cent at 24°C., and what remains in thin section is characterized by irregular development of indistinct deformation bands and by an internal rotation of r_1. This counterclockwise rotation of about 6° is consistent with negative translation on r_3 (Fig. 19, insert). Of the possible crystallographic forms, only r_3 and a second-order prism, $a\{11\bar{2}0\}$, are cozonal with the rotated lamellae. Gliding could not occur on the prism because it is parallel to the greatest principal stress. In contrast, the resolved shear-stress coefficient is 0.49 on r_3. Therefore, if one assumes negative translation gliding on r_3 in the direction $[01\bar{1}1 : \bar{2}021]$, as in calcite, the calculated strain should approximate the measured strain. From equation (2) and the values $S_0 = 0.49$, $\alpha = 65°$, $\beta = 71°$, and $\gamma = 52°$, a calculated strain of 7.5 per cent is obtained in good agreement with the measured value. There is

DISCUSSION

No general theory relates the translation gliding elements (plane T and direction t) to a particular crystal structure. However, in metals "it is invariably the most dense atomic row that serves as a direction of glide, and usually the planes of highest atomic density are the glide planes" (Schmid and Boas, 1950, p. 86). Thus planes and directions of low indices form the commonest gliding elements. The gliding line is the zone axis of several possible gliding planes, and it is seldom possible to predict which of these planes will be operative. A further restriction on translation in ionic crystals is possible. Ions of the same sign would not be likely to approach each other since this would lead to repulsions normal to the gliding line. This "forbidden" translation is, however, known in some crystals. These principles are

applied below to gliding in the rhombohedral carbonate minerals.

Figure 20 shows the generalized structure of the calcite type (symmetry, hexagonal scalenohedral). Magnesite ($MgCO_3$), rhodochrosite ($MnCO_3$), siderite ($FeCO_3$), and smithsonite ($ZnCO_3$) have the same structure. The figure also represents the structure of dolomite if it is understood that alternate layers of positive ions parallel to $c\{0001\}$ are composed of Ca and Mg and that as a consequence the symmetry (trirhombohedral) is lower than that of the calcite type.

The directions in which ions of like charge are most closely spaced are along the short diagonals of the rhombohedral faces. Thus if attention is focused on r_1, the line $[r_1{:}f_2] = [r_1{:}a_2]$ is the gliding line for the possible gliding planes of low indices $r_1(10\bar{1}1)$, $f_2(2\bar{2}01)$, $f_3(02\bar{2}1)$, and $a_2(\bar{1}2\bar{1}0)$. The three equivalent lines demanded by trigonal symmetry are $[r_1{:}f_2]$, $[r_1{:}f_3]$, and $[r_2{:}f_1]$.

The next most probable gliding direction is the long diagonal of the rhombohedral face. The line $[r_1{:}e_1] = [r_1{:}c] = [r_1{:}m_1]$ is the gliding line for the possible gliding planes of low indices $r_1(10\bar{1}1)$, $e_1(\bar{1}012)$, $c(0001)$, and $m_1(10\bar{1}0)$. The three equivalent lines are $[r_1{:}c]$, $[r_2{:}c]$, and $[r_3{:}c]$ which are the three crystallographic (horizontal) axes a_2, a_3, a_1.

The system ($T = r_1(10\bar{1}1)$, $t = [r_1{:}f_2]$) has been observed in calcite (Turner *et al.*, 1954a, p. 931; Handin *et al.*, 1957, p. 1223) and is first reported in magnesite in the present paper. The critical resolved shear stresses at room temperature differ widely, about 1500 and 2300 kg/cm² for calcite and magnesite, respectively. Moreover, in calcite the critical stress decreases to about 250 kg/cm² when the temperature is raised to 300°C. (Turner *et al.*, 1954a, Table 1); in magnesite the stress appears to increase with temperature.

In translation gliding each displacement is through an integral number of interionic distances, so that the configuration of the crystal structure remains unchanged. In a cubic metal, gliding in either sense is equally likely. However, in the carbonates one sense may be preferred over the other since the force field of a carbonate group is not spherical. The sense of r translation is observed to be negative in calcite, but the evidence is not unequivocal. Possibly failure to observe the positive sense is due to the fact that a force directed to induce gliding in this sense would much more readily induce e twinning. In our experiments twinning does not occur in magnesite, and r translation

---

PLATE 3.—THIN SECTIONS OF SPECIMENS LOADED PERPENDICULAR TO r_1

FIGURE 1.—Thin sections of specimens extended perpendicular to r_1. *A*. Specimen 160 extended 11.9 per cent at 24°C. Boundaries of the kink band are outlined by the lines WX and YZ. The section is perpendicular to r_1 and almost parallel to the plane of deformation. *B*. Specimen 170 extended 10.1 per cent at 300°C. The section is perpendicular to r_1. Slip bands parallel to $c\{0001\}$ are clearly visible and are illustrated in greater detail in Plate 4*A*, *B*. *C*. Specimen 174 extended 4.2 per cent at 400°C. Although incipient, f lamellae are more prominent than in 170. *D*. Specimen 559 extended 7.1 per cent at 500°C. The section is parallel to the plane of deformation. Lamellae parallel to f_1 are much more profuse than in either 170 or 174.

FIGURE 2.—Thin sections of specimens compressed perpendicular to r_1. *A*. Specimen 146 compressed 14.6 per cent at 24°C. The section is almost perpendicular to r_1 and parallel to the plane of deformation. *B*. Specimen 156 compressed 7.8 per cent at 300°C. The section is almost perpendicular to r_1 and parallel to the plane of deformation. *C*. Specimen 529 compressed 6.5 per cent at 400°C. The section is almost perpendicular to r_1. *D*. Specimen 504 (Griggs) compressed 10.8 per cent at 500°C. The section is almost perpendicular to r_1. Twinning on f_3 is almost complete in the central part.

PLATE 4.—PHOTOMICROGRAPHS OF SPECIMENS 170 (*A*, *B*), 174 (*C*, *D*), AND 161 (*E*, *F*)

A. Area in thin section of 170 (Pl. 3, fig. 1*B*) illustrating characteristics of the slip bands. Alternate bands contain rotated lamellae $L^c_{r_1}$. Plane polarized light with O-ray parallel to vibration direction of polarizing nicol. *B*. Same area as Plate 4*A* with the E-ray parallel to vibration direction of polarizing nicol. The f_1 lamellae occur in those slip bands containing $L^c_{r_1}$. *C*. Area in thin section of 174 illustrating slip bands parallel to $c\{0001\}$. There is a tendency for f lamellae to occur in alternate bands, but it is not so pronounced as in specimen 170 (Pl. 4*B*). *D*. Area in thin section of 174 illustrating the most common appearance of f lamellae in this specimen. *E*, *F*. Photomicrographs of specimen 161 from areas in the kink band (Pl. 6, fig. 1*A*) illustrating characteristics of internally rotated r_1 lamellae.

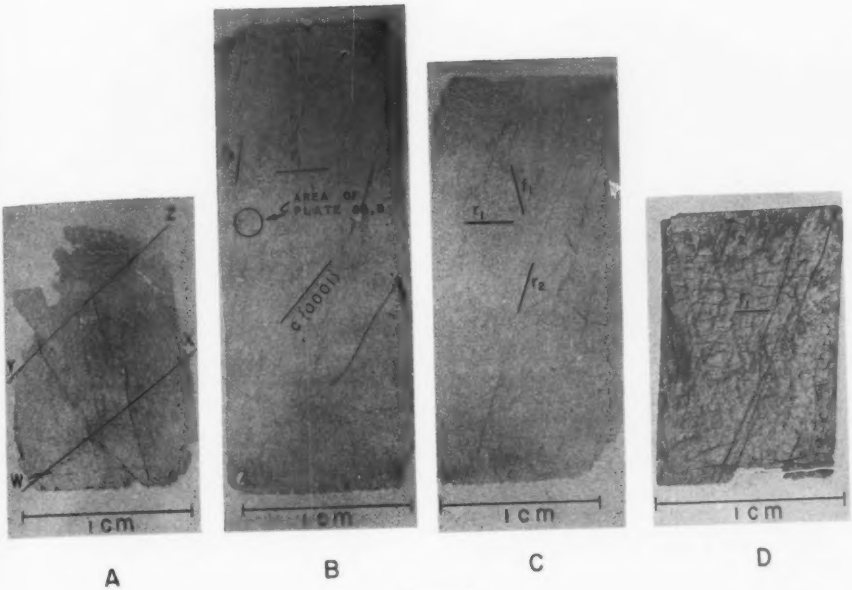

FIGURE 1

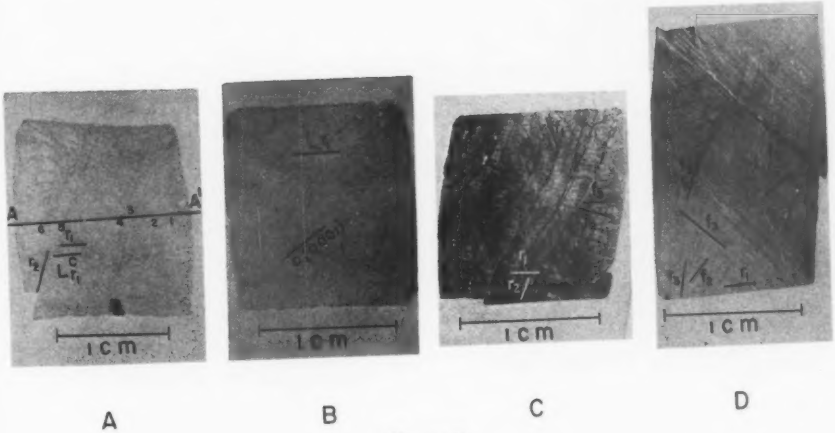

FIGURE 2

THIN SECTIONS OF SPECIMENS LOADED PERPENDICULAR TO r_1

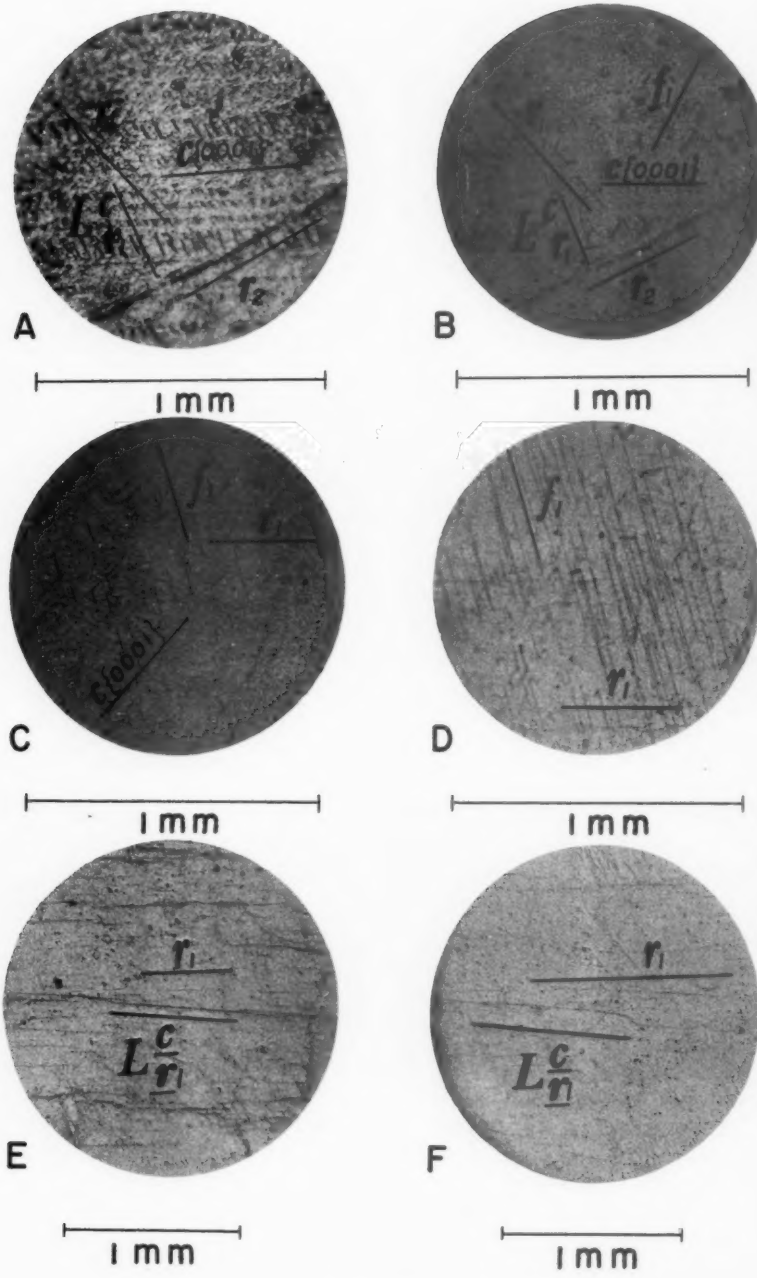

PHOTOMICROGRAPHS OF SPECIMENS 170, 174 AND 161

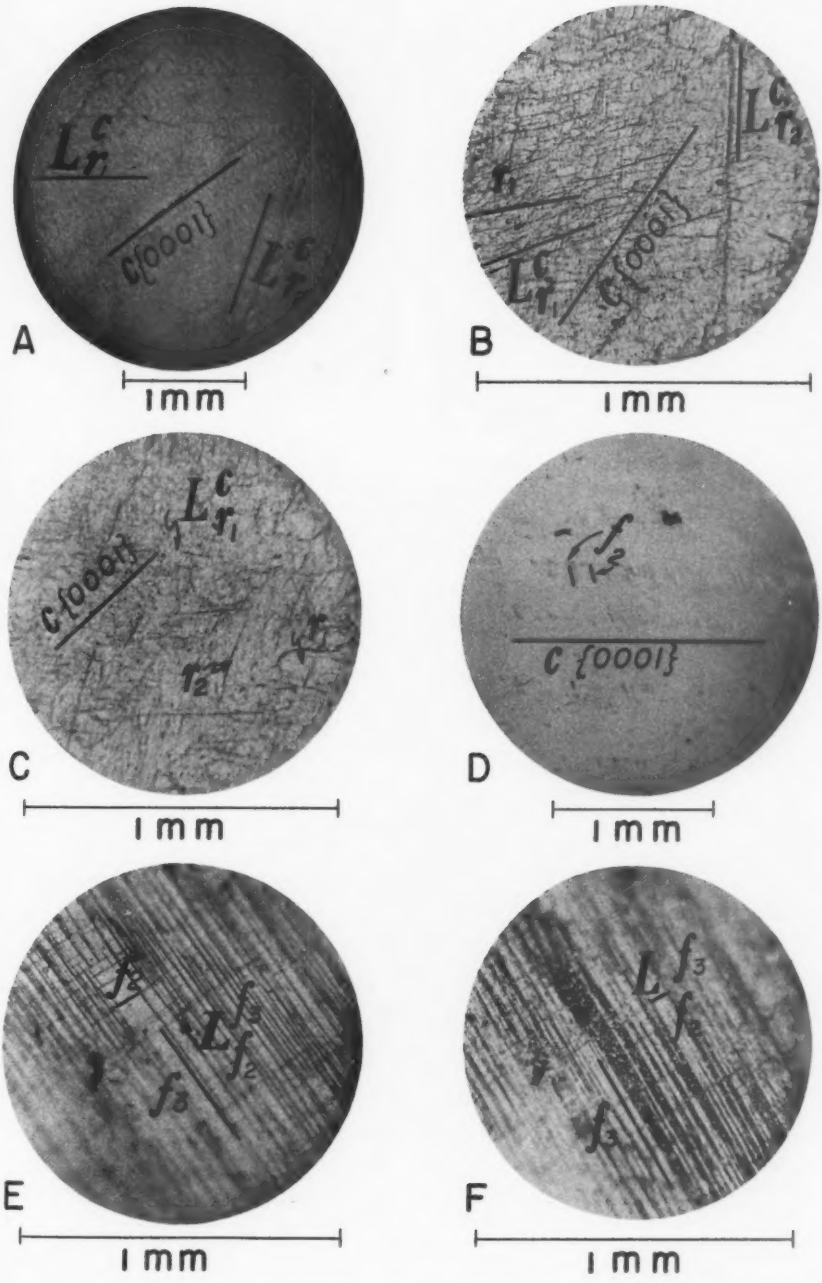

PHOTOMICROGRAPHS OF SPECIMENS LOADED PERPENDICULAR TO r_1

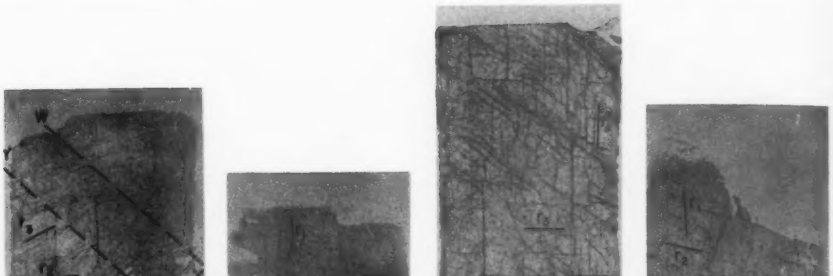

A B C D

FIGURE 1

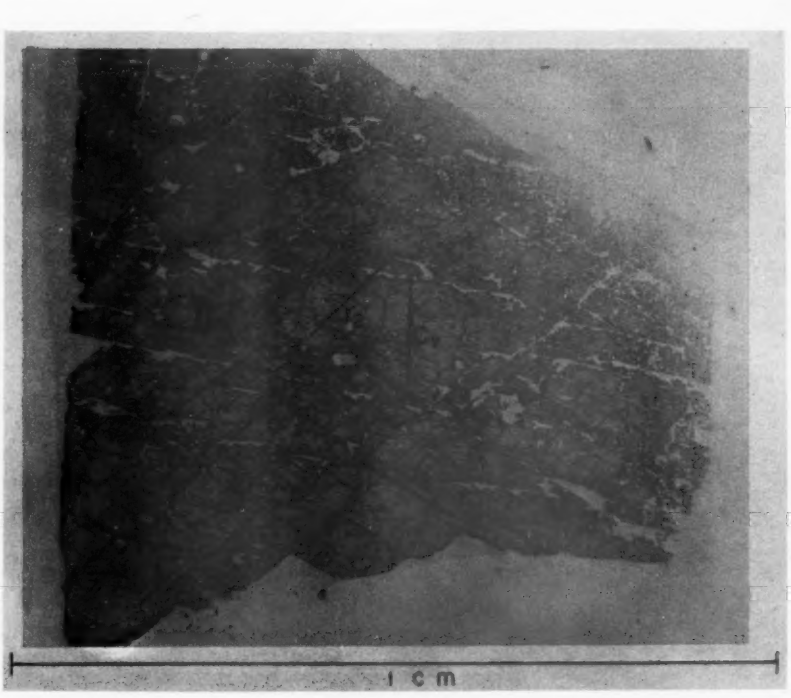

FIGURE 2

THIN SECTIONS OF DOLOMITE SPECIMENS LOADED PARALLEL TO $[f_2:f_3]$ AND MAGNESITE LOADED PARALLEL TO c_V

occurs in compression but not extension tests. This is evidence that translation is negative in magnesite also and is indeed restricted as to sense.

Translation ($T = f_2(2\bar{2}01)$, $t = [r_1{:}f_2]$) has been detected only in calcite and appears to be more effective at 24°C. than 300°C. (Turner *et al.*, 1954a, p. 931). The sense is again negative. Paterson (Personal communication, August 1957) reports the existence, as yet uncertain, of a_2 $(\bar{1}2\bar{1}0)$ translation in calcite.

None of the systems involving the long diagonal $[r_1{:}c]$ has been identified with certainty in calcite.[4] Their absence may be due to the ease of twinning in most orientations of specimens subjected to triaxial compression. Under the more severe restraint of a torsion experiment, it is possible, but not yet established, that gliding may occur on ($T = c(0001)$, $t = [r_1{:}c]$) or ($T = m_1(10\bar{1}0)$, $t = [r_1{:}m_1]$) (Handin, Higgs, and O'Brien, in manuscript). We are continuing work on the torsion of calcite single crystals.

Basal translation ($T = c(0001)$, $t = [r_1{:}c]$) has been reported for magnesite and siderite (Johnsen, 1902, p. 142) and for rhodochrosite and smithsonite (Veit, 1922, p. 128). It is the only system detected in dolomite, as might be predicted, since only layers parallel to c contain ions all of the same species. Gliding along $[r_1{:}c]$ on other possible planes or along $[r_1{:}f_2]$ involves rows made up alternately of Ca and Mg.[5] Basal translation in dolomite occurs with equal facility in either sense. This too might be anticipated, since displacements are parallel to the plane of the carbonate group containing the C and all three O atoms. This is the "smoothest" plane.

In calcite, twin gliding on $e_1(\bar{1}012)$ along $[e_1{:}r_2]$ in the positive sense has been long recognized. This system is known in siderite (Tertsch, 1949, p. 59) and might be expected in all the rhombohedral carbonates containing only one species of positive ions. This twinning cannot be ruled out for rhodochrosite and smithsonite but does not occur in magnesite, at least under our experimental conditions. This system would not be expected in dolomite. (*See* Handin and Fairbairn, 1955, p. 1258.) Twinning on $f_1(\bar{2}021)$ along $[f_1{:}a_2]$ is known only in dolomite.

In summary, the behaviors of calcite and dolomite differ as follows:

(1) At room temperature calcite twins readily on e; the critical resolved shear stress is only about 30 kg/cm². If the calcite is unfavorably oriented for twinning, it translates on r and f. The critical stress for r gliding is of the order of 1500 kg/cm². If it can twin, the calcite is very ductile under high confining pressure; strains of at least 30 per cent are achievable.

(2) At room temperature dolomite translates on c but does not twin. The critical stress is of the same order as that of r translation in calcite. However, the ductility of the dolomite is not so large as that of the calcite when the latter can twin.

[4] Translation of e_1 along a different gliding line, namely along $[r_2{:}r_3]$ in a sense opposite to that of e twinning, has been frequently mentioned in the literature but is now discredited (Turner, *et al.*, 1954a, p. 885).

[5] Table 7 shows that the resolved shear-stress coefficients for e and r translation are high in at least some of the orientations of the test cylinders.

PLATE 5.—PHOTOMICROGRAPHS OF SPECIMENS LOADED PERPENDICULAR TO r_1

A. Area in thin section 146 illustrating sharply defined slip bands that are parallel to $c\{0001\}$ *B*. Area in thin section 146 that exhibits both r_1 and $L^c_{r_1}$ lamellae. *C*. Area in thin section 156 illustrating rotated lamellae $L^c_{r_1}$. *D*. Area in thin section 156 which contains slip bands with concentrations of f_2 lamellae in alternate bands. *E*. Area in specimen 504 (Griggs) illustrating rotated lamellae resulting from twin gliding on f_2; plane polarized light. *F*. Same as *E* under crossed nicols.

PLATE 6.— THIN SECTIONS OF DOLOMITE SPECIMENS LOADED PARALLEL TO $[f_2{:}f_3]$ AND MAGNESITE LOADED PARALLEL TO c_v

FIGURE 1.—Thin sections of dolomite specimens loaded parallel to $[f_2{:}f_3]$. *A*. Specimen 161 extended 7.5 per cent at 24°C. *WX* and *YZ* mark the boundaries of the kink band. *B*. Specimen 153 compressed 12.0 per cent at 24°C. *C*. Specimen 575 extended 5.2 per cent at 300°C. *D*. Specimen 147 compressed 6.5 per cent at 300°C.

FIGURE 2.—Thin section of magnesite specimen 123 compressed 7.9 per cent at 24°C.

(3) At 300°C. calcite deforms by *e* twinning and *r* translation. The critical stresses are now only about 15 and 250 kg/cm², respectively. Heating has increased the ductility for all orientations of the crystals relative to the applied loads.

(4) At 300°C. the predominant mechanism in dolomite is still *c* translation; *f* twinning is subordinate. The critical stress for translation has, however, *increased* with temperature while the ductility is little affected by heating.

(5) At 500°C. the principal mechanisms in calcite are still *e* twinning and *r* translation. The critical stress for twinning approaches zero and for translation is less than 100 kg/cm². The ductility is enormous; strains of 100 per cent or more are attainable (Griggs *et al.*, in manuscript).

(6) At 500°C. *f* twinning in dolomite operates to the exclusion of *c* translation. The ductility of crystals unfavorably oriented for *c* gliding but favorably situated for twinning is much enhanced, for at lower temperatures these crystals are brittle. However, in no orientation is the dolomite as ductile as the calcite.

Contrasts in the deformational behavior of limestone and dolomite rock are now at least qualitatively explainable in the light of the information on single crystals.

At all temperatures the yield stress of limestone depends strongly upon the orientation of the load relative to the rock fabric if there is a preferred orientation of the constituent calcite grains. This is associated with the difference in yield stress of single crystals as twinning is possible or not. In limestone the yield stress decreases and the ductility increases as the test temperature is raised in accord with the behavior of the calcite crystals.

In dolomite crystals there is only one gliding mechanism at room temperature, and in dolomite rock also twinning does not occur at room temperature (Handin and Fairbairn, 1955, p. 1272). If there is a preferred grain orientation, some strength anisotropy in dolomite rock would be expected because statistically the resolved shear stress for basal translation would vary with the direction of the load relative to the rock fabric. However, the marked contrast observed in limestone would not be expected since there are not two potential gliding systems with vastly different critical stresses.

In dolomite rock the yield stress and ductility are affected little by heating to 300°C., just as these properties of single crystals are little influenced. The strength of the rock does not, however, *increase* with temperature. We have found that at 500°C. where twinning is important the ductility of dolomite rock is much greater than at 300°C. but still not nearly so great as that of limestone under the same conditions. The yield stress at 500°C. is appreciably lower than that at 300°C. as would be expected from the behavior of the single crystals. At 500°C. there is a pronounced strength anisotropy which is qualitatively correlatable with the loading direction relative to the rock fabric. Only one mechanism, *f* twinning, is important. But gliding can occur in only one sense, whereas the low-temperature translation-gliding mechanism is unrestricted in sense.

Conclusions

(1) Only two gliding systems have been observed in dolomite crystals: translation gliding on $c\{0001\}$ parallel to an a axis in either sense, and twin gliding on $f\{02\bar{2}1\}$ in a negative sense along a line defined by the intersection of the twin plane and $a\{11\bar{2}0\}$.

(2) Only one gliding mechanism has been detected in magnesite crystals which were loaded unfavorably for basal translation: translation gliding on $r\{10\bar{1}1\}$ in the direction $[10\bar{1}1:2\bar{2}01]$ in a negative sense. No twin gliding was produced.

(3) At temperatures below about 400°C., translation gliding on $c\{0001\}$ was the only intracrystalline mechanism that was detected in dolomite.

(4) The critical resolved shear stress for basal translation increased from about 900 kg/cm² at 24°C. to about 1200 kg/cm² at 400°C. This unusual behavior is not well understood and is in contrast to the behavior of most materials on which quantitative stress-strain data are available. However, since in calcite the critical stress for *r* translation decreases while in magnesite it increases with increasing temperature, the phenomenon may somehow be related to the magnesium ion.

(5) The critical resolved shear stress for *f* twinning decreases from a value of at least 2000 kg/cm² at 24°C. to about 500 kg/cm² at 500°C. The critical stresses for twinning and translation are equal at about 400°C. at which point twin gliding becomes important. At 500°C., twin gliding on $f\{02\bar{2}1\}$ is the only operative mechanism. This, too, is unusual, for according to Cahn (1954, p. 412), "It is a well established rule in metallurgy that as the temperature is raised, slip is favored at the expense of twinning, to the point where twinning may cease altogether."

References Cited

Bell, J. F., 1941, Morphology of mechanical twinning in crystals: Am. Mineralogist, v. 26, p. 247–261

Borg, I., and Turner, F. J., 1953, Deformation of Yule marble, Part VI: Geol. Soc. America Bull., v. 64, p. 1343–1352

Cahn, R. W., 1954, Twinned crystals: Advances in Physics, v. 3, p. 363–445

Fairbairn, H. W., and Hawkes, H. E., Jr., 1941, Dolomite orientation in deformed rocks: Am. Jour. Sci., v. 239, p. 617–632

Griggs, D., and Miller, W. B., 1951, Deformation of Yule marble, Part I: Geol. Soc. America Bull., v. 62, p. 853–862

Griggs, D. T., Turner, F. J., Borg, I., and Sosoka, J., 1951, Deformation of Yule marble, Part IV: Geol. Soc. America Bull., v. 62, p. 1385–1406

—— 1953, Deformation of Yule marble, Part V: Geol. Soc. America Bull., v. 64, p. 1327–1342

Handin, J., 1953, An application of high pressure in geophysics: Am. Soc. Mechanical Engineers Trans., v. 75, p. 315–324

Handin, J., and Fairbairn, H. W., 1953, Experimental deformation of Hasmark dolomite (Abstract): Geol. Soc. America Bull., v. 64, p. 1429–1430

—— 1955, Experimental deformation of Hasmark dolomite: Geol. Soc. America Bull., v. 66, p. 1257–1274

Handin, J. W., and Griggs, D., 1951, Deformation of Yule marble, Part II: Geol. Soc. America Bull., v. 62, p. 863–886

Handin, J., and Hager, R. V., Jr., 1957, Experimental deformation of sedimentary rocks under confining pressure: Tests at room temperature on dry samples: Am. Assoc. Petroleum Geologists Bull., v. 41, p. 1–50

Handin, J., Higgs, D. V., Lewis, D. R., and Weyl, P. K., 1957, Effects of gamma radiation on the experimental deformation of calcite and certain rocks: Geol. Soc. America Bull., v. 68, p. 1203–1224

Johnsen, A., 1902, Biegungen und Translationen: Neues Jahrbuch Mineralogie, Geologie, Palaeont., 1902, Teil II, p. 133–153

Pabst, A., 1955, Transformation of indices in twin gliding: Geol. Soc. America Bull., v. 66, p. 897–912

Palache, C., Berman, H., and Frondel, C., 1951, The system of mineralogy: 7th ed., v. 2, N. Y., John Wiley & Sons, 1124 p.

Schmid, E., and Boas, W., 1950, Plasticity of crystals: London, Hughes and Co., 353 p.

Tertsch, H., 1949, Die Festigkeitserscheinungen der Kristalle: Vienna, Springer-Verlag, 310 p.

Tschermak, G., 1881, Ueber die Isomorphie der rhomboedrichen Karbonate, etc.: Tschermaks Mineralog. u. Petrograph. Mitt. (Neue Folge), v. 4, p. 99–121

Turner, F. J., Griggs, D. T., and Heard, H., 1954a, Experimental deformation of calcite crystals: Geol. Soc. America Bull., v. 65, p. 883–934

Turner, F. J., Griggs, D. T., Heard, H., and Weiss, L. W., 1954b, Plastic deformation of dolomite rock at 380°C.: Am. Jour. Sci., v. 252, p. 477–488

Veit, K., 1922, Künstliche Schiebungen und Translationen in Mineralien: Neues Jahrbuch Mineralogie, Geologie, Palaeont., Beil.—Bd. 45, p. 121–148

Shell Development Co., 3737 Bellaire Blvd., Houston 25, Texas

Manuscript Received by the Secretary of the Society, June 23, 1958

Publication No. 161, Exploration and Production Research Division, Shell Development Co., Houston, Texas

BULLETIN OF THE GEOLOGICAL SOCIETY OF AMERICA
VOL. 70, PP. 279-290, 6 FIGS., 1 PL. MARCH 1959

TURBIDITY-CURRENT DEPOSITS IN SAN PEDRO AND SANTA MONICA BASINS OFF SOUTHERN CALIFORNIA

BY DONN S. GORSLINE AND K. O. EMERY

ABSTRACT

The floors of San Pedro and Santa Monica basins off southern California lie at a depth of nearly 1000 meters. Yet they contain layers of clean sand interbedded with normal deep-water green muds. The sands and their associated beds of silt and of fine gravel are believed to have been rapidly deposited by turbidity currents which started as mass movements at the shallow heads of submarine canyons and at the tops of basin slopes. A similar sequence is present in Pliocene sediments of completely filled basins now on land, for which the shales serve as source beds of petroleum and the sandstones as reservoir beds.

CONTENTS

TEXT

	Page
Introduction	279
Topography and water characteristics	281
Sediments	283
Samples	283
Continuous sediments	284
Discontinuous sediments	285
Correlation and age	286
Conclusions	288
Origin of the sediments	288
Geological significance	289
References cited	290

ILLUSTRATIONS

Figure	Page
1. San Pedro and Santa Monica basins	280
2. Flat floors of basins	282
3. Areal variation of texture	283
4. Typical cumulative grain-size curves of sediments	284
5. Schematic representation of typical sedimentary features	287
6. Manner of filling of basins with sediments	289
Plate	**Facing page**
1. Sand and silt layers	286

TABLE

Table	Page
1. Radiocarbon age determinations	287

INTRODUCTION

The sea floor off southern California is a block-faulted complex of basins separated by islands and banks (Shepard and Emery, 1941). The 14 basins range from ones that are about 200 km from shore and have received little sediment to others that are adjacent to shore and have received so much sediment that their floors are broad and flat. At least one of the latter basins has been filled so deeply that sediment is now spilling out of it into the next basin seaward. Additional basins occur on the adjacent mainland where four are completely filled and are now dry land; the gently sloping plain atop one of these basins is the site of the city of Los Angeles.

Coring of the sea-floor basins during the past 20 years has established the fact that each basin contains layers of clean sand or silt usually less than a few cm thick and interbedded with green muds (Shepard, 1951a; Emery and Rittenberg, 1952). Similar sequences of Pliocene age characterize the completely filled basins now on land as shown by outcrops and oil-well cores (Natland and Kuenen, 1951; Slosson, 1958, Ph.D. Dissertation, Univ. Southern Calif.). In 1954 an attempt to obtain cores at several places in San Pedro Basin (Fig. 1) resulted in bent core barrels and recovery of about a meter of sand. This experience led to a more detailed survey of the bottom materials in San Pedro and Santa Monica basins financed by a grant-in-aid from the Standard Oil Company of California (California Research Corporation) and supported by spare ship time provided by Captain Allan Hancock of the University of Southern California. Most of the

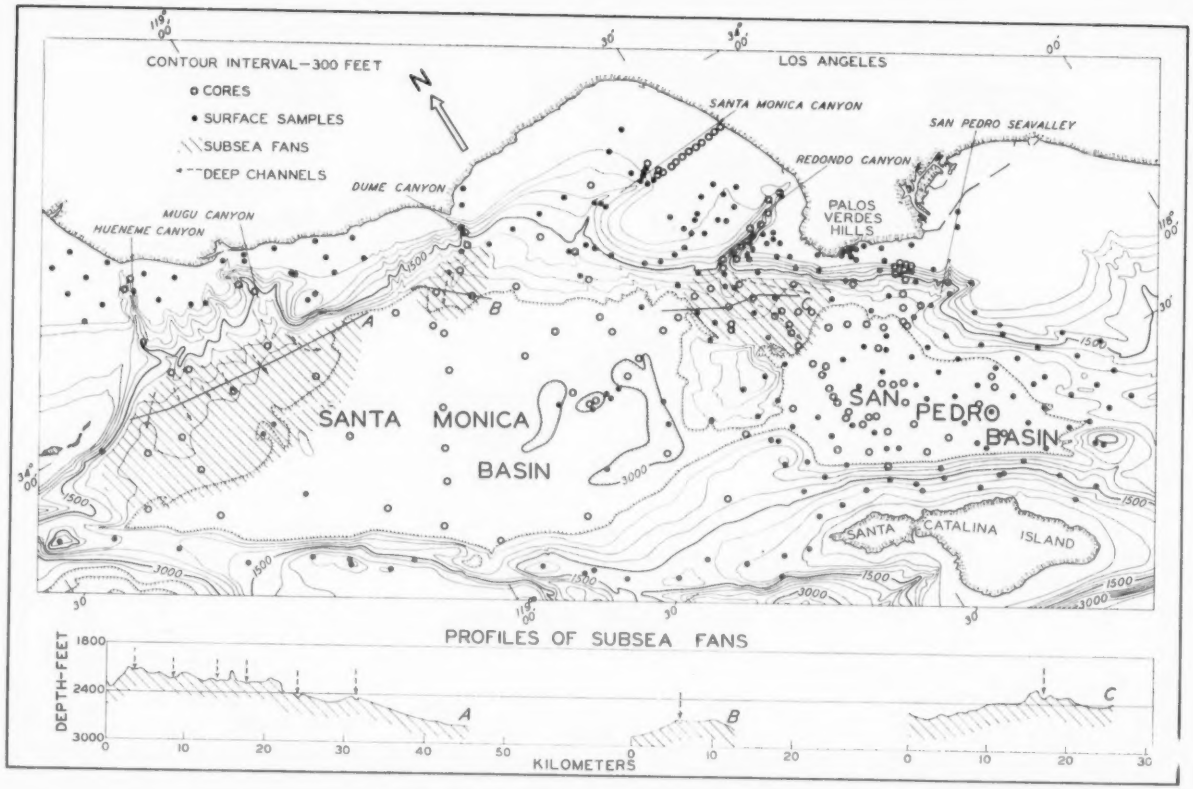

FIGURE 1.—SAN PEDRO AND SANTA MONICA BASINS

The 50-fathom (91.4-meter) contours are taken from Coast and Geodetic Survey Chart No. 5101. Subsea fans at mouths of Hueneme, Mugu, Dume, and Redondo Submarine canyons are crosshatched. Profiles across fans show typical transverse profiles of deep-sea channels that extend from the canyon mouths down the fans (dashed lines). Circles indicate positions of cores, and solid dots indicate positions of surface samples.

field and laboratory work was done by Gorsline as a doctoral dissertation (1958) under the guidance of Emery.

Topography and Water Characteristics

San Pedro and Santa Monica basins lie immediately south and west of the completely filled Los Angeles Basin. Maximum bottom depths of the two submarine basins are similar, 912 and 938 meters (2994 and 3078 feet) below sea level, respectively, and both basins have the same sill at 737 meters (2418 feet) near the southeastern end of San Pedro Basin (Fig. 1). Below this sill depth San Pedro Basin has an area of 655 km² and Santa Monica Basin an area of 1805 km²; about 90 per cent of both figures represents also the areas of flat floor. On the southwest both basins are limited by a single long fairly straight scarp that rises above sea level to form Santa Catalina Island. On the north and northeast the basins are limited by another scarp that is steep (2°–30°), smoothly curved, and rises to depths of 80–90 meters (260–295 feet) at the outer edge of the 1- to 15-km wide continental shelf. Each scarp is believed to be of fault origin.

The insular scarp meets the flat basin floor with no transition in slope. On the mainland side, however, the scarp has an apron of sediment at its base with an irregular hummocky surface. The upper edge of this scarp is indented by many small gullies, and both apron and gullies have been attributed to the effects of mass movements of sediment from the higher parts of the scarp (Emery and Terry, 1956).

Both the shelf and scarp along the mainland side of the basins are incised by submarine canyons, four of which reach to within 100 meters of shore: Hueneme, Mugu, Dume and Redondo (Fig. 1). Where the canyons debouch at the basin floor their mouths are at the apexes of half cones of sediment known as subsea fans. These fans have profiles with average gradients of about 1°, and their bases merge into the more gently sloping (about 0.2° southeastward) floors of both basins. Extending from the mouths of the canyons down the subsea fans and across part of the basin floors are deep-sea channels about 0.5 km wide, 10–20 meters deep, and bordered by natural levees (Fig. 1). Several generations of the channels appear to be present, indicating their changeable nature.

The volumes of subsea fans opposite the Hueneme-Mugu group, Dume, and Redondo submarine canyons are 24, 1.7, and 15 billion cubic meters respectively, about 1.8, 3.3, and 1.8 times the volumes of the empty adjacent canyons, and even more considering that part of each fan is buried under sediments of the basin floors. Beyond the subsea fans the floors of both San Pedro and Santa Monica basins are very flat (Fig. 2) according to recent surveys based on soundings by the Precision Depth Recorder (Luskin, Heezen, Ewing, and Landisman, 1954). Slopes of these floors are less than 0.33 per cent, or 0°11′.

Seismic surveys of the sediment thickness are lacking for San Pedro and Santa Monica basins, but such surveys for other basins that are farther offshore and are less flat and broad and therefore probably contain less sediment show the presence of as much as 3000 meters of sediment. Since their development the filled basins on land have received 2000–6000 meters of sediments. Both the land and sea-floor basins are believed to have been initiated during Middle and Late Miocene times, and they have received sediments ever since.

Sea water that fills the basins has a definite role in the production and preservation of the sand and silt layers. The dominant waves are swells moving from the storm centers of the northern Pacific Ocean southeastward into and through the region. Their movement causes extensive longshore drifting of beach sand, as revealed by the trapping of as much as 400,000 cubic meters annually against individual groins and breakwaters. Still more sand is trapped in the deep heads of the submarine canyons that reach close to shore. This sediment fill is known to slide away periodically down-canyon.

Between sill depth and the floors of San Pedro and Santa Monica basins the water is nearly isothermal at 5.05°C., isohaline at 34.3 ‰, and contains little dissolved oxygen, 0.25 ml/L, with no indication of seasonal or secular changes. These parameters are controlled by the fact that the water that enters the basins must enter at sill depth, which is also within the depth range of the oxygen minimum for this region (Emery, 1954). Owing to the low content of oxygen in bottom waters or to its absence in the interstitial waters of the sediment, bottom-living animals such as worms are virtually absent below the basin-sill depths (Hartman, 1955). Accordingly, thin layers of sediment deposited on the basin floors remain relatively undisturbed by animal activities.

the 30-fathom (91.4-meter) contours are taken from Coast and Geodetic Survey Chart No. 5101. Subsea fans at mouths of Hueneme, Mugu, Dume, and Redondo Submarine canyons are crosshatched. Profiles across fans show typical transverse profiles of deep-sea channels that extend from the canyon mouths down the fans (dashed lines). Circles indicate positions of cores, and solid dots indicate positions of surface samples.

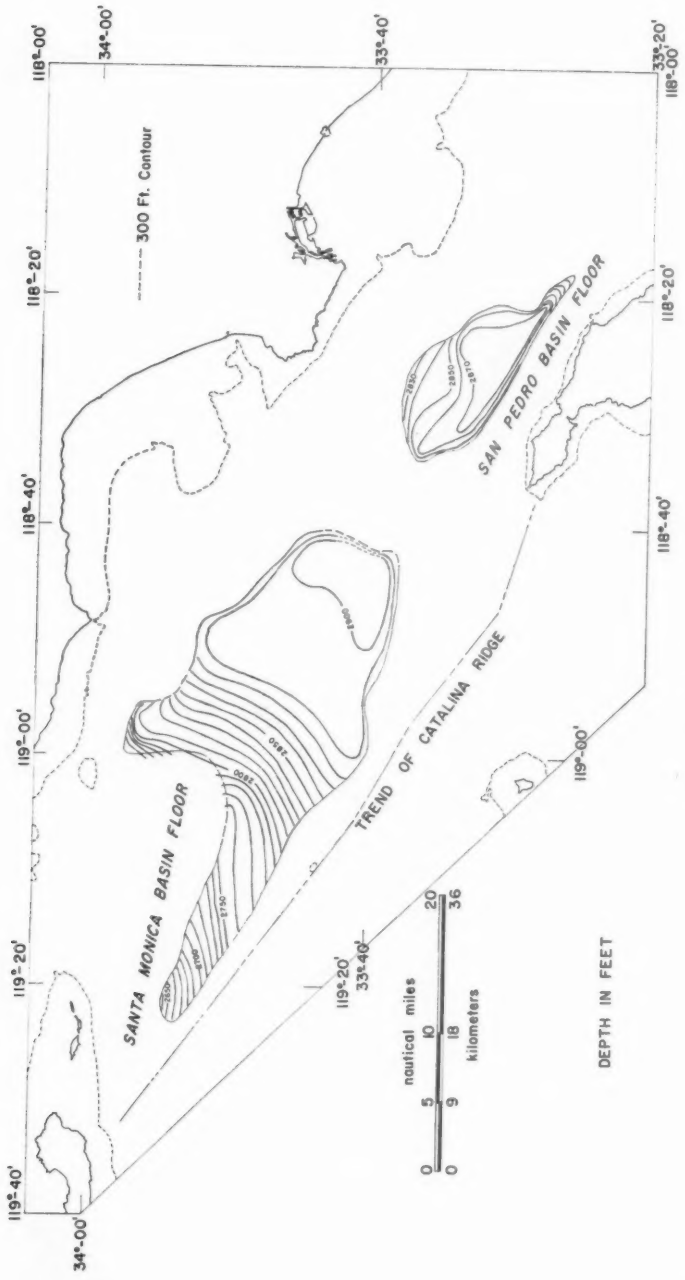

FIGURE 2.—FLAT FLOORS OF BASINS
From soundings by Precision Depth Recorder, uncorrected for velocity of sound in sea water

Sediments

Samples

About 260 bottom samples from San Pedro and Santa Monica basins were taken during the course of this study, and 210 additional samples were selected from more than 1500 collected during previous studies of the basins and the near-by continental and island shelves. Of these samples 136 were cores that ranged up to 6 meters in length (average was 3 meters); most of these were taken with a modified piston corer weighing about 500 kg (Kullenberg, 1947). The

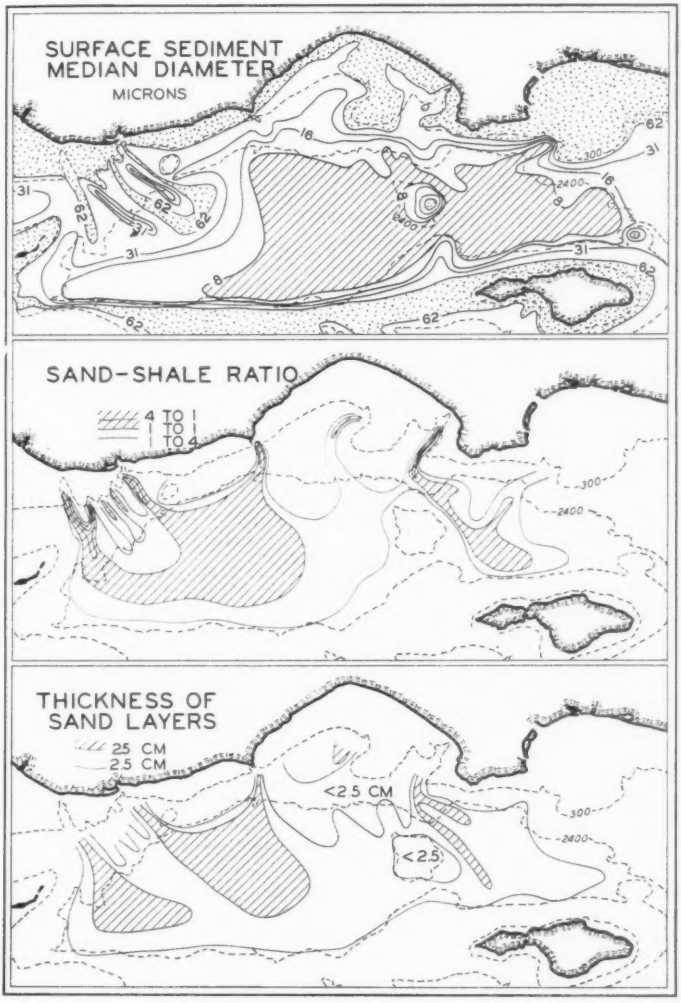

FIGURE 3.—AREAL VARIATION OF TEXTURE

Top—Median diameters of surface "continuous" sediments, showing general decrease from shore to the basin floors. Data from coarsest sediment omitted in interest of simplification.

Middle—Sand-shale ratio computed on basis of 2 meters of continuous green mud becoming eventually compacted to 1 meter of shale. Note close relationship of high ratios to submarine canyons and subsea fans.

Bottom—Average thickness of sand layers, showing seaward thinning.

cores were the only available means of detecting interbedded sand layers. All other samples were of surface sediments which were collected, using snappers and large orange-peel buckets, to provide information on the geographical variations of the muds that generally form the surface deposit.

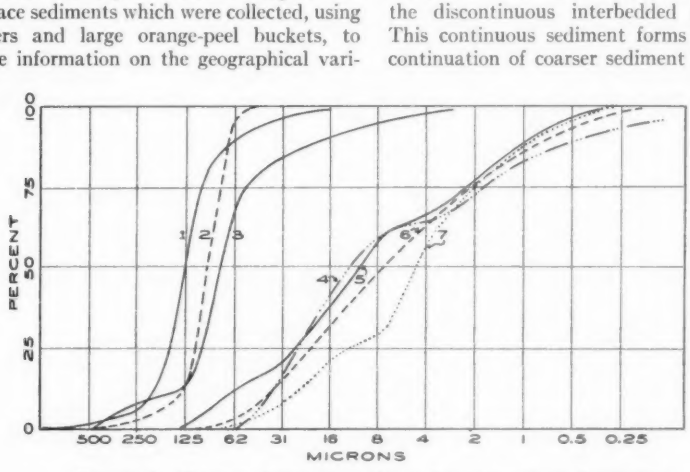

FIGURE 4.—TYPICAL CUMULATIVE GRAIN-SIZE CURVES OF SEDIMENTS

1. Lower portion of a graded sand layer (San Pedro Basin), 2. Nearshore shelf sand, 3. Middle portion of a graded sand layer (San Pedro Basin), 4. Silt layer including all parts of the layer, 5. Sandy clay silt from the fan periphery, 6. Green mud (clayey silt) from the floor of San Pedro Basin, 7. Green mud (clayey silt) from the deepest area of the floor of Santa Monica Basin.

After the cores were extruded from the core barrels they were cut into 1-meter lengths, split lengthwise, and allowed to dry for several days. This drying period accentuated textural differences but did not cause marked shrinkage. Following partial drying each core was described, measured, photographed, and sectioned for laboratory studies. Investigations in the laboratory consisted of more than 1200 grain-size analyses and microscopic examinations plus the impregnation of some layers with plastic for sectioning to exhibit microfabric.

Previous studies of the contents of moisture, nutrients, organic matter, and porphyrins in cores from these two basins as well as from elsewhere in the region provided considerable background experience for evaluating the new samples.

Continuous Sediments

Sediments that form the bulk of the deposit that has been cored in most basins off southern California are green muds (clayey silts). The same green muds occur in San Pedro and Santa Monica basins where they dominate on the seaward side of the floors and on all the side slopes. They are henceforth referred to as continuous or "normal" sediment in contrast to the discontinuous interbedded sand layers. This continuous sediment forms a basinward continuation of coarser sediment found at the surface of the adjacent slopes, shelves, and sea knolls. On the shelves and other high isolated areas sediment is coarse-grained because of the constant winnowing action of waves and currents. On high areas where modern detrital sediment accumulates slowly it becomes more or less diluted by coarse-grained organic components consisting of shell fragments and foraminiferal tests and by authigenic components consisting mostly of glauconite. As a result, the grain size of the continuous sediment ranges from an average of 250–500 microns on the beach, through 62–250 microns on the shelves, through 16–62 microns in the submarine canyons and on the subsea fans and basin slopes, to finer than 8 microns on the basin floors (Fig. 3, *top*). A sample from the floor of a deep-sea channel on Mugu Subsea Fan was 45 microns, whereas one from the fan beside it was only 8 microns. Average continuous sediments from the basin floor contain 7% sand, 59% silt, and 34% clay where the limiting divisions between these size grades are 62 and 4 microns, respectively. Continuous sediments of the basins also contain an average of 9% calcium carbonate, 8% biotite, 1.5% plant fibers, and 4.7% total organic matter. Foraminifera and fragments of the swimming *Cyclopectin* are present, and samples from the

side slopes contain in addition some radiolarians, sponge spicules, echinoid spines, and chitinous worm tubes. Typical cumulative curves of the continuous basin sediments exhibit much poorer sorting than do those of the coarser sediments from the shelves (Fig. 4).

Discontinuous Sediments

Interbedded with the continuous sediments of the basin floors and dominant in the upper parts of subsea fans and floors of submarine canyons are unusual deposits that are designated discontinuous sediments. They represent separate periods of large and geologically instantaneous deposition of coarser than usual sediment. Included are graded and/or laminated sand layers, gray silt layers, mud clasts, scattered gravels, and contorted beds.

Most typical of all are the sand layers (Pl. 1). These have a median thickness of about 1 cm, but the range is from mere partings to at least 1 meter—too thick for penetration by the heavy corer. The average median diameter of grains in the bedded sands of San Pedro Basin is 72 microns and for those of Santa Monica Basin, 58 microns. In both basins the sand beds are clearly coarser than the intervening continuous green muds and are more like the shelf sediments (Fig. 4). In general the sands are even coarser on the subsea fans, averaging 125, 64, and 78 microns for the Hueneme—Mugu, Dume, and Redondo subsea fans, respectively. Many of the thicker sand beds are graded from coarse at the bottom to fine at the top. A typical 18-cm bed from deep in a core near the middle of San Pedro Basin was arbitrarily subdivided into 9 sections 2 cm thick; median diameters from the bottom to the top section were: 89, 84, 85, 81, 78, 74, 70, 64, and 52 microns. Such a gradation strongly suggests deposition from a single suspension during a short period of time. Other sands (banded or laminated layers) contain thin partings of silt or several graded beds, which suggests repeated deposition during separate successive short time intervals. Others, particularly on the subsea fans, exhibit little vertical variation in grain size and have sharp tops, as though they had been truncated after deposition. Fine sands are typically laminated.

Most of the sand consists of quartz and feldspar in nearly the same ratio as on the adjacent shelves and beaches, about 2:1. Heavy minerals also have the same relative abundance of dominant species. A few grains of glauconite are present, but only in the sands, and glauconite also is an important constituent of the shelf sediments. Sand layers near the canyon mouths contain gravel consisting of sedimentary, igneous, and metamorphic types like rocks cropping out on the shelves. Unlike the continuous green muds, the sands contain little organic debris other than charcoal-like plant material that is concentrated in their upper portions.

Related to the sand layers are well-sorted massive gray silt layers that occur near the base of the slopes peripheral to the basin floors. These, like the sand layers, have a lower content of organic matter and calcium carbonate than the intervening green muds. Most of them have sharp upper surfaces, but others merge gradually into the green muds. A few silt layers have basal sections of sand. Muds containing locally derived pebbles occur in a few places in the same areas.

Mud clasts found in cores near the base of the slopes are round to flat and range from about 1 cm in diameter to sizes larger than the diameter of the core (Pl. 1). In the same areas many of the cores penetrated layers that were highly contorted in ways believed not to have resulted from the coring operations. Many contorted zones have a mixed appearance and contain small bits and pockets of sand. Possibly some zones are due to the destruction of sand layers by organisms (Moore and Scruton, 1957), but others are probably products of sliding and slumping. The undisturbed aspect of the overlying and underlying parts of these cores eliminates the possibility of the features being the result of the coring process.

The associations of sedimentary features with various parts of the topography may be summarized as follows:

(1) Canyons and upper subsea fans
  (a) Sand layers are graded and truncated.
  (b) Upper and lower boundaries of layers are sharp.
  (c) Massive layers with several superimposed graded portions probably represent repeated deposition and truncation.
  (d) Coarsest grains occur in lowest portions of layers (gravels are common in Hueneme—Mugu subsea fans and canyons).
  (e) Massive muddy sands with poorly developed internal structures are common on canyon floors.
  (f) A few large shells or pebbles are in the basal parts of the muddy sand layers but not necessarily at the base.

(g) Large quantities of plant debris (twigs, charcoal) occur in the upper fine silty sandy portions of the layers of the lower parts of subsea fans and interbedded within the coarse sediments of the upper parts of the fans.

(2) Subsea-fan margins
- (a) Fine-sand layers are graded and laminated.
- (b) Layers have sharply defined basal surfaces.
- (c) Coarsest grains are in the thickest layers.
- (d) Silty upper parts are preserved.
- (e) Gray silt layers occur on higher parts of subsea fans and peripheral areas of fans and have sharp top and bottom surfaces and massive internal structure.
- (f) Upper surfaces of fine sand layers have small-scale flow structures.
- (g) Modal bed thickness ranges from 2 to 5 cm.

(3) Basin floors
- (a) Most fine sands are laminated rather than graded, with top portions consisting of silt (particularly in Santa Monica Basin).
- (b) Fine to medium sand is in basal portions of sand layers and absent at a distance from subsea fans.
- (c) Top and bottom surfaces are sharply defined in sand and silty sand layers.
- (d) Gray silt layers became more frequent as the distance from subsea fans increases; silt is massive and has flow structures at the surface boundary.
- (e) In extreme ends of San Pedro Basin away from the subsea fan only gray silt layers appear, with gradational in addition to well-defined top surfaces.
- (f) In extreme ends of Santa Monica Basin away from subsea fans top portions of silt layers contain plant debris and have gradational surfaces.
- (g) On aprons at the coastal side of the basin floors parts of cores contain mud and sandy mud with scattered sand pockets and a "mixed" structure. Thick gray layers and discolored contorted clay silts appear. Sand layers are muddy and poorly defined.
- (h) In areas adjacent to the slope of the central Santa Monica Shelf cores contain contorted masses of pebbly muds without well-defined top or bottom surfaces.
- (i) Interbedded clay silts of all parts of the basin floors are massive and contain a few thin shells (*Cyclopectin*).
- (j) Modal bed thickness ranges from 0.25 to 2 cm.

(4) Slopes
- (a) Typical sediment is massive silty sandy mud with no apparent bedding.
- (b) Lower areas of slopes merge with the aprons in which contorted structures are present as noted above.
- (c) A few isolated pebbles or shells are present in the massive sandy clay silts.
- (d) At the lower part of the slope poorly defined gray silt layers are present as isolated units in many cores.
- (e) A microbreccia occurs in parts of a core near the base of the Santa Catalina Island slope, in an area of apronlike topography. Both the top and bottom of the breccia are poorly defined.

Correlation and Age

In spite of repeated attempts, correlation of individual layers from core to core proved unsuccessful. Correlation of sand layers in simple gravity cores taken by Ludwick (1950, Ph.D. dissertation, Univ. Calif. at Los Angeles) in an earlier related study off San Diego also failed, but it was thought that the thicker and more widespread sands in San Pedro and Santa Monica basins and the use of a piston corer would be more successful. Evidently, the sand and silt layers are discontinuous in space as well as in time. The fairly regular decrease in sand-shale ratio and thickness of the layers across the basin floor (Fig. 2), however, indicates that the discontinuous sediments are not haphazard. Probably the same layers occurred in many cores but were not recognized because they are absent in intervening areas. Adding to the difficulty of correlation are the variations in

---

PLATE 1.—SAND AND SILT LAYERS

The layers in cores 4663 (150–160 cm) and 4663 (122–128 cm) illustrate examples of fine-banded silty sand layers with flow structures in their upper surfaces. Core 4489 (135–150 cm) depicts a graded thick medium to coarse sand layer from a subsea fan. Core 4648 contains a group of gray mud layers (the downswept ends are the result of dragging along the walls of the core barrel) which are typical of the zones bordering steep slopes around the periphery of the central basin floor. The massive sandy silts with gravel and shallow-water invertebrate remains (Cores 4486 and 4683) are common on the upper parts of the subsea fans adjacent to the basin slopes. Core 4489 (30–33 cm) is another example of a coarse sand layer from the upper part of a subsea fan; note the grading and the absence of a silty graded zone at its top. Scale is in inches.

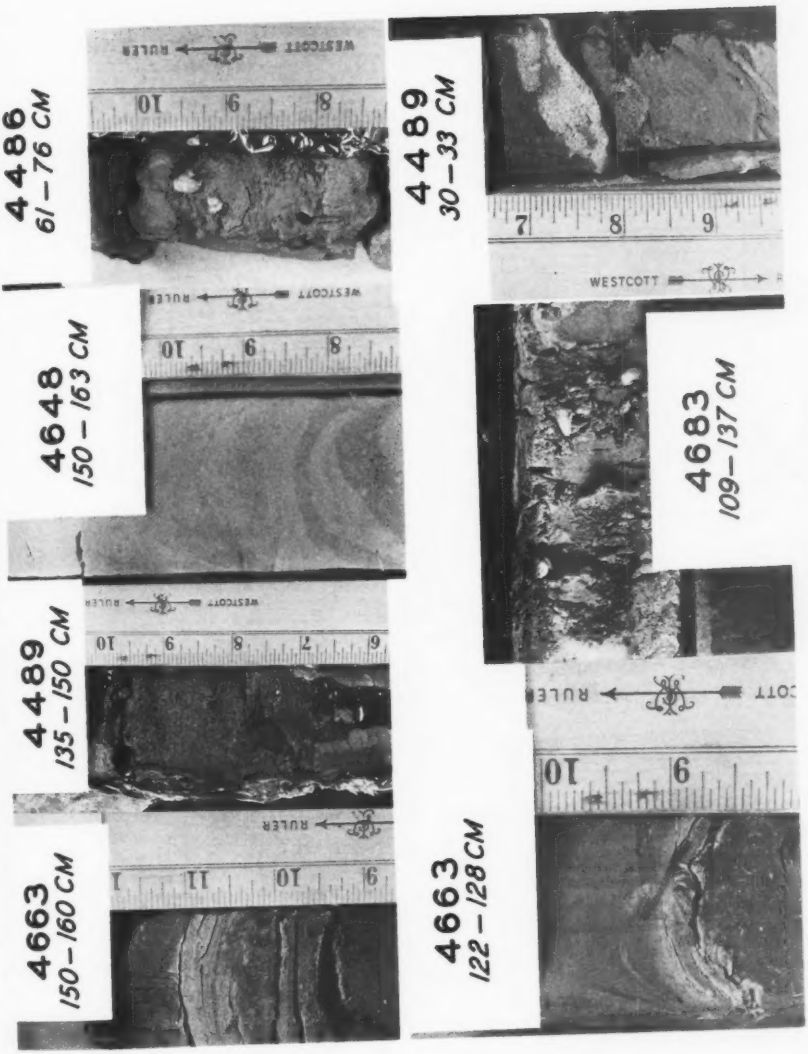

SAND AND SILT LAYERS

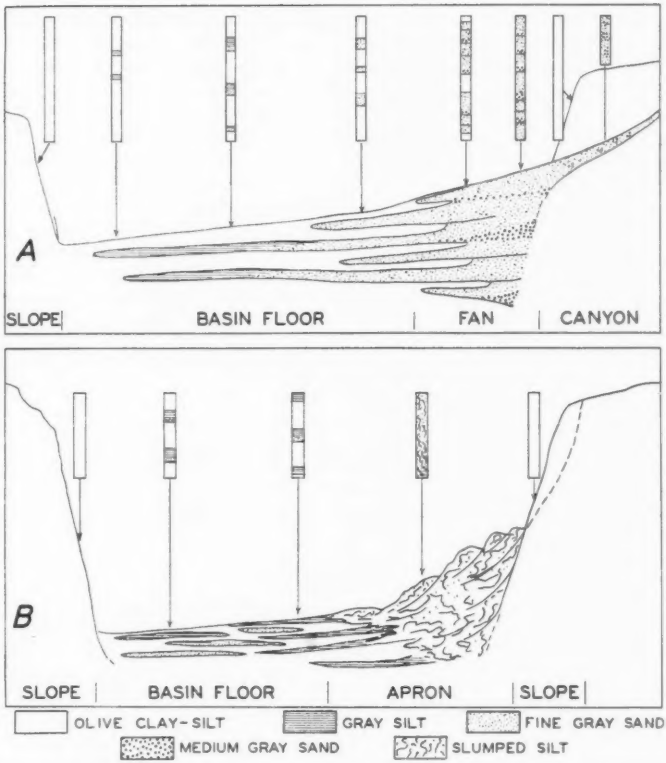

FIGURE 5.—SCHEMATIC REPRESENTATION OF TYPICAL SEDIMENTARY FEATURES
A. Canyon-Fan-Basin sequence, B. Slope-Apron-Basin sequence.

TABLE 1.—RADIOCARBON AGE DETERMINATIONS

AHF core no.	North latitude	West longitude	Water depth	Depth in core	C-14 age
4647	33°45.7′	118°47.5′	898 m	392 cm	4900 ± 140 years
4679	33°34.7′	118°24.8′	887 m	305 cm	9450 ± 250 years
4690	33°30.5′	118°22.4′	900 m	340 cm	7050 ± 120 years

thickness produced by original deposition and by later truncation, similarity of successive layers, and wide spacing of cores (average of one core per 28 km²). Although the sedimentary features in cores from various parts of the basins, aprons, fans, slopes, and canyons cannot be correlated in detail, they have a systematic geographical distribution that can be shown by a schematic diagram (Fig. 5).

Radiocarbon age determinations were made at the bottoms of three cores from near the middles of San Pedro and Santa Monica basins as part of a larger project supported by the National Science Foundation. The analyses, by T. A. Rafter (New Zealand Department of Scientific and Industrial Research), are based on organic carbon (Table 1).

Without question the sand layers in the sediment have been deposited within the past several thousand years. Graded bedding and low contents of organic matter and calcium carbonate provide ample evidence of extremely

rapid deposition of individual layers. The rate of deposition of the intervening green muds can be computed after correction of the radiocarbon ages for the "zero" age of the surface sediment (tentatively 2300 years) and correction of the core length for sand and silt layers. The resulting rates for green mud are 76, 26, and 53 mg/cm²/year, or an average of about 52 mg/cm²/year for the three cores. For sediment having a water content of 50 per cent by wet weight, this average rate corresponds to a thickness of 0.72 mm per year. With a typical interval of 0.3 meter of green mud between sand and silt layers near the middles of the basins, it is evident that the discontinuous sediments are commonly deposited there only at intervals of about 400 years. Banded sands on the fans and the canyon floors are indicative of deposition at much shorter intervals, possibly only 1–10 years. Owing to the discontinuous nature of deposition and to the great depth of water, the possibility of deposition being observed by existing types of cameras is remote; therefore, the mode and cause of deposition must be deduced from the various characteristics of the deposits.

Conclusions

Origin of the Sediments

The fine-grained green mud of San Pedro and Santa Monica basins as well as of other basins farther from shore is believed to reach its site of deposition by several different modes of transportation. Some is blown seaward during occasional brief periods of strong winds blowing from inland desert regions, and some is floated seaward in a lens of fresh water discharged to the ocean by streams during floods, but most of it is believed to make its way seaward from stream mouths and sea cliffs via diffusion through the water column and slow movement near the bottom on shelf areas. Movement of sediment across the continental shelf is indicated by ripple marks, by a continuous seaward decrease in grain size of present-day detrital sediment on shelves (Emery, 1952), by collection of fine sediment in various kinds of traps set on the shelves, and by a kind of haze, commonly observed by divers, just above the bottom.

Coarser-grained discontinuous sediment requires a different explanation. Landes (1952) postulated that such layers owe their origin to former shallow water, but the radiocarbon dating in addition to many other arguments (Emery and Natland, 1952) clearly shows that this explanation is incorrect.

The only hypothesis worthy of serious consideration that is known to the writers is that of turbidity currents. Streams that reach the coast adjacent to the two basins or west (and thus upcurrent) of them discharge great quantities of sediment—according to Handin (1951), about 1.3 million cubic meters of sand annually. This sand is moved alongshore to the southeast by the diagonally approaching waves (Johnson, 1956). Nowadays much of it is trapped by groins and breakwaters, but some is deposited in the heads of submarine canyons, as shown by shoaling depths in repeated hydrographic surveys. Sudden sliding away of the accumulated sediment has been noted at Redondo Canyon and at so many other canyons (Shepard and Emery, 1941, p. 94–103; Shepard, 1951b) that it appears to be a natural phenomenon. Beyond this point, the manner of transportation must be inferred. The mass movement down the axis of canyons is believed to become transformed into a turbidity current at some presently unknown depth in the canyons. The sediment-laden water, which is heavier than even the cold water at depth in the basins, is able to flow out of the canyons, down the subsea fans, and across a wide expanse of basin floor. For part of the distance the flow appears to be confined largely to the deep-sea channels, as proposed by many investigators of other deeper channels in the Atlantic, Pacific, and Indian oceans (Ericson, Ewing, and Heezen, 1952; Menard, 1955). En route, as the gradient decreases and the turbidity flow spreads laterally, its velocity decreases and its coarsest sediment is deposited. With the deposition of some sediment, the flow becomes less dense and moves less rapidly, so that finer sediment is deposited farther into the basins. Turbid water left behind drops its load of finer sediment to form graded bedding in the manner proposed by Kuenen and Migliorini (1951).

Additional mass movements also occur near the tops of basin slopes where a layer of sediments several meters thick may accumulate and finally slide away (Emery and Terry, 1956). Some of this sediment is deposited at the base of the slopes as irregular aprons that consist partly of large contorted slabs of sediment. Much sediment, however, moves beyond the aprons in the form of turbidity currents. Because little detrital sand from land reaches the basin slopes, the turbidity currents developed from the slopes form silt layers primarily

rather than the sand layers that are more typical of turbidity currents from the canyons. More slides and turbidity currents are produced on the slope bordering the mainland than on the slope at the seaward side of the basins because of the greater contribution of sediments by the mainland than by islands and banks.

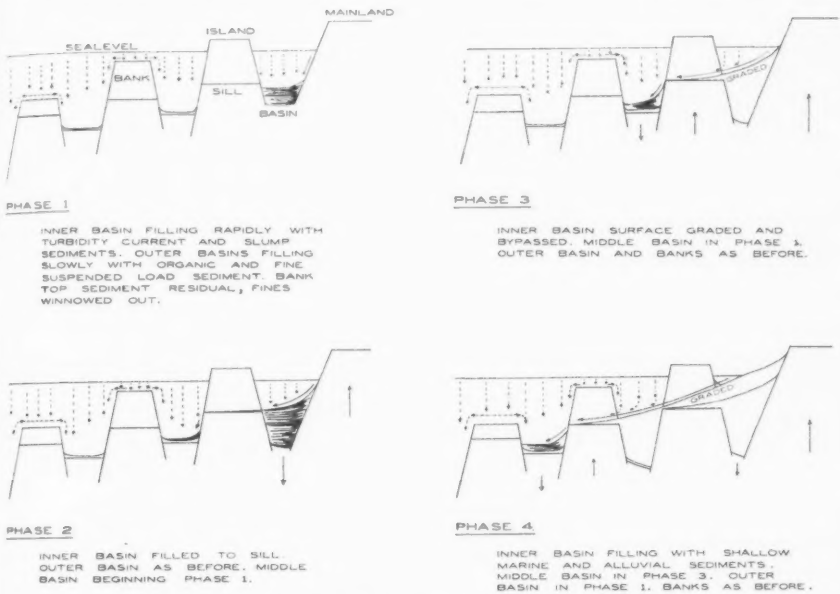
MAINLAND
ISLAND
SEALEVEL
BANK
SILL
BASIN
PHASE 1
INNER BASIN FILLING RAPIDLY WITH TURBIDITY CURRENT AND SLUMP SEDIMENTS. OUTER BASINS FILLING SLOWLY WITH ORGANIC AND FINE SUSPENDED LOAD SEDIMENT. BANK TOP SEDIMENT RESIDUAL, FINES WINNOWED OUT.
GRADED
PHASE 3
INNER BASIN SURFACE GRADED AND BYPASSED. MIDDLE BASIN IN PHASE 4. OUTER BASIN AND BANKS AS BEFORE.
PHASE 2
INNER BASIN FILLED TO SILL. OUTER BASIN AS BEFORE. MIDDLE BASIN BEGINNING PHASE 1.
GRADED
PHASE 4
INNER BASIN FILLING WITH SHALLOW MARINE AND ALLUVIAL SEDIMENTS. MIDDLE BASIN IN PHASE 3. OUTER BASIN IN PHASE 1. BANKS AS BEFORE.

FIGURE 6.—MANNER OF FILLING OF BASINS WITH SEDIMENTS

The greater rate of sedimentation in the nearshore basins owing to greater activity of turbidity cureents in them results in eventual spilling of sediments from basin to basin.

An approximate check on the sand budget can be made by comparing the rate of deposition of sand in the basins with its rate of supply by streams, because the rate of sea-cliff erosion is comparatively negligible. Assuming that the average sand-shale ratio of San Pedro and Santa Monica basins is 1 to 1 in terms of relative thickness, the long-term rate of intermittent deposition of sand and coarse silt must be equal to that of shale or half that of green mud, or about 0.36 mm/year. Since the cores that were dated are from near the middles of the basins, one can assume that the discontinuous sands on the landward side are deposited faster and those on the seaward side more slowly, so that the 0.36 mm/year can be applied to the entire basin floor as an approximate over-all average. At this rate, the 2460 km^2 of floor in the two basins must receive about 900,000 cubic meters of sand per year. This is about two-thirds of the estimated discharge of sand from streams, a remarkably close check considering the scanty base data.

Geological Significance

The discontinuous sands and silts in the San Pedro and Santa Monica basins have a total thickness just about as great as that of the continuous green muds, and the latter are deposited faster in nearshore basins than in others farther offshore; thus, the total rate of sedimentation in the nearshore basins must greatly exceed that in the other basins. As a result, the nearshore basins fill first and then spill over into the next adjacent basins. Not until the latter become filled, or until a damming basin slope is reached, can the nearshore basins become filled (Fig. 6).

A shallow rim around the Los Angeles Basin was responsible for its becoming completely filled during the Pliocene. In it are about 2000 meters of alternating sandstones and shales having a sand-shale ratio greater than 1 in the middle area of originally deepest water (Slosson, 1958, Ph.D. Dissertation, Univ. Southern Calif.) Both the shape of the lines of equal sand-shale ratio and the texture of the sands

indicate that the sands entered the basin from the north and east. A similar high sand-shale ratio exists in the Ventura Basin, which is also filled, located inshore from Hueneme Submarine Canyon. The strata include graded sand layers, contorted beds, deep ripple marks, pull-aparts, mud clasts, displaced faunas, and charcoal (Natland and Kuenen, 1951), like those of the modern basins. Similar features reported elsewhere (Kuenen, 1953; Crowell, 1957) are interpreted as produced by ancient representatives of the recent turbidity currents in San Pedro and Santa Monica basins.

The presence of both continuous and discontinuous sediments on the floors of San Pedro and Santa Monica basins causes these areas to have both the finest and the coarsest sediment of the region. This relationship has important implications with respect to the origin and accumulation of petroleum. The fine-grained sediments of these basins contain a very high content of hydrocarbons (Orr and Emery, 1956), even though their content of total organic matter is not so great as in basins farther offshore (Emery and Rittenberg, 1952). On compaction of the shales some of these hydrocarbons are probably squeezed out with the last of the interstitial water. Interbedded layers of clean sand provide convenient reservoirs for accumulation of the hydrocarbons from the shales. Thus the basins contain interbedded source beds and reservoir beds—an ideal situation for stratigraphic oil traps that can be enhanced by later folding into typical oil-field structures. The fact that Los Angeles and Ventura basins on land contain sediments similar to those of San Pedro and Santa Monica basins still under the sea is probably the reason why the two basins on land have proven to be such oil-rich areas, producing about an eighth of all the petroleum in the United States. We can expect that in a few million years the San Pedro and Santa Monica basins will become filled and exposed so that they too will be oil-rich provinces.

References Cited

Crowell, J. C., 1957, Origin of pebbly mudstones: Geol. Soc. America Bull., v. 68, p. 993–1010

Emery, K. O., 1952, Continental shelf sediments of southern California: Geol. Soc. America Bull., v. 63, p. 1105–1108

—— 1954, Source of water in basins off southern California: Jour. Marine Research, v. 13, p. 1–21

Emery, K. O., and Natland, M. L., 1952, Our shrinking globe—a discussion: Geol. Soc. America Bull., v. 63, p. 1069–1072

Emery, K. O., and Rittenberg, S. C., 1952, Early diagenesis of California basin sediments in relation to origin of oil: Am. Assoc. Petroleum Geologists Bull., v. 36, p. 735–806

Emery, K. O., and Terry, R. D., 1956, A submarine slope of southern California: Jour. Geology, v. 64, p. 271–280

Ericson, D. B., Ewing, M., and Heezen, B. C., 1952, Turbidity currents and sediments in North Atlantic: Am. Assoc. Petroleum Geologists Bull., v. 36, p. 489–511

Handin, J. W., 1951, The source, transportation, and deposition of beach sediment in southern California: Dept. of Army, Corps of Engineers, Beach Erosion Board, Tech. Memo. No. 22, 113 p.

Hartman, Olga, 1955, Quantitative survey of the benthos of San Pedro Basin, southern California, Part I, Preliminary results: Allan Hancock Pacific Exped., v. 19, no. 1, 185 p.

Johnson, J. W., 1956, Dynamics of nearshore sediment movement: Am. Assoc. Petroleum Geologists Bull., v. 40, p. 2211–2232

Kuenen, P. H., 1953, Significant features of graded bedding: Am. Assoc. Petroleum Geologists Bull., v. 37, p. 1044–1066

Kuenen, P. H., and Migliorini, C. I., 1950, Turbidity currents as a cause of graded bedding: Jour. Geology, v. 58, p. 91–127

Kullenberg, B., 1947, The piston core sampler: Svenska Hydrografiska-Biologiska Kommissionens Skr., 3rd ser., v. 1, pt. 2, 46 p.

Landes, K. K., 1952, Our shrinking globe: Geol. Soc. America Bull., v. 63, p. 225–240

Luskin, B., Heezen, B. C., Ewing, M., and Landisman, M. 1954, Precision measurement of ocean depth: Deep-Sea Research, v. 1, p. 131–140

Menard, H. W., 1955, Deep-sea channels, topography, and sedimentation: Am. Assoc. Petroleum Geologists Bull., v. 39, p. 236–255

Moore, D. G., and Scruton, P. C., 1957, Minor internal structures of some recent unconsolidated sediments: Am. Assoc. Petroleum Geologists Bull., v. 41, p. 2723–2751

Natland, M. L., and Kuenen, P. H., 1951, Sedimentary history of the Ventura Basin, California, and the action of turbidity currents: Soc. Econ. Paleontologists and Mineralogists Special Pub. No. 2, p. 76–107

Orr, W. L., and Emery, K. O., 1956, Composition of organic matter in marine sediments: Preliminary data on hydrocarbon distribution in basins off southern California: Geol Soc. America Bull., v. 67, p. 1247–1258

Shepard, F. P., 1951a, Transportation of sand into deep water: Soc. Econ. Paleontologists and Mineralogists Special Pub. No. 2, p. 53–65

—— 1951b, Mass movements in submarine canyon heads: Am. Geophys. Union Trans., v. 32 p. 405–418

Shepard, F. P., and Emery, K. O., 1941, Submarine topography off the California coast: Canyons and tectonic interpretation: Geol. Soc. America Special Paper 31, 171 p.

Oceanographic Institute, Florida State University, Tallahassee, Fla.; Department of Geology, University of Southern California, Los Angeles 7, Calif.

Manuscript Received by the Secretary of the Society, April 22, 1958

Allan Hancock Foundation Contribution No. 232

52, Early
ments in
Petroleum

ubmarine
Geology,

n, B. C.,
ments in
m Geolo-

portation,
southern
Engineers,
No. 22,

ey of the
n Califor-
llan Han-

hore sedi-
m Geolo-

of graded
Geologists

950, Tur-
bedding:

sampler:
Kommis-

obe: Geol.

d Landis-
t of ocean
31–140
ls, topog-
oc. Petro-
255
57, Minor
t uncon-
Petroleum

951, Sedi-
asin, Cali-
currents:
neralogists

mposition
ents: Pre-
ribution in
Geol Soc.

sand into
ogists and
53–65
ine canyon
ns., v. 32

Submarine
: Canyons
Soc. Amer-

TATE UNI-
RTMENT OF
RN CALI-

RY OF THE

ITION No.

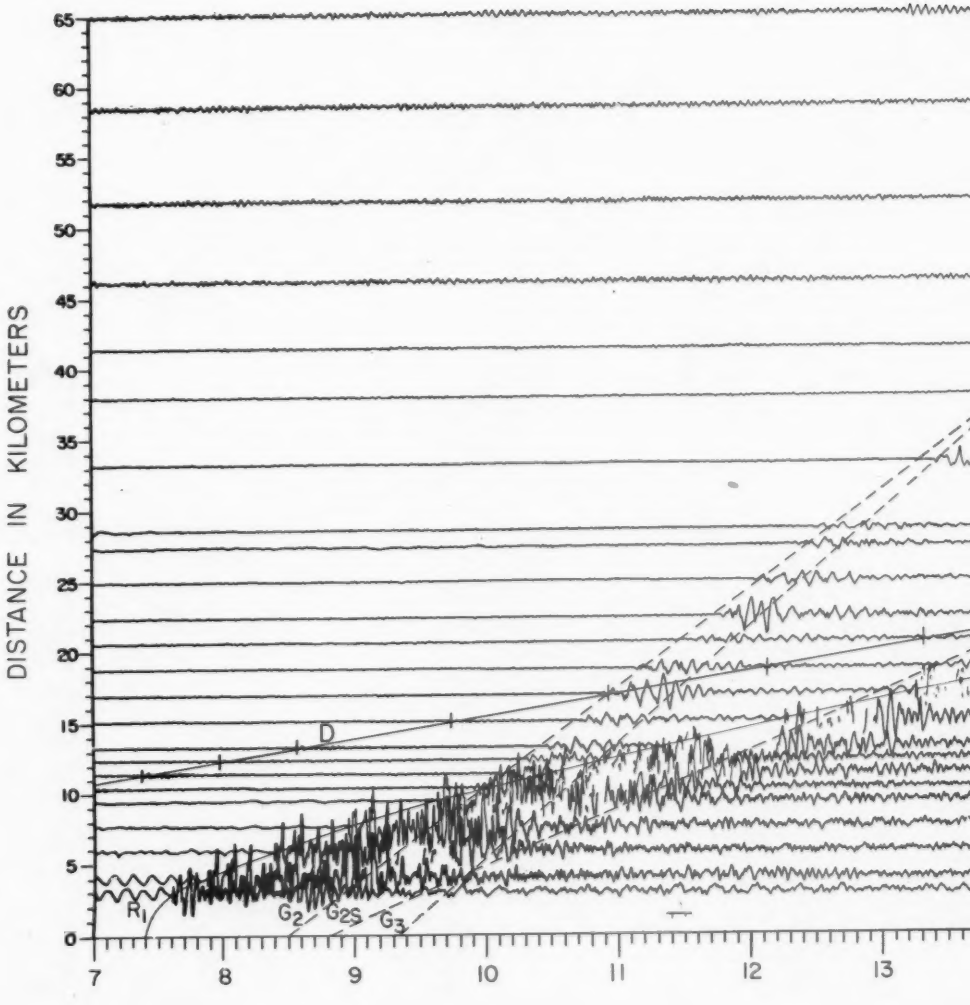
DISTANCE IN KILOMETERS
65
60
55
50
45
40
35
30
25
20
15
10
5
0
7
8
9
10
11
12
13
D
R1
G2
G2S
G3

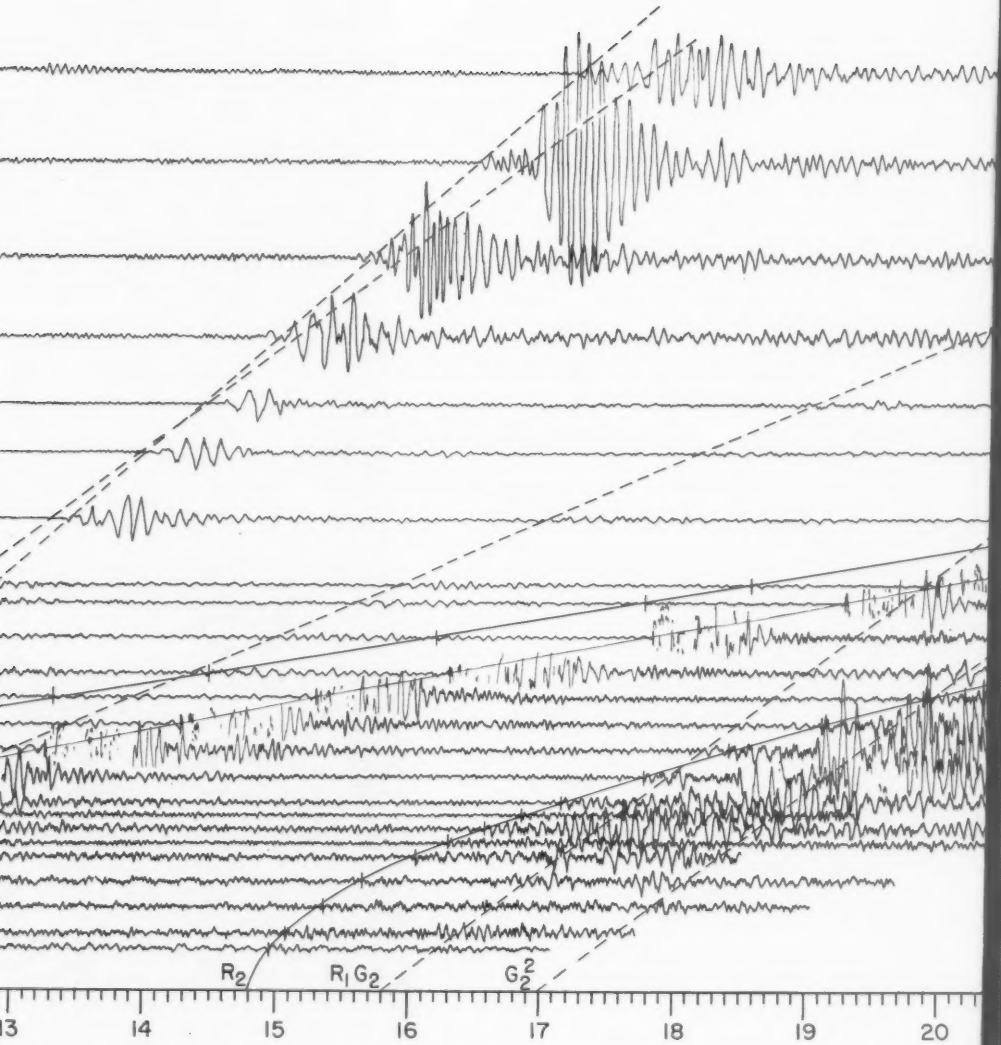

SEISMIC-REFRACTION STATION G-11a

Reproduction of a low-frequency trace from each seismogram on a common time scale and spaced according to shot distance.

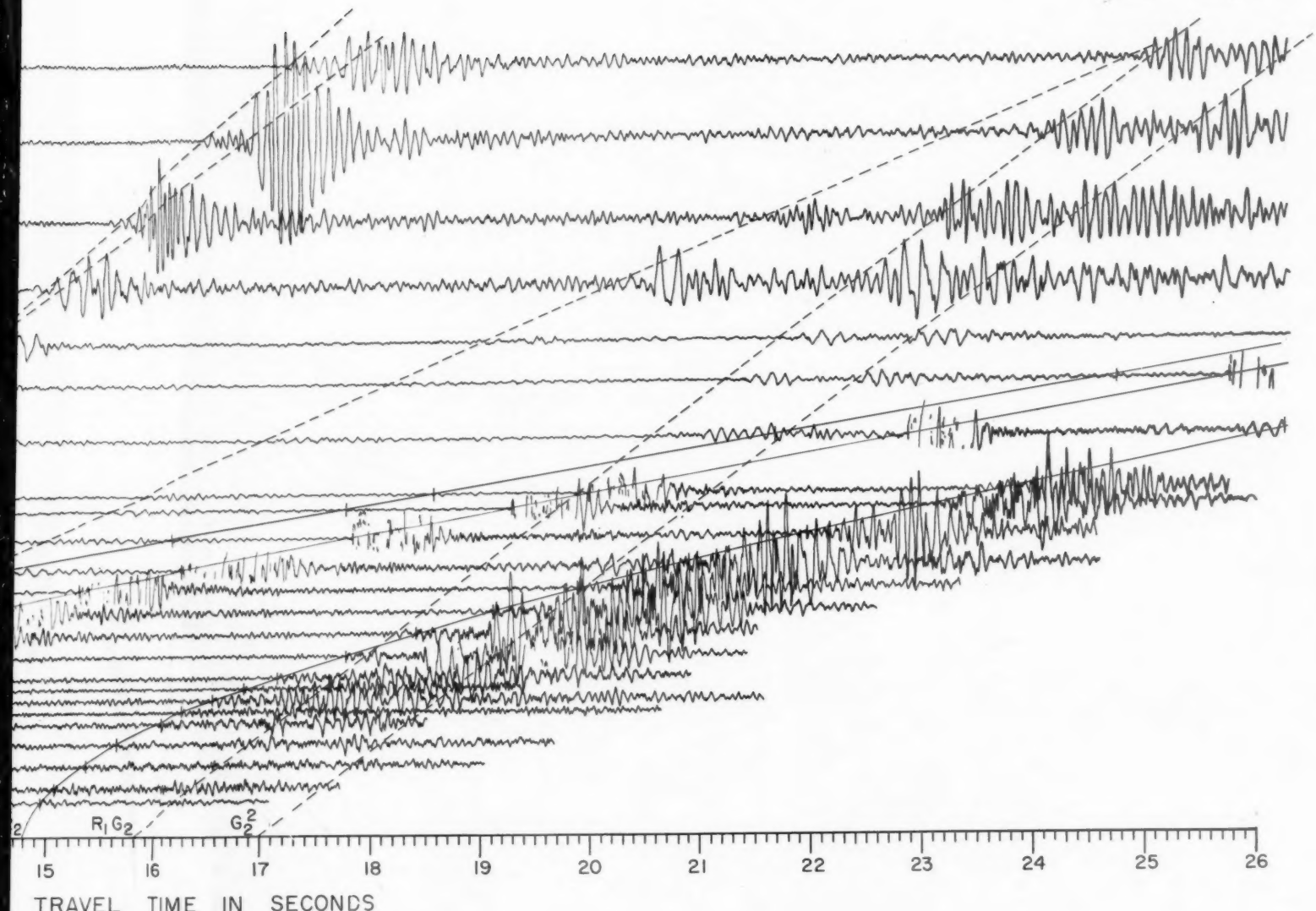

SMIC-REFRACTION STATION G-11a

uction of a low-frequency trace from each seismogram
mmon time scale and spaced according to shot distance.

BULLETIN OF THE GEOLOGICAL SOCIETY OF AMERICA
VOL. 70, PP. 291–318, 8 FIGS., 5 PLS. MARCH 1959

SEISMIC-REFRACTION MEASUREMENTS IN THE ATLANTIC OCEAN BASINS, IN THE MEDITERRANEAN SEA, ON THE MID-ATLANTIC RIDGE, AND IN THE NORWEGIAN SEA

BY JOHN EWING AND MAURICE EWING

ABSTRACT

Seismic-refraction measurements in the western basins of the North Atlantic Ocean show that an average crustal section consists of ½–1 km of low-velocity sediments and 4–6 km of oceanic crustal rock in which the seismic velocity is about 6.5 km/sec. There is good evidence from sub-bottom reflections and shear waves that in many places there is a layer with a velocity between 4.5 and 5.5 km/sec and a thickness of 1–2 km between the low-velocity sediments and the 6.5 km/sec layer, although it is not usually detected by refracted arrivals. These layers are underlain by the mantle which has an average seismic velocity near 8 km/sec. Measurements in the eastern basins show a similar crustal section, but the velocity below the deep discontinuity appears to be lower (7.7–7.8 km/sec).

Measurements in the Mediterranean Sea show only low-velocity sediments underlain by a refracting layer in which the average velocity is about 4.5 km/sec.

On the Mid-Atlantic Ridge the sediments are underlain by two refracting layers with velocities averaging 5.6 and 7.4 km/sec respectively. The results indicate that the ridge has been built by the upwelling of great amounts of basalt magma along a tensional fracture zone. Presumably the extensional forces and the supply of basalt magma come from convection currents deep in the mantle. Measurements in the Norwegian and Greenland seas show results very similar to those on the Mid-Atlantic Ridge, and, from this and the extension of the belt of active seismicity, it appears that the ridge structure continues through the Norwegian and Greenland seas into the Arctic Ocean.

The results of a few stations on the continental shelf of North America, Britain, and Norway are presented and compared with previously published results in these areas.

CONTENTS

TEXT

	Page
Introduction	292
Acknowledgments	292
Measurement and interpretation	292
Western Atlantic Ocean basins	293
Eastern Atlantic Ocean basin	302
Mediterranean Sea	303
Mid-Atlantic Ridge	305
Norwegian and Greenland seas	309
Continental shelf and slope of Britain and Norway	312
Continental margin of North America	314
Summary	315
References cited	315

ILLUSTRATIONS

Figure	Page
1. Location of seismic-refraction stations	294
2. Topographic profile and seismic section across the Mid-Atlantic Ridge south of the Azores	308
3. Generalized structure section and free-air anomaly profile across the Mid-Atlantic Ridge south of the Azores	308
4. Structure section along the Mid-Atlantic Ridge south of Iceland	308
5. Structure section between Bermuda and Madeira	309
6. Structure section in the Norwegian Sea	311
7. Comparison of continental, Atlantic Ocean Basin, and Norwegian Sea crustal sections	311
8. Structure section southeast of Cape May, New Jersey	315

Plate	Facing page
1. Seismic-refraction station G-11a	291
2. Seismic-refraction station F-1a, shots 6–10	296
3. Travel-time graphs, Western and Eastern Ocean basins	304
4. Travel-time graphs, Mediterranean Sea and Mid-Atlantic Ridge	308
5. Travel-time graphs, Norwegian and Greenland Seas; Continental Shelf of Britain and Norway; continental margin of North America	318

TABLE

Table	Page
1. Location of stations, seismic velocities, and layer thicknesses	296

Introduction

Seismic-refraction measurements were made on several cruises in the Atlantic Ocean and the Mediterranean and Norwegian seas during 1951, 1952, and 1953. These cruises provided the first opportunity to make seismic measurements in many parts of the ocean, and the data obtained allow comparisons of crustal structure among these and other, better-known areas. Included in this report are the results of 71 stations, of which 24 are in the western basins of the Atlantic, 6 are in eastern basins, 5 are in the Mediterranean Sea, 19 are on or near the Mid-Atlantic Ridge, 5 are in the Norwegian and Greenland seas, 8 are on the Continental Shelf of Britain and Norway, and 4 are on the continental margin of eastern North America.

Acknowledgments

This work was carried out under Contract Nonr 266(03) with the Office of Naval Research and Contract NObsr 43355 with the Bureau of Ships of the United States Navy. The field work at stations D-1 through D-16 was done by Maurice Ewing, Seymour Katz, and Robert Katz of the Lamont Geological Observatory and David Barnes of the U. S. Geological Survey. The measurements at stations E-1 through E-15 and F-1 through F-10 were made by John Ewing, Robert Katz, Edward Hazelwood, and George Shaffer; those at stations G-1 through G-16 by John Ewing, F. M. Brown, Edward Hazelwood, and Ezra Smith. Participating in the field work at the remainder of stations were Charles Bentley, James Dorman, Charles Drake, Bruce Heezen, John Hennion, David Warren, and J. L. Worzel. John Hennion assisted in the data reduction, and J. L. Worzel and others at Lamont Geological Observatory were of great assistance in reviewing and discussing the results.

Measurement and Interpretation

The methods of measurement and interpretation have been described previously (Ewing *et al.*, 1939; Officer *et al.*, 1952; Officer and Wuenschel, 1951; Sutton and Bentley, 1953), and only a short summary of them is given here. The corrections applied include shot depth, distance from shot to shooting ship, hydrophone depth, and topography. Unless stated to the contrary, the topographic corrections were made on the assumption that the irregularities in the water-sediment interface were duplicated in all deeper interfaces.

Throughout this work, the seismic detectors were crystal hydrophones suspended at a depth of 30–50 m in the water. The output of each hydrophone was amplified, filtered, and recorded by a photographic oscillograph on the receiving ship. During the operations, the receiving ship remained hove to while the shooting ship fired a line of shots out to the required distance. The functions of the ships were then reversed, and the former receiving ship fired shots on a line up to the new receiving position. This procedure is normally referred to as "reversing" the station. It would have been desirable to shoot short reverse profiles to determine the upper layers in addition to long reverse profiles to determine the deeper layers, but there was not time for this. Additional deviation from an ideal reversed station results from the drift of the receiving ships; this is minimized primarily by operating in favorable weather. All shots were fired with burning fuse, and the shot instant or "time break" was transmitted to the receiving ship by radio. As a safeguard against missed radio signals, events on both ships were related to absolute time by chronometers which were periodically checked against station WWV.

Sound waves radiating from each explosion reach the detectors by a number of paths. The sound which has travelled each path can be clearly distinguished. Definitions of the various phases and discussions of the place of each on the travel-time graph follow.

D—direct water wave, which has travelled horizontally in the water near the surface. Since the travel-time graph is a plot of arrival times on the ordinate against distance, in increments of direct water-wave travel time, on the abscissa, the *D* arrivals obviously fall on a straight line having a slope of 45° and a zero intercept on the time axis. Normally the points are not indicated on the graph, although the lines are drawn for convenience.

R_1, R_2, R_3, $\cdots$—water waves which have been reflected once, twice, etc., from the ocean floor. These arrivals form the hyperbolic curves shown on the travel-time graph.

R', R'' $\cdots$—reflected waves from interfaces below the ocean floor.

G_1, G_2, G_3, $\cdots$—compressional waves which have been refracted horizontally in successive layers beneath the ocean floor.

S_1, S_2, S_3, $\cdots$—transformed shear waves.

R_1G—reflected-refracted compressional waves which have been refracted in a layer beneath the ocean floor and in addition have been

reflected once. (See Ewing, Sutton, and Officer, 1954, for example.)

G^2—doubly refracted compressional waves.

The ground-wave arrivals determine straight-line segments which, when extended, intercept the time axis above the origin. The inverse slope of each segment gives the velocity of sound in the corresponding layer relative to that of the direct water wave, and the intercepts of these lines determine the layer thicknesses.

A line, rather than a point, on a travel-time graph shows the uncertainty in picking that particular arrival. In some cases the uncertainty results from almost simultaneous arrival time of the ground wave and the water wave. In others, excessive background noise or low signal strength has been the cause.

In the light of previous experience, a particular effort was made at stations F-1 to F-16 and G-1 to G-16 to space shots closely over the range at which refracted arrivals from the sedimentary layers can be observed. Still, there were at times no refracted arrivals through the upper (unconsolidated) layer. In such cases a velocity was assumed; the choice naturally was influenced by any available near-by measurements. Whenever a velocity has been assumed in this work, it is represented by a dashed line on the travel-time graph. The thickness of sediments at many of the stations, particularly in the earlier work, was calculated on the assumption that the velocity throughout the sedimentary column is 1.70–1.80 km/sec. In such cases the thickness possibly should be revised upward by as much as 10–15 per cent, in view of the appreciable number of detailed stations since occupied which show higher-velocity layers in the lower part of the sedimentary column. At present, it is not fully understood why the arrivals from the sediment layers are very strong at some stations and weak to nonexistent at others. Equally puzzling is a similar variation in the intensity of transformed shear waves.

Data for computing the speed of sound, both vertically and horizontally, in the water were obtained from hydrographic stations made at each seismic station, and from hourly bathythermograph observations made on both ships. As a check on the computed water velocities, R^2 vs. D^2 plots were made to confirm the ratio of horizontal to vertical velocity (Ewing, Worzel, Hersey, Press, and Hamilton, 1950).

Western Atlantic Ocean Basins

Several seismic-refraction studies have established that at many stations in typical deeper parts of ocean basins the crustal thickness is less than one-fifth that usually found in continents (Ewing *et al.*, 1954; Hersey *et al.*, 1952; Katz and Ewing, 1956; Raitt, 1956). A similar conclusion about oceanic crustal structure has been reached from studies of earthquake surface-wave dispersion, (Ewing and Press, 1952; Jardetzky and Press, 1953). A section representing the average of the results from 23 seismic-refraction stations (none of which is within 100 miles of shallow water) between North America and the Mid-Atlantic Ridge[1] shows the following:

5.15 km of water
1.49 km of sediment, velocity 1.7 to 4.5 km/sec
4.02 km of "oceanic-layer" rocks, mean velocity 6.53 km/sec
Subcrustal or mantle rock, mean velocity 7.95 km/sec

Although the values for the oceanic-layer velocity ranged between 5.50 and 7.08 km/sec, 80 per cent of them are in the range 6.36 to 6.88 km/sec. The range of values for mantle velocity is 7.68 to 8.50 km/sec, and of these 80 per cent are between 7.81 and 8.08 km/sec.

The work reported here includes 24 ocean-basin stations west of the Mid-Atlantic Ridge (Fig. 1). The travel-time graph and structure section for each station are shown. For convenience of discussion the receiving position on the left in each travel-time graph is designated *A*, and the one on the right is designated *B*. The symbols used in the structure sections are intended to represent velocity ranges rather than rock or sediment types since there is seldom opportunity to compare the seismic measurements with known geology.

Table 1 gives the location of all receiving positions, the velocity of sound in each layer, and the average layer thicknesses. Sample records are shown in Plates 1 and 2.

Station G-3 (Pl. 3)

This station is about 160 miles northeast of Bermuda. The bottom was almost flat at a depth of 2750 fathoms (5.02 km). At a depth of approximately 1.2 km below the ocean floor, a refracting crustal layer, called the oceanic layer in this paper, was found (velocity 6.93 km/sec). The depth to this layer was calculated using a velocity of 1.70 km/sec for the overlying sediments. In the *A* profile, a subcrustal layer was found with an apparent velocity of 7.86 km/sec. Although no long-range shots were received at *B*, a line (dashed) reversing the subcrustal line of the *A* profile was drawn to

[1] These values are taken from Officer *et al.* (1952), Ewing *et al.* (1954), and Katz and Ewing (1956).

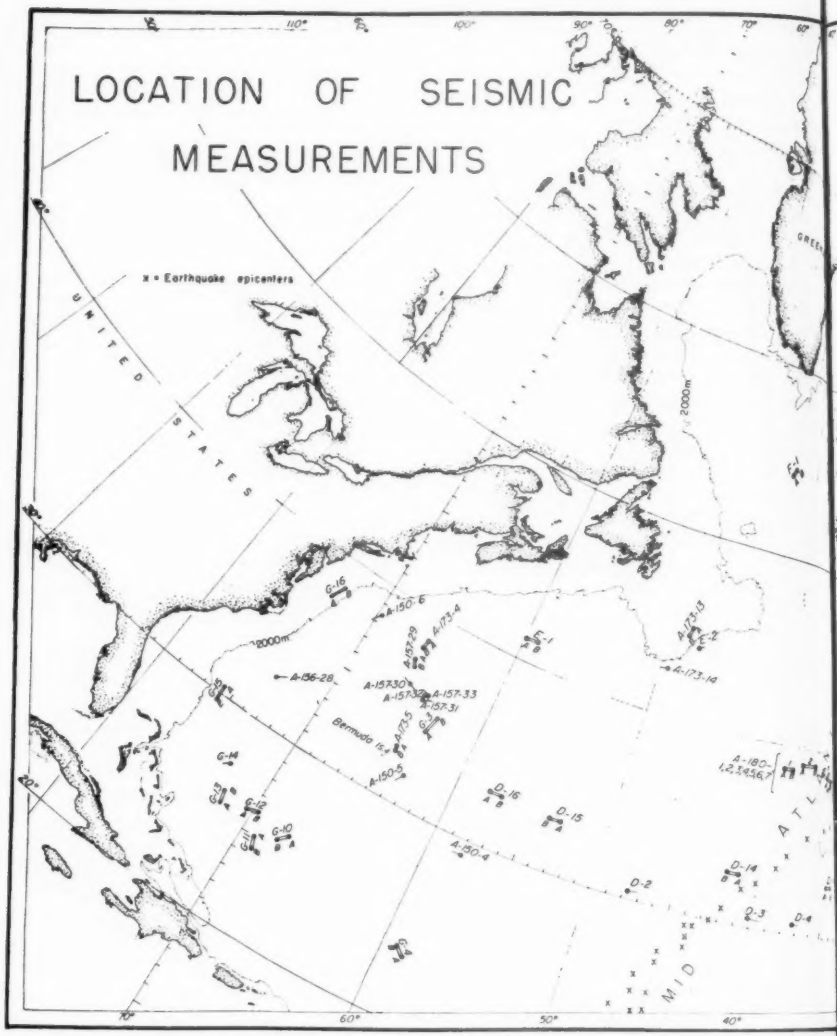

FIGURE 1.—LOCATION [illegible]

pass through the last point in the *B* profile. This determines a minimum velocity of 7.84 km/sec for the subcrust and a minimum thickness (average) of 4.08 km for the oceanic layer.

The velocity in the sediments is not well determined by the refraction data, although in each profile there is a ground-wave arrival just preceding the R_1 arrival at a D range of about 16 seconds. On the assumption that these arrivals propagated through the topmost sedimentary layer, it indicates a velocity of about 1.7 km/sec. In the *B* profile, distinct sub-bottom reflections were received which determine a pair of hyperbolic curves on the travel-time graph with intercepts of 0.6 and 1.3 seconds above the R_1 intercept. These correspond to reflecting horizons whose depths beneath the ocean floor are 0.3 V_1 and 0.3 V_1 + 0.3 V_2, where V_1 is the average vertical velocity in the top layer, and V_2 is the average velocity in the second layer. Possibly the later reflection is a multiple of the first (*i.e.*, reflected twice through the upper layer), although this is very doubtful in view of the relative strength of the signals; the second is stronger than the first. The deeper reflector may be the top of the oceanic layer, which is determined by the refraction lines $G_2 = D/4.49 + 7.64$ in the *A* profile and $G_2 = D/4.63 + 7.90$ in the *B* profile. This would mean, however, that the refraction line should be tangent to the sub-bottom reflection curve. This conditoin is approxi-

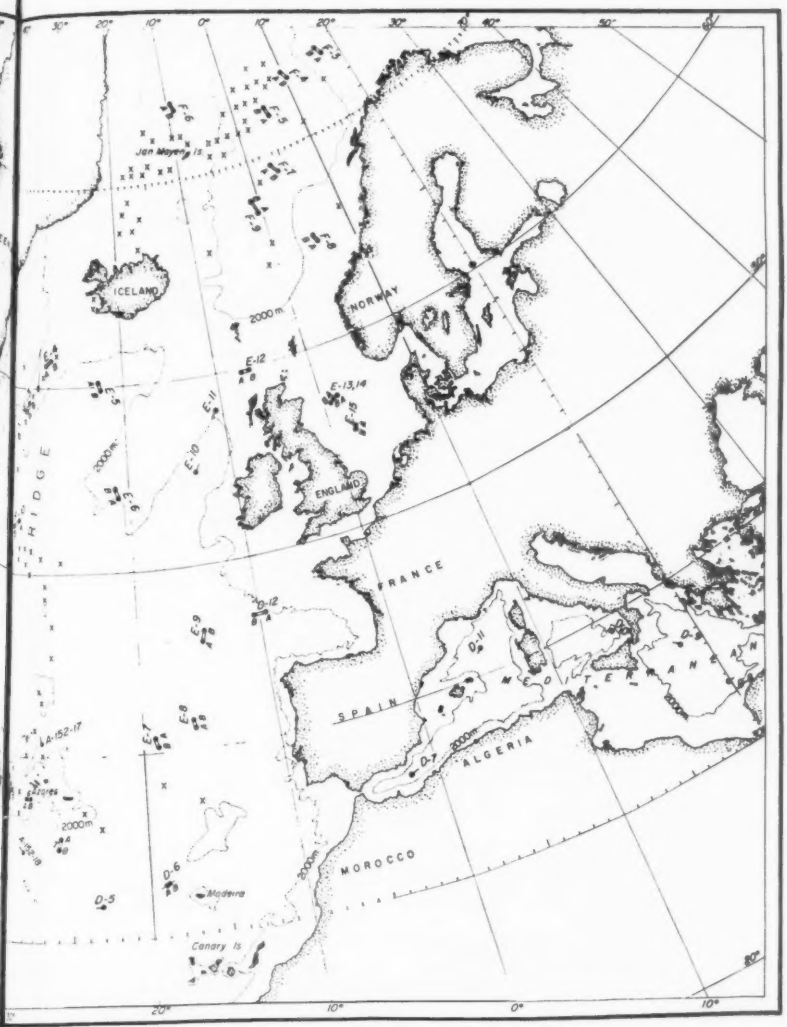

OCATION OF SEISMIC-REFRACTION STATIONS

mately satisfied here, and, if this were the only station to be considered in this respect, the deviation from tangency would probably be considered as experimental error. However, other stations to be discussed in this report have better control, and in every instance, the strong sub-bottom reflections, when observed, come from a horizon above the oceanic layer as determined by the refracted arrivals—*i.e.*, the sub-bottom reflection curve is cut by the extended line of refracted arrivals from the oceanic layer.

Sub-bottom reflections are also seen in the *A* profile but are difficult to pick accurately, because of overloading of the low-frequency channels by the R_1 arrivals. The points shown on the travel-time graph in that profile result from measuring the R_2'–R_2 interval (sub-bottom reflection delay following the second bottom-reflected arrival) and applying it as R_1'–R_1 at approximately half the range. It is frequently possible to see the sub-bottom reflection clearly following R_2 when high-gain levels have caused it to be obscured by overloading following R_1.

Station G-4 (Pl. 3)

This station is about 500 miles northeast of Puerto Rico in a depth of 3100 fm (5.67 km). The bottom was quite rough along the shot lines, and the arrival times of the ground waves have been

TABLE 1.—LOCATION OF STATIONS, SEISMIC VELOCITIES, AND LAYER THICKNESSES

Station	LOCATION OF STATION A Lat.	A Long.	B Lat.	B Long.	VELOCITIES (km/sec) Sediments 1	Sediments 2	Sediments 3	High Velocity Rocks 1	High Velocity Rocks 2	High Velocity Rocks 3	Water Depth	THICKNESSES (km) Sediments 1	Sediments 2	Sediments 3	High-Velocity Rocks
WESTERN OCEAN BASINS															
G-3	34° 08'N	63° 18'W	34° 48'N	62° 46'W	1.70			6.93	7.84		5.01	1.15			4.00
G-4	23° 19'N	58° 33'W	23° 40'N	58° 57'W	(1.70)			6.60	8.14		5.65	0.63			5.05
G-5	18° 13'N	56° 54'W	17° 40'N	57° 51'W	(1.72)			6.82	8.23		5.49	0.75			6.48
G-10	25° 53'N	67° 26'W	25° 39'N	67° 45'W	(1.70)	2.46*		6.57	8.29		5.49	0.19	0.60		5.90
G-11	24° 51'N	69° 07'W	24° 28'N	69° 24'W	(1.71)			6.76	8.04		5.76	0.87			5.15
G-12	25° 51'N	70° 27'W	26° 25'N	69° 51'W	(1.71)	2.03		6.90	8.14		5.49	0.35	1.08		4.28
G-13	25° 23'N	71° 52'W	26° 05'N	72° 02'W	(1.70)	1.99		6.85	8.32		5.43	0.42	0.97		4.19
G-14	27° 25'N	72° 41'W	-	-	(1.71)			6.58*	7.75*		5.06	1.34			5.72
D-2	30° 25'N	47° 39'W	-	-	(1.72)			6.62*	7.94*		4.36	0.56			3.11
D-15	32° 53'N	53° 01'W	32° 51'N	53° 51'W	(1.71)			6.82	8.25		5.40	0.89			3.65
D-16	32° 51'N	57° 55'W	32° 52'N	57° 05'W	(1.71)			6.85	8.06		4.87	1.17			4.73
F-1	54° 27'N	43° 19'W	55° 12'N	42° 30'W	(1.70)			6.94	(8.00)		3.39	1.06			3.50
A-156-28	32° 29'N	73° 24'W	-	-	1.74*			6.59*	-		5.02	2.36			-
A-173-4	38° 35'N	66° 05'W	38° 07'N	66° 16'W	(1.70)	1.88		6.62	7.70		4.73	0.48	1.41		4.35
A-157-29	37° 21'N	66° 08'W	37° 00'N	65° 57'W	1.62	1.82		6.82	-		5.05	0.44	1.09		-
A-157-30	36° 00'N	65° 40'W	-	-	(1.80)			6.66	(8.00)		4.85	1.45			5.40
A-157-31	35° 35'N	64° 28'W	-	-	(1.80)			6.65*	-		5.05	1.76			-
A-157-32	35° 55'N	64° 28'W	-	-	(1.80)			6.21*	8.10*		5.02	0.71			4.41
A-157-33	35° 58'N	64° 12'W	-	-	1.80*			6.63*	-		5.05	0.77			-
G-15	30° 25'N	75° 46'W	29° 40'N	75° 31'W	(1.73)	1.98	3.05*	6.81	8.12		4.57	0.27	0.90	2.36	6.71
E-1	41° 13'N	59° 58'W	41° 20'N	59° 16'W	1.83	2.05	3.97	6.69	8.22		4.79	0.33	1.79	3.43	5.25
A-150-4	29° 12'N	57° 59'W	-	-	(1.80)			(6.50)	-		5.63	1.23			-
A-150-5	31° 31'N	63° 06'W	-	-	(1.80)			(6.50)	-		4.67	0.71			-
A-150-6	38° 25'N	69° 40'W	-	-	(1.80)		(5.00)	-	-		3.49	2.57			-
EASTERN OCEAN BASINS															
E-7	40° 49'N	19° 01'W	40° 18'N	18° 54'W	(1.73)			6.46	7.68		5.49	0.86			4.31
E-8	41° 10'N	16° 01'W	41° 39'N	16° 03'W	(1.74)			6.28	7.77		4.85	0.88			3.81
E-9	45° 52'N	15° 23'W	46° 25'N	15° 19'W	(1.72)			6.26	7.65		4.39	0.89			3.62
D-12	46° 57'N	09° 25'W	46° 50'N	10° 17'W	(1.71)	2.24*		6.14	7.77		4.50	1.17	0.50		6.49
D-5	31° 55'N	23° 02'W	-	-	(1.71)			6.49*	8.04*		5.17	1.10			4.41
D-6	32° 49'N	18° 58'W	32° 51'N	18° 55'W	(1.69)			6.64	-		3.45	1.50			-
MEDITERRANEAN SEA															
D-8	33° 44'N	20° 00'E	-	-	(1.71)		4.80*	-	-		2.42	2.2-1.5			-
D-9	36° 29'N	18° 25'E	-	-	(1.71)		4.20*	-	-		3.66	0.34			-
D-10	39° 04'N	14° 36'E	-	-	(1.72)		4.9-5.7		-		3.43	0.87			-
D-11	41° 23'N	05° 52'E	-	-	(1.71)		4.79*	(6.50)	-		2.50	1.30			4.39
D-7	35° 50'N	01° 58'W	-	-	(1.71)		-	6.08	-		2.01	2.05			-
MID-ATLANTIC RIDGE															
D-13	32° 50'N	34° 46'W	32° 50'N	34° 04'W	(1.71)		5.01*	7.21	-		3.66	0.39			3.12
D-14	32° 52'N	41° 04'W	32° 52'N	41° 35'W	(1.71)		4.97*	7.27	-		3.20	0.56			2.09
D-3	30° 27'N	40° 04'W	-	-	(1.72)		5.38*	7.42*	-		2.76	0.22			3.33
D-4	30° 31'N	37° 16'W	-	-	(1.72)		(4.55)	6.26*	-		3.21	0.31			1.16
A-152-16	34° 47'N	39° 13'W	-	-	(1.70)		5.23*	-	-		3.34	0.22			-
A-152-17	40° 42'N	27° 51'W	-	-	(1.70)		6.08*	-	-		2.38	0.52			-
A-180-1	38° 45'N	39° 25'W	38° 45'N	38° 40'W	(1.80)		5.49	-	8.11		5.12	0.50			4.60
A-180-2	39° 05'N	37° 40'W	39° 10'N	36° 35'W	(1.80)		6.10	-	8.00		4.44	0.80			2.43
A-180-3	38° 50'N	35° 40'W	38° 40'N	34° 55'W	(1.80)		4.31	-	7.91		3.91	0.36			2.79
A-180-4	38° 40'N	34° 55'W	38° 40'N	34° 20'W	-		4.04	7.30	-		3.90	-			2.72
A-180-5	38° 05'N	31° 45'W	38° 20'N	31° 05'W	(1.80)		4.86	7.24	-		1.72	0.58			1.77
A-180-6	37° 45'N	29° 20'W	37° 40'N	28° 55'W	-	3.15	5.42	-	-		0.70	-	1.66		-
A-180-7	35° 35'N	26° 00'W	35° 00'N	26° 05'W	(180)		4.47	6.21	7.97		4.02	0.09			5.25
F-10	52° 43'N	32° 30'W	52° 44'N	33° 42'W	(1.72)		-	7.36	-		3.38	0.78			-
E-3	58° 45'N	32° 16'W	59° 14'N	31° 38'W	(1.70)		5.60	7.24	-		1.52	0.38			2.87
E-4	61° 03'N	29° 07'W	61° 30'N	28° 28'W	(1.75)		5.83	7.63	-		1.37	0.39			4.32
E-5	60° 14'N	22° 54'W	59° 45'N	22° 45'W	(1.72)	1.94	5.71	7.47	-		2.38	0.19	0.82		2.84
E-6	54° 01'N	21° 15'W	54° 34'N	21° 23'W	1.81*	2.79	5.80	7.43	-		2.98	0.87	1.24		4.30
A-173-5	32° 46'N	64° 31'W	32° 30'N	64° 29'W	-	- 4.04	5.36	-	-		2.22	-	-	2.68	-
NORWEGIAN AND GREENLAND SEAS															
F-9	67° 32'N	00° 21'W	68° 07'N	01° 00'W	(1.70)	1.87	5.36	-	8.04		3.37	0.14	0.76		2.76
F-7	69° 38'N	02° 28'E	69° 07'N	03° 45'E	1.80	2.00	5.37	6.94	-		3.18	0.43	0.63		3.01
F-6	73° 47'N	10° 03'W	73° 28'N	08° 37'W	(1.72)		5.06	7.38	-		3.05	0.49			3.04
F-5	71° 38'N	05° 36'E	72° 07'N	04° 44'E	(1.70)	2.01	3.60	5.26	7.69	-	2.96	0.23	0.49	1.38	2.56
F-4	73° 23'N	09° 27'E	72° 58'N	10° 16'E	1.79*	2.23		4.96	7.55	-	2.27	0.57	0.95		2.40
CONTINENTAL SHELF OF BRITAIN AND NORWAY															
E-10	54° 59'N	14° 06'W	-	-	(1.71)	2.65*	3.22*		6.96*		2.75	0.42	1.42	3.55	-
E-11	58° 15'N	10° 33'W	-	-	(1.71)	2.08*		4.97*	-		1.95	0.14	2.48		-
E-12	59° 48'N	07° 09'W	59° 56'N	06° 29'W	1.73*	2.24*		4.91	-		0.55	0.25	1.56		-
E-13	57° 07'N	01° 51'E	57° 04'N	01° 25'E	1.71	2.26		4.96	-		0.09	0.61	2.64		-
E-14	57° 04'N	01° 25'E	57° 00'N	00° 58'E	1.71	2.26		4.85	-		0.09	0.54	2.58		-
E-15	55° 27'N	02° 21'E	55° 16'N	02° 19'E	1.73	2.03	3.00	(4.90)	-		0.04	0.39	0.54	3.40	-
F-3	73° 22'N	17° 15'E	73° 48'N	16° 41'E	(1.77)		3.56	5.11	-		0.42	0.70	-	1.88	-
F-8	64° 55'N	05° 19'E	65° 14'N	04° 35'E	1.66	2.08	3.44	4.01*	-		0.64	0.36	1.78	2.12	-
CONTINENTAL MARGIN OF NORTH AMERICA															
G-16	37° 46'N	73° 30'W	38° 21'N	72° 56'W	(1.68)	2.54	4.12	5.46	7.13		2.28	0.68	1.89	3.73	5.20
E-2	44° 02'N	47° 51'W	-	-	1.73*	2.04*	3.32*	-	6.22*		3.67	0.08	1.50	2.90	-
A-173-14	42° 32'N	49° 25'W	-	-	(1.70)	2.46*	3.80*	5.80*	-		2.45	0.62	2.02	1.06	-
A-173-13	44° 55'N	48° 26'W	44° 31'N	48° 41'W	(1.70)	2.66	4.28	5.69	-		2.39	0.49	2.14	2.31	-

A - Receiving position on left of travel-time graphs
B - Receiving position on right of travel-time graphs

* Unreversed measurement
( ) Assumed velocity

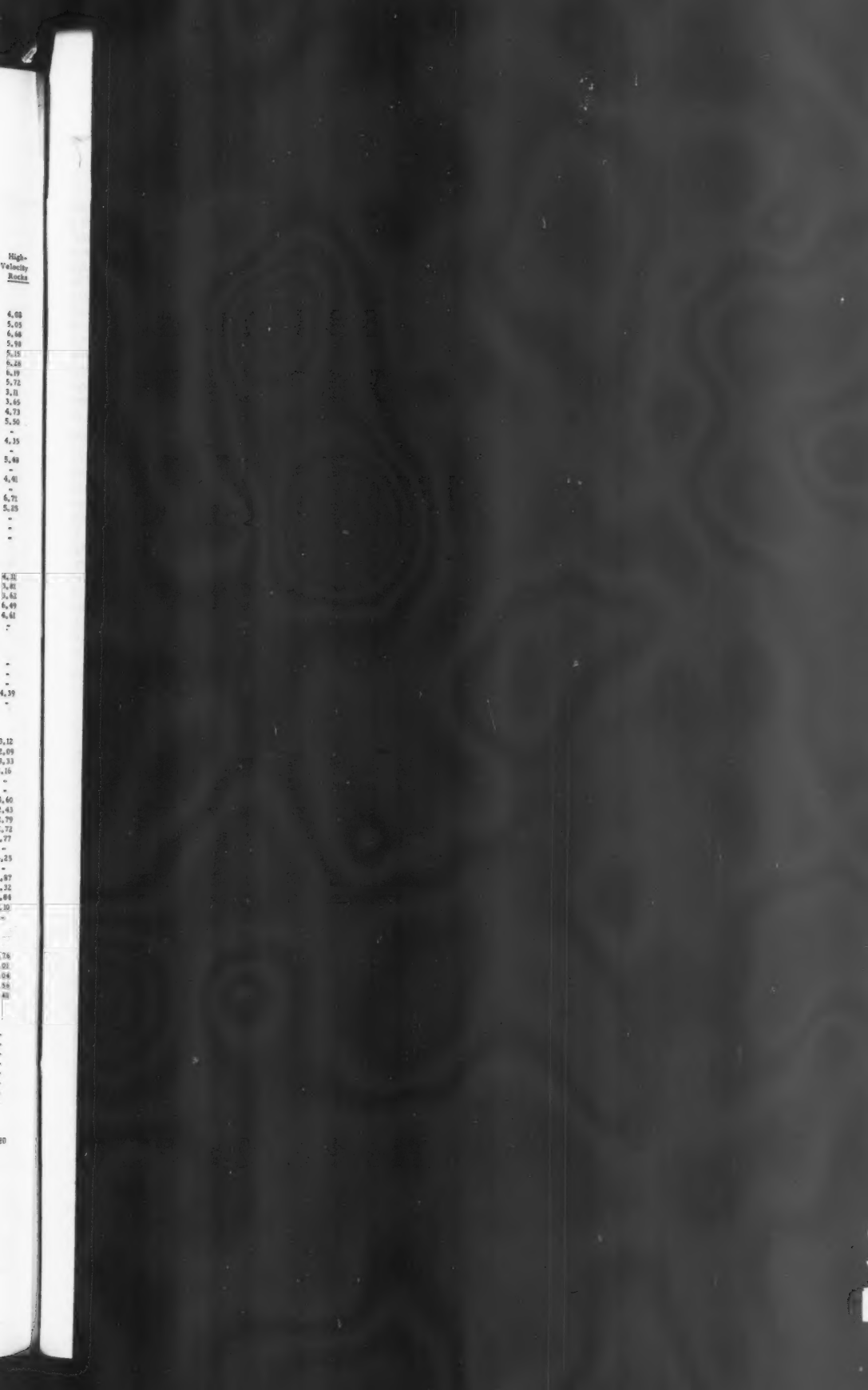

Bull.

0.90

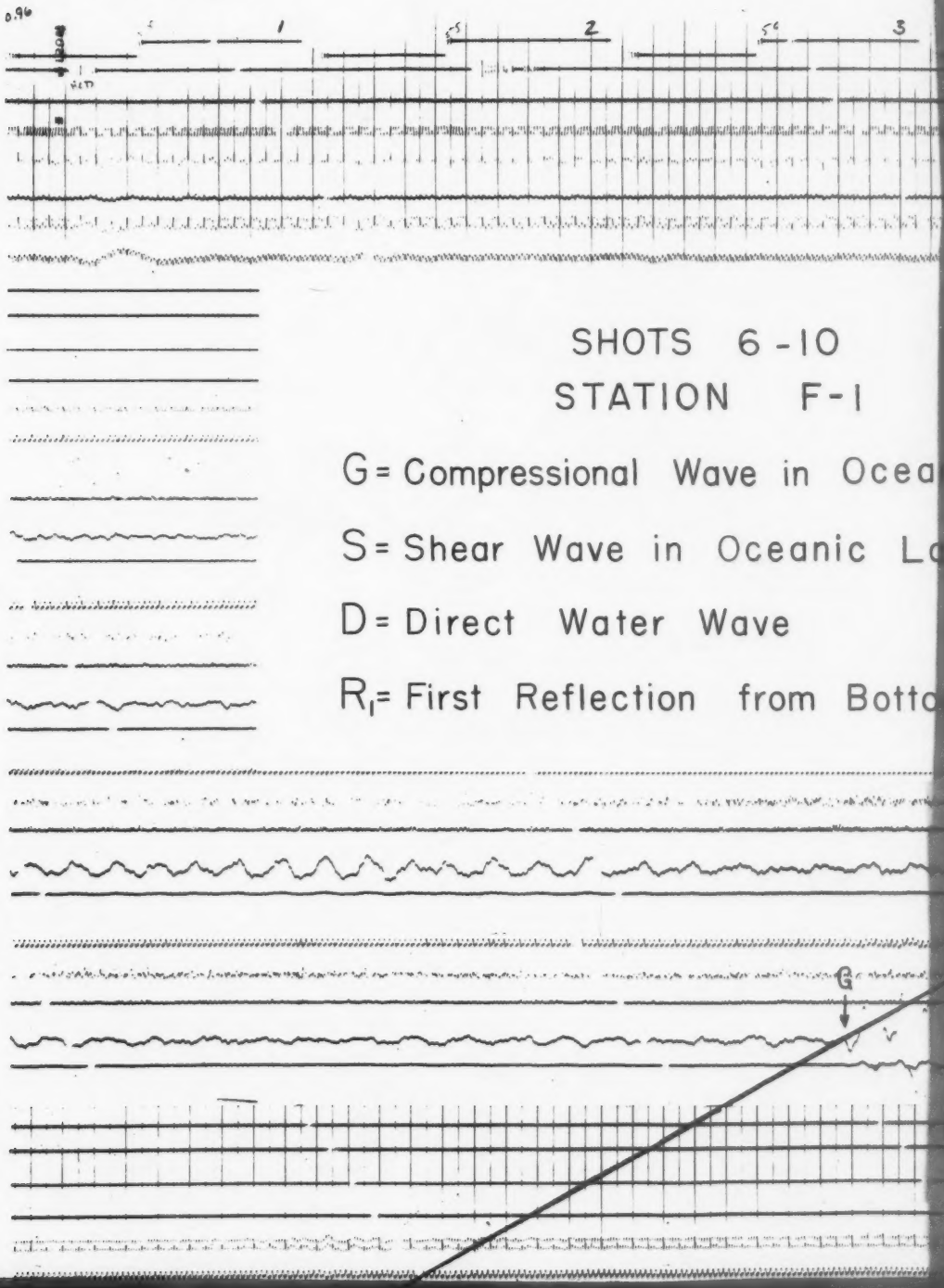
SHOTS 6 - 10
STATION F-1
G = Compressional Wave in Ocean
S = Shear Wave in Oceanic La
D = Direct Water Wave
R1 = First Reflection from Botto
G

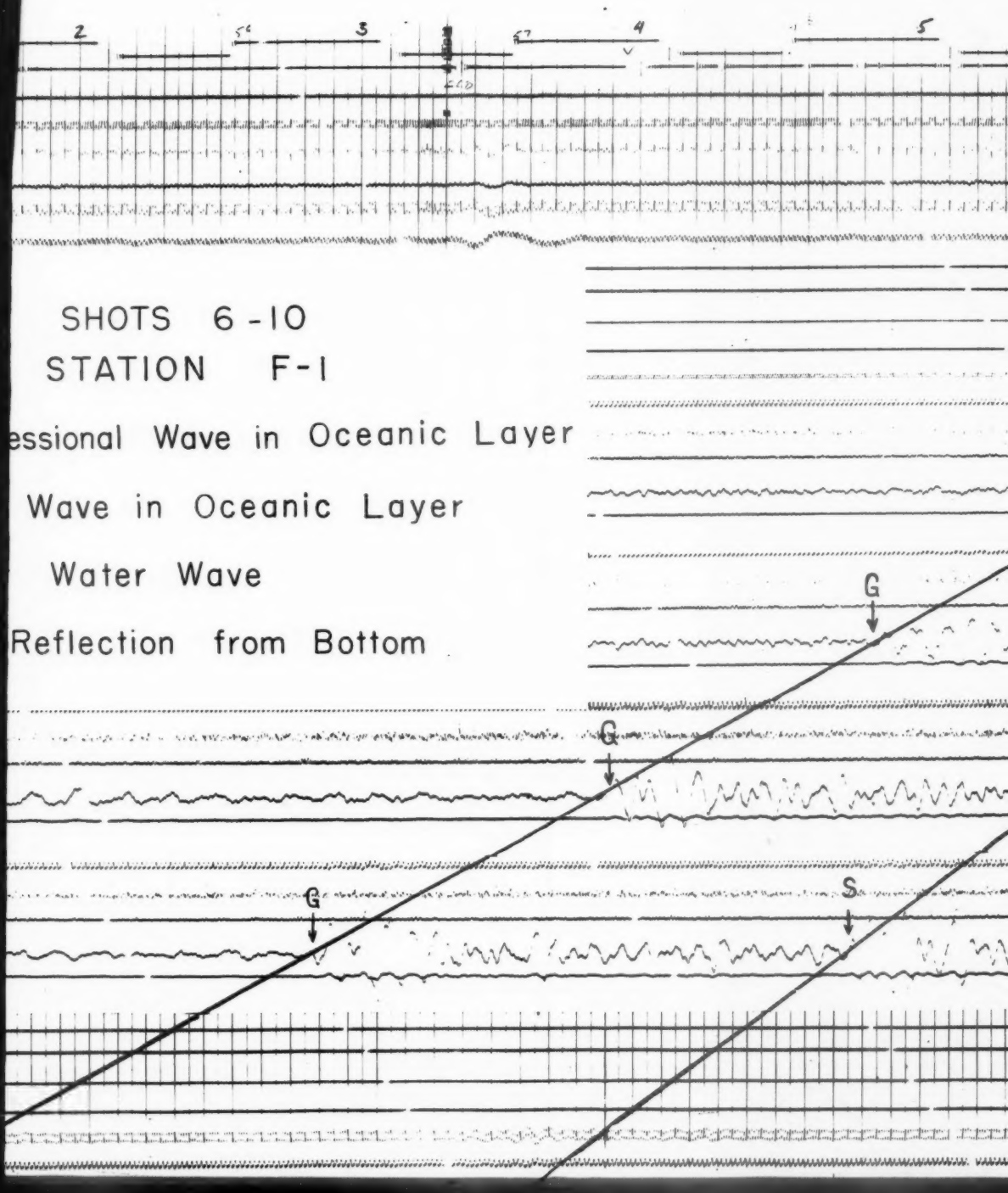
SHOTS 6 - 10
STATION F-1
essional Wave in Oceanic Layer
Wave in Oceanic Layer
Water Wave
Reflection from Bottom
G
G
G
S

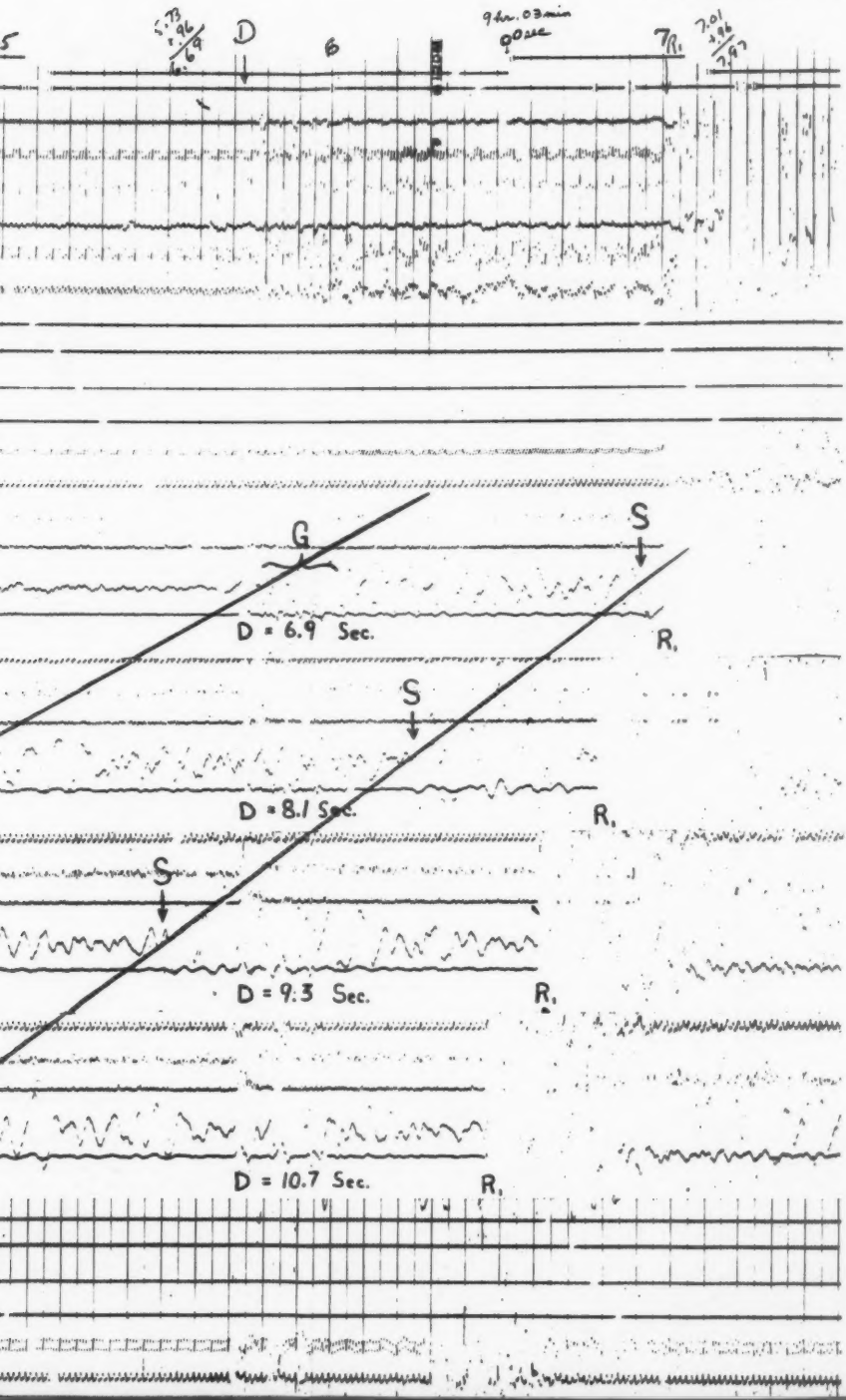
D
9 hr. 03 min
00 sec
R1
G
S
D = 6.9 Sec.
R1
S
D = 8.1 Sec.
R1
S
D = 9.3 Sec.
R1
D = 10.7 Sec.
R1

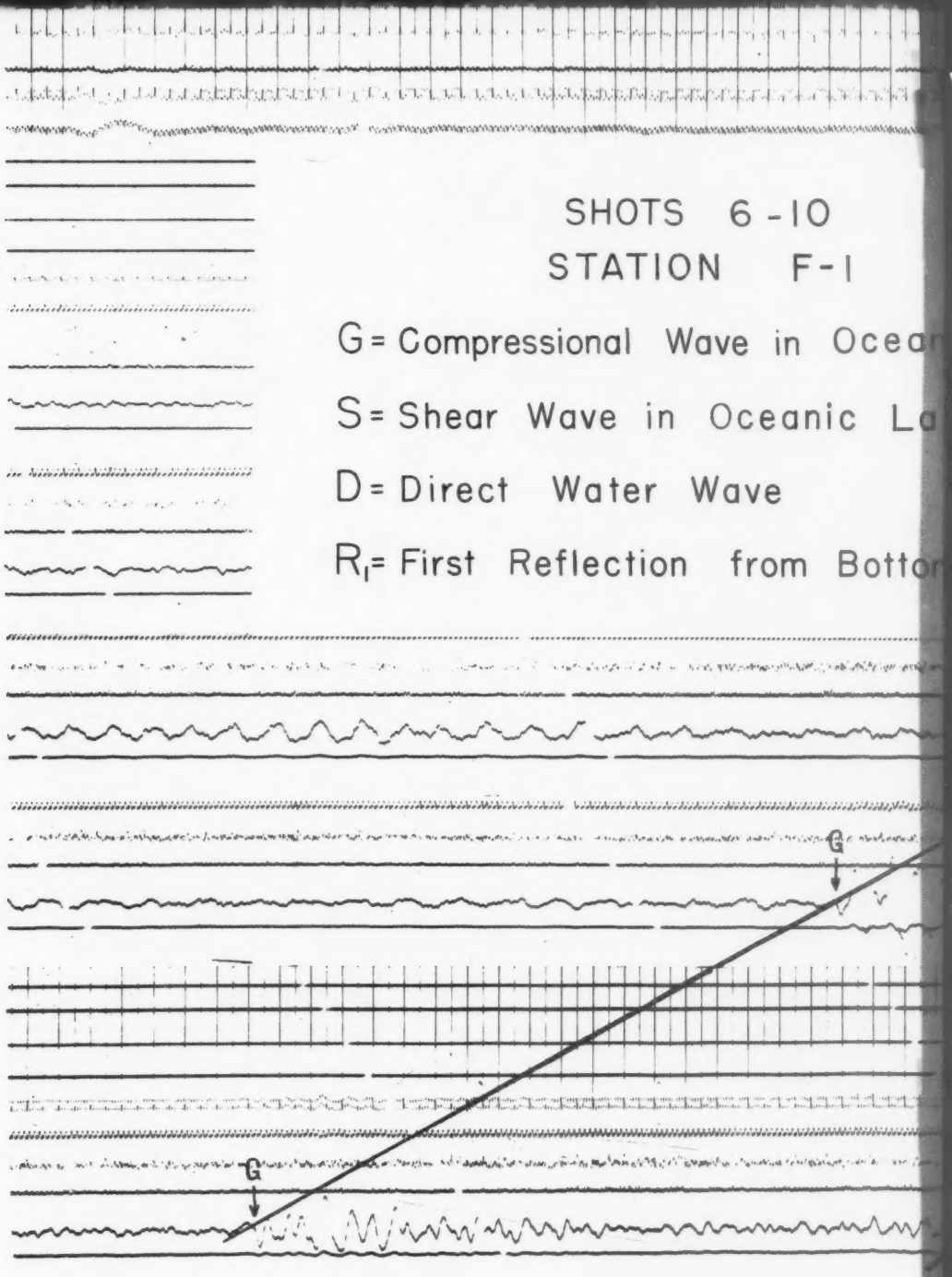
SHOTS 6 - 10
STATION F-1
G = Compressional Wave in Ocean
S = Shear Wave in Oceanic La
D = Direct Water Wave
R1 = First Reflection from Botto
G
G

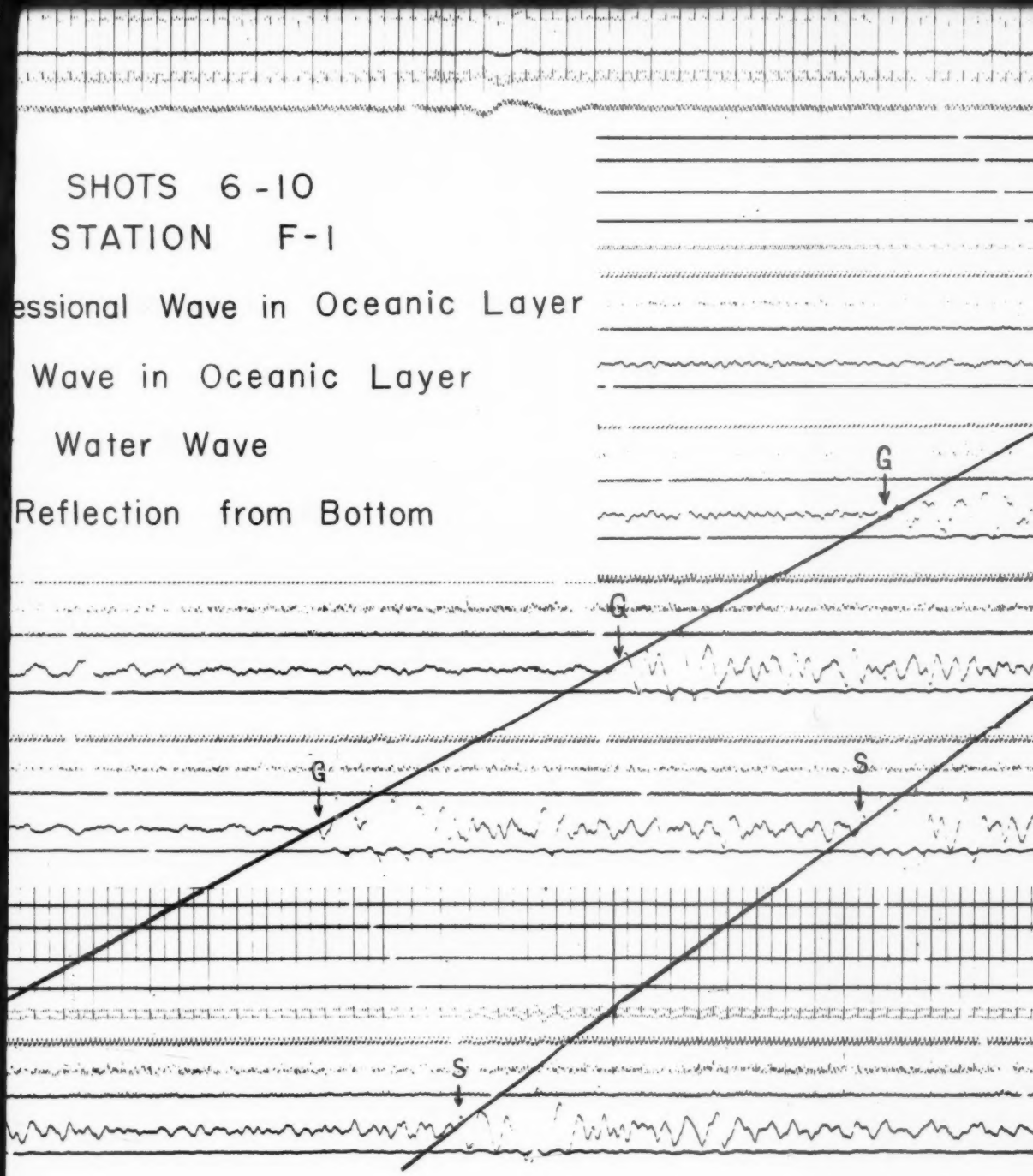

SEISMIC-REFRACTION STATION F-1a, SHOTS 6-10

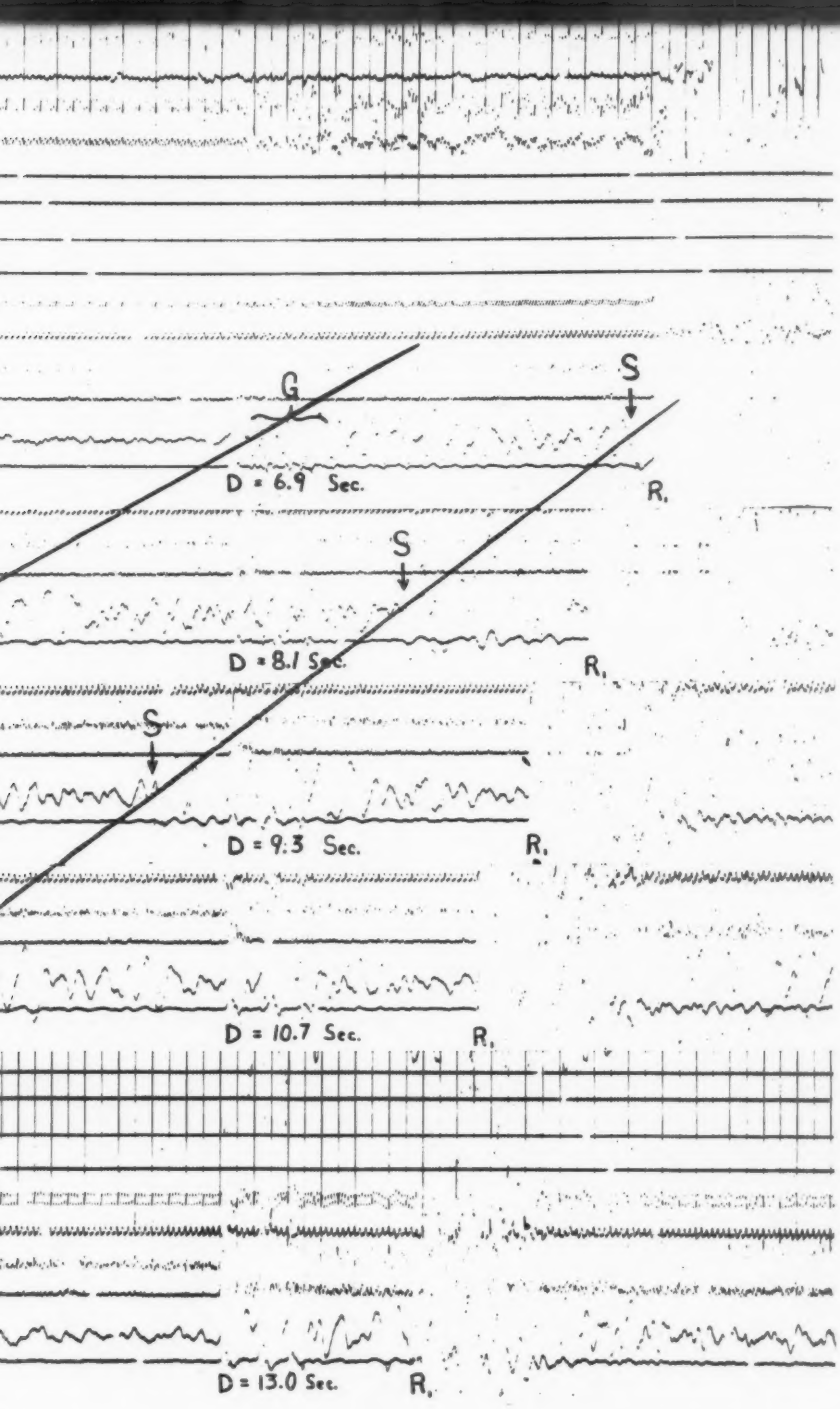
G
S
D = 6.9 Sec.
R,
S
D = 8.1 Sec.
R,
S
D = 9.3 Sec.
R,
D = 10.7 Sec.
R,
D = 13.0 Sec.
R,

corrected for the topographic irregularities, assuming that the oceanic layer has comparable relief.

The velocity in the sediments (not measured) was assumed to be 1.70 km/sec. On this basis, the average sedimentary thickness was computed to be 0.63 km. The oceanic layer has a velocity of 6.60 km/sec and an average thickness of 5.05 km. The velocity of 8.14 km/sec shown for the subcrust was not well determined, because of an insufficient number of shots at long range.

No persistent sub-bottom reflections were observed here, undoubtedly in part because of the irregularities in the bottom. These produce prolonged R_1 arrivals which obscure possible reflections from a deeper horizon.

Station G-5 (Pl. 3)

This station is about 250 miles northeast of Martinique in about 3000 fathoms of water. The bottom was fairly rough, necessitating topographic corrections of up to 0.25 sec on some arrival times.

The velocity in the sediments was assumed to be 1.72 km/sec, and the average thickness was calculated to be 0.75 km. The velocity in the oceanic layer is 6.82 km/sec, and the average thickness is about 6.7 km. The thickness of the oceanic layer and the velocity in the subcrust (8.23 km/sec) are inaccurately determined as a result of insufficient shots at long range.

No sub-bottom reflections were seen at this station.

Station G-10 (Pl. 3)

This station is just north of the abyssal plain in the Nares Basin, about 450 miles due north of Mona Passage. The average water depth along the shot lines was 3000 fathoms (5.49 km) with variations up to 200 fathoms.

The velocity 1.70 km/sec was assumed for the topmost layer of sediments. A layer of semiconsolidated sediments (velocity 2.46 km/sec) was clearly determined in the *B* profile by the line $G_2 = 5.85 + D/1.60$, and a corresponding line was assumed in the *A* profile. It is not unusual for a long refraction station to show sedimentary arrivals such as these—clearly observed at one receiving position and very poorly or not at all at the other. This may be the result of horizontal gradients or velocity changes in the sediments or of the pinching out of the refracting layers in the sedimentary column. An explanation believed to be more likely, however, is that, in the areas of good sedimentary refractions, the transition from a lower to a higher velocity is sharp, whereas it is more gradual in the other areas. Of equal importance is the character of the boundary between the two media; a smooth boundary obviously is more efficient than a rough one. These arguments also apply in the consideration of sub-bottom reflections.

The oceanic-layer and mantle velocities are well determined to be 6.57 and 8.29 km/sec respectively. A considerable amount of relief in the oceanic layer is indicated in the area around 17 seconds from *B*, where the points fall below the line by as much as 0.3 sec. This represents a rise in the refracting interface on the order of 0.5 km above the mean level. The feature is not seen in the *A* profile, probably because of the wide shot spacing in that portion of the track.

The lines $G_n = D/2.37 + 7.58$ in the *A* profile and $G_n = D/2.36 + 7.50$ in the *B* profile are determined by strong second arrivals which are identified as transformed shear waves travelling horizontally in the oceanic layer. These, with reflected-refracted and doubly refracted arrivals, have been described in earlier papers (Ewing *et al.* 1954) and are discussed in some detail in this report.

Some sub-bottom reflections were observed at *A*, but the irregular bottom topography complicates and prolongs R_1 to such an extent that the deeper reflections are uncertain.

Station G-11 (Pl. 3)

This station is on the abyssal plain in the Nares Basin about 330 miles north of the eastern end of Hispaniola. The average water depth was 3120 fathoms (5.70 km).

The *A* profile produced very good records in which a number of secondary phases could be read in addition to the first arrivals. These are identified as transformed shear waves travelling in the oceanic layer and as reflected-refracted and doubly refracted arrivals from that layer. The shear waves determine the line $G_n = D/2.63 + 8.90$; the reflected-refracted arrivals determine the line $R_1G_2 = D/4.52 + 15.80$; and the doubly refracted arrivals determine the line $G_2^2 = D/4.52 + 16.95$. These phases are discussed in another section of this report. The records in the *B* profile were made at low gain and did not show these secondary phases.

Strong sub-bottom reflections were seen in both profiles. These determine reflection hyperbolas which intercept the time axes above R_1 by 0.9 sec at *A* and 0.6 sec at *B*. In both profiles, the sub-bottom reflection curves are cut by the extended refraction lines representing the oceanic layer, indicating that the reflecting horizon is above that layer.

The structure section shows that the average thickness of sediments is 0.87 km, calculated for an assumed velocity of 1.71 km/sec. The oceanic-layer velocity is 6.76 km/sec, and the velocity in the mantle, determined primarily by the *A* profile, is 8.04 km/sec. The average thickness of the oceanic layer is 5.15 km.

To illustrate the correlation of the various phases from shot to shot, one low-frequency trace from each seismogram of the *A* profile has been reproduced on a common time scale in Plate 1, with trace spacing proportionate to shot distance. All except the last four are low-sensitivity traces and do not show some of the arrivals distinctly—the shear waves for example. All arrivals can be picked with much more certainty when all the traces, which have a variety of filter settings and sensitivities, are utilized.

Station G-12 (Pl. 3)

This station is on the abyssal plain of the Nares Basin about 100 miles northwest of station G-11. The water depth was 3000 fathoms (5.49 km).

Both profiles produced reflected-refracted and doubly refracted arrivals, and in addition the *A* profile showed transformed shear waves for several of the shots determining the line $G_n = D/2.60 + 8.62$. Prominent sub-bottom reflections are seen in both profiles, determining reflection hyperbolas which intercept the time axes above R_1 by 1.0 sec at *A* and 0.9 sec at *B*.

A value of 1.71 km/sec was assumed for the velocity in the unconsolidated sediments. In pro-

file *B*, three distinct arrivals (one almost coincident with *R*) were received. These determine a refracting layer with an apparent velocity of 2.03 km/sec lying at a depth of 0.35 km beneath the ocean floor. The *A* records, which consistently had a higher sensitivity than the *B* records, did not show these arrivals. This again demonstrates the inconsistency of refractions in the sedimentary column. As at station G-10, the semiconsolidated sediments here (2.03 km/sec layer) are assumed to be present at *A*, even though not detected, and the average thickness is calculated to be 1.08 km. The velocity in the oceanic layer is 6.90 km/sec, and the apparent velocity in the mantle determined by the *A* profile is 8.12 km/sec.

Station G-13 (Pl. 3)

This station is about 350 miles north of Haiti and about 100 miles west of G-12. The water depth ranged from 2990 fathoms (5.46 km) at the south end to 2950 fathoms (5.40 km) at the north end of the shot lines.

This is one of the clearest and most detailed deep-sea refraction stations known. The structure is typically oceanic. The sedimentary column consists of 0.42 km of unconsolidated material (assumed velocity 1.70 km/sec) overlying a semiconsolidated layer which has a velocity of 1.99 km/sec and an average thickness of 0.97 km. Here, the semiconsolidated sediments are clearly determined at both ends of the station. The velocity in the oceanic layer is 6.85 km/sec, and its average thickness is 6.19 km. The velocity in the mantle is 8.32 km/sec.

Reflected-refracted and doubly refracted arrivals from the oceanic layer are seen in both profiles, determining the lines R_1G_3 and G_3^2. In the *B* profile, still later arrivals are seen which correspond approximately to travel times involving one reflection and two refractions and triple refractions. On the longer shots, these two phases cannot be separated, and the points on the travel-time graph roughly show the arrival times of maximum energy.

Reflected-refracted and doubly refracted arrivals are also seen for the layer of semiconsolidated sediment. These are labeled R_1G_2 and G_2^2 respectively on the travel-time graph. Since the range of observation of these phases is short, only one or two arrivals are seen for each. However, the arrivals are very strong and distinct, and there is little doubt that they are correctly interpreted.

Strong sub-bottom reflections are seen in both profiles, indicating a reflecting horizon above the oceanic layer.

The longest shots of this station clearly show the constant frequency R_{ib} arrivals reported by Hersey *et al.* (1952), Katz and Ewing (1956), and Officer (1955). The arrivals here have a frequency of 63 cycles per second.

No transformed shear waves were observed at this station.

Station G-14 (Pl. 3)

This station is about 230 miles northeast of Eleuthera Island at 2760 fathoms (5.06 km) water depth. No reverse profile was shot, so the velocities are apparent, and the layer thicknesses were calculated assuming no component of dip in the direction of the shot line.

The refraction data show that the structure consists of 1.34 km of unconsolidated sediment (assumed velocity 1.71 km/sec) overlying the oceanic layer, which is 5.72 km thick and has an apparent velocity of 6.58 km/sec. The velocity determined for the layer beneath the oceanic layer is 7.75 km/sec, which is low for mantle velocity. The discrepancy could be due to slope in the layer or simply to the fact that the station was not long enough for an accurate velocity determination.

An unusually strong set of sub-bottom reflections was recorded at this station, again showing that the reflecting horizon is above the oceanic layer. These arrivals determine the R_1' curve from the once-reflected signals and the R_2' and R_2'' curves from the twice-reflected signals. Also observed on some shots were reflected-refracted and doubly and triply refracted arrivals from the oceanic layer. These determine the lines R_1G_2, G_2^2, G_2^3, respectively, on the travel-time graph.

Station D-2 (Pl. 3)

This station is west of the Mid-Atlantic Ridge at Lat. 30.5°N. on a 2400-fathom terracelike feature which forms the first approach to the ridge. No reverse profile was obtained, but, since the topography was generally flat along the shooting track, it is probable that no serious error in determining the velocities was introduced by slope in the layers.

The approximate depth to the oceanic layer was computed to be 0.56 km by assuming that the entire sedimentary column was unconsolidated and has a velocity of 1.72 km/sec. The oceanic layer has an apparent velocity of 6.62 km/sec and a thickness of approximately 3.11 km. The apparent velocity in the mantle is 7.94 km/sec.

Station D-15 (Pl. 3)

This is a reversed station in the North American Basin east of Bermuda at a water depth of about 2950 fathoms (5.40 km). Oceanic layer and mantle velocities are 6.82 and 8.25 km/sec respectively. The average thickness of overlying sediments is computed to be 0.89 km for an assumed velocity of 1.71 km/sec. The average thickness of the oceanic layer is 3.65 km.

Station D-16 (Pl. 3)

This station is also in the North American Basin about 200 miles west of station D-15. The actual topographic profile here is approximated by a line sloping from 2450 fathoms (4.50 km) at *A* to 2825 fathoms (5.23 km) at *B*. The ground-wave arrival times were corrected to this datum plane, and a satisfactory alignment of the points on the travel-time graph was obtained. Oceanic layer and mantle velocities are 6.85 and 8.06 km/sec respectively. The sediments were assumed to have a velocity of 1.71 km/sec, from which the average thickness was computed to be 1.17 km. The average thickness of the oceanic layer is 4.73 km.

Station F-1 (Pl. 3)

The shot lines were run over a fairly level bottom in the northern edge of the Labrador Basin; the water depth was about 1850 fathoms (3.39 km). All shots of sufficient range produced good arrivals through the oceanic layer, determining a velocity of 6.94 km/sec. No mantle arrivals were obtained, and the minimum thickness of the oceanic layer is 5.50 km.

No sedimentary arrivals were obtained, but the

sedimentary layer was computed as 1.06 km using an assumed velocity of 1.70 km/sec.

The line in the *A* profile, $G_s = D/2.46 + 5.40$, is determined by prominent arrivals identified as shear waves which have been transformed from compressional waves apparently near the base of the sedimentary layer. Some of these arrivals, labeled "*S*", are illustrated in Plate 2. There are indications of shear waves also in the *B* profile, but they could not be picked accurately, because all records received at *B* are comparatively weak.

Station A-156-28 (*Pl. 3*)

This unreversed whaleboat profile shows typical velocities 1.74 and 6.59 km/sec for the sedimentary and oceanic layers but was slightly too short to give data for the mantle. The great thickness of the sediment layer, 2.4 km, is attributed to proximity to the continental rise.

Station A-173-4 (*Pl. 3*)

This station is about 270 miles southeast of Cape Cod near the foot of the continental rise in 2590 fathoms (4.73 km) water depth. The unconsolidated sediments, 1.70 km/sec assumed velocity, are 0.5 km thick and overlie a 1.4 km-thick layer of semiconsolidated sediment, velocity 1.88 km/sec. The oceanic layer, velocity 6.62 km/sec, is 4.35 km thick. The deepest refracting layer is at a depth of about 10.8 km and has a velocity of 7.70 km/sec. Although the depth to this layer is very near that at which the mantle is usually found in ocean-basin areas, the velocity is significantly lower than standard mantle velocity. Other stations in this general area which have shown a subnormal velocity at about normal mantle depth are A-164-24, A-179-11, A-179-12 (Katz and Ewing, 1956), and A-172-29 (Ewing *et al.*, 1954).

Station A-157 - C-10-29 (*Pl. 3*)

This station, in 2760 fathoms (5.05 km) about 300 miles north-northwest of Bermuda, shows standard velocities 1.62 to 1.82 km/sec for the sedimentary layer (2.1 km thick) and 6.82 km/sec for the oceanic layer. The station did not have long-range shots for detection of the mantle (assumed velocity 8.03 km/sec) but gives a minimum thickness of 4.6 km for the oceanic layer.

Station A-157 - C-10-30 (*Pl. 3*)

This is an end-to-end station about, 70 miles south-southeast of A-157-29 in 2650 fathoms (4.85 km) water depth. A layer of sediments 1.5 km thick with an assumed velocity of 1.80 km/sec is underlain by the oceanic layer (velocity 6.6 km/sec). The minimum thickness of the oceanic layer is computed to be 6.75 km, assuming it to be underlain by the mantle with a velocity of 8.0 km/sec.

The accuracy of these measurements is considerably reduced by indeterminable firing delays[2] at two of the shot points.

Station A-157 - C-10-31 (*Pl. 3*)

This unreversed profile, about 60 miles east-southeast of A-157-30, showed 1.7 km of sediment, assumed velocity 1.80 km/sec, overlying the oceanic layer, velocity 6.65 km/sec.

Sedimentary arrivals are present, but confused.

[2] At stations A-157-29 through A-157-33, the charges were fired with electric blasting caps.

Station A-157 - C-10-32 (*Pl. 3*)

This is an unreversed profile about 20 miles north of A-157-31. The oceanic layer (velocity 6.21 km/sec) is overlain by 0.71 km of sediment (assumed velocity 1.80 km/sec). An apparent velocity of 8.1 km/sec determined by the two longest shots is identified as the mantle. The oceanic layer is 4.41 km thick.

Station A-157 - C-10-33 (*Pl. 3*)

This is an unreversed profile a few miles northeast of A-157-32 showing 0.71 km of sediment (assumed velocity 1.80 km/sec) overlying the oceanic layer (velocity 6.63 km/sec).

The sediments thin almost 1 km from stations A-157-29, 30, and 31 to stations A-157-32 and 33. This suggests that there is an appreciable amount of relief on the top of the oceanic layer, which, because of sedimentary filling, is not expressed in the ocean-bottom topography. Other good examples of buried relief are shown in stations E-5, F-9, and G-10.

Station G-15 (*Pl. 3*)

This station is just off the Blake Plateau at about the latitude of Jacksonville, Florida. The water depth ranged from 2340 fathoms (4.29 km) at *A* to 2660 fathoms (4.87 km) at *B*. There was very little topographic variation other than the general slope.

A layer of semiconsolidated sediments (velocity 1.98 km/sec) was clearly detected at both receiving positions. This layer is overlain by 0.47 km of unconsolidated sediments (assumed velocity 1.73 km/sec) at *A* and by 0.07 km at *B*. A deeper sedimentary layer is indicated at *A*, both by refraction and reflection data, in which the apparent velocity is 3.05 km/sec. Although this layer was not seen in the *B* profile, it was assumed in the calculations since the records there were fairly weak, and the signals (judging by the *A* profile) were not strong. Station A-164-15 (Katz and Ewing, 1956), located at almost the same position as receiving position B here, also fails to show the 3.05 km/sec layer, but those records also are weaker than the records made at *A* in this station. Additional evidence for a high-velocity sediment here comes from stations A-164-13 and -14, (Katz and Ewing, 1956), about 80 miles to the east, which show a layer 1.5 km thick with a velocity of 2.5 km/sec, underlying the unconsolidated sediments.

Oceanic-layer and mantle velocities are 6.81 and 8.12 km/sec respectively. An oceanic-layer velocity (unreversed) of 6.73 km/sec is reported for Station A-164-15, and mantle velocity was not determined.

A few strong arrivals were recorded at *A* which can be identified only as transformed shear waves traveling in the oceanic layer. These determine the line $G_s = D/2.70 + 9.20$ on the travel-time graph.

Station E-1 (*Pl. 3*)

This station is about 160 miles directly south of Sable Island near the 2600-fm curve (4.79 km). The reception was good throughout the *A* profile, but several records were lost in the *B* profile because of equipment failure, and none of the four good records had time breaks. However, the bottom topography was flat enough that the method of recovering time breaks from the D-R_1-R_2 intervals (Ewing, Worzel, Hersey, Press, and Hamilton,

1950), in conjunction with the ship's navigation, provides a usable reverse for the *A* profile.

The structure section shows five layers in the ocean floor: unconsolidated sediments (1.83 km/sec), semiconsolidated sediments (2.05 km/sec), consolidated sediments (3.97 km/sec), oceanic layer (6.69 km/sec), and mantle (8.22 km/sec). These results agree very closely with the seaward end of the Grand Banks profile (Bentley and Worzel, 1956), the end point of which is about 160 miles east of this station at about the same water depth. Similar results were obtained from the Halifax section (Officer and Ewing, 1954), although the seaward end of that profile shows no semiconsolidated or consolidated sediments.

The great thickness of the sedimentary layers and the increased depth to mantle found at this station are common as one approaches the continental boundary from the sea.

Station A-150-4, 5, and 6 (Pl. 3)

These are three short whaleboat stations, each of which produced only one record of a ground wave. The sedimentary thicknesses for these stations are listed in Table 1 but were not included in the average for the ocean-basin stations. The thicknesses were computed by assuming velocities (governed by the values measured at the closest standard station) for the sediments and for the subsedimentary layer.

DISCUSSION OF RESULTS: The measurements at 21 of the ocean-basin stations in the Western North Atlantic reported in this paper give the following average values:

	Km	*No. of Measurements*
Water depth	5.02	21
Thickness of sediments	1.07	17*
Depth to oceanic layer	6.15	17*
Velocity (km/sec) in oceanic layer	6.71	21
Thickness of oceanic layer	5.16	15
Depth to mantle	11.25	15
Velocity (km/sec) in mantle	8.08	15

* Stations G-15, A-156-28, and A-173-4 were not used in determining average sediment thickness or depth to the oceanic layer because of their location on the continental rise.

There is good overall agreement between these and the earlier results in ocean basins reported by Officer *et al.* (1952), Ewing *et al.* (1954), Katz and Ewing (1956), Hersey *et al.* (1952), Hill (1952), Gaskell and Swallow (1951; 1952; 1952), and Raitt (1956). From the study of sub-bottom reflections (Hill, 1952; Officer, 1955; Nafe and Ewing, unpublished), and from laboratory experiments (Laughton, 1954), it is evident that velocity usually increases with depth in the sediments. For this reason, the sediment thickness at many stations, particularly where the velocity was assumed, may need revision upward. However, there is also good evidence that, because of the possible presence of a masked intermediate-velocity layer or because of a velocity gradient in the oceanic layer, part of the geologic column computed with sediment velocity is actually high-velocity rock. In this sense, the listed sediment thickness is excessive. Therefore it appears that about 1 km average thickness is as accurate a number as can be given until more precise determinations are made by measuring directly on the sea floor where the water waves will not mask the early refracted arrivals.

In Plate 1, one low-frequency trace from each of the seismograms of station G-11A is reproduced on a common time scale, and spaced according to shot distances, to demonstrate the correlations involved in identifying any given arrival over a range of distances. The phases of interest are labeled on the diagram.

The multiple phases R_1 G and G_2 have been discussed in earlier papers (*e.g.*, Ewing, Sutton, and Officer, 1954). The $R_1 G$ phase has the same apparent velocity as G and is delayed by the time required by the simple geometrical theory, approximating that for one reflection from the ocean bottom. The G^2 phase is simply a multiple refraction, hence has the same apparent velocity and twice the time intercept of G. These phases are generally strong when all refracting layers are nearly horizontal. Although some conclusions may be drawn from these phases, the principal reason for studying them is that they sometimes tend to obscure more important ones, which may be identified more readily if the multiples are understood.

Shear waves, propagated through the oceanic layer, have been identified at seven of the stations reported here, and in some cases their amplitude is large compared to that of all other refracted phases. At nine stations the shear waves are judged to be present but are not shown on the travel-time curves because they are seen on only a few records. At 17 stations they are either absent or too weak to be identified, while at the remainder of the stations the data are inadequate or too complicated to indicate presence or absence of the shear waves. Many in the latter group are shallow-water stations at which shear waves would be difficult to identify because of numerous multiple-refracted phases.

The marked variation in intensity of the

shear waves merits further study. At present no correlation with other observed factors, such as geographical location, sediment type, or topographic province, has been found. Neighboring stations, apparently similar in all other respects, may differ radically in shear-wave transmission.

Identification of a given arrival as a shear wave depends on the time intercept and apparent velocity attributed to the arrival on the travel-time curve. The velocity is approximately $1/\sqrt{3}$ times the observed compressional wave velocity in the same layer, and the time intercept agrees approximately with the theoretical intercept computed for arrivals which have been transformed from compressional to shear waves at the depth of the sediment–rock interface. Sample records of shear waves obtained at station G-11 and station F-1 are illustrated in Plates 1 and 2.

It is difficult to demonstrate how much of the scatter in the velocity is real and how much is experimental error. The mean of the observed values reported here gives V_p/V_s = 1.80, and 80 per cent of the values are included between 1.72 and 1.99. The periods of the shear waves are not usually noticeably different from those of compressional waves found on the same records.

Similar observations of shear waves at deep-water stations have been mentioned by Raitt (1949), Hersey *et al.* (1952), Ewing *et al.* (1954), and Katz and Ewing (1956). In the last three of these papers it was reported that the thickness of sediments, as computed from the shear waves on the assumption that transformation occurred at the interface between the sediments and the oceanic layer, was somewhat greater than that computed from the compressional-wave data. As with the results reported in the present paper, the apparent discrepancy in depth disappears if the transformation to shear waves is assumed to be at a suitable horizon above the oceanic layer.

Two other phases, which are related to a horizon above the oceanic layer are frequently observed. They are sub-bottom reflections and refracted arrivals from semiconsolidated sedimentary layers. They also show large variations in intensity from station to station, which have not been correlated with any other properties. In some cases, the sub-bottom reflections correlate fairly well with refracted arrivals from within the sedimentary column; in other cases they correlate approximately, but not exactly, with refracted arrivals from the oceanic layer. In still other cases, strong sub-bottom reflections observed cannot be correlated with any refracted arrivals. The travel-time graphs of stations G-3 and G-14 show examples of sub-bottom reflections correlating more closely than usual with the top of the oceanic layer. Both show that the reflecting horizon is above that determined by the refracted arrivals since the R_1' curve is cut by the G_2 line. Therefore, both shear waves and sub-bottom reflections indicate that an important horizon exists above the top of the oceanic layer at which transformation from compressional to shear waves can occur and which is a good reflector.

The discrepancies in depth to the horizon indicated by the two types of refracted waves and the reflected wave may indicate that an additional layer, intermediate in velocity between the oceanic layer and the sediments, exists but is masked by the water waves. Explanation of the large variations in intensity seems to be more difficult. There are some indications that the horizon in question is a transition zone in the sediments separating the material above, which behaves as a fluid, from that below, which has rigidity. The degree of abruptness of this transition probably would have greater effect on the intensity of reflected signals than on refracted signals.

At a few stations (*e.g.*, G-11, G-12, G-13) a dotted line, indicating a velocity of about 5 km/sec, has been drawn to show the possibility of a masked layer between the sediments and the oceanic layer. If this layer is present, attenuation in it must be high because its travel-time curve cannot be extended to greater distances by the use of second arrivals. Perhaps a better explanation is that the upper part of the oceanic layer has a velocity gradient which would bend down the masked portion of the refraction line into a position of tangency to the R' hyperbola. This would eliminate the discrepancy between the depth determined by reflected and by refracted waves and would account for the failure to observe the postulated intermediate-velocity material as a second-arrival refracted phase. At Atlantic stations (in deep basins) there is usually no direct evidence from refracted waves for the presence of a 5-km/sec layer, whereas such evidence is frequently found in the Pacific.[3] The sediment-layer thickness in the Atlantic is sufficient to mask the postulated layer at

[3] Raitt (1956) reports a layer 1–2 km thick with an average velocity of about 5.2 km/sec at many locations in the Pacific Ocean.

most of the stations, but its presence is frequently indicated by shear waves and subbottom reflections and occasionally by compressional arrivals.

Eastern Atlantic Ocean Basin

The seismic-refraction data hitherto available for the crustal structure of the eastern basin of the Atlantic are those reported by Hill (1952), Gaskell and Swallow (1951), and Hill and Laughton (1954).

Most of their measurements are near the basin margins. Their stations and those of the present report are all north of 30° N. Lat., where the eastern basin is narrow and interrupted by numerous seamounts and submarine ridges. Probably this accounts for the difference between the results found here and those reported for the broad western basins.

Station E-7 (*Pl. 3*)

Station E-7 is in the western edge of the Iberian Basin between Spain and the Azores. This general area has quite complex topography; variations of as much as several hundred fathoms are common even within relatively short distances. For example, an 1800-fathom peak was crossed a short time before arriving at the station.

Unconsolidated sediments about 0.9 km thick are found, assuming a velocity of 1.73 km/sec. Beneath the sediments are two refracting layers, the upper 4.3 km thick, with velocity 6.46 km/sec, the lower with velocity 7.68 km/sec. Although the accuracy of the measurements is low here, the results are in good agreement with near-by stations, E-8 and E-9.

Station E-8 (*Pl. 3*)

This station is in the Iberian Basin in 2660 fm (4.85 km). It is on the northern slope of a large topographic rise which gave a minimum sounding of 1800 fathoms about 40 miles south of the station. The arrival times were corrected to a sloping bottom approximating the slope of the main topographic feature.

The seismograms recorded at *A* are very good and, although only five ground-wave arrivals were received at *B*, these reverse the station satisfactorily. The structure section consists of a layer of unconsolidated sediment which averages 0.88 km thick, assuming a sedimentary velocity of 1.74 km/sec. The oceanic layer has a velocity of 6.28 km/sec and an average thickness of 3.81 km. The velocity 7.77 km/sec found for the deepest layer is below accepted values for the mantle.

Station E-9 (*Pl. 3*)

This station is in the West European Basin west of the Bay of Biscay. The water depth averaged 2400 fathoms (4.39 km), and the bottom topography was relatively flat along the shot lines.

The velocities in the oceanic layer and in the layer below it are 6.26 and 7.65 km/sec respectively, and 1.72 km/sec was assumed for the velocity in the sediments. The velocity 7.65 km/sec is below the accepted values for the mantle.

Station D-12 (*Pl. 3*)

This station is located in deep water about midway between the northwestern tip of Spain and southern Ireland. The shot lines cut obliquely across the bottom contour lines; the depth increases from 2250 fathoms (4.10 km) at *A* to 2600 fathoms (4.85 km) at *B*. Topographic corrections were applied for deviations from a sloping line which approximates the bottom profile. The velocities found for the oceanic layer and the layer beneath are 6.14 and 7.77 km/sec, respectively, in good agreement with the values found at Stations E-7, E-8, and E-9. The average sedimentary column is considerably thicker here than at E-7, E-8, and E-9 (1.6 vs. 0.9 km), a reasonable result considering the proximity of this station to the continental shelf.

The velocity in the topmost layer of sediments was assumed to be 1.71 km/sec at both ends of the station. A semiconsolidated layer (2.24 km/sec) was clearly seen in the *B* profile but was not detected at *A*. The structure section, intended to show the average layer thicknesses, shows this layer about half as thick as indicated at *B*.

The results at Stations E-7, E-8, E-9, and D-12 agree well among themselves and may be compared with the profiles near stations E-9 and D-12 reported by Hill and Laughton (1954). Two of their stations will not be discussed here—No. 9 is on the continental slope, and No. 18 is reported as inaccurate. For their stations 10, 11, and 17, the velocities reported for the oceanic layer range from 6.49 to 6.75 km/sec and are considered to be in reasonable agreement with the values 6.14 to 6.46 km/sec reported in the present paper. For stations 16 and 17 Hill and Laughton report velocities 8.18 and 7.80 km/sec for a deeper layer which may be compared with the values 7.65 to 7.77 found in the present work.

Station D-5 (*Pl. 3*)

This unreversed station is in the Canary Basin west of Madeira. The water depth along the shot line was constant at 2830 fathoms (5.17 km). Apparent velocities of 6.49 and 8.04 km/sec were determined for the oceanic layer and mantle respectively. The sedimentary thickness of 1.10 km was computed on the assumption that the entire column is unconsolidated and has a velocity of 1.72 km/sec.

Station D-6 (*Pl. 3*)

This station is about 100 miles west-northwest of Madeira over a relatively flat bottom on the slope between the Canary Basin and Madeira. The water depth was about 1900 fathoms (3.45 km). Only 9 km of the station line was reversed, but, since the apparent velocity for the oceanic layer is about the same in each profile, 6.62 km/sec is probably reliable. The sedimentary thickness of 1.5 km± was computed assuming the velocity in the sediments to be 1.70 km/sec. According to this result, the oceanic layer is 5.15 km below sea level here, compared with 6.27 km at station D-5. Possibly because of the presence of volcanic rocks, a higher velocity for sediments should be used. If so the oceanic layer would probably be a little deeper at D-6 than at D-5. The material which forms this rise apparently originated at or near Madeira and built up the rise as a superficial load on normal crust. In contrast, the oceanic layer and the mantle show deviations from typical basin structure over

a large area surrounding Bermuda. The same is true for the flanks of the Mid-Atlantic Ridge and for many parts of the West Indian island arc.

DISCUSSION OF RESULTS: The scarcity of long reversed stations here makes it difficult to determine a good average crustal section in the eastern North Atlantic for comparison with that in other areas. Station D-5 appears to show results typical of ocean basins elsewhere, although the accuracy is not high because the station is short and unreversed. Much the same can be said for D-6, despite the shallow depth of water, but this is a poor station which is only partially reversed and has only a few shots.

Stations D-12, E-7, E-8, and E-9 show consistent results and suggest that the structure is slightly different from that in other basin areas. This might be expected in view of the fact that the basins in which these stations are located are relatively constricted, lying between the Mid-Atlantic Ridge, Britain, and southern Europe. The results reported by Hill (1952) and by Hill and Laughton (1954) are combined with those reported here to give the following average crustal section:

	Km
Water depth	4.56
Sediment thickness	1.18
Oceanic-layer thickness	4.87
Oceanic-layer velocity (km/sec)	6.52
Mantle velocity (km/sec)	7.81

The only significant difference in structure between this and other, larger basin areas is in the velocity below the oceanic layer. Compared with the normal mantle velocity of about 8.0–8.1 km/sec found in the large basins, the average velocity here is 7.8 km/sec. As in the western basins, a masked 4.5–5.5 km/sec layer could have been missed in these stations. Similar structure has been found in the Venezuelan Basin of the Caribbean Sea (Officer *et al.*, 1957; J. Ewing *et al.*, 1957; G. Sutton and M. Ewing, unpublished) and at other places such as the Bermuda Rise and the Continental Rise of North America (Officer *et al.*, 1954; Katz and Ewing, 1956). There is increasing evidence that only the broad, deep-ocean basins display the simple structural configuration of sediments–oceanic layer–mantle. In the intermediate areas, the structure deviates slightly toward the continental type, possibly as a result of intrusion, differentiation, changes of state, or a combination of these processes in the crust and upper mantle.

MEDITERRANEAN SEA

Previous seismic work in the Mediterranean Sea was done by Gaskell and Swallow during the world cruise of H.M.S. CHALLENGER in 1950–1952. Eight stations were occupied, two near the coast of Cyprus, two near Malta, three in deep water in the eastern basin, and one in shallow water southwest of Malta. At the deep stations, only one refracting layer was found (velocity 4.42 to 4.57 km/sec) underlying the low-velocity sediments. The shallow stations showed a wider range of refracting velocities—2.96 to 6.70 km/sec. Four of the stations reported here are in general agreement with the deep-water station of Gaskell and Swallow; the fifth, near Alboran Island, shows a higher refracting velocity.

Station D-8 (*Pl.* 4)

The shot line of this unreversed station was run down the eastern slope of a large, flat-topped seamount (at least 20 miles across) about 60 miles off the coast of Cyrenaica in the Ionian Basin. The receiving position was near the top of the mountain at about 700 fathoms water depth. The bottom sloped downward at 6.5° from the receiving position to the fifth shot, at the foot of the mountain, then upward at 2° from that point to the last shot. The water depth thus ranged from a minimum of 700 fathoms (1.28 km) at the receiving position to 1950 fathoms (3.56 km) at the deepest point. The effect of the change in slope of the bottom is clearly seen in the travel-time graph in which the line of ground-wave arrivals breaks from an inverse slope of 2.30 to 4.00.

If the observed slope of the bottom is introduced into the calculations, the velocity in the refracting layer at the receiving end of the shot line is 4.61 km/sec. The corresponding calculation for the upslope portion of the shot line (shots 5–8) gives a velocity of 5.18 km/sec. In applying the corrections for slope in these calculations, it was assumed that the refracting layer is parallel to the bottom topography.

There are two obvious structural interpretations of the data:

(1) The refracting layer on the seamount is the same as that found under the surrounding sea bed —*i.e.*, the mountain might have been formed by the intrusion of an igneous mass which raised the upper layers of the sea bed to the observed configuration. In that case, the velocities determined from the downslope and from the upslope portions of the shot line should agree, and their failure to do so means that the slopes used in calculating the velocities were incorrect, and the refracting layer is not parallel to the bottom topography. Agreement in this respect requires that the refracting layer (velocity 4.8± km/sec) slopes more steeply than the sea floor. The sedimentary thickness at the deep end was assumed to be 0.35 km on the basis of measured thicknesses at three stations north of this location.

(2) The seamount is volcanic and differs in composition from the refracting layer in the surrounding sea bed. In this case the break in the

ground-wave line could represent a change in velocity as well as a change in slope.

Station D-9 (*Pl.* 4)

This is an unreversed station in the Ionian Sea about 150 miles east of Sicily. The water depth was about 2000 fathoms (3.66 km), and the bottom topography is generally flat along the line of shots. A single refracting layer is detected at a depth of 0.34 km below the sea floor; the depth is calculated by assuming a velocity of 1.71 km/sec for the overlying sediments. The apparent velocity in the refracting layer is 4.20 km/sec.

The results from this station are in good agreement with the deep-water stations occupied in the Mediterranean from H.M.S. CHALLENGER in 1950–1952 (Gaskell and Swallow, 1953). Two CHALLENGER stations, 28 and 29, located slightly south and west of this station, show velocities in the refracting layer of 4.57 and 4.42 km/sec respectively and thickness of the sediments as 0.37 km. A velocity in the range of 4.2–5.0 km/sec is found in many other widely separated places in the Mediterranean: 4.36 km/sec at CHALLENGER station 31 south of Malta, 4.79 km/sec at station D-11 west of Sardinia. The true velocity at stations D-8 and D-10 may also lie within this range, but those determinations were very inaccurate owing to topographic complications. The layer represented by this velocity range is apparently characteristic of the deep-water areas throughout the Mediterranean. The only deep-water station which shows conflicting results is D-7, located beyond the western limit of the deep basin. The apparent velocity found there is not well determined but seems to be higher than 5.0 km/sec.

Station D-10 (*Pl.* 4)

This is an unreversed station in the Tyrrhenian Sea about 60 miles north of Sicily, which unfortunately ran over a seamount, since found to be a volcanic cone (VEMA Expedition, 1956). The water depth was about 1875 fathoms (3.43 km) for the first four shots, then decreased rapidly to 500 fathoms at the fifth shot, and increased again to 1800–1900 fathoms. The ground-wave intensity decreased abruptly when the seamount was reached, as often happens, and ground waves could be read only to the fourth shot.

Obviously the structure at this station was not accurately determined. The two solid lines on the travel-time graph show the reasonable limits for lining up the ground-wave points. The apparent velocity in the refracting layer is between 4.9 and 5.7 km/sec, and the depth of the layer below the sea floor is between 0.9 and 1.2 km. Further uncertainty is introduced, as it is in all unreversed stations, by the possibility that the refracting layer is sloping, a particularly strong possibility here.

Station D-11 (*Pl.* 4)

This is an unreversed station in the basin about 150 miles west of Corsica and Sardinia. The water depth was constant at 1370 fathoms (2.50 km). A refracting layer, in which the apparent velocity is 4.79 km/sec, was detected at a depth, calculated by assuming a sediment velocity of 1.71 km/sec, of 1.30 km below the sea floor. According to Heezen and Ewing (1955) the basin in which this station lies is an abyssal plain which receives turbidity-current deposits. The sediment layer here is thicker than at any other Mediterranean basin station.

A minimum thickness of 4.4 km was calculated for the 4.79 km/sec layer assuming that the layer beneath has a velocity of 6.50 km/sec and is too deep to be detected by the longest shot. A similar result would be obtained for Station D-9 by ignoring the longest shot, which was weak. As Gaskell and Swallow (1953) point out, possibly the refracting layer is a thin band underlain by additional low-velocity material. If so, a 6.5 km/sec layer would not have been detected as a first arrival in these measurements if it were more than 6 km below sea level.

Station D-7 (*Pl.* 4)

This is an unreversed station in about 1100 fathoms (2.01 km) of water 60 miles east of Alboran Island. The first three shots produced fairly good ground-wave arrivals, but the last two were weak. If all five arrivals are considered valid and represent the same layer, the apparent velocity in the layer is 6.08 km/sec. This interpretation of the data gives a sedimentary thickness of 2.05 km, assuming the velocity in the sediments to be 1.71 km/sec. It is equally possible, however, that only the first three points on the graph should be used, in which case the refracting velocity would be about 5.2 km/sec and the thickness of the sediments about 1.6 km. The first interpretation was used in computing the structure section.

DISCUSSION OF RESULTS: A refracting layer with a velocity between 4.2 and 5.0 km/sec is found at all the deep-water stations in the Mediterranean. None of these stations was long enough to penetrate to a deeper, higher-velocity layer. The available data indicate that the low-velocity sediments are appreciably thicker in the western end of the sea than in the eastern end. Station D-9 and CHALLENGER stations 27, 28, and 29, all of which are east of Sicily, show 0.3–0.4 km; D-10, and CHALLENGER station 31 which are at the same longitude as Sicily, show about 1 km; D-11, west of Sardinia, shows 1.3 km; and D-7, just east of Alboran Island, shows 1.6–2.0 km. Although this trend is indicated, the coverage is inadequate to justify speculating on its geological significance.

The identification of the 4.2–5.0 km/sec refracting layer should be one of the primary objects of future work in the Mediterranean. If this layer marks the bottom of the sedimentary column, the thickness of sediments apparently averages only slightly more than 1 km, which seems surprisingly thin in view of the large land area which drains into the Mediterranean. If, on the other hand, the refracting layer is a relatively thin layer of consolidated sediments, limestone, or possibly volcanic rock within the sedimentary column, it is equally significant since this boundary must represent

TRAVEL TIME IN SECONDS

40
35
30
25
20
15
10
5

40
35
30

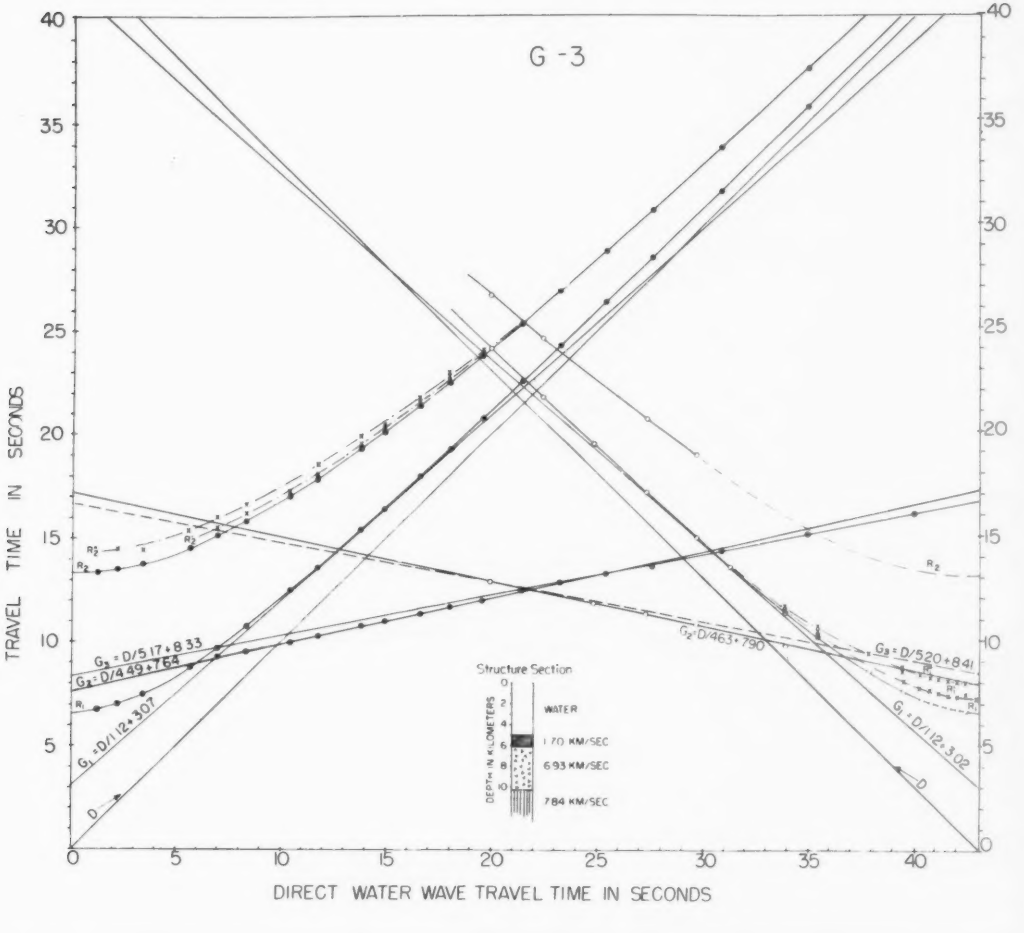
G-3
TRAVEL TIME IN SECONDS
DIRECT WATER WAVE TRAVEL TIME IN SECONDS
$G_3 = D/5.17 + 8.33$
$G_2 = D/4.49 + 7.64$
$G_1 = D/1.12 + 3.07$
$G_2 = D/4.63 + 7.90$
$G_3 = D/5.20 + 8.41$
$G_1 = D/1.12 + 3.02$
D
Structure Section
DEPTH IN KILOMETERS
WATER
1.70 KM/SEC
6.93 KM/SEC
7.84 KM/SEC

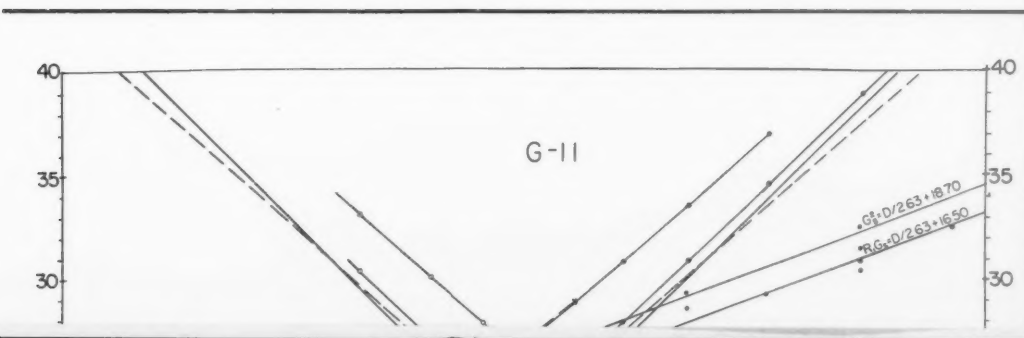
G-11
$G_3 = D/2.63 + 18.70$
$RG = D/2.63 + 16.50$

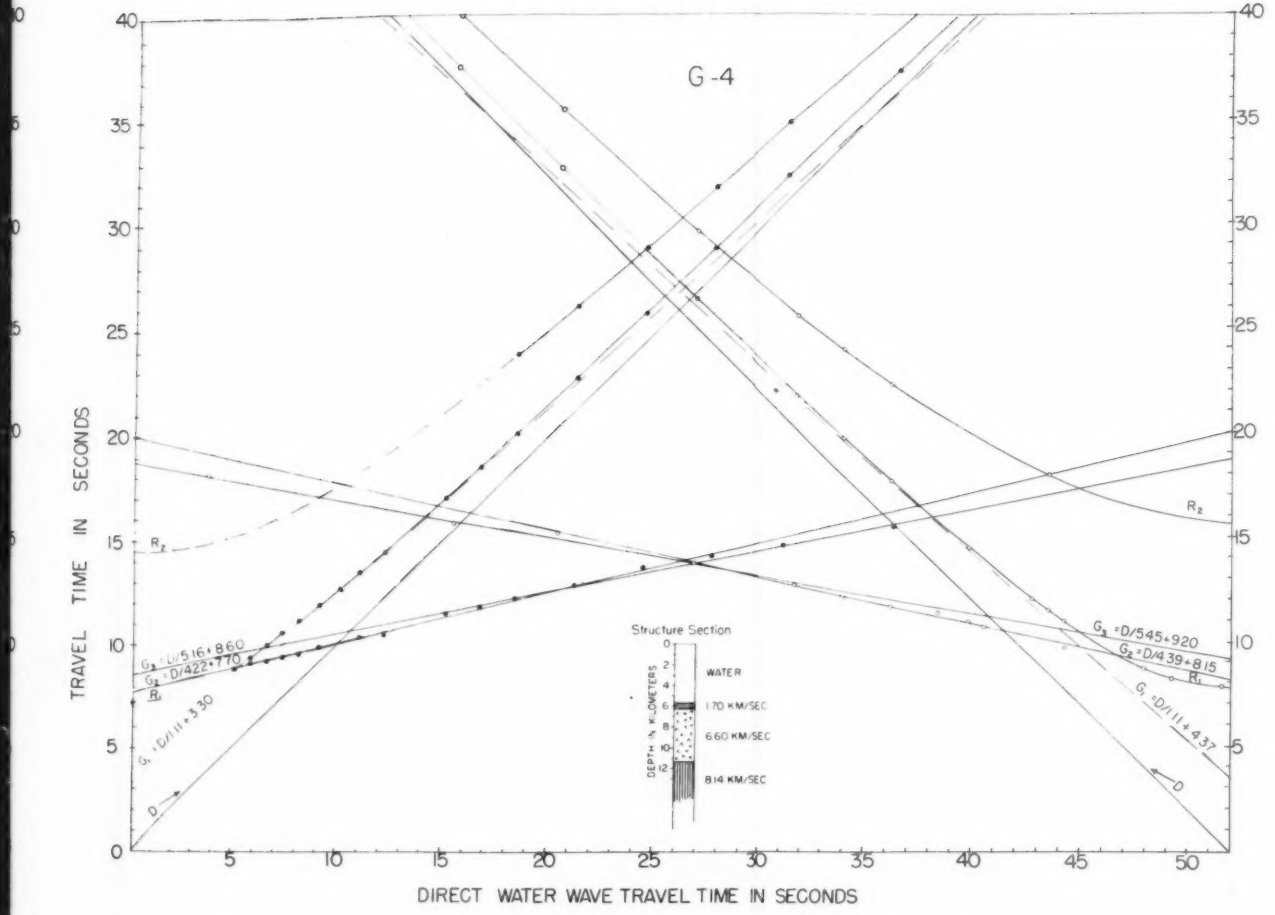
G-4
TRAVEL TIME IN SECONDS
DIRECT WATER WAVE TRAVEL TIME IN SECONDS
Structure Section
DEPTH IN KILOMETERS
WATER
1.70 KM/SEC
6.60 KM/SEC
8.14 KM/SEC
G3 =D/5.16+8.60
G2 =D/4.22+7.70
G1 =D/1.11+3.30
G3 =D/5.45+9.20
G2 =D/4.39+8.15
G1 =D/1.11+4.37
R2
R1
D

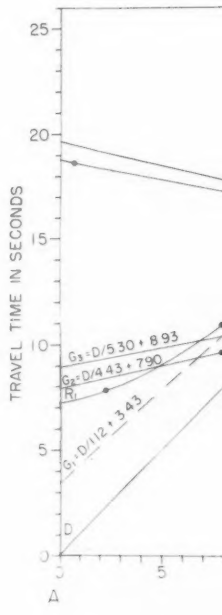
TRAVEL TIME IN SECONDS
G3 =D/5.30+8.93
G2 =D/4.43+7.90
G1 =D/1.12+3.43
R1
D
A

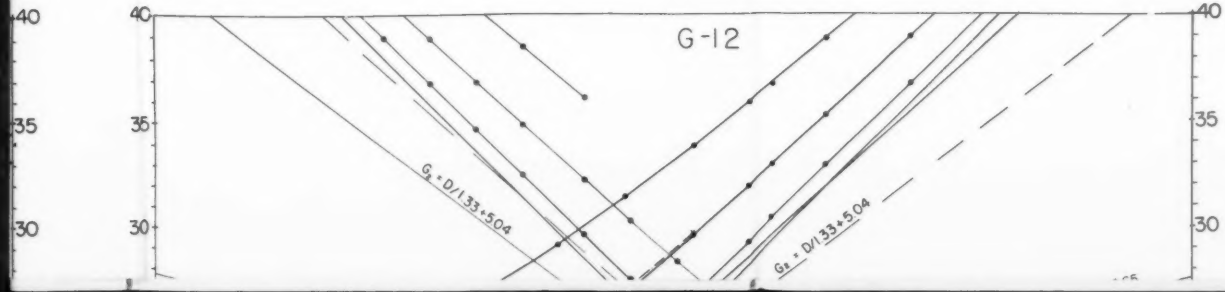
G-12
G2 =D/1.33+5.04
G2 =D/1.33+5.04

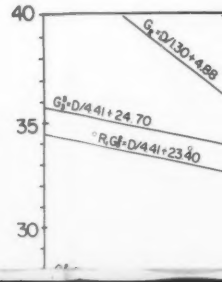
G2 =D/1.30+4.88
G2 =D/4.41+24.70
R G2 =D/4.41+23.40

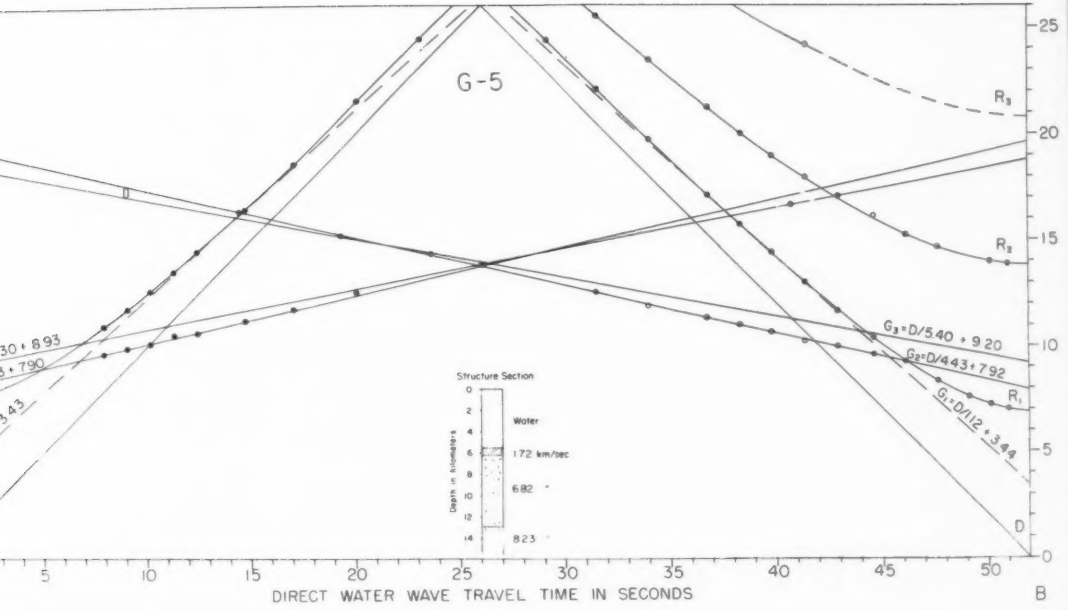
G-5
R3
R2
R1
D
G3=D/5.40 + 9.20
G2=D/4.43+7.92
G1=D/1.12 + 3.44
Structure Section
Depth in kilometers
Water
1.72 km/sec
6.82 "
8.23 "
DIRECT WATER WAVE TRAVEL TIME IN SECONDS
B

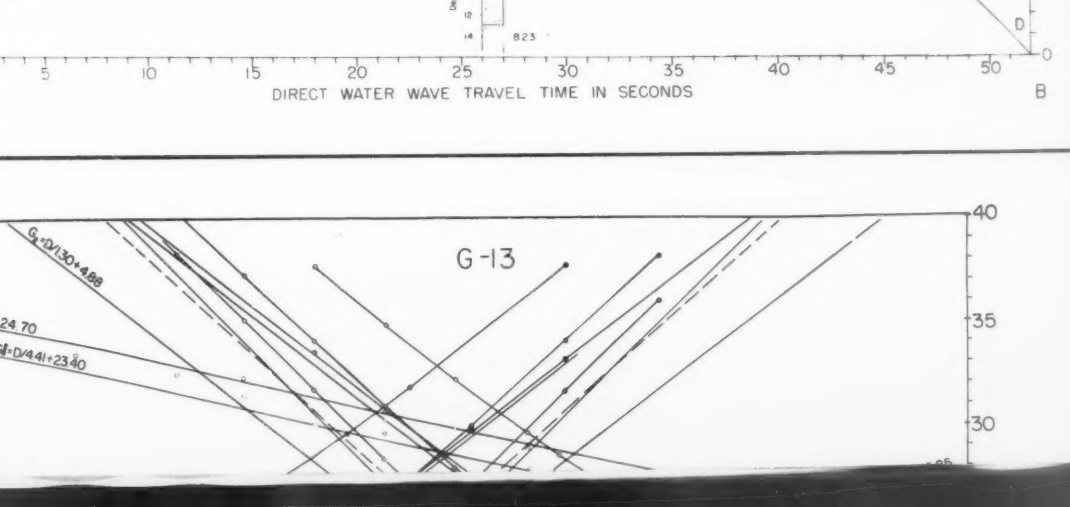
G-13
G=D/1.30+4.88
24.70
=D/4.41+23.40

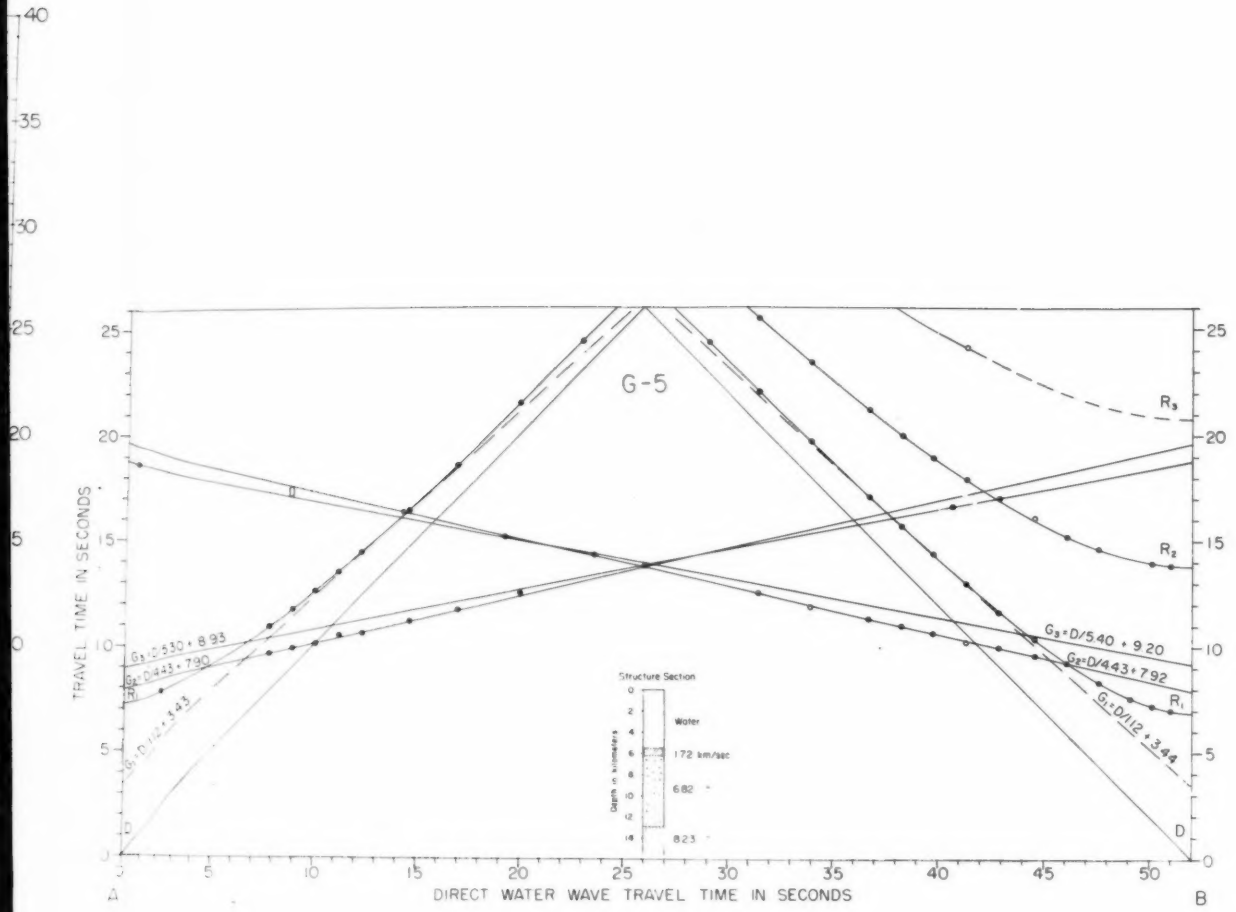
G-5
TRAVEL TIME IN SECONDS
DIRECT WATER WAVE TRAVEL TIME IN SECONDS
A
B
G_3=D/5.30+8.93
G_2=D/4.43+7.90
G_1=D/1.12+3.43
G_3=D/5.40+9.20
G_2=D/4.43+7.92
G_1=D/1.12+3.44
R_3
R_2
R_1
D
Structure Section
Depth in kilometers
Water
1.72 km/sec
6.82
8.23

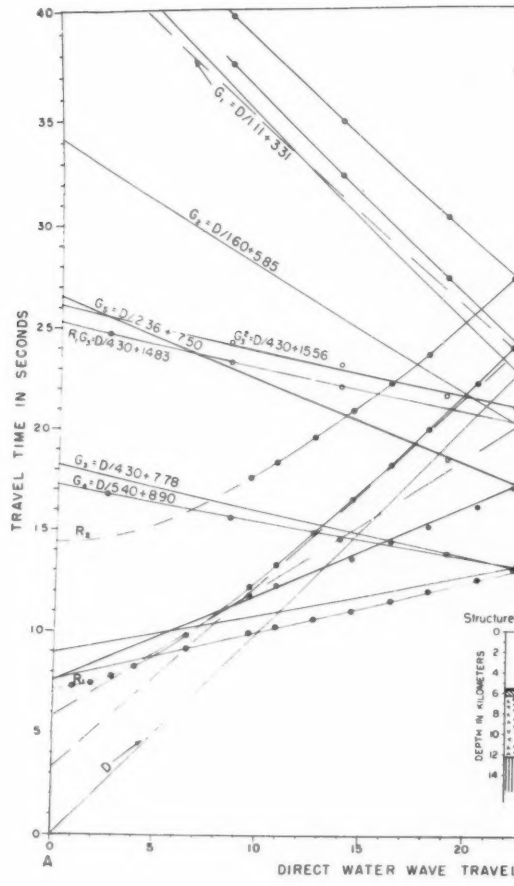
TRAVEL TIME IN SECONDS
G_1=D/1.11+3.31
G_2=D/1.60+5.85
G_3=D/2.36+7.50
R_3G_3=D/4.30+14.83
G_3^2=D/4.30+15.56
G_3=D/4.30+7.78
G_4=D/5.40+8.90
R_2
R_1
D
DIRECT WATER WAVE TRAVEL
Structure
DEPTH IN KILOMETERS

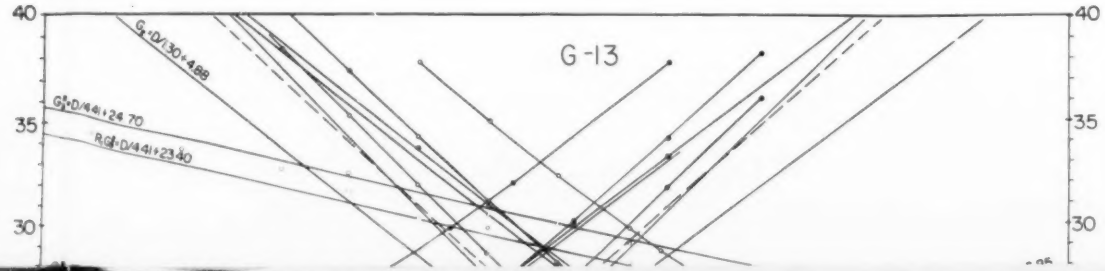
G-13
G_3=D/4.30+4.88
G_2^2=D/4.41+24.70
$R_3G_2^2$=D/4.41+23.40

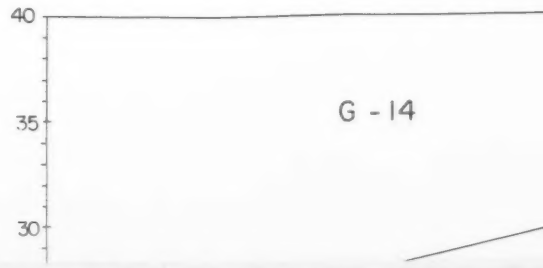
G - 14

Ewing and Ewing, Pl. 3

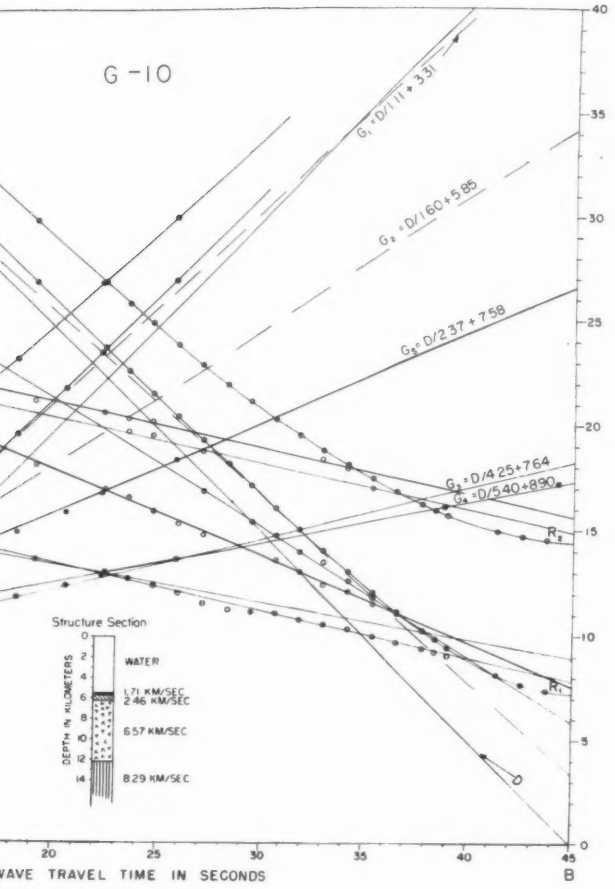

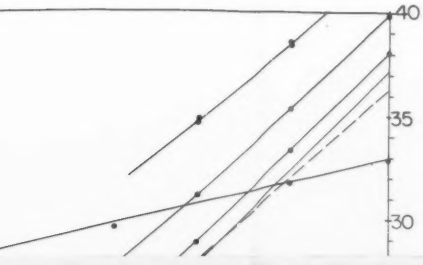

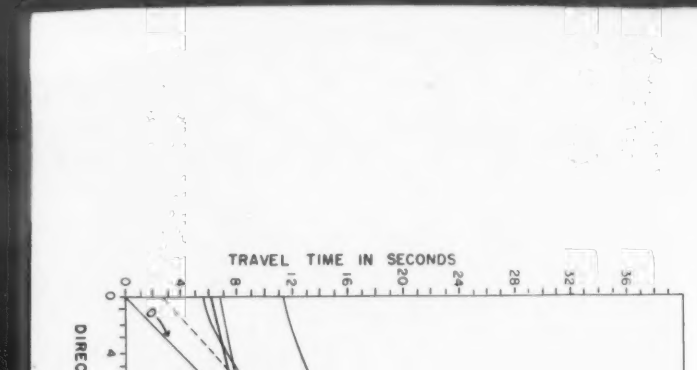
TRAVEL TIME IN SECONDS
0
4
8
12
16
20
24
28
32
36
DIREC

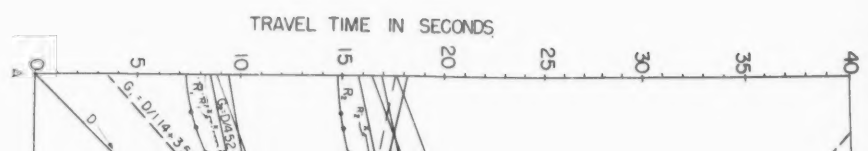
TRAVEL TIME IN SECONDS
0
4
5
10
15
20
25
30
35
40

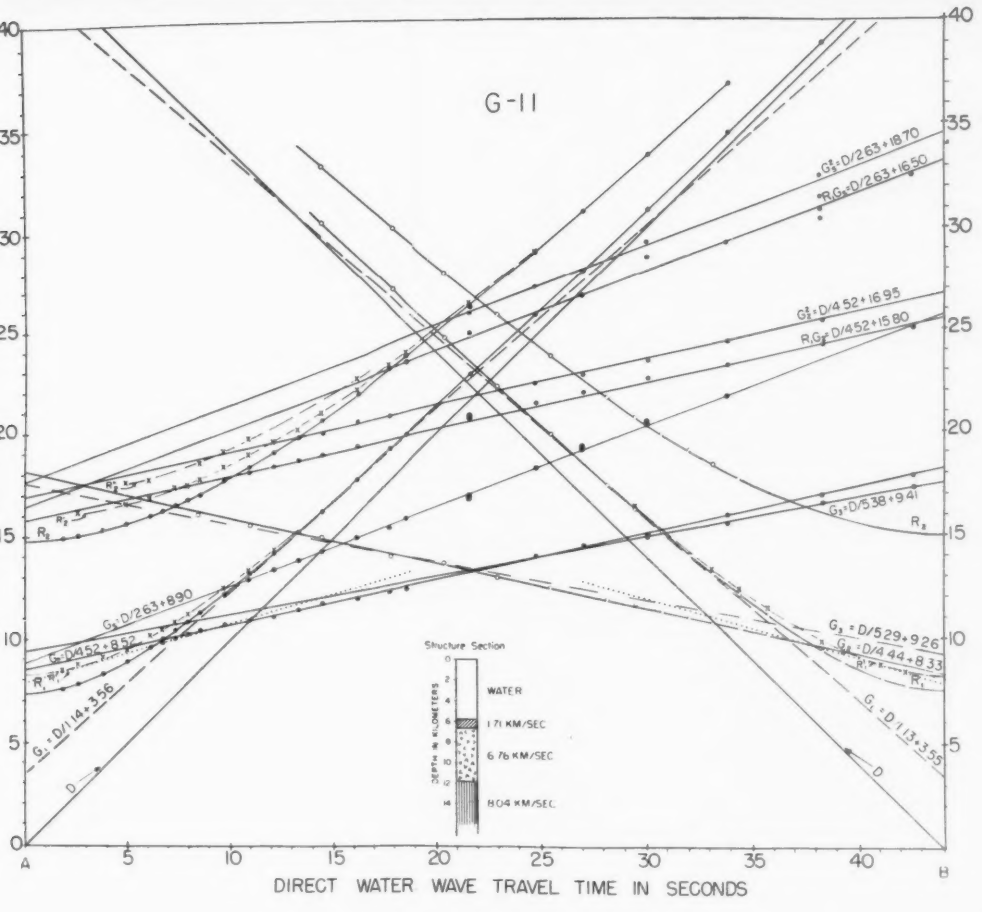
G-11
G_3^1=D/263+1870
RG_2=D/263+1650
G_3^1=D/452+1695
RG_2=D/452+1580
G_3=D/538+941
G_3=D/529+926
G_3=D/444+833
G_1=D/113+355
G_2=D/263+890
G=D/452+852
G_1=D/114+356
Structure Section
WATER
1.71 KM/SEC
6.76 KM/SEC
8.04 KM/SEC
DEPTH in KILOMETERS
DIRECT WATER WAVE TRAVEL TIME IN SECONDS
TRAVEL TIME IN SECONDS

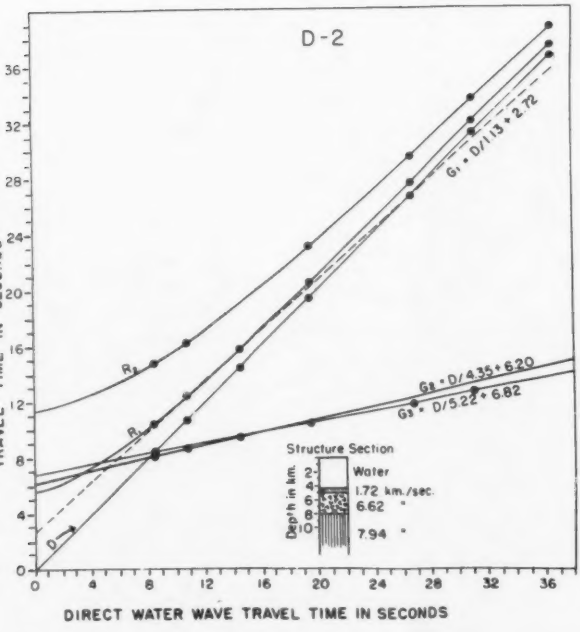
D-2
G_1=D/113+272
G_3=D/435+620
G_3=D/522+682
Structure Section
Water
1.72 km./sec.
6.62 "
7.94 "
Depth in km.
DIRECT WATER WAVE TRAVEL TIME IN SECONDS

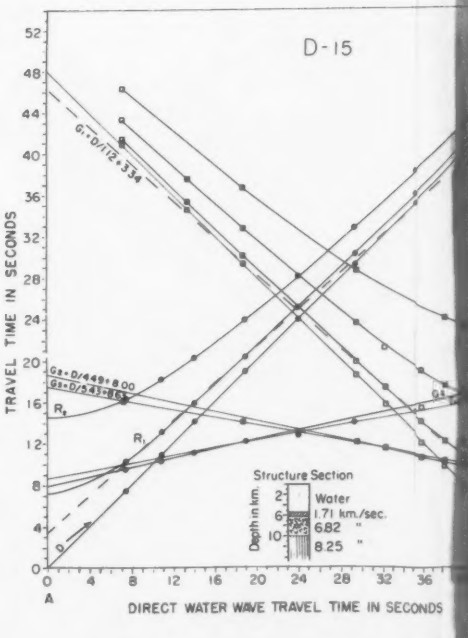
D-15
G_1=D/172+334
G_3=D/449+800
G_3=D/541+665
Structure Section
Water
1.71 km./sec.
6.82 "
8.25 "
Depth in km.
TRAVEL TIME IN SECONDS
DIRECT WATER WAVE TRAVEL TIME IN SECONDS

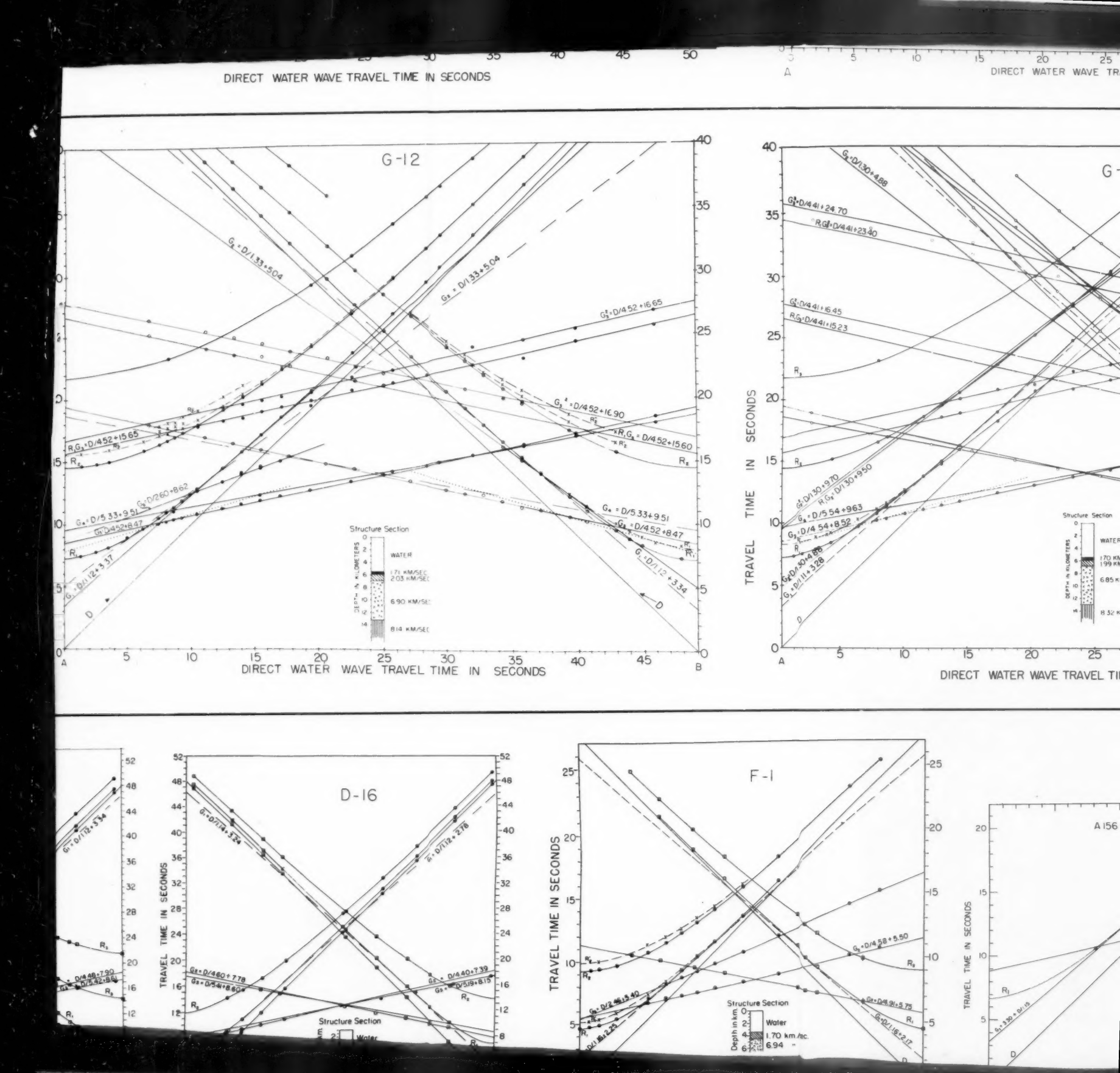
DIRECT WATER WAVE TRAVEL TIME IN SECONDS
G-12
TRAVEL TIME IN SECONDS
DIRECT WATER WAVE TRAVEL TIME IN SECONDS
Structure Section
WATER
1.71 KM/SEC
2.03 KM/SEC
6.90 KM/SEC
8.14 KM/SEC
D-16
F-1
Water
1.70 km./sec.
6.94 "

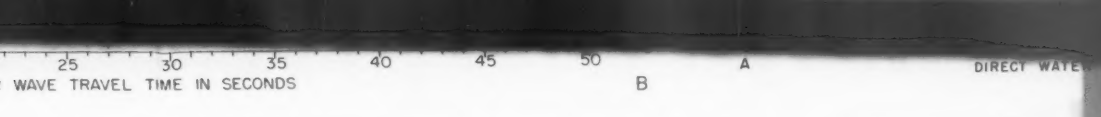
25
30
35
40
45
50
A
DIRECT WATE
WAVE TRAVEL TIME IN SECONDS
B

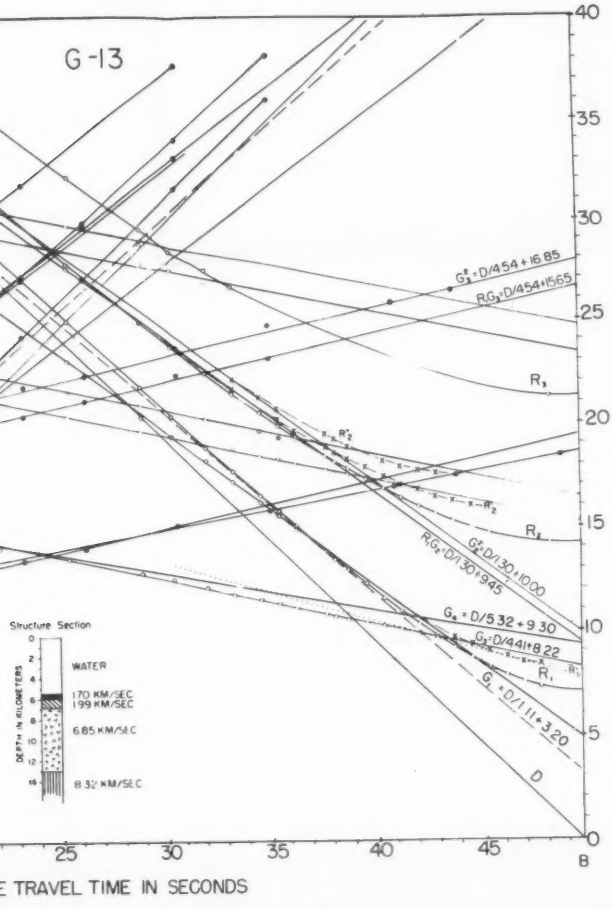
G-13
40
35
30
25
20
15
10
5
0
G_3^2=D/454+16.85
RG$_3$=D/454+1565
R$_3$
R'$_2$
R$_2$
R$_1$G$_2$=D/130+945
G$_2^2$=D/130+1000
G$_3$=D/532+9.30
G$_2$=D/441+8.22
R$_1$
R'$_1$
G$_1$=D/1.11+3.20
D
Structure Section
DEPTH IN KILOMETERS
WATER
1.70 KM/SEC
1.99 KM/SEC
6.85 KM/SEC
8.32 KM/SEC
25
30
35
40
45
B
E TRAVEL TIME IN SECONDS

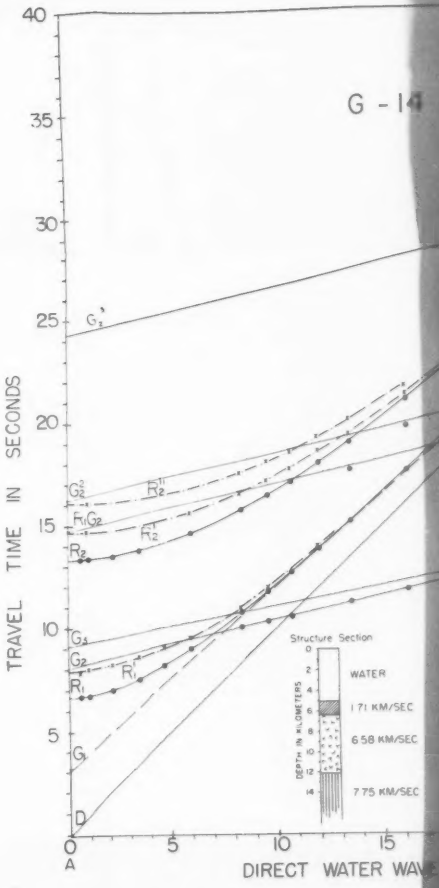
G - 14
40
35
30
25
20
15
10
5
0
TRAVEL TIME IN SECONDS
G$_3$'
G$_2^2$
R'$_2$
R$_1$G$_2$
R'$_1$2
R$_2$
G$_3$
G$_2$
R$_1$
R'$_1$
G$_1$
D
Structure Section
DEPTH IN KILOMETERS
WATER
1.71 KM/SEC
6.58 KM/SEC
7.75 KM/SEC
0
5
10
15
A
DIRECT WATER WAV

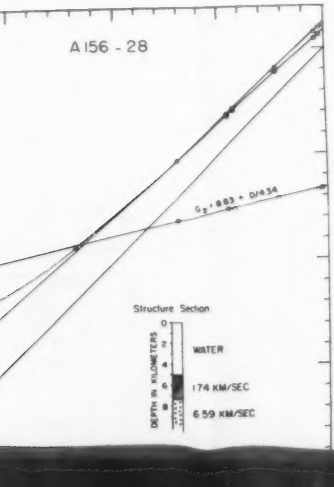
A 156 - 28
G$_2$=.883 + D/434
Structure Section
DEPTH IN KILOMETERS
WATER
1.74 KM/SEC
6.59 KM/SEC

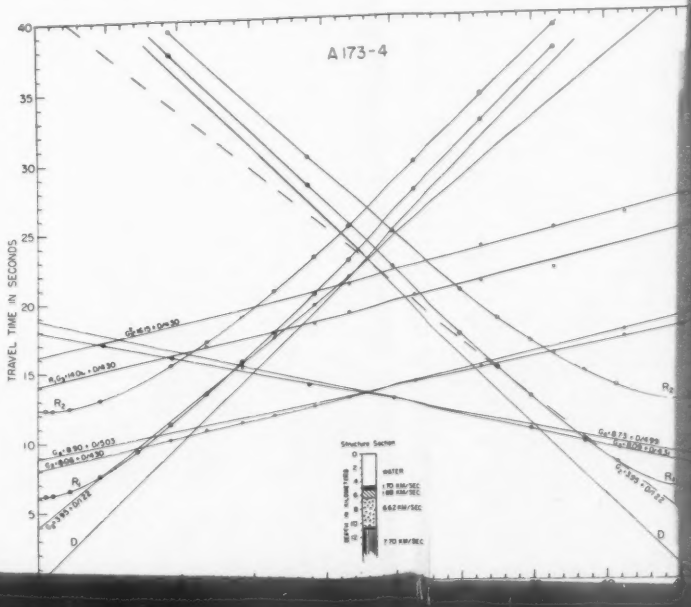
A 173-4
40
35
30
25
20
15
10
5
TRAVEL TIME IN SECONDS
R$_2$
R$_1$
D
Structure Section
DEPTH IN KILOMETERS
WATER
1.70 KM/SEC
6.62 KM/SEC
7.70 KM/SEC

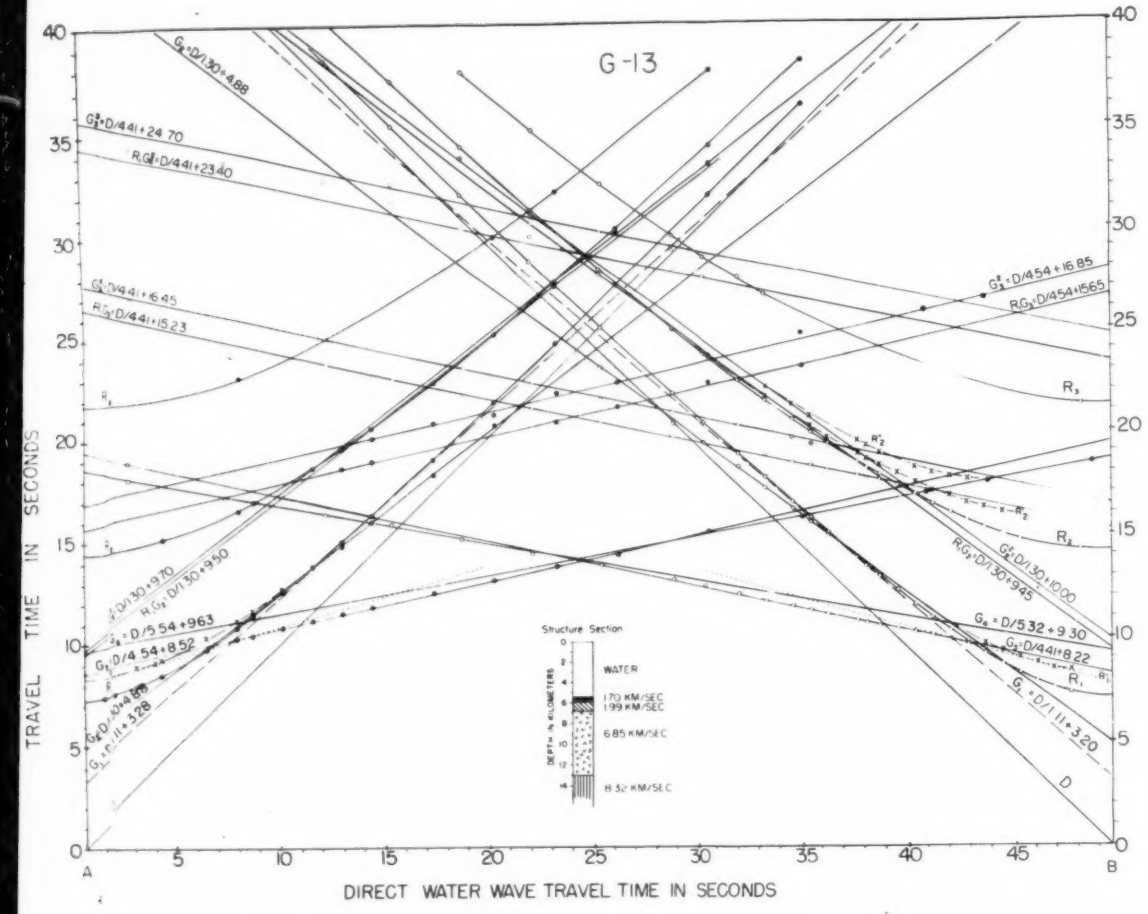
G-13
TRAVEL TIME IN SECONDS
DIRECT WATER WAVE TRAVEL TIME IN SECONDS
A
B
Structure Section
WATER
1.70 KM/SEC
1.99 KM/SEC
6.85 KM/SEC
8.32 KM/SEC
DEPTH IN KILOMETERS

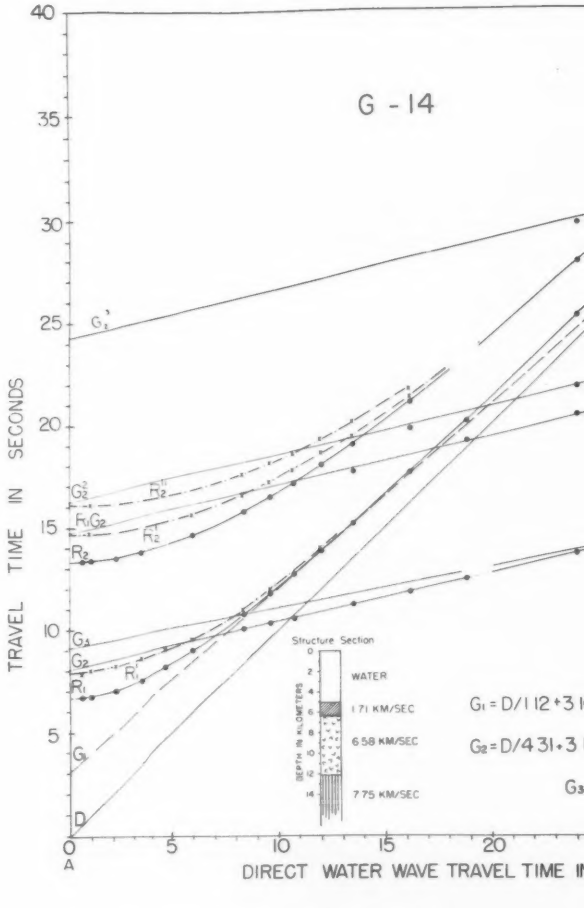
G - 14
TRAVEL TIME IN SECONDS
DIRECT WATER WAVE TRAVEL TIME IN
A
Structure Section
WATER
1.71 KM/SEC
6.58 KM/SEC
7.75 KM/SEC
DEPTH IN KILOMETERS

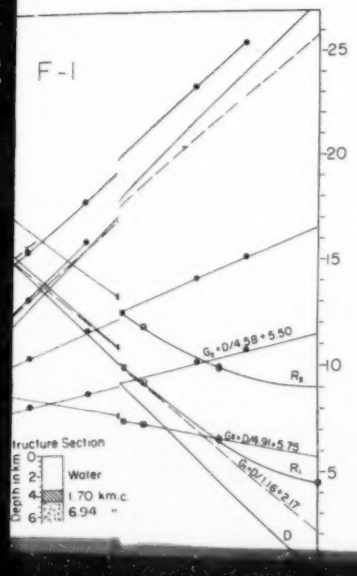
F-1
Structure Section
Water
1.70 km.c
6.94 "

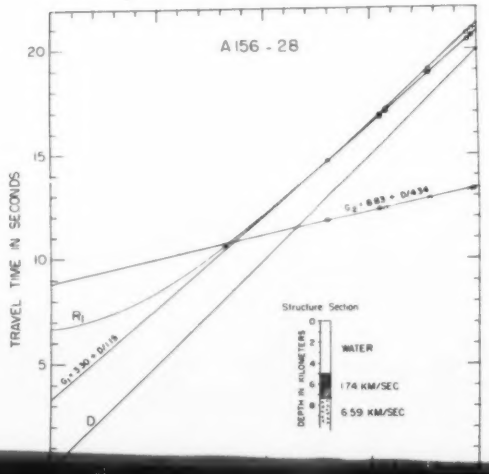
A 156 - 28
TRAVEL TIME IN SECONDS
Structure Section
WATER
1.74 KM/SEC
6.59 KM/SEC
DEPTH IN KILOMETERS

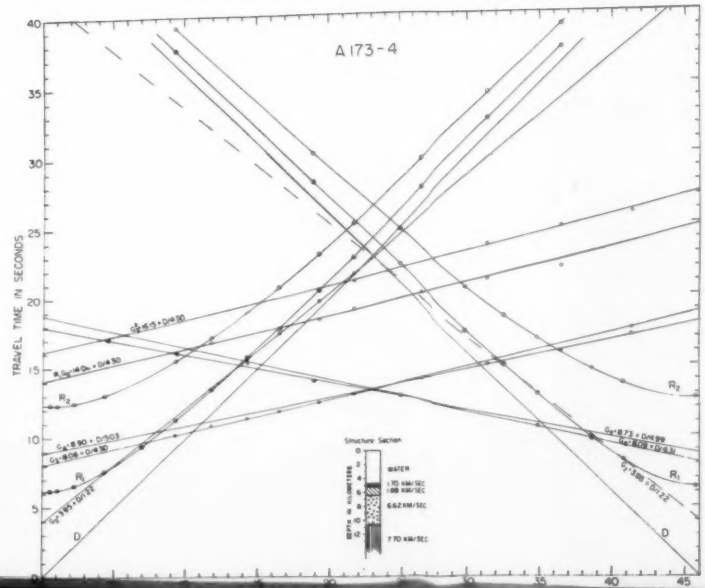
A 173 - 4
TRAVEL TIME IN SECONDS
Structure Section
WATER
1.70 KM/SEC
1.88 KM/SEC
6.62 KM/SEC
7.70 KM/SEC
DEPTH IN KILOMETERS

TRAVEL TIME IN SECONDS

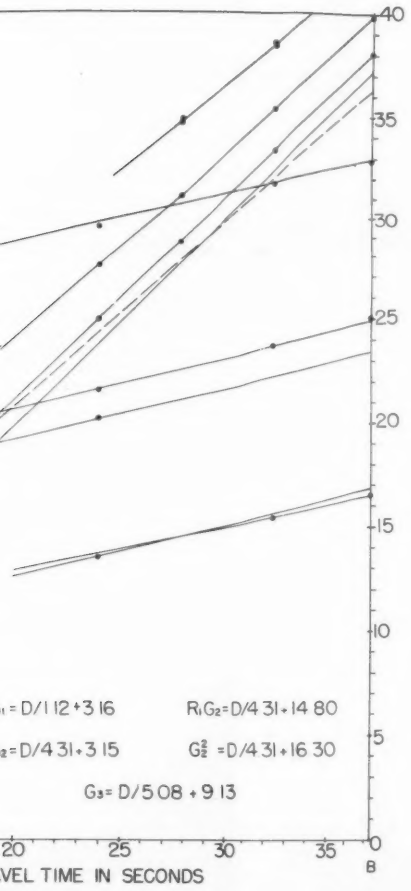
40
35
30
25
20
15
10
5
0
= D/1 12 + 3 16
R1G2 = D/4 31 + 14 80
= D/4 31 + 3 15
G2 = D/4 31 + 16 30
G3 = D/5 08 + 9 13
20
25
30
35
B
VEL TIME IN SECONDS

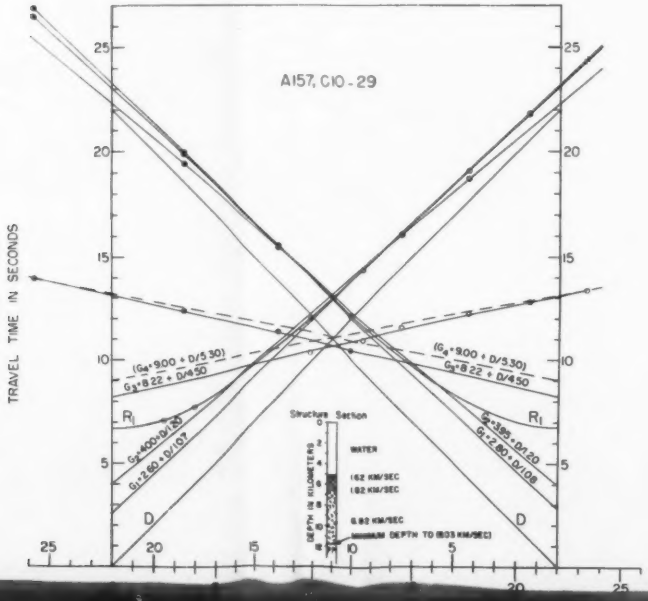
A157, C10 - 29
TRAVEL TIME IN SECONDS
25
20
15
10
5
(G4 = 9.00 + D/5.30)
G3 = 8.22 + D/4.50
R1
G4 = 4.00 + D/1.80
G2 = 2.80 + D/1.07
D
Structure Section
WATER
1.62 KM/SEC
1.82 KM/SEC
6.82 KM/SEC
MINIMUM DEPTH TO (8.03 KM/SEC)
DEPTH IN KILOMETERS
G4 = 3.99 + D/1.20
G2 = 2.80 + D/1.08

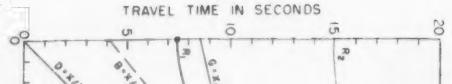
TRAVEL TIME IN SECONDS
0
5
10
15
20

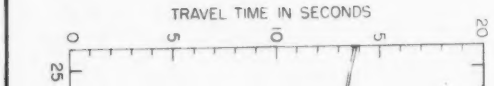
TRAVEL TIME IN SECONDS
0
5
10
5
20
25

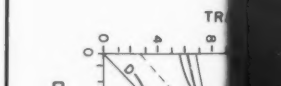
TR
0
4
8

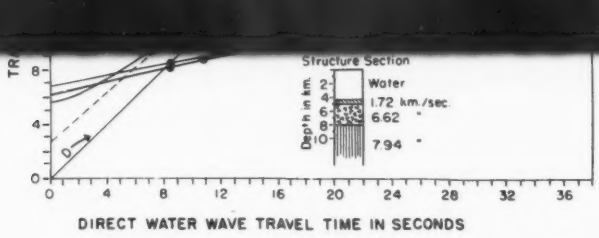
Structure Section
Depth in km.
Water
1.72 km./sec.
6.62 "
7.94 "
DIRECT WATER WAVE TRAVEL TIME IN SECONDS

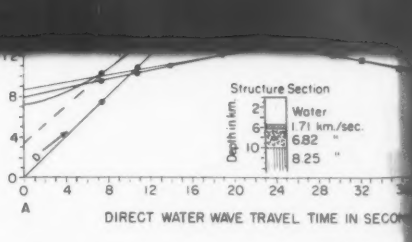
Structure Section
Depth in km.
Water
1.71 km./sec.
6.82 "
8.25 "
DIRECT WATER WAVE TRAVEL TIME IN SECON

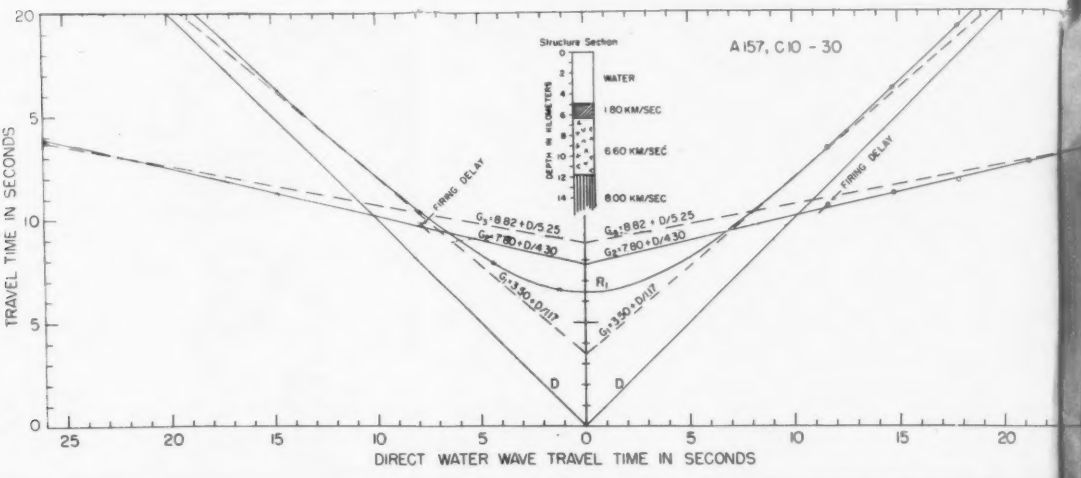
A 157, C10 - 30
Structure Section
DEPTH IN KILOMETERS
WATER
1.80 KM/SEC
6.60 KM/SEC
8.00 KM/SEC
FIRING DELAY
FIRING DELAY
R1
D
D
TRAVEL TIME IN SECONDS
DIRECT WATER WAVE TRAVEL TIME IN SECONDS

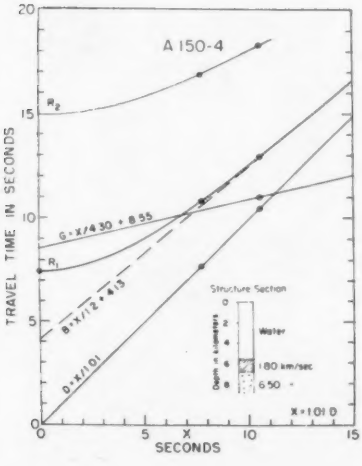
A 150-4
R2
R1
Structure Section
Water
1.80 km/sec
6.50 "
X=1.01 D
TRAVEL TIME IN SECONDS
X
SECONDS

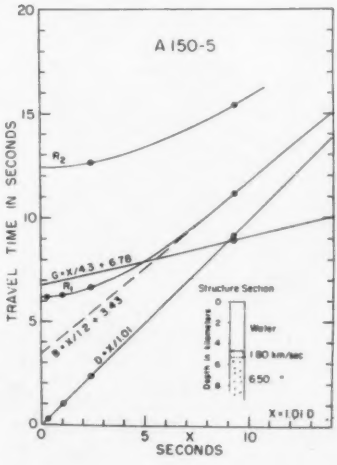
A 150-5
R2
R1
Structure Section
Water
1.80 km/sec
6.50 "
X=1.01 D
TRAVEL TIME IN SECONDS
X
SECONDS

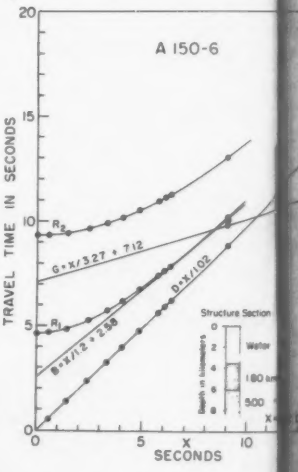
A 150-6
R2
R1
Structure Section
Water
TRAVEL TIME IN SECONDS
X
SECONDS

32
36

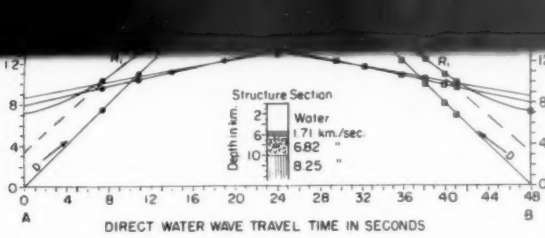
Structure Section
Depth in km.
Water
1.71 km./sec.
6.82 "
8.25 "
A
B
DIRECT WATER WAVE TRAVEL TIME IN SECONDS

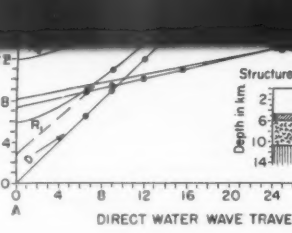
Structure
Depth in km.
DIRECT WATER WAVE TRAVE

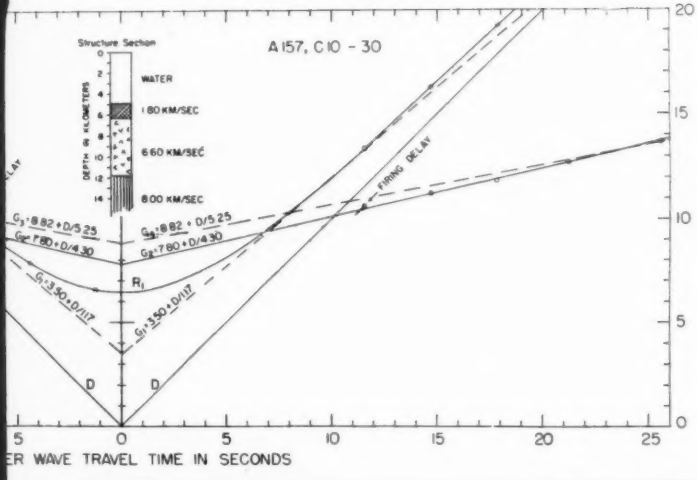
A 157, C 10 - 30
Structure Section
WATER
1.80 KM/SEC
6.60 KM/SEC
8.00 KM/SEC
FIRING DELAY
R1
D
ER WAVE TRAVEL TIME IN SECONDS

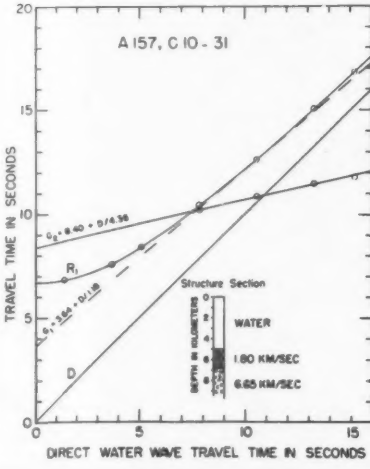
A 157, C 10 - 31
TRAVEL TIME IN SECONDS
Structure Section
WATER
1.80 KM/SEC
6.65 KM/SEC
R1
D
DIRECT WATER WAVE TRAVEL TIME IN SECONDS

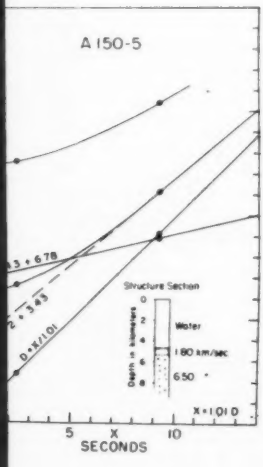
A 150-5
Structure Section
Water
1.80 km/sec
650 "
X=1.01 D
SECONDS

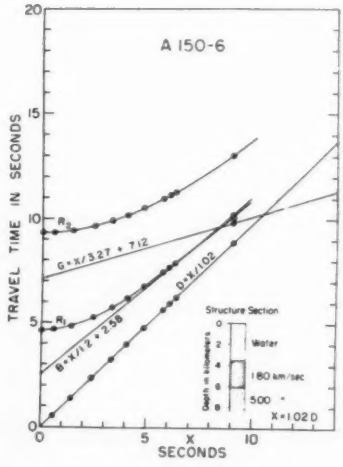
A 150-6
TRAVEL TIME IN SECONDS
R2
R1
G=X/3.27 + 7.12
D=X/1.02
Structure Section
Water
1.80 km/sec
500 "
X=1.02 D
SECONDS

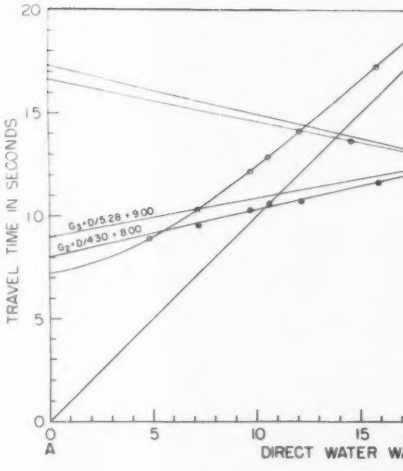
TRAVEL TIME IN SECONDS
G3=D/5.28 + 9.00
G2=D/4.30 + 8.00
A
DIRECT WATER WA

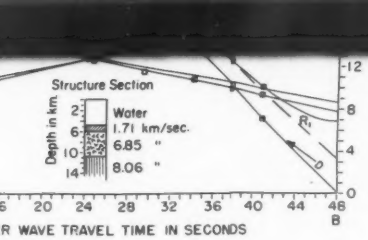

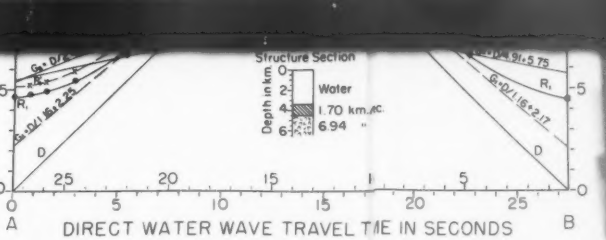

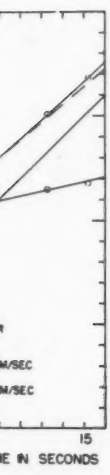

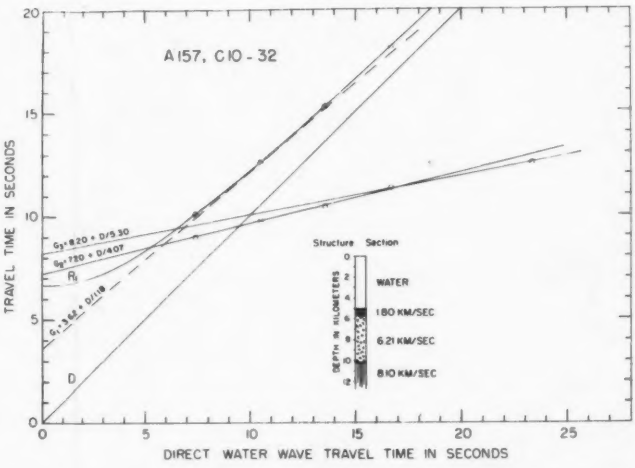

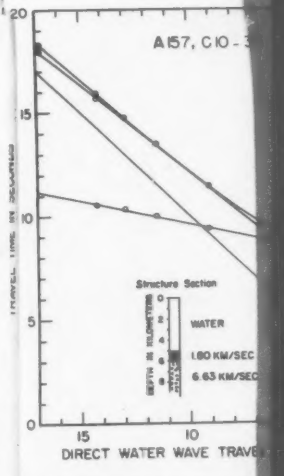

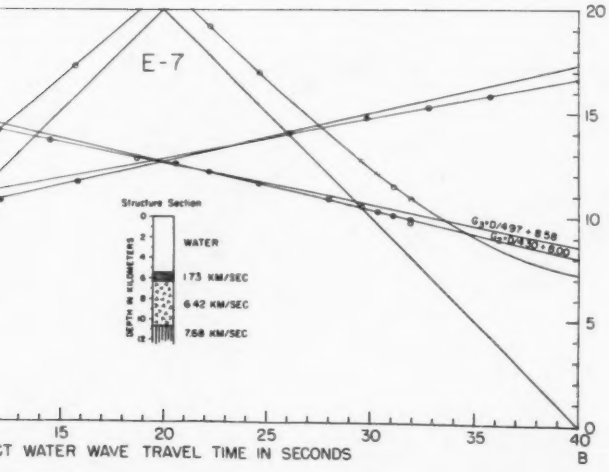

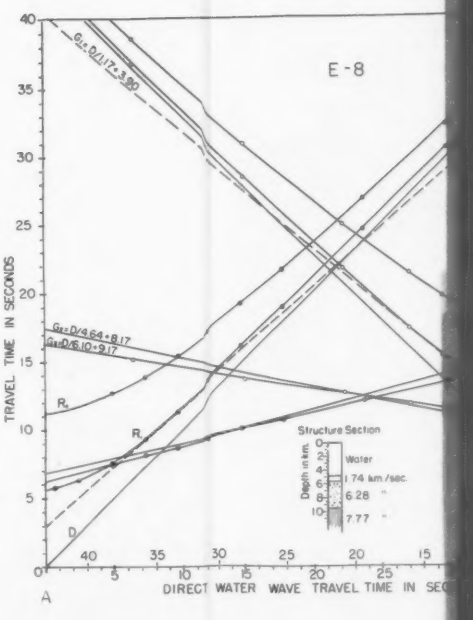

TRAVEL-TIME GRAPHS, WESTE

Distance on the abscissa is plotted in increments of direct water-wave time, *i. e.*, 1 second is approximately 5000 feet. The lines G_1, G_2, G_3 ....

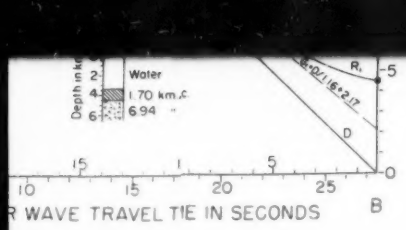

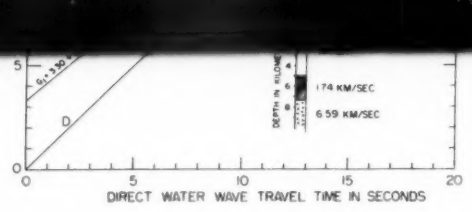

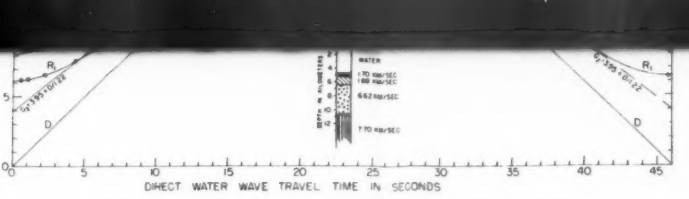

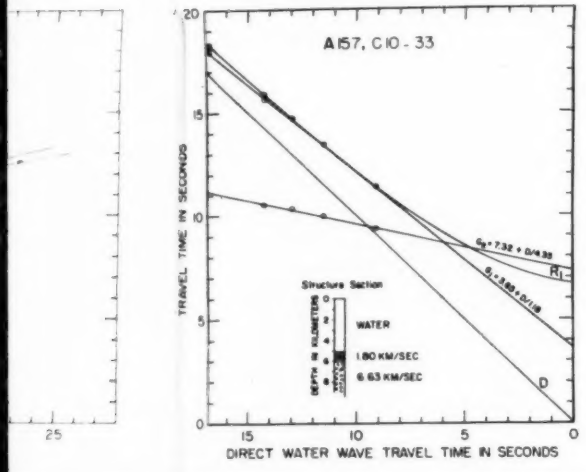

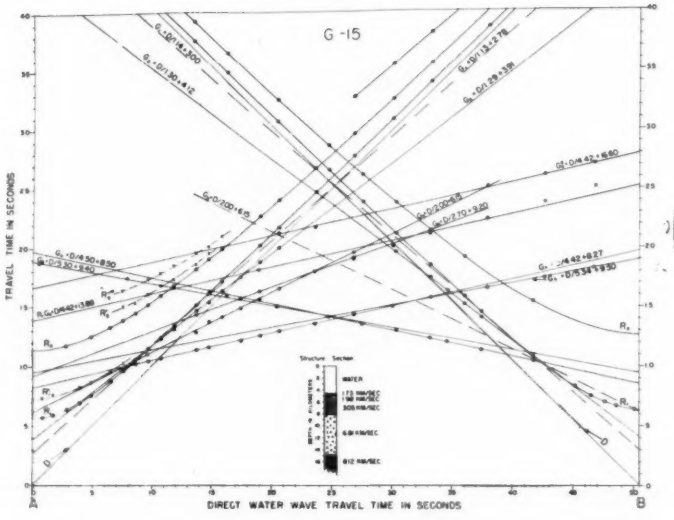

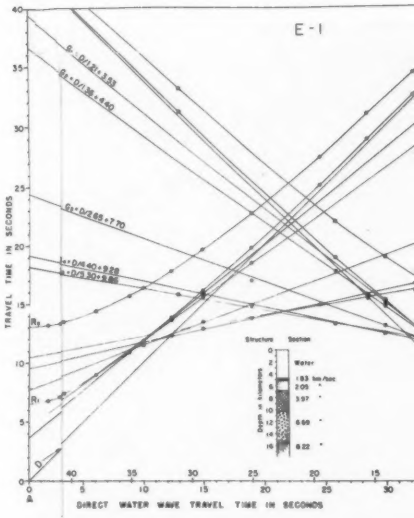

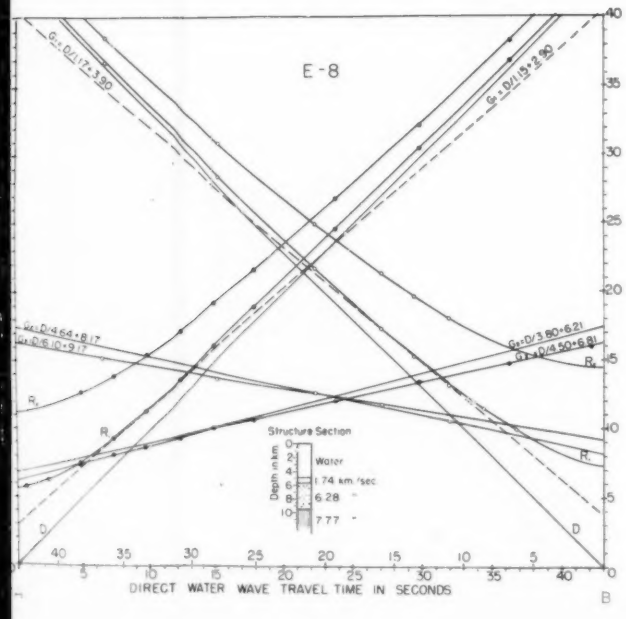

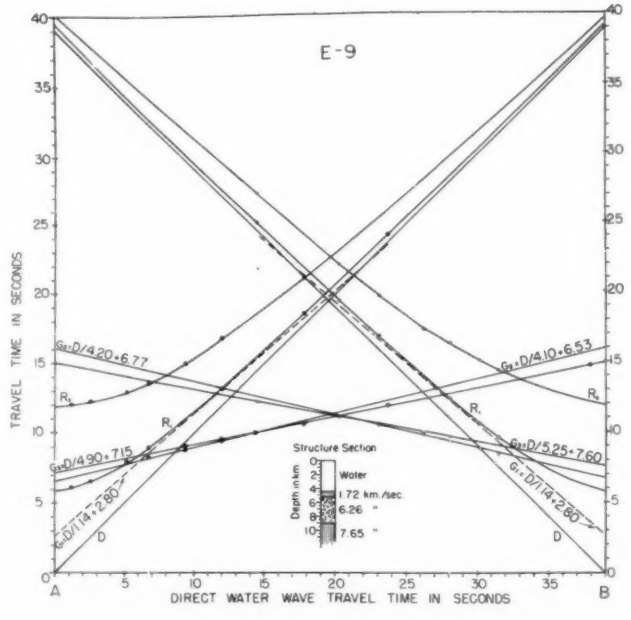

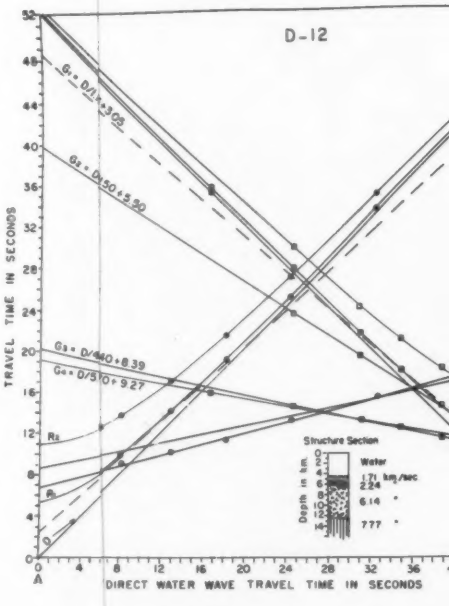

IE GRAPHS, WESTERN AND EASTERN OCEAN BASINS

e abscissa is plotted in increments -wave time, *i. e.*, 1 second is 00 feet. The lines G_1. G_2. G_3 .... are determined by refracted arrivals in successive layers beneath the ocean floor. When G is dashed or absent, the velocity in the top layer was assumed.

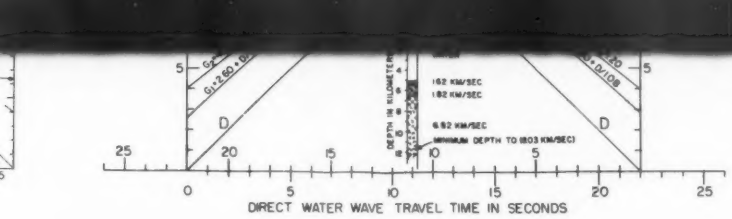
1.62 KM/SEC
1.82 KM/SEC
6.92 KM/SEC
MINIMUM DEPTH TO (8.03 KM/SEC)
DEPTH IN KILOMETERS
D
D
DIRECT WATER WAVE TRAVEL TIME IN SECONDS

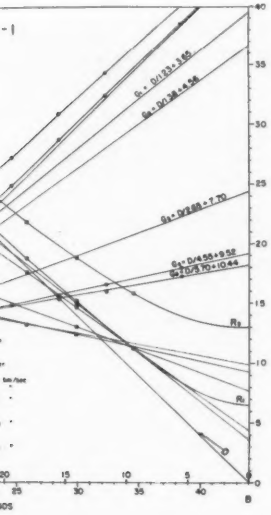

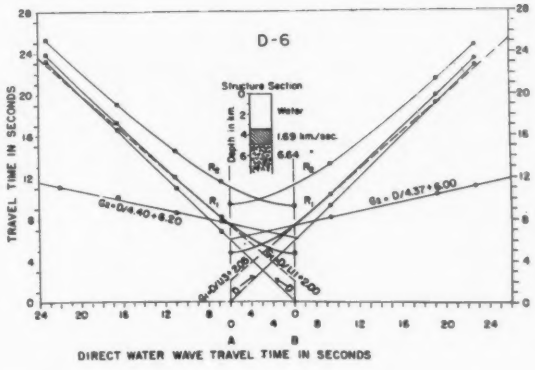
D-6
Structure Section
Water
1.69 km/sec.
6.64 "
Depth in km
TRAVEL TIME IN SECONDS
DIRECT WATER WAVE TRAVEL TIME IN SECONDS

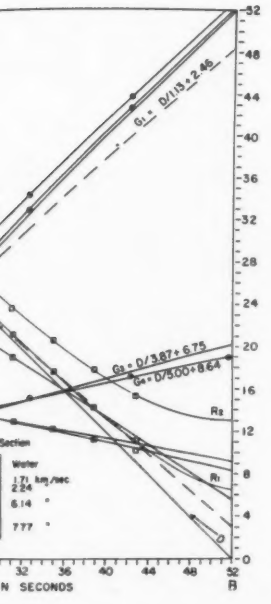

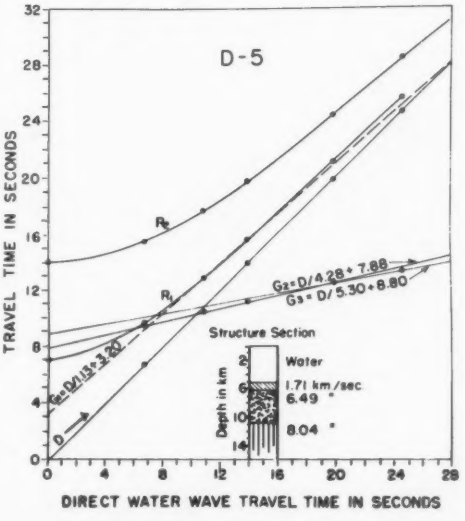
D-5
TRAVEL TIME IN SECONDS
Structure Section
Water
1.71 km/sec
6.49 "
8.04 "
Depth in km
DIRECT WATER WAVE TRAVEL TIME IN SECONDS

an important change in events in the history of the area.

Seismic results from the deeper parts of the Caribbean show about 2 km of low-velocity sediment, 2–4 km of consolidated sedimentary or igneous rocks, and a crustal velocity of 6–7 km/sec (J. I. Ewing, J. F. Hennion, and C. B. Officer (in preparation)).

In the deeper part of the Gulf of Mexico approximately 6 km of sediment overlies crustal rocks with velocities of 5–6 km/sec (Ewing *et al.*, 1955).

In all three basins there is great need for information about the crustal thicknesses and the subcrustal velocities.

Mid-Atlantic Ridge

The Mid-Atlantic Ridge extends the full length of the north and south Atlantic oceans, approximately equidistant from the bordering continents. It is a broad swell, several hundred miles wide, with a rugged crest which rises about 2000 fathoms above the eastern and western Atlantic basins. Ewing and Heezen (1956) have suggested that this ridge extends into the Arctic Ocean in one direction and into the Indian and Pacific oceans in the other. They have pointed out that practically all available sounding traverses of this ridge are characterized by a median rift zone which follows the crest of the ridge very accurately, and that, within the accuracy of epicentral determinations, the earthquake belt coincides with the median rift.

Olivine basalts are the predominant rocks of the volcanic islands of this ridge system. Hess (1954, p. 344) has pointed out that "Peridotite xenoliths are the only foreign rocks brought to the surface in volcanoes on the ridges, and peridotite is known to outcrop at two points on the Mid-Atlantic Ridge."

Despite similarities with the cordilleran mountain systems in length, height, and general pattern the Mid-Atlantic Ridge shows no evidence of andesite or of geosynclinal development. Seismic-refraction measurements on the ridge have been difficult on account of the great topographic relief, but definitive results are now available.

Station D-13 (*Pl.* 4)

This station is on the eastern flank of the Mid-Atlantic Ridge at about the latitude of Bermuda. The water depth along the shot lines varied by as much as 700 fathoms, and corrections were applied to the ground-wave arrivals to remove the effects of topographic variations from the mean depth of 2000 fathoms (3.66 km). The structure section determined here consists of a thin layer of low-velocity sediments (0.39 km), 3.12 km of material with velocity 5.01 km/sec, and a substratum with velocity 7.21 km/sec. The 5.01 km/sec layer is determined only in the *B* profile, and that determination is not good, owing to an uncertain time break on the closest shot. Because of the exceptionally rough topography and the failure to record shots at close range, the upper part of the structure section reported here may be inaccurate. The *B* profile indicates that very little unconsolidated sediment is present, since the line representing the 5 km/sec layer is approximately tangent to R_1. Therefore the assumed G_2 line in the *A* profile was drawn with the lowest possible intercept, indicating a minimum thickness of sediments there. Additional evidence for a thin sedimentary cover at *A* lies in the fact that the receiving position was over a 500-fathom peak.

Station D-14 (*Pl.* 4)

This station is on the western flank of the Mid-Atlantic Ridge about 370 miles west of station D-13. Although the bottom topography was rough, topographic corrections to the mean depth of 1750 fathoms (3.20 km) produced good alignment of the points on the travel-time graph.

As at station D-13, the failure to record shots at close range has resulted in uncertainty about the upper part of the structure section. The velocity in the deep refracting layer (7.27 km/sec) was well determined, but the velocity in the material above was not. The dashed lines (G_2) represent a layer approximately 2 km thick (velocity 4.97 km/sec) which could be present but undetected. Assuming that the remainder of the overlying material is unconsolidated sediment with a velocity of 1.7 km/sec, the thickness was computed to be 0.56 km.

Station D-3 (*Pl.* 4)

This is an unreversed station near the crest of the Mid-Atlantic Ridge at Lat. 30.4° N. The water depth under the receiving position was 1500 fathoms (2.74 km), and the bottom sloped down uniformly from west to east at an angle of 1.4°.

Two refracting layers were found here, indicated on the travel-time graph by the lines $G_2 = D/3.30 + 3.75$ and $G_3 = D/4.50 + 4.42$. These represent velocities of 5.38 and 7.42 km/sec after slope correction. The thickness of the overlying sedimentary layer is computed to be 0.22 km assuming a velocity of 1.72 km/sec.

Station D-4 (*Pl.* 4)

This unreversed station is slightly east of the crest of the Mid-Atlantic Ridge at Lat. 30.5° N. The water depth along the shot line was fairly constant, near 1750 fathoms (3.21 km). The four recorded shots determine a line on the travel-time graph representing a velocity of 6.26 km/sec. The dashed line $G_2 = D/3.00 + 4.40$ represents a layer with apparent velocity 4.55 km/sec which could be present but was undetected because of the lack of shots at close ranges. The sedimentary thickness is calculated to be 0.31 km assuming that the velocity is 1.72 km/sec and that the 4.55 km/sec layer is present.

Station A-152 - 18 (*Pl.* 4)

This unreversed station is on the western flank of the Mid-Atlantic Ridge at about Lat. 35° 47′ N.

This station and station A-152-17 were made by the whaleboat technique (Tolstoy *et al.*, 1953); hence water depth is known only from an echo-sounding survey made subsequently, and no detailed topographic corrections are made. The water depth was about 1800 fm (3.3 km), the sediment-layer thickness was 0.2 km (assuming a velocity of 1.70 km/sec), and the apparent velocity in the refracting layer is 5.23 km/sec.

Station A-152 - 17 (*Pl.* 4)

This unreversed whaleboat station is near the crest of the Mid-Atlantic Ridge in a depth of about 1300 fm (2.36 km). The sediment-layer thickness is 0.58 km (assuming a velocity of 1.70 km/sec), and the apparent velocity in the refracting layer is 6.08 km/sec.

Stations A-180, KM-1-1 through 7 (*Pl.* 4)

These seven stations were made along a traverse across the Mid-Atlantic Ridge south of the Azores. The topographic section and the seismic results are shown in Figure 2. Because of the rough topography on the ridge, the accuracy of the individual measurements is not high; but, since reasonably consistent results have been obtained at most of the stations, the major structural features are probably approximately as shown in the generalized cross section, (Fig. 3).

The arrival times were corrected in the normal manner (assuming all interfaces to be parallel to the bottom topography) for stations 2, 3, 6, and 7. For stations 1 and 4, the uncorrected plots indicated that an appreciable amount of unconsolidated sediment was present at the west end while high-velocity rocks outcropped at the east end. Therefore, the arrival times at these stations were corrected to conform to horizontal layering for the purpose of computing thicknesses; then the interfaces were adjusted in the section to show the amount of relief indicated by the uncorrected measurements. At station 5, in order to obtain a satisfactory reverse and a satisfactory alignment of the points, it was necessary to assume that the receiving ship at the west end of the line drifted over a peak. This cannot be confirmed because of lack of soundings by the receiving ship, but it is probable in view of the known topography and direction of drift.

Station F-10 (*Pl.* 4)

This station is on the Mid-Atlantic Ridge at about 52° 40′ N. Lat. The water depth increased from 1600 fathoms (2.93 km) at the eastern end, *A*, to 2100 fathoms (3.84 km) at the western end, *B*. Great topographic relief was encountered along the shot lines, and the arrival times have been corrected as usual on the assumption that the same relief exists in the refracting layer. The alignment of the points on the travel-time graph is improved by the topographic correction, but there are still some fairly large residuals.

The average thickness of the sediments was 0.78 km (assuming a velocity of 1.72 km/sec), and the measured velocity for the underlying rock is 7.36 km/sec. Possibly the section should include an additional layer 1–2 km thick with a velocity between 4.5 and 5.5 km/sec. There is no indication of a break into a higher velocity even on the longest shot which is at a range of 70 km. Assuming that the charge size (220 pounds) on the longest shot was sufficient to penetrate the mantle, it was calculated that the minimum depth at which a velocity of 8.0 km/sec (assumed mantle velocity) would be found is 12.0 km below sea level.

Station E-3 (*Pl.* 4)

Both sets of seismograms were very good at this station, producing one of the best refraction stations to date on the Mid-Atlantic Ridge. It is located on the western flank of the ridge about 400 miles southwest of Iceland. The shot lines were run parallel to the trend of the ridge in order to reduce to a minimum complications introduced by topographic irregularities, and, although the bottom was rough, the water depth did not change appreciably from the average of 830 fathoms (1.52 km).

Two refracting layers showed velocities of 5.60 and 7.24 km/sec respectively. The sedimentary cover was 0.38 km thick, assuming a velocity of 1.70 km/sec. The average thickness of the upper refracting layer was 2.86 km.

Strong arrivals identified as transformed shear waves traveling in the deeper refracting layer were recorded at both receiving positions. These determine the lines on the travel-time graph represented by the equations $G_s = D/2.50 + 3.43$ and $G_s = D/2.45 + 3.17$. The ratio of compressional to shear velocity is 1.99. Although this number is higher than average, the identification of these arrivals as other than transformed shear waves is not possible in view of the velocity and time intercept—*i.e.*, their identification as compressional waves in another layer would result in negative values in the calculation of layer thickness.

The travel-time graph shows that the intercepts of the shear-wave lines are higher than those of the corresponding compressional-wave lines. This relationship can exist only if the transformation from compressional to shear waves occurs at a level higher than the depth of horizontal refraction. In the present case, it would not have been possible to observe shear waves transformed from compressional waves at the interface between the two high-velocity layers since the velocity of shear waves in the lower layer is less than that of compressional waves in the upper one. Here the propagation is compressional in the water and sediments, and shear in both refracting layers; horizontal refraction takes place in the deeper layer. A calculation based on this interpretation gives the depth to the 7.24 km/sec layer as 4.52 km as compared with 4.67 km computed from compressional arrivals.

Station E-4 (*Pl.* 4)

This is a good reversed station about 150 miles northeast of Station E-3. The shot lines were run parallel to the trend of the ridge near the crest. As at Station E-3, the bottom along the shot lines was rough but with no general slope. The average water depth was 750 fathoms (1.37 km).

The average sedimentary thickness is 0.39 km calculated for an assumed velocity of 1.75 km/sec. Although the velocities found here are somewhat higher than at Station E-3 (5.83 and 7.63 *vs.* 5.60 and 7.24 km/sec), they probably represent the same layers.

Some of the records from the *B* profile showed large-amplitude second and third arrivals, some of which can be interpreted as transformed shear waves traveling in the sub-basement, as at Station E-3, and others as twice-refracted compressional waves.

Figure 4 shows a north-south structure section along the crest of the Mid-Atlantic Ridge south of Iceland. Although the extrapolation over such a great distance is speculative, the results indicate that the 5-km/sec layer, presumably volcanic rock, thickens toward Iceland. At Station F-10, this layer is either absent or masked, and if masked it is not thicker than 1–2 km.

Station E-5 (*Pl.* 4)

This station is about 240 miles south of Iceland. The shot lines were run in a north-south direction with the water depth nearly constant at 1300 fathoms (2.38 km). The structure section consists of unconsolidated sediments (1.72 km/sec assumed), semiconsolidated sediments (1.94 km/sec), and two deeper layers with velocities of 5.71 km/sec and 7.47 km/sec respectively. The thickness of the sedimentary layers is about 1 km, that of the 5.71 km/sec layer about 2.8 km.

Although soundings showed no appreciable change in depth along the shot lines, some of the points on the travel-time graph have large residuals. This is probably the result of relief, in one or both of the refracting layers, which has been obscured by the sediments. A conspicuous example is the region 10–20 seconds from point *A* where the lines for the 7.47 km/sec layer are offset by 0.3 sec. The most plausible structural interpretation is that the offset represents a graben fault or synclinal feature in which the vertical displacement is on the order of 0.5 km.

Possibly an additional line with an inverse slope of 1.9–2.1 should be drawn in the *A* profile passing through the first ground-wave point. This arrival, which is quite distinct and plots conspicuously low on the travel-time graph, may indicate an additional layer with a velocity around 3 km/sec beneath the semiconsolidated sediments. However, in view of rather large residuals elsewhere in this station, believed to be due to relief in the refracting layers, this was not considered sufficient evidence for another layer.

Station E-6 (*Pl.* 4)

This station is near the tip of the prominent topographic rise which extends southwesterly from Rockall Bank. The water depth decreased slightly from north to south (*A* to *B*). The *A* profile was well recorded, but unfortunately the close-range shots in the *B* profile were too small to penetrate to the deeper layers. The shots at ranges of 7.5 and 9.8 sec gave clear arrivals from the semiconsolidated sediments but were apparently not strong enough to reach the deeper layers.

Four layers are determined here. The unconsolidated sediments are 0.87 km thick with a velocity of 1.81 km/sec, and the semiconsolidated layer is 1.24 km thick with a velocity of 2.79 km/sec. The basement and sub-basement velocities are 5.80 and 7.43 km/sec respectively in the two deeper layers—significantly close to the velocities found at stations E-3, E-4, and E-5. This similarity of crustal layering is as striking as the similarity in rock types in this part of the Brito-Arctic petrographic province (Turner and Verhoogen, 1951, p. 188).

Three profiles about 120 miles east of this location (Hill, 1952) show a velocity of 2.5 km/sec for the semiconsolidated sediments, 5.0 km/sec as the average of three determinations of the velocity in the upper refracting layer, and 6.3 km/sec as the average of two velocity determinations for the lower refracting layer.

Station A-173-5 (*Pl.* 4)

This station is over a lesser peak on the northern flank of Bermuda. It is included in the section on the Mid-Atlantic Ridge on the basis of structural similarity. As shown in the structure section, a satisfactory interpretation of the data is that two velocities were measured: 4.04 km/sec and 5.36 km/sec. An alternate interpretation, perhaps equally as good, is that only one kind of material is present, and the velocity in it is between the values listed above.

Because of the rough topography, it was not possible to determine whether or not any low-velocity sediments were present. If so, there could be only a thin layer.

DISCUSSION OF RESULTS: The crustal layering in the Mid-Atlantic Ridge is significantly different from that under the adjacent ocean basins. The ridge structure and the comparison with ocean-basin structure is shown in the cross sections (Figs. 2, 3, 4, 5). The oceanic layer is believed to be olivine basalt. This belief is based principally on the fact that the rocks brought up in oceanic volcanoes throughout the world are predominantly olivine basalts. Since these rocks also are the predominant constituent of the exposed portions of the Mid-Atlantic Ridge, the view is taken that the ridge has been built by volcanism in a formerly oceanic area.

The upper layer of the ridge, 5.15 km/sec average velocity, is identified as basaltic volcanic rock. This velocity agrees well with values given by Birch *et al.* (1942) and with the velocity measured on Bermuda (Officer *et al.*, 1952). The deeper layer with average velocity 7.21 km/sec is tentatively identified as a mixture of mantle and oceanic layer. Assuming a simple mixture of approximately equal parts, the mean density may be estimated as 3.07. If isostatic equilibrium is assumed and the average height of the ridge above the sea floor is taken to be 1500 fathoms (or about 3 km), the thickness of the 7.3 km/sec material is about 30 km, as indicated by the dashed lower interface in Figure 3. The free-air anomaly profile shown in this figure is taken from Vening Meinesz (1948). The fact that the anomaly is relatively small indicates that the ridge is largely compensated.

The formation of the ridge requires the addition of a great quantity of basalt magma and raises the question of its source. This is attributed to a rising convection current in the mantle, as described by Hess (1954, p. 345). We suggest that a convection-current system has contributed the basalt magma and has applied

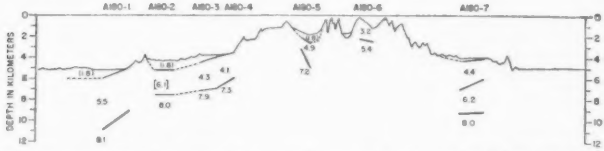

FIGURE 2.—TOPOGRAPHIC PROFILE AND SEISMIC SECTION ACROSS THE MID-ATLANTIC RIDGE SOUTH OF THE AZORES

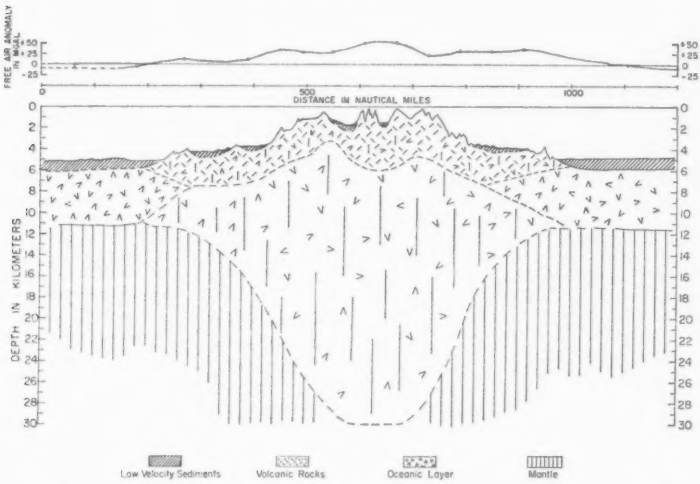

FIGURE 3.—GENERALIZED STRUCTURE SECTION AND FREE-AIR ANOMALY PROFILE ACROSS THE MID-ATLANTIC RIDGE SOUTH OF THE AZORES
Gravity anomalies taken from Vening Meinesz (1948)

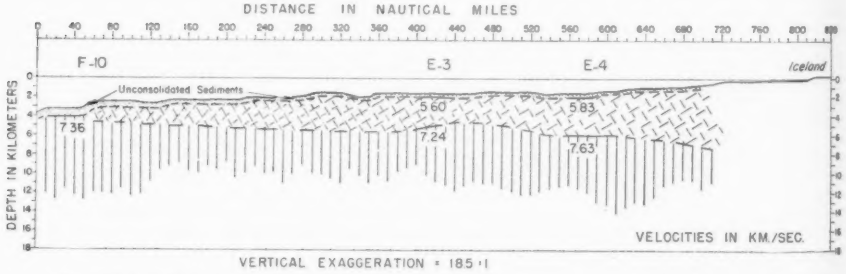

FIGURE 4.—STRUCTURE SECTION ALONG THE MID-ATLANTIC RIDGE SOUTH OF ICELAND

the extensional forces to the crust to produce the axial rift.

The rift and the earthquake activity indicate that the area is now under tension. This in turn indicates that the present convection system is such that material is rising along a belt approximately following the axis of the north and south Atlantic oceans. The fact that the ridge follows the axis of the oceans has been discussed by numerous authors. The convection pattern envisioned here can best be related to this fact on the assumption that the positions of North America and South America relative to Europe and Africa have been determined by the current system rather than that the current system was determined by the location of the continents. To explain the relative location of the continents (with respect to the Mid-Atlantic

RIDGE

THE

vection
ated to
sitions
elative
ned by
urrent
of the
ion of
lantic

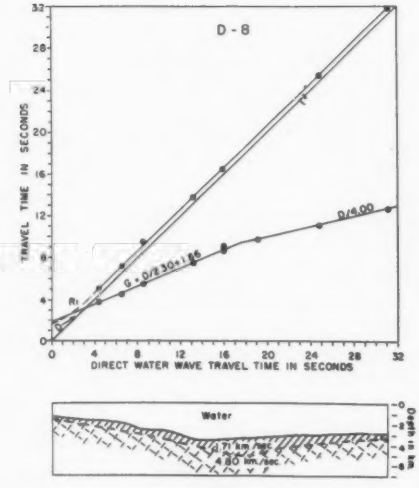
D - 8
TRAVEL TIME IN SECONDS
DIRECT WATER WAVE TRAVEL TIME IN SECONDS
R1
G = D/2.30+1.86
D/4.00
Water
4.80 km/sec

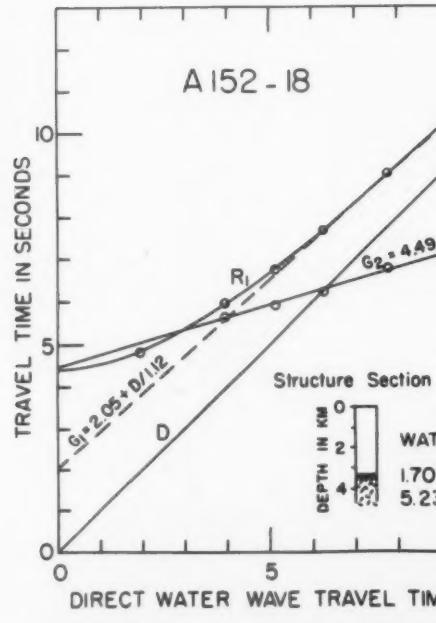
A 152 - 18
TRAVEL TIME IN SECONDS
R1
G1 = 2.05 + D/1.12
D
Structure Section
DEPTH IN KM
WAT
1.70
5.23
DIRECT WATER WAVE TRAVEL TIM

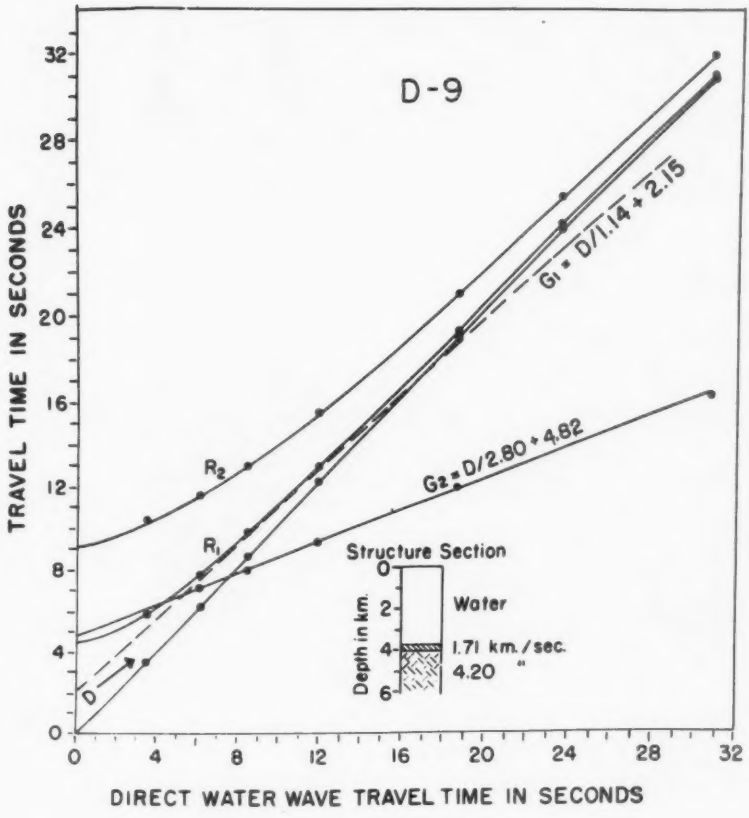
D-9
TRAVEL TIME IN SECONDS
DIRECT WATER WAVE TRAVEL TIME IN SECONDS
$G_1 = D/1.14 + 2.15$
$G_2 = D/2.80 + 4.82$
R_2
R_1
D
Structure Section
Depth in km.
Water
1.71 km./sec.
4.20 "

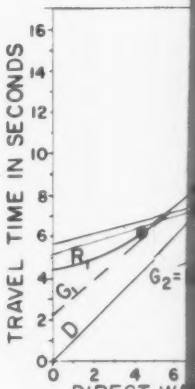

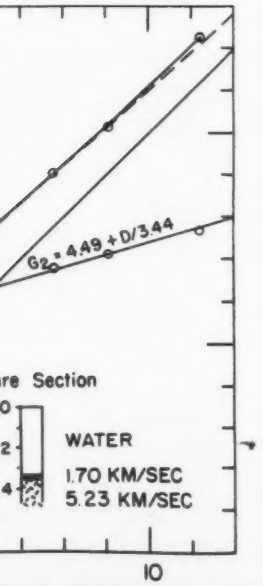
$G_2 = 4.49 + D/3.44$
WATER
1.70 KM/SEC
5.23 KM/SEC
RAVEL TIME IN SECONDS

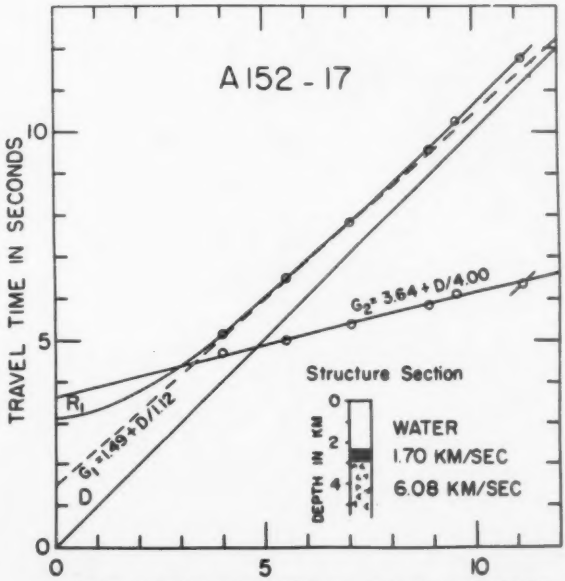
A152 - 17
TRAVEL TIME IN SECONDS
DIRECT WATER WAVE TRAVEL TIME IN SECONDS
$G_1 = 1.49 + D/1.12$
$G_2 = 3.64 + D/4.00$
R_1
D
Structure Section
DEPTH IN KM
WATER
1.70 KM/SEC
6.08 KM/SEC

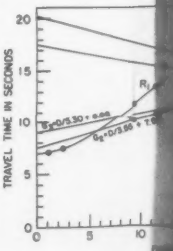

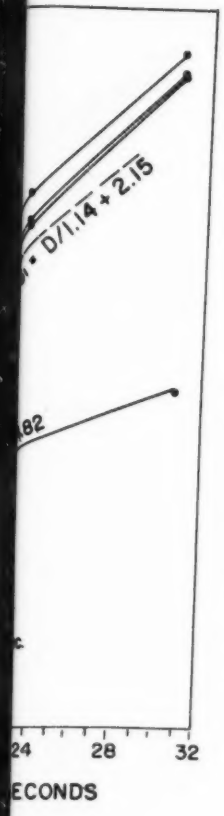

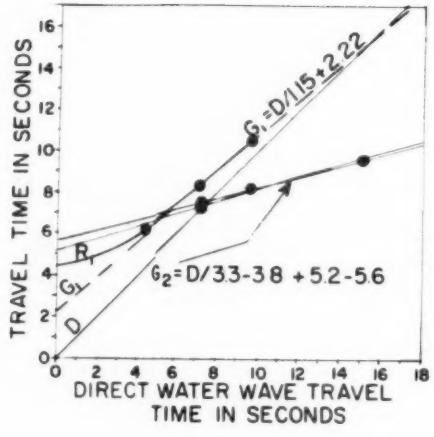

D-10

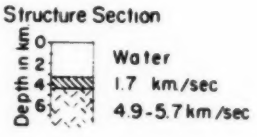

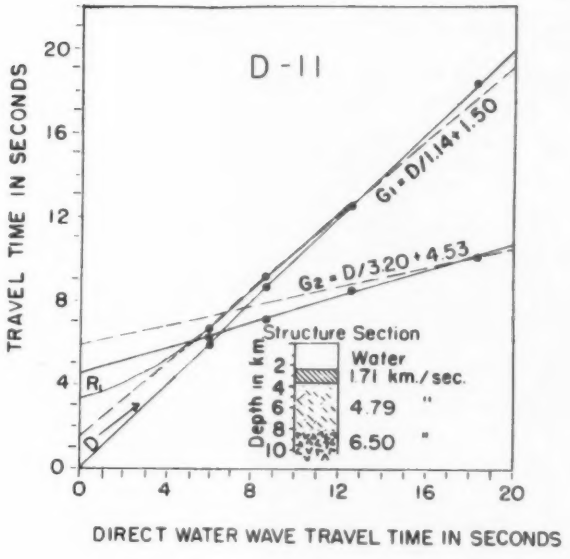

TRAVEL TIME IN SECONDS

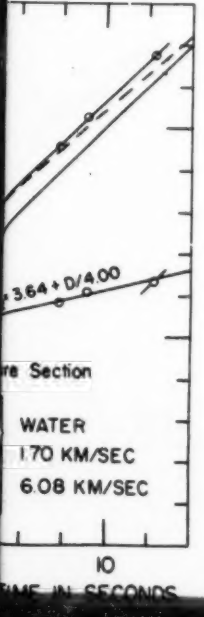

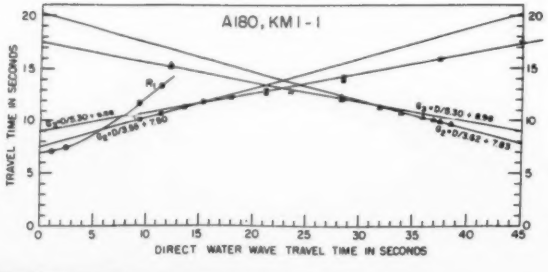

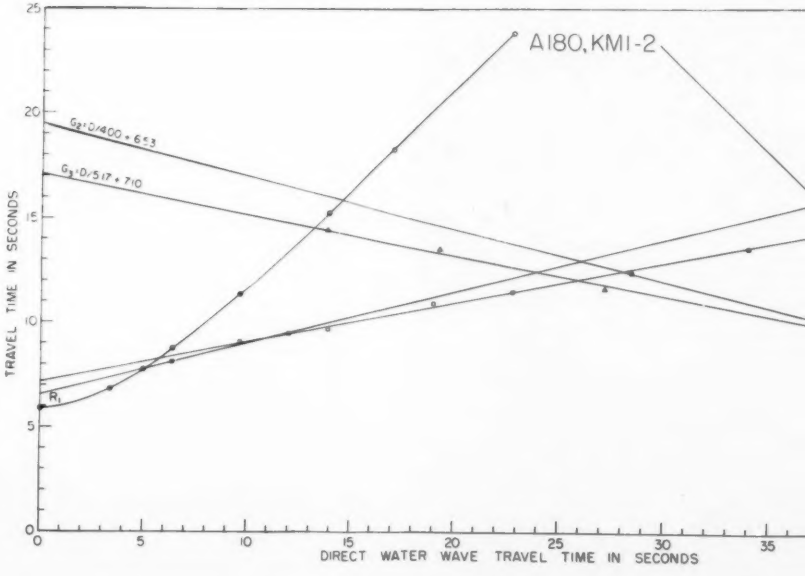

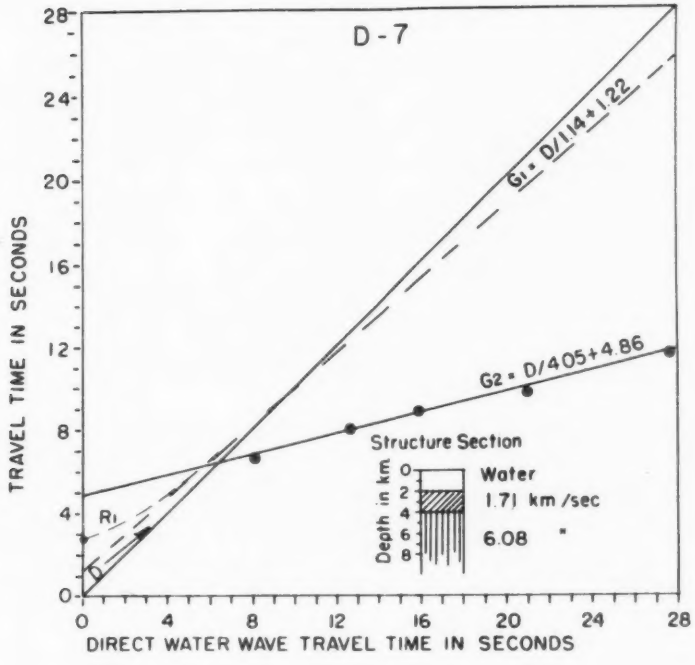
D - 7
TRAVEL TIME IN SECONDS
DIRECT WATER WAVE TRAVEL TIME IN SECONDS
G1 = D/1.14 + 1.22
G2 = D/4.05 + 4.86
R1
Structure Section
Depth in km
Water
1.71 km /sec
6.08 "

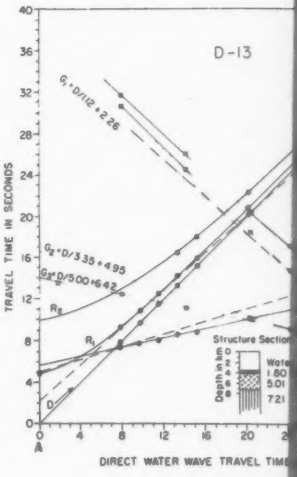
D-13
TRAVEL TIME IN SECONDS
DIRECT WATER WAVE TRAVEL TIME
G1 = D/1.12 + 2.26
G2 = D/3.35 + 4.95
R1

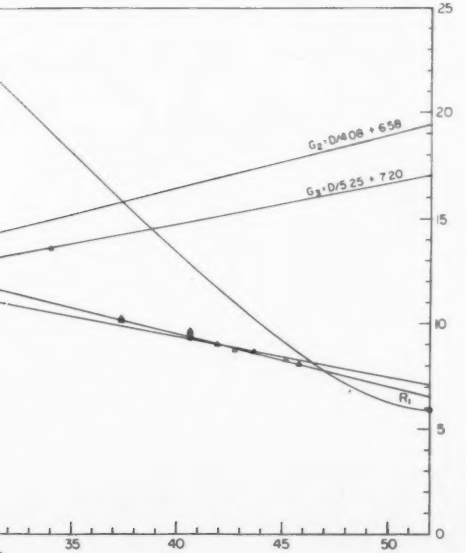
G2 = D/4.08 + 6.58
G3 = D/5.25 + 7.20
R1

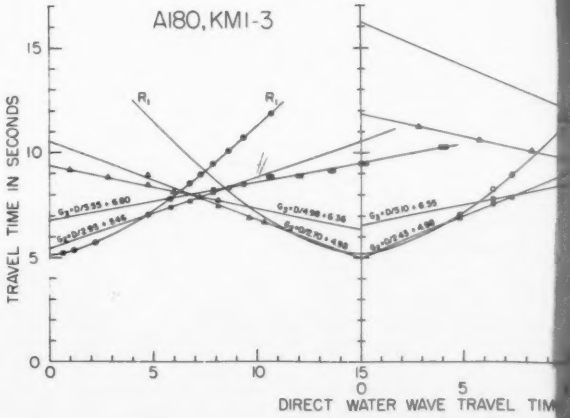
A180, KM1-3
TRAVEL TIME IN SECONDS
DIRECT WATER WAVE TRAVEL TIME
R1
R1

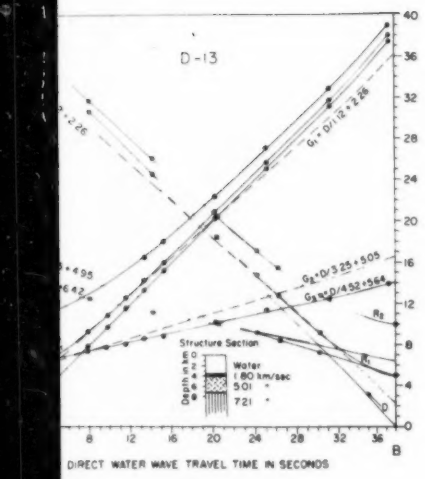

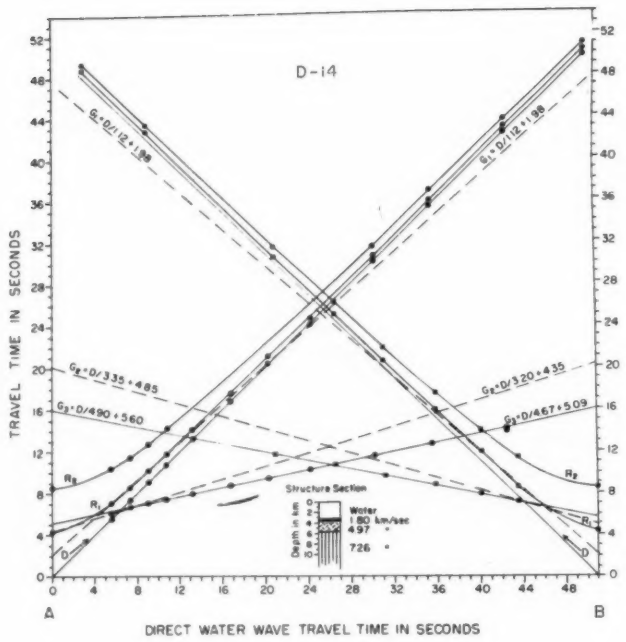

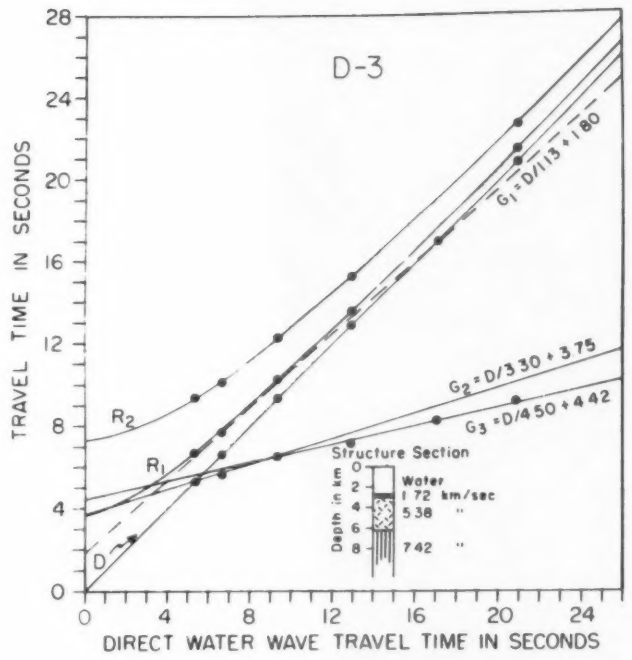

TRAVEL TIME IN SECONDS

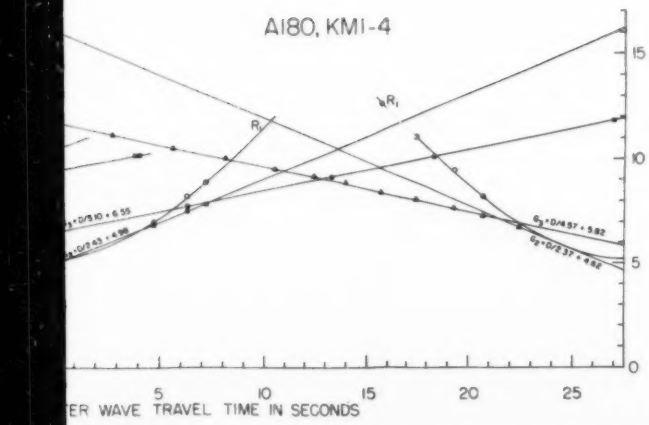

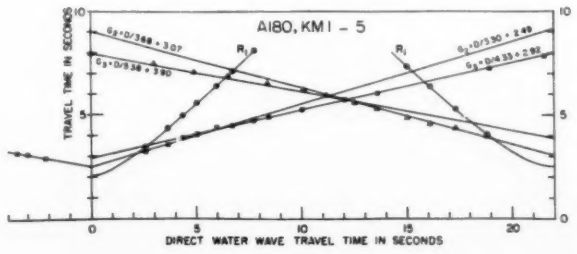

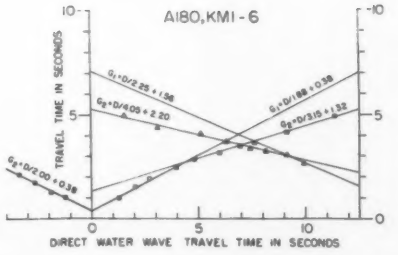

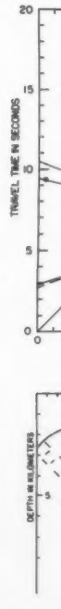

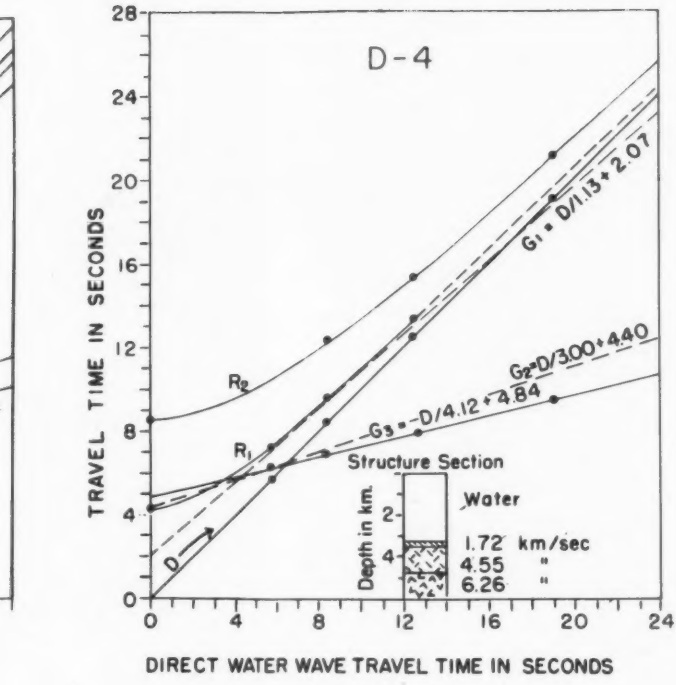
D-4
TRAVEL TIME IN SECONDS
DIRECT WATER WAVE TRAVEL TIME IN SECONDS
R2
R1
D
G1 = D/1.13 + 2.07
G2=D/3.00+4.40
G3 = D/4.12 + 4.84
Structure Section
Depth in km.
Water
1.72 km/sec
4.55 "
6.26 "

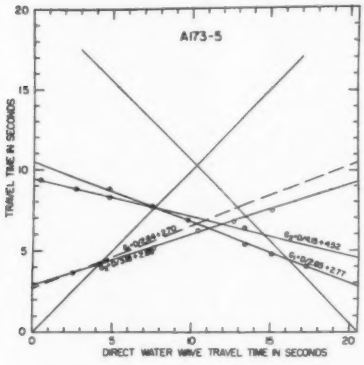
A173-5
TRAVEL TIME IN SECONDS
DIRECT WATER WAVE TRAVEL TIME IN SECONDS

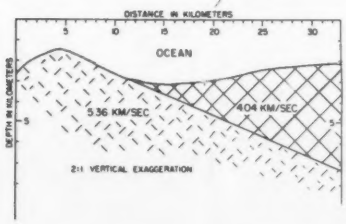
DISTANCE IN KILOMETERS
OCEAN
5.36 KM/SEC
4.04 KM/SEC
DEPTH IN KILOMETERS
2:1 VERTICAL EXAGGERATION

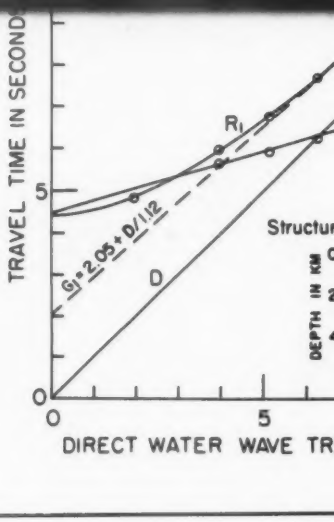
TRAVEL TIME IN SECOND
R1
G1 = 2.05 + D/1.12
D
Structur
DEPTH IN KM
0
5
DIRECT WATER WAVE TR

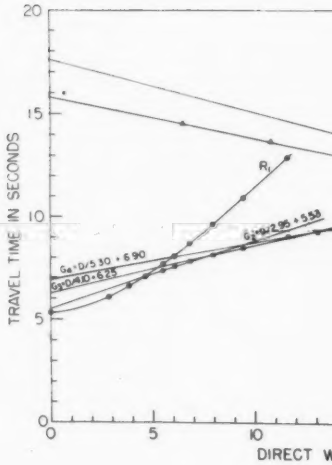
20
15
10
5
0
TRAVEL TIME IN SECONDS
R1
G2=D/5.30 + 6.90
G3=0.410+6.25
0
5
10
DIRECT W

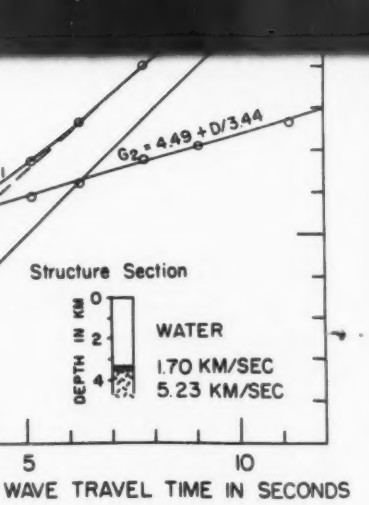
$G_2 = 4.49 + D/3.44$
Structure Section
DEPTH IN KM
0
2
4
WATER
1.70 KM/SEC
5.23 KM/SEC
5
10
WAVE TRAVEL TIME IN SECONDS

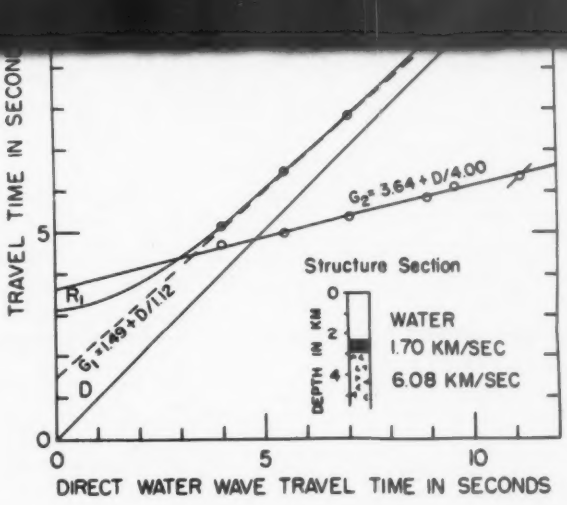
TRAVEL TIME IN SECON
5
$G_2 = 3.64 + D/4.00$
R_1
$G_1 = 1.45 + D/1.12$
D
Structure Section
DEPTH IN KM
0
2
4
WATER
1.70 KM/SEC
6.08 KM/SEC
0
5
10
DIRECT WATER WAVE TRAVEL TIME IN SECONDS

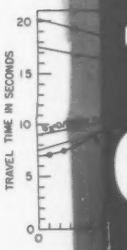
TRAVEL TIME IN SECONDS
20
15
10
5
0

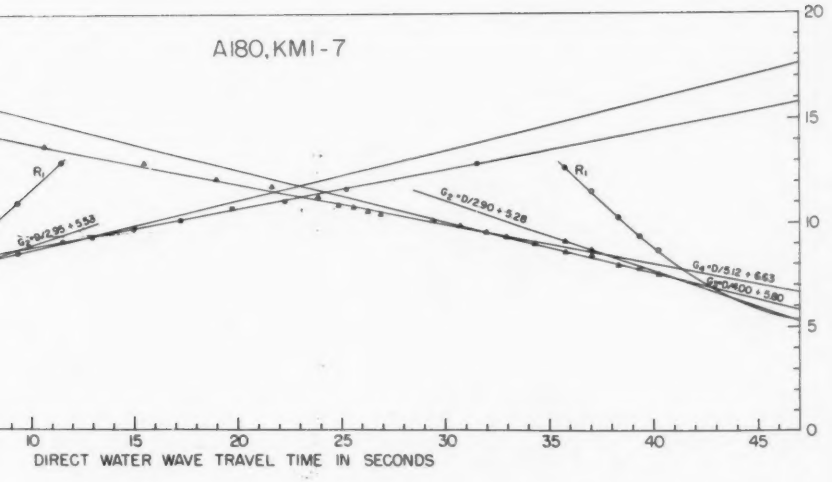
A180, KM1-7
R_1
$G_2 = D/2.35 + 5.53$
R_1
$G_2 = D/2.90 + 5.28$
$G_2 = D/5.12 + 6.63$
$G_2 = D/4.00 + 5.80$
20
15
10
5
0
10
15
20
25
30
35
40
45
DIRECT WATER WAVE TRAVEL TIME IN SECONDS

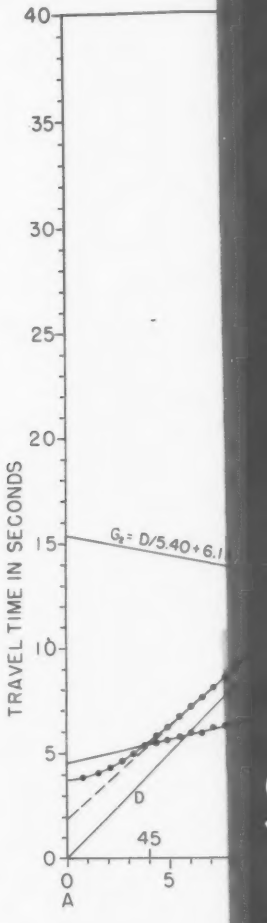
40
35
30
25
20
15
10
5
0
TRAVEL TIME IN SECONDS
$G_2 = D/5.40 + 6.1$
D
45
0
5
A

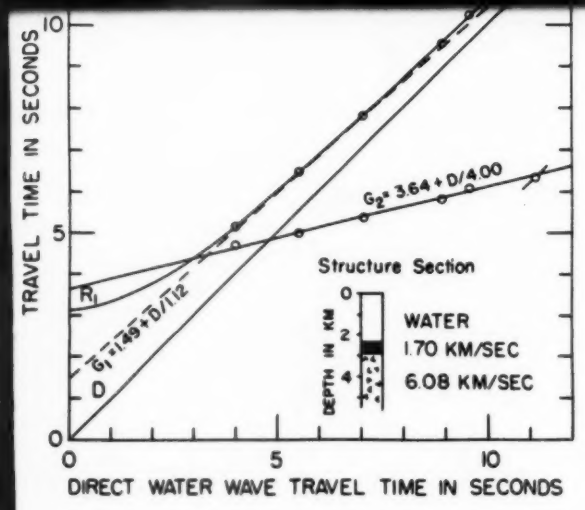
TRAVEL TIME IN SECONDS
DIRECT WATER WAVE TRAVEL TIME IN SECONDS
$G_2 = 3.64 + D/4.00$
$G_1 = 1.45 + D/1.12$
R_1
D
Structure Section
DEPTH IN KM
WATER
1.70 KM/SEC
6.08 KM/SEC

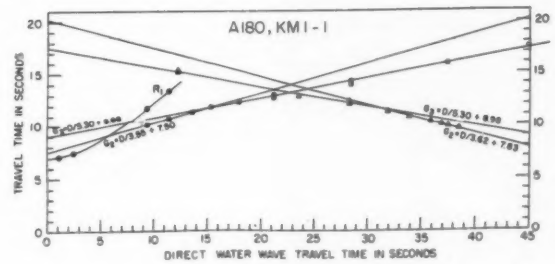
A180, KM1-1
TRAVEL TIME IN SECONDS
DIRECT WATER WAVE TRAVEL TIME IN SECONDS
R_1
$G_3 = D/5.30 + 8.96$
$G_2 = D/3.62 + 7.69$

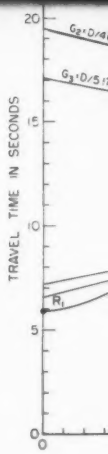
TRAVEL TIME IN SECONDS
$G_2 = D/4$
$G_3 = D/5$
R_1

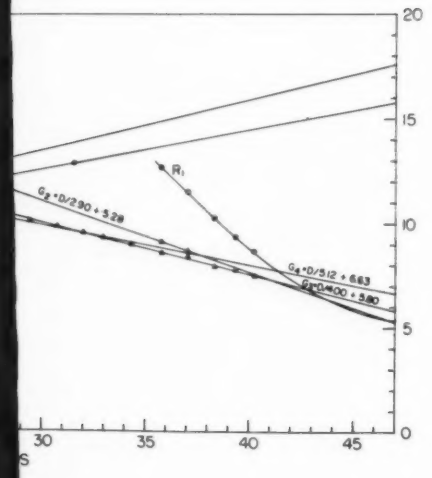
R_1
$G_2 = D/2.90 + 5.28$
$G_3 = D/5.12 + 6.63$
$G_2 = D/4.00 + 5.80$

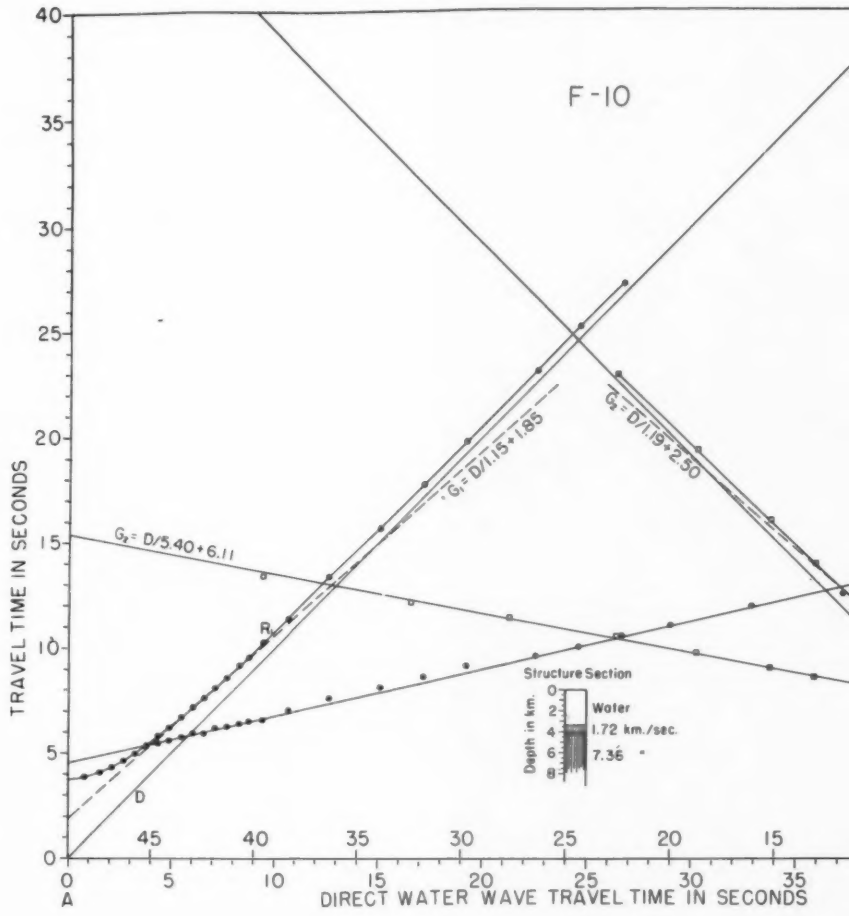
F-10
TRAVEL TIME IN SECONDS
DIRECT WATER WAVE TRAVEL TIME IN SECONDS
$G_2 = D/5.40 + 6.11$
$G_1 = D/1.15 + 1.85$
$G_2 = D/1.19 + 2.50$
R_1
D
Structure Section
Depth in km.
Water
1.72 km./sec.
7.36

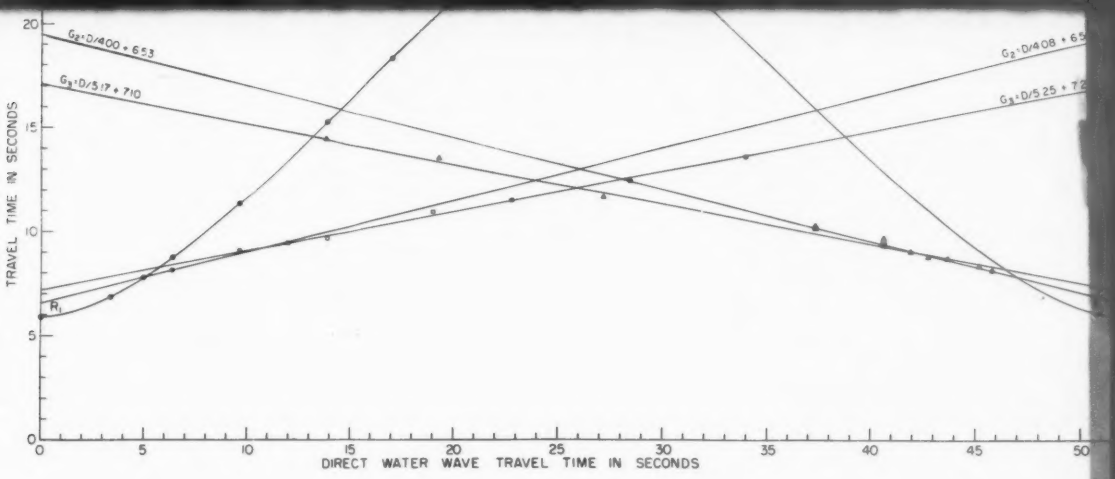

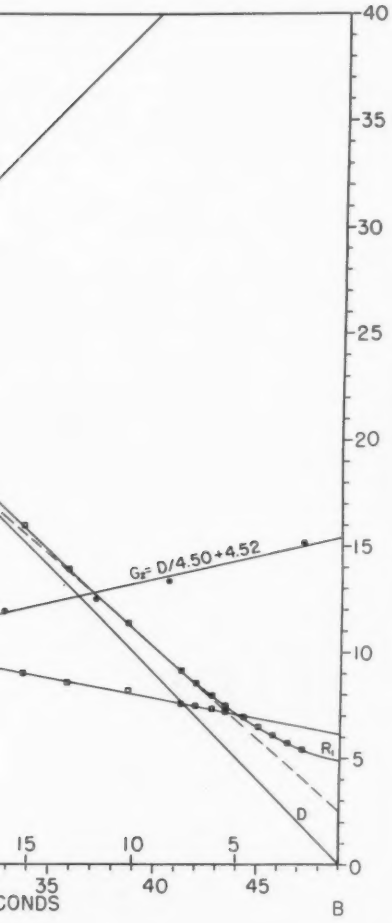

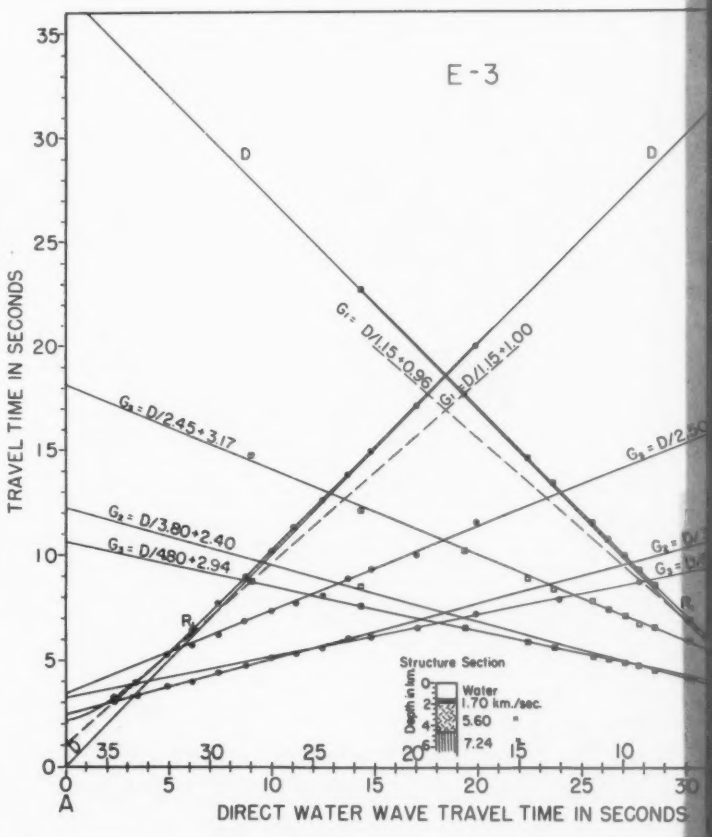

TRAVEL-TIME GRAPHS, MEDITERRA

Distance on the abscissa is plotted in increments of direct water-wave time, *i. e.*, 1 second is approximately 5000 feet. The lines G_1, G_2, G_3 ....

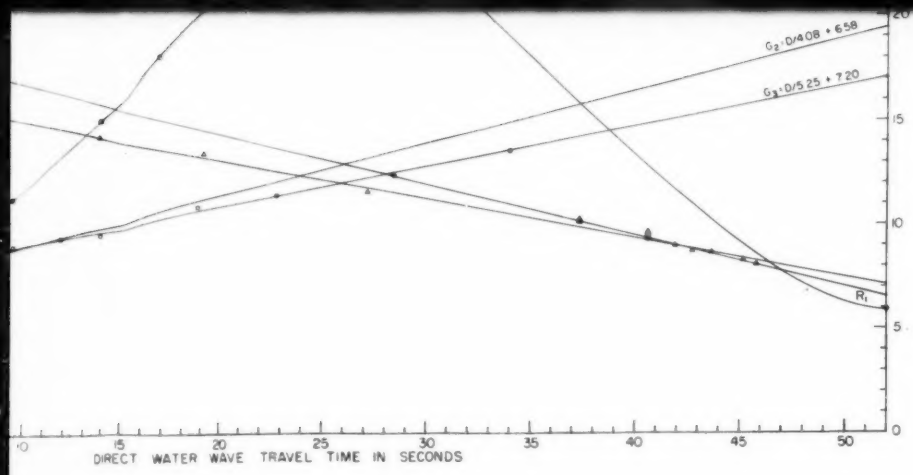

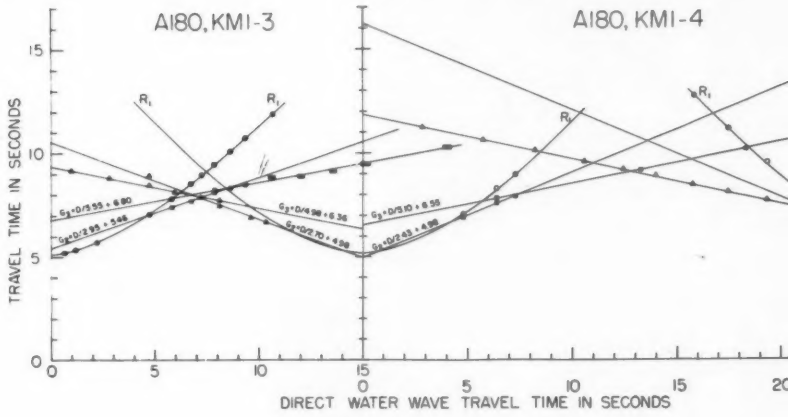
A180, KMI-3
A180, KMI-4
TRAVEL TIME IN SECONDS
R_1
$G_1 = D/3.55 + 6.80$
$G_2 = D/2.95 + 5.48$
$G_2 = D/4.98 + 6.36$
$G_3 = D/2.70 + 4.98$
$G_2 = D/5.10 + 6.55$
$G_3 = D/2.63 + 4.98$
DIRECT WATER WAVE TRAVEL TIME IN SECONDS

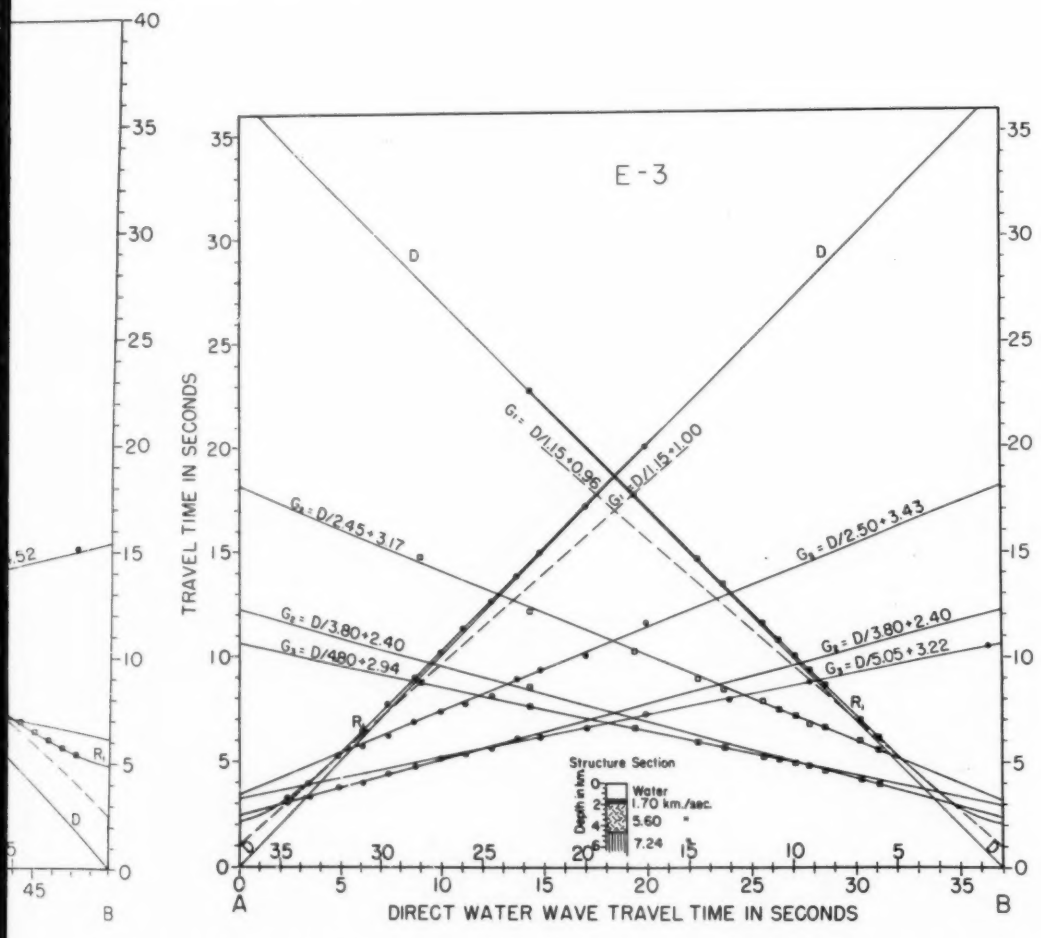

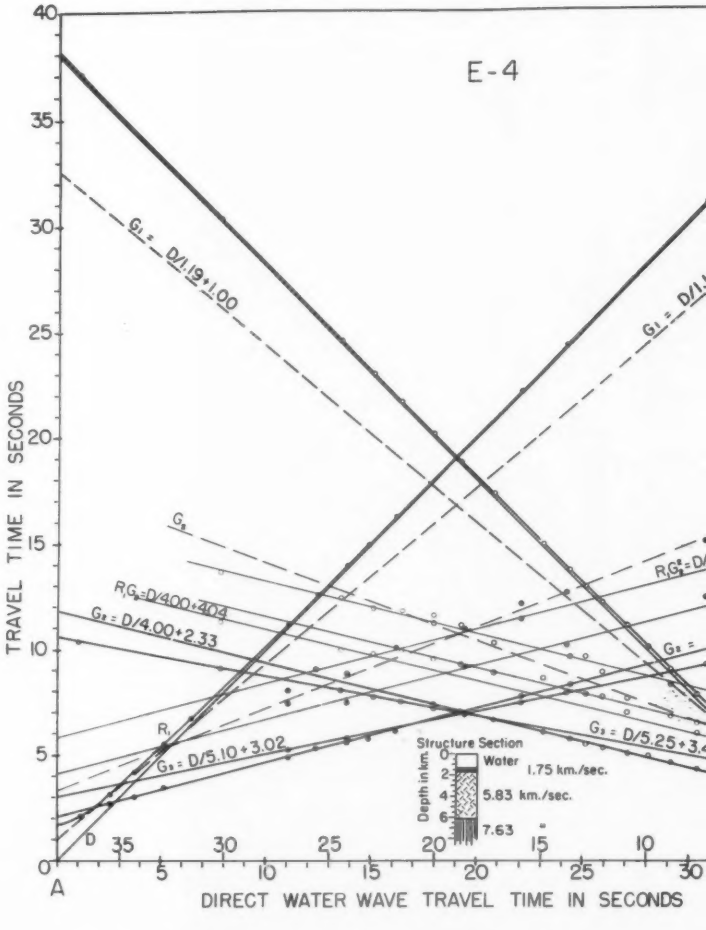

TRAVEL-TIME GRAPHS, MEDITERRANEAN SEA AND MID-ATLANTIC RIDGE

Distance on the abscissa is plotted in increments of direct water-wave time, *i. e.*, 1 second is approximately 5000 feet. The lines G_1, G_2, G_3 .... are determined by refracted arrivals in successive layers beneath the ocean floor. When G is dashed or absent, the velocity in the top layer was assumed.

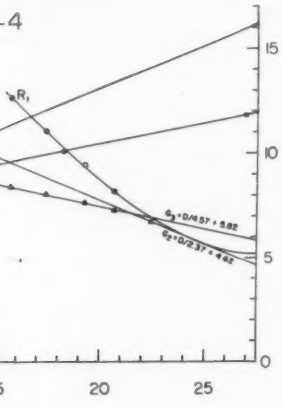
-4
R1
G2=D/4.97+5.82
G3=D/2.37+4.62
15
10
5
0
20
25

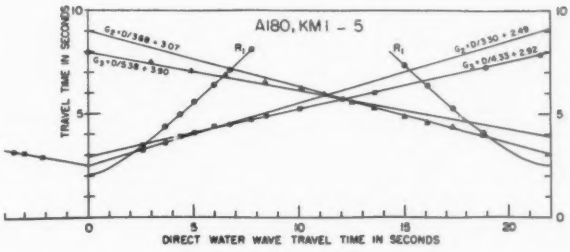
A180, KM1 - 5
TRAVEL TIME IN SECONDS
G2=D/3.68+3.07
G3=D/5.38+3.90
R1
G2=D/3.30+2.69
G3=D/4.33+2.92
10
5
0
5
10
15
20
DIRECT WATER WAVE TRAVEL TIME IN SECONDS

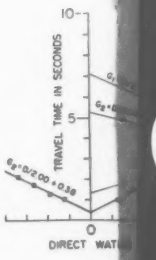
TRAVEL TIME IN SECONDS
G3=D/2.00+0.38
10
5
0
DIRECT WATE

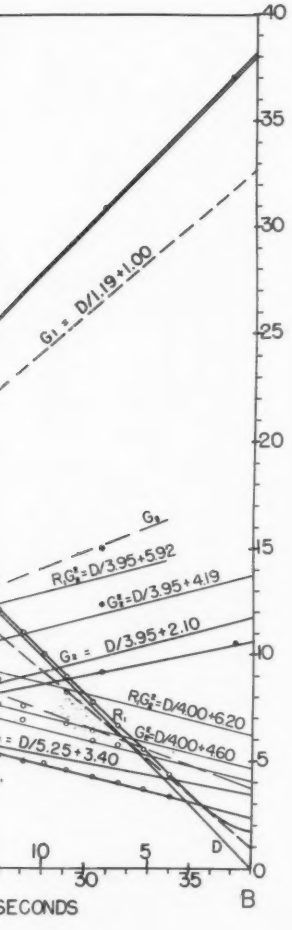
G1 = D/1.19+1.00
G2
RG2=D/3.95+5.92
G2=D/3.95+4.19
G3 = D/3.95+2.10
RG3=D/4.00+6.20
R1
G3=D/4.00+4.60
= D/5.25+3.40
D
40
35
30
25
20
15
10
5
0
10
5
30
35
SECONDS
B

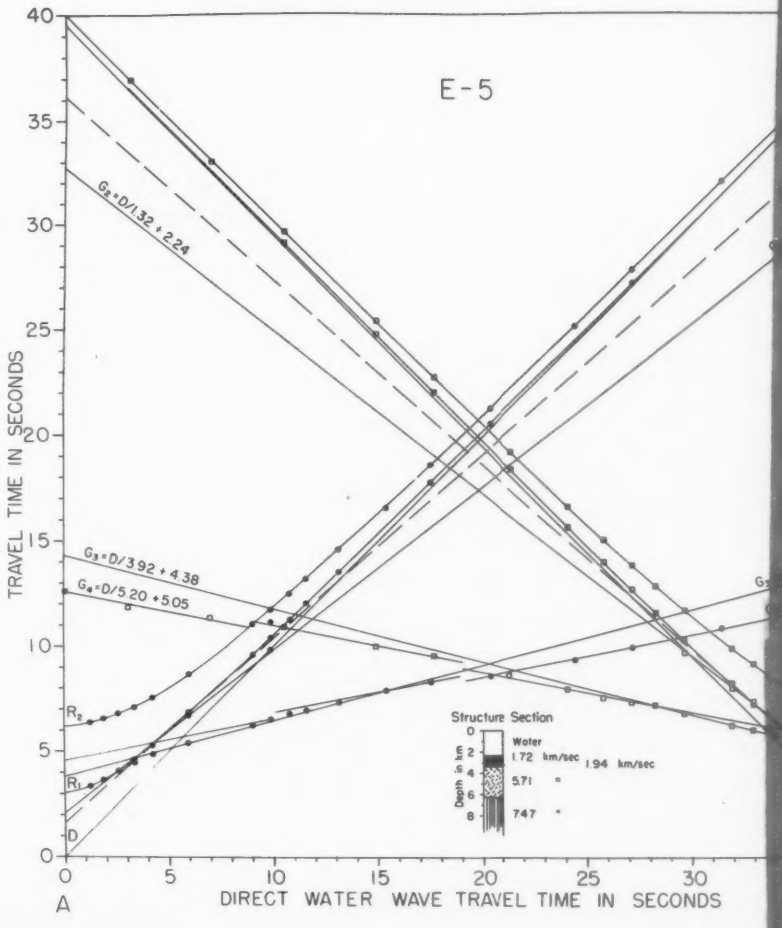
E-5
G2=D/1.32+2.24
G3=D/3.92+4.38
G4=D/5.20+5.05
R2
R1
D
TRAVEL TIME IN SECONDS
Structure Section
Depth in km
Water
1.72 km/sec
1.94 km/sec
5.71
7.47
0
2
4
6
8
40
35
30
25
20
15
10
5
0
0
5
10
15
20
25
30
A
DIRECT WATER WAVE TRAVEL TIME IN SECONDS

GE

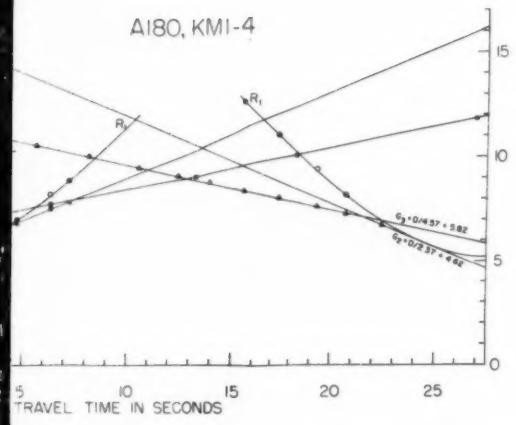

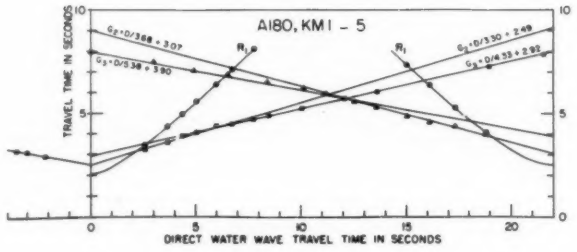

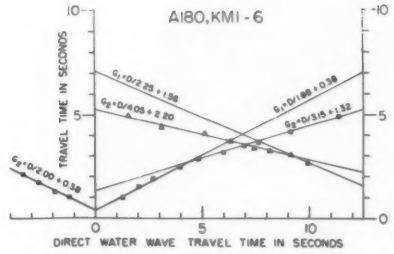

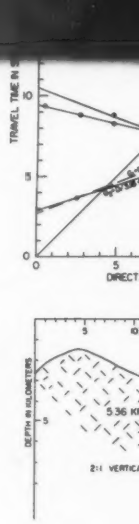

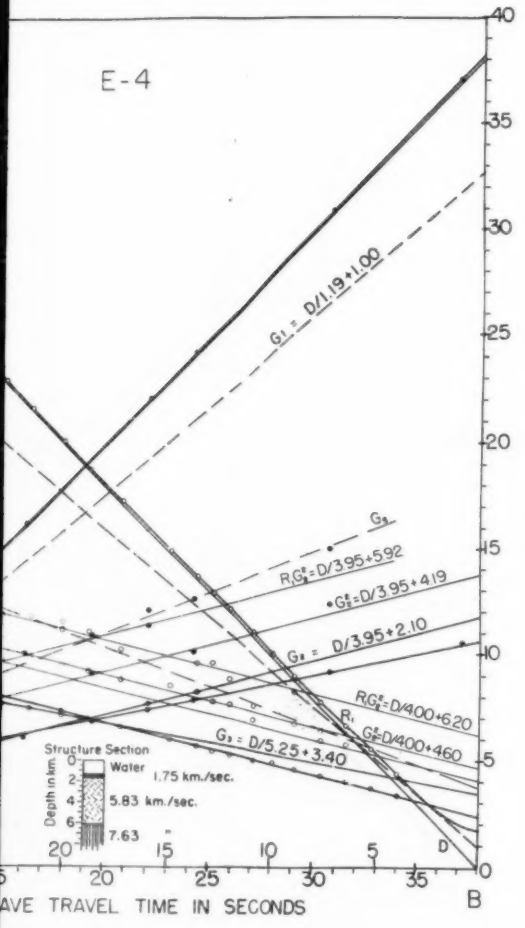

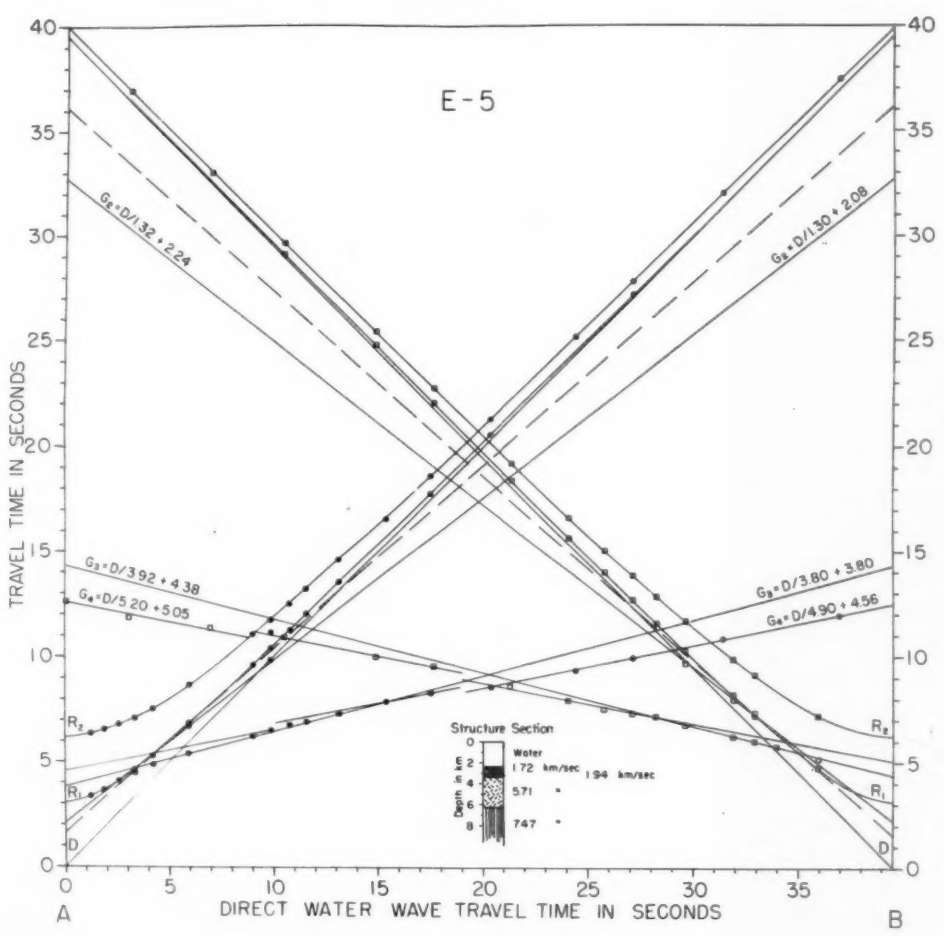

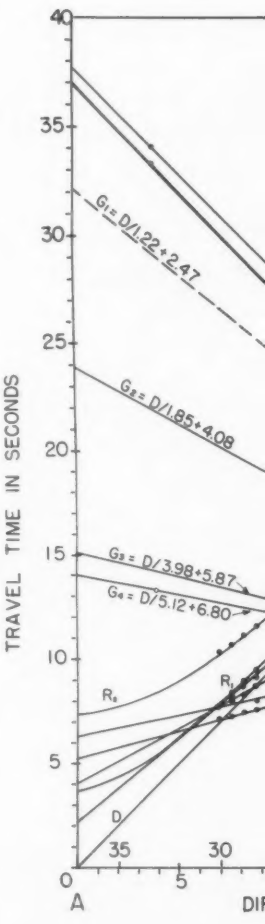

NTIC RIDGE

successive
dashed or
assumed.

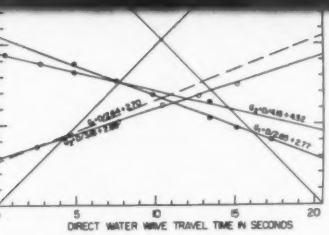
DIRECT WATER WAVE TRAVEL TIME IN SECONDS

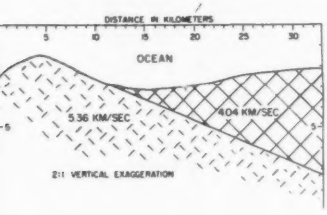
DISTANCE IN KILOMETERS
OCEAN
5.36 KM/SEC
4.04 KM/SEC
2:1 VERTICAL EXAGGERATION

E-6

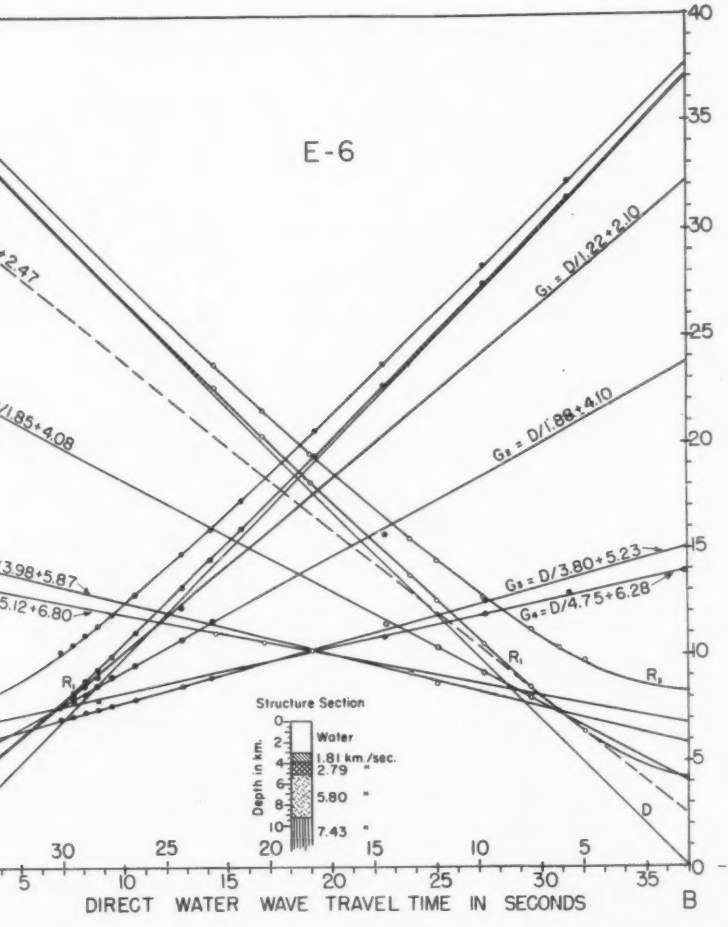
G1 = D/1.22+2.10
G2 = D/1.88+4.10
G3 = D/3.80+5.23
G4 = D/4.75+6.28
R1
R2
D
Structure Section
Depth in km.
Water
1.81 km./sec.
2.79 "
5.80 "
7.43 "
DIRECT WATER WAVE TRAVEL TIME IN SECONDS
B

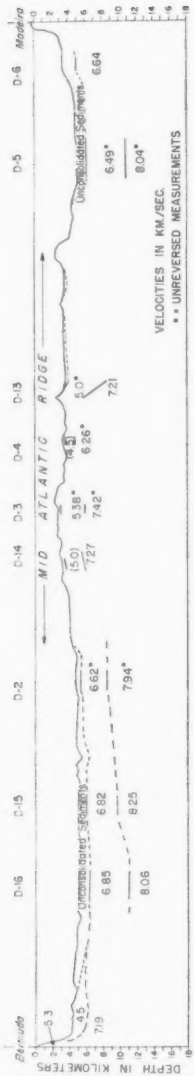

FIGURE 5.—STRUCTURE SECTION BETWEEN BERMUDA AND MADEIRA

Ridge) by this current system, we assume, following Vening Meinesz (1957, p. 133), that all sialic crustal material was collected in one hemisphere by the initial current system. The second current system, whose pattern is assumed to persist to the present, contained a number of convection cells. These broke the original continental mass into fragments which moved prior to the solidification of a competent oceanic crust, to areas of subsiding current in the present pattern.

Many writers have suggested that convection currents of the present should rise beneath continents, because of local heating. This would require that a reversal of the second convection pattern occurs after the formation of an oceanic crust. Possibly it could account for the accumulation of basaltic magma along the Mid-Atlantic Ridge, but it could hardly account for the tension indicated by the rift.

NORWEGIAN AND GREENLAND SEAS

Five deep-water stations and the two shallow-water stations, discussed in the following section, are the only measurements in this area. The results are reasonably consistent, and, in spite of the small number of measurements, some conclusions appear justified.

Station F-9 (*Pl.* 5)

This station is in the northeastern edge of the basin (about 2000 fathoms deep) between Iceland and southern Norway. Rough topography along the shot lines greatly complicated the interpretation of the data. Sedimentary arrivals were recorded in both profiles. At A the apparent velocity is 1.76 km/sec, and this clearly represents the topmost layer; the G_1 line is tangent to R_1. The measured sedimentary velocity at B is 2.02 km/sec (apparent velocity), and, since the line representing this layer crosses the R_1 curve, the topmost layer was not observed at this end of the station. The dashed line, $G_1 = D/1.17 + 2.50$, represents the inferred upper layer here. The sedimentary layers are not uniform over any appreciable distance in this area, and the thickness and velocity of each individual layer shown in the section are considered to be representative only in the broadest sense. The section is reasonably accurate, however, in representing the average thickness of sediments. As mentioned earlier, even in regions of featureless topography, many of the sedimentary layers vary both in velocity and thickness over the range covered by the measurements, and, in regions such as this where the depth along the shot lines ranges as much as 550 fathoms, it is difficult to determine a representative section.

The first refracting layer beneath the sediments, primarily determined by the A profile, has a velocity of 5.36 km/sec and an average thickness of 2.76 km.

The lines representing the deepest refracting layer are offset in the middle portion of the travel-

time graph by about 0.6 sec, which seriously reduces the accuracy of the measurements. These high points are over a valley whose flat floor suggests turbidity-current filling and an even deeper valley in the underlying rocks. When interpreted in this way, the high points indicate that the sediment thickness in the region of the offset is about 1.2 km greater than elsewhere. This is a good illustration of the way in which long reversed refraction profiles can indicate buried topography.

The highest velocity indicated here, 8.04 km, is considerably higher than at any of the other stations in the area. Normally a velocity of this order is identified with the mantle, which is generally at a depth of 10–12 km in oceanic areas. Since the depth, 7.2 km, is unusual for the mantle, it is doubtful if the velocity has been correctly measured. Where such large topographic corrections are required, the accuracy of the velocity determination is greatly reduced, and the velocity in the deepest layer here may be as low as 7.4 km/sec, the average for the deepest layer in the Norwegian and Greenland seas.

Station F-7 (*Pl.* 5)

This station is about 250 miles southeast of Jan Mayen Island. The soundings were constant at 1750 fathoms (3.18 km) throughout both shooting runs. Sedimentary arrivals recorded at both receiving positions determined two layers with velocities of 1.80 and 2.00 km/sec. Velocities in the deeper refracting layers were 5.37 and 6.97 km/sec respectively.

A distinct offset is noticed in the G_3 line in profile *A* at a water-wave travel time of 9.5 seconds. Unfortunately, the range of shots in the *B* profile is not sufficient to cover this region, and dashed lines are drawn on the travel-time graph to show a similar behavior of the corresponding lines in that profile. The amount of relief necessary to cause the travel times to deviate by the observed 0.3 second is about 0.6 km.

Since this is the longest and most heavily shot station in the area, a calculation was made to determine the minimum undetectable depth below sea level of an assumed mantle layer with the velocity 8.0 km/sec. The results show that such a layer is more than 15 km deep.

Station F-6 (*Pl.* 5)

This station is about 150 miles north of Jan Mayen Island in the Greenland Sea. Except for a 200-fathom rise near *B*, the topography was generally flat along the shot lines, and the arrival times have been corrected to a level bottom at a depth of 1670 fathoms (3.05 km).

Since no sedimentary arrivals were received in either profile, an assumed velocity of 1.72 km/sec was used in the calculations. The refracting layers have velocities of 5.06 and 7.38 km/sec respectively. The section thus produced shows a thickness of 0.49 km for the sediments and 3.04 km for the upper refracting layer.

The G_s lines are determined by shear waves travelling in the 7.38 km/sec layer. The ratio of compressional to shear velocity is about 1.91, and the depth calculations indicate transformation from compressional to shear waves near the base of the sediments. The line *Rt* in the *A* profile is determined by strong arrivals containing abundant high and low frequencies which are identified as topographic echoes (Luskin *et al.*, 1952). These could arise from a hill in the neighborhood of point *A* similar to that found at *B*.

Station F-5 (*Pl.* 5)

This station is near the flank of the ridge northeast of Jan Mayen Island. The soundings deviated only slightly from 1600 fathoms (2.92 km) along the shot lines, and no topographic corrections were made. Several of the arrivals from the deeper refracting layers had large residuals, which are probably due to buried relief. The structure section consists of three sedimentary layers overlying two deeper, high-velocity layers. Velocities were determined for all but the unconsolidated sediments, for which a value of 1.70 km/sec was assumed. Including the deeper-sediment layers, velocities 2.01 and 3.60 km/sec, the total thickness of sediment is about 2 km. Beneath the sediments are found a refracting layer 2.6 km thick with velocity 5.26 km/sec and a layer with velocity 7.69 km/sec which is about 7.6 km below sea level.

This is the only deep-water station in the area at which the 3.60 km/sec layer (presumably consolidated sediments) is detected, but a velocity close to this is found at Stations F-3 and F-8, both of which are in shallow water. The arrivals for this layer in the *B* profile are highly questionable owing to interference from stronger basement arrivals at the range where they should be observed. The layer is clearly determined in the *A* profile by distinct arrivals. The fact that consolidated sediments were found here and at Station F-3 led to the speculation that they could also be present at station F-4 which lies between these two stations.

Station F-4 (*Pl.* 5)

This station is on the continental slope southwest of Bear Island. The bottom had a uniform slope from 1300 fathoms at *A* to 1200 fathoms at *B*. Although most of the ground waves were strong enough to be picked accurately, some of the arrival times had residuals as high as 0.2 sec, particularly among those from the deeper refracting layers. This is characteristic of the stations occupied in the Norwegian and Greenland seas and is probably the result of relief in the deeper interfaces.

The section consists of two layers of sediment with velocities 1.79 and 2.23 km/sec and two deeper layers with velocities 4.96 and 7.55 km/sec. The upper layer of sediment was not recorded at *B*, although indicated by G_2 crossing the R_1 hyperbola, but it is well determined in the *A* profile. The semiconsolidated layer (velocity 2.23 km/sec), however, was well determined at *B*, while only two arrivals could be picked at *A*. This again demonstrates the erratic behavior of refracted arrivals from the sediments.

There is a good possibility, based on comparison with Stations F-3 and F-5, that an additional layer with a velocity in the neighborhood of 3.6 km/sec should be shown for this station. The thickness of such a layer could not be more than about 1 km, and the total sedimentary thickness would be changed very little by computing thicknesses according to that assumption.

DISCUSSION OF RESULTS: The crustal structure under the Norwegian Sea is significantly

different from that usually found under the deeper oceanic areas. The region is characterized by unusually large residuals in the ground-wave arrivals from the deeper layers. These probably result primarily from large irregularities in the deeper interfaces, although some of the scatter may be due to lateral velocity changes in the layers. As a result of these complications, some of the individual velocity determinations may have errors as great as 20 per cent. However, the five deep-water stations occupied in the area give results which are similar in many respects and for this reason the arithmetical average of the velocities is considered significant. The upper high-velocity layer (5.2 km/sec average) is fairly consistent, both in velocity and thickness; the velocities range between 4.96 and 5.37 km/sec, and the thickness between 2.5 and 3.0 km. The determinations of velocity in the deepest layer fall within a much wider range, 6.97–8.04 km/sec. The average velocity is 7.5 km/sec, and the depth of the layer is quite consistently 7 km ± 0.7 km below sea level.

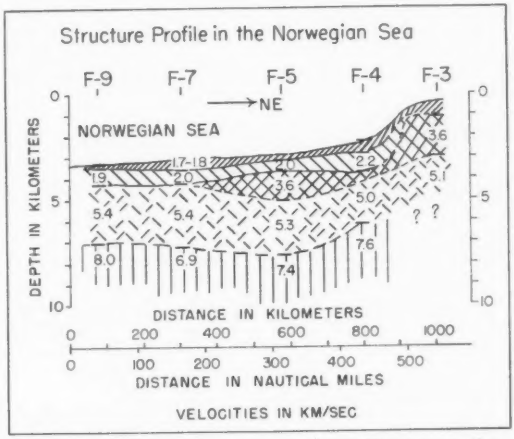

FIGURE 6.—STRUCTURE SECTION IN THE NORWEGIAN SEA

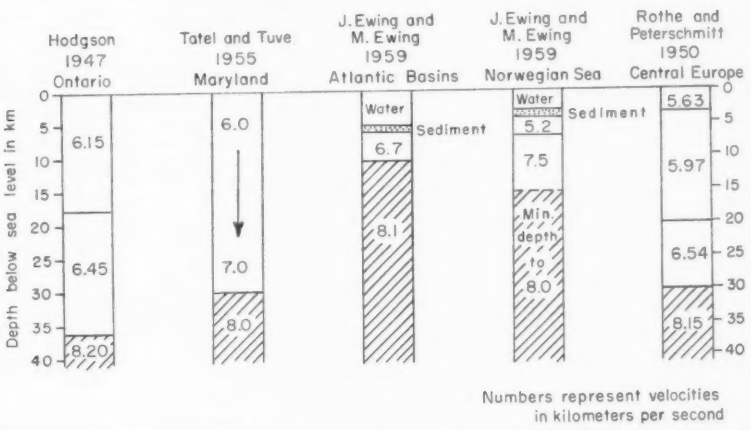

FIGURE 7.—COMPARISON OF CONTINENTAL, ATLANTIC OCEAN BASIN, AND NORWEGIAN SEA CRUSTAL SECTIONS

The similarity of the structure of this area (a 2- to 3-km basement, velocity 5.2 km/sec over a substratum, velocity about 7.5 km/sec) with that of the Mid-Atlantic Ridge strongly

supports the conclusion, based on the extension of the earthquake belt, that the Ridge structure extends far north of Iceland. The width of the Mid-Atlantic Ridge, as shown in Figure 3, is approximately equal to the width of the Norwegian Sea. Hence the entire Brito-Arctic petrographic province (*e.g.*, Turner and Verhoogen, 1951, p. 188–194) may be considered as a Mid-Atlantic Ridge province, probably modified at both edges by contact with continental rocks. Oceanic and continental crustal sections are compared with a representative section from the Norwegian Sea (Fig. 7); the minimum depth to an assumed 8.0 km/sec velocity is taken from Station 7. Figure 6 shows a cross section running approximately northeast from Station F-9 in the basin to F-3 on the shelf near Bear Island.

Continental Shelf and Slope of Britain and Norway

Five stations were occupied on the continental slope of Britain and Scandinavia, and three in the North Sea. Previous seismic work on the continental shelf and slope of the British Isles has been reported by Bullard and Gaskell (1941), Hill and King (1953), and Hill and Laughton (1954). These measurements, made in the English Channel and southwest of the Channel, determined average velocities of 2.09, 3.01, 4.51, and 6.22 km/sec for unconsolidated sediment, semiconsolidated sediment, consolidated sediment, and basement, respectively. A decrease in velocity in the upper two layers is noticed on going from the Channel toward the edge of the shelf. The basement velocities which they report are somewhat higher than those (5 to 6 km/sec) found in most areas of the continental shelf of eastern North America—*e.g.*, Drake *et al.* (1957). In the present work, the highest velocity measured is about 5 km/sec (excepting an apparent value of 6.9 at Station E-10). In the discussion which follows, the material with velocity 4.85 to 5.11 km/sec is called "basement," but velocities in this range were described by Hill and Laughton as consolidated sediment. Velocities close to 5 km/sec were found for rocks of the Paleozoic floor in southeastern England (Bullard *et al.*, 1940).

Station E-10 (*Pl.* 5)

This is an unreversed profile in the trough which extends southwesterly between Rockall Bank and Porcupine Bank west of the British Isles. It is not clear to which province this station should be assigned. The shot line follows the trough, with the receiving position in 1500 fm (2.75 km) at the southwest end of the line. The water depth varied only slightly along the line.

Unreversed velocities of 2.65, 3.22, and 6.96 km/sec were found for the semiconsolidated sediments, consolidated sediments, and basement. A velocity of 1.71 km/sec was assumed for the unconsolidated sediments. The velocities and layer thicknesses listed for the station in Table 2 were calculated on the assumption that the strata had no component of dip in the direction of the shot line. In drawing the G_4 line on the travel-time graph for this station, the strongest points were satisfied. However, the few points in the range between 14 and 26 seconds of D indicate an apparent velocity of about 5.5 km/sec. The line was not drawn through these points, primarily because it would have passed well below the very strong arrival at range $D = 11$ seconds. In spite of this difficulty, the alternate interpretation should be considered. It would produce a section consisting of the same sedimentary layers (the 3.22 km/sec layer about 1 km thinner) overlying a 5.5 km/sec layer, and a poorly determined deeper layer in which the velocity might be as high as 8 km/sec. Possibly this station belongs with the continental-rise group or the Mid-Atlantic Ridge group, but the difficulties of interpretation and the lack of a reversed profile make its status uncertain.

Station E-11, (*Pl.* 5)

Station E-11 is approximately 180 miles northeast of Station E-10 and is also unreversed; the listening point is at the northeast end of the shot line. The water depth was approximately constant at 1100 fathoms (2.01 km). This is a very weak station.

The results here show two refracting layers, identified as semiconsolidated sediments and basement, in which the velocities are respectively 2.08 and 4.97 km/sec. The unconsolidated sediments were assumed to have a velocity of 1.71 km/sec. The semiconsolidated sediments are determined by strong arrivals for most of the shots, but some shots were apparently too small to produce good arrivals through the basement. The basement velocity is determined by two reasonably good and three weak arrivals. The better ones are at ranges of 11.1 and 22.7 seconds. As in the preceding station, the accuracy of the results reported here depends on the assumption of no component of dip of the refracting layers in the direction of the shot line.

The arrivals through the semiconsolidated layer (2.08 km/sec) were remarkably strong and consistent at this station.

Station E-12 (*Pl.* 5)

This station is about midway between the Faeroe Islands and the northern tip of Scotland. The water depth decreased from 600 fathoms (1.10 km) at *A* to 200 fathoms (0.37 km) at *B*; the bottom slopes at a fairly uniform rate except for a rather sharp rise of 200 fathoms near *B*.

Most of the seismograms in the *A* profile were good, although the shots at ranges of 4.9 and 6.2 sec were too small to show the basement arrivals. The unconsolidated and semiconsolidated sediments are well determined here; the velocities are 1.72 and 2.24 km/sec respectively. These velocities are apparent (unreversed) since no sedimentary arrivals were recorded at *B*. Both ships recorded good basement arrivals which determine a true velocity of 4.91 km/sec.

The failure to record sedimentary arrivals at *B* was due in part to equipment trouble. One set of

apparatus became inoperative before the station was finished, and it was probably responding poorly on some of the later shots where the arrivals should have been observed. It is also possible that the sharp topographic rise near point *B* acted as a baffle for the sedimentary arrivals. In any event, it was necessary to make some assumptions about the sediments at *B*. Since this point is on the ridge which connects Faeroe Bank and Bill Bailey Bank with the mainland, it was assumed that there would be no unconsolidated sediments here; the very existence of the ridge suggests material fairly resistant to erosion. Accordingly, no unconsolidated sedimentary line is shown on the travel-time graph, and the assumed line representing the semiconsolidated sediments was drawn tangent to R_1. The average thicknesses of the layers are thus 0.25 km for the unconsolidated and 1.56 km for the semiconsolidated layer.

Stations E-13 and E-14 (Pl. 5)

Stations E-13 and E-14 are in the North Sea about 180 miles northeast of the Firth of Forth. The azimuth of the shot lines is approximately east–west. The water depth remained constant at 50 fathoms (0.09 km) during all shooting runs. Although the stations are given separate numbers, they will be discussed jointly because of the end-to-end arrangement of the shot lines.

In both locations the unconsolidated sediments have a velocity of 1.71 km/sec, and the semiconsolidated sediments a velocity of 2.26 km/sec. A basement velocity of 4.96 km/sec was found at E-13 and 4.85 km/sec at E-14.

The total thickness of unconsolidated and semiconsolidated sediments averages about 3.2 km. A considerable amount of buried relief in the underlying basement rock is indicated by the fact that the extensions of the basement lines in the travel-time graph intercept the time axis at position *B* by different amounts. Since the basement is masked for first arrivals over a range of about 20 km in the area surrounding point *B*, it is not possible to determine the exact configuration of the sediment–basement interface, but it apparently is faulted or otherwise offset by about 1 km in the neighborhood of *B*, and the west side is down relative to the east side. On each side of *B* the interface has an apparent slope upward from *A* to *C* (east to west) of about 3° to 5°.

Station E-15 (Pl. 5)

This station is in the North Sea at the northern edge of Dogger Bank in 20 fathoms of water. The velocities for the two upper layers (1.73 km/sec for unconsolidated sediments and 2.03 km/sec for semiconsolidated sediments) are in close agreement with E-13 and E-14, and probably those layers are continuous between the two locations. The combined thickness of the two layers, however, has diminished from approximately 3 km at E-13 and E-14 to about 1 km here, and the velocity in the next deeper layer is 3.00 km/sec as compared with 4.90 km/sec at Stations 13 and 14. On the assumption that the 3.00 km/sec layer (presumably consolidated sediments) is underlain by the 4.90 km/sec basement found at Stations 13 and 14, the minimum thickness of consolidated sediments has been computed to be 3.4 km. In view of the thinner cover of low-velocity sediments found here, it might be expected that, on the shallowest part of Dogger Bank, the consolidated sediments are exposed on the sea floor, and their greater resistance to erosion accounts for the existence of the bank.

Station F-3 (Pl. 5)

This station is on the continental shelf between Norway and Spitsbergen. The bottom sloped uniformly along the shot lines from a depth of 250 fathoms (457 m) at *A* to 200 fathoms (366 m) at *B*. The first few shots at *A* indicate a velocity of 3.48 km/sec (presumably consolidated sediments). Assuming a velocity of 1.77 km/sec, the unconsolidated sediment is calculated to be 0.30 km thick at this end of the station. No shots at short range were received at *B*, hence data on sediment layers are missing. The dashed line on the travel-time curve represents the minimum velocity of 3.56 km/sec for the consolidated sediments and a minimum thickness of 1.11 km for the unconsolidated sediments at this end of the station. The average thickness of the unconsolidated sediments is 0.70 km. A single-refracting layer, velocity 5.11 km/sec, was found beneath the sediments. Both G_2 lines are offset by 0.2–0.3 sec near point *A*, indicating an increase of about 0.5 km in the depth to this layer.

Station F-8 (Pl. 5)

This station is on the continental slope west of Trondheim. Soundings showed a uniform slope from 330 fathoms (0.60 km) at *A* to 370 fathoms, (0.67 km) at *B*.

The section consists of unconsolidated (1.66 km/sec), semiconsolidated (2.08 km/sec), and consolidated sediments (3.44 km/sec) overlying the basement (4.01 km/sec apparent velocity).

All shots of the *B* profile produced strong ground-wave arrivals, but owing to equipment failure none was recorded in the *A* profile beyond a range of 13 km (8.5 sec of direct water-wave travel time). The line representing basement in that profile was drawn to reverse the corresponding line in the *B* profile. The value 4.01 km/sec represents only the lower limit of possible velocities for the basement.

DISCUSSION OF RESULTS: Reasonably good determinations of sediment velocity were made at most of the stations in this group. The velocity in the unconsolidated sediments was measured at five stations (average 1.7 km/sec) and was assumed at the others. In all except F-3, a semiconsolidated layer was found in which the average velocity is 2.2 km/sec; in all except E-11, E-12, E-13, and E-14, a consolidated layer with a velocity of 3.3 km/sec was present. The average velocity in the basement is 5.11 km/sec if all measurements are included and 4.96 km/sec if we exclude stations E-10 and F-8, which are unreversed and deviate most from the average. As mentioned earlier, this velocity is intermediate between the values found for consolidated sediment and basement in the neighborhood of the English Channel (Bullard and Gaskell, 1941; Hill and King, 1953; Hill and Laughton, 1954).

Within the rather wide limits imposed by the weakness of the data and the wide spacing of stations, Stations E-12, F-8, and F-3 offer no

contrast to typical continental-shelf stations elsewhere. The velocities in the central North Sea at Stations E-13, E-14, and E-15 are about the same as at the shelf stations mentioned above. Basement was not reached at Station E-15, but its depth is greater than 4 km, consistent with the concept of the North Sea as a sedimentary basin. The velocities found at the North Sea station are consistent with those reported for the adjacent stations in northwest Germany by Muhlen and Tuchel (1953), and in southeast England by Bullard *et al.* (1940).

Stations E-10 and E-11, both unreversed, give only apparent velocities. If the basement slope is simply related to the topography, the true basement velocity might lie between the values found at these two stations (6.96 and 4.97 km/sec). But if the apparent basement velocity at Station E-10 is not affected by slope, the similarity of this station to E-6 is noteworthy.

Continental Margin of North America

The present work includes four stations on the continental slope of North America, one southeast of Cape May, New Jersey, and the other three near the southeastern tip of the Grand Banks. The results are in general agreement with the findings of other investigators who have worked in these areas (Ewing, Worzel, Steenland, and Press, 1950; Officer and Ewing, 1954; Bentley and Worzel, 1956; Press and Beckmann, 1954; Drake *et al.*, 1957).

Station G-16 (*Pl.* 5)

This station is on the continental slope off New Jersey, extending the Cape May profile (Ewing, Worzel, Steenland, and Press, 1950) to the 1250-fathom contour.

The Cape May section is shown in Figure 8. The velocities found for the consolidated sediments and the basement complex (4.12 and 5.46 km/sec respectively) are in close agreement with the earlier work. The upper sediments are distinctly stratified in Station G-16, showing an unconsolidated layer (assumed velocity 1.68 km/sec) 0.68 km thick overlying a semiconsolidated layer (2.53 km/sec) 1.89 km thick. The stations on the shelf show the unconsolidated sediments to be 1.52 km thick near the slope, and no semiconsolidated sediments were found.

The profiles on the shelf were not long enough to penetrate to a sub-basement layer. Station G-16, however, shows that the basement complex is 5.2 km thick and is underlain by material with a velocity of 7.13 km/sec. Although no deeper refracting layer was found, a minimum depth calculation shows that the mantle with an assumed velocity of 8.0 km/sec must lie at a depth of at least 18 km.

Station E-2 (*Pl.* 5)

This is an unreversed station about 15 miles in length along the 2000-fathom curve east of the Grand Banks. The layer thicknesses are calculated on the assumption that there is no dip in the direction of the shot line. The section thus obtained shows 0.1 km of unconsolidated sediment (1.73 km/sec), 1.5 km semiconsolidated sediment (2.04 km/sec), 2.9 km of consolidated sediment (3.32 km/sec) overlying the basement (6.22 km/sec).

Station A-173-14 (*Pl.* 5)

This unreversed station is on the continental slope at the southern tip of the Grand Banks at the northwestern end of the Newfoundland Rise. The water depth is 1340 fathoms (2.45 km). The section shows 0.62 km of unconsolidated sediment (1.70 km/sec, assumed), 2.02 km of semiconsolidated sediment (2.46 km/sec), 1.06 km of consolidated sediment (3.80 km/sec) overlying the basement (5.80 km/sec).

Station A-173-13 (*Pl.* 5)

This station is on the continental slope east of the Grand Banks in 1310 fathoms (2.39 km). The section shows 0.49 km of unconsolidated sediment (1.70 km/sec, assumed), 2.14 km of semiconsolidated sediment (2.66 km/sec), 2.31 km of consolidated sediment (4.28 km/sec) overlying the basement (5.69 km/sec).

The measurements at the last three stations may be summarized by the following averages:

	Velocity km/sec	*Thickness km*
Unconsolidated sediments	(1.7)	0.6
Semiconsolidated sediments	2.4	1.9
Consolidated sediments	3.8	2.1
Basement	5.9	—

These should be compared with observations at several stations on the Grand Banks and along a line reaching beyond the foot of the continental slope south of Cape Race reported by Press and Beckmann (1954) and Bentley and Worzel (1956).

DISCUSSION OF RESULTS: In the Grand Banks area a semiconsolidated sediment layer, velocity about 2.5 km/sec, is present at all stations on the continental slope and extends well up on the continental shelf. A consolidated-sediment layer, velocity about 4.0 km/sec, is found at all stations. A basement layer, velocity about 5.6 km/sec, is found at all stations except A-173-6, the most southerly one on the line reported by Bentley and Worzel. This station is in 2600 fathoms and is an ocean-basin station. Despite the velocity, 6.2 km/sec, the deepest layer in the unreversed station E-2 is correlated with the 5.6 basement on the assumption that slope has produced a high apparent velocity.

In the three stations reported here the maximum shot distances were insufficient to show the sub-basement layer (7.5 ± km/sec) found at the three offshore stations of Bentley and Worzel.

Station G-16 extends the Cape May, New Jersey, section (Ewing, Worzel, Steenland, and Press, 1950) to the 1200-fathom curve on the

continental slope. There is good agreement with the earlier work of the velocities in the sedimentary layers and in crystalline basement. In addition, the new station measures the thickness of the basement complex and determines the Mid-Atlantic Ridge and its admixture with mantle material.

The mid-ocean ridge system is worldwide in extent (Ewing and Heezen, 1956) and generally follows a course midway between continental

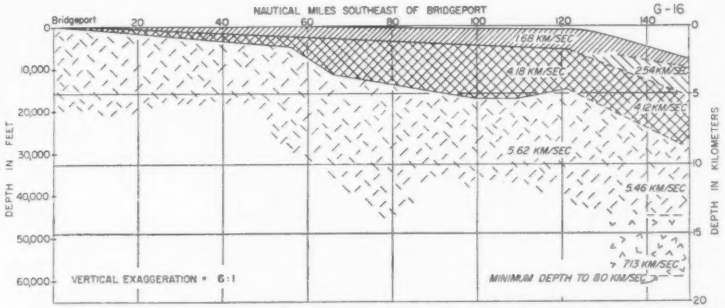

FIGURE 8.—STRUCTURE SECTION SOUTHEAST OF CAPE MAY, NEW JERSEY
Section from 0 to 120 miles taken from Ewing, Worzel, Steenland, and Press (1950)

a velocity of 7.13 km/sec for the sub-basement. The entire Cape May section is shown in Figure 8.

SUMMARY

The seismic measurements described in this paper have produced considerable data on the crustal and subcrustal structure of the earth at several locations in the Atlantic Ocean and in the Norwegian Sea. The observations made on the continental margins and in the Mediterranean Sea are inadequate for a comprehensive study of these areas but should be useful as a guide in future investigations or for comparison with other data.

The present work gives additional evidence that the oceanic crust is basaltic and generally about 5 km thick. It also shows that the Mid-Atlantic Ridge is a zone about 700 miles wide in which the crustal thickness is 25–30 km. From observed velocities and outcrops it is concluded that the upper 3–4 km are basaltic volcanic rocks which are underlain by a layer 20–25 km thick which is considered to be a mixture of basalt and mantle material.

Wager (1958), in a review of the petrological evidence on the composition of the crust and mantle, concluded that the solid mantle formed by settling of crystals, leaving an interprecipitate basaltic liquid which formed the oceanic crust. He attributes present-day basaltic lavas to the continued expulsion of interprecipitate liquid. Some additional mechanism is required to account for the concentration of basalt under masses, suggesting that it is as old as the continents themselves. A narrow median rift is apparently a characteristic feature. The seismic epicenter belt and the recent volcanoes follow the median rift very closely. The thermal flux through the ridges is several times greater than the average for ocean basins (Revelle, 1958; M. N. Hill, personal communication). On the East Pacific Rise, which Revelle reports as a region of definitely high heat flow, no seismic velocities greater than 7.5 km/sec were recorded, in good agreement with the Mid-Atlantic Ridge seismic results.

All these conditions would result from convection with rising currents under the mid-ocean ridges. These currents are now supplying magma and exerting extensional forces on the ridges. Apparently this is the convection system which determined the location of the continents.

REFERENCES CITED

Bentley, C. R., and Worzel, J. L., 1956, Geophysical investigations in the emerged and submerged Atlantic Coastal Plain. Part X: Continental Slope and Continental Rise south of the Grand Banks: Geol. Soc. America Bull., v. 67, p. 1–18

Birch, F., Schairer, J. F., and Spicer, H. C., *Editors*, 1942, Handbook of physical constants: Geol. Soc. America Special Paper 36, 325 p.

Bullard, E. C., and Gaskell, T. F., 1941, Submarine seismic investigations: Roy. Soc. London Proc., ser. A, no. 971, v. 177, p. 476–499

Bullard, E. C., Gaskell, T. F., Harland, W. B., and Kerr-Grant, C., 1940, Seismic investigations on the Palaeozoic floor of east England: Royal Soc. London Philos. Trans., ser. A, v. 239, p. 29–94

Drake, C. L., Sutton, G. H., and Ewing, M., 1957,

Continental margins and geosynclines: East coast of North America north of Cape Hatteras (Abstract): Geol. Soc. America Bull., v. 68, p. 1718–1719

Ewing, J. I., Officer, C. B., Johnson, H. R., and Edwards, R. S., 1957, Geophysical investigations in the eastern Caribbean: Trinidad Shelf, Tobago Trough, Barbados Ridge, Atlantic Ocean: Geol. Soc. America Bull., v. 68, p. 897–912

Ewing, M., and Heezen, B. C., 1956, Some problems of Antarctic submarine geology: Antarctica in the International Geophysical Year, Geophys. Mon. 1

Ewing, M. and Press, F., 1952, Crustal structure and surface-wave dispersion. Part II: Seismol. Soc. America Bull., v. 42, p. 315–325

Ewing, M., Sutton, G. H., and Officer, C. B., 1954, Seismic refraction measurements in the Atlantic Ocean. Part VI: Seismol. Soc. America Bull., v. 44, p. 21–38

Ewing, M., Woollard, G. P., and Vine, A. C., 1939, Geophysical investigations in the emerged and submerged Atlantic Coastal Plain. Part III: Barnegat Bay, N. J., section: Geol. Soc. America Bull., v. 50, p. 257–296

Ewing, M., Worzel, J. L., Ericson, D. B., and Heezen, B. C., 1955, Geophysical and geological investigations in the Gulf of Mexico. Part I: Geophysics, v. 20, p. 1–18

Ewing, M., Worzel, J. L., Steenland, N. C., and Press, F., 1950, Geophysical investigations in the emerged and submerged Atlantic Coastal Plain. Part V: Woods Hole, New York and Cape May section: Geol. Soc. America Bull., v. 61, p. 877–892

Ewing, M., Worzel, J. L., Hersey, J. B., Press, F., and Hamilton, G. R., 1950, Seismic refraction measurements in the Atlantic Ocean Basin. Part I: Seismol. Soc. America Bull., v. 4, p. 233–242

Gaskell, T. F., and Swallow, J. C., 1951, Seismic refraction experiments in the North Atlantic: Nature, v. 167, p. 723

—— 1952, Seismic refraction experiments in the Pacific: Nature, v. 170, p. 1010

—— 1953, Seismic refraction experiments in the Indian Ocean and in the Mediterranean Sea: Nature, v. 172, p. 535

Heezen, B. C., and Ewing, M., 1955, Orleansville earthquake and turbidity currents: Am. Assoc. Petrol. Geologists Bull., v. 39, p. 2505–2514

Hersey, J. B., Officer, C. B., Johnson, H. R., and Bergstrom, S., 1952, Seismic refraction observations north of the Brownson Deep: Seismol. Soc. America Bull., v. 42, p. 291–306

Hess, H. H., 1954, Geological hypotheses and the earth's crust under the oceans: Roy. Soc. London Proc., ser. A, v. 222, p. 341–348

Hill, M. N., 1952, Seismic refraction shooting in an area of the eastern Atlantic: Roy. Soc. London Philos. Trans., ser. A, v. 244, p. 561–596

Hill, M. N., and King, W. B. R., 1953, Seismic prospecting in the English Channel and its geological interpretation: Geol. Soc. London Quart. Jour., v. 109, pt. 1, p. 1–18

Hill, M. N., and Laughton, A. S., 1954, Seismic observations in the eastern Atlantic: Roy. Soc. London Proc., ser. A, v. 222, p. 348–356

Hodgson, J. H., 1947, Analysis of travel times from rockbursts at Kirkland Lake, Ontario: Seismol. Soc. America Bull., v. 37, p. 5–17

Jardetzky, W. S., and Press, F., 1953, Crustal structure and surface-wave dispersion. Part III: Seismol. Soc. America Bull., v. 43, p. 137–144

Katz, S., and Ewing, M., 1956, Seismic refraction measurements in the Atlantic Ocean. Part VII: Atlantic Ocean Basin, west of Bermuda: Geol. Soc. America Bull., v. 67, p. 475–510

Laughton, A. S., 1954, Laboratory measurements of seismic velocities in ocean sediments: Roy. Soc. London Proc., ser. A, v. 222, p. 336–341

Luskin, B., Landisman, M., Tirey, G. B., and Hamilton, G. R., 1952, Submarine topographic echoes from explosive sound: Geol. Soc. America Bull., v. 63, p. 1053–1068

Muhlen, W. von Zur, and Tuchel, G., 1953, A study of well velocity data in northwest Germany: Geophys. Prospecting, v. 1, p. 159–170

Officer, C. B., 1955, A deep-sea seismic reflection profile: Geophysics, v. 20, p. 270–282

Officer, C. B., and Ewing, M., 1954, Geophysical investigations in the emerged and submerged Atlantic Coastal Plain. Part VII: Continental Shelf, Continental Slope, and Continental Rise south of Nova Scotia: Geol. Soc. America Bull., v. 65, p. 653–670

Officer, C. B., and Wuenschel, P. C., 1951, Reduction of deep-sea refraction data: Palisades, N.Y., Lamont Geol. Observatory Tech. Rept. 1, 12 p.

Officer, C. B., Ewing, M., and Wuenschel, P. C., 1952, Seismic refraction measurements in the Atlantic Ocean. Part IV: Bermuda, Bermuda Rise and Nares Basin: Geol. Soc. America Bull., v. 63, p. 777–808

Officer, C. B., Ewing, J. I., Edwards, R. S., and Johnson, H. R., 1957, Geophysical investigations in the eastern Caribbean: Venezuelan basin, Antilles island arc, and Puerto Rico trench: Geol. Soc. America Bull., v. 68, p. 359–378

Press, F., and Beckmann, W., 1954, Geophysical investigations in the emerged and submerged Atlantic coastal plain. Part VIII: Grand Banks and adjacent shelves: Geol. Soc. America Bull., v. 65, p. 299–314

Raitt, R. W., 1949, Studies of ocean-bottom structure off southern California with explosive waves (Abstract): Geol. Soc. America Bull., v. 60, p. 1915

—— 1956, Seismic refraction studies of the Pacific Ocean basin. Part I: Geol. Soc. America Bull., v. 67, p. 1623–1640

Revelle, Roger, 1958, The DOWNWIND expedition to the Southeast Pacific (Abstract): Am. Geophys. Union, Tr., v. 39, No. 3, p. 528

Rothe, J. P., and Peterschmitt, E., 1950, Etude seismique des explosions d'Haslach: Ann. de l'Inst. de Physique due Globe de Strasbourg, Tome 5, p. 31

Sutton, G. H., and Bentley, C. R., 1953, Topographic correction curves: Palisades, N.Y., Lamont Geol. Observatory Tech. Rept. 3, 5 p.

Tatel, H. E., and Tuve, M. A., 1955, Seismic exploration of a continental crust, p. 35–50, *in* Poldervaart, Arie, *Editor*, Crust of the earth: Geol. Soc. America, Special Paper 62, 762 p.

Tolstoy, I., Edwards, R. S., and Ewing, M., 1953, Seismic refraction measurements in the Atlantic Ocean. Part III: Seismol. Soc. America Bull., v. 43, p. 35–48

Turner, F. J., and Verhoogen, J., 1951, Igneous and metamorphic petrology: N.Y., McGraw-Hill Book Co., 602 p.

Vening Meinesz, F. A., 1948, Gravity expeditions at sea, 1923–1938: Delftsche Uitgevers Maatschappy, Delft, v. 4, 233 p.

—— 1957, The geophysical history of a geosyncline. I: Proc. Roy. Netherlands Acad. Sci., ser. B, v. 60, p. 126–140

Wager, L. R., Beneath the earth's crust: The Advancement of Science, no. 58

LAMONT GEOLOGICAL OBSERVATORY (COLUMBIA UNIVERSITY), PALISADES, N. Y.

MANUSCRIPT RECEIVED BY THE SECRETARY OF THE SOCIETY, MARCH 11, 1958

LAMONT GEOLOGICAL OBSERVATORY CONTRIBUTION No. 327

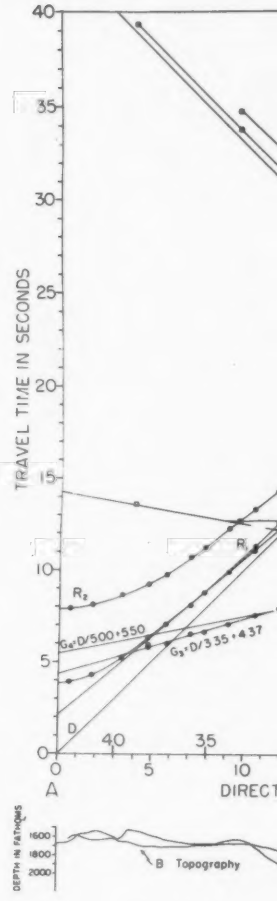
TRAVEL TIME IN SECONDS
40
35
30
25
20
15
10
5
0
R_1
R_2
G_2+D/500+550
G_3+D/335+437
D
0
5
10
40
35
A
DIRECT
DEPTH IN FATHOMS
1600
1800
2000
B Topography

TRAVEL TIME IN SECONDS
35
30
25
20
15
10
5
R_1

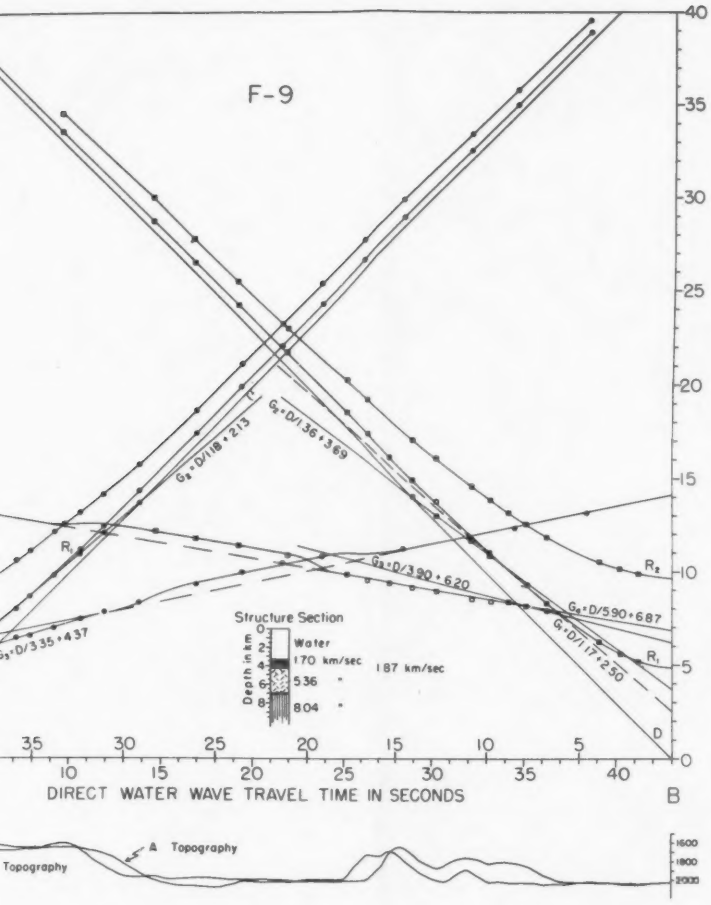
F-9
Structure Section
Water
1.70 km/sec
5.36 "
8.04 "
1.87 km/sec
Depth in km
DIRECT WATER WAVE TRAVEL TIME IN SECONDS
B
A Topography
Topography

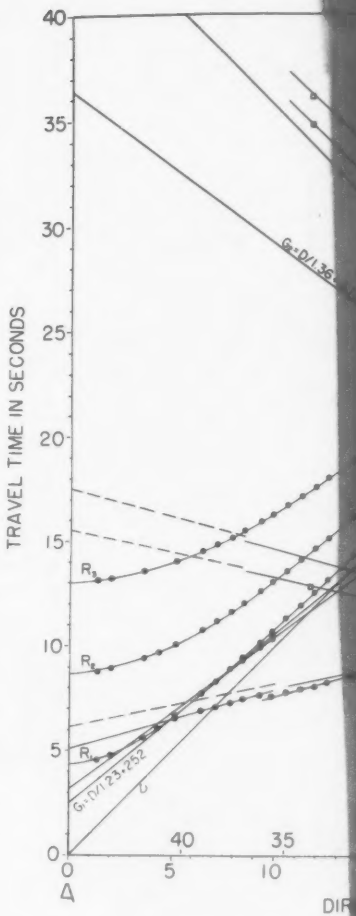
TRAVEL TIME IN SECONDS
A

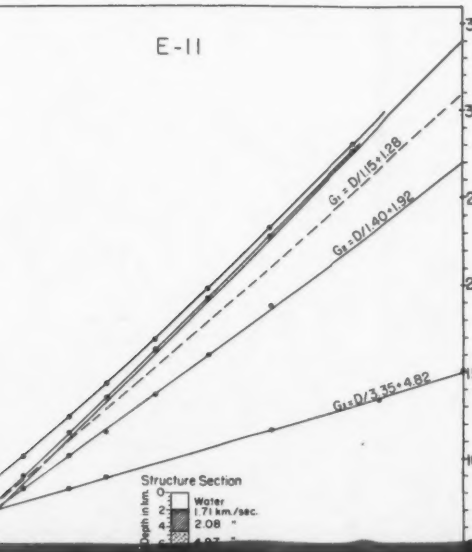
E-11
Structure Section
Water
1.71 km/sec.
2.08 "

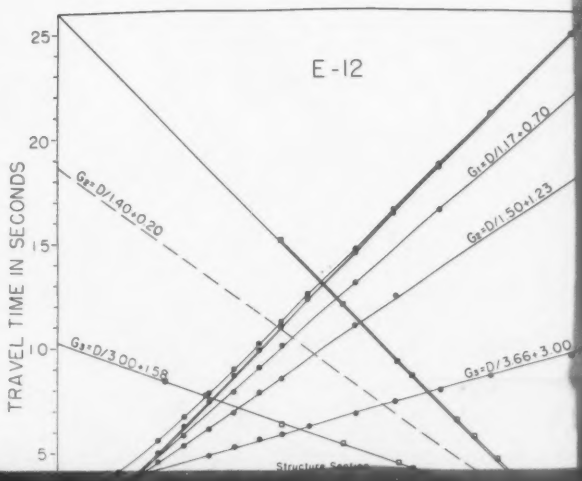
E-12
TRAVEL TIME IN SECONDS

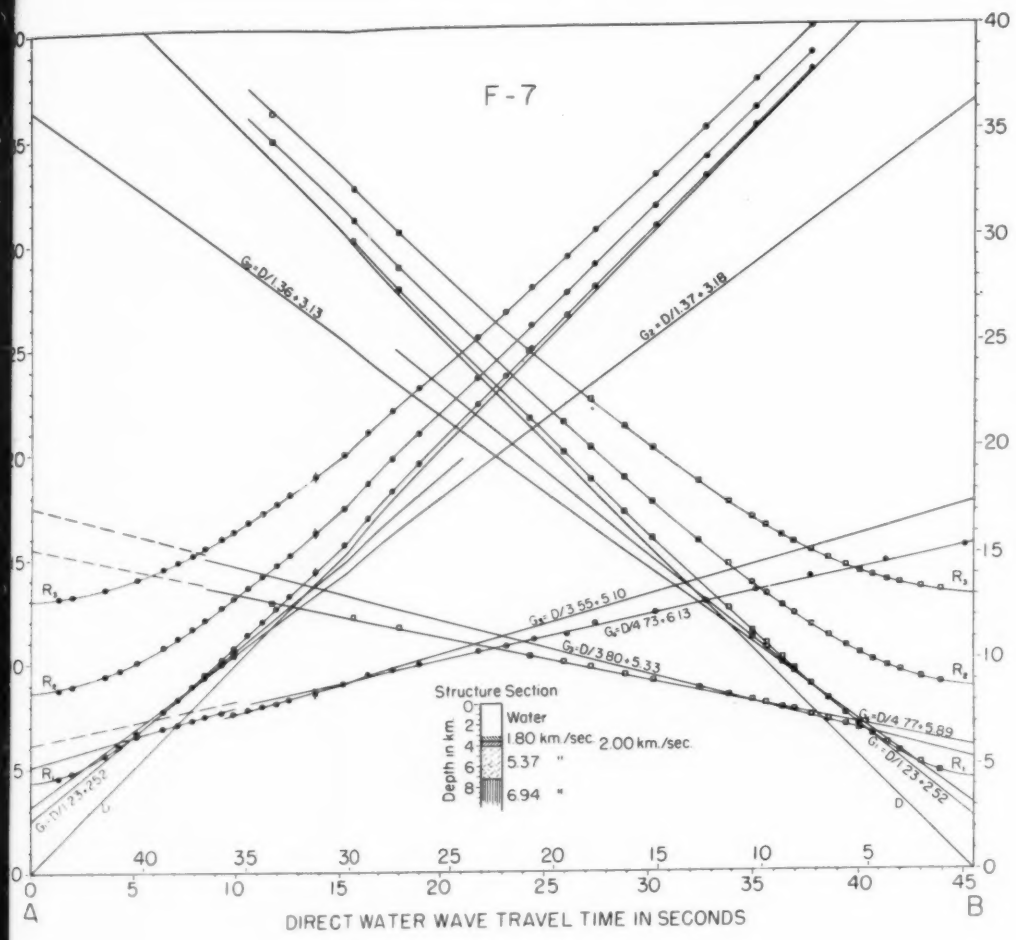
F-7
G=D/1.36+3.13
G=D/1.37+3.18
G=D/3.55+5.10
G=D/4.73+6.13
G=D/3.80+5.33
G=D/4.77+5.89
G=D/1.23+2.52
G=D/1.23+2.52
R3
R2
R1
D
Structure Section
Depth in km.
Water
1.80 km./sec.
2.00 km./sec.
5.37 "
6.94 "
A
B
DIRECT WATER WAVE TRAVEL TIME IN SECONDS

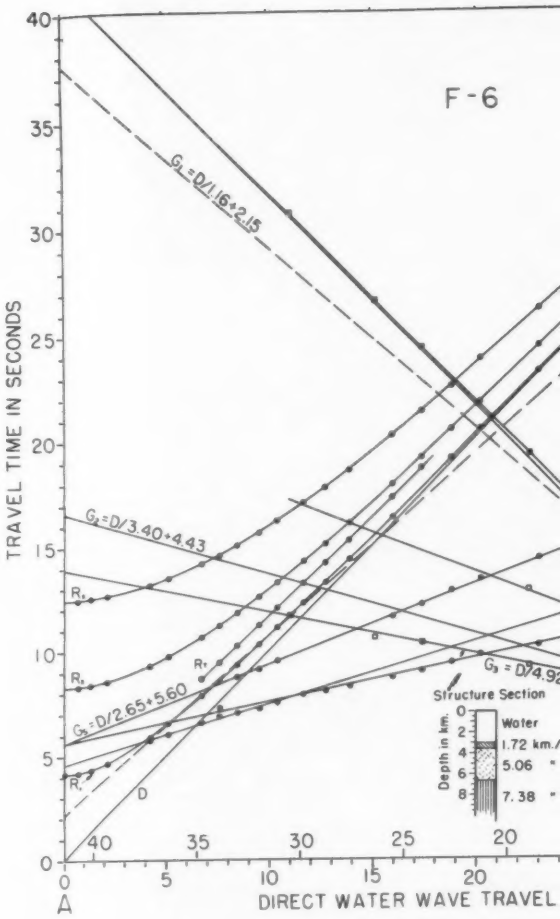
F-6
TRAVEL TIME IN SECONDS
G=D/1.16+2.15
G=D/3.40+4.43
G=D/2.65+5.60
R3
R2
R1
D
Structure Section
Depth in km.
Water
1.72 km./
5.06 "
7.38 "
A
DIRECT WATER WAVE TRAVEL

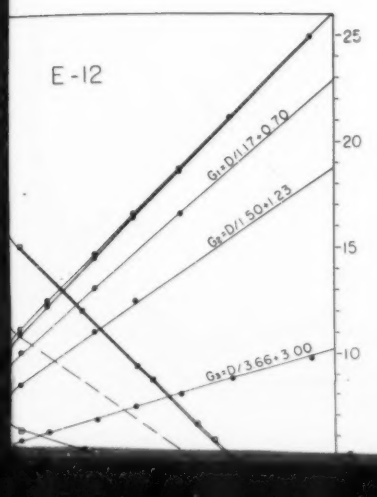
E-12
G=D/1.17+0.70
G=D/1.50+1.23
G=D/3.66+3.00

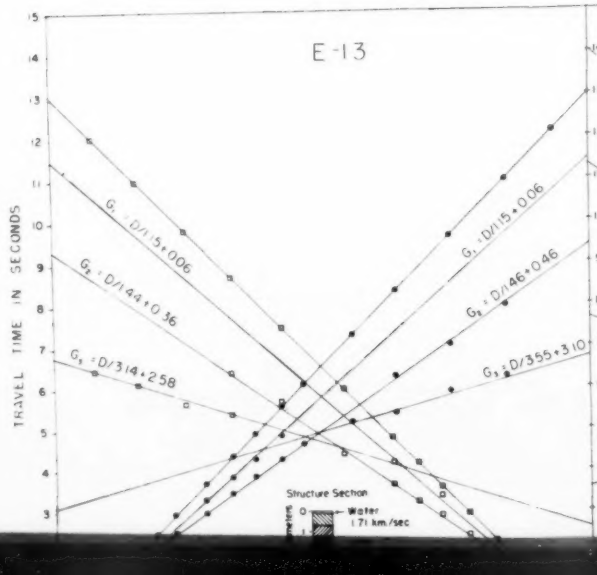
E-13
TRAVEL TIME IN SECONDS
G=D/1.15+0.06
G=D/1.44+0.36
G=D/3.14+2.58
G=D/1.46+0.46
G=D/3.55+3.10
Structure Section
Water
1.71 km/sec

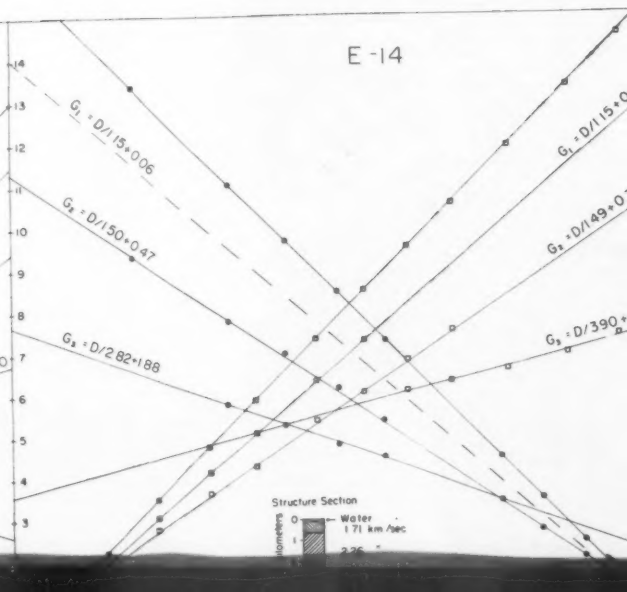
E-14
G=D/1.15+0.06
G=D/1.50+0.47
G=D/2.82+1.88
Structure Section
Water
1.71 km/sec

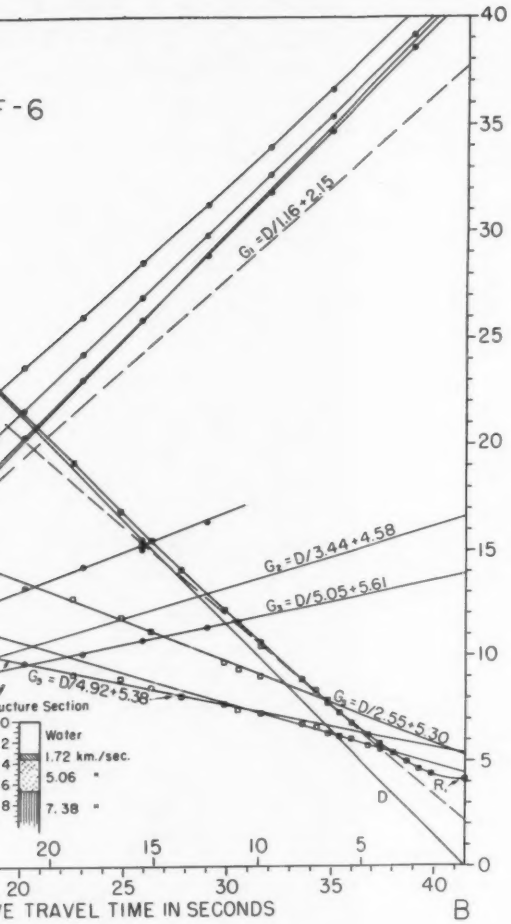
F-6
G1=D/1.16+2.15
G2=D/3.44+4.58
G3=D/5.05+5.61
G4=D/4.92+5.38
G5=D/2.55+5.30
D
R1
Structure Section
Water
1.72 km./sec.
5.06 "
7.38 "
TRAVEL TIME IN SECONDS
B

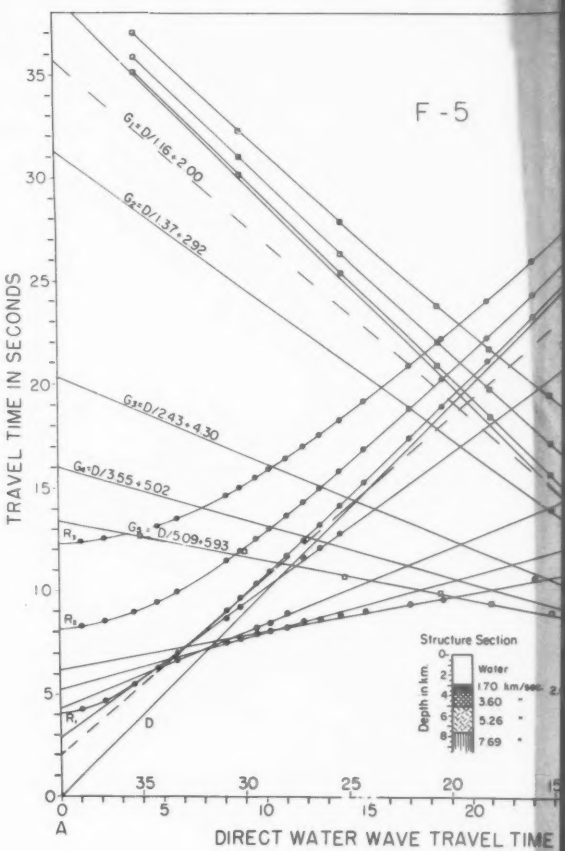
F-5
G1=D/1.16+2.00
G2=D/1.37+2.92
G3=D/2.43+4.30
G4=D/3.55+5.02
G5=D/5.09+5.93
R1
R2
R3
D
Structure Section
Depth in km.
Water
1.70 km./sec.
3.60 "
5.26 "
7.69 "
TRAVEL TIME IN SECONDS
A
DIRECT WATER WAVE TRAVEL TIME

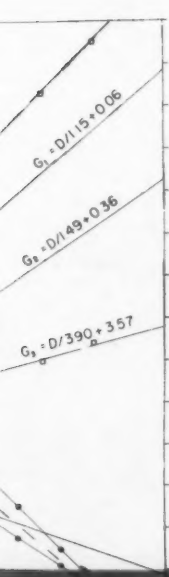
G1=D/1.15+0.06
G2=D/1.49+0.36
G3=D/3.90+3.57
TRAVEL TIME IN SECONDS

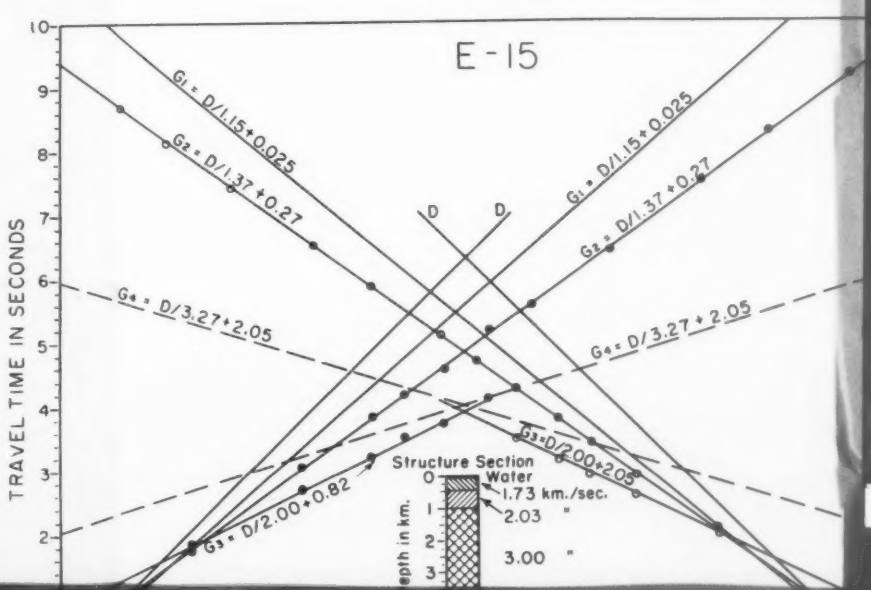
E-15
G1=D/1.15+0.025
G2=D/1.37+0.27
G3=D/2.00+0.82
G4=D/3.27+2.05
G5=D/2.00+2.05
D
D
Structure Section
Water
1.73 km./sec.
2.03 "
3.00 "
Depth in km.
TRAVEL TIME IN SECONDS

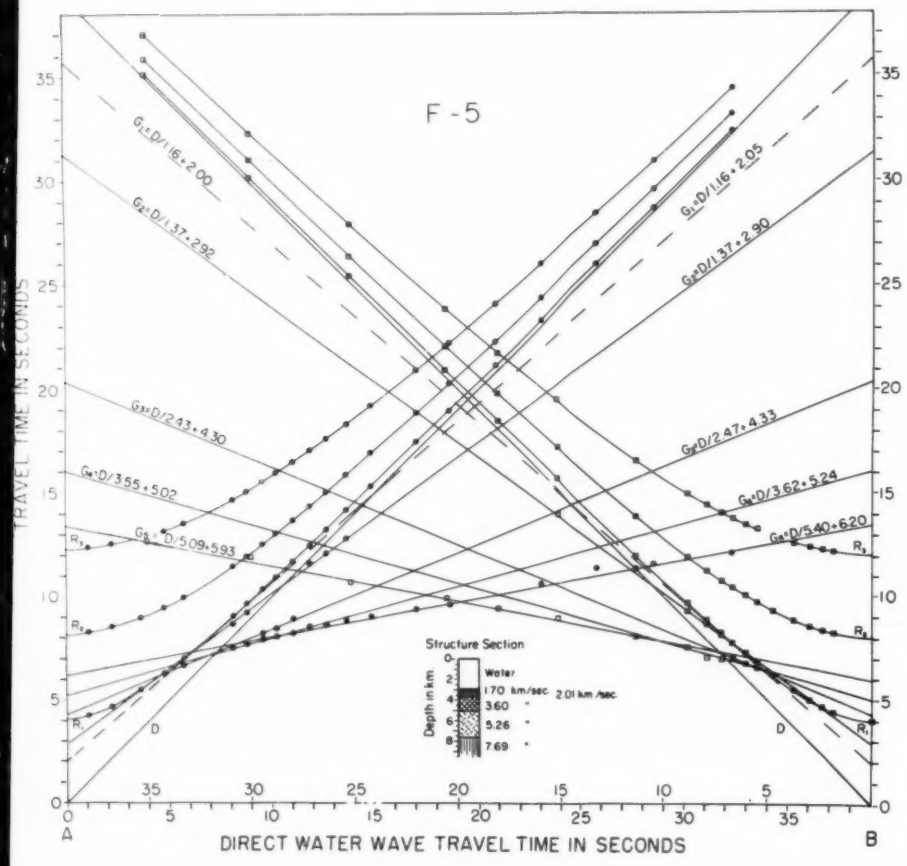
F-5
TRAVEL TIME IN SECONDS
DIRECT WATER WAVE TRAVEL TIME IN SECONDS
A
B
D
$G_1 = D/1.16 + 2.00$
$G_2 = D/1.37 + 2.92$
$G_3 = D/2.43 + 4.30$
$G_4 = D/3.55 + 5.02$
$G_5 = D/5.09 + 5.93$
$G_1 = D/1.16 + 2.05$
$G_2 = D/1.37 + 2.90$
$G_3 = D/2.47 + 4.33$
$G_4 = D/3.62 + 5.24$
$G_5 = D/5.40 + 6.20$
Structure Section
Depth in km.
Water
1.70 km/sec.
2.01 km/sec.
3.60 "
5.26 "
7.69 "

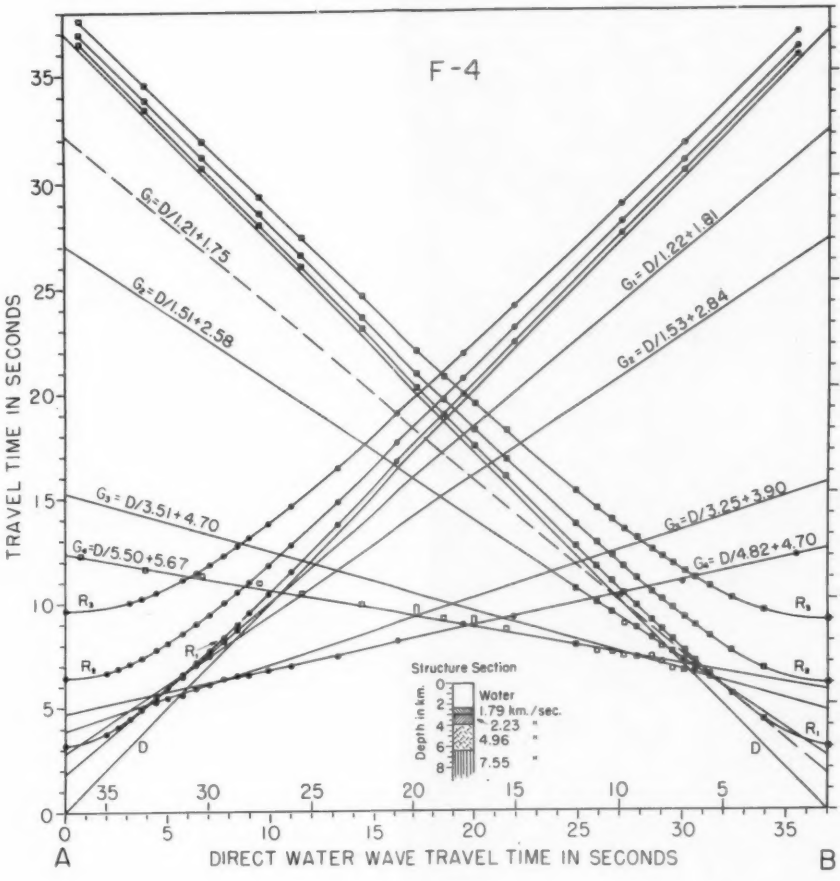
F-4
TRAVEL TIME IN SECONDS
DIRECT WATER WAVE TRAVEL TIME IN SECONDS
A
B
D
$G_1 = D/1.21 + 1.75$
$G_2 = D/1.51 + 2.58$
$G_3 = D/3.51 + 4.70$
$G_4 = D/5.50 + 5.67$
$G_1 = D/1.22 + 1.81$
$G_2 = D/1.53 + 2.84$
$G_3 = D/3.25 + 3.90$
$G_4 = D/4.82 + 4.70$
Structure Section
Depth in km.
Water
1.79 km./sec.
2.23 "
4.96 "
7.55 "

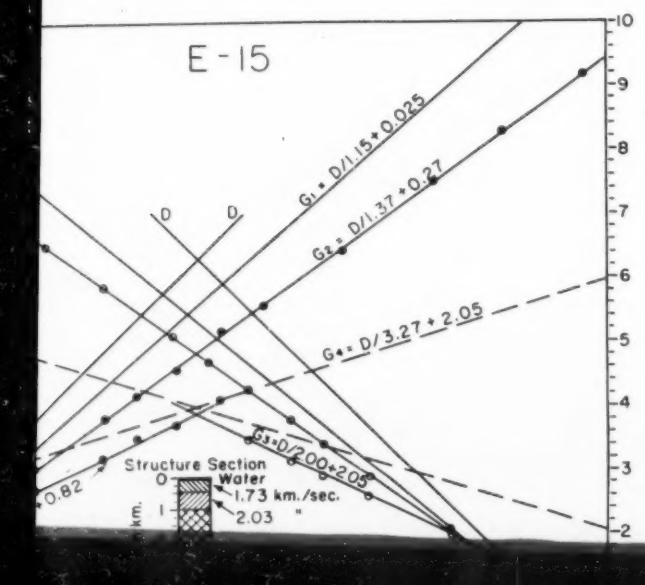
E-15
D
D
$G_1 = D/1.15 + 0.025$
$G_2 = D/1.37 + 0.27$
$G_4 = D/3.27 + 2.05$
$G_3 = D/2.00 + 2.05$
Structure Section
Water
1.73 km./sec.
2.03 "

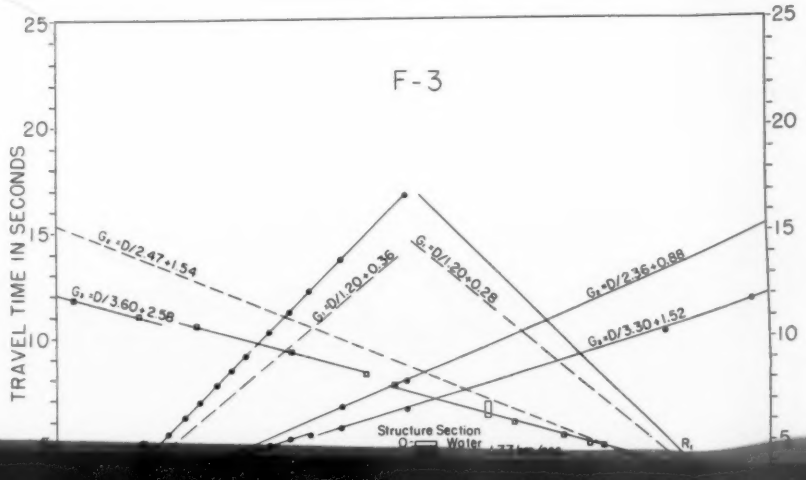
F-3
TRAVEL TIME IN SECONDS
$G_1 = D/2.47 + 1.54$
$G_2 = D/3.60 + 2.58$
$G_3 = D/1.20 + 0.36$
$G_4 = D/1.20 + 0.28$
$G_5 = D/2.36 + 0.88$
$G_6 = D/3.30 + 1.52$
Structure Section

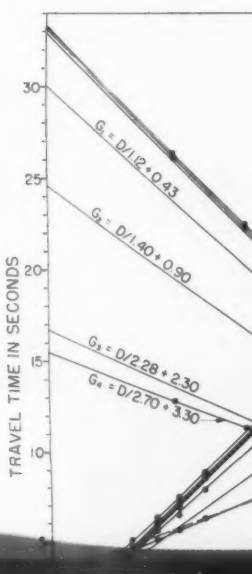
TRAVEL TIME IN SECONDS
$G_1 = D/1.12 + 0.43$
$G_2 = D/1.40 + 0.90$
$G_3 = D/2.28 + 2.30$
$G_4 = D/2.70 + 3.30$

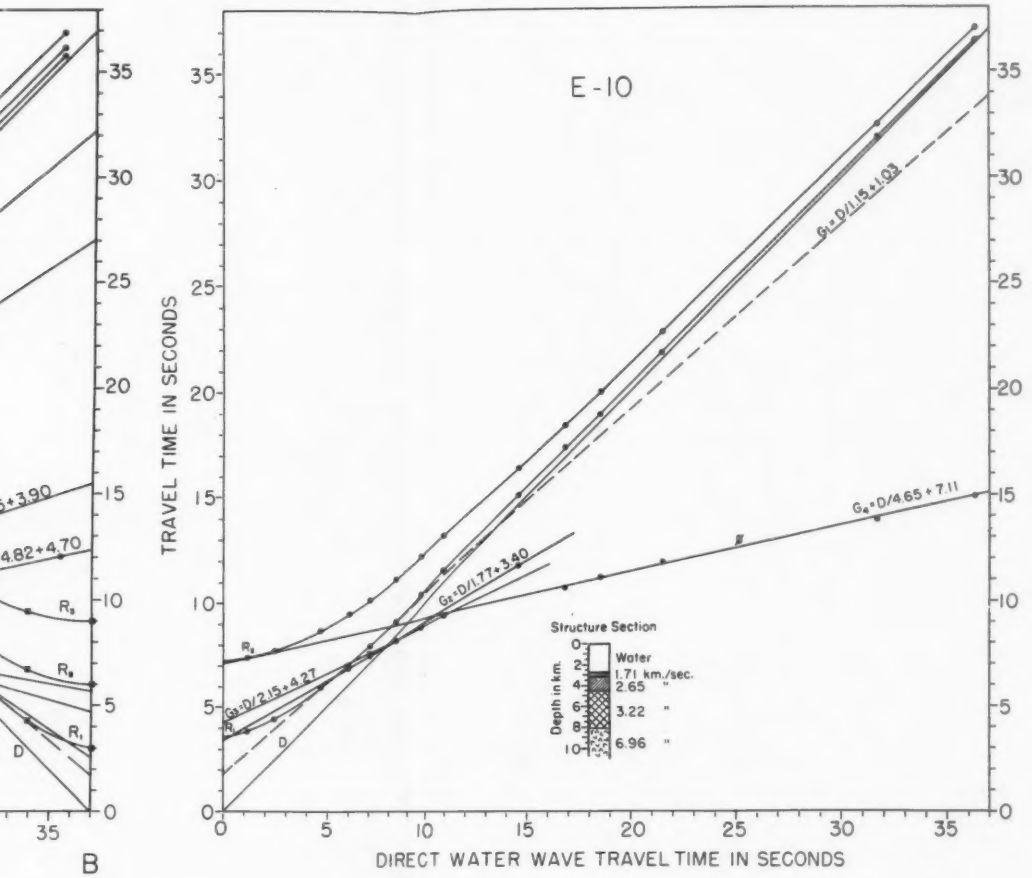
E-10
TRAVEL TIME IN SECONDS
DIRECT WATER WAVE TRAVEL TIME IN SECONDS
G₁=D/1.15+1.93
G₂=D/1.77+3.40
G₃=D/2.15+4.27
G₄=D/4.65+7.11
Structure Section
Depth in km.
Water
1.71 km./sec.
2.65 "
3.22 "
6.96 "
R₁
R₂
R₃
R₄
D
B

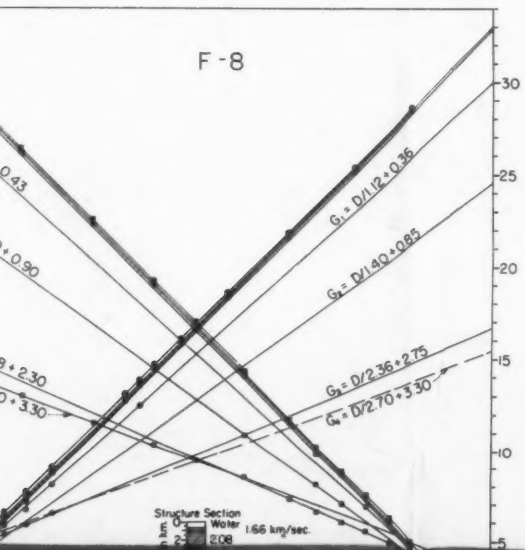
F-8
G₁=D/1.12+0.36
G₂=D/1.40+0.85
G₃=D/2.36+2.75
G₄=D/2.70+3.30
Structure Section
Water
1.66 km/sec.

TRAVEL TIME IN SECONDS
15
10
5
0
R1
R
D
5
10
DIRECT WATER

TRAVEL TIME IN SECONDS
40
35
30
25
20
15
10
5
0
G4 =D/170+3.21
G3 =D/276+4.79
G2 =D/366+6.18
G1 =D/475+7.90
R3
G5
G4
R2
G3
G2
R1
G
D
A
5
10

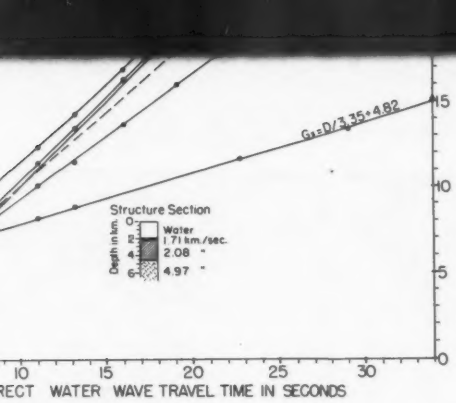
G_2=D/3.35+4.82
Structure Section
Depth in km
Water
1.71 km./sec.
2.08 "
4.97 "
RECT WATER WAVE TRAVEL TIME IN SECONDS

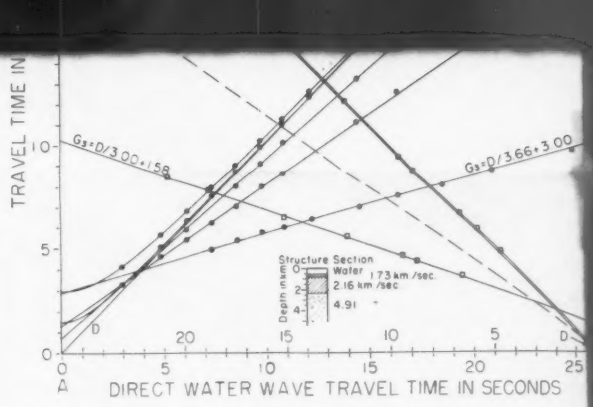
TRAVEL TIME IN
G_2=D/3.00+1.58
G_3=D/3.66+3.00
Structure Section
Water 1.73 km./sec.
2.16 km./sec.
4.91 "
A
DIRECT WATER WAVE TRAVEL TIME IN SECONDS

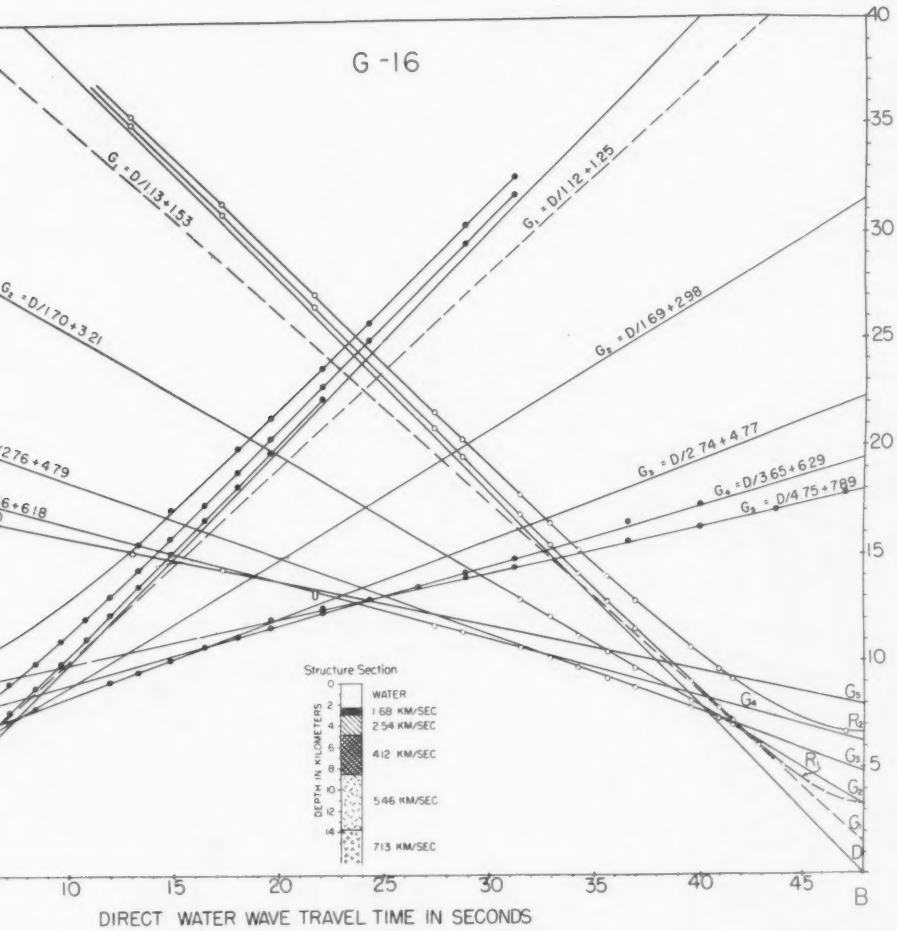
G-16
G_1=D/1.13+1.53
G_1=D/1.12+1.25
G_2=D/1.70+3.21
G_2=D/1.69+2.98
G_3=D/2.74+4.77
G_4=D/3.65+6.29
G_5=D/4.75+7.89
Structure Section
DEPTH IN KILOMETERS
WATER
1.68 KM/SEC
2.54 KM/SEC
4.12 KM/SEC
5.46 KM/SEC
7.13 KM/SEC
B
DIRECT WATER WAVE TRAVEL TIME IN SECONDS

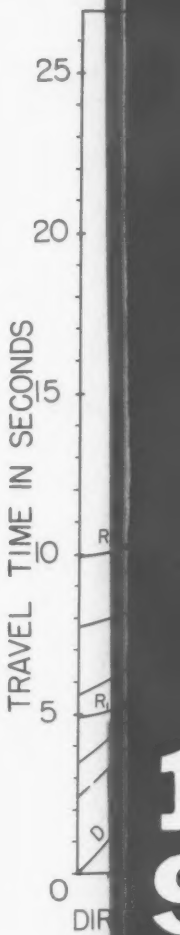
TRAVEL TIME IN SECONDS
DIR

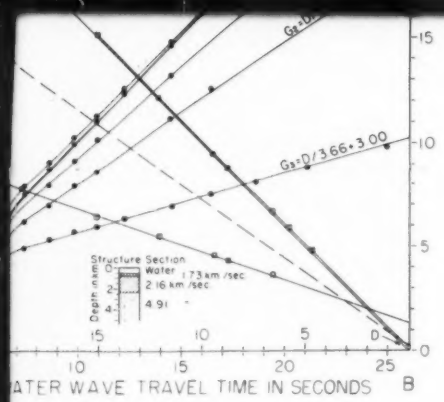

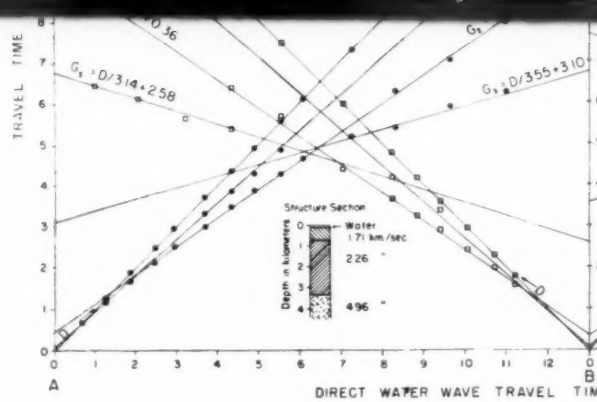

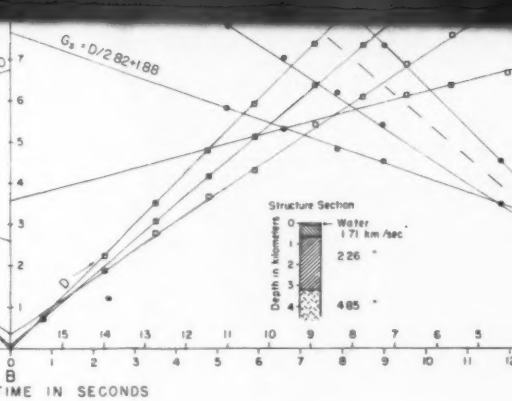

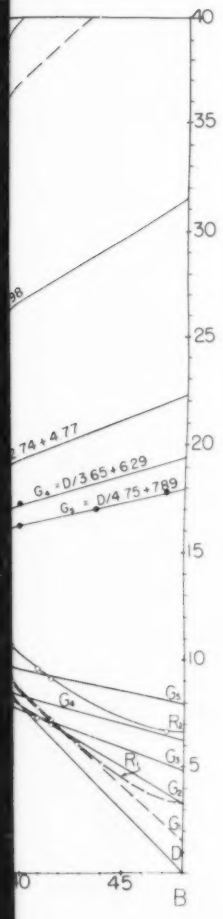

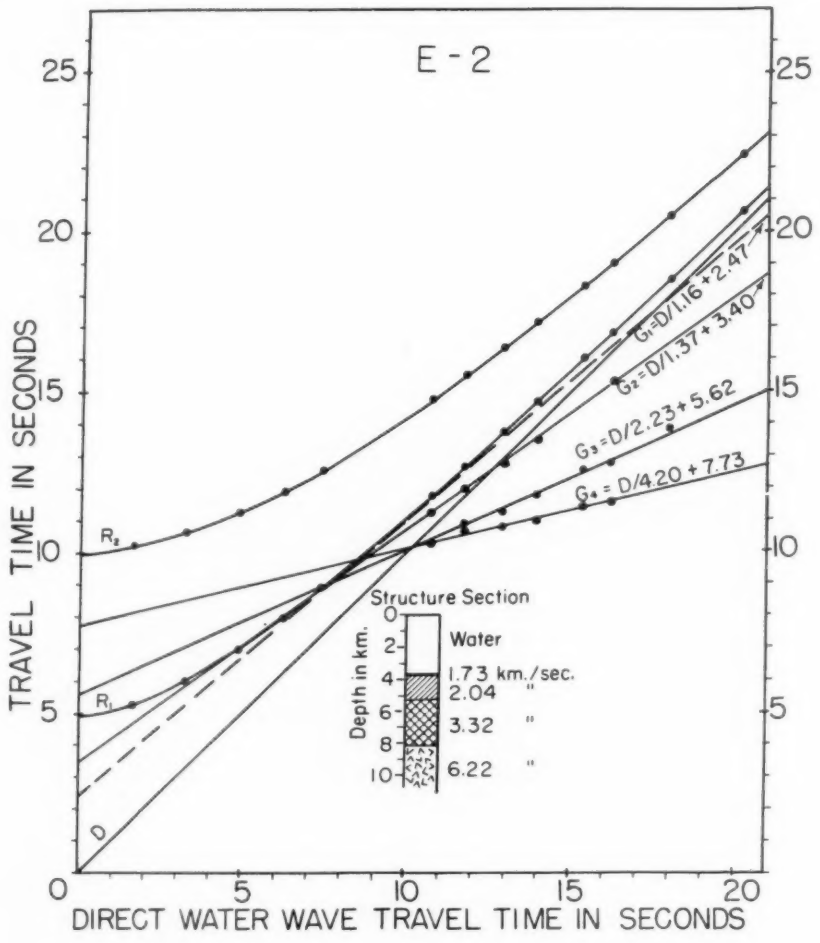

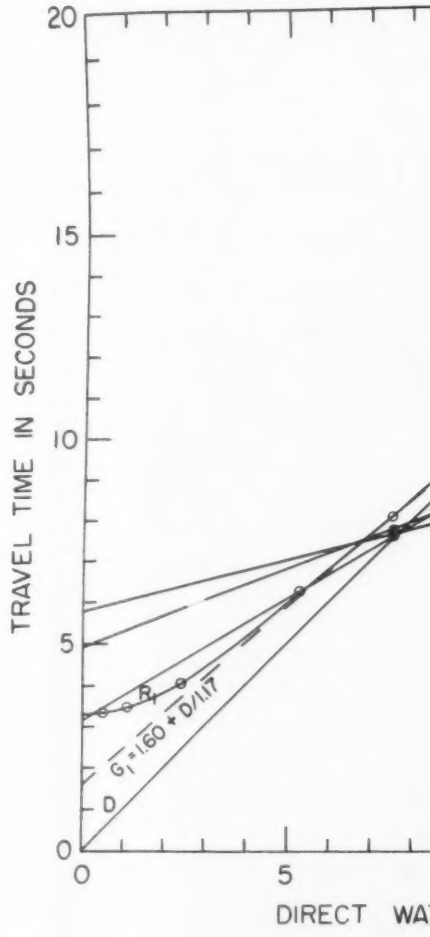

TRAVEL-TIME GRAP
SHELF OF BRITAIN A

Distance on the ab
of direct water-wa
approximately 5000 f

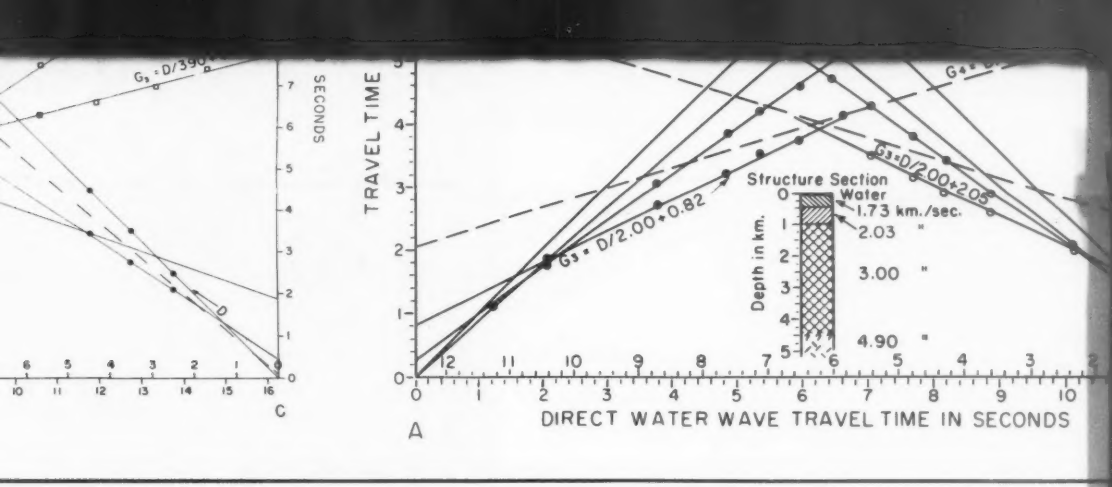

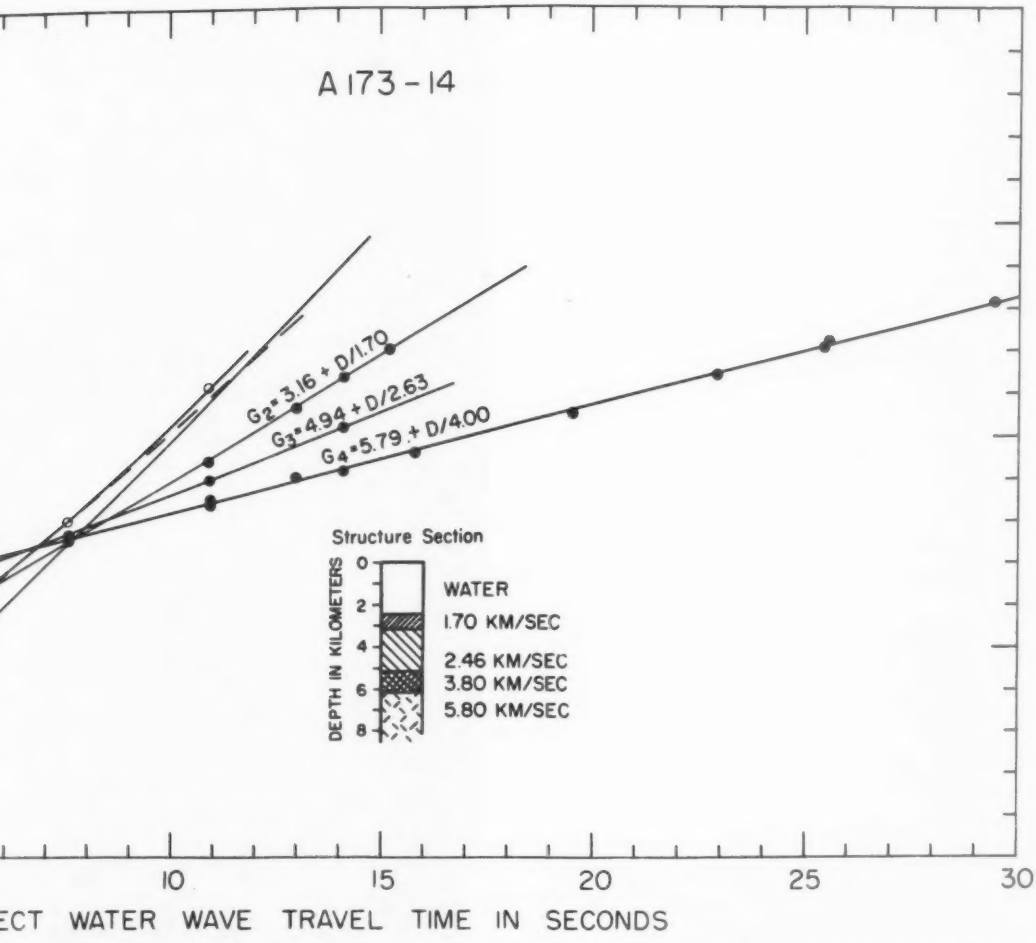

GRAPHS, NORWEGIAN AND GREENLAND SEAS; CO
AIN AND NORWAY; CONTINENTAL MARGIN OF NO

on the abscissa is plotted in increments water-wave time, *i. e.*, 1 second is ly 5000 feet. The lines G_1, G_2, G_3 .... are determined by refracted arrivals in su layers beneath the ocean floor. When G is d absent, the velocity in the top layer was a

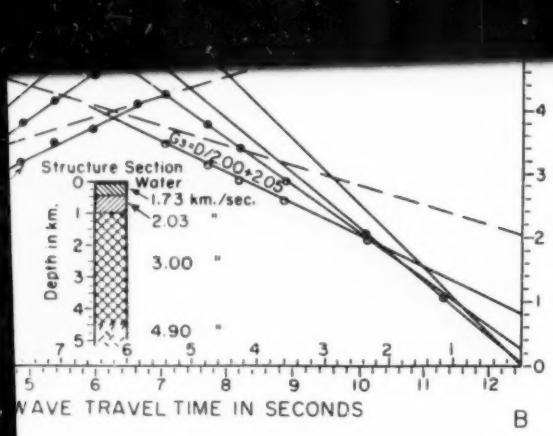

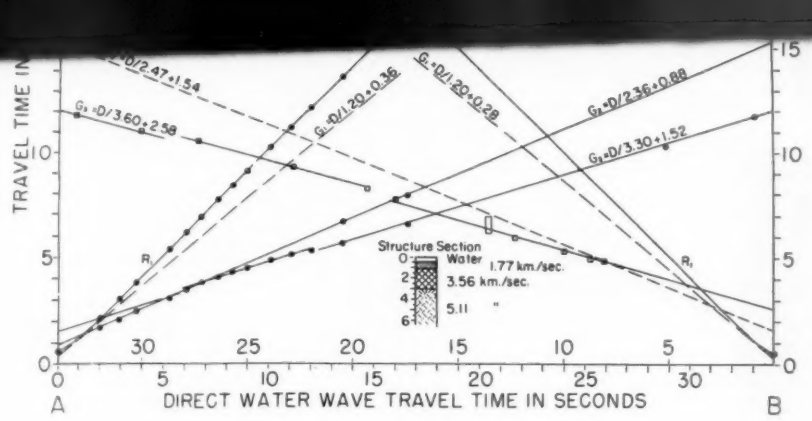

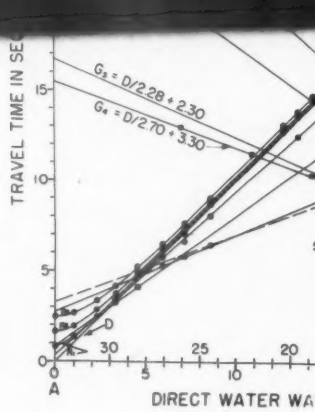

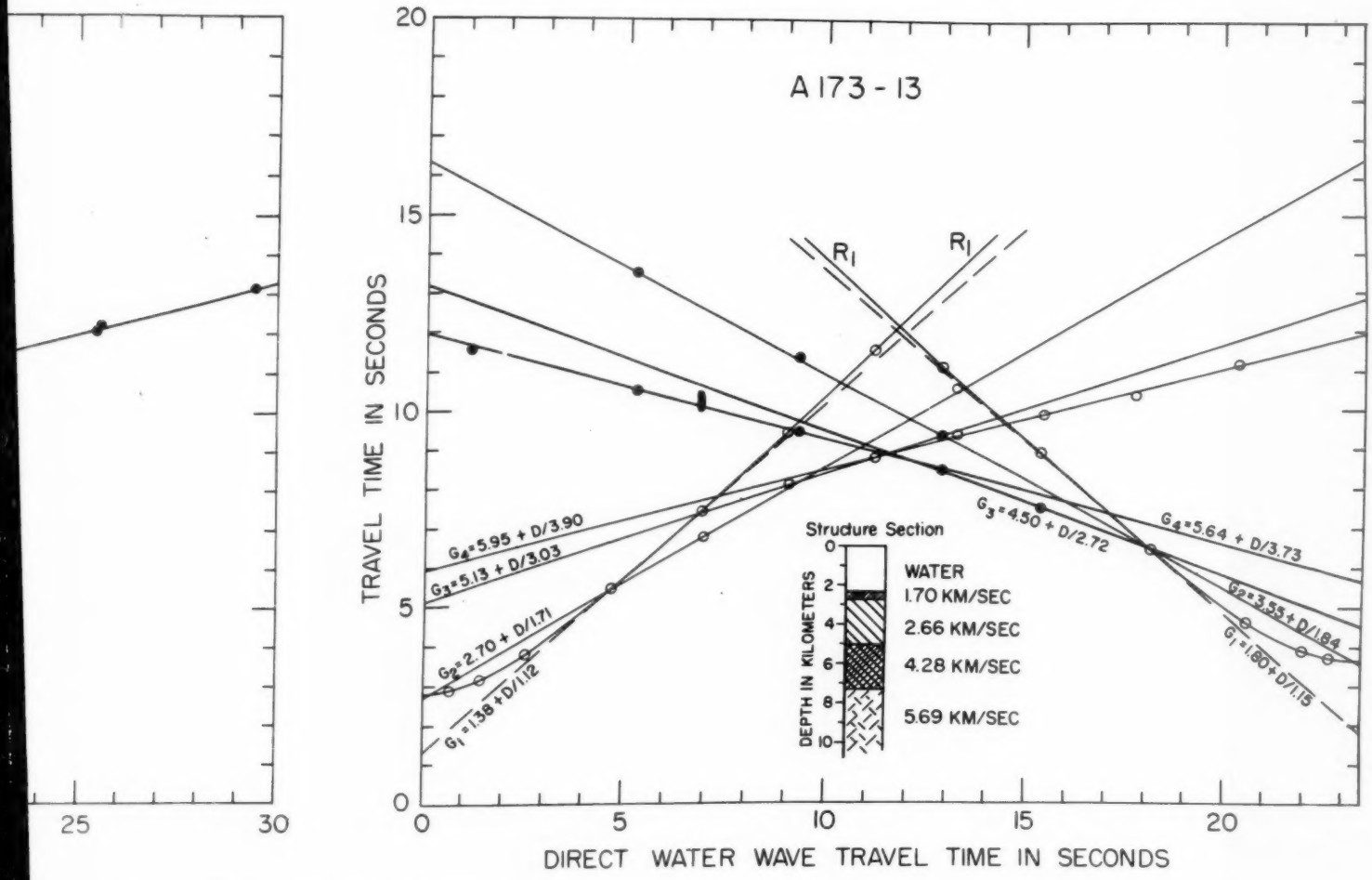

LAND SEAS; CONTINENTAL MARGIN OF NORTH AMERICA

y refracted arrivals in successive
e ocean floor. When G is dashed or
ty in the top layer was assumed.

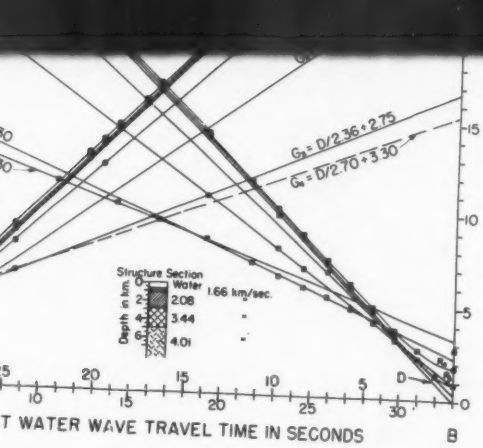

T WATER WAVE TRAVEL TIME IN SECONDS

B

I
A
P
F
S
C
R

BULLETIN OF THE GEOLOGICAL SOCIETY OF AMERICA
VOL. 70, PP. 319-342, 9 FIGS., 2 PLS. MARCH 1959

QUATERNARY GEOLOGY OF THE BENGAL BASIN, EAST PAKISTAN AND INDIA

BY JAMES P. MORGAN AND WILLIAM G. MCINTIRE

ABSTRACT

Reconnaissance of the Bengal provinces of East Pakistan and India indicates that structural activity, primarily faulting, has significantly influenced Quaternary geology. Two areas of Pleistocene terrace border the Bengal basin on the east and west and flank Tertiary and older hills of India. Two large inliers of Pleistocene sediments within the basin are surrounded by Recent flood-plain deposits of the Ganges and Brahmaputra rivers and their combined deltaic plain.

Block faulting and echelon faulting have so disturbed the topography of the Pleistocene terrace that the reconnaissance was insufficient to permit determination of whether multiple terraces are present within the basin. Faulting and structural uplift have continued into the Recent epoch, necessitating a physiographic subdivision into an early and a late phase.

Changes in the courses of the Ganges and Brahmaputra rivers through Bengal during the last few hundred years can be attributed to faulting and resultant tilting of fault blocks. These changes have caused the Ganges to abandon numerous western distributaries in favor of joining the Brahmaputra-Meghna system to the southeast. At present about 12,000 square miles of former Ganges deltaic plain in southwest Bengal has been abandoned.

A series of surface echelon faults plus evidence of structural control of stream courses suggest the presence of a subsiding structural trough or major fault at depth. This active structural zone apparently has controlled both the Brahmaputra and Ganges rivers in their lower reaches. Subsurface information is lacking, but this subsiding trough may possibly be related to the arcuate chain of mountains in adjacent Burma.

CONTENTS

TEXT

	Page
Introduction	320
Acknowledgments	321
Physical characteristics of Bengal	321
Physiographic units of the Bengal Basin	323
Pleistocene	323
General statement	323
Multiple terrace concept	324
Terraces flanking the Bengal Basin	326
The Barind	326
Madhupur Jungle area	329
Minor Pleistocene units	331
Summary	332
Recent flood plain	333
General statement	333
Alluvial fans	333
Tippera surface	333
Sylhet Basin	334
Bengal deltaic plain	335
Structural modification of Quaternary sediments	335
Faulting and folding in the Bengal Basin	335
Causes of echelon faulting	335
Conclusions	340
References cited	340

ILLUSTRATIONS

Figure	Page
1. Location map of the Bengal Basin	320
2. Index map showing locations within the Bengal Basin	322
3. Quaternary geology of the Bengal Basin	324
4. Composite grain-size curves of Pleistocene and Recent sediments of Bengal	325
5. Drainage map of the Pleistocene Barind surface	327
6. Profiles across Pleistocene and Recent surfaces	328
7. Rectangular drainage pattern of uplifted, early Recent surface contrasted with adjacent drainage	334
8. Map of earthquake epicenters since 1900	337
9. Structural forces affecting the Bengal Basin	338

Plate	Facing page
1. Fault scarps of the Sylhet Basin and Madhupur Jungle	330
2. Pleistocene terrace characteristics	331

TABLE

Table	Page
1. Evidence of subsidence in the Recent deltaic plain	336

Introduction

A geological reconnaissance of the Bengal provinces of East Pakistan and India was made from November 1955 through April 1956, principally to determine the morphology of the deltaic complex of the Ganges, Brahmaputra, and Meghna rivers and their distributaries (Fig. 1). Field techniques established through studies of the Mississippi River delta were applied to this larger, relatively unknown deltaic complex. Subsequent publications will compare these deltaic regions. Three major problems were recognized at the onset. First, the Ganges - Brahmaputra - Meghna delta, roughly twice the size of the Mississippi delta, has not been building seaward into the Bay of Bengal at anything like a normal rate for the last 200 years. This has been emphasized in the literature and is easily established by map comparisons. Second, lunar tides affecting the Bengal delta average 10 feet or more; those of the Mississippi River delta average 2 feet or less. Correlation of high tides with deltaic sedimentation will be considered in a subsequent paper. The third problem concerned the "older alluvium" of earlier writers (Ball, 1877, p. 69; Hirst, 1916, p. 10; Majumdar, 1942, p. 58; Oldham *et al.*, 1859, p. 266; Spate, 1954, p. 24). A. I. H. Rizvi (1955, unpub. PhD thesis, Louisiana State Univ.) and Wadia (1949, p. 287) have suggested that the "older alluvium" of Bengal is Pleistocene terrace material. The present writers hoped to establish conclusively whether or not this was correct and, if so, whether there were multiple Pleistocene terraces in Bengal similar to those mapped in the Mississippi Alluvial Valley.

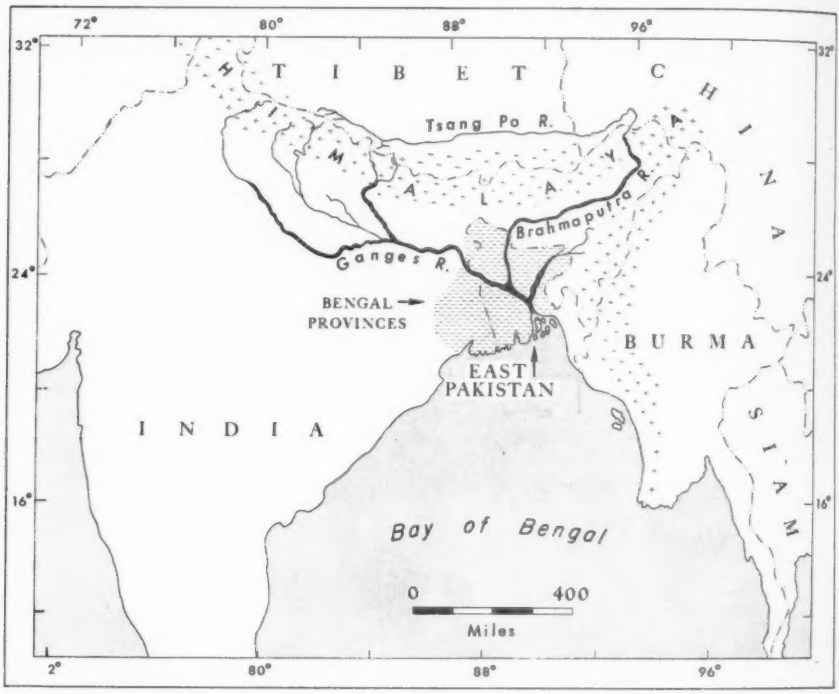

Figure 1.—Location Map of the Bengal Basin

There are four major areas of "older alluvium" in Bengal. The first area studied was the Madhupur Jungle, north of Dacca. Preliminary field work revealed that the Madhupur "old alluvium" is almost identical with the terrace material of the Gulf Coast. It stands appreciably higher than the surrounding flood plains, is composed of well-oxidized alluvial

sediments, compares in grain size with Recent flood-plain sediments, and displays sedimentary properties (such as stream cross-bedding) indicative of alluvial origin.

Prior to making aneroid barometer profiles to establish terrace surface levels, the writers studied aerial photographs of the region which showed that the western border of the Madhupur Pleistocene block (approximately 60 miles long) is delineated by six echelon faults. In addition, 10 or more secondary faults subdivide the block. Further interpretation of aerial photographs established that alluvial processes in northern Bengal have been controlled by Quaternary structural activity. The field program was modified to permit evaluation of this activity.

The area studied exceeds 70,000 square miles. Climatic conditions limited the field season to about 4 months and prevented the writers from making more than a reconnaissance study. Aerial photographs and observations were used extensively and conclusions are based upon interpretation of photographs coupled with as much field work as was possible within the time available.

Acknowledgments

This is one of a number of deltaic and coastal studies of the Coastal Studies Institute of Louisiana State University (R. J. Russell, Director). It was sponsored by the Geography Branch of the Office of Naval Research under Project No. N7 onr 35608, Task Order No. NR 388 002. The Bengal project was made possible by an affiliation with the University of Dacca, East Pakistan, through A. I. H. Rizvi, who had done graduate work with the writers at Louisiana State University. While in Pakistan Rizvi contributed immeasurably toward making preparations for and in assisting with field work. Co-operation of the University of Dacca through Dr. W. A. Jenkins, Vice Chancellor, and Dr. Nafis Ahmed, Geography Department, is greatly appreciated. Many governmental agencies of East Pakistan and India were exceedingly co-operative. Thanks are due especially to Mr. A. R. Quirashi of the Pakistan Survey, East Pakistan, and to V. P. Sondhi and K. Jacob of the Geological Survey of India for assistance and encouragement. Capt. H. A. Vazir, Chief Transportation Officer of the Home Department, East Pakistan, made boats available for field use. Much of the work would have been impossible without the friendly co-operation of Standard Vacuum Oil Company and Geophysical Services International personnel, too numerous to mention individually.

Appreciation is expressed to personnel of the Coastal Studies Institute who helped in the compilation of this paper. The writers especially acknowledge the valuable help and constructive criticisms of Richard J. Russell, who reviewed the manuscript. J. Hoover Mackin of the University of Washington and Richard Foster Flint of Yale University read the manuscript and made numerous thoughtful suggestions which are appreciated.

Physical Characteristics of Bengal

Bengal consists primarily of a large alluvial basin floored with Quaternary sediments deposited by the Ganges and Brahmaputra rivers and their numerous associated streams and distributaries. Much has been written about the physical characteristics of the Bengal area (Ascoli, 1910; Bagchi, 1944; Colebrooke, 1803; Muckerjee, 1938; Vredenburg, 1908; Willcocks, 1930). Figure 2 indicates the extent of the Bengal Basin.

The Geologic Map of India (West, 1949) indicates the Rajmahal Hills, which border the basin on the northwest and west, are composed of trap and are considered to be Lower Jurassic of the Upper Gondwana system (Ball, 1877, p. 1–94). The hills and trap plateaus range from 500 to 800 feet above sea level, although some individual hills exceed 1500 feet in elevation. Physiographically the hill section is sharply differentiated from the lower, flat, Quarternary alluvial and deltaic surfaces to the east.

The Bengal Basin is bounded on the northeast by the Shillong or Assam Plateau, locally known, from west to east, as the Garo, Khasi, and Jaintia hills. The plateau measures about 60 miles from north to south, about 150 miles from east to west, and is surrounded on the north, west, and south by low river basins. The basement rocks of the Shillong Plateau are intensely contorted Archean quartzites, slates, and schists, with masses of granitic intrusions and basic interbedded traps (Wadia, 1949, p. 76). The basement rocks are overlain by horizontal Eocene sandstones and nummulitic limestones (Wadia, 1949, p. 249). Elevations of the plateau summit range between 4500 and 6000 feet. The slope, approximating 500 feet per mile in places, breaks off abruptly from the plateau to the Sylhet Basin. It is an eroded fault scarp in the west (Pl. 1, fig. 1) and passes into a monoclinal fold toward the east (Krishnan, 1953, p. 58).

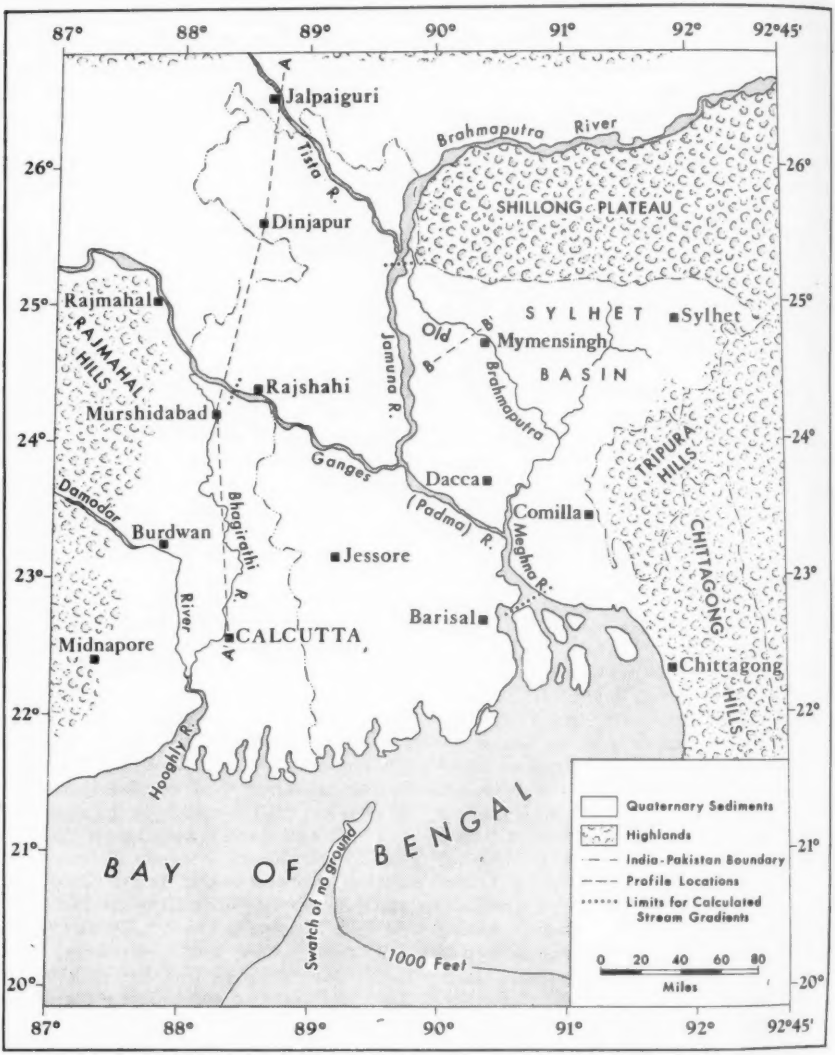

FIGURE 2.—INDEX MAP SHOWING LOCATIONS WITHIN THE BENGAL BASIN

Bengal Basin eastern limits are the Tripura Hills to the north and the Chittagong Hills to the south. The Geological Map of India (West, 1949) indicates they are composed of sediments of Paleocene through Pliocene age and include a representative section of Siwalik system sediments. The Chittagong-Tripura Hills are formed by folded sediments whose folding axes form an arc convex toward the west. The northern Tripura Hills include a series of plunging anticlines which die out under the overlapping Recent sediments of the Sylhet Basin. The Pakistan-India border follows the base of the hills, and border restrictions limited the field work in the hills proper. The folded terrane ranges from a few hundred feet to about 2000 feet above sea level. The folded, forested, sparsely populated hill tracts differ radically from the flat alluvial plains to the west.

The Bengal Basin is floored with Quaternary

sediments deposited by the Ganges, Brahmaputra, and Meghna rivers and their numerous distributaries. The Ganges discharges into the basin from the northwest after having drained the foothills of the Himalaya Mountain System over more than 1500 miles (Fig. 1). The Brahmaputra enters the basin from the northeast. It drains the northern slope of the Himalaya system by way of its principal tributary, the Tsangpo River of Tibet. The combined length of the Tsangpo and Brahmaputra rivers is 1800 miles. Headwaters of both the Ganges and Brahmaputra systems lie in the vicinity of the crest of the Himalaya Mountains. The Meghna river system drains the Sylhet Basin and parts of the adjacent Shillong Plateau and Tripura Hills (Fig. 2).

Discharge and sedimentary load figures are, in general, unavailable for the Bengal rivers, but for comparison, maximum flow of the Ganges River is on the order of 1.5 million cubic feet per second, whereas the Brahmaputra maximum flow probably exceeds 2 million cubic feet per second (Chatterjee, 1949, p. 10-11). The maximum measured flood on the Mississippi River carried about 2.4 million cubic feet per second; thus the Bengal deltaic plain has been developed by two rivers which are of the same order of magnitude as the Mississippi River.

Physiographic Units of the Bengal Basin

Pleistocene

General statement.—Figure 3 shows the distribution of Pleistocene alluvial terraces in the Bengal Basin. The four main areas of Pleistocene sediments and several smaller outliers stand topographically above the active flood plains. Of the four areas, two flank the basin; one is east of the Rajmahal Hill system, and the other is west of the folded Tripura Hills. Time did not permit more than a casual investigation of these areas.

The other two major areas of Pleistocene sediments lie within the Bengal Basin and are known as the Barind and the Madhupur Jungle. In addition to these are three small outliers which must be considered separately, namely the Lalmai Hills near the eastern flank of the Bengal Basin, the Sylhet Hills north of the town of Sylhet, and the Chhatak Hills 15 miles northwest of Sylhet. These areas have been mapped as Pleistocene (Fig. 3) because of their sedimentary properties and physiographic expression. The Lalmai Hills consist of an uplifted Pleistocene block bounded by faults. The other two areas may have had similar origins, but no faults are evident, possibly because of the rapid destruction of fault scarps by the monsoonal rainfall.

Sediments examined in the Pleistocene areas of Bengal were deposited as flood plains of earlier Ganges-Brahmaputra river systems. As far as grain size and mineral content are concerned, Pleistocene sediments are almost identical with those of the Recent flood plain. Grain-size analyses of 39 samples of Recent sediments collected over the entire Bengal Basin are plotted as two composite curves (*A* of Fig. 4), one representing well-sorted beach and towhead-island sands, and the other representing poorly sorted flood-plain and deltaic-plain sediments. Well-sorted sand is not as abundant in the Bengal Basin as might be inferred from the cumulative curves. Cumulative curves made from 16 samples of Pleistocene sediments are given in *B* of Figure 4. These are subdivided into average terrace samples and a few analyses of Pleistocene terrace sands (probably remnant towhead islands). Pleistocene and Recent samples do not differ in maximum grain size, but an excess of very fine-grained material is found in the Pleistocene samples. This could be related to weathering or pedogenesis.

Despite the similarity in grain size between Pleistocene and Recent sediments, field differentiation is simple. Recent sediments are typically dark, loosely compacted, and have a high water content and variable but appreciable quantities of organic material. Pleistocene sediments, on the other hand, are well oxidized and typically are reddish, brown, or tan, and are mottled. They commonly contain ferruginous or calcareous nodules. Water content is lower, resulting in firmer, more compacted material. Organic material in Pleistocene sediments is commonly confined to the surface soil profile.

The Pleistocene sediments are flood-plain deposits of earlier Ganges and Brahmaputra rivers. That they occur in several extensive areas above the level of present flood plains indicates that there has been differential movement between Pleistocene and Recent time. Differential relief between Pleistocene and Recent flood plains is extremely variable. Where fault scarps occur, as along the west flank of the Madhupur Jungle and around the Lalmai Hills, the relief is obvious. Where the Ganges River flows close to the southern end of the Barind, the relief is considerable. In other places, notably along the Pleistocene areas which flank the Bengal Basin on the east

and west, along the northeast and west sides of the Barind, and along the eastern and southern sides of the Madhupur, the Pleistocene slopes entrenched, meandering courses. Local relief is much greater. In order to cultivate rice, the staple commodity of Bengal, natives have

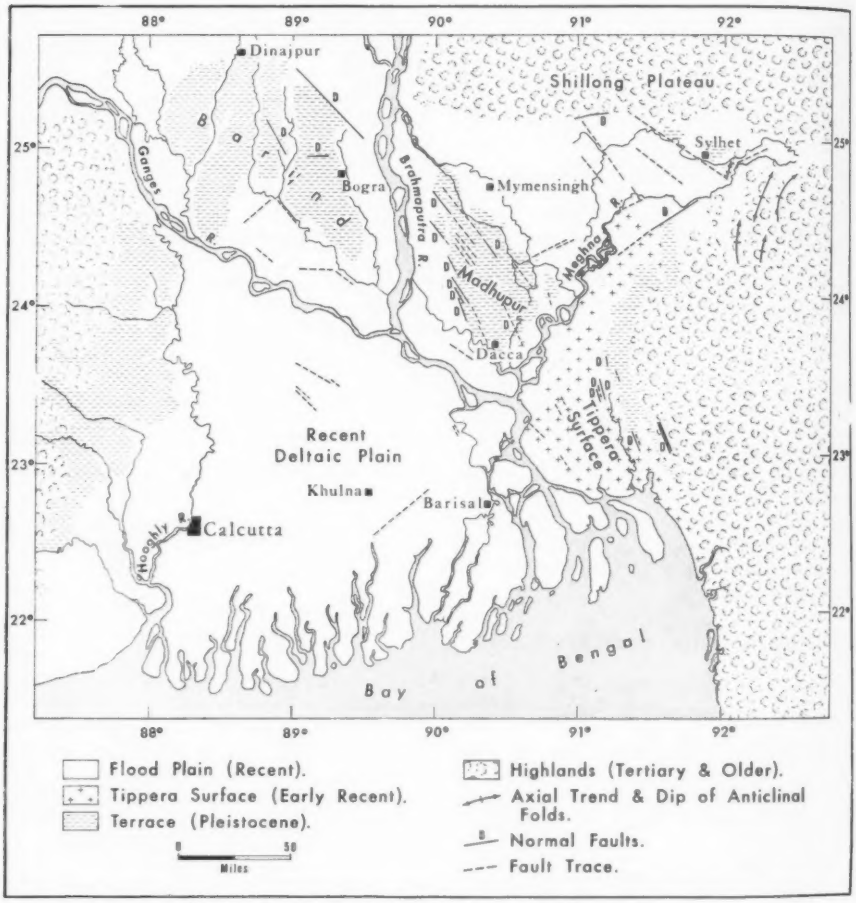

FIGURE 3.—QUATERNARY GEOLOGY OF THE BENGAL BASIN

gradually beaneath the overlapping Recent sediments.

Pleistocene and Recent surfaces can be differentiated readily on aerial photographs on the basis of tone, texture, and drainage patterns. Most of the Recent flood plain of the Bengal Basin is under water during the monsoon, and the surface is covered with stream scars of active and abandoned stream systems. The Pleistocene areas stand above monsoonal floods and are drained by a relatively few small streams which have developed distinctive, laboriously leveled and paddied the valleys of the small tributary dendritic streams; this leads to a distinctive pattern on aerial photographs which emphasizes minor local relief (Pl. 1, fig. 2).

Multiple terrace concept.—The development of Quaternary multiple alluvial terraces in major deltaic areas has been established in several parts of the world (Barbour, 1935; DeTerra, 1943, p. 271–339; Fisk, 1944; LeBlanc and Bernard, 1954; Russell, 1940, 1942). The development of multiple terraces, as recon-

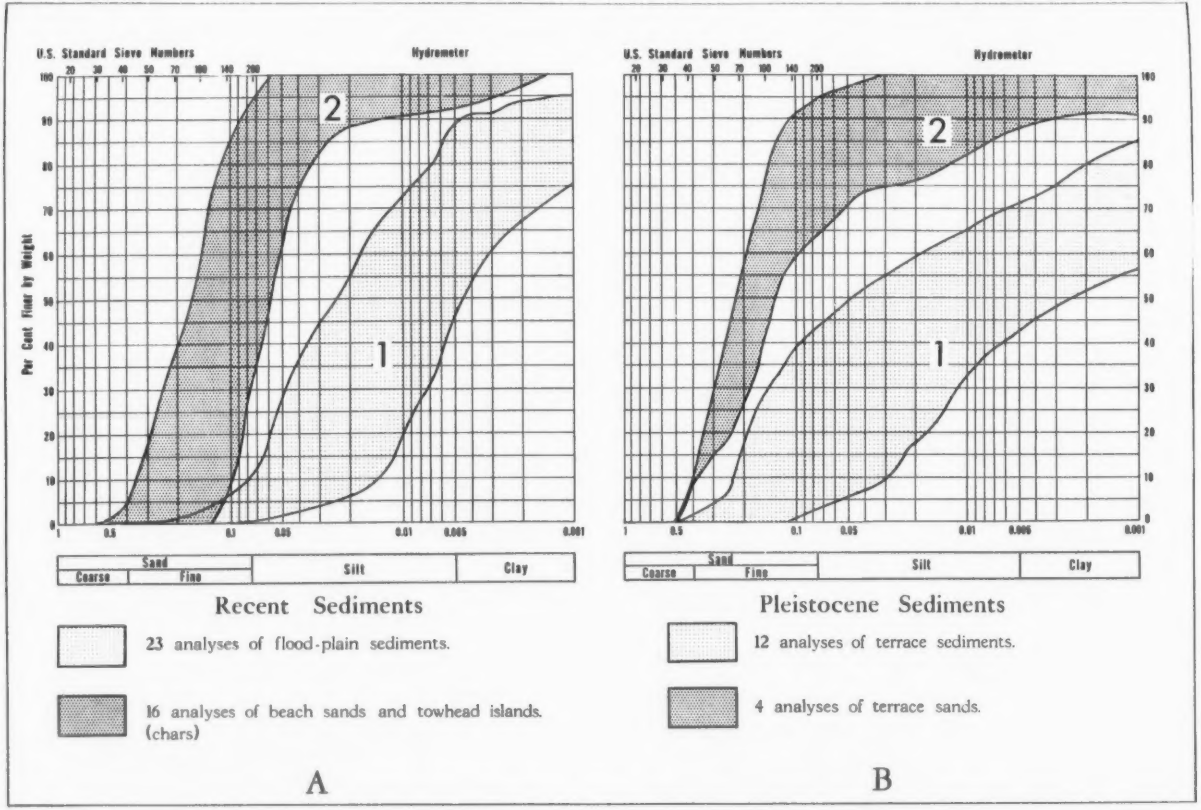

FIGURE 4.—COMPOSITE GRAIN-SIZE CURVES OF PLEISTOCENE AND RECENT SEDIMENTS OF BENGAL

structed from the Mississippi River deltaic region, is summarized herein.

During Pleistocene time, sea level fluctuated in response to the quantity of glacial ice on the continents. With each glacial advance, sea level dropped. In the Gulf Coast there were five such sea-level lowerings. During each, the gradients of major streams discharging into the Gulf abruptly increased. This resulted in rapid headward erosion and scour of stream valleys to a new base level 400 to 500 feet lower than that at present. With waning of the glaciers, sea level came back to a higher stand, and the entrenched valleys gradually lost their estuarine character through filling with alluvial sediments.

The interglacial periods, however, were of much greater duration than the glacial periods. During the long interglacial periods, the Gulf Coast geosyncline, a long, broad, sediment-filled trough roughly paralleling the coast line, continued subsiding, and compensatory inland uplift occurred. The combined effects of seaward subsidence and landward uplift have caused a warping of the older alluvial deposits. Four Pleistocene terraces and a Recent alluvial surface in the Gulf Coast can be related to five glacial and interglacial periods. The oldest terrace has been subjected to greater uplift landward and corresponding subsidence seaward, with the result that it is physiographically the highest-standing terrace surface inland, and seaward it is the most deeply buried Pleistocene geologic unit. The youngest terrace for the same reasons is lowest physiographically and shallowest in the subsurface. There is then a series of four alluvial terraces inland passing through respective hinge lines into buried alluvial and deltaic sequences seaward. In the Gulf Coast of the United States, the oldest terrace, because of its age and greater elevation, has been weathered and eroded most. Hence its sediments are more completely oxidized, and physiographically it is more rolling and exhibits greater relief.

The four-terrace system has been based upon detailed mapping and recognition of a series of alluvial flats with elevations sloping seaward toward each respective hinge line. Seaward slopes of the four terraces steepen from youngest to oldest, indicating the increasing length of time they have been subjected to tilting through geosynclinal downwarping.

Prior to field work in the Bengal Basin the possibility of multiple Pleistocene terraces was anticipated. Earlier writers (A.I.H. Rizvi, 1955, unpub. PhD thesis, Louisiana State Univ.) had described the "old alluvium" as high-standing, highly oxidized, and possessing many properties of Gulf Coast Pleistocene terraces. The east-west-trending Ganges-Brahmaputra Valley has been described as a foredeep flanking the front of the convex Himalaya Mountain chain (Krishman, 1953, p. 81–82). The subsiding trough has accumulated sediments perhaps on the order of 10,000 feet thick (Krishman, 1953, p. 82). The relationship of the Bengal Basin to this trough is not known, but during the Quaternary the Ganges, Brahmaputra, and Meghna rivers have been contributing enormous quantities of alluvium to the basin. The problem was to determine whether the Bengal Basin has been subsiding like the Gulf Coast Geosyncline, with compensating uplift and tilting of the Pleistocene to the north.

Terraces flanking the Bengal Basin.—No field work was done in the far western area flanking the Rajmahal Hills or the far eastern area flanking the Tripura Hills. They have been mapped (Fig. 3) as Pleistocene for the following reasons. Topographically they stand lower than the flanking hills on the sides but higher than the adjacent flood plain. On aerial photographs distinct tonal differences separate the Tertiary or older-hill areas and the areas mapped as Pleistocene. The drainage patterns of the valley-flank areas are similar to those of the Barind and Madhupur Jungle which have been studied. Modification of the dendritic stream valley bottoms into rice paddies indicates relief similar to that of known Pleistocene areas. Earlier workers have described both old and new alluvium as flanking the hills but did not attempt to differentiate or map the units (Ball, 1877; Oldham *et al.*, 1859).

The Barind.—The Pleistocene area called the Barind is the largest of the Bengal Basin units; it covers about 3600 square miles (Fig. 3). It has long been recognized as "old alluvium" differing from the surrounding Recent flood plain. Figure 5 shows the limits of the Barind and its relationship to the regional drainage system. It has been mapped as four distinct Pleistocene bodies separated by long, narrow Recent alluvial river valleys. The flood plain of the Mahananda River flanks the west side; the Karatoya River delineates the eastern margin. The Purnabhaba, Atrai, and Jamuna rivers with headwaters in the Himalaya foothills have cut across the Pleistocene, and their flood plains delineate the four units. These and numerous other streams have deposited a

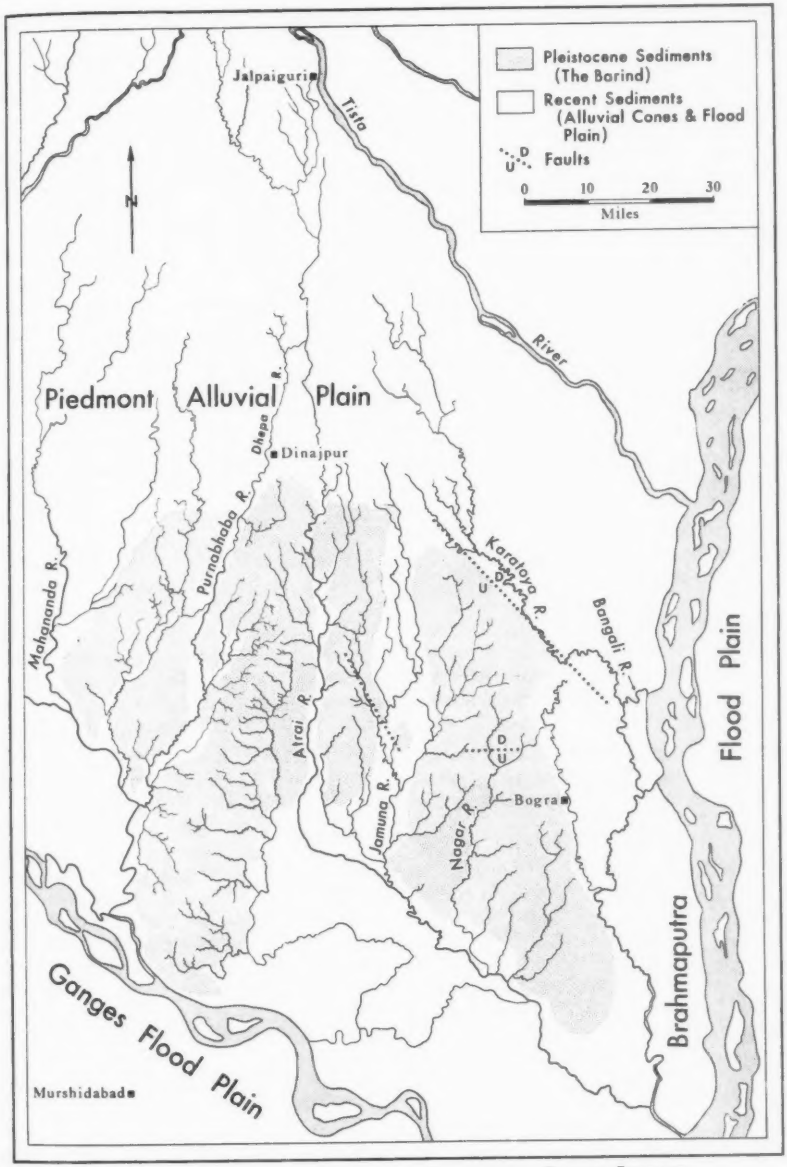

FIGURE 5.—DRAINAGE MAP OF THE PLEISTOCENE BARIND SURFACE

broad piedmont alluvial plain which overlaps the northern flank of the Barind.

Figure 6*A* is an approximate north-south profile across the alluvial plain and through the cities of Jalpaiguri, Dinajpur, Murshidabad, and Calcutta. The profile illustrates three main physiographic units of the Barind and adjacent areas. To the north is the alluvial fan surface of the Himalaya foothills which has a southerly slope of approximately 2.3 feet per mile. This

surface overlaps the Barind, which has essentially a flat or slightly domed surface. South of the Barind is the Recent flood plain with a southerly slope of approximately 0.3 feet per mile. Not enough surveyed elevations exist on the Barind surface to establish accurate slopes; however, the domed appearance in the profile is probably typical.

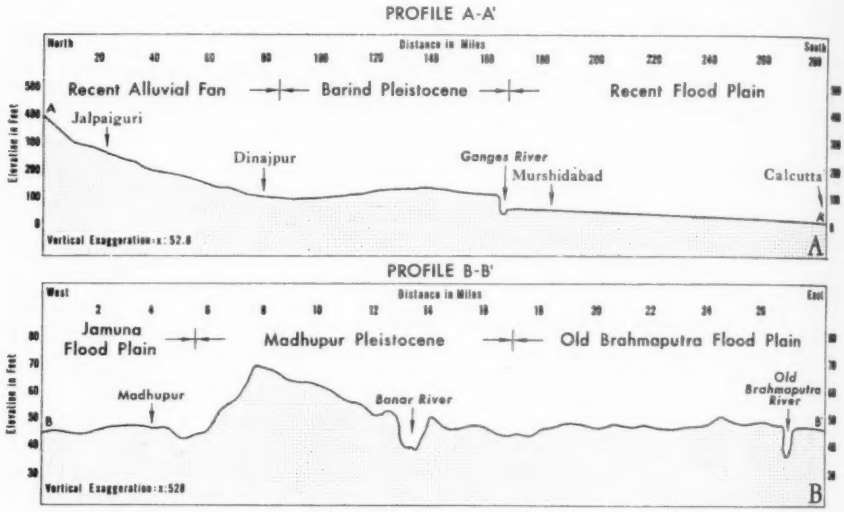

FIGURE 6.—PROFILES ACROSS PLEISTOCENE AND RECENT SURFACES
(Profile locations shown on Figure 2)

In the Barind, three distinctive stream-pattern types are evident (Fig. 5). North of the Pleistocene Barind are many small braiding streams which have built a broad piedmont alluvial plain along the foothills of the Himalaya. Major streams of this alluvial plain (including the Atrai and Purnabhaba) have entrenched valleys across the Barind surface. Numerous small, tightly meandering streams on the Pleistocene have developed an over-all dendritic pattern and flow into the more important north-south rivers (Pl. 2, fig. 1). Flanking the remainder of the Pleistocene inlier are low-gradient, sluggish, meandering and braiding streams of the Recent flood plain.

Bounding the northeast flank of the Barind is a northwest-southeast fault 40 miles long, upthrown to the southwest (Fig. 5). This fault has controlled the course of the Karatoya River. All minor streams draining the eastern portion of the Barind flow southwest into the Jamuna River, suggesting southwest tilting of the uplifted block.

From 1764 to 1773, Major James Rennell mapped Bengal for the British Government (Rennell, 1781). His surveys were exceedingly accurate for the time, and many geologists have used Rennell's maps to determine river changes since his time. The present writers have compared overlays of these maps (scale 4 miles to the inch) with modern maps of the Barind region. Several differences become immediately apparent. The Karatoya River has maintained essentially the same course along the northeast flank of the Barind. Its southern extension past Bogra, however, has been abandoned in favor of a more direct route to the Brahmaputra by way of the Bangali River (Fig. 5).

About 10 miles north of Bogra is another small river (the Nagar) that in Rennell's time was connected with the Karatoya and carried appreciable flow southwest across the Barind to the Jamuna River (Fig. 5). Its junction with the Karatoya is now virtually severed, and it serves primarily as local drainage for the Barind.

At the time of Rennell's mapping (1770), the foothills in this region were drained principally by the Tista River which, near Jal-

paiguri, branched and followed the course of the Dhepa-Purnabhaba to the southwest, the Atrai due south, and the Jamuna to the southeast. These streams discharged into the Ganges River. The Atrai seems to have been the major channel in the late 1700's, the Purnabhaba of secondary importance, and the Jamuna well on its way toward extinction. On Rennell's map "Teestah Creek" was a small unimportant distributary of the Tista River which discharged southeast from the Atrai near Jalpaiguri. The fact that it was named Teestah Creek is taken by some to imply that it was an old abandoned channel of the main river. Subsequent to Rennell's mapping, Tista Creek has taken the full low-water flow of the entire Tista system at the expense of the Purnabhaba, Atrai, and Jamuna rivers and now discharges into the Brahmaputra system rather than the Ganges. According to LaTouche (1910, p. 22) the change occurred suddenly in 1787 during a single flood. At present the Purnabhaba, Atrai, and Jamuna rivers still carry some flood flow, but they can be considered as antecedent streams carrying mainly local runoff waters of the Barind surface.

Although changes in the Karatoya, Nagar, and Tista rivers occurred during floods and seemingly were normal alluvial stream diversions, it is significant that they can be integrated with the Karatoya River fault. Numerous earthquakes have affected the region, suggesting active structural movements. Gupta (1910, p. 74) notes major earthquakes in 1885, 1888, and 1897. The Gazetteer of the Dacca district (Allen, 1912, p. 130–131) noted that there were also major quakes in 1762, 1775, and 1812.

Periodic disastrous earthquakes, the major changes in stream diversions, and the southwestward tilting of the eastern part of the Barind along a major fault all suggest the importance of structural activity in this region.

The southwest part of the Barind and adjacent flood plain has recently been surveyed by field parties of the Standard Vacuum Oil Company. Contouring of the surveyed portion of the Barind suggests that two terrace levels may be present. One level occurs at 130 feet above sea level; a second, less definite surface is at 65 to 75 feet above sea level. Available data permit only a suggestion that two terraces may be present. It is not known whether the surfaces are an indication of multiple terraces in Bengal or if they reflect structural activity.

Madhupur Jungle area.—The fourth major unit of Pleistocene terrace in the Bengal Basin is the region north of the city of Dacca called the Madhupur or Madhupur Jungle (Fig. 3). This 1585 square mile area for many years has been recognized as "old alluvium." A.I.H. Rizvi (1955, unpub. PhD thesis, Louisiana State Univ.) and Wadia (1949, p. 287) recognized that it could be Pleistocene terrace. Elevations on the Madhupur surface range from about 20 feet on the south and east to a maximum of about 100 feet above sea level. Generally the higher elevations are on the west, and the entire unit dips east and south beneath the overlapping Recent flood plain. Structural implications of the eastward dip of the "old alluvium" were recognized by Fergusson (1863), Hirst (1916), and others. Fergusson believed that the Madhupur region had been uplifted in very recent times and referred to the earthquake of 1762 which was accompanied by elevation and subsidence of large tracts of land. He suggested (p. 329) that the Madhupur Jungle occurs along the "axis of the belt of volcano action" which extends northwest through Chittagong and Dacca from the Sunda Island arc. Fergusson considered that the numerous low lakes in the Sylhet Basin may have been caused by subsidence compensatory to the elevation of the Madhupur Jungle.

Hirst (1916, p. 9–10) suggested that both the Barind and Madhupur Jungle areas were elevated

> "as compensation to a line of subsidence passing approximately from Jalpaiguri to the sea, down the alignment of the present Meghna River".

He considered the elevated tracts to be "old alluvium" representing a formerly continuous surface which had been uplifted locally. As evidence he cited a few borings which indicate similar stratigraphic sections in widely separated areas and also called attention to "hanging stream beds" in the Madhupur north of Dacca. Hirst further cited several points as proof for a zone of subsidence along a line passing from "Jalpaiguri to a point to the east of Barisal" (Fig. 2). Some of his observations concerning river changes and abnormally slow delta growth at the mouth of the Meghna River are pertinent and will be mentioned later.

A remarkable characteristic of the Madhupur is the abrupt western margin separating the low, flat, flood plain from the uneven, highly dissected Pleistocene surface. The entire, irregular western margin is formed by a series of six echelon faults ranging from 6 to 13 miles long (Fig. 3). The eastern side of each fault is upthrown, and surface relief indicates a

minimum throw of 20 to 60 feet. Figure 2 of Plate 1 is an aerial view of three echelon faults toward the northern end of the Madhupur. The flood plain is on the west, and the highly dissected Pleistocene of the uplifted block is on the east. The dendritic stream pattern of the Madhupur is emphasized by the dense jungle cover on the ridges and artificially flattened paddied stream valleys. Figure 2 of Plate 2 is a view south along the most northerly of the group of echelon faults. The fault scarp at this locality has a surface throw in excess of 50 feet. A line of elevations, furnished by the Standard Vacuum Oil Company, has been used to compile an east-west profile across the Madhupur Jungle. The profile (Fig. 6*B*) runs northeast from the flood plain of the Brahmaputra River toward the town of Mymensingh (see Fig. 2 for location of profile). This profile does not show the maximum relief of the Madhupur, for it follows a road which takes advantage of a stream valley across the scarp face. Nevertheless it illustrates graphically the eastward tilting which has taken place in the Madhupur Pleistocene block.

The Madhupur Pleistocene island has figured prominently in the Recent history of the Brahmaputra River. The earliest evidence of the Brahmaputra River in the Bengal Basin consists of a group of large Brahmaputra-size river scars which extend into the Sylhet Basin flanking the southern edge of the Shillong Plateau. One of the low, flooded areas (called haors) is shown on Figure 3 (Matian-Sanir Haor). The main river apparently extended east beyond this locality and then swung south into the Bay of Bengal. By the time of Rennell's mapping, this course had been abandoned in favor of a shorter route down what is still called the Old Brahmaputra River past Mymensingh. Northwest of the town of Mymensingh a distributary called the Banar River left the right bank of the Brahmaputra. On Rennell's map this stream flows south about 50 miles and joins the Lakhya River, which was another right-bank distributary of the Brahmaputra (Fig. 3). Both streams are of interest, because through a part of their distance they follow entrenched courses across the Pleistocene. The road from Mymensingh southwest to the town of Madhupur crosses the entrenched Banar River (Fig. 6*B*). Along this stream valley at least 3 feet of highly oxidized red sediment of Pleistocene age is exposed. Capping this is a layer of Recent gray silts and sands, 10–15 feet thick. These are Banar River flood-plain sediments, but they exhibit a dissected, rolling surface which suggests they were uplifted recently.

By the early 1770's the major diversion of the Brahmaputra into its present channel west of the Madhupur Jungle had occurred. There is no complete agreement as to when this diversion down the Jenai River of Rennell occurred. Hirst (1916, p. 14) indicates that it took place gradually between 1720 and 1830. Buchanan Hamilton (*in* Fergusson, 1863, p. 334) observed in 1810, however, that the Brahmaputra threatened to divert into its present course. Apparently by 1830 the diversion of low-river flow down the new channel was complete. Cause for the diversion according to Fergusson was uplift of the Madhupur Jungle block. Hirst (1916) agreed and advanced the concept of a zone of sinking and compensatory uplift of the Barind and Madhupur.

Hirst's concept, however, was violently attacked by Hayden and Pascoe (1919, p. 17–21), who preferred the more "rational" explanation of LaTouche (1910, p. 21 and 22). LaTouche suggested that the Brahmaputra diversion resulted directly from a major increase in water volume of the river. He postulated that the Dihang as a tributary of a then-small Brahmaputra beheaded the Tsangpo River of Tibet (Fig. 1), and through the resulting "enormous accession of water began to exert itself." LaTouche stated that the Old Brahmaputra flowed east of the Madhupur Jungle, which was a "relic of the old delta face of the Ganges." In other words he considered the entire Bengal Basin (excluding the Sylhet Basin) as the sole regime of the Ganges prior to the sudden increase in Brahmaputra volume.

PLATE 1.—FAULT SCARPS OF THE SYLHET BASIN AND MADHUPUR JUNGLE

FIGURE 1.—Shillong Plateau fault scarp north of Sylhet basin. Shallow lakes at base of escarpment have elevations of less than 10 feet above sea level.

FIGURE 2.—Echelon faulting of Madhupur Jungle. Three of a series of echelon faults (dotted) which delineate uplifted Pleistocene Madhupur Jungle. Strike of faults distorted by oblique aerial view. Note dendritic, paddied stream valleys in right foreground.

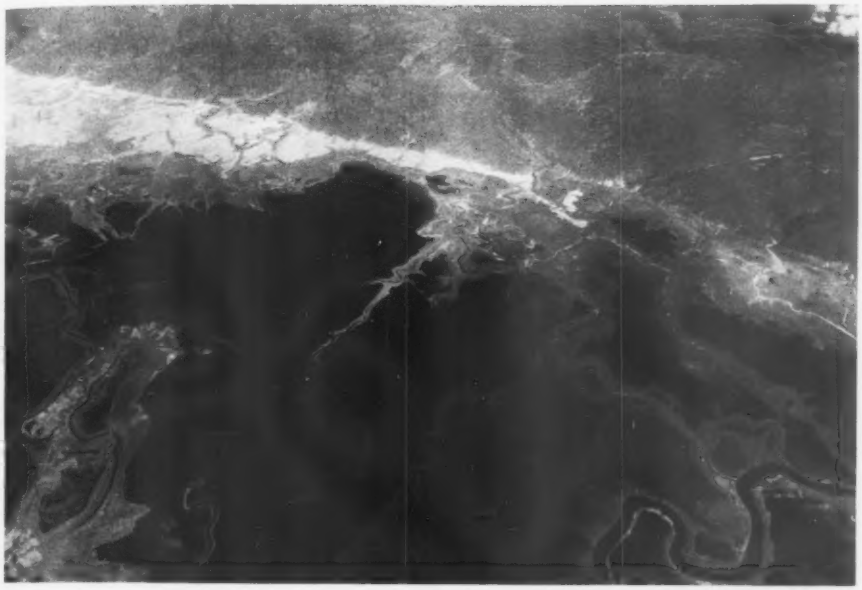

FIGURE 1

FIGURE 2

FAULT SCARPS OF THE SYLHET BASIN AND MADHUPUR JUNGLE

FIGURE 2

FIGURE 4

FIGURE 1

FIGURE 3

PLEISTOCENE TERRACE CHARACTERISTICS

He suggested that the sudden diversion of Tista River water from the Ganges to the Brahmaputra in 1787 was the final action that triggered the diversion into the Jenai channel west of the Madhupur Jungle. Subsequent writers have generally accepted LaTouche as representing the opinion of the Geological Survey of India.

Probably the diversion of the Brahmaputra was gradual, as most major river diversions are, and was caused in part by gradual tilting of the Madhupur block. This tilting caused the Old Brahmaputra River to become antecedent in places, necessitating river scour into slowly or periodically rising, comparatively resistant Pleistocene sediments. The sudden change of course by the Tista River with resulting addition of its waters to the Brahmaputra River may well have been a contributing factor toward diversion.

Additional evidence from field studies necessitates a re-evaluation of the somewhat discredited concepts of Hirst and widely accepted ideas of LaTouche. The echelon fault system along the west face of the Madhupur and the Karatoya River fault flanking the northeast edge of the Barind indicate that the intervening area, the flood plain of the Brahmaputra, has been actively subsiding. The eastward slope of the Madhupur Jungle of 3.6 feet per mile (Fig. 6*B*) indicates considerable eastward tilt of the Pleistocene unit. In addition, the antecedent nature of the Banar and Lakhya rivers attests to regional uplift in addition to eastward tilt. Not enough elevations are available for construction of a profile across the eastern portion of the surface of the Barind, but the predominant southwest drainage on this surface indicates southwest regional dip. Therefore, all available evidence substantiates the importance of structural activity in the Brahmaputra River basin and the Pleistocene areas along its flanks.

Aerial photographs of the Sylhet Basin show river scars of at least one ancient Brahmaputra River course occupied prior to the Old Brahmaputra course past Mymensingh. These scars are almost obscured by subsequent sedimentation and subsidence of the region. The remaining scars are comparable in size to the present river, indicating greater antiquity of the Brahmaputra than has been recognized by LaTouche and others. It should be pointed out that rapid subsidence both in the Sylhet Basin and in the area between the Barind and Madhupur Pleistocene units makes it entirely possible that older courses of the Brahmaputra were present but have subsequently become obscured. Pending proof of "enormous accession of water" as a result of Brahmaputra piracy of the Tsangpo and field evidence for its beheaded downstream segment, it seems that this river has been as important during the Recent period as the Ganges has. In other words while the Ganges has been building a broad lateral deltaic mass, the Brahmaputra, because of structural activity, has been building a thicker mass of sediment in structurally subsiding basins. Only deep detailed borings across the Brahmaputra River Valley and Sylhet Basin will clarify the geologic history.

Minor Pleistocene Units.—The Lalmai Hills, commonly called the Red Banks near the town of Comilla (Fig. 3), merit discussion. The hills are an uplifted block of highly oxidized, red Pleistocene sediments. Bounded on both east and west by faults, the entire structural unit can be considered a horst. The block is about 13 square miles in area; some individual peaks are more than 150 feet high, although the average elevation is in the neighborhood of 70 feet above sea level. The eastern margin is bounded by a single continuous fault, upthrown to the west. The scarp on this side is dissected by numerous rainfall drainage channels discharging toward the east. The western margin

PLEISTOCENE TERRACE CHARACTERISTICS

PLATE 2.—PLEISTOCENE TERRACE CHARACTERISTICS

FIGURE 1.—Vertical aerial view of Barind Pleistocene. Uplifted terrace surface has dendritic, tightly meandering drainage pattern. The numerous "tanks" (artificial ponds) are for water storage during dry season.

FIGURE 2.—Aerial view along echelon fault. Differential relief between Brahmaputra flood plain (lower left) and tilted, uplifted Madhupur Jungle (right) exceeds 50 feet at this location.

FIGURE 3.—West fault scarp of Lalmai Hills. Differential relief between Tippera surface (left) and hills is in excess of 100 feet.

FIGURE 4.—Angular unconformity in Pleistocene deposits. Lalmai Hills exposure reveals organic particles in upper (Pleistocene) sediments and east dip in lower (older Pleistocene or Tertiary) sediments.

is determined by two parallel faults about a mile apart; both are upthrown on the east. The range of hills is about 1 mile wide in the northern area and 2 miles wide to the south. The flanking fault in the north extends through the center of the block in the south, forming, in places, a fairly well-defined valley.

The fault scarp bounding the western side of the hills in places has a surface throw in excess of 100 feet (Pl. 2, fig. 3). A number of small permanent springs discharge along the scarp foot. The accordant submits of the dissected block indicate a slight tilting of the entire unit to the east. Consequently the highest hills are on the western margin, and most drainage finds its way to the east.

Lalmai sediments are predominantly sands and silts, but toward the west side of the hills, near the bottom of the exposed sections, are layers of gravels and cobbles. Most pebbles consist of ironstone or calcareous nodules with some quartz and considerable quantities of petrified wood fragments. Numerous large blocks of petrified wood, some 24 inches by 12 inches, are present in the gravel layers. The completely silicified wood invariably shows stream transport and with the gravel layers is highly suggestive of torrential stream transport and deposition. All gravel layers observed dip east, and, since they are low in the stratigraphic section, are found exposed only in the central and western parts of the hills. Higher in the section is a well-defined angular unconformity (Pl. 2, fig. 4), which occurs over an appreciable area. The underyling unit dips steeply eastward, whereas the overlying younger sediments are either horizontal or dip only slightly eastward. The upper unit contains a relatively high concentration of well-disseminated organic particles, which was not observed in the lower unit. The degree of oxidation of these sediments seems to be unrelated to stratigraphic position. Hilltops are redder and more highly oxidized than beds lower in elevation. Intense oxidation reflects high local relief rather than age, as the oxidation boundary transects the stratigraphic boundaries.

In the Sylhet Basin north and northeast of the city of Sylhet are the Sylhet Hills and Chhatak Hills, which also are classed with the minor Pleistocene units (Fig. 3). The Sylhet Hills cover 72 square miles and attain maximum elevations of 260 to 300 feet above sea level. The unit is elongate and trends northeast-southwest. The southeast front of the hills is abrupt and may well be fault-controlled, but because of the extremely heavy rainfall (180–200 inches per year) and the unconsolidated, sandy nature of the sediments, it is extremely dissected and eroded. A reconnaissance of two areas along the southeastern margin of the hills revealed sands, silts, and clays of fluviatile origin. As in the Lalmai area, the hilltops in regions of high relief were most highly oxidized. A quarry within the hills north of Sylhet was inspected briefly. Here, beneath oxidized Pleistocene sediments were banded clays, silts, and sands, highly compacted, tilted, and faulted. These sediments are probably Tertiary.

In summary it should be stated that the relatively high-standing Sylhet and Chhatak Hills are associated with numerous low, swampy areas (haors) in the Sylhet Basin. Air photographs indicate a number of fault scars, most of which are shown on Figure 3. The Sylhet Basin is probably the most active part of Bengal structurally, but much of the tectonic story is obscured by the monsoonal floods with their resulting veneer of alluvial sediments. Additional work is necessary to differentiate Pleistocene from Tertiary deposits in the Sylhet and Chhatak Hills and to determine the tectonic history of the region. Figure 3 identifies these deposits as Pleistocene because of their surficial similarity, but much more work is needed in the Sylhet Basin before its geologic history can be defined accurately.

Summary.—There are four major and three minor Pleistocene areas in the Bengal Basin. The two major units flanking the east and west valley walls have not been sufficiently investigated to establish whether they exhibit evidence of the development of multiple terraces.

The two major Pleistocene units in the central part of the Bengal Basin, the Barind and the Madhupur, may exhibit evidences of multiple terraces, but active and continuing faulting have obscured the record. The development of readily recognizable terraces in a marginal deltaic region results from slow warping and tilting of the flank of a subsiding sedimentary trough during a period of sea-level fluctuations, as in the Gulf Coast of the United States. In the central and eastern part of the Bengal Basin, faulting, resulting in tilted fault blocks, has obscured the slow regional tilting which would normally result in a multiple-terrace sequence. For this reason more than a single Pleistocene terrace cannot be determined with certainty until more factual data are accumulated.

The Recent Flood Plain

General statement.—Within the Bengal Basin as limited by the Tertiary and older hills are the alluvial Pleistocene deposits discussed in the previous section, and Recent flood-plain sediments. The Recent deposits, which comprise the combined deltaic masses and flood plains of the Ganges, Brahmaputra, and Meghna rivers, cover more than 50,000 square miles. This enormous region is divisible into four categories to be considered individually.

Alluvial fans.—The Tista, Atrai, Mahananda, Purnabhaba, Old Jamuna, and Karatoya rivers which flank and subdivide the Barind Pleistocene surface (Fig. 5) rise as a part of the drainage system of the Himalaya foothills. These and many other streams of a similar nature have developed an extensive piedmont alluvial plain. Down-slope these same streams gradually flatten their gradients and ultimately become tributaries of the Ganges and Brahmaputra systems. No attempt has been made to differentiate alluvial fan sediments from flood-plain sediments.

Tippera surface.—In the eastern part of the Bengal Basin, flanking the Tripura Hills and surrounding the Lalmai Hills is a distinctive alluvial physiographic unit (Fig. 3). This unit, 3000 square miles in area, has been named the Tippera surface, because it covers most of the district of Tippera and small parts of the adjacent districts. For several reasons the Tippera surface is a mappable unit.

On aerial photographs or detailed maps, the drainage system of the Tippera surface displays a well-developed rectangular pattern in contrast to the braiding and meandering pattern of the Recent flood plain and the dendritic pattern of the hill regions (Fig. 7). In addition to the rectangular system are a few small meandering streams which form the drainage system for the adjacent hills. In contrast to meandering streams of the Barind Pleistocene surface, however, these exhibit numerous cutoff and oxbow lakes, indicating that the deposits are less consolidated. The rectangular pattern upon detailed examination proved to be due entirely to man's activity. Because of its flat surface, relatively low elevation, and heavy seasonal rainfall, the entire Tippera area is uniformly inundated. For agricultural purposes a series of low dikes has been constructed throughout the area. The ditches resulting from excavation for dike material have subsequently become the rectangular drainage network. Through continuous use, the artificial canals have been expanded, and natural drainage has declined in importance. High land values, coupled with the need for flat rice paddies, have resulted in artificial filling in of most of the abandoned natural drainage channels. Although the Tippera surface exhibits a high degree of cultural modification, its alluvial origin is still evident on aerial photographs. Traces and remnants of curved meander scars and loops are emphasized by concentrations of trees and houses along former natural levees. However, intensive agriculture for countless generations has nearly erased such evidences of origin and has led to formation of the rectangular drainage net.

The Tippera surface is delineated on the north by an important northeast-southwest trending fault (Fig. 3). It is uplifted to the southeast a few feet higher than the adjacent flood plain of the Meghna River. A branch of the Meghna impinging against the Tippera surface along the fault scarp has caused appreciable local erosion. Most of the western limit of the Tippera likewise is being eroded by the Meghna or its branches. Along the southwest and southern margin the Tippera is flanked by a narrow band of Recent river deposits. The eastern limit of the Tippera surface is the abrupt boundary with the Pleistocene hills.

Field examination revealed that sediments of the Tippera surface correspond physically with the Recent flood-plain sediments, except that they are more compacted and are slightly oxidized. The sediments display higher oxidation than Recent flood-plain deposits but are not comparable with the reddish-brown Pleistocene terrace materials.

Surveyed elevations are scarce on available maps of the Tippera surface and adjacent flood plain, but all available elevations have been averaged. Based on 65 elevations, the Tippera surface averages about 21 feet above sea level in contrast to an average of less than 15 feet for 45 elevations on the near-by flood plain.

All evidence suggests slight uplift of the entire Tippera surface. Cultural modifications of the natural drainage system, displacement along the bordering fault to the north, and oxidation of sediments all indicate that the Tippera surface has been uplifted during Recent time. Amount and nature of uplift are not precisely known, but future work will probably verify a differential elevation on the order of 4 to 6 feet

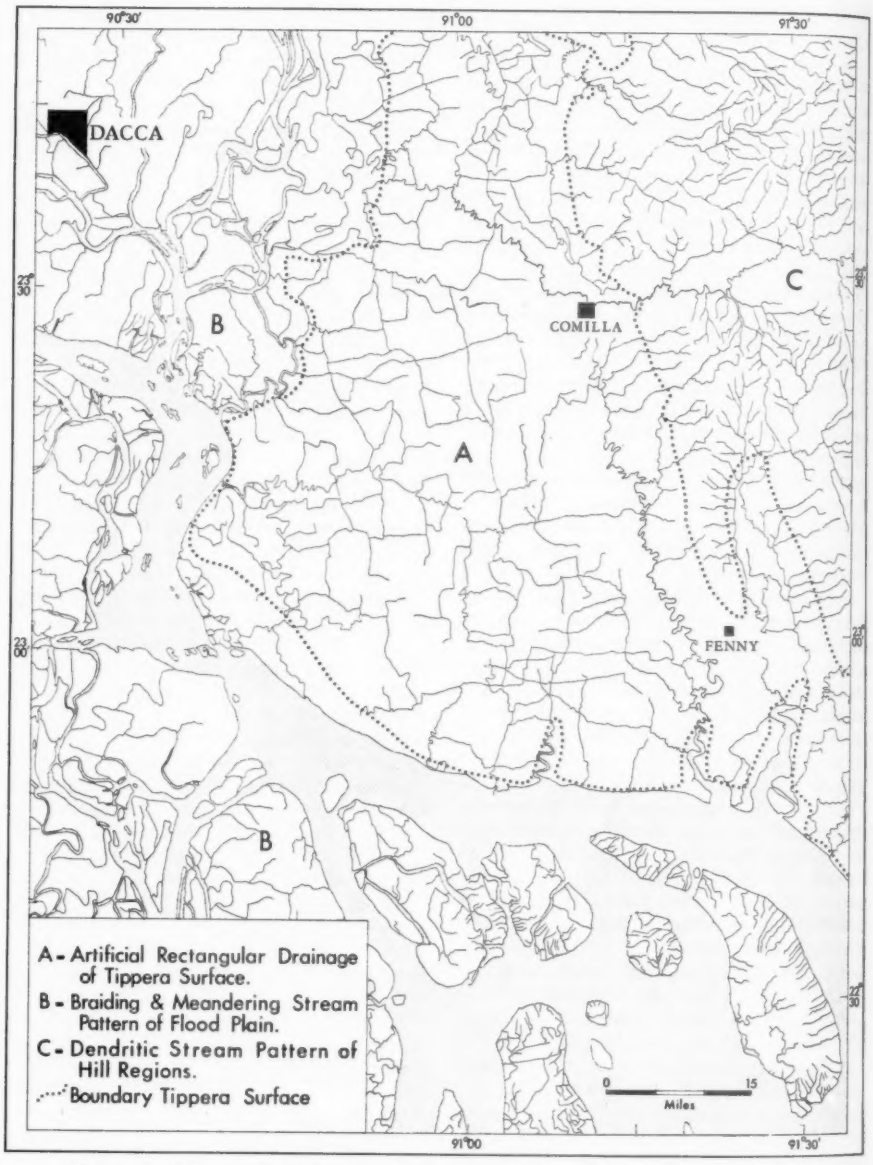

FIGURE 7.—RECTANGULAR DRAINAGE PATTERN OF UPLIFTED, EARLY RECENT TIPPERA SURFACE CONTRASTED WITH ADJACENT DRAINAGE

between the Tippera surface and the adjacent flood plain.

Sylhet Basin.—The Sylhet Basin has been mentioned previously as a subsidiary part of the Bengal Basin, bounded on the north by the Shillong Plateau and on the east and south by the plunging, anticlinically folded Tripura Hills. The south flank of the Shillong Plateau

is delineated in part by a major fault scarp which is dissected by numerous steep valleys (Pl. 1, fig. 1). New topographic maps of the Sylhet Basin are being compiled by the Pakistan Survey, and their advance sheets indicate that much of the area in the northern part of the basin is less than 10 feet above sea level, for example the vicinity of Matian-Sanir Haor (Pl. 1, fig. 1, and Fig. 3). In the same immediate area are meander scars left by an old course of the Brahmaputra River which antedates the recently abandoned course past Mymensingh. Maximum elevations on the residual levees of this old stream course average about 15 feet above sea level. At a comparable distance from base level (the Bay of Bengal), the other Brahmaputra River courses have elevations in excess of 50 feet above sea level. This suggests that the Sylhet Basin has subsided about 30–40 feet within the last several hundred years. Information furnished by personnel of Geophysical Services International indicates that stumps and wood were encountered in at least three shallow holes at depths of 60–65 feet, 60 feet, and 50–55 feet in the northern part of the Sylhet Basin. Rapid subsidence, probably still occurring, has exceeded the rate of sedimentary fill of the basin. A calculated gradient for the Brahmaputra river course passing through the low part of the basin is about 0.11 feet per mile. This gradient is much flatter than that of the Old Brahmaputra past Mymensingh (0.25 feet per mile), the Jamuna (0.26 feet per mile), the Ganges (0.26 feet per mile), the Mississippi (0.25 feet per mile), or any other known major river.

Although sediments are probably undergoing compaction, the subsidence of the Sylhet Basin is probably primarily tectonic and is undoubtedly related to the major fault system bounding the northern side of the basin. The many lakes (haors) immediately adjacent to the fault scarp suggest that the downthrown block has been rotated, carrying the Sylhet Basin down more rapidly than it is being alluviated.

Bengal deltaic plain.—The remaining region of Bengal, bounded by the Pleistocene terrace on the west, the Barind and Madhupur Jungle on the north, and the Tippera surface on the east, consists of the Recent deltaic plain. No attempt will be made in this paper to detail the physical characteristics of the delta. It is complex in that it has been the site of sedimentary deposition by two of the world's major rivers. It, like other major deltas, is composed of a number of overlapping subdeltas. The deltaic region is constantly subsiding, owing mainly to compaction of Recent sediments and possibly to structural downwarping. Numerous instances of subsidence have been recorded in the literature. Table 1 includes these data plus additional field observations. The effect of deltaic plain subsidence upon the adjacent Pleistocene of the Madhupur Jungle is considered in the following section.

Structural Modification of Quaternary Sediments

Faulting and Folding in the Bengal Basin

Figure 3 shows that eastern and northern parts of the Bengal Basin have been subjected to more structural modification than have western and southern parts. Nearly all faults and folds mapped are north of the Ganges River. A similar distribution applies to recorded seismic phenomena. Figure 8 shows epicenters of recorded earthquakes in the Bengal Basin and adjacent regions. These data, modified from Gutenberg and Richter (1949, p. 119–267) and from Krishnan (1953, Pl. 2) indicate that the distribution of Recent seismic activity in the region resembles that of the Quaternary faults and folds revealed by the present field work.

Active, Recent faults of the magnitude present in the Bengal Basin are unusual. Throws of similar magnitude are not known to occur in the Mississippi River deltaic region, although faulting which involves displacements of the modern flood plain has been recognized (Fisk, 1944, p. 24 and Pl. 15). The most impressive structure noted is the series of echelon faults flanking the west side of the tilted Madhupur Jungle. In addition there is notable subsidence in the Sylhet Basin, faulting, tilting, and uplift of the eastern Barind, relative uplift of the Tippera surface, and Recent folding in the Tripura Hills. These structural phenomena and a general subsidence of the deltaic plain are believed to be interrelated.

Causes of Echelon Faulting

Two general theories have been proposed to explain echelon faulting. The first assumes a major fault at depth, along which a couple is acting, with the result that a number of secondary echelon faults develop at the surface. This theory is represented in Figure 9*A*, the fault at depth following the trend shown by the pair of dotted lines.

Considerable evidence suggests the presence of such a "zone of weakness" passing between the Barind and Madhupur Pleistocene inliers.

TABLE 1.—EVIDENCE OF SUBSIDENCE IN THE RECENT DELTAIC PLAIN

Location of Data and Type Information			Evidence	Subsidence Indicated (In feet)	Source of Information
Calcutta and Vicinity	Near Hooghly River	Water-well boring	Rotten wood	32–55	East, 1818, 544–46
	Chowrhinghee Road	Tank excavation	Decayed wood	35	East, 1818, p. 547
	Sialdah	Tank excavation	*Sundri* trees *in situ*	30	Hunter, 1875, p. 291
	King George dock	Excavation	Wood (*Ceriops* sp.)	40	Curtis, 1933, p. 11
	Fort Williams	Water-well boring	Peat and *Sundri* trees	30–50	Smith, 1841, p. 342
	Port Canning on Matla River	Tank excavation	Large trees in Place (*Sundri*)	10	Hunter, 1875, p. 291
Khulna and Vicinity	At Khulna, about 12 mi. N. Sundarbans	Tank excavation	Large *Sundri* trees in place and layer of vegetable mould	18	Hunter, 1875, p. 291
	Khulna shipyard docks	Foundation Borings:			
		No. 4	Decayed wood	86.5–99	R. Troiana, personal communication
		No. 6.....	Decayed wood	4–18	
		No. 6.....	Decayed vegetation	23–48	
		No. 6.....	Decayed wood	97–99	
Sundarbans (Coastal Region)	Near Kobadak Forest station	Shallow hand auger boring	Wood (*Sundri*)	12–14	Borings made by writers December-March, 1956
	Talpatti Khal	Shallow hand auger boring	Peat layer	14	Borings made by writers December-March, 1956
	Near mouth of Raimangal River	Shallow hand auger boring	Intermittent organic down to 20 feet	20	Borings made by writers December-March, 1956
	Dhaki Khal boring	Shallow hand auger boring	Peat layer	13–16	Borings made by writers December-March, 1956
			Wood (*Sundri*)	18	
			Peat layer	21–22	
	Dhaki Khal ¼ mile from boring	Tank excavation	Wood (*Sundri*)	18	Field observation
	Dhaki Khal 200 yards from boring	Tank excavation	Human artifact (Milling or grinding stone)	13	Field observation
	Dubla Island	Shallow hand auger boring	Intermittent organic down to 20 feet	20	Borings made by writers December-March, 1956
	Shekretak Ruins near Sibsa River	Shallow hand auger boring	Peat	6	Borings made by writers December-March, 1956
			Wood	16	
			Wood	20–23	
			Organic	23–34.5	

putra River abandoned its channel east of the Madhupur in favor of its present channel undoubtedly in response to a shorter course of steeper gradient to the Bay of Bengal. The Tista River (Fig. 5) abandoned its course straight south across the Barind to the Ganges in favor of a southeast course into the present Brahmaputra channel. Lastly the Ganges has abandoned numerous deltaic distributaries to the southwest in favor of joining the Brahmaputra to form the combined Meghna River. Such a change again suggests a more advantageous course with steeper gradient.

Hirst (1916, p. 9–12) and Fergusson (1863, p. 329), as mentioned, suggested such a zone. The available evidence can be itemized as follows:

(1) Change in stream courses. The Brahma-

(2) Sediment and water of the combined Ganges-Brahmaputra-Meghna rivers have been pouring into the active (eastern) part of the delta for the last 200 years or more with no appreciable build-out of the deltaic front. A comparison of Rennell's map with modern maps covering a span of approximately 175 years does not show appreciable deltaic growth. This suggests that the rate of subsidence has kept pace with the rate of sedimentary deposition.

(3) The northeastern flank of the Barind surface is terminated by a fault with the northeast side downthrown. This again could be

related to a subsiding trough passing between the Barind and the Madhupur.

(4) Several papers have been published concerning the "Garo-Rajmahal gap," and the possibility of a former connection of the Garo Hills part of the Shillong Plateau across to the Rajmahal Hills of peninsular India (Hora, 1944; Auden, 1949; Dey, 1949). Although little factual information is available, most writers agree that the Garo-Rajmahal gap represents a sag in the once-continuous crystalline rock barrier. Krishnan (1953, p. 38) suggests that the western side of the Shillong Plateau may be marked by fracturing, which would agree with other evidence for the "zone of weakness" which follows approximately the trend of the Jamuna-Padma-Meghna river system (Figs. 2 and 9).

This evidence points either to a subsiding trough or to a single major fault at depth. However, there is no suggestion of a couple which might cause relative movement of the northeast side toward the north. The only apparent evidence is the folding in the Tripura Hills east of the Sylhet Basin (Fig. 9*A*). This folding indicates compression of the crust in a west-northwest direction. No data are available about the structure of the southern area of the Tripura Hills in India and in Burma, but the Lalmai Hills to the west are a horst. Horst formation suggests local tension of the crust rather than compression. It can be inferred, then, that west-northwest compression across the Sylhet Basin could have a component of force which would act as a couple along the "zone of weakness" (Fig. 9*A*). At least five fault scars are obvious in the Recent sediments of the Sylhet Basin between the folded Tripura Hills and the Madhupur Jungle. Unfortunately, neither field work nor examination of aerial photographs yielded evidence as to the type of movement along these faults. They cannot be used at present to confirm or refute the effect of compression upon establishment of a couple.

The second theory used to explain echelon faulting demands torsion or warping of a surface to produce tear faults. In the Bengal Basin a major deltaic sedimentary mass is subsiding, as

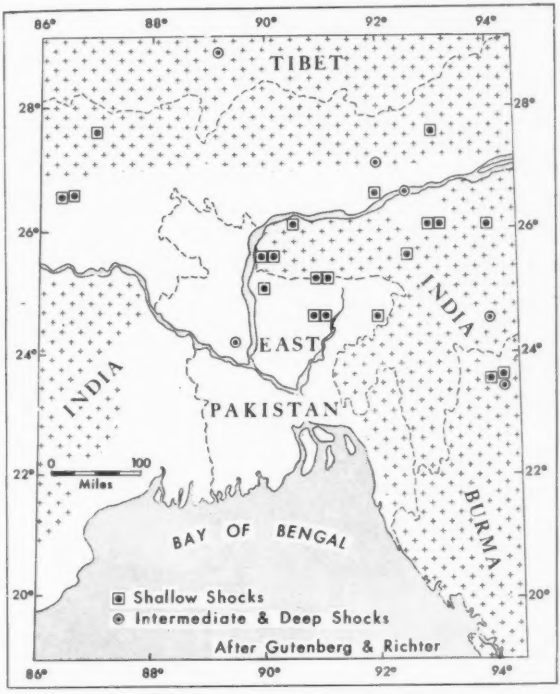

FIGURE 8.—MAP OF EARTHQUAKE EPICENTERS SINCE 1900

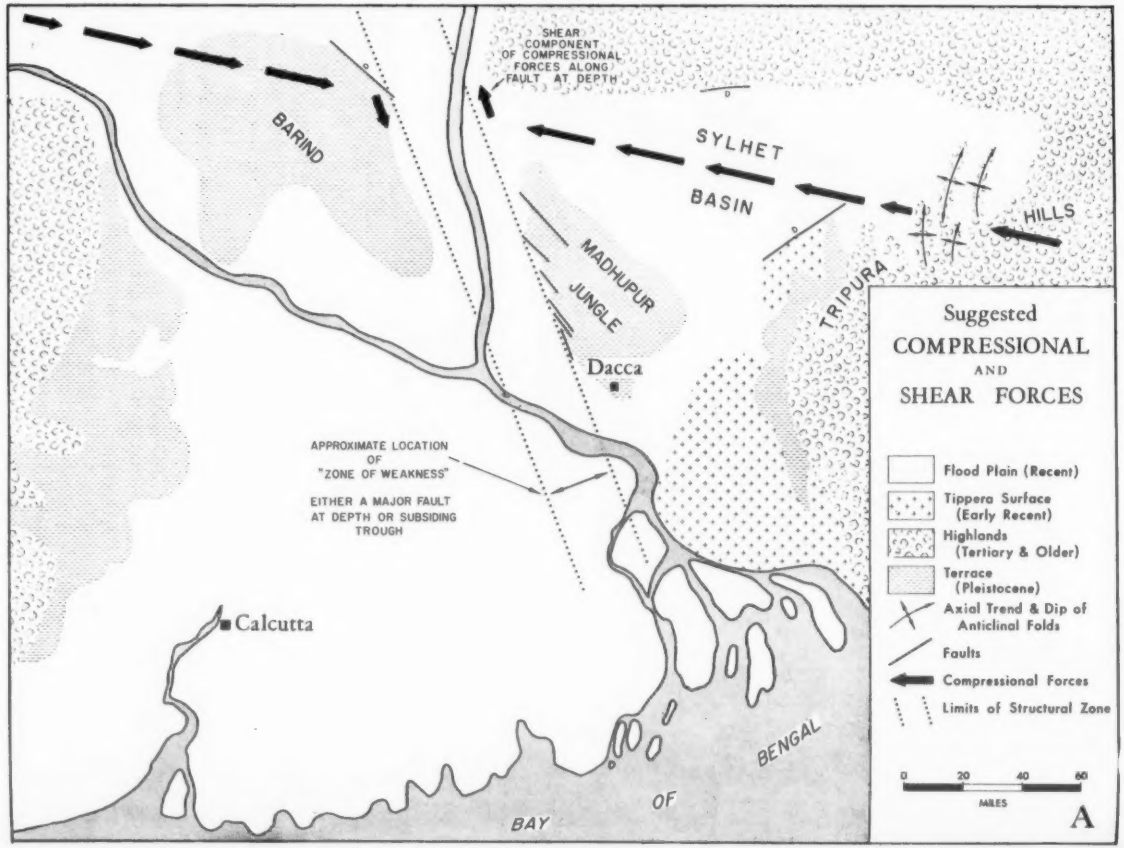
SHEAR COMPONENT OF COMPRESSIONAL FORCES ALONG FAULT AT DEPTH
BARIND
SYLHET
BASIN
HILLS
MADHUPUR
JUNGLE
TRIPURA
Dacca
APPROXIMATE LOCATION OF "ZONE OF WEAKNESS"
EITHER A MAJOR FAULT AT DEPTH OR SUBSIDING TROUGH
Calcutta
BAY
OF
BENGAL
Suggested
COMPRESSIONAL
AND
SHEAR FORCES
Flood Plain (Recent)
Tippera Surface (Early Recent)
Highlands (Tertiary & Older)
Terrace (Pleistocene)
Axial Trend & Dip of Anticlinal Folds
Faults
Compressional Forces
Limits of Structural Zone
0 20 40 60
MILES
A

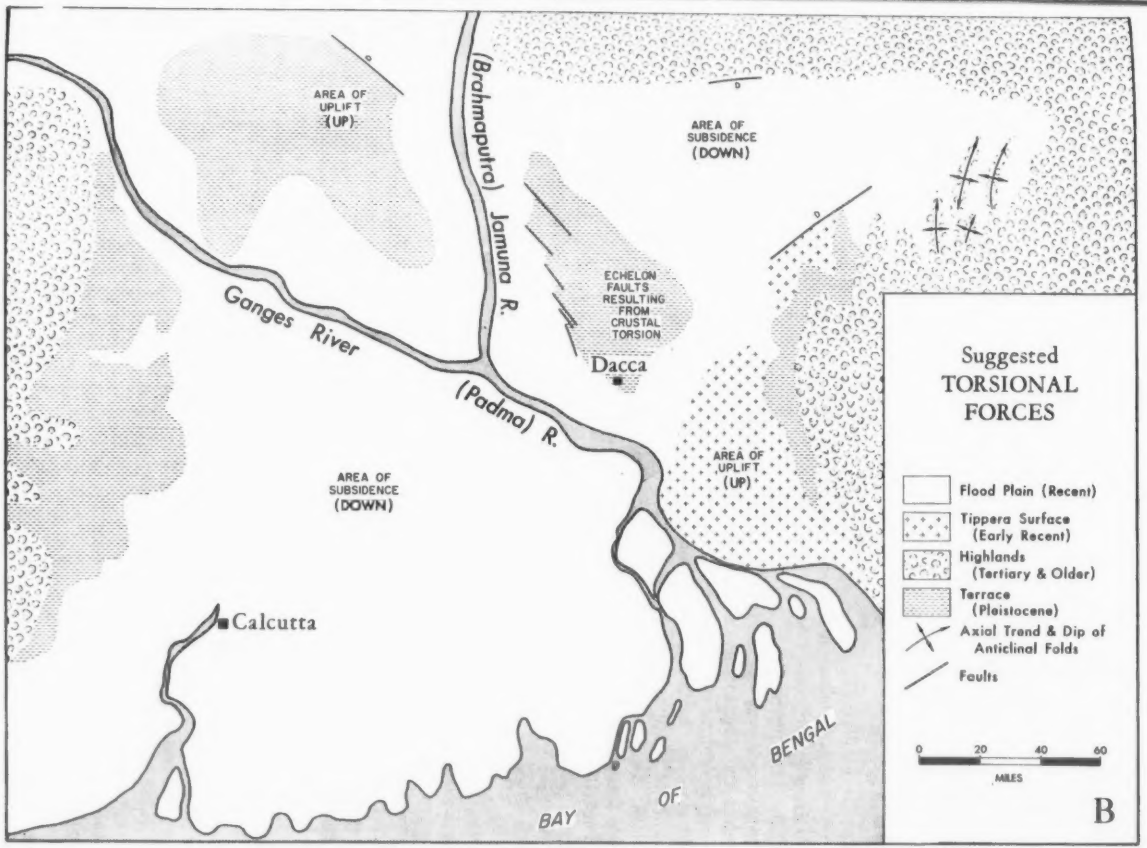

FIGURE 9.—STRUCTURAL FORCES AFFECTING THE BENGAL BASIN

previously mentioned. The Sylhet Basin is also subsiding. These two areas however are counterbalanced by the Barind to the northwest and the Recent Tippera surface to the southeast, which are not subsiding and may be rising slightly. Such warping could result in a broad area subjected to torsion, which would tend to be relieved through echelon faulting (Fig. 9*B*).

Therefore either of the theories, or possibly a combination of the two, may explain echelon faulting.

Conclusions

The Bengal Basin is flanked on the east and west by areas of Pleistocene terrace. Two other main areas of Pleistocene deposits, the Barind and the Madhupur, lie within the basin. A reconnaissance was not sufficient to establish whether the Pleistocene of Bengal may be differentiated into more than a single terrace. Field work in the Bengal Basin suggests the presence of multiple terraces, but they are not obvious. Detailed surface mapping in the upper Ganges and Brahmaputra valleys and evidence of detailed borings may reveal buried alluvial sequences. Terrace surfaces of the central-basin Pleistocene inliers have been drastically modified by major structural activity. The areas of pronounced Recent faulting and folding can be correlated directly with known seismic areas of Assam and adjacent regions. The Barind Pleistocene has apparently experienced domal uplift. The western part is higher toward its center and slopes both to the north and south (Fig. 6*A*). A suggestion of two terrace levels is found in this high-standing region. The eastern Barind is lower and consists of a uniform surface tilted southwest. The Madhupur Pleistocene unit, bounded on the west by a series of echelon faults, has been uplifted and tilted northeast. One measured profile indicates a northeast slope in excess of 3.5 feet per mile. The uplift has caused some of the Old Brahmaputra distributaries to become antecedent, which probably helped effect the diversion of the river to its present channel.

Areas adjacent to the Madhupur have also been affected by structural activity. The Sylhet Basin is rapidly sinking, showing in some places subsidence on the order of 35 feet within the last few hundred years. This rapid subsidence rate is probably related to movement along the major fault flanking the uplifted Shillong Plateau. The Sylhet Basin suggests a tilted fault block because of the numerous broad shallow lakes and streams which hug the Shillong fault scarp. A large area of Recent flood plain south and east of the Madhupur has been slightly uplifted, resulting in establishment of a distinct and mappable portion of the flood plain, which has been named the Tippera surface.

Uplift of the Barind Pleistocene unit and the Tippera surface coupled with subsidence of the Sylhet Basin and the deltaic plain has resulted in torsion of the crust in East Bengal. Additional indirect evidence indicates either a major fault at depth or a subsiding trough following approximately the axis of the Jamuna-Ganges (Padma)-Meghna river system. Folding of the northeastern part of the Tripura Hills suggests forces that may have established a couple, affecting the buried fault or trough. Surface echelon faulting of the Madhupur has probably resulted either from torsion of the region or the effect of shear along a postulated buried fault, or possibly a combination of both forces. The subsiding structural zone may, in part, represent a foredeep flanking the west side of the north-south convex arc of the Burmese Mountains. It may have the same relationship to this mountainous chain as the Gangetic trough or foredeep bears to the Himalayan arc.

Krishnan (1953, p. 12–13) summarizes existing knowledge of the Assam (Shillong) Plateau and surrounding areas and emphasizes how little is known about the geology of the Eastern Himalaya and its relationship to the Burmese Mountains and the Shillong Plateau. The plateau, bounded by major fault scarps, is related geologically to peninsular India and is composed for the most part of materials older than the adjacent Himalayan and Burmese mountains. This peninsular outlier is located at the approximate junction of a known and a postulated downwarped foredeep and may be related genetically to the same tectonic causes. Certainly this is one of the most active tectonic regions of the world, and the presence of a subsiding trough in the Bengal Basin must be related to activity in the adjacent mountain chains.

References Cited

Allen, B. C., 1912, Dacca district gazetteer: Allahabad, Pioneer Press, 131 p.

Ascoli, F. D., 1910, The rivers of the delta: Asiatic Soc. Bengal, Jour. and Proc., v. VI, no. 10, p. 543–556

Auden, J. B., 1949, Geological discussion of the Satpura hypotheses and Garo-Rajmahal gap: Natl. Inst. Sci. India, Proc. v. 15, p. 315–340

Bagchi, Kanangopal, 1944, The Ganges delta: Calcutta, Calcutta Univ. Press, 157 p.

Ball, F., 1877, Geology of the Rajmahal Hills: Geol. Survey India Mem., v. 13, p. 1–94

Barbour, George B., 1935, Correlation by fluviatile terraces; physiographic history of the Yangtze: Geol. Survey China Mem., serial A, no. 14, 112 p.

Chatterjee, S. P., 1949, Bengal in maps: Calcutta, Orient Longmans Ltd., 105 p.

Colebrooke, Major R. H., 1803, On the course of the Ganges through Bengal: Asiatik Researches, v. 7, p. 1–32

Curtis, S. J., 1933, Working plan for the forests of the Sundarbans division: Calcutta, Bengal Govt. Press, v. I, parts I and II, p. 7–22

DeTerra, Hellmut, 1943, The Pleistocene of Burma: Am. Philos. Soc. Trans., new ser., v. 33, p. 271–339

Dey, A. K. 1949, The age of the Bengal gap: Natl. Inst. Sci. India, Proc. v. 15, p. 409–410

East, Sir Edward Hyde, 1818, Abstract of an account, containing the particulars of a boring made near the river Hooghly, in the vicinity of Calcutta, from May to July 1814 inclusive in search of a spring of pure water: Asiatik Researches, v. XII, p. 544–547

Fergusson, J., 1863, Delta of the Ganges: Geol. Soc., London Quart. Jour., v. XIX, p. 321–354

Fisk, H. N., 1944, Geological investigation of the alluvial valley of the lower Mississippi River: Vicksburg, Mississippi River Comm., 78 p.

Gupta, J. N., 1910, Bogra district gazetteer: Allahabad, Pioneer Press, 79 p.

Gutenberg, B., and Richter, C. F., 1949, Seismicity of the earth: Princeton, Princeton Univ. Press, p. 119–267

Hayden, H. H., and Pascoe, E. H., 1919, Report on the Hooghly River and its headwaters: Calcutta, The Bengal Secretariat Book Depot, v. 1, App. 1, p. 17–21

Hirst, Major F. C., 1916, Report on the Nadia Rivers 1915: Calcutta, The Bengal Secretariat Book Depot, 39 p.

Hora, S. L., 1944, On the Malayan affinities of the fresh-water fish fauna of peninsular India and its bearing on the probable age of the Garo-Rajmahal gap: Natl. Inst. Sci. India, Proc. v. 10, p. 423–439

—— 1951, Some observations on the paleogeography of the Garo-Rajmahal gap as evidenced by the distribution of Malayan fauna and flora to peninsular India: Natl. Inst. Sci. India, Proc. v. 17, no. 6, p. 437–444

Hunter, W. W., 1875, A statistical account of Bengal: London, Trubner and Co., v. I, p. 22–34, 285–289

Krishnan, M. S., 1953, The structural and tectonic history of India: Geol. Survey India Mem., v. 81, 109 p.

LaTouche, T. H. D., 1910, Relics of the great Ice Age in the plains of northern India, *reprinted* (1919) *in* Report on the Hooghly River and its headwaters: Calcutta, The Bengal Secretariat Book Depot, v. I, p. 21–22

LeBlanc, R. J., and Bernard, H. S., 1954, Resumé of late Recent geological history of the Gulf Coast: Geol. en Mijnb. v. 16, no. 6, p. 185–195

Majumdar, S. C., 1942, Rivers of the Bengal delta: Calcutta, Calcutta Univ. Press, 124 p.

Muckerjee, Radhakamal, 1938, The changing face of Bengal, study in riverine economy: Calcutta, Calcutta Univ. Press, 288 p.

Oldham, Thomas, *et al.*, 1859, On the geological structure and physical features of the districts of Bancoorah, Midnapore and Orissa—Bengal: Geol. Survey India Mem. v. 1, p. 249–279

Rennell, James J., 1781, The Ganges and Brahmaputra rivers: Royal Soc. London Philos. Trans., v. LXXI, p. 91–103

—— 1793, An account of the Ganges and Burrampooter rivers, Appendix to Memoir of a map of Hindoostan or the Mogul Empire: London, W. Bulmer and Co., p. 336–364

Russell, Richard J., 1940, Quaternary history of Louisiana: Geol. Soc. America Bull., v. 51, p. 1119–1134

—— 1942, Geomorphology of the Rhone delta: Assoc. Amer. Geographers, v. XXXII, no. 2, p. 151–255

Smith, Lt. R. Baird, 1841, On the structure of the delta of the Ganges as exhibited by the boring operations in Fort Williams, A. D. 1836–40: Calcutta Jour. Nat. History, v. I, p. 324–343

Spate, O. H. K., 1954, India and Pakistan, A general and regional geography: London, Methuen and Co., 827 p.

Vredenburg, E., 1908, The geological history of the alluvial plain of Bengal: Hemchandra Memorial Series, Part I, p. 24–59

Wadia, D. N., 1949, Geology of India: 2d edition, MacMillan and Co., Ltd., London, 460 p.

West, W. D., 1949, Geological map of India: India Geol. Survey Records, v. 81, pt. 1, 222 p.

Willcocks, Sir William, 1930, Lectures on the ancient system of irrigation in Bengal: Calcutta, Calcutta Univ. Press, 128 p.

COASTAL STUDIES INSTITUTE, LOUISIANA STATE UNIVERSITY, BATON ROUGE, LOUISIANA

MANUSCRIPT RECEIVED BY THE SECRETARY OF THE SOCIETY, JUNE 21, 1957

BULLETIN OF THE GEOLOGICAL SOCIETY OF AMERICA
VOL. 70, PP. 343-374, 8 FIGS. MARCH 1959

PLEISTOCENE CLIMATES IN EASTERN AND SOUTHERN AFRICA

BY RICHARD FOSTER FLINT

ABSTRACT

Pleistocene climates in the southern half of Africa are indicated by evidence of lakes in regions now dry, ancient soils for whose development the climate is now too dry or too wet, inactive wind-blown sand now covered by vegetation, and signs of former glaciation. Such features indicate climates different from those now prevailing. In addition, anomalies in the distribution of living organisms seem to support the assumption of climatic change.

Most of the evidence indicates change in annual amount or seasonal distribution of rainfall, but some suggests former temperatures lower, possibly by as much as 5°C., than those of today. Few of the features discussed are well fixed stratigraphically, but most of them are probably late Pleistocene.

The atmospheric-circulation pattern shows that annual amount and seasonal distribution of rainfall differ markedly in various regions in the subcontinent. The current literature contains a start toward a reconstruction of former patterns which are compatible with the geologic and biogeographic evidence, based on analogies with modern anomalies.

Although probable, the theory that pluvial climates in Africa were contemporaneous with glacial climates in Europe remains unsupported by geologic evidence, mainly because data are very few.

CONTENTS

TEXT

	Page
Introduction and acknowledgments	344
Statement of problem and definition of terms	344
Morphology and Pleistocene geology	346
Climatic system	347
Kinds of evidence of Pleistocene climates	351
Glaciation	351
Evidence of relatively wet climates	353
Rainfall and temperature	353
Lacustrine features in Rift Valleys	353
Cavern stratigraphy	357
Travertine aprons	358
Changes in grain size of colluvium; lag concentrates	359
Soils with ferric oxides	359
Plants occurring as fossils at stations where today's climate is too dry or too warm for them	361
Disjunctions of living ecologic groups	362
Stream gravel	362
Evidence of relatively dry climates	363
Limitations of the term	363
Wind-blown sand	363
Deflation basins	366
Soils with secondary carbonates	366
Erosional unconformities within lake sediments	367
Biogeography of fresh-water faunas	368
Cutting and filling by streams	368
Evidence of relatively warm climates	369
Summary	370
Meteorologic theory	371
References cited	372

ILLUSTRATIONS

Figure		Page
1.	Sketch map of eastern and southern Africa	345
2.	Mean positions of high- and low-pressure areas over Africa in January and July	348
3.	Mean fronts and air streams over equatorial and southern Africa in January and July	349
4.	Distribution of rainfall in eastern and southern Africa, shown by isohyets	350
5.	East-west profiles of East African mountains, showing glacial data	352
6.	Map showing locations of places and features in the Eastern Rift Valley	354
7.	Diagrammatic section through cavern in Twin Rivers Kopje, Northern Rhodesia	358
8.	Sketch map showing distribution of Kalahari Beds and orientation of elongate sand dunes	364

Introduction and Acknowledgments

This paper represents the first part of the results of a study tour in Africa near and south of the equator, sponsored by the Wenner-Gren Foundation of New York. The four months, May-August, 1957, were spent in the field with geologists and archeologists. The objective was to assess the existing state of knowledge of the climatic implications and stratigraphic correlation of Pleistocene sediments and other features. The physical, not the stratigraphic aspects, are discussed in this paper; neither sequence nor chronology of former climates is considered.

Travel between principal centers was by air; local travel was by Land Rover, boat, and foot. The territory visited (Fig. 1) includes Ruanda-Urundi, eastern Belgian Congo, Uganda, Kenya, Tanganyika, Zanzibar, areas in Northern and Southern Rhodesia, southern Moçambique, Swaziland, Transvaal, Orange Free State, and Cape Province. The Congo basin, Angola, and South-West Africa were not visited and hence are not discussed.

Besides the Wenner-Gren Foundation, which financed the tour and laid the groundwork for many contacts, I have to thank members of the geological surveys of Uganda, Kenya, and Moçambique, the administration of the Parc National Albert, personnel of the museums at Livingstone, Bulawayo, Pretoria, and Bloemfontein and the universities of The Witwatersrand and Cape Town, and employees of the Northern Lime Company for transportation, housing, and other facilities. To the following people my thanks are due for time spent in the field, guidance, planning of arrangements, and invaluable discussion: B. H. Baker, Lereno Barradas, W. W. Bishop, Geoffrey Bond, C. K. Brain, J. D. Clark, H. B. S. Cooke, R. A. Dart, A. de Kock, M. B. Dias, Jean de Heinzelin, A. C. Hoffman, Raymond Inskeep, L. S. B. Leakey, B. D. Malan, Revil Mason, F. O. Mouta, Merrick Posnansky, J. T. Robinson, Ronald Singer, Philip Tobias, E. M. van Zinderen Bakker, and E. J. Wayland. Finally I acknowledge assistance of many kinds from Margaret C. H. Flint, experienced field companion and good ambassadress.

Thanks are due to these persons who read and commented helpfully on the manuscript or parts of it: B. H. Baker, W. W. Bishop, Geoffrey Bond, J. D. Clark, H. B. S. Cooke, Charles Downie, and members of the University of Sheffield Kilimanjaro Expedition 1957, Jean de Heinzelin, D. M. Hopkins, E. B. Kraus, R. E. Moreau, Merrick Posnansky, I. I. Schell, E. J. Wayland, J. H. Wellington, and H. E. Wright.

Statement of Problem and Definition of Terms

There is little doubt that climatic change occurred in equatorial and southern Africa during the Pleistocene; however, little is known about Pleistocene climates in that region. Questions that should be answered are: (1) How many major changes have occurred? (2) What amplitudes of precipitation and temperature change do they imply? (3) What is their relationship in time to the European glacial and interglacial climates? (4) Did the changes have varying intensity in various regions, and if so, how were the changes distributed in area? (5) What changes, if any, in the existing wind systems are implied? Answers to (1) and (3) are implicit in the climatic sequence (e.g., Leakey, 1948, p. 63) proposed for East Africa and widely quoted.[1]

At least as early as the beginning of the twentieth century, the German literature carried the theory that glacial climates in northern middle latitudes should have been accompanied in low latitudes by pluvial[2] conditions of increased rainfall; the theory was applied to southwestern Africa as early as 1904 (Passarge, 1904, p. 648, 651). After it appeared in the English literature (Brooks, 1914), the theory was applied to equatorial Africa, with reference to sediments and other physical features in that region. Although it became widely accepted, only rarely was there a reminder that, whereas inference from African field data might imply former different climates, correlation of such climates with European climates remained theoretical, however reasonable some particular correlation might seem. Brooks (*in* Leakey, 1931a, p. 267–270) thought the correlation probable but did not claim that it had been established.

As early as 1863 Jamieson (1863, p. 258) suggested a genetic relationship between large former lakes in central Asia and glaciations. Two years later Whitney (1865, p. 452) made a similar suggestion as to lakes in desert basins in western United States; this was subsequently supported by stratigraphic evidence and later by C^{14} dates. However, in both North America

[1] An evaluation of the basis on which the sequence is erected will appear in a later paper.

[2] The term appears in a paper by Blanckenhorn (1901, p. 393).

FIGURE 1.—SKETCH MAP OF EASTERN AND SOUTHERN AFRICA

and Asia most of the lakes referred to lie no nearer to the equator than the 35th parallel of latitude, in a zone which today is subject to a wind system different from those which characterize equatorial and southern Africa. Therefore, although C^{14} dates support the coincidence of European with North American glaciations, it does not follow necessarily that pluvials in low latitudes in Africa were synchronous with glaciations in Europe.

African pluvials are of great importance for climatic history, for Pleistocene correlation, and for meteorologic theory, and deserve more thorough analysis than they have received. Apparently only one scientist working in Africa has

attempted to define the terms formally. Sir Frank Dixey (*in* Clark, 1950, p. 11) defined pluvial as

"a climate of long extent, consistently wetter (though allowing for minor fluctuations within the whole) than the climate pertaining today....."

Interpluvial (a term introduced apparently by Wayland, 1934, p. 347) was defined by Dixey as a major climatic phase drier than the climate of today, Wayland (*in* Leakey, 1952, p. 59) wisely noted that these terms, meaning "more rain" and "less rain", can be used only relatively, and that their relationship to glacial and interglacial climates is not established.

So that ambiguity may be avoided, one of these terms should be altered slightly, and the definitions of both should be sharpened. I suggest that pluvial, used as noun or adjective, should refer to a climatic regimen sufficiently long enduring to be clearly recorded in physical or organic evidence, and having an average effective rainfall distinctly greater than that of today[3] in the same area. I suggest that nonpluvial, also used as a noun or adjective, should be substituted for interpluvial, which implies that the climate is both preceded and followed by pluvial climates, an implication rarely justified. Nonpluvial should refer to a climatic regimen having an average effective rainfall either (1) recognizably less than that of today, or (2) distinctly less than that of a preceding or following pluvial regimen. No absolute duration, no particular stratigraphic position, and no specific relationship to glacial and nonglacial ages in other parts of the world should be implicit in these terms. Their merit is that they should simplify discussion while affording considerable flexibility through the avoidance of unsupported implications. Although conceivably it might become desirable to discontinue the use of existing climate as a standard of reference, in the present state of knowledge it is the obvious choice.

No doubt further changes in definitions and usage will be made. For example temperature may come to be included, for there is evidence that temperature as well as precipitation varied in Africa during the Pleistocene. Also it may appear that in some parts of Africa, at least, a nonpluvial climate was drier than a pluvial but not significantly drier than the climate of today.

Further deduction from theory must await refinement of the theory by climatologists. What is needed now is thorough evaluation of field evidence. The evaluation should exclude both the influence of theory and the possibility of tectonic or other nonclimatic origin of the features under consideration. A principal objective should be the setting of quantitative limits to any inferred changes of precipitation, temperature, and seasonality of climate. However, general inferences must be based on good areal distribution of data; inferences from a single locality should not be applied to a wide region. Two possibilities must be kept in mind. First, departures from existing values, even though they may be everywhere of the same sign, might vary considerably in amplitude from one area to another, although probably in a systematic way. Second, departures might prove to be small.

Finally it is advisable to concentrate on the most recent pluvial, where more than one is recorded, for at least three reasons: (1) Evidence of it is likely to be best preserved. (2) The possibility of control by C^{14} dates is greatest. The predominantly dry climate that prevails over most of the subcontinent results in a generally low water table. In consequence fossil wood, charcoal, peat, and other organic substances used to obtain C^{14} dates commonly have been destroyed by oxidation. Most of the objects of this kind that have been collected have come from relatively young stratigraphic units or from local environments that are wet. (3) Topography and altitudes are most likely to have resembled those of today. As rainfall in much of Africa changes sensitively with changes in altitude, serious errors could result from the interpretation of earlier Pleistocene features whose relative altitude at the time they were made is not known.

The body of data gathered within a few decades by a small number of workers in the vast southern half of Africa is truly remarkable. However, the effort to synthesize the data has perhaps been overambitious. In Europe a large corps of scientists, working through a much longer time, has as yet reconstructed only a crude picture of the climate and vegetation of even the last glacial age. We should attempt to produce at least a comparable reconstruction for Africa. The more nearly complete it is, the more value it will have as a guide to earlier climates.

Morphology and Pleistocene Geology

Africa near and south of the equator is mostly plateau more than 3000 feet above sea level. At least two broad pre-Pleistocene ero-

[3] By "today" is meant the period of instrumental record since the settlement of equatorial and southern Africa by Europeans.

sion surfaces, warped up steeply near the coasts but deformed relatively little throughout the vast interior, are prominent. (For a summary of current concepts of African landscape evolution and a discussion of erosion surface, *see* King, 1948a.) The surfaces are cut by the two Rift Valleys, belts of active faulting having the aspect of long, complex grabens with depths of hundreds to thousands of feet. Lower Pleistocene sediments locally postdate the main faulting; minor faulting has occurred even in very late Pleistocene time. Related to the Rift Valleys are many lava flows, as well as volcanic cones that include some of the world's loftiest.

With local exceptions the subcontinent is predominantly dry, and possesses a coarse-textured drainage pattern. Glaciation is confined to the highest parts of the high mountains, and apart from wind-blown sand there are no broad continuous blankets of Pleistocene sediment. The Pleistocene deposits are confined mainly to valleys and consist mostly of dissected bodies of alluvium of varying, but usually small, thickness. In tectonic basins within the Rift Valleys Pleistocene lake sediments occur. Colluvium is present in many areas.

These bodies of sediment cannot be correlated by continuous tracing in the field because in most cases they are not continuous. Some contain fossil mollusks and mammals, but only a few localities have yielded good collections, and only three faunal stratigraphic zones, the boundaries of which are not sharply defined, have been distinguished. As noted, prevailingly dry climates have induced oxidation of organic matter that would have been datable by C^{14}. Stone tools are abundant and have been employed as guides to stratigraphic zones for lack of anything better.[4] Empirically, correlation on this basis seems to work, but opinion is still divided as to its validity.

These, in essence, are the broad characteristics of the Pleistocene in equatorial and southern Africa, a region which in consequence poses problems quite different from those in Europe and North America, the continents in which Pleistocene features are best understood.

Climatic System

Africa is the world's warmest continent. It is divided by the equator and lies mainly between the subtropical belts of high pressure, which strongly influence its climates. Local topographic influences on climate are less important than in Eurasia and the Americas, because mountains are few; the greater part of southern Africa is plateau more than 3000 feet above sea level. Hence African climates depend chiefly on the broad atmospheric-circulation pattern and have relatively few local variations.

Theoretically Africa lies within the two trade-wind belts on either side of the equator. The symmetry of this arrangement is, however, distorted by the presence over tropical Africa, and in summer over Asia, of an area of low pressure set up by the greater heating of the land than of the sea surface. It is distorted further by seasonal shifting of this equatorial pressure trough over Africa, as well as by shifting of the belts of subtropical highs. The result is a seasonal system of winds and precipitation.

The zone of greatest heating, coinciding with the overhead position of the sun, shifts from the southern hemisphere in January to the northern in July. The pressure trough follows, lagging about a month behind. The subtropical highs shift in the same directions, but less far. The inflow of maritime air, occurring as discrete air streams associated with the subtropical highs over the ocean, brings moisture onto the continent, precipitating it according to season. The precipitation is both orographic and convective, according to locality, temperature, and time. In southern Africa the traveling weather systems common in middle latitudes are weakly developed and are confined mainly to the far south and to the winter.

The seasonal character of the climates of equatorial and southern Africa is best seen in a comparison of the January and July air-circulation patterns. In January (Figs. 2 and 3) the pressure trough lies close to the equator and often merges with a monsoon low centered near 20°S. over Rhodesia. Winds are relatively strong. Three air streams dominate the circulation.

(1) Along the west coast from the Cape to the mouth of the Congo the southeast trade-wind air stream is deflected so as to parallel the coast, giving rise to southerly and offshore winds. Southerly winds activate the cold Benguela Current in the Atlantic Ocean; the current flows north along the west coast of South Africa. Offshore winds drag surface water westward away from the coast; this water is replaced by cold water welling up from moderate depth close inshore. Over the adjacent land the wind system, aided by the slope of the ground toward the coast, causes a general descent of air from the plateau in the interior to the coast, and cloudless skies result. Except

[4] For the general sequence of stone-age cultures, *see* Cole, 1954, p. 193.

over the extreme southern tip of the continent, the same is true in July. In consequence much of southwestern Africa ranges from semiarid to intensely arid.

over Eurasia, crosses the equator at the height of summer and penetrates southern Africa as far as the Tropic of Capricorn. As this air is mainly of continental origin, it is compara-

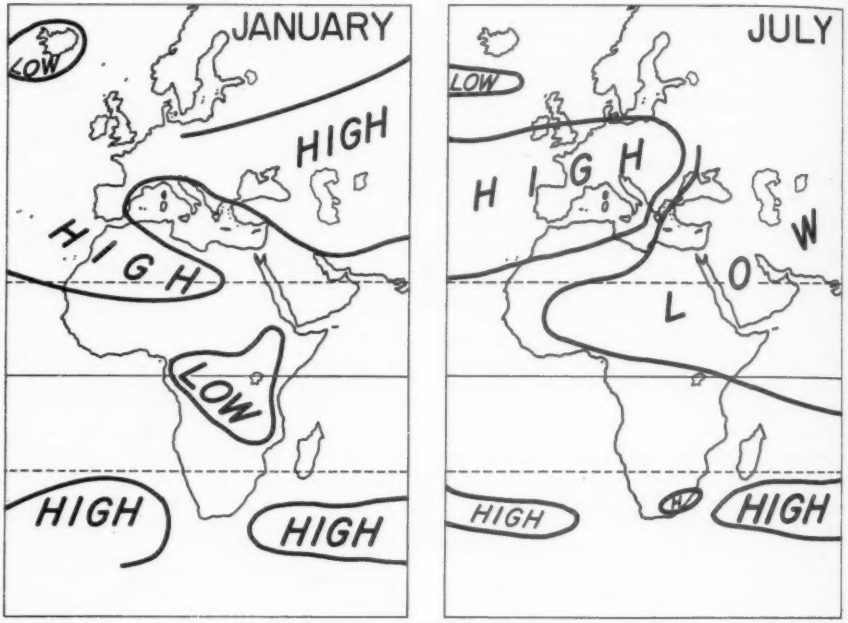

FIGURE 2.—MEAN POSITIONS OF HIGH- AND LOW-PRESSURE AREAS OVER AFRICA IN JANUARY AND JULY (After Kendrew, 1941)

On the southeast coast, in Natal and southern Moçambique, the southeast trade-wind air stream is accelerated by monsoonal indraft. Being onshore and having passed over ocean water about 5°C. warmer than the water off the west coast, it is quite unstable and precipitates rain on southeastern Africa, particularly on highlands. This is the cause of the rainy season (November to March) in that region.

(2) Farther north along the east coast during the northern winter, an air stream that begins as the Asiatic northeast monsoon and merges into the trade-wind system is drawn south across the equator by monsoonal indraft. This air stream brings rain, chiefly convectional, to Kenya; most of the rain falls in November, immediately following the overhead passage of the sun. This air stream contributes similarly to the southern summer rains in southern Tanganyika and Rhodesia.

(3) Meanwhile the third air stream, associated with the flow from subtropical-high cells

tively dry; rain is scarce except on the high, cool East African mountains.

The intertropical front, separating the southeast trade-wind air stream from the two northern air streams, and the convergence zone separating the two northern air streams from each other, are shown in Figure 3. It is evident that most of the precipitation in southern Africa originates in the Indian Ocean.

By July (Figs. 2 and 3) the equatorial pressure trough and the intertropical front have migrated well north of the equator. The southern subtropical high-pressure belt likewise has shifted northward closer to the Tropic of Capricorn. The westerly wind system of the southern hemisphere, with its traveling cyclones, brings rain to the southern tip of the continent. With northward migration of the sun, the interior of southern Africa becomes cooler than the adjacent Indian Ocean and has developed a high-pressure system characterized by descending and outflowing air rather than by indraft of

FIGURE 3.—MEAN FRONTS AND AIR STREAMS OVER EQUATORIAL AND SOUTHERN AFRICA IN JANUARY AND JULY
(January modified from Wellington, 1955; July from Brooks and Mirrlees, 1932; *see also* Garbell, 1947)

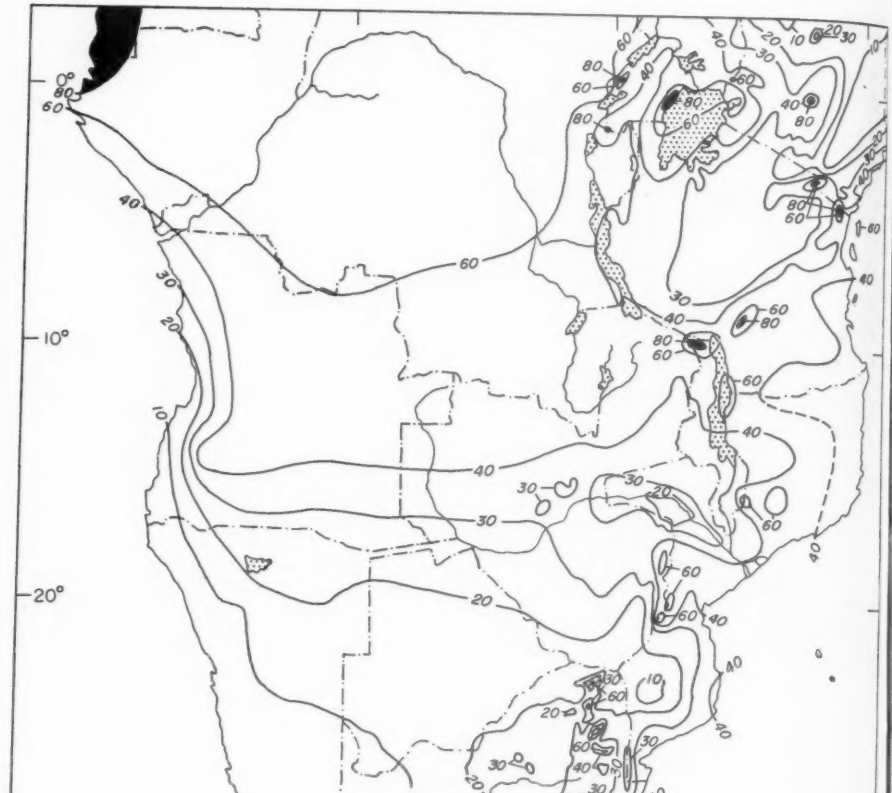

FIGURE 4.—DISTRIBUTION OF RAINFALL IN EASTERN AND SOUTHERN AFRICA, SHOWN BY ISOHYETS IN INCHES PER YEAR

Areas receiving more than 80 inches per year are shown in solid black. Stippled area are lakes. (Compiled from Wellington, 1955, map 3; Walter, 1938; Kendrew, 1941, Fig. 7.) For place names see Figure 1.

maritime air masses; this results in a dry season. Farther north, however, the equatorial east coast escapes the high-pressure system, and, being also open to the southeast trade winds without interference by the island of Madagascar, receives rainfall from air masses flowing in from the Indian Ocean. On the west coast dry southwest winds prevail as in January.

The distribution of mean annual rainfall resulting from this circulation pattern is shown in generalized form in Figure 4.

In summary, the climates that characterize

the various regions of the subcontinent are seasonal, but the seasons throughout the subcontinent do not coincide. Southwestern Africa experiences little seasonal change in wind direction and is dry throughout the year. The western part of the coast of South Africa has a Mediterranean climate with a winter rainy season (May-August). The rest of South Africa, with most of Rhodesia and Moçambique, has a pronounced summer rainy season and a dry winter season. Much of equatorial eastern Africa has two rainy seasons, each intermediate between summer and winter. These accompany the passage of the overhead sun, centering in April-May and October-November, respectively. The former season, because it partly coincides with the northeast monsoon, is the wetter of the two.

Kinds of Evidence of Pleistocene Climates

Glaciation

Equatorial East Africa contains the three volcanic cones Kilimanjaro, Kenya, and Elgon and also the Ruwenzori, an uplifted-block mountain mass. As shown in Figure 5, the highest of these approximates 5900 m, and three of them are capped by glaciers. Reported altitudes of the lowest moraines identified (not necessarily the lowest limit of former glaciation) are 1000 m and more below the termini of existing glaciers, showing that former glaciers were much more extensive than those of today.[5] However, comparison of lower limits affords little basis for climatic inference beyond the statement that the climate was more favorable for glaciation in former times than it is today. This is because topography can influence the form and downward extent of local glaciers.

Published and unpublished observations indicate that despite differences in topographic detail, former glaciers descended lower on the eastern than on the western flanks of Elgon and the Ruwenzori. A similar relationship appears to have existed on Kilimanjaro during the last major glaciation, but altitudes reached on the southern flank were even lower than those on the east. For Mt. Kenya no data are available. In the absence of information on the existing climates on these mountains, the relative influence of distribution of snowfall and intensity of heating on the differences mentioned cannot be evaluated.

The climatic snow line is a more meaningful parameter than is the lower limit of glaciation. B. H. Baker (personal communication) placed the climatic snow line on Mt. Kenya in 1957 at about 5100 m; on Kilimanjaro in the same year Charles Downie (personal communication) placed it above the top of the mountain. As the floors of cirques crudely approximate the minimum altitude of the snow line when the cirques were last actively occupied, it can be seen from the altitudes of the lowest cirques shown in Figure 5 that during glacial maxima the climatic snow line must have been at least 900 m lower than it is now on Mt. Kenya, and at least 1300 m lower than it is now on Kilimanjaro. This difference compares with 1200–1400 m, according to age of the glaciation, in the northwestern Alps. On Mt. Kenya the direction of slope of the existing snow line is not known because all the larger existing glaciers are on the western side of the summit.

The eastward slope of the lower limit of former glaciation reported on Elgon and the Ruwenzori suggests that on them the related snow line might also slope eastward. The only actual measurement known to me is 4750 m(?) for the existing snow line on the west side of Ruwenzori, measured before 1953 (Heinzelin, 1953, p. 4). The values given by Nilsson (1940, p. 63) are estimated.

Determination of the altitudes of today's snow line and of the floors of the lowest cirques on the eastern and western slopes of the mountains should show whether the former snow line parallels that of today; if it does, the former climatic regimen probably differed only in the amounts of accumulation and ablation, not in distribution in terms of compass direction. Parallelism would imply that the local wind system had much the same directions then as now, and that the equator was in approximately the same position. Furthermore, parallelism of existing and former snow lines would favor the inference that precipitation values at a glacial maximum were not greatly different from those of today, and hence that the lower snow line resulted primarily from reduction of temperature rather than from increase in precipitation. Assuming parallel snow lines and no change in precipitation, descent of the snow line through 900 m (Mt.

[5] The most comprehensive reference on glaciated mountains in equatorial Africa is by Nilsson (1931, p. 255–287, Pl. 3; *see also* Nilsson, 1929, 1940). Additional references: Mt. Kenya—Nilsson (1935, p. 10–12); Gregory (1921, p. 149–153); Ruwenzori—Heinzelin (1953); Aberdare Range—Nilsson (1935, p. 10). In connection with the International Geophysical Year 1957–1958, scientific expeditions mapped glacial features on Mts. Kilimanjaro and Kenya.

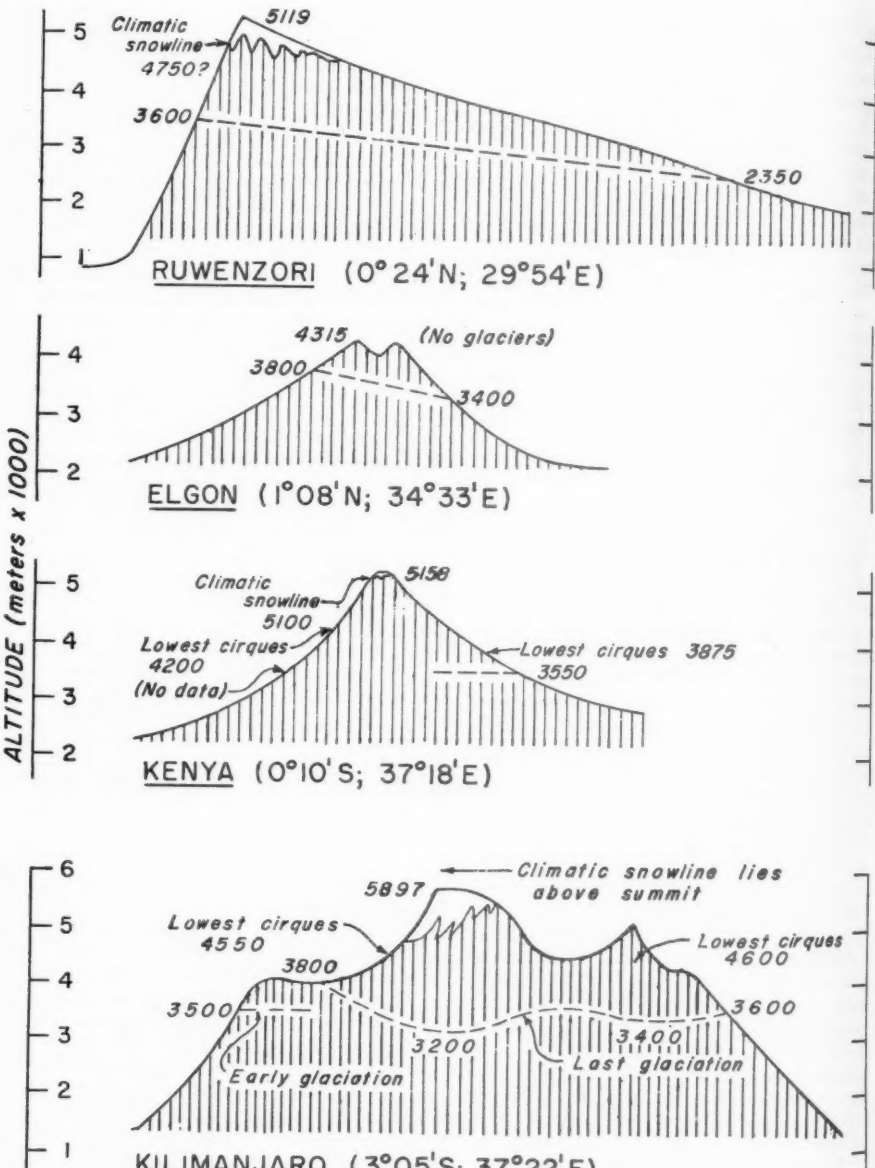

FIGURE 5.—EAST-WEST PROFILES OF EAST AFRICAN MOUNTAINS, SHOWING GLACIAL DATA

Shown are existing glaciers (white), altitudes of lowest-identified limits of glaciation (connected by broken line), climatic snow line (where known), and lowest cirques on Mt. Kenya. Figure is diagrammatic—horizontal scale not true. Sources: Bergström (1955); Heinzelin (1953); Nilsson (1931, 1940); for Mt. Kenya, B. H. Baker (personal communication); for Kilimanjaro, Charles Downie (personal communication).

Kenya data) would imply a temperature reduction of ~5°C.; on the basis of Kilimanjaro data the reduction would be ~7°C. These calculations neglect the influence of change in amount of snowfall with altitude, a factor not yet measured.

During recent decades glaciers on both the Ruwenzori (Heinzelin, 1953) and Mt. Kenya (B. H. Baker, personal communication) have been shrinking. Apparently, however, no data on local or regional trends of temperature or precipitation during these decades are available.

Drift bodies of two ages were recognized on Mt. Kenya, on the basis of weathering differences, by Nilsson (1931, p. 270); the difference was confirmed by B. H. Baker (personal communication). The older drift extends somewhat lower. The presence of two drifts implies that there were two periods of glacier expansion on that mountain.

Correlation of end moraines through outwash bodies with nonglacial sediments in the lower country surrounding the mountains does not afford much promise of success. On the Ruwenzori, the only mountain I ascended, stream valleys on the western flank are steep canyons, cut in bare rock, with no obvious outwash remnants. Indeed they contain little sediment other than stream-bed boulders and cobbles. If the valleys radiating from the summits of the volcanic cones are comparable, correlation of the glaciations with nonglacial sediments will have to be accomplished in some other way.

Evidence of Relatively Wet Climates

Rainfall and temperature.—Some of the evidence in southern Africa indicates that rainfall was greater than it is in the same areas today. The extent to which temperature changes may have accompanied change in amount of rainfall cannot be evaluated from existing evidence. At some places high lake levels and other features may have resulted not only from increased rainfall but also in part from decreased evaporation caused by lowered temperatures. At others red tropical soils might have developed because of increase in seasonal temperatures through threshold values, with or without conspicuous increase in rainfall. No attempt can be made here to separate the factors of rainfall and temperature, but it should be understood that temperature changes of unknown amount may have accompanied the inferred rainfall changes.

Lacustrine features in Rift Valleys.—Although lake-floor sediments stand above the levels of existing lakes in both the Western and Eastern Rift Valleys, abandoned strand lines are probably the best measure of the depths of former lakes. Such strand lines have been reported from a number of lake basins in the Eastern Rift Valley (Fig. 6). Former higher lakes implied by this kind of evidence could have resulted from tectonic movements or from dams, principally volcanic. The draining of such a lake could result from tilting, in which case any strand lines affected would not be horizontal, or from erosion of an outlet, in which case evidence of the erosion should remain. Hence horizontal strand lines, unrelated to any former outlet, are ideal evidence of climatic change. However, slightly deformed strand lines, sufficiently continuous to permit evaluation, are acceptable.

The reconnaissance nature of most of the geologic work published on strand lines in the Rift Valleys leaves little basis for conclusions on this matter. However, the high strand lines of Lake Magadi and of the Naivasha-Elmenteita-Nakuru sector are probably records of climatically controlled lakes; both are in the Eastern Rift Valley, in Kenya.

LAKE MAGADI[6]: Lake Magadi (area about 35 square miles) is fed by alkaline springs and is rising on the surface of its evaporites. As mean annual rainfall on the lake is only 14 inches and air temperatures are high, the lake is believed to exist only because of the springs. About 40 feet above the present lake surface is a conspicuous embankment of laminated lacustrine silt. Of volcanic origin, but transported to the lake by streams and wind, the silt contains fish remains. This embankment records an older, higher lake. Its surface, where in contact with bedrock, is believed to be essentially the strand line of the higher lake. Evidence of crustal warping or temporary dams is negative, nor is there evidence of a former outlet. By elimination, and unless the springs have fluctuated independently of climate, a climatic origin of the former higher lake becomes probable.

The lacustrine silt unconformably overlies two older sequences of lake beds, each having at its upper surface a soil rich in secondary carbonate. As both these older sequences are

[6] Data on Lake Magadi are from B. H. Baker, Kenya Mines and Geological Department, and were communicated during a visit to the lake with Mr. Baker.

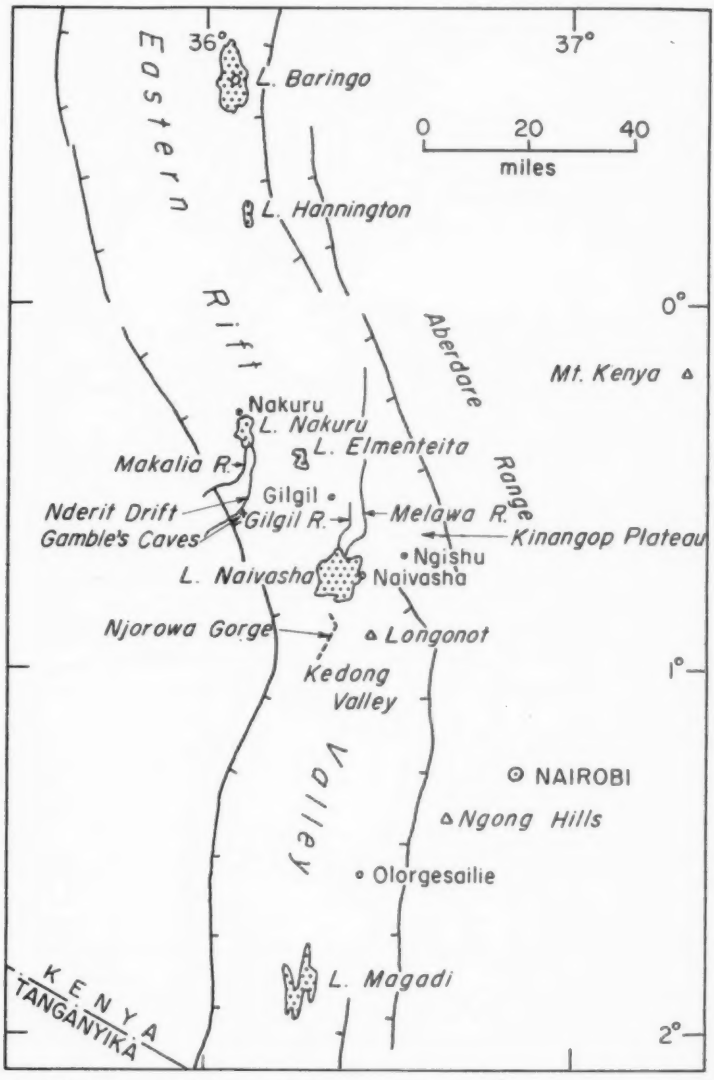

FIGURE 6.—MAP SHOWING LOCATIONS OF PLACES AND FEATURES IN THE EASTERN RIFT VALLEY

deformed by faulting and tilting, it is not evident whether the lakes they represent were controlled by climate or by other factors.

OLORGESAILIE BASIN: In Kenya, 31 miles southwest of Nairobi, the Olorgesailie lake beds occupy a former basin, about 50 square miles in area, of fault-block origin. They are about 170 feet thick and consist mainly of tuffaceuos silts, marls, and diatomites, with at least 14 disconformities as well as alternations of littoral and deep-water sediments. Fossil mammals place the sequence as mid-Pleistocene; at some of the disconformities hand axes and other artifacts occur also. The lake appears to have been drained by erosion, stimulated by minor faulting, at its outlet. As rainfall today

is estimated at 18–20 inches, and as the watershed tributary to the former basin is small, substantially greater rainfall seems demanded by the existence of the lake. Climatic fluctuation is suggested by the disconformities; although the influence of earth movement cannot be ruled out, the number of disconformities and lack of angular unconformity makes this seem improbable. Conceivably the Olorgesailie lake beds are equivalent to one of the older lake sequences at Magadi.

On the basis of both fossil mammals and hand-ax cultures, the Olorgesailie lake is substantially older than the highest lake recorded by strand lines in the Naivasha basin, described hereafter, and was not recreated because, after having been drained, the basin no longer existed.

NAIVASHA SECTOR: The Naivasha sector of the Eastern Rift Valley lies in Kenya, between Nairobi and Nakuru. The three existing lakes, Naivasha, Elmenteita, and Nakuru, occupy basins that contain the strand lines and sediments of former much expanded lakes. The basins are in part tectonic, in part the result of volcanic dams.[7] They are believed to be mid-Pleistocene, although correlation is not precise. The strand lines, although discontinuous, actually are more nearly continuous than is shown on sketch maps (Nilsson, 1931, p. 291; Leakey, 1931b, p. 499) made before 1935. The strand lines were measured as to altitude by leveling in 1927–1928 and were briefly described by Nilsson (1931, p. 290–300; *see also* J. D. Solomon *in* Leakey, 1931a, p. 258).

The shore features consist of surf-cut benches, small deltas, and beaches; the latter consist in places of small pebbles of pumice. The strand lines are broadly comparable in "freshness" to those in the Basin and Range region in western United States.

Nilsson's mapping shows that the highest lake identified in the sector was confluent through the three existing basins. It stood about 375 feet above the 1956 surface of Lake Naivasha and more than 600 feet above Lake Nakuru, and spilled southward around the western base of the volcano Longonot and its satellites into the Kedong Valley,[8] whose floor is at least 1200 feet lower than the highest lake shore line. The lake outlet is represented by the Njorowa Gorge, a canyon 5 miles long cut into flows and lacustrine tuffs (Nilsson, 1940, Pl. 1C, p. 16). Features in the gorge suggest that there were at least two episodes of lake outflow during which substantial erosion occurred; these were separated by a time when the lake surface was lower than the spillway, which today is about 180 feet above the 1956 surface of Lake Naivasha. The relationships of the inferred outflows to specific strand lines remain to be established.

Because the divide between the Naivasha basin and the Nakuru-Elmenteita basin, near Gilgil, is higher than all but the highest shore lines (Nilsson, 1931, p. 300), it is probable that the lakes in the two basins ceased very early to be confluent; after the early outflow, Njorowa Gorge was deepened by outflow from the Naivasha basin only. From plots of the strand lines surveyed, Nilsson (1940, p. 26–27) inferred similar subsequent histories for the lakes in the two basins. This is surprising, as the basins are at different altitudes, and their watersheds are quite different in area.

The published results of leveling data on the strand lines are not easy to understand. Nilsson's reconstruction, based on by far the greatest number of stations occupied, implies gentle, not wholly systematic deformation of these originally horizontal features (Nilsson, 1931, p. 294–301, 1940, p. 24–28). Although it is not unreasonable to expect signs of recent deformation in the unstable Rift Valley, the inclination of the strand lines as plotted might result from some systematic instrumental error.

In either case general inferences on the lake sequence would remain the same. As to what caused fluctuation of the lakes, the observed strand lines postdate all the volcanic rocks except for thin deposits of ash; hence the creation and erosion of a succession of volcanic dams is not admissible. Further, deformation of the shore lines, if real, is too slight to explain the succession of lakes through tectonic movements alone. In other words, although earth movements and volcanic activity could reasonably explain the basins, they are inadequate in themselves to explain the succession of strand lines. By elimination, climatic change seems to be demanded.

But could the climatic change itself be the result of tectonics? It is probable that downfaulting of the floor of the Rift Valley has reduced the rainfall on the area thus lowered, for

[7] A useful generalized N–S profile along the Rift Valley floor, showing the relative positions of these and other basins, is given by Leakey (1934, p. 300, Fig. 3 (2)). However, Lake Elmenteita is about 50 feet higher than Lake Nakuru, not lower as shown in the profile. It is only a few feet deep.

[8] The Kedong Valley drains southward into other basins, whose relationship to the history of the Naivasha basin has not yet been clarified.

there is conspicuously less rainfall on the valley floor than on the plateau into which the valley is sunk, and this difference is clearly reflected in the contrasting assemblages of plants that cover the two areas. Therefore it is true that earth movement has resulted in climatic desiccation within a limited belt of country. All or nearly all this movement, however, antedates both the strand lines and the floor sediments mentioned hereafter, all of which are late Pleistocene. The succession of lakes does not seem explicable in this way, and again general climatic change seems to be the probable cause.

Climatic control of lakes in the Rift Valley was first suggested by Gregory (1921). It was supported by Nilsson in all his papers, and by J. D. Solomon (*in* Leakey, 1931a) after field work in the Naivasha sector in 1928. However, following additional studies in Uganda, Solomon (*in* O'Brien, 1939) expressed doubt as to the exclusive climatic control of lakes in the region and favored crustal movement as a factor in the creation and draining of Rift-Valley basins. Fuchs (1950) expressed similar views. The evidence in the Naivasha sector, however, supports climatic control as a significant factor.

The existing lakes are shallow. Maximum depths in 1932 were: Nakuru, 9 feet; Elmenteita, 6 feet (1929); Naivasha, 34 feet. The first two are saline; Naivasha is nearly fresh. A curve based on annual measurements (Nilsson, 1940, p. 34) shows that Naivasha subsided irregularly from 1916 to 1937. This could have resulted from climatic change, but the possible effects of human interference (deforestation and other vegetation changes, withdrawal of tributary water for irrigation) have not been evaluated. With a surface area that is large in proportion to its tributary drainage area, the lake can be expected to fluctuate sensitively with changes in temperature and precipitation, on which, unfortunately, precise data are not available. Precipitation varies sharply with altitude, ranging from 21 inches at 6200 feet (the altitude of Lake Naivasha) to 41 inches at 9500 feet (A. O. Thompson, unpublished manuscript). Nilsson 194a0, p. 35) explained the low salinity of (Naivsha as the result of desiccation followed by rebirth within the last few millenia. There is, however, no direct evidence on this hypothesis. In summary, the few facts available on the regimens of the modern lakes seem compatible with the concept of large fluctuations resulting from small changes in precipitation and temperature sustained over periods of hundreds or even thousands of years.

In addition to strand lines, other evidence of former larger lakes consists of floor sediments (tuff, silt, clay, and diatomite) distributed widely through the basins. In cuts made by tributary streams these sediments, nowhere known to be more than 200 feet thick, are exposed in a sequence of stratigraphic units separated by erosional unconformities. The sequence, set forth by Solomon (*in* Leakey, 1931a, p. 245) and by Nilsson (1931, p. 300-313), is constructed from sections exposed in and near Nderit Drift, Melawa Gorge, and the valleys of the Makalia and Little Gilgil rivers and also from the Gamble's Cave II section listed by Leakey (1931a, p. 116–119) but not yet published in detail. The local sections are correlated by the succession of Upper Paleolithic and post-Paleolithic artifacts they contain. The sequence shows that living sites along the shores shifted back and forth as the later lakes expanded and shrank.

The floor sediments are not yet correlated precisely with the strand lines, mainly because artifacts occur in definite relation to strand lines at only a few places, where strand lines occupy caves. However, we are concerned here, not with the stratigraphy, but only with noting that sections in the floor sediments, like the strand lines, indicate repeated lake fluctuations during late- and post-Paleolithic (very late Pleistocene) time.

The evidence from the Naivasha and Magadi sectors, from which the most abundant data are available, implies that late Pleistocene climatic changes have occurred. But the facts now known do not afford an adequate basis for estimating the magnitude of the changes.

OTHER BASINS: Elsewhere in the Eastern Rift Valley similar lake features have been reported from the Baringo-Hannington basin (Nilsson, 1931, p. 316–322; Fuchs, 1950) and Lake Rudolf basin, and from other basins farther north in Ethiopia (Nilsson, 1935, p. 5–9, 1940, p. 36–49). But such features cannot be accepted as evidence of climatic change without detailed analysis. Fuchs (1939) held that the basin of Lake Rudolf had been altered by faulting early in the Pleistocene, and that late Pleistocene movements had brought about a substantial rise of the lake surface. Later (1950, p. 170) he maintained that post-mid-Pleistocene faulting and volcanism had resulted in both upward and downward fluctuations of lake surfaces in the Baringo and Rudolf basins.

If detailed study demonstrates strand lines that are essentially horizontal and unrelated to a lake outlet, the hypothesis of climatic change is warranted. Lake Rudolf, receiving a mean rainfall of only about 8 to 10 inches and fed by streams draining high areas of much greater precipitation, should be sensitive to regional climatic changes.

Emerged beaches are reported also from Lakes Natron and Manyara in Tanganyika, but the meager data from them do not justify inferences as to their history.

In the Western Rift Valley the basin of Lake Rukwa, in Tanganyika, contains well-marked strand lines, apparently horizontal, up to about 625 feet above the present lake (Grantham *in* Leakey, 1952, p. 78–82). Lake sediments without strand lines also occur farther north in the Western Rift Valley, within the Belgian Congo (Cahen, 1954; Heinzelin, 1957). Artifacts in them imply fluctuations of lake level extending back into the middle Pleistocene.

Between the Eastern and Western Rift Valleys is the dissected plateau that contains the basin of Lake Victoria, in area the world's second largest lake, despite the fact that it is rather shallow. The basin could possibly have originated by simple gentle downwarping of the plateau after the "End-Tertiary" partial peneplane had been developed on it and then dissected, for that surface seems to pass beneath the western shore of the lake.

Emerged benches and beaches occur at various places around the coast of Lake Victoria. Near Homa Mountain on the east coast there are strand lines at 20 feet (said to be contemporaneous with a Mesolithic culture), 35 feet, and 100 feet (Saggerson, 1952, p. 45). Patches of rounded pebbles at about 300 feet were reported by Oswald (1918) and were thought by him to be beach gravel. However, along the southern coast no strand lines higher than 60 feet have been found (Grantham *in* Leakey, 1952, p. 81). Post-strand-line warping, therefore, may have occurred.

On the west coast, between Entebbe and the mouth of the Kagera River, persistent strand lines at 200 feet, 110 feet, 65 feet, 40 feet, and 12 feet have been mapped.[9] The two higher strands appear to rise westward, but the three lower ones are essentially horizontal. Therefore, although warping may have affected this part of the coast before the 65-foot strand line was fashioned, the lower strands could be related to climatic changes or to erosion at the outlet at Jinja, at the northern end of the lake. As no direct evidence of either has been reported, climatic change cannot yet be confidently inferred from the strand-line evidence at hand.

In theory, however, a moderate decrease in rainfall could cause Lake Victoria to fall below its outlet level and become temporarily an undrained lake. As it receives mean rainfall of about 40 inches, a value greater than that for the Great Lakes in North America, such a fall may seem unlikely at first. Yet when estimated inflow from streams is added to rainfall, and the total compared with discharge at the outlet, it appears that about 85 per cent of the water received by the lake is lost by evaporation (Brooks, 1925). Hence if rainfall were reduced only moderately, Lake Victoria might be lowered below its outlet. According to Worthington (1932) and Greenwood (1951), the distribution of existing lake and river faunas, detailed elsewhere in this report, is compatible with the concept of former partial desiccation of Lake Victoria.

Lakes older than those recognized mainly from strand lines are inferred from eroded lake sediments in both Rift Valleys and in the Lake Victoria basin between them. In the Eastern Rift Valley from Lake Magadi north to Lake Baringo the sediments are believed to date from mid-Pleistocene time; near Lake Rudolf older Pleistocene sediments are present. Near Lakes Albert and Edward in the Western Rift lower Pleistocene lake beds occur, and on the northeastern coast of Lake Victoria both lower and middle Pleistocene lacustrine strata have been identified. Owing to erosion or tectonic movements or both, the limits of the basins that contained these ancient lakes are either poorly defined or not defined at all.

Cavern stratigraphy.—In a steep-sided hill named Twin Rivers Kopje, 15 miles southwest of Lusaka, Northern Rhodesia, a fissurelike cavern (Clark, 1955, p. 29–31) affords probable evidence of former precipitation greater than today's 35 inches of seasonal rainfall. The hill, 170 feet high, consists of steeply dipping coarsely crystalline Precambrian limestone. Thirty feet below its top is a small sinklike cavern (Fig. 7), largely filled with breccia, that subsequently has been partly eroded. Beneath the breccia is a partial pavement of flowstone. The breccia includes a fine-grained facies (reddish probably because of washed-in red-clay soil), grading into an overlying coarse facies, with fallen roof blocks, broken stalactites, and thin lenses of flowstone. Both facies con-

[9] These and following data from W. W. Bishop, with whom I visited strand-line localities.

tain mammal bones and artifacts suggesting the proto-Stillbay culture. Exposed surfaces of the breccia contain solution cavities of various sizes. Some of those in the lower part are filled with the insoluble residue (including stone tools) resulting from re-solution of the breccia. Cavities in the upper part are filled with fine-grained gray earth containing artifacts of the Wilton culture. Calcareous cement has converted both breccia and post-breccia filling into firm rock.

As the surface watershed tributary to the cavern has an area of less than 800 square yards, factors other than direct rainfall are minimized. Changes in rainfall, then, should be reflected sensitively in the cavern regimen.

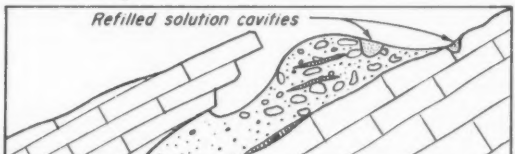

FIGURE 7.—DIAGRAMMATIC SECTION THROUGH CAVERN IN TWIN RIVERS KOPKE, NORTHERN RHODESIA
Not to scale

A cursory inspection of the cavern suggests these events:

(1) Excavation of cavern with a roof more extensive than now; climate probably as wet as or wetter than today.

(2) Partial filling with dripstone and flowstone; climate at least as wet as in (1).

(3) Beginning of unroofing; concomitant filling with insoluble red earth plus a few roof fragments; cementation of filling. Climate possibly drier than in (2), as suggested by apparent cessation of flowstone making and by implied conspicuous erosion of red soil upslope from the cave.

(4) Rapid unroofing; nearly complete stripping of red-clay soil from watershed area upslope; cementation of filling and deposition of flowstone. Climate possibly wetter than (3), as suggested by renewal of flowstone making.

(5) Localized re-solution of filling exposed by unroofing; continued relatively wet climate, suggested by renewed solution.

(6) Partial refilling, with gray earth, of solution cavities in breccia and bedrock; climate possibly drier than (5), as suggested by reduced solution and implied increase in erosion upslope.

In summary, fluctuation of rainfall is suggested although not proved by the features observed, but magnitude of fluctuation is not indicated. The process of unroofing may have been simply a result of long-continued erosion, in itself possessing no climatic significance. The associated cultures suggest that (6), a relatively dry time, may have been the Hypsithermal, and that the breccias may be many times older.

Travertine aprons.—The Kaap escarpment in Bechuanaland, northwest of Kimberley, consists of Precambrian dolomite. Along parts of its extent it is characterized by remarkable accumulations of travertine. This calcium carbonate issued from springs in small valleys and was precipitated as the water evaporated or as its CO_2 was absorbed by aquatic plants. Extensively exposed by large-scale quarrying, the travertine is seen to fill valleys. Evidently it blocked them and forced the streams to cut new channels. It also forms great carapaces built outward and downward over cliffs, with beds 100 feet or more in aggregate thickness and having dips as great as 75°, like the foreset beds of a classical delta. At some places at cliff edges the deposits are outright dripstones.

Peabody (1954) contributed significantly to clarifying the origin of the travertines. He showed that there were four deposits, separated in time by episodes of stream erosion. Little travertine is forming today, probably because of generally small spring discharges, for evaporation at the nearest station, Kimberley,

is great, approximating 96 inches annually. Hence during precipitation of travertine, rainfall probably exceeded today's value of 15 to 20 inches. On the other hand, as fossil plants in one of the massive travertine units are essentially the semiarid assemblage of today, the rainfall was not sufficiently greater to alter substantially the regional flora. Hence the travertines are ascribed by Peabody to the late, waning segments of relatively rainy periods, with whose peaks the episodes of valley cutting are correlated. In this scheme today's climate falls near the dry end of the range of Pleistocene climates indicated by the assembled evidence. If the greater rainfall demanded by the presence of the travertine had been part of a climate characterized also by even drier or longer dry seasons than those characteristic of today's climatic regimen, travertine deposition should have been even more rapid.

The oldest travertine contains a cavern, in the breccia of which *Australopithecus africanus* and other extinct mammals have been found. As the cavern antedates valley cutting, which in turn antedates the next oldest of the four travertines, several alternations of climate extending back into middle or early Pleistocene time are indicated.

Changes in grain size of colluvium; lag concentrates.—In moist areas with considerable relief, clay-rich mantle formerly believed to be residual soil is now recognized as colluvium, transported down-slope through considerable distances. The occurrence in vertical sequence of two or more bodies of such colluvium, separated by lag concentrates of the coarsest particles present, implies changes in the erosion-deposition conditions on slopes, such as alternations of soil creep and sheet erosion (Heinzelin, 1955a). These changes very likely include changes in climate. Other possible causes are impairment of grass cover by fire and trampling by prehistoric people at campsites or by animals.

These features, exposed in road cuts and stream banks, are widespread in hilly parts of western Uganda, Ruanda-Urundi, and eastern Belgian Congo. They are exposed also in railway cuts near Victoria Falls Station, Livingstone, Northern Rhodesia, overlain by sediment containing a Sangoan culture. The phenomena deserve detailed study, one of the objects of which would be determination of the areal extent of individual sheets of colluvium and the form of the lag concentrates, some of which suggest the presence of small gullies.

The value of intensive study of colluvium is illustrated by the archeologic site at Khami waterworks, 13 miles west of Bulawayo, Southern Rhodesia, investigated by Bond (1957). The site is at the base of a dissected scarp consisting of steep domelike hills of fine-grained granite, largely bare of mantle. At the site are sediments consisting of grains of quartz, feldspar, and other minerals mechanically disaggregated from the granite and transported mainly by rills and sheetfloods. The sediments, 10 feet thick, overlie a pedimentlike granite floor. Bond took samples of the sediment at close vertical intervals, separated the feldspar grains out of each, and weighed 600 grains from each sample. Weights were plotted against vertical position. On the assumption that runoff is proportional to rainfall and that competence of rills and sheetfloods ranges between the third and sixth power of velocity, he derived possible former rainfall maxima of about 36 inches per year and minima of about 22 inches per year, compared with today's value of 25 inches per year. The possibility exists, however, that storm intensities rather than annual rainfall totals are indicated by these data.

The 10-foot section was subdivided on the basis of six successive cultures. Largest diameters occurred at the interface separating the Stillbay culture zone from the overlying Magosian zone. In the section at Gamble's Cave II in Kenya the Stillbay culture postdates by an apparently short interval a high stand of the lake in the Nakuru Basin, representing a wet climatic phase.

Although bold, this kind of measurement and reasoning are promising and should be applied to other sites where analogous conditions permit.

Soils with ferric oxides.—Actively developing "red"[10] tropical soils and weathering profiles are distinctively distributed relative to climate. Their distribution shows that such soils require relatively high temperatures, at least at one season, and moderate to great rainfall. Although it has been rather widely thought that markedly seasonal rainfall is an additional requirement, there is reason to believe that various kinds of red loams in tropical regions can form without seasonal rainfall, but that the development of concretions and hard crusts of hydrated iron oxides does demand alternating wet and dry seasons.[11]

[10] Some so-called red soils are brown (5YR to 10YR in the Munsell color system).

[11] The supporting argument is stated in Mohr and van Baren, 1954, p. 365–373.

Development of red soils and weathering profiles of both kinds is favored by free subsurface drainage and an acid-soil environment. They develop best in rocks of basic to intermediate composition. Under this combination of conditions silicate minerals rapidly decompose to bases, silica, and iron and aluminum oxides. Bases, followed by silica, are leached out of the surface zone, leaving sesquioxides of iron, aluminum, and manganese as residuum.

With some red tropical soils the process seems to stop here. But with strongly seasonal rainfall and consequent fluctuation of the water table, the development appears to be more complicated. Leaching-out of bases and silica and their movement downward take place mainly during wet seasons. During dry seasons the water table subsides, but moisture moves upward by capillarity and evaporates in the zone between the water table and the surface. Its solutes are oxidized and are precipitated, in a zone parallel with the surface, as small pelletlike concretions or as continuous crusts, some of them pisolitic or slaglike, of hydrous oxides of iron and aluminum. The crusts are sometimes erroneously termed laterite and are also known as lateritic ironstones, a better designation, but the term *ferricrete* (Lamplugh, 1907. p. 198) is preferable.

The sequence of events outlined is very generalized. The varieties and degrees of development of red tropical soils and weathering profiles are many. They result from variations in such factors as temperature, amount and seasonality of rainfall, parent materials, topography, and time. Lower limits of rainfall necessary for the production of various kinds of red tropfcal soils are not found in the literature, probably because the climate within the soil depends on all these factors, of which climate above the ground is only one. Nevertheless the principle seems valid that residual accumulation of iron sesquioxides in a developing soil requires high temperatures and moderate to high rainfall and does not take place under continuously dry conditions. On this basis we can say that an ancient red soil, or components such as iron concretions or ferricrete layers in a moderately dry tropical area where such soil is not forming today, probably indicate former greater rainfall. At present seasonality does not appear to be a critical factor, as the climates of the African subcontinent are seasonal.

The areal distribution of red tropical soils now actively forming and that of ancient Pleistocene soils of similar character should be determined. A large map showing the distribution of red tropical soils in Africa—presumably modern soils still actively forming—appears in Schokalskaja (1953).[12] It is difficult to distinguish between modern soils and relict soils that are at the present surface, as well as between red-loam soils in place and colluvium derived from such soils where the occurrence is on slopes. Thick ferricretes are widely developed in East Africa at or near the summits of hills that mark the positions of extensive pre-Pleistocene erosion surfaces and are present, although less well developed, in materials whose stratigraphic relationships imply a Pleistocene age. Probably most of these ferricretes are relict, and in most cases it is not known what soils are developing today in the same localities. However, according to Janmart (1953, p. 61), ferricrete is forming now in high northeastern Angola and in some places is thickening at a rate of about 1 mm per year.

Despite the probable inclusion of some relict soils, the map referred to appears to represent the general distribution of red tropical soils now actively forming. Such soils extend from 10°N. Latitude to 24°S. Latitude and when compared with rainfall maps are seen to be confined to areas receiving more than 40 inches of rainfall annually; the soils labeled "laterite" (ferricrete?) receive 60 inches or more. These values might be taken as provisional rough guides to the minimum rainfall implied by the occurrence of ancient red tropical soils elsewhere in the subcontinent.

Ancient soils of red-tropical character are found to be more extensive than what are believed to be their modern counterparts. They occur not only in higher latitudes but also at lower altitudes where rainfall is less than the values deduced from the Schokalskaja map. These statements, based only on widely scattered observations, are subject to refinement, for no systematic survey of ancient soils has been made. Localities at which red-tropical soils are known to occur (mostly in alluvium) include the following, listed in condensed form:

Red-tropical soil profiles without ferricrete or ferruginous nodules

(1) High terrace of Semliki River, Belgian Congo, immediately north of Lake Edward; altitude, 3000 feet; rainfall approximately 20 inches (Heinzelin, 1955b, p. 99, 128).

[12] *See also* the sketch map reproduced in Mohr and van Baren, 1954, p. 374.

(2) Rwindi plain, south of Lake Edward; Lubilia River plain and Kazinga Channel north of Lake Edward; east and west bases of the Ruwenzori. All at 3000–3300 feet; rainfall 20–30 inches. Similar soils are common at least 2000 feet higher, under 40–60-inch rainfall; even these may be relict in part.

Soils with zones of ferruginous nodules or thin ferricrete

(3) Kinangop Plateau east of Naivasha, Kenya; altitude, 8500 feet; rainfall about 35 inches. (Reference on stratigraphy: Shackleton, 1955.)

(4) Lusaka district, Kalomo district, and Victoria Falls (Clark, 1955, p. 19) in Northern Rhodesia; Bulawayo district (Jones, 1944, p. 39) in Southern Rhodesia; rainfall about 25 inches.

(5) Magude, Moçambique; Elandsfontain, Transvaal; rainfall 25 inches.

(6) Southeastern Bechuanaland (Söhnge, Visser, and Lowe, 1937, p. 51); rainfall 18 inches.

(7) Hopefield, northwest of Cape Town (two horizons; Mabbutt, 1956); rainfall 12 inches.

In addition, the very fine-grained red interstitial material in the Older Gravels (*see*, for example, Cooke, 1946) along the Vaal River, mainly in the western Transvaal, is probably the residuum of a much-eluviated ancient soil. No soil profile remains, but the color (5YR4/4 to 5R3/4) of the residuum, which coats the quartzose pebbles constituting the gravel, suggests that the former soil was rich in iron sesquioxides, probably derived from the diabasic Ventersdorp lava flows that underlie much of the region. The implied rainfall during the time of soil development is substantially greater than present values, which range from about 10 inches in the west to more than 20 inches in the eastern part of the area of occurrence.

All these occurrences are in areas where the mean annual rainfall is smaller, by widely varying amounts, than the minimum believed necessary for their development, and where the soils now forming are appropriate to the present drier climate.

Ferricrete, developed in Precambrian rocks and in colluvium derived from them, is exposed at various places along the west side of Lake Victoria. At some localities the ferricrete may be related to a broad pre-Pleistocene erosion surface, apparently warped down so as to pass beneath the lake. At others, however, it appears to be Pleistocene, postdating emerged surf-cut cliffs of former higher shores of the lake. It seems possible that in such positions ferricrete (as at the Magude locality mentioned earlier) is not necessarily indicative of former greater rainfall. It might have resulted from alternate spray from surf during storms and drier local air during calms, the two conditions simulating a microclimate with seasonally high rainfall. The amount of spray created can be judged from the observation (W. W. Bishop, oral communication) that storm waves dash water against shore cliffs to heights as great as 15 feet above mean lake level.

Apart from the presence or absence of ferricrete, soil color appears to be related systematically to climate in southern Africa. According to C. K. Brain (oral communication), sampling of modern soils developed in the existing surface in Precambrian dolomite shows this relation of color to rainfall, which is strongly seasonal throughout the region:

Mean annual rainfall (Range in inches)	*Predominant color (Munsell scale) (Approx.)*	
60–28	Moderate brown	5YR3/4
28–15	Light brown to moderate brown	5YR5/6 to 5YR4/4
15–3	Dusky yellow	5Y6/4

This seems to imply a change, with decreasing rainfall, from iron and manganese sesquioxides through iron sesquioxides to hydrous iron oxides. It suggests a means whereby ancient soils, buried within the Pleistocene stratigraphic sequence and developed from a single kind of rock might afford evidence of the climate prevailing when and where the soils developed.

In summary, red tropical soils, ferricrete, and ferruginous concretions related to such soils seem to indicate Pleistocene climates that were wetter than those of today, provided Pleistocene age is established and local microclimates created by spray can be ruled out. An attempt should be made to determine within narrower limits the minimum rainfall, temperature, and seasonality under which such soil features will form; such an effort could be related to the soil-mapping programs of government agencies, for the soils now forming in any region must be well understood before the quantitative implications of the ancient soils can be realized. Although it has been asserted (e.g. Smuts, 1945, p. 43) that ferricrete is indicative of diminished precipitation following a phase of wet climate, it is not clear why this should be true. The climatic relationships of ferricrete seem to require only that temperature be relatively high and that rainfall be above a certain minimum, and markedly seasonal.

Plants occurring as fossils at stations where today's climate is too dry or too warm for them.—The biogeography of southern Africa is so little

known that few comparisons of existing and former ranges of critical organisms have yet been made. A discovery at the southeast end of Lake Tanganyika promises useful data on climatic change. The site (Clark, 1954b) is Kalambo Falls, at the boundary between Northern Rhodesia and Tanganyika. There sediments of a former local lake, stratigraphically identified by evolved Acheulean and Sangoan cultures, contain fossil wood and pollen. Much pollen is present, and wood (*Cynometra* sp.) associated with it has been dated by C^{14} at >53,000 years B.P. At present *Podocarpus* grows in the surrounding region only on ridge tops more than 5500 feet in altitude, where rainfall is of the order of 80 inches, and temperature is low. The altitude of the fossil locality is 3500 to 4000 feet and receives much less rainfall than do the ridge tops.

Furthermore there is no adjacent higher land on which the trees could have grown and from which the wood could have been washed down to the locality in which it was found. The nearest known living *Podocarpus* forest is 60 miles distant, at an altitude of more than 7500 feet. The inference is justified that the fossil trees indicate a formerly greater rainfall at the Kalambo locality. Unfortunately comparative temperature data are lacking, so that although a former lower temperature can be reasonably assumed, it is unconfirmed by measurement as yet.

Disjunctions of living ecologic groups.—Moreau (1933, 1952) developed an argument leading to the concept that rainfall was greater and temperature less than they are at present in equatorial and subequatorial Africa. It runs thus: Montane forests of tall evergreen trees are confined to highlands with altitude sufficient to receive more than 40 inches of rain; such forests, shown on a sketch map (Moreau, 1933, Fig. 1) are widely scattered from Lake Nyasa north and west to the Ituri highland in the Belgian Congo. At high altitudes in these forests is a temperate bird fauna, believed to be incapable of adapting to nonforest conditions. Accordingly it is suggested that the distribution of both forest flora and birds, now isolated and patchy, was formerly continuous.

The country that now separates the highlands is mostly savanna and drier terrain at altitudes of from 4000 feet down to less than 2000 feet and receiving about 30 inches of rain or less. As evergreen forest will grow anywhere in East Africa with 45–50 inches of rainfall, a sustained regional increase of 10–15 inches should have resulted in continuous forest. Increase in rainfall would have been favored by lowered temperature.

As most of the highlands seem to have been formed in Plio-Pleistocene time, the forests occupying such highlands are inferred to be no older than Plio-Pleistocene. They can be reasonably assumed to have been continuous when large lakes occupied the basins in the Naivasha segment of the Eastern Rift Valley.

A similar isolated forest, containing many species identical with East African species, occurs in the Cameroun, 1200 miles northwest of the Ituri highland; here also former interchange of montane organisms, across what is now mostly low-altitude savanna, seems to be implied. In this case, especially, increased rainfall alone is not enough, for the high temperatures at the low intervening altitudes would have constituted a barrier. If mean temperature had been at least 5°C. lower than its present value of around 25°C., communication should have been possible (Moreau, 1952, p. 907).

Although this kind of evidence hardly compels the inference of formerly lowered temperature at the equator, it should be considered in any evaluation of late Pleistocene climatic changes. Its bearing on the rationale of Pleistocene climatic change put forth by Simpson (1957), according to which wet periods in the tropics should have been not cooler but warmer than dry periods, is worth noting also.[13]

A study of the distribution of living waterbugs in Africa (Hutchinson, 1933) suggests that climates both wetter and drier than the present climates affected the continent during the Pleistocene.

Stream gravel.—Although coarse stream gravel in several localities in East Africa has been cited as evidence of former increased rainfall, the implied argument (more runoff, greater stream discharge, greater competence) is fraught with uncertainty. Even were it satisfactorily established that such gravel is never moved today, even during exceptional floods, the distribution in time as well as the annual amount of inferred former rainfall would have to be considered. It could be argued that a given mean annual rainfall so spaced as to create a few flash floods could result in alluvium coarser than that obtainable from the same

[13] The isotopic temperatures of tropical surface sea water, determined by Emiliani (1958) as about 5°C. lower during glacial maxima than existing temperatures in the same region, point in the same direction.

rainfall occurring in equal daily increments. Even this is an oversimplification, for weathering and mass-wasting also would be affected by climate and would in turn influence both mean and maximum diameters of the rock particles constituting stream loads. So many variables are involved that for the present, at least, it seems best to avoid direct and simple inferences from diameter measurements in coarse alluvium. When detailed data on entire stream systems are developed, it may become possible to draw significant inferences from grain-size distribution in ancient alluvium.

Former Relatively Dry Climates

Limitations of the term.—A different group of sediments, land forms, and other phenomena affords evidence of former climates that were relatively dry. The expression "relatively dry" is preferable to "drier than today" because in some instances, at least, it can be inferred only that the climate was dry relative to a climate that preceded or followed it; its relationship to today's conditions is not known. None of the existing evidence indicates certainly that any Pleistocene climate in southern Africa was radically drier than today's, although slightly drier conditions seem probable.

The evidence of "relatively dry" climate over the subcontinent cannot be expressed in mean annual rainfall values with assurance. Quite possibly such evidence could be attributed in part to a dry season that was formerly relatively longer, with less change in over-all annual precipitation than would otherwise be implied. In fact it is conceivable that lengthening of the dry season, with no change at all in the annual rainfall, might give rise to features of the kind described in the following paragraphs.

Wind-blown sand.—Pleistocene or mainly Pleistocene sand of chiefly eolian character has been recognized widely in northwestern South Africa, the western part of the Rhodesias, eastern Angola, and the southern part of the Belgian Congo. Most of it is reddish or brownish (typical samples are classified as 10R4/6 to 5YR4/4). Its thickness varies, and locally it is present as two or three stratigraphic units separated by units of other origins. Its Pleistocene age is established at various points by its relationship to stream terraces, to culture horizons, and to a dissected, End-Tertiary(?) broad erosion surface. The greatest unbroken extent of the sand is in Bechuanaland and southern Angola. In most of the region in which such sand is at the surface, it is covered with vegetation, mainly grass and shrubs, and is not actively moving. Hence former drier conditions are implied.

Throughout most of its extent the Pleistocene sand is underlain unconformably by a sequence of sediments, a few tens to a few hundreds of feet thick, known as the Kalahari Beds (South Africa and Bechuanaland) or Kalahari System (Belgian Congo). The name is derived from the Kalahari region, a dry region roughly coincident with the Bechuanaland Protectorate. Said to be late Tertiary because of its relationship to erosion surfaces, this sequence consists primarily of sandstone but includes also conglomerate, siltstone, clay, and marl. Some samples of the sand are rounded, frosted, and well sorted; this is perhaps the basis of a belief that all the sand is eolian. Undoubtedly much of it is, but extensive alluvial and lacustrine sediments are recognized also. The Kalahari beds appear to have been deposited in shallow basins and on plains surfaces. They are now mainly a plateau cap or cover with a distinct margin that is being actively dissected. Unquestionably the cover originally was more extensive.

Although there are clearly two major stratigraphic units, one Pleistocene and one pre-Pleistocene, the name "Kalahari sand" (Passarge, 1904) has been applied to both, with resulting confusion. Recently occurrences of the Pleistocene sand have been referred to as Kalahari-type sand and as redeposited Kalahari sand, terms that at least represent an effort at discrimination. Understanding of the eolian sediments would be furthered if they were not called Kalahari sands. They are not part of the Kalahari Beds (Kalahari System), which are pre-Pleistocene. Nor is it established, nor even likely, that all such sediments—the extensive sands in coastal Moçambique, for example—were derived from the Kalahari region. They should be called Pleistocene eolian sands until they can be given local formation names.

The main region of Pleistocene sand is marked in some areas by massive longitudinal dunes, whose trend, broadly west-east with variations, apparently indicates wind directions at the times when they were built; but, as they have been mapped only locally (*see*, for example, Lewis, 1936), little is known about them. Where closely observed, the dunes postdate deep dissection of the Kalahari Beds. Du Toit (1954, p. 462) speculated that the Pleistocene sand was blown mainly from arid South-West Africa, but it seems more probable that it was derived from many local sources, chiefly in the

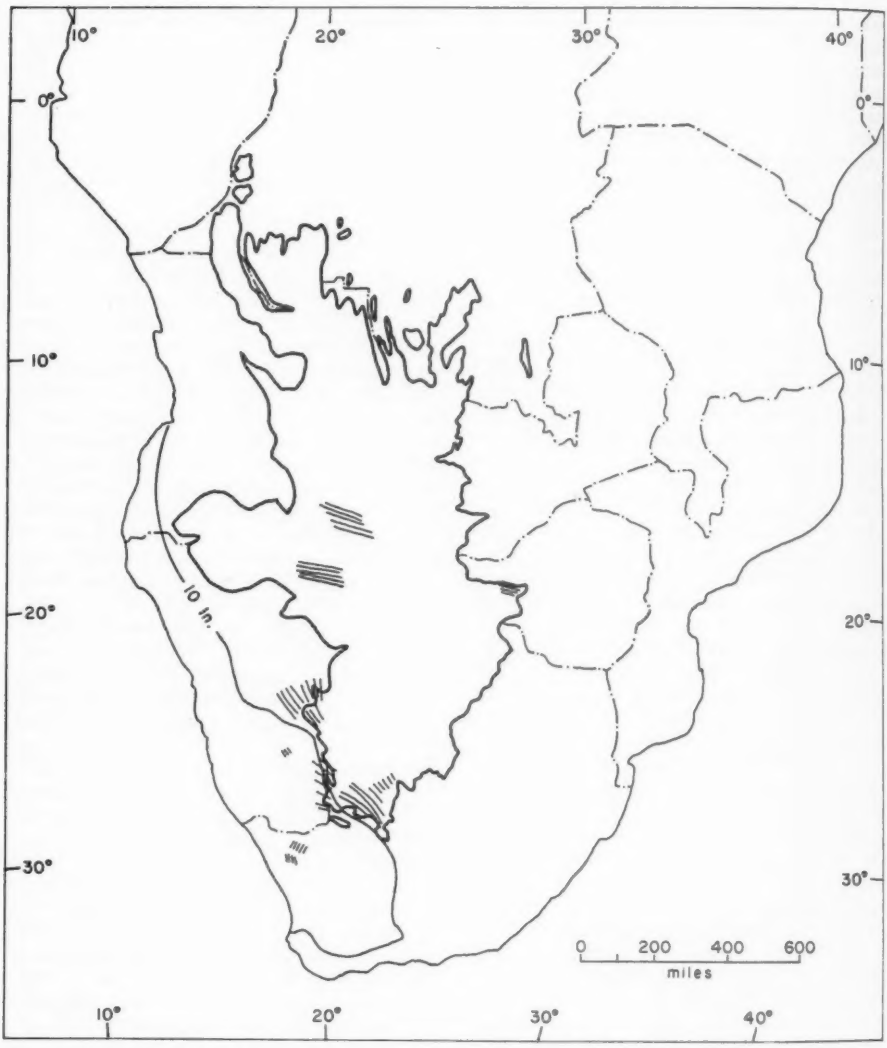

FIGURE 8.—SKETCH MAP SHOWING DISTRIBUTION OF KALAHARI BEDS AND ORIENTATION OF ELONGATE SAND DUNES

Dunes (mostly of the longitudinal type) are undoubtedly far more extensive than shown. Area of Kalahari Beds compiled from several geologic maps. Dunes compiled from data in Lewis (1936), Clark (1957), and direct observation. The 10-inch isohyet is shown also.

Kalahari Beds, and that it has been reworked repeatedly. Mineral-provenance studies of limited areas, such as the study of samples from marginal areas in Bechuanaland made by Arie Poldervaart (*in* Clark, 1957, p. 106–114) are the best way to determine the origin of the sand. Studies of the shape, character of surface, and sorting of the sand grains, such as the study of samples from Victoria Falls made by Geoffrey Bond (*in* Clark, 1957, p. 115–122), are the best way to make sure the sand bodies dealt with are eolian.

The orientations of longitudinal dunes (Fig. 8) should indicate effective wind direc-

tions during dune building. Wellington (1955, p. 55, 197) showed that dunes in the southern part of the Kalahari region are parallel with light northwesterly winds that are strongest in the afternoon in both summer and winter. If the dunes were built by these winds, no radical change in the atmospheric circulation in this region is indicated.

What are the climatic implications of the Pleistocene sands of Kalahari type? Clearly these sediments were laid down at times when the mantle of vegetation (mostly grass and shrubs) that now covers them was discontinuous or lacking. Very probably the times of deposition were marked by climates sufficiently dry to have impaired the vegetation cover. How dry were they? Today, vegetation thins toward the southwest in the direction of decreasing rainfall. It becomes thin enough to permit active deflation where rainfall is less than 10 inches, and probably also at higher values, but the data are so scattered that it is difficult to fix a threshold value. In other parts of the world sand in continental interiors is known to lose its grass cover in places and to begin to move under as much as 16 inches of rainfall. This comparison of crude annual values is, however, weakened by the differences imposed by distribution of rainfall within the year. A strongly seasonal distribution should permit sand movement at higher annual precipitation values than would a less seasonal climate.

A distinction should be drawn between longitudinal dunes and eolian sand having other surface forms. Areas of active longitudinal dunes in southwestern United States and in central Australia are limited approximately by the 10-inch isohyet. It may be, therefore, that at the times of most active former deflation the parts of southern Africa that are marked by longitudinal dunes received rainfall of 10 inches, or possibly more if, as is likely, rainfall was seasonal.

We have, then, suggested crude maximum values of 10 inches or more for longitudinal-dune areas and 16 inches or more for other sand. Comparison of these values with today's rainfall is met in order. Inactive longitudinal dunes occur in the southwestern region, with as little as 10 inches of rainfall, and as far east as the western part of Southern Rhodesia, which receives as much as 25 inches. Hence it could be inferred that at dry times in the past, annual rainfall may have been 15 inches less than it is today, differences due to changes in seasonality being neglected.

Inactive sand not in longitudinal dunes is more widespread and occurs through a greater range of present-day rainfall values. In parts of southeastern Belgian Congo and northeastern Angola such values reach 60 inches but with markedly seasonal distribution. At Elisabethville, northeast of the sand region, the annual mean is 47 inches, but of this amount only 1.3 inches falls during the 6-month dry season. Because of this strong seasonality it would be unrealistic to apply a 16-inch threshold deduced from less seasonal areas on other continents and suggest that annual rainfall was formerly 30 inches less than today. It is more likely that, with such seasonality, only a moderate reduction of today's rainfall could cause movement of sand during the dry season.

The foregoing discussion shows what a slender basis exists as yet for quantitative climatic influence from eolian sand. One special kind of study, however, has been made by C. K. Brain (*in* Clark, 1957, p. 143–148; also unpublished data) on the sediments found in breccias filling the early Pleistocene caves in dolomite at Sterkfontein, Swartkrans, Kromdraai, and Makapan in the Transvaal, where Australopithecine fossils have been found. The sand-size particles occurring as incomplete mantles on dolomite hillsides in that region consist of a mixture of (1) minute chert nodules from the dolomite, released by solutional weathering, plus other local mineral grains, and (2) quartz particles less angular and reasonably inferred to have been wind-blown from sources outside the district. Samples of hillside mantles on dolomite in the vicinity of the caves (rainfall 28 inches) show good agreement among themselves in the proportion of eolian to other grains, suggesting that the proportion depends on climate. Samples of the sand fraction removed from the cave breccias vary systematically with stratigraphic position in the breccias, suggesting corresponding changes in rainfall if eolian sand is assumed to increase with drier climate. That the assumption is reasonable is indicated by samples of hillside mantles at many localities throughout southern Africa; with decreasing rainfall, the proportion of rounded quartz grains increases. This seems to make possible an approximate calibration of rainfall changes with time during accumulation of the breccias, a process of probably early Pleistocene date as suggested by the fossil mammals found in them. Variations through an amplitude of about 10 inches on each side of today's rainfall of 28 inches or so are recorded, three on the dry side and one on the wet side. On this evidence alone it would seem that

today's rainfall value is not far from an average value for the part of middle Pleistocene time represented by the breccias.

Brain's study implies that the relative concentration of eolian sand grains on the present surface is related to present annual rainfall values, and the use of this relationship for calibrating variations in former rainfall seems soundly based. However, Pleistocene eolian sand might have resulted in part from lengthening of the dry seasons, with correspondingly smaller change in total yearly precipitation values. No systematic means of investigating this possibility seems evident, other than accurate observation of the results of present-day variations in rainfall seasonality and rainfall totals, as well as of groups of unusually effective "soil storms" like those reported by V. L. Bosazza (*in* Clark, 1957, p. 131). If annual rainfall and seasonal distribution of rainfall are recognized as two different things, serious errors are not likely to be made.

Deflation basins.—Basins universally known as pans occur throughout a wide region of the subcontinent, extending from South-West Africa to the eastern Transvaal and from the Orange Free State to Northern Rhodesia. The basins range in shape from subcircular to oval to irregular, in diameter from a few tens of yards to several miles, and in depth from 2 or 3 feet to as much as 200 feet. Their slopes are generally smooth and little indented by minor drainage lines. The pans occur mainly in areas of clay, silt, or fine sand or in rocks yielding such sediments as they become weathered. Examples are Pleistocene alluvium and the Dwyka and Ecca shales of the Karroo system. Pans are found also in dolomite. Distribution of pans is irregular both in detail and in general. They occur in shallow alluvium-filled valleys but more commonly on broad flat interfluves that represent a mid-Tertiary(?) erosion surface. Throughout the region of their occurrence, mean rainfall ranges from 5 inches in the extreme west to 30 inches[14] in eastern Transvaal, and in Rhodesia is as much as 35 inches. A few now contain shallow lakes, and most are at least partly clothed with vegetation.

Although some of the pans that occur in relatively soluble rocks may be wholly or partly products of solution, most are, by elimination, the result of deflation, as has been widely recognized. Wallowing animals may have helped deepen some of the smaller basins (Du Toit, 1954, p. 466), but animal wallows imply the pre-existence of a basin. The pans in the eastern and northeastern part of the region are inactive today; many of those in the arid west are still active.

Little is known as to limiting dates of origin of the pans. A few basins are excavated in bodies of alluvium that on culture evidence must be very late Pleistocene. As some of these are apparently inactive today, it is reasonable to infer that a climate drier than today's prevailed (although not necessarily for long) quite recently, possibly within the last 10,000 years. Excavation of selected pans might repay test excavation in the hope that alternating dry and moister climates might have left a record in the form of a thin stratigraphic sequence, perhaps with culture remains, from which age and history might be read.

The pans are much like the basins that occur by the thousands on the Great Plains in the United States, from Montana south to New Mexico and western Texas, in a belt in which rainfall ranges between 10 and 20 inches. Many of the American basins are now inactive, but during the dry years in the 1930's some were activated and new ones were created, and it is probable that many were active during the warmest and driest part of the Hypsithermal time between about 9000 and about 3000 B.P. African and North American basins cannot be compared with confidence, because the seasonal African rainfall permits deflation at higher annual values than would be possible in western United States. Probably a slight decrease in the rainfall now prevailing would reactivate large numbers of pans.

Soils with secondary carbonates: In parts of western North America, northern India, central Australia, and other dry regions in which evaporation exceeds precipitation, there occur soils whose *B* horizons contain secondary calcium (and in some cases magnesium) carbonates, accumulated a few inches to a few feet below the surface. Zonal soils that commonly possess secondary carbonates include Chernozems, Chestnut soils, and Desert soils. The carbonates occur as nodular or concretionary bodies of various sizes or as subhorizontal lenticular masses (caliche) cementing the rock particles among which they form. These soils occur under covers of grass or desert shrubs; in the United States mean annual precipitation in the region of their occurrence is commonly 25 inches or less.

In southern Africa and in parts of equatorial Africa analogous soils occur, with concretions of

[14] Of which about 80 per cent falls within a 5-month wet season.

olive-gray calcium carbonate (*kunkur*[15]) or, less commonly, as more massive layers (*calcrete*; Lamplugh, 1907). The concentration of carbonate depends on a number of variables, including quantity of available calcium in the parent material as well as air temperatures and amount and seasonal distribution of rainfall. Other, unevaluated geochemical factors may be significant also.

The distribution, within southern Africa, of soils in which calcium carbonate is actively accumulating apparently has not yet been defined. About 18 inches can be suggested tentatively as the annual rainfall below which carbonate in soils can be expected. That this value is lower than the value prevailing in western United States is probably attributable, despite higher temperatures, to the strong seasonality of southern African rainfall, in consequence of which fewer alterations of wetting and drying of soils are likely to occur.

Carbonate in the form of kunkur is widespread in ancient soils, developed mainly in Pleistocene alluvium, in areas where rainfall ranges between 20 and 30 inches; in places it occurs where rainfall exceeds 30 inches. It has been generally inferred that rainfall values were smaller than today's at the times of accumulation, some of which are fixed relatively by associated artifacts.

Ancient soils with kunkur, developed in bodies of alluvium exposed in stream terraces and commonly overlain by younger alluvium, are widespread in the Rhodesias and in many parts of the Union of South Africa. In the Rhodesias and the Transvaal, at least, the zones of kunkur occur persistently at the same horizons as determined by cultures and by stream-terrace stratigraphy and morphology; these kinds of evidence are internally consistent. As rainfall on much of the region ranges between 20 and 30 inches, and in some areas is less than 20 inches, no great former decrease is demanded by the presence of kunkur zones. However, kunkur occurs at places in coastal Moçambique where rainfall today reaches 35 inches.

In East Africa, kunkur zones were seen exposed principally in areas which even today are rather dry. In Kenya the Olorgesailie lake beds, already described, overlie two such zones, implying that the climate was at least as dry as it is today shortly before the inception of the lake. In the Magadi basin, also described earlier, kunkur zones are developed immediately below the two interfaces of unconformity that separate the three lake sequences; the climatic implication is the same as at Olorgesailie. In the sequence exposed in the Olduvai Gorge in Tanganyika, one or two such zones, locally with calcrete, postdate Bed 5 and postdate a culture of Capsian aspect. Farther west, at various localities on the floor of the Western Rift Valley near Lake Edward, kunkur zones are exposed in the upper part of the Kaiso beds of early Pleistocene age and also in upper Pleistocene sediments. On the northeast shore of Lake Victoria kunkur occurs at surfaces cut across the lower Pleistocene Kanam beds and the mid-Pleistocene Kanjera beds but may postdate both beds. The nearest station with a rainfall record, Kisumu, 20 miles to the north, reports 40–48 inches of rainfall, but in this case crustal uplift as a partial cause of climatic change is less readily ruled out than in the case of the more recent carbonates.

The problem of the distribution of soils with carbonates is complicated by the presence at the surface of degraded ancient soils, which can be distinguished from actively forming soils only through detailed examination. In large areas of East Africa, absence of secondary carbonates expectable under today's dry climate has been attributed to loss of mobile bases by leaching under an earlier wetter climate (G. Milne, *cited in* Mohr and van Baren, 1954, p. 452). In such cases geology as well as soil morphology must be considered, because scarcity of available calcium in parent material might possibly explain the lack of calcium carbonate in an ancient savanna soil.

A soil without carbonates, but suggesting a history similar to that implied by the soils with kunkur, is exposed in the Lusaka district in Northern Rhodesia, where present rainfall is about 35 inches. The soil appears to be a Chernozem, now degraded by oxidation of iron, developing a reddish hue. It suggests a former drier climate (G. W. Bain, personal communication).

In summary, secondary carbonates in soils appear to offer a promising means of identifying relatively dry Pleistocene climates, provided other influences can be eliminated. When at least moderately detailed maps can be compiled, showing the distribution of (1) such soils in the active state, (2) ancient soils of similar character, and (3) present-day rainfall, they should afford a clue to a former rainfall pattern.

Erosional unconformities within lake sedi-

[15] Spelled thus in Page (1865, p. 269), and as *kankar* or *kunkur* in the early description by Medlicott and Blanford (1879, pt. 1,p. 381); the word is of Hindu origin, and means gravel.

ments.—Unconformities within lake sediments imply fluctuation of lake levels. Fluctuation is explained most simply by climatic desiccation. Such unconformities have been mentioned as occurring in the Magadi, Olorgesailie, and Naivasha-Nakuru basins. They occur also in the sequence at Kalambo, Northern Rhodesia, mentioned in a preceding section. Some of the unconformities are characterized by groups of artifacts, which may make correlation among basins possible.

Biogeography of fresh-water faunas.—In lakes and streams in East Africa there are two distinct vertebrate faunas separated by a sinuous east-west line. North of the line, Lakes Rudolf and Albert and the Albert Nile contain a varied fauna including Nile perch and other distinctive fishes. South of it, Lakes Kioga, Victoria, and Edward lack these fishes but possess an endemic fauna developed from only a few genera. The dividing line passes through the Murchison Falls on the Victoria Nile and the rapids of the Semliki River, which flows from Lake Edward into Lake Albert. Moreover Lake Edward lacks crocodiles, although the lower Pleistocene Kaiso beds, exposed near the lake, contain fossil crocodiles and Nile perch as well. Lungfish and catfish, both capable of surviving desiccation, are found on both sides of the line.

According to Worthington (1932), a reasonable explanation of these facts is the hypothesis that the Nile fauna was once common to all the lakes, but that in a dry middle part of Pleistocene time Victoria, Kioga, and Edward shrank and became swamps, extinguishing many of the aquatic vertebrates. With subsequent re-establishment of the dried-up lakes, repopulation from the Nile system was prevented by the falls and rapids downstream. If Lakes Albert and Rudolf dried during the same time, they could have been recolonized from the Nile, which lacks falls.

Greenwood (1951, p. 20) believed that species evolution had occurred in two parts, of which only the second is referable to post-middle Pleistocene time. He emphasized the view that middle Pleistocene desiccation was not complete, and that Lake Victoria, at least, was probably then a small body of water with flanking swamps.

No evidence in the published record suggests that the outlet of Lake Victoria has ever been elsewhere than at Jinja, the present outlet, marked by a falls and shallow gorge cut into Precambrian crystalline rocks.

The possible reversal of the Semliki River (Heinzelin, 1955b, p. 119) occurred, if at all, in late Pleistocene time and is therefore unlikely to have been related to the suggested desiccation of Lakes Edward, Victoria, and Kioga. Heinzelin placed the latter event much earlier in the Pleistocene, presumably to allow time for speciation within the fish faunas after those lakes had been re-established.

Cutting and filling by streams.—In parts of Rhodesia, Moçambique, and the Union of South Africa the Pleistocene sequence consists mainly of dissected alluvium, occurring as several bodies and constituting fill terraces and veneers on rock terraces in valleys both large and small. Although the sequences vary locally, they show broad regional similarities which, together with similarities in the sequence of artifacts found in and upon them, afford a basis on which correlation from one major valley to another has been attempted.

In general the sequences consist of one or more bodies of high-level gravel and a group of lower and younger sediments ranging from gravel to silt according to valley and locality. In most places the older, high-level gravels have been altered by differential weathering, eluviation, settling, and creep to a quartzose residuum whose individual pebbles and cobbles are no longer in the positions in which they were deposited. In places the residuum includes pebble tools of Oldowan character (e.g. Clark, 1954a, p. 13, 14), similar to those found elsewhere in association with mid-Pleistocene mammals. The younger and lower terrace sediments contain, in places, more developed cultures such as the Fauresmith and Sangoan.

At localities along the Vaal River the two groups of sediments are separated by wind-blown sand indicative of a climatic phase dry enough to have impaired the cover of vegetation. Such a phase need not have been much drier than the climate of today. Reworked sand of the same character occurs in places within or upon the younger group of alluvial units, implying at least two, possibly quite minor, dry phases of comparatively late date.

The sequence as a whole represents episodes of alluviation alternating with episodes of downcutting, with eolian activity immediately following some downcutting episodes. Although the relationship of eolian activity to climate is fairly evident, the climatic inferences to be drawn from stream cutting and filling are less clear. As a rule no fossils are found in the alluvial sediments, and the artifacts occurring in and upon them do not in themselves afford evidence of the climatic conditions, other than that sufficient water was present to support bands of people occupying at least temporary

habitations. It has been repeatedly held that the general similarity of the sequences in several valleys having different orientations precludes crustal movements and other local or one-directional causes and by elimination implies climatic change. Although very broad epeiric uplift of southern Africa, such as has manifestly occurred since Pliocene time, is not excluded as at least a partial cause of the cutting that separates the two chief groups of terrace sediments, climate can be accepted as a probably significant factor in cutting and filling.

Doubtless few would deny that a given change in climate could be expected to have variable results in the stream channels of any particular district, according to variations in such factors as bedrock, soil, slope angle, kind of vegetation, and area of watershed. It has been claimed that much of southern Africa is so nearly uniform in these respects that factors other than climate are minimal. It is questionable, however, whether knowledge is sufficient to support this claim.

On the assumption that climate is the dominant factor, the following argument has been employed.[16] In southern Africa, owing to generally low rainfall values and seasonal rainfall distribution, the vegetation cover today tends to be discontinuous except at relatively high altitudes. Most of the continuous grassland or forest is in Natal and along the south coast of the Cape Province; the rest is mainly savanna and semidesert with discontinuous plant cover. Assuming, then, a terrain that lacks a continuous cover of vegetation, increased rainfall or increased length of the rainy season should result in increased sheet erosion and gully cutting on the unprotected surface. This in turn would increase rates of transport of sediment on slopes and in headwater areas. If major streams were already in approximate equilibrium, the result should be alluviation in major valleys. Hence bodies of ancient alluvium are correlated with times of relatively great rainfall; conversely incision by major streams is attributed to drier episodes.

This scheme correlates marked headwater erosion with marked valley alluviation but does not consider differences in grain size that might be expected, such as the production, on appropriate rocks, of joint-block fragments reached by the floors of gullies cut completely through the weathered mantle. Nor does it consider the effect of increase of area of continuous vegetation as the postulated high rainfall develops; this might give a result different from the one deduced. Again, the base from which the rainfall increase starts may be significant. If discontinuity of vegetation is slight, an increase in annual rainfall of, say, 10 inches might produce less conspicuous results than would a similar increase in a region of very discontinuous cover.

An example of the apparent effect of a continuous grass cover and high rainfall on stream loads was shown me by Mr. B. H. Baker in the Ngong Hills, Kenya. This area, underlain by volcanic rocks at an altitude of 7000–8000 feet and with an estimated rainfall of 50 inches seasonally distributed, is completely covered with tough grass plus sparse trees. The plant cover is continuous from hill summits down to stream banks, and a thin mantle of rock waste is moving down-slope by soil creep. Slopes are smooth, and there are no gullies. Sheet erosion surely could not occur under these conditions. The stream is clear.

It seems unlikely that any generalization on the relationship of climatic change to stream regimens on the subcontinent can have wide value until systematic measurements have been made in selected drainage basins, so that what is happening today can be clearly understood. Until this has been done it would seem best to draw inferences as to former climates from features other than alluvial stratigraphy. Observations on bodies of alluvium should be continued as supplements to the useful ones already in the literature. Meanwhile the probably large part played by strength and continuity of plant cover in the erosion of surfaces, particularly slopes, whether by deflation or by running water, should be noted. When alluvium, colluvium, and eolian sediments are considered, a change in rainfall sufficient to convert a continuous plant cover into a discontinuous one, or vice versa, might result in substantial geologic changes. Possibly even a change in the seasonality of rainfall, without change in its annual total, might have similar results in an area that is critical, or a threshold, in terms of vegetation.

Evidence of Relatively Warm Climates

Data assembled by Krige (1927, p. 67–72) during a study of emerged marine strand lines along the coast of South Africa show discrepancies in the distribution of fossil and

[16] The argument is implicit in Smuts (1945, p. 43); Bond and others (1955, p. 1–3); and Cooke (1946, p. 257–258). *See also* King (1948b, p. 217–218. I have benefited from discussion of it with Dr. J. D. Clark.

living marine invertebrates. Sediments identified as related to a former sea level at +20 feet contain a fossil fauna, some species of which are living today only at temperatures higher than those characteristic of the localities of their occurrence as fossils. It is inferred that at the time of higher sea level the climate was warmer than that of today. The fossils are not dated but are held to be of recent aspect. Judging from today's surface sea-water temperatures, the differences referred to are of the order of 1°C.–3°C.

Summary

Evidence of former Pleistocene climates in eastern and southern Africa consists mainly of features that are not now forming actively in some particular area but are forming elsewhere under different climatic conditions. On the classical principle of uniformity of process, many of these features are considered as indicative of climates different from those now prevailing. Other lines of evidence are biogeographic, consisting of anomalies in the distribution of living organisms, which seem explicable only on the assumption of climatic change. Most of the evidence pertains to changes in rainfall, but some of it suggests former climates cooler than those of today. In the equatorial region indications of former moister climate predominate over indications of former greater aridity, whereas in southern Africa the reverse is true. The cause of this difference is not yet apparent.

The evidence is fragmentary, and its reliability varies widely; at present it is difficult to evaluate in quantitative terms. Soils, whether buried or merely degraded at the present surface, seem to offer the best promise of quantifying climatic parameters. Sediments of former lakes, buried soils, and beds of wind-blown sand, occurring in stratigraphic sequence, seem most likely to afford the best evidence of the number of climatic changes that have occurred.

The observation cited earliest in the literature as evidence of a pluvial climate—coarse stream gravel—is a less sure line of evidence than most or all of the observations cited here. The Magadi and Olorgesailie lakes imply repeated changes in the precipitation-evaporation ratio, as do the travertines of the Kaap escarpment. The distribution and amounts of wind-blown sand, as well as deflation basins, suggest decreased rainfall or a lengthened dry season, although the change might have been small. Soil morphology (red tropical soils, ferricrete, calcrete) suggests rainfall fluctuation through a possible range extending from less than 18 inches to more than 45 inches (or, in part, fluctuation of seasonal distribution of rain) at various localities, although the data need refinement. At one locality grain size of colluvium suggests former greater intensity of runoff. Forest distribution in general suggests former greater rainfall and possibly lower temperature as well.

The data evolved by C. K. Brain (*in* Clark, 1957) imply that in The Transvaal the existing climate is closer to the drier than to the wetter inferred former climates.

Ancient lower temperatures are suggested by the extent of former glaciation on equatorial East African mountains and by forest biogeography at Kalambo and in the region between the Ituri highland and The Cameroun. Both kinds of evidence suggest mean annual temperatures about 5°C. less than those of today.

In this connection isotopic temperatures derived by Emiliani (1958) from sea-floor sediments suggest that Pleistocene tropical surface sea-water temperatures fluctuated between $\sim +1$°C. and -5°C. compared with those of today. Presumably average tropical air at sea level should have been in approximate thermal equilibrium with sea water and should have had similar temperatures. The very scanty temperature indications from southern Africa therefore seem consistent with the sea-floor data developed thus far.

The climatic data, as far as they go, are compatible with the concept that the African continent has not changed its position with respect to the equator during the part of Pleistocene time they represent.

This review of the evidence suggests that periods of rainfall both greater and less than today's values formerly characterized parts of the subcontinent. It suggests also the possibility of former lower temperatures, perhaps coinciding with times of increased rainfall. But it does not indicate whether increased rainfall occurred simultaneously throughout the subcontinent; possibly changes of opposite sign occurred simultaneously in different areas. Nor is it known whether the region of dry climate now centered in the Kalahari region shifted equatorward and then poleward with changing Pleistocene climates, or merely contracted when a pluvial climate prevailed and expanded during a nonpluvial regimen, as suggested by Flohn (1952; *see also* Butzer, 1957) for the Sahara region. In this particular case more

detailed geologic knowledge might answer the question. In other words, comparison of the data with the five questions put forward at the beginning of this paper shows that although attempts have been made at answering them, the results to date are not very satisfactory.

Meteorologic Theory

What more can be done with the data at hand, pending the accumulation of additional knowledge? Deduction from meteorologic theory affords a useful basis of comparison with the direct evidence. The climatic regimen of the subcontinent today, described briefly near the beginning of this paper, is the logical starting point for an attempt to apply the field evidence of former climates that were different. What changes in today's atmospheric circulation could be expected to result in the differences in annual and seasonal rainfall and temperature values that are reasonably inferred from the field data? A partial answer to this question may lie in the circulation anomalies that appear from analysis of the atmospheric patterns developed during the period of instrumental record.

The rainfall data assembled by Kraus (1958) are pertinent. Selecting six areas within the subtropical belt (three south of the equator, in South Africa and Australia, and three north of it, in northeast Africa, India, and North America), he showed that during about the first half of the twentieth century, climates were conspicuously drier than in the later part of the nineteenth century. The change to drier climates was accompanied by widening of the low-latitude dry belts and by shortening of the rainy seasons (Kraus, 1955, p. 202). At climatically corresponding stations the change was simultaneous in both equatorial hemispheres. At several stations on the fringes of the dry belt the decrease in mean annual rainfall amounted to more than 30 per cent. The data show that substantial changes in rainfall means, lasting through several decades, actually occur in southern Africa, and that in some regions at least the changes are accompanied by widening and narrowing of low-latitude dry belts and by shortening and lengthening of the rainy seasons.

Another analysis of modern circulation anomalies was made by Flohn (1952). He found that the pattern developed during unusually severe winters in the Northern Hemisphere today is a low-index or meridional pattern, in contrast with the high-index or zonal pattern characteristic of much less severe conditions. The meridional circulation is accompanied by reduced temperatures in the tropics and increased rainfall on low-latitude dry belts, which become narrower.

If patterns of the kinds dealt with by Kraus and by Flohn are basically similar to the patterns that occurred during glacial maxima in Europe, they are worth comparing with the evidence of former climates in equatorial and southern Africa. Qualitatively there appears to be nothing in the evidence that could not be satisfied by the assumption that very low-index circulation patterns formerly prevailed over the subcontinent. If such patterns affected both polar hemispheres simultaneously, the equatorward limit of Antarctic pack ice at its annual maximum (today about 56°S. Latitude in the longitude of Cape Town) could have reached much farther north, accompanying and in part causing the activities mentioned heretofore, as described by Flohn for the northern hemisphere. This would have favored the reduced temperatures, the increased rainfall over the broad territory in southern Africa that is now dry, and the glaciation of high equatorial mountains that are indicated by the field evidence.

Even though conflicts are not apparent, application of the pattern to a glacial maximum is only a theory based on analogy. The theory implies that glacial ages are contemporaneous with pluvial ages, the relationship urged by Brooks in 1914 and considered reasonable by other students of the problem. The validity of the theory might be tested best by C^{14} dating and by the detailed and continuous measurement and correlation of Pleistocene marine strand lines and other emerged marine features from Mediterranean Europe southward down the African coasts. It might then be possible to relate bodies of alluvium along major streams, and even perhaps ancient soils, to particular strand lines. Some strand-line research has been done along African coasts south of the Mediterranean; this includes the South African study by Krige (1927).

While the meteorologic study is being refined, as it undoubtedly will be, the accumulation and evaluation of direct evidence—absolutely essential to the reliability of the over-all results—should be actively pursued. This should include: (1) attempts at stratigraphic correlation of Pleistocene sediments and other features having climatic implications; (2) intensification of attempts to set quantitative limits to rainfall and temperature of former

climates and to discriminate between evidence of former changes in (a) annual rainfall and (b) length of dry seasons; and (3) study of cores drilled from Pleistocene sediments beneath selected lakes and areas of swamp or exceptionally high water table. In such places long or complete Pleistocene sequences could reasonably be expected. Fossil pollen should afford invaluable ecologic and hence climatic data, lake microfauna might afford depth data, and similarity of sequence should make correlation possible. In these special wet environments included organic matter should have escaped oxidation and hence should make possible dating and correlation by C^{14}, at least within the upper and younger part of the sequence. Among lakes, Naivasha and Victoria are obvious candidates; other wet basins, of which there are many, include the Kafue Flats west of Mazabuka and the Lake Bangweulu swamps east of Fort Rosebery, both in Northern Rhodesia.

When the stock of data has been enlarged and refined in these ways, it should become possible to construct more detailed models of former circulation patterns that would satisfy the evidence and at the same time be dynamically reasonable. This is a long-term geophysical objective. Equally important for the anthropologist is the light that research in this direction would throw on the environments of early man in equatorial and southern Africa.

References Cited

Bergström, Erik, 1955, British Ruwenzori expedition, 1952; glaciological observations—preliminary report: Jour. Glaciology, v. 2, p. 469–476

Blanckenhorn, Max, 1901, Neues zur Geologie und Paleontologie Aegyptens, IV. Das Pliocän- und Quartärzeitalter in Aegypten ausschliesslich des Rothen Meergebietes: Zeitschr. der Deutschen Geol. Gesell., v. 53, p. 307–502

Bond, Geoffrey, 1957, The geology of the Khami Stone Age sites: Southern Rhodesia Nat. Mus. Occasional Papers, v. 3, no. 21A, p. 44–55

Bond, Geoffrey, and others, 1955, Excursion handbook, Southern Rhodesia: Pan-African Cong. on Prehistory, 3d, Livingstone, 1955, 28 p.

Brooks, C. E. P., 1914, The meteorological conditions of an ice-sheet and their bearing on the desiccation of the globe: Royal Meteorol. Soc. Quart. Jour., v. 40, p. 53–70

—— 1925, The fluctuations of Lake Victoria: East Africa and Uganda Nat. Hist. Soc. Jour., no. 22, p. 47–55

Brooks, C. E. P., and Mirrlees, S.T.A., 1932, A study of the atmospheric circulation over tropical Africa: Great Britain, Meteorol. Office Geophys. Mem. 55, 15 p.

Butzer, K. W., 1957, The recent climatic fluctuation in lower latitudes and the general circulation of the Pleistocene: Geografiska Annaler, v. 39, p. 105–113.

Cahen, L., 1954, Géologie du Congo Belge: Liège, Belgium, H. Vaillant-Carmanne, 577 p.

Clark, J. D., 1950, The Stone Age cultures of Northern Rhodesia: Claremont, Cape Province, South African Archaeol. Soc., 157 p.

—— 1954a, A provisional correlation of prehistoric cultures north and south of the Sahara: South African Archaeol. Bull., v. 9, p. 3–17

—— 1954b, An early Upper Pleistocene site at the Kalambo Falls on the Northern Rhodesia-Tanganyika border: South African Archaeol. Bull., v. 9, p. 51–56

—— 1955, Excursion handbook, Northern Rhodesia: Pan-African Cong. on Prehistory, 3d, Livingstone, 1955, 42 p.

—— *editor*, 1957, Proceedings of the Third Pan-African Congress on Prehistory, Livingstone, 1955: London, Chatto and Windus, 440 p.

Cole, Sonia, 1954, The prehistory of East Africa: Baltimore, Penguin Books, 301 p.

Cooke, H. B. S., 1946, The development of the Vaal River and its deposits: South Africa Geol. Soc. Trans., v. 49, p. 243–259

—— 1958, Observations relating to Quaternary environments in east and southern Africa: Geol. Soc. South Africa Bull., v. 20, annexure, 73 p.

Du Toit, A. L., 1954, The geology of South Africa: 3d edition, Edinburgh, Oliver and Boyd, 611 p.

Emiliani, Cesare, 1958, Paleotemperature analysis of core 280 and Pleistocene correlations: Jour. Geology, v. 66, p. 264–275

Flohn, Hermann, 1952, Allgemeine atmosphärische Zirkulation und Paläoklimatologie: Geol. Rundschau, v. 40, p. 153–178.

Fuchs, V. E., 1939, The geological history of the Lake Rudolf basin, Kenya Colony: Royal Soc. London Philos. Trans., ser. B, v. 229, p. 219–274

—— 1950, Pleistocene events in the Baringo basin, Kenya Colony: Geol. Mag., v. 87, p. 149–174

Garbell, M. A., 1947, Tropical and equatorial meteorology: N. Y., Pitman Publ. Corp., 237 p.

Greenwood, P. H., 1951, Evolution of the African cichlid fishes; the *Haplochromis* species-flock in Lake Victoria: Nature, v. 167, p. 19–20

Gregory, J. W., 1921, The Rift Valleys and geology of East Africa: London, Seeley, Service and Co. Ltd., 479 p.

Heinzelin, Jean de, 1953, Les stades de récession du Glacier Stanley Occidental, Exploration du Parc National Albert, 2me Série, Fascicule 1: Brussels, Institut des Parcs Nationaux du Congo Belge, 25 p.

—— 1955a, Observations sur la genèse des nappes de gravats dans les sols tropicaux: Pub. Inst. Natl. pour l'Étude Agronomique du Congo Belge, ser. sci., no. 64, 37 p.

—— 1955b, Le fossé tectonique sous le parallèle d'Ishango, Exploration du Parc National Albert, Fascicule 1: Brussels, Institut des Parcs Nationaux du Congo Belge, 150 p.

—— 1957, Les fouilles d'Ishango, Exploration du Parc National Albert, Fasciscule 2: Brussels, Institut des Parcs Nationaux du Congo Belge, 128 p.

Hutchinson, G. E., 1933, The zoo-geography of the African aquatic Hemiptera in relation to past

climatic change: Internat. Revue der gesamten Hydrobiologie u. Hydrographie, v. 28, p. 435–468

Jamieson, T. F., 1863, On the parallel roads of Glen Roy, and their place in the history of the glacial period: Geol. Soc. London Quart. Jour., v. 19, p. 235–259

Janmart, J., 1953, The Kalahari sands of the Lunda: Lisbon, Companhia de Diamantes de Angola, Publicacaõs Culturais, no. 20, 62 p.

Jones, Neville, 1944, The climatic and cultural sequences at Sawmills, Southern Rhodesia: Southern Rhodesia Natl. Mus. Occasional Papers, v. 2, p. 39–46

Kendrew, W. G., 1941, The climates of the continents: 3d ed., Oxford Univ. Press, 473 p.

King, L. C., 1948a, On the ages of African landsurfaces: Geol. Soc. London Quart. Jour., v. 104, p. 439–459

—— 1948b, South African landscape and early man: Royal Soc. South Africa, Robert Broom Commemorative Volume, p. 217–224

Kraus, E. B., 1955, Secular changes of tropical rainfall regimes: Royal Meteorol. Soc. Quart. Jour., v. 81, p. 198–210

—— 1958, Recent climatic changes: Nature, v. 181, p. 666–668

Krige, A. V., 1927, An examination of the Tertiary and Quaternary changes of sea-level in South Africa, with special stress on the evidence in favour of a recent world-wide sinking of ocean-level: Univ. Stellenbosch Ann., v. 5, sec. A, no. 1, 80 p.

Lamplugh, G. W., 1907, The geology of the Zambezi basin around the Batoka Gorge (Rhodesia): Geol. Soc. London Quart. Jour., v. 63, p. 162–214

Leakey, L. S. B., 1931a, The Stone Age cultures of Kenya Colony: Cambridge Univ. Press, 287 p.

—— 1931b, East African lakes: Geog. Jour., v. 77, p. 497–508

—— 1934, Changes in the physical geography of East Africa in human times: Geog. Jour., v. 84, p. 296–305

—— 1948, The lower limit of the Pleistocene in Africa: 18th Internat. Geol. Cong., London, 1948, Proc., pt. 9, p. 62–65

—— *editor*, 1952, Proceedings of the Pan-African Congress on Prehistory, 1st, Nairobi, 1947: N. Y., Philosophical Library, 239 p.

Lewis, A. D., 1936, Sand dunes of the Kalahari within the borders of the Union: South African Geog. Jour., v. 19, p. 22–32

Mabbutt, J. A., 1956, Physiography and surface geology of the Hopefield fossil site: Royal Soc. South Africa Trans., v. 35, p. 21–58

Medlicott, H. B., and Blanford, W. T., 1879, A manual of the geology of India: Calcutta, Supt. Govt. Print., 2 pts., 817 p.

Mohr, E. C. J., and van Baren, F. A., 1954, Tropical soils: N. Y., Interscience Publishers, Inc., 498 p.

Moreau, R. E., 1933, Pleistocene climatic changes and the distribution of life in East Africa: Jour. Ecology, v. 21, p. 415–435

—— 1952, Africa since the Mesozoic, with particular reference to certain biological problems: London Zool. Soc. Proc., v. 121, p. 869–913

Nilsson, Erik, 1929, Preliminary report on the quaternary geology of Mount Elgon and some parts of the Rift Valley: Geol. fören. Stockholm Förh., v. 51, p. 253–261

—— 1931, Quarternary glaciations and pluvial lakes in British East Africa: Geografiska Annaler, v. 13, p. 249–349

—— 1935, Traces of ancient changes of climate in East Africa: Geografiska Annaler, v. 17, p. 1–21

—— 1940, Ancient changes of climate in British East Africa: Geografiska Annaler, v. 22, p. 1–79

O'Brien, T. P., 1939, The prehistory of the Uganda Protectorate: Cambridge Univ. Press, 319 p.

Oswald, Felix, 1918, Notes on the former level of Victoria Nyanza: East Africa and Uganda Nat. Hist. Soc. Jour., no. 13, p. 300–302

Page, David, 1865, Handbook of geological terms, geology and physical geography: 2d ed., Edinburgh, William Blackwood and Sons, 506 p.

Passarge, Siegfried, 1904, Die Kalahari: Berlin, Dietrich Reimer, v. 1, 822 p., v. 2, plates.

Peabody, F. E., 1954, Travertines and cave deposits of the Kaap escarpment of South Africa, and the type locality of *Australopithecus africanus* Dart: Geol. Soc. America Bull., v. 65, p. 671–706

Saggerson, E. P., 1952, Geology of the Kisumu district: Kenya Geol. Survey Rept. 21, 86 p.

Schokalskaja, S. Ju., 1953, Die Böden Afrikas: Berlin, Akademie-Verlag, 408 p.

Shackleton, R. M., 1955, Pleistocene movements in the Gregory rift valley: Geol. Rundschau, v. 43, p. 257–263

Simpson, G. C., 1957, Further studies in world climate: Royal Meteorol. Soc. Quart. Jour., v. 83, p. 459–485

Smuts, J. C., 1945, Climates and pre-Palaeolithic artifacts of the Witwatersrand: Royal Soc. South Africa Trans., v. 31, p. 39–65

Söhnge, P. G., Visser, D. J. L., and Lowe, C. V., 1937, The geology and archaeology of the Vaal River basin: South Africa Geol. Survey Mem., v. 35, 184 p.

Walter, A., 1938, The climate of British East Africa: Royal Meteorol. Soc. Quart. Jour., v. 64, p. 97–116

Wayland, E. J., 1934, Rifts, rivers, rains and early man in Uganda: London, Royal Anthropol. Inst. Jour., v. 64, p. 333–352

Wellington, J. H., 1955, Southern Africa, a geographical study, Volume 1—Physical geography: Cambridge Univ. Press, 528 p.

Whitney, J. D., 1865, Geological survey of California: Geology, v. 1: Geol. Survey Calif., 498 p.

Worthington, E. B., 1932, The lakes of Kenya and Uganda: Geog. Jour., v. 79, p. 275–297

Department of Geology, Yale University, New Haven, Connecticut

Manuscript Received by the Secretary of the Society, July 1, 1958

Short Notes

BULLETIN OF THE GEOLOGICAL SOCIETY OF AMERICA
VOL. 70, PP. 375-378, 1 FIG. MARCH 1959

BLANCAN MAMMALIAN FAUNA FROM RIO GRANDE VALLEY, HUDSPETH COUNTY, TEXAS

BY W. S. STRAIN

An early Pleistocene age can now be assigned to a part of the basin fill in the Rio Grande Valley, Hudspeth County, Texas. Previously no precise age was known because of a lack of fossils. Bones are extremely rare, but a sufficient number have recently been found to determine that, in part, a local fauna of Blancan age is present.

The area considered is northeast of McNary, Texas, in the southeastern part of the Hueco Bolson. The Rio Grande traverses the Hueco Bolson from El Paso to the Quitman Mountains, and the principal exposures are in intermittent tributary streams. The basin fill that yielded the bones originated as channel, flood-plain, playa, and possibly alluvial-fan deposits. They are composed of claystone, siltstone, sand, and gravel. Wells have indicated a thickness of more than 4000 feet in places, but only 600 feet of the upper part of the section is exposed in the stream valleys near McNary. The significant fossil-bearing strata crop out in the Campo Grande, Diablo, Madden, and Balluco arroyos.

Albritton (1938, p. 1768) remarked that the sedimentary fill had no formal name, although Baker (1927, p. 39) and Bryan (1938, p. 205) had vaguely referred it to the Sante Fe formation, and Sayre and Livingston (1945, p. 39) followed Bryan's suggestion. The writer concurs with Albritton and will propose formal names for the formations in a forthcoming paper.

The lower part of the section forms a distinct unit, herein referred to as Unit A (Fig. 1). It is composed of red, brown, and gray claystone and siltstone and contains some bentonite and gypsum. The fill is rather evenly bedded and was formed from sediment deposited by streams with very low gradients. The preliminary faunal list for Unit A is as follows: *Testudo*, *Geomys*, *Nannippus*, *Sigmodon*, *Citellus*, *Scalopus*.

Because *Testudo* and *Sigmodon* are forms which today are restricted to warm climates, it is reasonable to assume that the climate of this area was warm at the time these animals lived.

The upper part of the section, Unit B, lies unconformably on Unit A and is composed of poorly consolidated gray sand and brown clayey sand, volcanic ash, and silt. Gravel is also present in channels and lenses, but it constitutes only a small part of the total volume of the fill. Unit B represents principally stream channel and flood-plain environments, but playa and aeolian environments are indicated to a lesser degree. The volcanic ash in the middle of Unit B occurs in isolated lenses and was probably preserved in playas or oxbow lakes. It is petrographically distinct and is tentatively identified as Pearlette ash. If further research proves this identification to be correct, this will provide a means of precise correlation with the Great Plains geologic section of the Pleistocene. The preliminary faunal list for Unit B, below the Pearlette (?) ash, is as follows: *Equus* (*Plesippus*), *Nannippus*, *Testudo*, *Tapirus*, *Megalonyx*, *Glyptodon*.

At least the fossiliferous part of Unit B is thought to be Pleistocene, early Kansan or older. The species of *Plesippus* from Unit B is very similar to, if not identical with, *P. idahoensis*, which is known to be Pleistocene. *Plesippus-Nannipus* association is not known to occur later than early Kansan. *Tapirus* and *Testudo* suggest the climate was warm at the time these animals lived in the area, which would indicate that Unit B is probably Aftonian.

Unit A is believed to be younger than medial Pliocene because the gophers and ground squirrels are more advanced than those of Hemphillian age. If the evidence previously enumerated is accepted as indicating a warm climate, the geologic age of Unit A could be

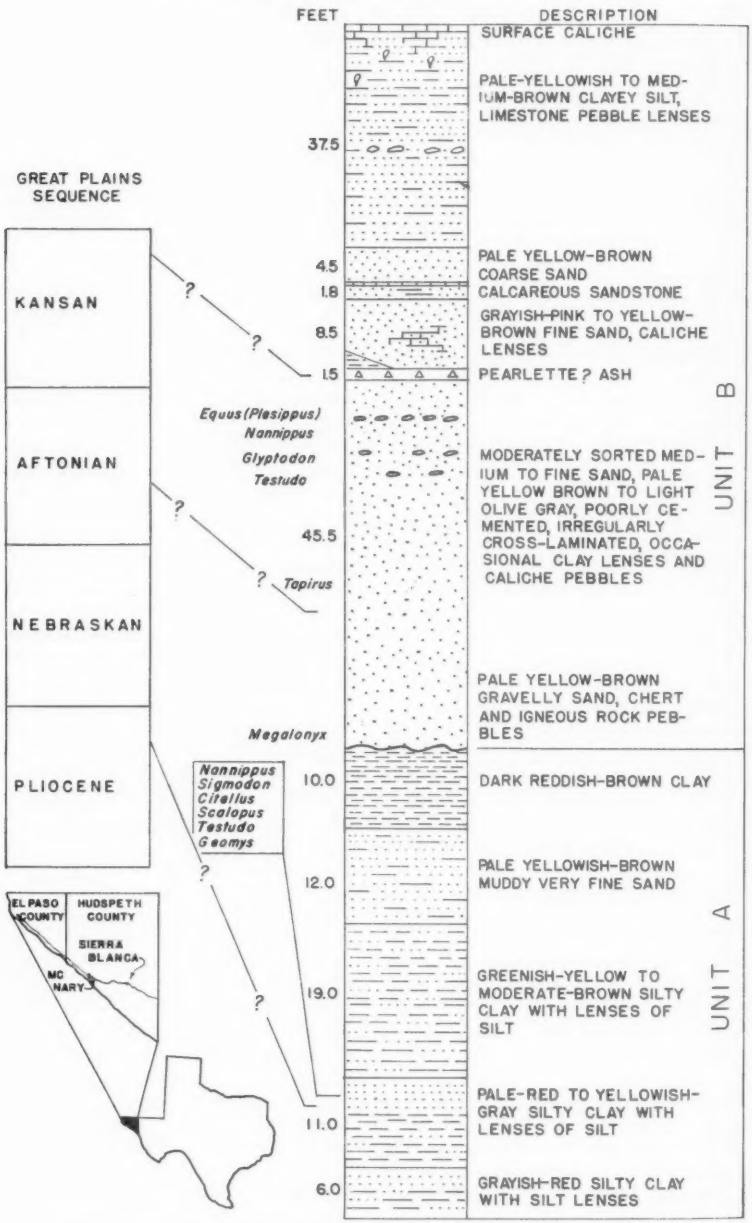

FIGURE 1.—TYPICAL SECTION OF BASIN FILL, RIO GRANDE VALLEY, TEXAS

Pliocene; or it may represent an interglacial age in the Pleistocene, probably Aftonian.

In the area under discussion, Unit B is capped by surface caliche. To the northwest in the vicinity of El Paso, a gravelly sand, just below the surface caliche, contains *Equus* (*sensu stricto*) and *Mammuthus*, but *Bison* has not been recognized in it. In North America

these forms are not known to occur in deposits older than late Kansan (Hibbard, 1958, p. 6), and *Bison* is not recognized in deposits older than medial Illinoian (Flint, 1957, p. 469).

From these data it is logical to conclude that the gravelly sand near El Paso was deposited at some time between early Kansan and medial Illinoian; that the Rio Grande, in the Hueco Bolson, began to entrench itself in the older basin fill after late Kansan and probably before medial Illinoian time.

Regardless of the uncertainty concerning the age of Unit A, the information here presented represents a definite advance in knowledge. A Blancan age can now be assigned to a part of the exposed Cenozoic strata in the Hueco Bolson, Hudspeth County, Texas.

References Cited

Albritton, C. C., Jr., 1938, Stratigraphy and structure of Malone Mountains, Texas: Geol. Soc. America Bull., v. 49, p. 1747–1805

Baker, C. L., 1927, Exploratory geology of a part of southwestern Trans-Pecos Texas: Univ. Texas Bull. 2745, 69 p.

Bryan, Kirk, 1938, Regional planning: Part VI, The Rio Grande joint investigation in the upper Rio Grande Basin in Colorado, New Mexico and Texas 1936–1937: Natl. Res. Comm., U. S. Govt. Printing Office, Washington, D. C., 566 p.

Hibbard, Claude W., 1958, Summary of North American Pleistocene mammalian local faunas: Papers of the Mich. Acad. Sci., Arts, Letters, v. XLIII, p. 3–32, 1 pl.

Flint, Richard F., 1957, Glacial and Pleistocene geology: New York, John Wiley and Sons, 553 p., 133 figs., 51 tables, 5 pls.

Sayre, A. N., and Livingston, Penn, 1945, Groundwater resources of the El Paso area, Texas: U. S. Geol. Survey Water-Supply Paper 919, 190 p.

Texas Western College, El Paso, Texas

Manuscript Received by the Secretary of the Society, August 4, 1958

BULLETIN OF THE GEOLOGICAL SOCIETY OF AMERICA
VOL. 70, PP. 379-382 MARCH 1959

QUANTITATIVE STUDY OF COLUMNAR JOINTING

BY C. NOBLE BEARD

Wherever columns or joints are caused by shrinkage in tabular igneous rocks during cooling, prisms occur in a variety of geometric forms. Descriptions, diagrams, and pictures frequently imply that in practically all outcrops hexagonal prisms predominate. Authors generally hasten to add that the development of perfect or nearly perfect hexagonal columns is dependent upon many conditions. A few authors mention similarity of origin of mud cracks through tension set up by desiccation, but photographs and descriptions of such fractures demonstrate that playas are practically the only sites where well-formed polygons may be found.

Theoretically, the easiest relief of tension that is equal in all directions within a layer of mud or lava is by the formation of numerous regularly spaced centers having three fractures that make angles of 120° with each other; thus hexagonal columns are the only type formed (Billings, 1954, p. 115–117), but this is the ideal condition dependent upon slow, uniform shrinkage of homogeneous material.

Significantly, F. E. Matthes, famous for his studies of topography in the Sierra Nevada of California, recorded in his notes on the Sequoia National Park region that in one Pleistocene lava flow just outside the park "Perfect columns are six-sided, exactly hexagonal; but such columns are rare. The great majority have five sides, and some have only four." (Matthes, 1956, Fig. 124).

The writer noticed in volcanic districts of the United States that the columns in ordinary exposures of basalt or similar igneous rock generally consisted largely of pentagons with some quadrilaterals and that hexagons were hard to find. Consequently, in 1955 he visited localities in America and Europe celebrated for their jointing to gather data on shapes, sizes, and attitudes of the rock pillars. Furthermore, evidence was sought as to the reasons for the shapes of the columns and the degree of approach to ideal conditions of cooling.

Since the writer believes that the ordinary outcrop tends to have a predominance of polygons that are not hexagonal, counts from three typical exposures are presented (Table 1).

The outcrop in the Craters of the Moon region was about 5 miles north of the Monument boundary, since the Monument itself has no locality noted for columnar jointing. The columns were fairly well defined, but care had to be taken in choosing columns that could be counted because of rounding of the columns between faces. Such rounding permits almost any interpretation as to the number of sides represented. Dominance of pentagons (56 per cent) and small percentage of hexagons (16 per cent) characterize this outcrop.

The second locality, in a railroad cut at Dunsmuir, California, is in basalt (Pleistocene?) that flowed southward from Mount Shasta; erosion by the Sacramento River has exposed the basalt for more than half a mile. The dominance of pentagons over hexagons is marked.

The data from Lewiston, Idaho, were compiled from a typical jointed portion of the Miocene basalt of the Columbia Plateau. There is a slight dominance of pentagons over hexagons, tending to support the writer's assumption.

As a type of control, columnar joints were examined in several famous localities, and counts of the number of sides were compared with counts recorded in the literature. In addition, any pertinent facts regarding size and attitude were recorded. Table 2 shows the results of the counts. An attempt was made to get counts from the Palisades in the region around Fort Lee, New Jersey, but the jointing was rather crudely developed and was considered nondiagnostic.

The Giant's Causeway seemingly has the best developed jointing in the world, since it has the highest percentage of hexagons. The outcrop is about 300 yards long by 200 yards wide and, according to Rohleder (1929, p. 21), is the lower part of an ancient flow (believed to be Miocene) that was faulted and dropped downward to sea level. The columns have a maximum diameter of 27 inches and a maximum height of 36 feet. In an outcrop about half a mile east of the Causeway and believed to be part of the same flow, the columns are bent (in the feature called the Giant's Organ) in the supposed direction of flowage.

The writer's count of pentagons and hexagons compares favorably with a count made

by a Mr. O'Reilly in 1879 and recorded in the literature. Mr. O'Reilly found 31 per cent of pentagons and 48 per cent of hexagons.

Tomkeieff (1940) considered the Giant's Causeway region a type locality for columnar jointing. He divided every flow of the area into (1) a lower basal "colonnade" having regular vertical columns of the largest diameter, and (2) an upper "entablature" composed of three subzones which from top to bottom were vesicular, pseudo-columnar, and sheeted with some curved and relatively small diameter columns. He considered the Giant's Causeway a fine example of the "colonnade", developed through slow, uniform cooling at the base of a rather thick flow (about 120 feet).

The Auvergne region of central France was examined under the general guidance of Dr. Maurice Roques of the Laboratoire de Géologie, Clermont-Ferrand. Excellent jointing was seen only at the top of Mount Rodeix, and the predominance of pentagonal columns there was very evident. The average diameter of the pillars was about 1 foot, and the maximum diameter was 19 inches; the maximum height was 45 feet. The outcrop reminds one of the Devil's Postpile in California.

At the Devil's Tower in Wyoming, the huge mass of intrusive rock (865 feet high) shows marvelous development of some of the largest columnar joints in the world. The rock pillars are vertical or nearly so in the upper two-thirds of the butte, but in the lower or basal portion they bend outward into a broad shoulder area and give way to vertical, inclined, and horizontal joint sets which divide the rock into many blocks and sheets. The largest column observed was 16½ feet in diameter, but the average diameter was 7–8 feet. A count was difficult because most of the columns found as talus are rounded; thus some of the columns had to be viewed as they formed a part of the Tower itself.

The dominance of pentagons over hexagons at the Tower apparently has little relation to the origin of columns in general, since authorities are divided as to whether the structure was a laccolith or a volcanic neck. The presence near by of the Missouri Buttes, which generally have been called laccoliths, led the National

TABLE 1.—COUNTS OF COLUMNAR JOINTS IN ORDINARY EXPOSURES

Locality	Number of sides and percentage						Total columns counted
	3	4	5	6	7	8	
Pleistocene basalt flow, Craters of Moon region, Idaho	....	14 (28%)	28 (56%)	8 (16%)	....	... ...	50
Pleistocene basalt flow, Dunsmuir, California	1 (.5%)	29 (14.5%)	92 (46%)	67 (33.5%)	9 (4.5%)	2 (1%)	200
Miocene basalt flow, Lewiston, Idaho*	....	5 (7.5%)	30 (45%)	28 (41.5%)	7 (6%)	... ...	67

* Count through the courtesy of Dr. C. D. Campbell, State College of Washington

TABLE 2.—COUNTS OF COLUMNAR JOINTS IN FAMOUS LOCALITIES

Locality	Number of sides and percentage						Total columns counted
	3	4	5	6	7	8	
Giant's Causeway basalt, north Ireland	....	18 (4.5%)	140 (35%)	204 (51%)	37 (9.25%)	1 (.25%)	400
Mount Rodeix basalt, Auvergne region, France	....	30 (15%)	100 (50%)	65 (32.5%)	5 (2.5%)	....	200
Devil's Tower phonolite, eastern Wyoming	....	17 (17%)	42 (42%)	35 (35%)	6 (6%)	....	100
Devil's Postpile basalt, eastern California	2 (.5%)	38 (9.5%)	150 (37.5%)	178 (44.5%)	32 (8%)		400

Parks Service for many years to call the intrusion a laccolith, but recent opinion seems to favor considering the Tower a volcanic neck. The Tower resembles several necks of the Navajo-Hopi country of Arizona and a neck about 500 feet high near Catania, Sicily.

The Devil's Postpile of eastern California shows numerous columns that are bent laterally, thus giving the name to the lava remnant. The pillars are up to 60 feet high and 3½ feet in diameter. The cause of the bending is not known to the writer, but presumably it is related to proximity to irregular cooling surfaces of the Pleistocene flow, probably in the middle or near the base.

In making the count presented in Table 2, care was taken to avoid columns with rounded surfaces; this procedure undoubtedly accounts for the difference between the writer's count and one made by a ranger naturalist of the National Parks Service (Hartesveldt, 1952, p. 145). The writer's count showed only 44½ per cent of hexagons, whereas Hartesveldt's count had 55½ per cent of hexagons. However, both counts demonstrate that hexagons dominate; therefore there was a close approach to ideal cooling conditions.

It is difficult to place the Devil's Postpile vertically within the lava flow, but from field observations it seems to be basal; consequently it would belong in the "colonnade" of Tomkeieff.

An important analysis of the probable factors bearing upon the origin of columns ranging up to 120 feet in height in the basalt of the Sydenham region near Melbourne, Australia, was made by James (1920). Counts of several hundred columns gave the following percentages: quadrilaterals 3, pentagons 22, hexagons 40, heptagons (7 sides) 22, and octagons 13. James did not speculate on probable causes of the percentages, but it is noteworthy that he found such high percentages of heptagons and octagons. He was emphatic in his belief that bending of the columns could not occur by flowage after the columns formed.

Thus, in most outcrops of columnar jointing pentagonal prisms are dominant. It is only in such localities as the Devil's Postpile, the Giant's Causeway, and the flows of Sydenham, Australia, that exceptionally favorable circumstances produced more hexagons than any other form.

References Cited

Billings, M. P., 1954, Structural geology: N. Y., Prentice Hall, 514 p.

Hartesveldt, R. J., 1952, The geologic story of the Devil's Postpile: Yosemite Nature Notes, v. 31, p. 140–149

James, Albert V. G., 1920, Factors producing columnar structure in lavas and its occurrence near Melbourne, Australia: Jour. Geology, v. 28, p. 458–469

Matthes, F. E. (edited by Fritiof Fryxell), 1956, Sequoia National Park; a geological album: Berkeley, Univ. of Calif. Press, 136 p.

Rohleder, Herbert P. T., 1929, Geological guide to the Giant's Causeway and the north coast of Antrim: Belfast, Wm. Sweeney, 32 p.

Tomkeieff, S. I., 1940, The basalt lavas of the Giant's Causeway District of northern Ireland: Bull. Volcanologique, v. 6, p. 89–143

Fresno State College, Fresno, Calif.

Manuscript Received by the Secretary of the Society, September 16, 1958